

MASTER
MSC-PA-R-68-7
Copy No.

T77-12951



NATIONAL AERONAUTICS AND SPACE ADMINISTRATION

C.

MSC-PA-R-68-7

APOLLO 5 MISSION REPORT

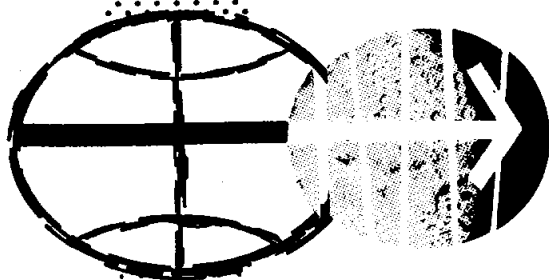
LIBRARY COPY

JUL 14 1977

JOHNSON SPACE CENTER
HOUSTON, TEXAS

DISTRIBUTION AND REFERENCING

This paper is not suitable for general distribution or referencing. It may be referenced only in other working correspondence and documents by participating organizations.



MANNED SPACECRAFT CENTER
HOUSTON, TEXAS
MARCH 1968

APOLLO SPACECRAFT FLIGHT HISTORY

<u>Mission</u>	<u>Spacecraft</u>	<u>Description</u>	<u>Launch date</u>	<u>Launch site</u>
PA-1	BP-6	First pad abort	Nov. 7, 1963	White Sands Missile Range, N. Mex.
A-001	BP-12	Transonic abort	May 13, 1964	White Sands Missile Range, N. Mex.
AS-101	BP-13	Nominal launch and exit environment	May 28, 1964	Cape Kennedy, Fla.
AS-102	BP-15	Nominal launch and exit environment	Sept. 18, 1964	Cape Kennedy, Fla.
A-002	BP-23	Maximum dynamic pressure abort	Dec. 8, 1964	White Sands Missile Range, N. Mex.
AS-103	BP-16	Micrometeoroid experiment	Feb. 16, 1965	Cape Kennedy, Fla.
A-003	BP-22	Low-altitude abort (planned high- altitude abort)	May 19, 1965	White Sands Missile Range, N. Mex.
AS-104	BP-26	Micrometeoroid experiment and service module RCS launch environment	May 25, 1965	Cape Kennedy, Fla.
PA-2	BP-23A	Second pad abort	June 29, 1965	White Sands Missile Range, N. Mex.
AS-105	BP-9A	Micrometeoroid experiment and service module RCS launch environment	July 30, 1965	Cape Kennedy, Fla.
A-004	SC-002	Power-on tumbling boundary abort	Jan. 20, 1966	White Sands Missile Range, N. Mex.
AS-201	SC-009	Supercircular entry with high heat rate	Feb. 26, 1966	Cape Kennedy, Fla.
AS-202	SC-011	Supercircular entry with high heat load	Aug. 25, 1966	Cape Kennedy, Fla.

(Continued inside back cover)

APOLLO 5 MISSION REPORT

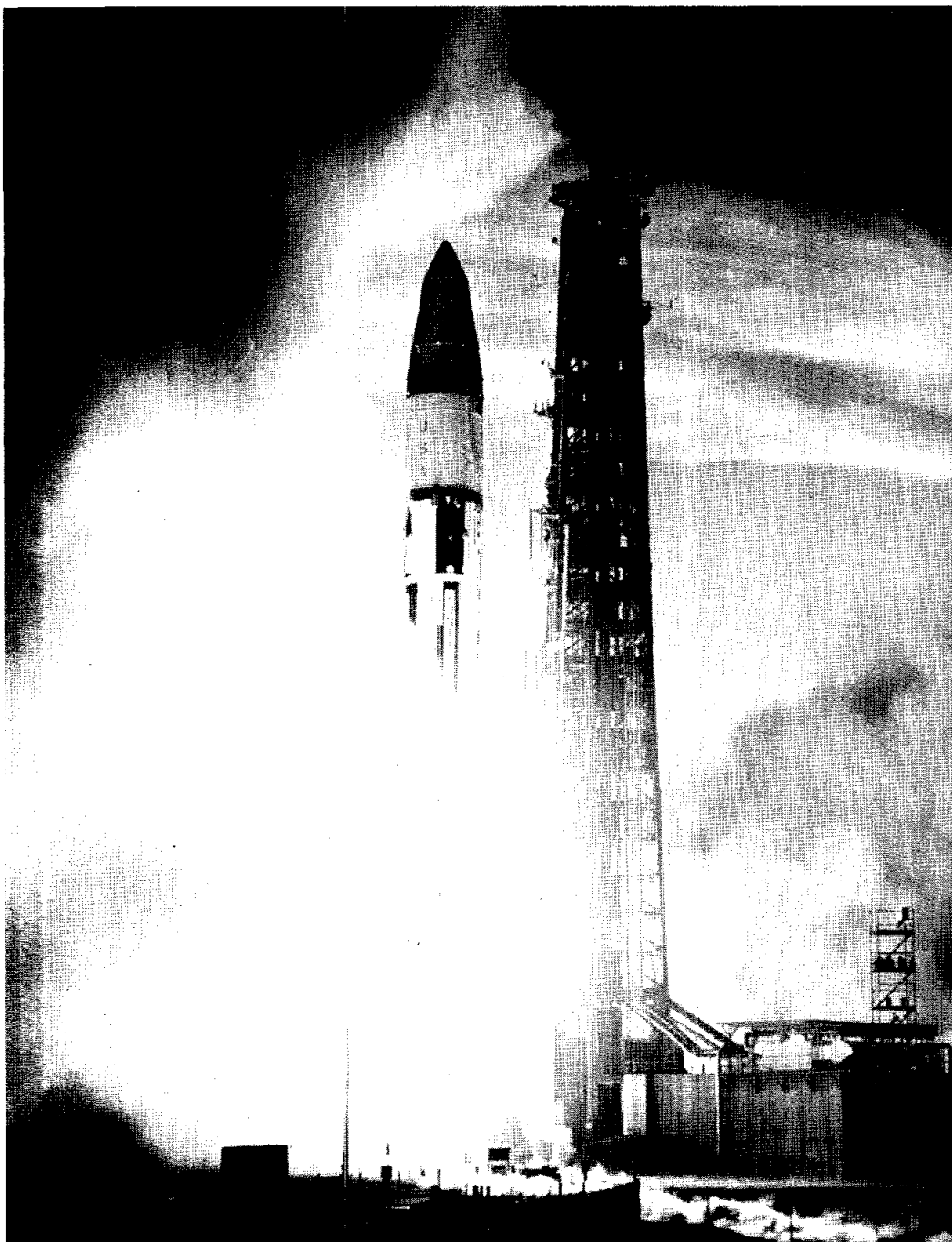
Prepared by: Apollo 5 Mission Evaluation Team

Approved by: George M Low
George M Low
Manager
Apollo Spacecraft Program

3-27

March 27, 1968

NATIONAL AERONAUTICS AND SPACE ADMINISTRATION
MANNED SPACECRAFT CENTER
HOUSTON, TEXAS



Lift-off of Apollo 5 space vehicle.

CONTENTS

Section		Page
	TABLES	ix
	FIGURES	xi
	ABBREVIATIONS AND ACRONYMS	xxii
1.0	<u>SUMMARY</u>	1-1
2.0	<u>MISSION DESCRIPTION</u>	2-1
	2.1 PLANNED MISSION	2-1
	2.2 ACTUAL MISSION	2-1
3.0	<u>TRAJECTORY DATA</u>	3-1
	3.1 LAUNCH	3-1
	3.2 ORBIT	3-2
	3.2.1 Trajectory Profile Analysis	3-2
	3.2.2 Lunar Module/S-IVB Stage Separation	3-3
	3.2.3 Maneuver Profile Analysis	3-4
4.0	<u>LAUNCH VEHICLE PERFORMANCE SUMMARY</u>	4-1
5.0	<u>COMMAND AND SERVICE MODULE PERFORMANCE</u>	5-1
6.0	<u>LUNAR MODULE PERFORMANCE</u>	6.1-1
	6.1 STRUCTURES	6.1-1
	6.1.1 Loads	6.1-1
	6.1.2 Vibrations	6.1-3
	6.2 THERMAL CONTROL	6.2-1
	6.2.1 Launch Phase Thermal Response	6.2-1
	6.2.2 Control Engine Plume Impingement	6.2-1

Section	Page
6.2.3 Descent Stage Heat Shield	6.2-2
6.2.4 Abort Staging	6.2-3
6.2.5 Ascent Stage Structure	6.2-4
6.2.6 Second Ascent Engine Firing	6.2-5
6.3 LANDING GEAR	6.3-1
6.4 PYROTECHNIC	6.4-1
6.5 ELECTRICAL POWER	6.5-1
6.6 MISSION PROGRAMMER	6.6-1
6.7 INSTRUMENTATION	6.7-1
6.7.1 Development Flight Instrumentation . . .	6.7-1
6.7.2 Operational Instrumentation	6.7-3
6.7.3 Calibration	6.7-4
6.7.4 Launch Vehicle Instrument Unit	6.7-4
6.8 COMMUNICATIONS	6.8-1
6.8.1 LM Communications Performance	6.8-1
6.8.2 LM/Network Communications System Performance	6.8-2
6.9 RADAR	6.9-1
6.10 GUIDANCE AND CONTROL	6.10-1
6.10.1 Summary	6.10-1
6.10.2 Integrated System Performance	6.10-1

Section	Page
6.10.3 Primary Guidance, Navigation, and Control System Performance	6.10-5
6.10.4 Stabilization and Control System Performance	6.10-7
6.11 REACTION CONTROL	6.11-1
6.11.1 System Pressures and Temperatures . . .	6.11-1
6.11.2 Propellant Utilization	6.11-3
6.11.3 Control Engine Performance	6.11-5
6.12 DESCENT PROPULSION	6.12-1
6.12.1 Start Characteristics	6.12-1
6.12.2 Transient Characteristics	6.12-2
6.12.3 Engine Throttle Response	6.12-2
6.12.4 Steady-State Characteristics	6.12-2
6.12.5 Shutoff Valve Phasing	6.12-3
6.12.6 Propellant Quantity Gaging	6.12-4
6.12.7 Supercritical Helium Pressurization	6.12-4
6.13 ASCENT PROPULSION	6.13-1
6.13.1 Propellant Loading	6.13-1
6.13.2 Steady-State Performance	6.13-1
6.13.3 Chamber Pressure Oscillations	6.13-2
6.13.4 Propellant Pressurization	6.13-4
6.14 CREW STATION	6.14-1
6.15 ENVIRONMENTAL CONTROL	6.15-1

Section		Page
	6.15.1 Cabin Pressure	6.15-1
	6.15.2 Water System	6.15-2
	6.15.3 Heat Transport Section	6.15-2
	6.16 CONSUMABLES	6.16-1
	6.17 ABORT STAGING	6.17-1
7.0	<u>FLIGHT CREW</u>	7-1
8.0	<u>BIOMEDICAL EVALUATION</u>	8-1
9.0	<u>MISSION SUPPORT PERFORMANCE</u>	9-1
	9.1 FLIGHT CONTROL	9-1
	9.1.1 Prelaunch Operations	9-1
	9.1.2 Powered Flight	9-2
	9.1.3 Orbital Flight	9-3
	9.2 NETWORK PERFORMANCE	9-14
	9.2.1 Telemetry	9-14
	9.2.2 Tracking	9-14
	9.2.3 Command	9-14
	9.2.4 Mission Control Center Central Processors	9-15
	9.2.5 Miscellaneous Problems	9-15
	9.3 RECOVERY OPERATIONS	9-17
10.0	<u>EXPERIMENTS</u>	10-1
11.0	<u>CONCLUSIONS</u>	11-1
12.0	<u>ANOMALY SUMMARY</u>	12-1

Section	Page
12.1 ERRATIC FREON COOLING DURING COUNTDOWN	12-1
12.2 PREMATURE SHUTDOWN OF THE FIRST DESCENT ENGINE BURN	12-2
12.3 ABRUPT CHANGE IN CABIN PRESSURE LEAK RATE.	12-3
12.4 OUT-OF-PHASE INDICATION FROM DESCENT ENGINE PROPELLANT SHUTOFF VALVES	12-4
12.5 ABRUPT CHANGES IN RECEIVED UHF SIGNAL STRENGTH	12-4
12.6 EXCESSIVE CONTROL ENGINE PROPELLANT USAGE	12-5
12.6.1 Discrepant Manifold Pressure Indications	12-5
12.6.2 Inadvertent Closure of Oxidizer Shutoff Valve	12-6
12.6.3 Thrust Chamber Failure	12-6
12.6.4 High Cluster Temperatures	12-7
12.7 FAILURE OF DESCENT STAGE FIBERGLASS THERMAL SHIELD	12-7
12.8 INSTRUMENTATION DISCREPANCIES	12-8
12.8.1 Adapter Panel Deployment	12-8
12.8.2 Separation Distance Monitors	12-8
12.8.3 Pressure and Temperature Sensors	12-9
12.8.4 Vibration Measurement	12-9
13.0 <u>VEHICLE AND SYSTEMS DESCRIPTION</u>	13-1
13.1 COMMAND AND SERVICE MODULES	13-3
13.2 LUNAR MODULE	13-4
13.2.1 Structures	13-6

Section	Page
13.2.2 Thermal Control	13-7
13.2.3 Pyrotechnics	13-8
13.2.4 Electrical Power	13-9
13.2.5 Instrumentation	13-10
13.2.6 Communications	13-12
13.2.7 Guidance and Control	13-15
13.2.8 Reaction Control	13-18
13.2.9 Descent Propulsion	13-19
13.2.10 Ascent Propulsion	13-21
13.2.11 Environmental Control	13-23
13.3 LAUNCH VEHICLE	13-52
13.3.1 S-IB Stage	13-52
13.3.2 S-IVB Stage	13-52
13.3.3 Instrument Unit	13-53
13.4 ADAPTER AND NOSE CONE	13-56
13.5 WEIGHT AND BALANCE DATA	13-60
14.0 <u>VEHICLE HISTORIES</u>	14-1
15.0 <u>SUPPLEMENTAL REPORTS</u>	15-1
16.0 <u>REFERENCES</u>	16-1
17.0 <u>DISTRIBUTION</u>	17-1

TABLES

Table		Page
2-I	APOLLO 5 MISSION EVENTS	2-3
3-I	DEFINITION OF TRAJECTORY AND ORBITAL PARAMETERS	3-6
3-II	LAUNCH PHASE PLANNED AND ACTUAL TRAJECTORY PARAMETERS	3-7
3-III	ORBITAL PHASE PLANNED AND ACTUAL TRAJECTORY PARAMETERS	3-9
3-IV	MISSION PROGRAMMER SEQUENCES III AND V STATE VECTOR COMPARISON	3-12
3-V	NAVIGATION STATE VECTOR COMPARISONS	3-13
3-VI	ORBITAL ELEMENTS	3-14
6.1-I	LM MAXIMUM LOADING CONDITIONS	6.1-7
6.1-II	LM OUTRIGGER LOADS AT END OF S-IB BOOST (MAXIMUM AXIAL ACCELERATION)	6.1-8
6.1-III	LM/ADAPTER INTERACTION LOADS AT END OF S-IB BOOST (MAXIMUM AXIAL ACCELERATION)	6.1-9
6.1-IV	PEAK SURFACE PRESSURES AT STAGING	6.1-10
6.1-V	VIBRATION MEASUREMENTS	6.1-11
6.1-VI	VIBRATION LEVELS TO WHICH EQUIPMENT MOUNTED ON THE AFT EQUIPMENT RACK WAS TESTED AT 210 Hz	6.1-12
6.6-I	MISSION PROGRAMMER SEQUENCE III	6.6-2
6.6-II	MISSION PROGRAMMER SEQUENCE V	6.6-4
6.7-I	USABLE PULSE CODE MODULATED DATA	6.7-5
6.8-I	S-BAND RF SYSTEM PERFORMANCE	6.8-7
6.8-II	NETWORK/LM S-BAND TRANSMISSION COMBINATION SUMMARY	6.8-9

Table		Page
6.10-I	STATE VECTOR COMPARISON AT 00:10:00.86 IN LM-1 INERTIAL COORDINATE SYSTEM	6.10-8
6.10-II	PERFORMANCE CHARACTERISTICS DURING MISSION PROGRAMMER SEQUENCE III	6.10-9
6.10-III	PRELIMINARY INERTIAL MEASUREMENT UNIT ERROR SOURCES	6.10-10
6.10-IV	INFLIGHT BIAS COMPUTATION	6.10-11
6.10-V	LM-1 MAJOR MODE TIMELINE	6.10-12
6.11-I	ASCENT PROPELLANT USED BY THE REACTION CONTROL ENGINES	6.11-10
6.11-II	REACTION CONTROL ENGINE INJECTOR TEMPERATURES . . .	6.11-11
6.12-I	DESCENT ENGINE TRANSIENT CHARACTERISTICS	6.12-6
6.12-II	SUPERCRITICAL HELIUM HEAT EXCHANGER PERFORMANCE	6.12-7
6.13-I	ASCENT ENGINE TRANSIENT ANALYSIS SUMMARY	6.13-5
6.16-I	CONSUMABLES	6.16-2
13.2-I	LM-1 INSTRUMENTATION PARAMETERS	13-25
13.5-I	MASS PROPERTIES	13-61

FIGURES

Figure		Page
2-1	Planned and actual Apollo 5 mission	2-7
2-2	Apollo 5 mission detailed timeline	
	(a) 00:00:00 to 02:00:00	2-8
	(b) 02:00:00 to 04:00:00	2-9
	(c) 04:00:00 to 06:00:00	2-10
	(d) 06:00:00 to 07:00:00	2-11
	(e) 07:00:00 to 08:00:00	2-12
3-1	Apollo 5 mission ground track	3-15
3-2	Trajectory parameters during the launch phase	
	(a) Latitude, longitude, and altitude	3-16
	(b) Space-fixed flight-path angle and velocity . .	3-17
	(c) Earth-fixed flight-path angle and velocity . .	3-18
	(d) Mach number and dynamic pressure	3-19
3-3	Statistical summary of tracker residuals	3-20
3-4	Space-fixed velocity, flight-path angle, and altitude during the orbital phase	3-21
3-5	Apogee and perigee altitude profile	3-22
3-6	Space-fixed velocity, space-fixed flight-path angle, and altitude during maneuvers	
	(a) Second and third descent engine firings, and first ascent engine firing	3-23
	(b) Second ascent engine firing	3-24
6.1-1	Launch winds	6.1-13
6.1-2	Comparison of adapter body loads at the LM/adapter interface with limit design body load capabilities	6.1-14
6.1-3	Comparison of adapter body loads at the adapter/ instrument unit interface with limit design body load capabilities	6.1-15

Figure		Page
6.1-4	Adapter vent pressure	6.1-16
6.1-5	Lift-off accelerations	
	(a) X-axis translation and rotation, and Y-axis translation	6.1-17
	(b) Y-axis rotation, and Z-axis translation and rotation	6.1-18
6.1-6	S-IB shutdown	
	(a) X-axis translation and rotation, and Y-axis translation	6.1-19
	(b) Y-axis rotation and Z-axis translation and rotation	6.1-20
6.1-7	LM/adapter interaction loads sign convention and strut identification	6.1-21
6.1-8	Typical outrigger strut launch loads	6.1-22
6.1-9	Ascent stage base heat shield pressure measurement locations	6.1-23
6.1-10	Descent stage upper surface pressure measurement locations	6.1-24
6.1-11	Comparison of navigation base vibration response at lift-off to current flight vibration and actual qualification test levels	6.1-25
6.1-12	Comparison of the landing radar antenna vibration response at lift-off to current flight vibration criteria and acceptance vibration test responses	6.1-26
6.1-13	Comparison of ascent stage oxidizer tank bottom cover vibration response at lift-off to current flight criteria	6.1-27
6.1-14	Comparison of ascent stage aft equipment rack vibration response at lift-off to current flight vibration criteria	6.1-28

Figure		Page
6.1-15	Vibration measurements during mission programmer sequence III	
	(a) Instrumentation/telemetry noise floor (engines not operating)	6.1-29
	(b) Descent engine thrust chamber, ascent engine support structure, and inertial measurement unit during ignition and 10-percent throttle for descent engine third firing	6.1-30
	(c) Descent engine thrust chamber, ascent engine thrust chamber, ascent stage support structure, and inertial measurement unit during abort staging	6.1-31
	(d) Ascent engine thrust chamber, ascent engine support structure, and inertial measurement during shutdown of first ascent engine firing	6.1-32
6.2-1	Descent stage quadrant I control engine plume impingement sensor locations and configuration. . .	6.2-6
6.2-2	Descent stage quadrant III control engine plume impingement sensor locations and installation . . .	6.2-7
6.2-3	Descent stage insulation blanket temperatures during LM/S-IVB stage separation	
	(a) Sensors GB3033T and GB3025T	6.2-8
	(b) Sensors GB3031T and GB3021T	6.2-8
	(c) Sensor GB3023T	6.2-9
	(d) Sensors GB3027T and GB3029T	6.2-10
6.2-4	Descent stage base heat shield sensor locations . . .	6.2-11
6.2-5	Descent stage upper surface temperature instrumentation	6.2-12
6.2-6	Temperature measured on upper surface of descent stage	6.2-13
6.2-7	Ascent stage heat shield sensor location	6.2-14
6.2-8	Cabin floor and ascent engine cover temperatures . .	6.2-15
6.2-9	Cabin wall temperatures	6.2-16

Figure		Page
6.2-10	Ascent stage helium tank temperature	6.2-17
6.2-11	Temperature of steerable S-band antenna	6.2-18
6.2-12	Temperature of VHF inflight antenna	6.2-19
6.5-1	Electrical power characteristics	6.5-2
6.5-2	AC voltage transients	6.5-3
6.5-3	Battery load sharing during mission programmer sequence III	6.5-4
6.8-1	Communication system configurations	6.8-10
6.8-2	Received unified S-band downlink carrier power, Carnarvon, revolution 1	6.8-11
6.8-3	Primary to secondary unified S-band system switchover, Texas, revolution 1	6.8-12
6.8-4	Received unified S-band uplink carrier power, Texas, revolution 1	6.8-13
6.8-5	Received unified S-band downlink carrier power, Texas, revolution 1	6.8-14
6.8-6	Received unified S-band uplink carrier power, MILA, revolution 1-2	6.8-15
6.8-7	Received unified S-band downlink carrier power, MILA, revolution 1-2	6.8-16
6.8-8	Received unified S-band uplink carrier power, Redstone, revolution 2	6.8-17
6.8-9	Received unified S-band downlink carrier power, Redstone, revolution 2	6.8-18
6.8-10	Received unified S-band downlink carrier power, Guaymas, revolution 2	6.8-19
6.8-11	Received unified S-band uplink carrier power, MILA, revolution 2-3	6.8-20

Figure		Page
6.8-12	Received unified S-band downlink carrier power, MILA, revolution 2-3	6.8-21
6.8-13	Received unified S-band uplink carrier power, Carnarvon, revolution 3	6.8-22
6.8-14	Received unified S-band downlink carrier power, Carnarvon, revolution 3	6.8-23
6.8-15	Received unified S-band downlink carrier power, Goldstone, revolution 4	6.8-24
6.8-16	Received unified S-band uplink carrier power, Guaymas, revolution 4	6.8-25
6.8-17	Received unified S-band downlink carrier power, Guaymas, revolution 4	6.8-26
6.8-18	Received unified S-band uplink carrier power, Texas, revolution 4	6.8-27
6.8-19	Received unified S-band downlink carrier power, Texas, revolution 4	6.8-28
6.8-20	Received unified S-band uplink carrier power, Hawaii, revolution 5	6.8-29
6.8-21	Received unified S-band downlink carrier power, Hawaii, revolution 5	6.8-30
6.8-22	Typical range code acquisition sequence (128 inte- grations per step)	6.8-31
6.8-23	S-band RF spectrum	6.8-32
6.8-24	Turned-around unified S-band up-data signal-to-noise ratio, MILA, revolution 1-2	6.8-33
6.8-25	Turned-around unified S-band up-voice signal-to-noise ratio, Guaymas, revolution 2	6.8-33
6.8-26	Turned-around unified S-band up-voice signal-to-noise ratio, MILA, revolution 2-3	6.8-33
6.8-27	Unified S-band PCM bit error probability, Carnarvon, revolution 1	6.8-34

Figure		Page
6.8-28	Unified S-band bit error probability, Guaymas, revolution 4	6.8-34
6.8-29	Unified S-band PCM bit error probability, Hawaii revolution 5	6.8-34
6.8-30	Total received VHF power, Guaymas, revolution 4 . .	6.8-35
6.8-31	Total received VHF power, Texas, revolution 4 . . .	6.8-36
6.8-32	VHF PCM bit error probability, Carnarvon, revolution 1	6.8-37
6.8-33	VHF PCM bit error probability, Guaymas, revolution 4	6.8-37
6.8-34	VHF PCM bit error probability, Hawaii revolution 5	6.8-37
6.8-35	Total received UHF and VHF power, Carnarvon, revolution 1	6.8-38
6.10-1	LM/S-IVB stage separation sequence of events . . .	6.10-13
6.10-2	Spacecraft dynamics - separation and maneuver to cold-soak attitude	6.10-14
6.10-3	Gimbal angle comparison - maneuver to cold-soak attitude	6.10-15
6.10-4	Typical limit cycle during cold-soak attitude hold	6.10-16
6.10-5	Pitch and roll phaseplane	6.10-17
6.10-6	Spacecraft dynamics - maneuver to attitude for first descent engine firing	6.10-18
6.10-7	Gimbal angle comparison - maneuver to attitude for first descent engine firing	6.10-19
6.10-8	Spacecraft dynamics - maneuver to attitude for second descent engine firing	6.10-20
6.10-9	Gimbal angle comparison - maneuver to attitude for second descent engine firing	6.10-21

Figure		Page
6.10-10	Spacecraft dynamics - mission programmer sequence III	6.10-22
6.10-11	Mission programmer sequence III	6.10-23
6.10-12	Abort staging dynamics	6.10-24
6.10-13	Spacecraft dynamics - second ascent engine firing	
	(a) Ignition and initial portion of firing, with rate control	6.10-25
	(b) Control propellant depletion	6.10-26
6.10-14	Inertial measurement unit coefficient history	
	(a) X-axis accelerometer	6.10-27
	(b) Y-axis accelerometer	6.10-28
	(c) Z-axis accelerometer	6.10-29
	(d) X-axis gyro	6.10-30
	(e) Y-axis gyro	6.10-31
	(f) Z-axis gyro	6.10-32
6.10-15	Inertial measurement unit prelaunch alignment orientation	6.10-33
6.10-16	Launch phase velocity comparisons	
	(a) X-axis	6.10-34
	(b) Y-axis	6.10-35
	(c) Z-axis	6.10-36
6.11-1	Manifold pressure during system activation sequence	6.11-12
6.11-2	Manifold pressures at main A closure	6.11-13
6.11-3	B system manifold pressures at propellant depletion	6.11-14
6.11-4	Helium B tank pressure (corrected to 70° F) during period of propellant depletion	6.11-15
6.11-5	Manifold pressures during A system reactivation . .	6.11-16

Figure		Page
6.11-6	Manifold pressures during period of A system reactivation and crossfeed valve opening	6.11-17
6.11-7	Manifold pressures after interconnect valve closure	6.11-18
6.11-8	Propellant expended	6.11-19
6.11-9	Performance of propellant quantity measuring device	6.11-20
6.11-10	Engine chamber pressures during first firings (separation sequence)	6.11-21
6.11-11	Chamber pressure of engines 4-down and 4-up during high propellant usage following first ascent engine firing	6.11-22
6.11-12	Engine 4-up chamber pressure at B system oxidizer depletion	6.11-24
6.11-13	Ignition pressure spike (detonation) in engine 3-down during operation with two-phase oxidizer at 50 psia manifold pressure and with helium in fuel manifold	6.11-24
6.11-14	Cluster temperatures during the mission	6.11-25
6.11-15	Cluster 1 and engines 1-down and 1-forward injector head temperatures at LM/S-IVB stage separation. .	6.11-26
6.11-16	Cluster 1 and engines 1-down and 1-forward injector head temperatures during mission programmer sequence III	6.11-27
6.11-17	Cluster 2 and engines 2-down and 2-up injector head temperatures during mission programmer sequence III	6.11-28
6.11-18	Cluster 1 and engines 1-down and 1-forward injector head temperatures during second ascent engine firing	6.11-29
6.11-19	Comparison of thermal response of clusters 3 and 4 to control engine activity during second ascent engine firing	6.11-30

Figure		Page
6.12-1	Chamber pressure during start sequence of descent engine firings	6.12-8
6.12-2	Descent propulsion parameters during transition from 10-percent throttle to full throttle (typical of second and third firings)	6.12-9
6.12-3	Chamber pressure during second descent engine firing	6.12-10
6.12-4	Descent engine schematic	6.12-11
6.12-5	Supercritical helium supply pressure during first descent engine firing	6.12-12
6.12-6	Supercritical helium supply pressure during second descent engine firing	6.12-13
6.12-7	Supercritical helium supply pressure during third descent engine firing	6.12-14
6.12-8	Supercritical helium supply pressure during coast period between second and third firings	6.12-15
6.13-1	Chamber pressure during ascent engine firings	
	(a) First firing	6.13-6
	(b) Second firing	6.13-7
6.13-2	Ascent engine chamber pressure oscillations	6.13-8
6.15-1	Pressure of cabin and internal pressure of cabin pressure relief valve	6.15-4
6.15-2	Cabin pressure profile	6.15-5
6.15-3	Water/glycol pump inlet temperature	6.15-6
6.16-1	Water usage	6.16-3
6.16-2	Electrical power consumption	6.16-4
6.16-3	Ascent engine propellant usage	6.16-5
6.16-4	Descent engine propellant usage	6.16-6

xx

Figure	Page
6.16-5 Reaction control propellant usage	6.16-7
6.17-1 Abort staging characteristics	6.17-2
6.17-2 Abort staging sequence, pyrotechnic system A . . .	6.17-3
9.1-1 Real-time decision logic	9-13
13.0-1 Apollo 5 space vehicle	13-2
13.2-1 Lunar module configuration	13-30
13.2-2 Ascent and descent stages of LM-1	13-31
13.2-3 Dimensions of lunar module	13-32
13.2-4 LM ascent stage structure	13-33
13.2-5 LM ascent stage structure (top view)	13-34
13.2-6 Aft equipment bay structure	13-35
13.2-7 Descent stage structure (top view)	13-36
13.2-8 Descent stage structure (side views)	13-37
13.2-9 Locations of explosive devices	13-38
13.2-10 AC power system (contact positions shown are as-flown)	13-39
13.2-11 DC power system (contacts shown in as-flown configuration)	13-40
13.2-12 Operational instrumentation functional block diagram	13-41
13.2-13 Development flight instrumentation data conditioning and processing system	13-42
13.2-14 Development flight instrumentation data transmission system	13-43
13.2-15 Development flight instrumentation ranging and tracking RF system	13-43

Figure		Page
13.2-16	Communication system schematic	13-44
13.2-17	Control paths	
	(a) Primary guidance, navigation, and control . .	13-45
	(b) Backup	13-46
13.2-18	Reaction control system	13-47
13.2-19	Descent propulsion system schematic	13-48
13.2-20	Ascent propulsion propellant/pressurization schematic	13-49
13.2-21	Ascent engine schematic	13-50
13.2-22	Schematic of environmental control system	13-51
13.3-1	S-IB stage	13-54
13.3-2	S-IVB stage	13-55
13.4-1	Location of lunar module within adapter	13-57
13.4-2	Adapter panel separation lines	13-58
13.4-3	Nose cone jettison controller, schematic diagram of system A of a redundant A and B system	13-59
14-1	LM-1 history at Bethpage	14-2
14-2	LM-1 history at Kennedy Space Center	14-3

ABBREVIATIONS AND ACRONYMS

ac, AC	alternating current
ADIA	drift due to acceleration along the input axis
ADOA	drift due to acceleration along the output axis
ADSRA	drift due to acceleration along the spin reference axis
a.m.	ante meridian
amp-hr	ampere hours
amps	amperes
ANT	Antigua tracking station
ASC	Ascension tracking station
BDA	Bermuda tracking station
CAL	California tracking station
cm/sec	centimeter per second
cm/sec ²	centimeter per second per second
CRO	Carnarvon tracking station
CSQ	Coastal Sentry Quebec tracking ship
CYI	Canary Islands tracking station
D	down firing
dB	decibel
dBm	decibels
dc, DC	direct current
deg	degree
° F	degree Fahrenheit

$^{\circ} R$	degree Rankine
DFI	Development Flight Instrumentation
deg/sec	degree per second
E	East
EMU	Eraseable Memory Unit
e.s.t.	eastern standard time, fifth time zone west of Greenwich
F	force
f	fore/aft firing
f_d	doppler frequency
fig.	figure
FM	Frequency Modulation
ft	feet
ft-lb	foot pound
ft/sec	feet per second
ft^3	cubic feet
g	gravity, 32.2 ft/sec^2
GBI	Grand Bahama Island tracking station
GDS	Goldstone tracking station
G.m.t.	Greenwich mean time
GWM	Guam tracking station
GYM	Guaymas tracking station
HAW	Hawaii tracking station
hr	hour

xxiv

Hz	hertz, equivalent to one cycle per second
in.	inch
in-lb	inch pounds
k	kilo-, 1000
KSC	Kennedy Space Center, Florida
lb	pounds
lb/hr	pound per hour
lb/ft ²	pound per square foot
lb/ft ³	pound per cubic foot
lb/min	pound per minute
lb/sec	pound per second
lb-sec	pound-seconds
LH ₂	liquid hydrogen
LM	Lunar Module
LTA	Lunar Module Test Article
M	mega-, 1,000,000
m	milli-, 0.0001
mERU	milli Earth radius units
MIL	Merritt Island tracking station
MILA	Merritt Island Launch Area
min	minute
MLA	Merritt Island tracking station
MSC	Manned Spacecraft Center
msec	millisecond

MSFC	Marshall Space Flight Center
MSFN	Manned Space Flight Network
N	North
NBD	null bias drift
N_2H_4	hydrazine
N_2O_4	nitrogen tetroxide
n. mi	nautical mile
NRZ	non return to zero
n_X, n_Y, n_Z	loads along the X, Y, and Z axes
o.d.	outside diameter
PA-1	ascent propulsion test article
PAT	Patrick Air Force Base tracking station
P_c	chamber pressure
PCM	pulse code modulation
PCMTEA	pulse code modulation and timing electronics assembly
p.m.	post meridian
PM	phase modulation
ppm	parts per million
psfa	pounds per square foot, absolute
psia	pounds per square inch, absolute
psid	pounds per square inch, differential
q	dynamic pressure
R	radius

xxvi

rad	radian
rad/sec ²	radians per second
range zero	integral second before lift-off
RED	Redstone tracking ship
ref.	reference
RF	radio frequency
RKV	Rose Knot Victor tracking ship
R _X , R _Y , R _Z	reactions along X, Y, and Z axes
rms	root mean square
s	side firing
scc/hr	standard cubic centimeter per hour
sec	seconds
S-IB	Saturn IB, launch vehicle
S-IVB	Saturn second stage
sq. in.	square inch
T	time of lift-off
TAN	Tananarive tracking station
TEL IV	telemetry station at KSC
TEX	Texas tracking station
time	referenced to range zero
U	up firing
UDMH	unsymmetrical dimethylhydrazine
UHF	ultrahigh frequency
V	volts

V ac	volts
V dc	volts direct current
VHF	very high frequency
WHS	White Sands tracking station
WTN	Watertown tracking ship
X_A	spacecraft body stations, in.
X, Y, Z	axes
α	angle of attack
ΔV	change in velocity

1.0 SUMMARY

The Apollo 5 mission, the first mission of a flight configuration lunar module (LM-1), was successfully flown on January 22 and 23, 1968. The primary objectives of the Apollo 5 mission were to flight-verify the ascent and descent propulsion systems and the abort staging function for manned flight. These objectives were met.

Lift-off occurred at 22:48:08 G.m.t. (05:48:08 p.m. e.s.t.). The S-IVB stage inserted the lunar module/S-IVB combination into an earth orbit after 10 minutes 3 seconds of powered flight. The lunar module loads and vibrations measured during this phase of the flight were within the design capability of the structures. Cooling commenced after S-IVB stage cutoff, and the equipment temperatures were properly regulated by the coolant system for the remainder of the mission. The lunar module was separated from the S-IVB stage at 00:53:50, using the control engines. Separation disturbances were small. The lunar module was maneuvered to a cold-soak attitude which was maintained by the guidance system until early in the third revolution. A minimal control engine duty cycle was required to maintain the desired attitude.

Midway through the third revolution, the first descent engine firing was initiated. The planned duration of this firing was 38 seconds; however, after only 4 seconds, the guidance system shut down the engine. Both the guidance system and the propulsion system operated properly, and the premature shutdown resulted from incomplete systems coordination.

After the premature shutdown, a planned alternate mission which provided minimum mission requirements was selected. At approximately 06:10:00, the automatic sequencer within the onboard mission programmer initiated the sequencing for the second and third descent engine firings, the abort staging, and the first ascent engine firing. Attitude rate control was maintained with the backup control system. The descent engine gimbaled properly and responded smoothly to the commands to full throttle. The thermal aspects of the supercritical helium pressurization system could not be adequately evaluated because of the short duration of the three descent engine firings. During abort staging, all system operations and vehicle dynamics were satisfactory for manned operations.

After the first ascent engine firing, the primary control system was reselected to control the spacecraft attitudes and rates. Because the primary system had been passive during the abort staging sequence, the computer program did not reflect the change of mass resulting from staging. Therefore, computations of control engine firing times were based on the mass of a two-stage vehicle and resulted in an extremely high propellant usage by the control engines, eventually causing propellant

depletion. Because of excessive control engine activity, the control engine cluster temperatures exceeded the upper red-line limits but without any detrimental effects.

The reaction control system was subjected to abnormal operating conditions as a result of low manifold pressures after propellant depletion. Continued operation under these abnormal conditions resulted in three malfunctions within the system; none had any appreciable effect on the mission.

The second firing of the ascent engine, initiated by the automatic sequencer, began at 07:44:13 and continued until thrust decay at 07:50:03. During the initial portion of the firing, attitude rate control was maintained using propellants from the ascent propulsion tanks through interconnect valves to the control engines. However, the sequencer automatically closed the interconnect valves, thus depleting control propellants. With the loss of rate control, the vehicle began tumbling while the ascent engine was firing. All tracking was lost within 2 minutes after thrust decay. The lunar module had been in a retrograde orientation during the controlled portion of the firing, and trajectory simulations show that the lunar module entered over the Pacific Ocean soon after firing. The predicted point of impact was approximately 400 miles west of the coast of Central America.

The overall performance of the lunar module was good and met all requirements for manned orbital flight. All operational systems were successfully verified, and the abort staging sequence was demonstrated.

2.0 MISSION DESCRIPTION

2.1 PLANNED MISSION

The Apollo 5 mission was planned to consist of two descent engine maneuvers, two ascent engine maneuvers, and an abort staging. The overall planned and actual missions are shown in figure 2-1 and the event times are given in table 2-I. The first descent engine maneuver duration was to be 38 seconds (26 seconds at 10-percent throttle and 12 seconds at full throttle). The second descent engine maneuver thrust profile was to be representative of the profile expected for lunar landing. The profile was to consist of five phases extending over 734 seconds. The abort staging sequence was to be initiated at the end of the random throttling phase with the descent engine operating at full throttle and controlled by the guidance computer. The abort staging sequence was to include descent engine shutdown and ignition of the ascent engine for a 5-second firing.

The second ascent engine maneuver, to propellant depletion (approximately 445 seconds), was to be the termination of the primary mission. Extended mission activities were planned to continue until the remaining consumables were expended.

2.2 ACTUAL MISSION

The actual mission is compared with the planned mission in figure 2-1. All major events during the actual mission are shown in figure 2-2.

Lift-off occurred at 22:48:08 G.m.t. (05:48:08 p.m. e.s.t.) on January 22, 1968 (fig. 2-1). The lunar module was separated from the S-IVB stage at 00:53:50 and was maneuvered to a cold-soak attitude. After two and a half revolutions, the first descent engine maneuver was initiated by a discrete from the guidance computer. As planned prior to flight, the maneuver was begun with less than normal pressure in the propellant tanks. However, as a result, the computer shut down the engine after only 4 seconds because the thrust buildup did not satisfy the programmed velocity/time criteria. Both the guidance system and the propulsion system operated properly, and the premature shutdown was the result of incomplete systems coordination.

After the premature shutdown, an alternate mission — the minimum mission requirements sequence — was selected. The major differences between the planned and the alternate mission were deletion of the 734-second descent engine firing and substitution of mission programmer control for guidance computer control during all firings.

A 33-second firing of the descent engine was initiated at 06:10:46 by an automatic sequence within the mission programmer. The sequence continued with a third descent engine firing, an abort staging, and the first ascent engine firing. The sequence was stopped by ground command after the first ascent engine firing.

A second mission programmer sequence was used to initiate the second ascent engine firing. The firing was planned to continue until propellant depletion. During the initial portion of the firing, rate control was maintained by the control engines, using propellant from the ascent propulsion system through interconnect valves. The sequencer automatically closed the interconnects, and since the control engine propellants were already depleted, the vehicle began to tumble. Vehicle rates became of such magnitude that propellants could not flow into the engine, and helium ingestion caused thrust decay prior to propellant depletion. All tracking was lost about 2 minutes after thrust decay, thus terminating the mission.

TABLE 2-I.- APOLLO 5 MISSION EVENTS

Event	Mission elapsed time, hr:min:sec	
	Planned	Actual
Launch Phase		
Range zero - 22:48:08 G.m.t.	00:00:00	00:00:00
Maximum dynamic pressure	00:01:14.2	00:01:11.5
S-IB stage inboard engine cutoff	00:02:19.3	00:02:19.0
S-IB stage outboard engine cutoff	00:02:22.3	00:02:22.3
S-IB/S-IVB stage separation	00:02:23.6	00:02:23.5
S-IVB stage start command	00:02:25.0	00:02:24.9
S-IVB stage cutoff signal	00:09:58.4	00:09:53.3
Orbital Phase		
Orbital insertion	00:10:08.4	00:10:03.3
Nose cone jettison	00:10:43.5	00:10:38.5
Adapter panel deployment	00:19:58.5	00:19:53.5
Initiate +X translation	00:54:01.5	00:53:50.1
LM/S-IVB stage separation	00:54:06.5	^a 00:53:55.7
Initiate maneuver to cold-soak attitude	00:55:53	00:54:32.3
Initiate maneuver to attitude for first descent engine firing	03:55:31	03:55:09.6
+X translation	03:59:47	03:59:33.9
"Engine on" discrete	03:59:54	03:59:41.4
Engine on	03:59:54	^a 03:59:41.7
"Engine off" discrete	04:00:32	03:59:45.6
Engine off	04:00:32	^a 03:59:45.7

^aBecause of parameter sample intervals, the events shown could have occurred any time in the second previous to the time shown.

TABLE 2-I.- APOLLO 5 MISSION EVENTS - Continued

Event	Mission elapsed time, hr:min:sec	
	Planned	Actual
Mission Programmer Sequence III		
Sequence III initiate	06:10:00	
+X translation on	06:10:05	06:10:07.4
+X translation off	06:10:15	06:10:17.5
+X translation on	06:10:20	06:10:22.4
+X translation off	06:10:25	06:10:27.2
+X translation on	06:10:31	06:10:33.4
Descent engine on (second firing)	06:10:39	^a 06:10:41.7
+X translation off	06:10:44	06:10:46.3
Descent engine to full throttle	06:11:05	06:11:07.8
Engine off	06:11:12	^a 06:11:14.7
+X translation on	06:11:36	06:11:38.4
Descent engine on (third firing)	06:11:44	^a 06:11:46.7
+X translation off	06:11:49	06:11:51.3
Descent engine to full throttle	06:12:10	06:12:12.8
Abort staging	06:12:12	06:12:14.3
Descent engine off	06:12:12	^a 06:12:14.7
Ascent engine on (first firing)	06:12:12	06:12:14.7
Ascent engine off	06:13:14	06:13:14.3

^aBecause of parameter sample intervals, the events shown could have occurred any time in the second previous to the time shown.

TABLE 2-I.- APOLLO 5 MISSION EVENTS - Concluded

Event	Mission elapsed time, hr:min:sec	
	Planned	Actual
Mission Programmer Sequence V		
Sequence V initiate	07:43:55	
+X translation on	07:43:57	07:44:00.3
Ascent engine on (second firing)	07:44:09	07:44:12.7
Engine fire override command		07:44:15
+X translation off	07:44:14	07:44:17.3
+X translation on	07:45:08	07:45:11.3
+X translation off	07:45:24	07:45:27.3
Ascent engine thrust decay		07:50:03

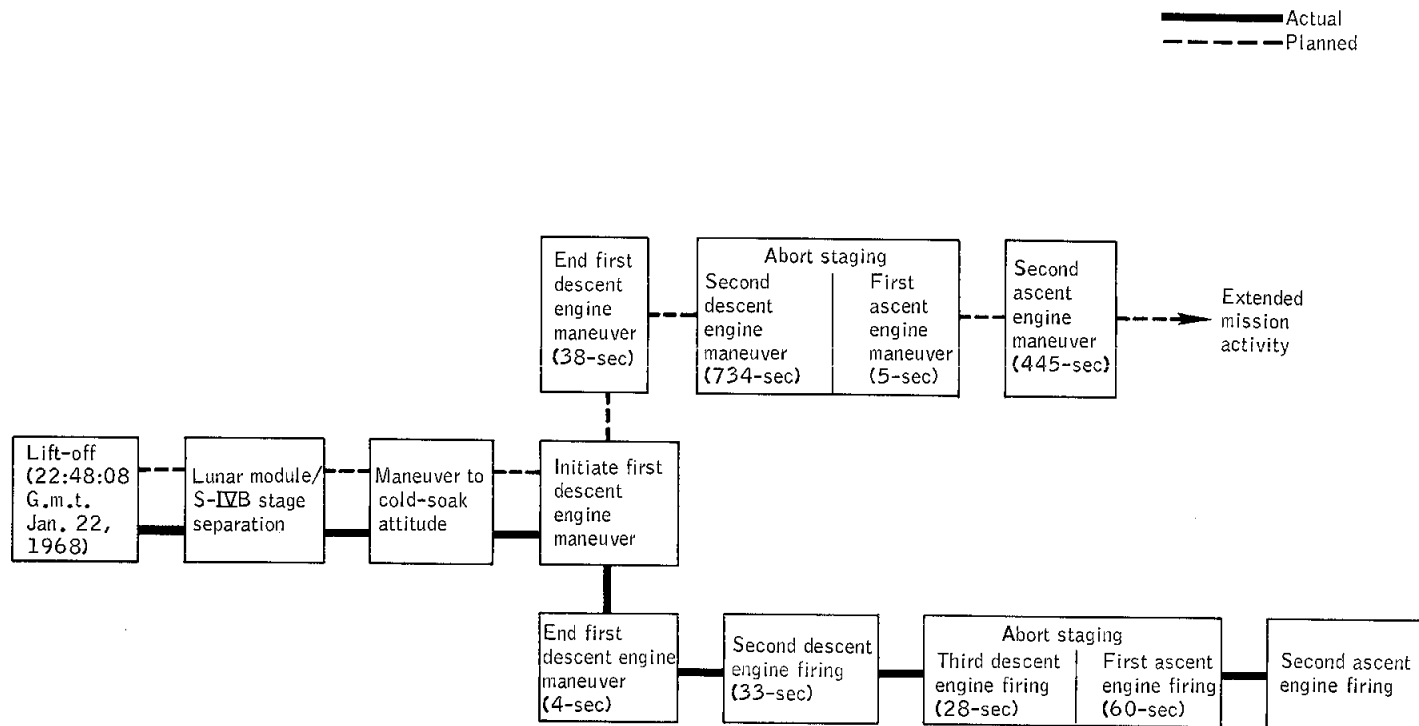
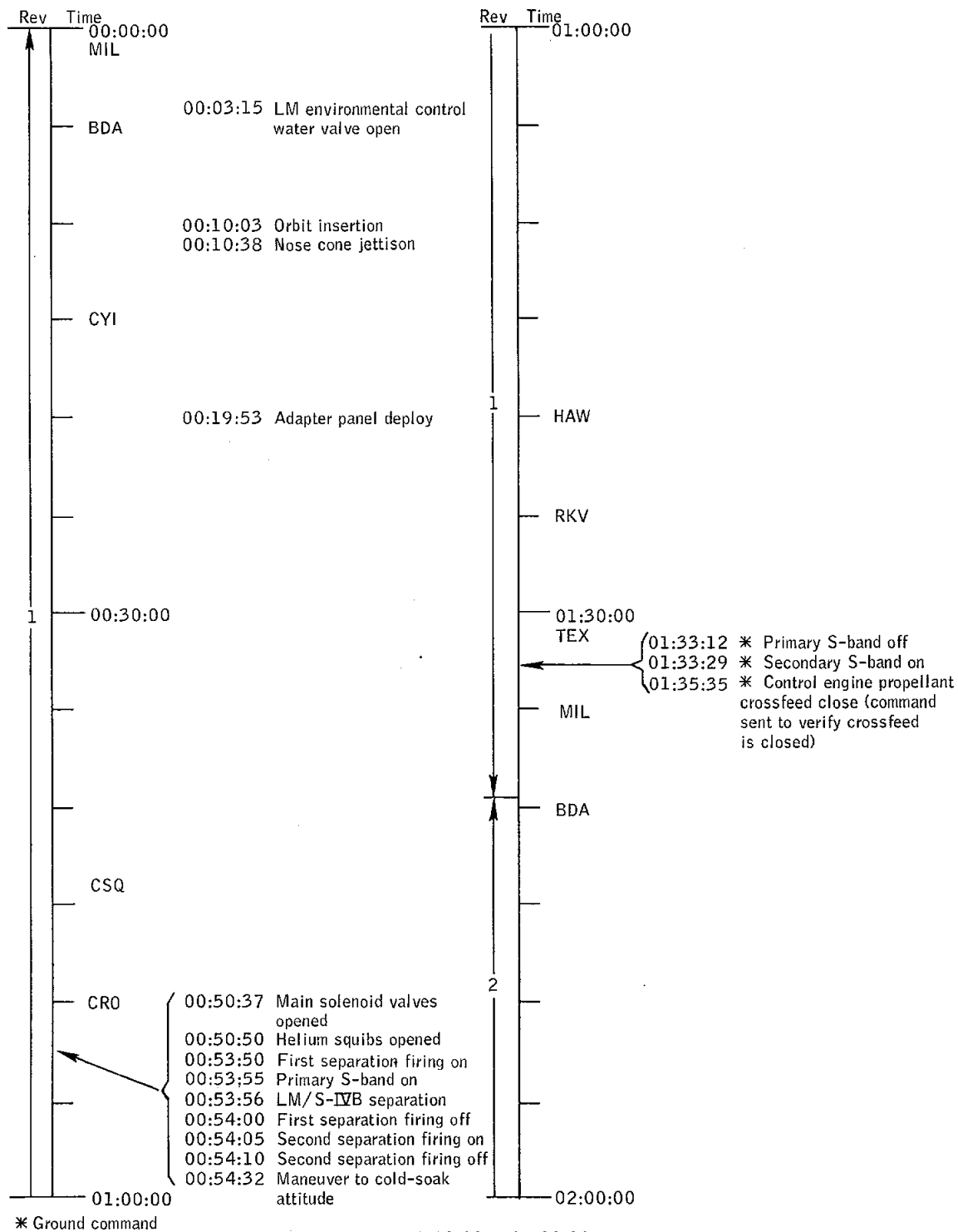


Figure 2-1.- Planned and actual Apollo 5 mission.

NASA-S-68-1923



(a) 00:00:00 to 02:00:00.

Figure 2-2.- Apollo 5 mission detailed timeline.

NASA-S-68-1924

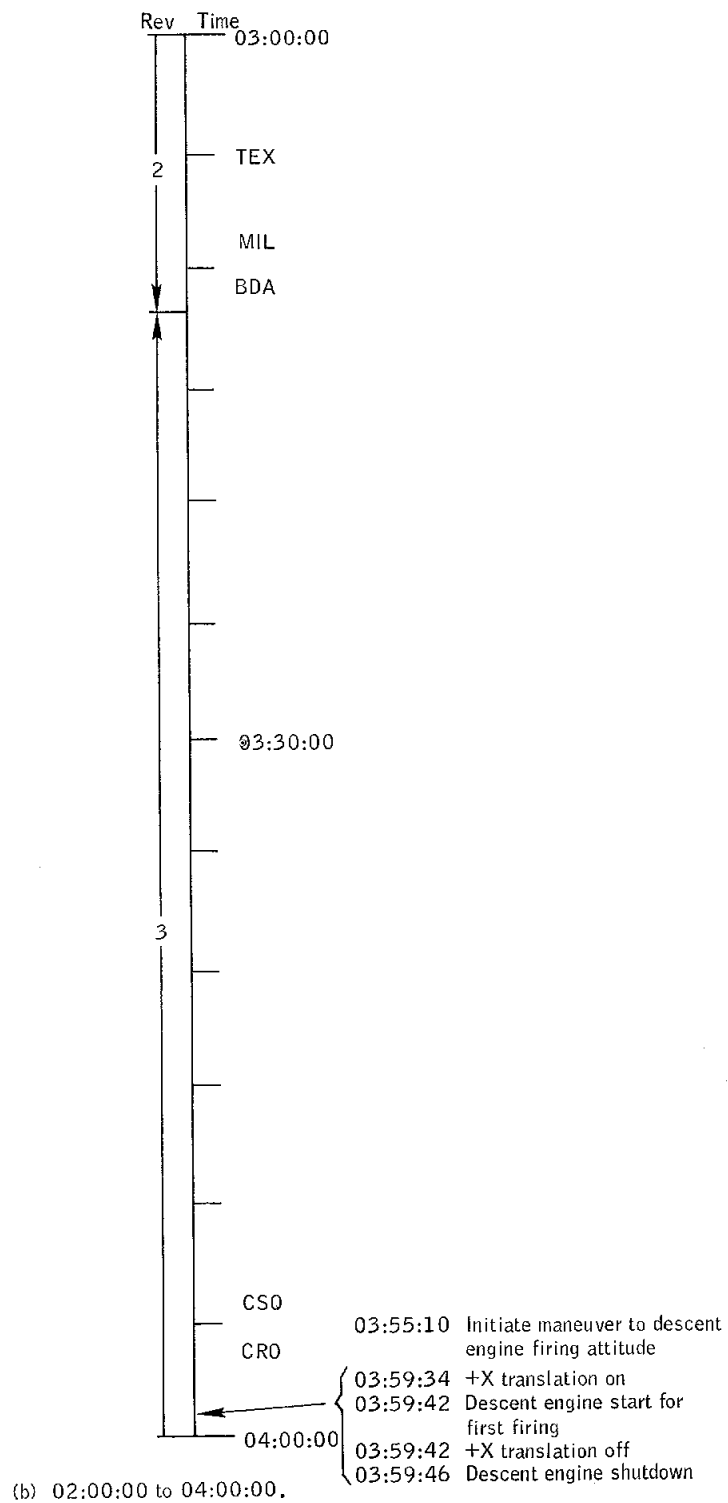
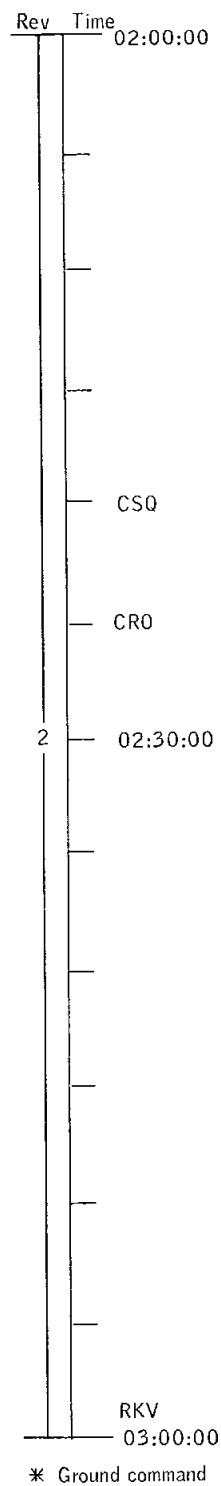
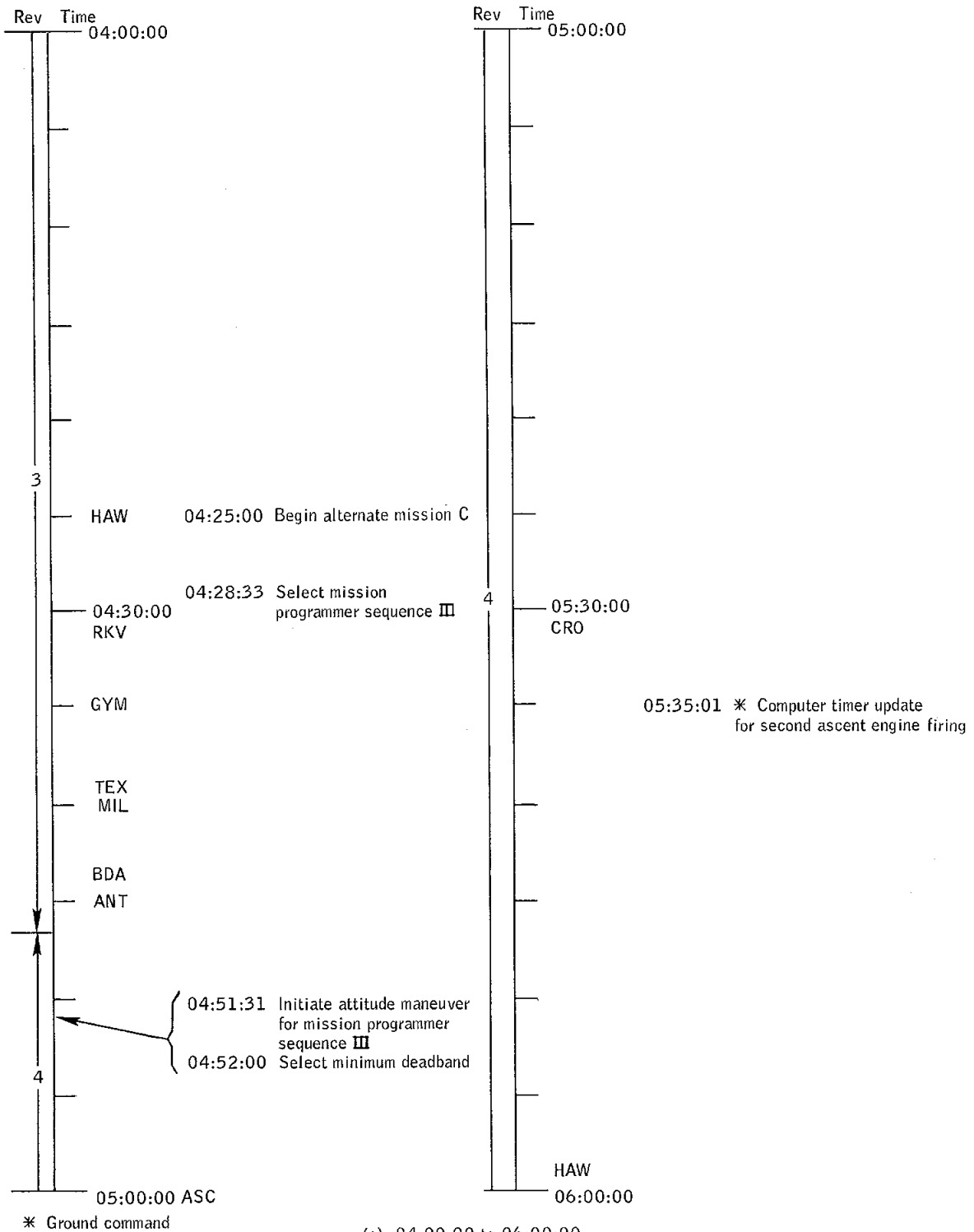


Figure 2-2.- Continued.



(c) 04:00:00 to 06:00:00.

Figure 2-2.- Continued.

NASA-S-68-1926

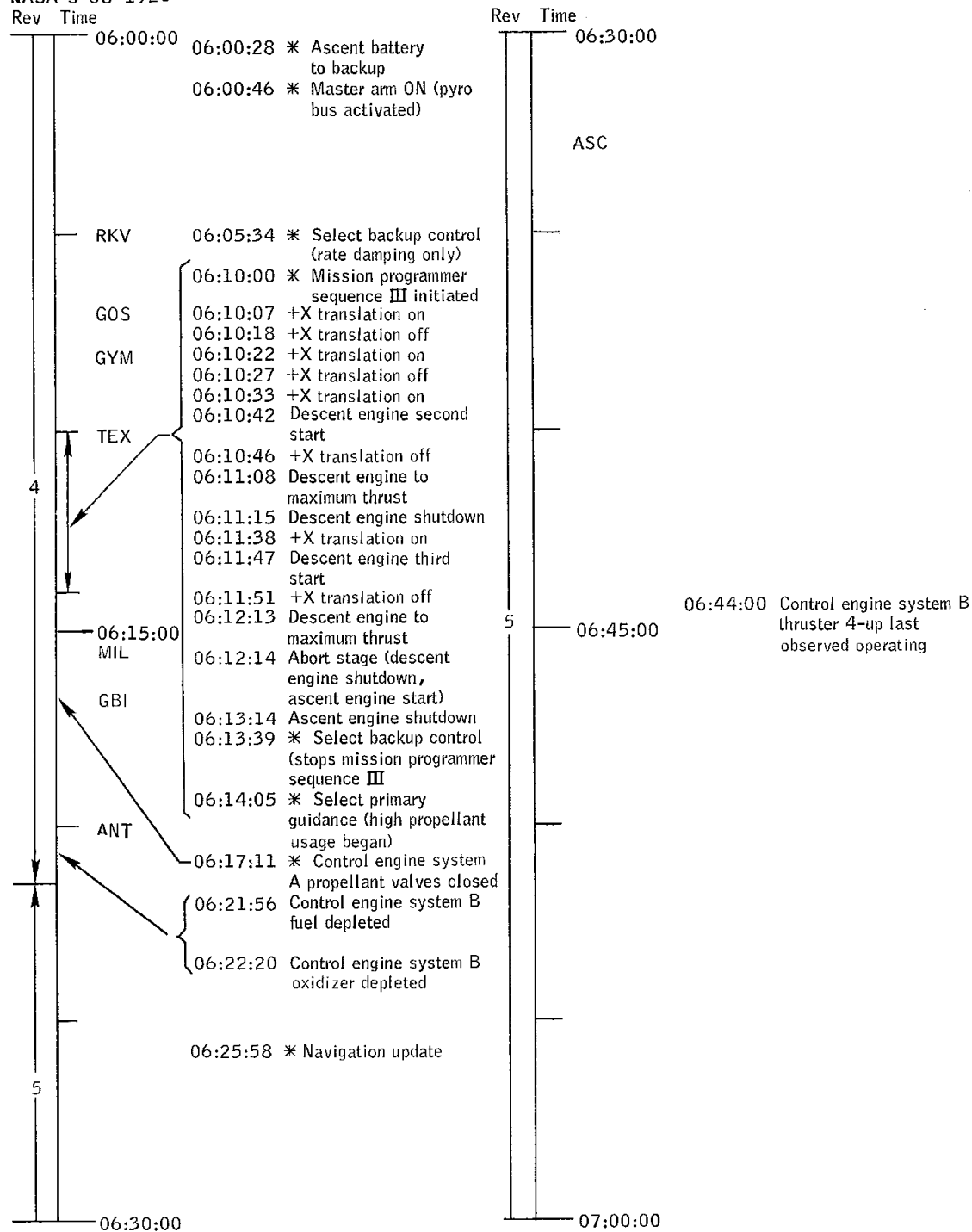
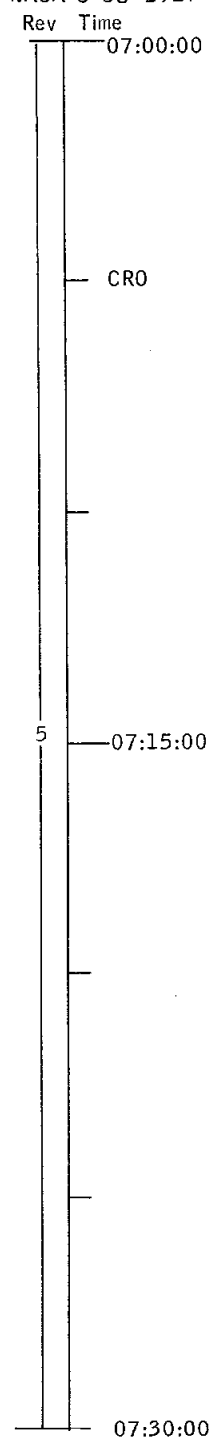
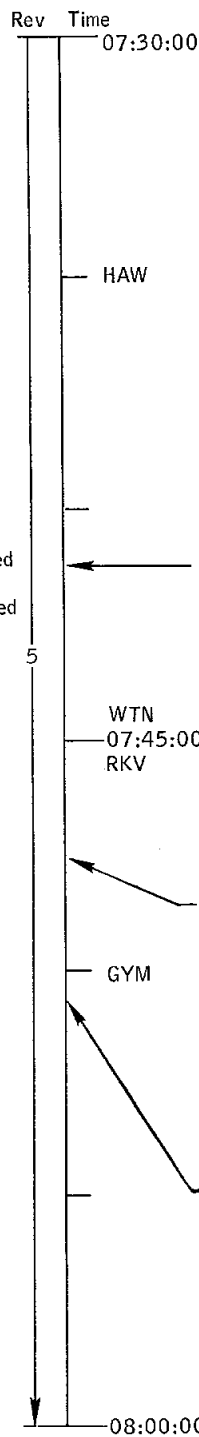


Figure 2-2.- Continued.

NASA-S-68-1927



* Ground command



(e) 07:00:00 to 08:00:00.

Figure 2-2.- Concluded.

3.0 TRAJECTORY DATA

A comparison of the planned and actual trajectories of the Apollo 5 mission is presented in this section. The trajectories referred to as planned are preflight-calculated trajectories obtained from references 1 and 2. The actual trajectories are based on tracking data from the Manned Space Flight Network and on the actual spacecraft data. Marshall Space Flight Center (MSFC) supplied the trajectory data for the launch phase up to the time of lunar module/S-IVB separation, and a detailed analysis is presented in reference 3. The orbital analysis in this section is based on the preliminary best estimate trajectory data generated in 21 days after the end of the mission; the final trajectory data will be released in supplement 2 to this report.

The earth model for all trajectories and analyses of the trackers contained geodetic and gravitational constants representing the Fischer ellipsoid. The state vectors for the events are based on results from the orbital analysis in section 3.2. These vectors are in the Geographic Coordinate system defined in table 3-I. The ground track of the orbit and the location of the tracking network sites for this mission are shown in figure 3-1.

3.1 LAUNCH

Launch phase conditions were nominal as shown in figure 3-2. Mach 1 occurred at 00:00:59.8 at an altitude of 24 574 feet and was approximately 0.2 second earlier than expected but occurred at the planned altitude. The maximum dynamic pressure of 655 lb/ft² occurred at 00:01:11.5. This was 2.7 seconds earlier and 2862 feet lower in altitude than planned.

The actual cutoff times for the inboard and outboard engines were within 0.3 second of the planned times. The conditions at outboard engine cutoff, as presented in table 3-II, were 11 ft/sec low in velocity, 2339 feet high in altitude, and 0.23 degree high in flight-path angle, when compared with the planned conditions. The S-IVB stage engine cutoff was 5 seconds earlier than planned but was within the 3-sigma limits. The velocity and flight-path angle were low by 2 ft/sec and 0.01 degree, respectively, and altitude was high by 766 feet, when compared with the planned conditions in table 3-II. Orbital insertion occurred 10 seconds after S-IVB stage engine cutoff. The insertion conditions listed in table 3-II were based on launch vehicle powered-flight data and S-IVB stage first-revolution tracking data.

The Goddard Space Flight Center provided tracking solutions of the S-IVB stage after lunar module/S-IVB stage separation. A lifetime of 15 hours 32 minutes was computed for the S-IVB stage, with predicted entry in the 10th revolution near the east coast of Australia.

3.2 ORBIT

3.2.1 Trajectory Profile Analysis

Trajectory reconstruction was divided into the four free flight phases defined by the following maneuvers: (1) lunar module/S-IVB stage separation, (2) first descent engine firing, (3) second descent engine firing (mission programmer sequence III), and (4) second ascent engine firing (mission programmer sequence V).

The preliminary C-band evaluation is based on individual station performance for each tracker used in calculating the trajectory profile. Figure 3-3 is a summary of the C-band evaluation in the form of residual statistics. The bias magnitude was calculated as the mean value of the residuals for the observations in a given phase. The noise magnitude was calculated as the rms value of the residuals. All residuals were obtained by subtracting the observed values from the computed values for each tracker, based on the data fit.

The preliminary S-band evaluation is based on total system performance rather than on individual station performance. This evaluation was accomplished by comparing the orbital vectors obtained from selected S-band data with comparable C-band data.

During the pre-separation phase, the data from the two Bermuda trackers and Tananarive provided a usable fit, although not as good as desired. However, at Tananarive there appeared to be a 0.06-degree azimuth bias, which was subsequently rejected (fig. 3-3). S-band data were not available for this phase; therefore, no comparisons can be made between the S-band and C-band state vectors.

Phase 1 extended from lunar module/S-IVB stage separation to the first descent engine firing. As shown in figure 3-3, a good data fit was obtained with data from Antigua, Bermuda, Patrick, Merritt Island, and the first pass over White Sands. White Sands, Merritt Island, and Bermuda exceeded the theoretical noise limits, but the bias was well within theoretical limits and the data were acceptable. A comparison of the converged S-band and C-band state vectors for this phase agreed within 150 feet in position and 0.21 ft/sec in velocity.

Phase 2 extended from cutoff of the first descent engine firing to the second descent engine firing. Here again, as shown in figure 3-3, a

good fit was obtained with data from Grand Bahama, Merritt Island, Carnarvon, and White Sands. The converged S-band and C-band state vectors agreed within 420 feet in position and 0.62 ft/sec in velocity.

Phase 3 (first ascent engine firing to second ascent engine firing) had greater inaccuracies because of low radar elevation angles and the excessive firing cycle of the control engines. Tananarive and Ascension provided sufficient C-band tracking data for satisfactory orbit determination, even though Tananarive again had an undesirable azimuth bias. For the first time, Ascension data were usable. The Ascension S-band residuals (the only S-band data) for phase 3 agreed favorably with the two C-band residuals for this phase.

Tracking data which were available but not used in the best estimate trajectory were deleted for various reasons. Canary Island data in the pre-separation phase were inconsistent with the other three stations. In phase 1, the Carnarvon range data degraded the solution, and White Sands appeared to be locked on a side-lobe of the antenna during the second pass. In phase 2, the Hawaii data were inconsistent with the fit, and Ascension data contained discontinuities in range and azimuth similar to the range discontinuity exhibited for the high ellipse portion of the Apollo 4 mission.

Time histories of space-fixed velocity, flight-path angle, and altitude for the four trajectory phases previously described are presented in figure 3-4. Figure 3-5 shows a profile of apogee and perigee altitudes during the mission.

3.2.2 Lunar Module/S-IVB Stage Separation

The separation conditions contained in table 3-III were obtained by simulating the separation sequence using a phase 1 vector and integrating this back through the sequence by using platform gimbal angles and acceleration data, and actual spacecraft mass characteristics. The validity of this simulated solution is indicated by comparing an orbital analysis pre-separation-phase vector to a phase-1 vector at the time of separation, then comparing the pre-separation-phase vector to the simulation, and finally comparing the phase-1 vector to the simulation. The pre-separation-phase vector and the phase-1 vector agreed to within 7200 feet in position and 6 ft/sec in total velocity. The pre-separation-phase and simulation vectors agreed to within 7900 feet in position and 8 ft/sec in total velocity. The phase-1 and simulation vectors agreed to within 600 feet in position and 2 ft/sec in total velocity. The separation conditions computed by MSFC agreed with the conditions in this report to within 3200 feet in position and 5 ft/sec in velocity; however, the MSFC conditions were computed using complete first revolution tracking data on the S-IVB stage only.

3.2.3 Maneuver Profile Analysis

The actual event time history of the maneuvers performed during the two mission programmer sequences is shown in table 2-I. Figure 3-6 shows space-fixed velocity, flight-path angle, and altitude for mission programmer sequences III and V. Figure 3-1 shows the simulated ground track for entry of the ascent stage. Table 3-IV presents a comparison of state vectors reconstructed from guidance and navigation accelerometer data, radar tracking data (best estimated trajectory), and the simulated trajectory program. Table 3-V includes state vector comparisons between the onboard guidance computer, the real time computer complex, and the best estimated trajectory. The three times chosen for the comparisons in table 3-V were (1) orbital insertion, (2) immediately prior to the onboard-computed first descent engine firing, and (3) the state vector time for the navigation update sent prior to the second ascent engine firing.

Mission programmer sequence III maneuvers.- The mission programmer sequence III maneuvers were reconstructed using two independent post-flight trajectory programs. The two reconstruction programs used in extrapolating the maneuvers were the guidance and navigation trajectory reconstruction program which processes accelerometer data, and a quasi six-degree-of-freedom operational trajectory simulation program. The guidance and navigation accelerometer reconstruction program, which is considered the most reliable source for generating the maneuver reconstruction, did not include the finalized set of inertial measurement unit performance errors including misalignments, but did include the preflight-predicted accelerometer scale factor and bias terms. The mission programmer sequence III maneuver profile is shown in figure 3-6. The third and most accurate method of determining the conditions at the beginning and end of a maneuver is integration of the free flight tracking vector (best estimated trajectory) to the specific event. The comparisons of state vectors derived from the three data sources are presented in table 3-IV for the first ascent engine firing (abort staging) and cut-off of the first ascent engine firing. A state vector established from tracking data during free flight phase 2 at 06:09:52 was used to initialize the simulated sequence III maneuver. Actual gimbal angles for sequence III maneuvers were implemented into the simulation program to provide an equivalent six-degree-of-freedom orbital integration/attitude control profile. The thrust profiles for the second and third descent engine firings and the first ascent engine firing were based on chamber pressures, vehicle propellant weights, and the rate of propellant usage. During the start and shutdown of the first ascent engine firing, the simulated results agree closely with the guidance and navigation reconstruction and the radar tracking (best estimate trajectory) conditions, as can be seen from table 3-IV.

The conditions presented for the tracking vector comparison at abort staging were obtained from the NORAD skin tracking vector of the descent stage integrated back to the time of abort staging. The best estimate tracking vector presented for cutoff of the first ascent engine firing was determined by integrating a phase-3 vector back to cutoff. This vector agreed with the guidance and navigation accelerometer reconstructed and simulated state vectors. The orbital elements at the completion of the first ascent engine firing are presented in table 3-VI.

Mission programmer sequence V maneuver.- The second ascent engine firing was initiated at a retrograde orientation with a subsequent decrease in velocity up to the time of reaction control propellant depletion. Gimbal lock occurred at 07:47:30, after which time the accelerometer and angle data were meaningless. The maneuver profile for the second ascent engine firing to the time of gimbal lock, shown in figure 3-6, was obtained from the guidance and navigation accelerometer reconstruction program. Using a state vector from phase 3, the maneuver profile for the second ascent engine firing was also reconstructed by means of the simulation program which used gimbal angles and the actual thrust profile to the time of gimbal lock. The comparison of the results at gimbal lock between the two programs is good. The differences shown are attributed to control engine thrust effects on the state vector, and radical changing of the gimbal angles, and the uncertainty in the preliminary thrust profile.

The position and velocity vector at gimbal lock obtained from the guidance and navigation accelerometer reconstruction program was integrated to ascent stage impact, assuming a ballistic entry. Another profile was reconstructed, using the position and velocity vector from the trajectory simulation program results at gimbal lock, by integrating a tumbling non-thrusting ascent stage to thrust decay and then a ballistic entry to impact. The results of these two cases, representing the conditions at thrust decay, entry (400 000 feet), and the impact coordinates are shown in table 3-IV. The impact coordinates are within approximately 110 n. mi. The ground track of the second ascent engine firing and the entry of the ascent stage that immediately followed are shown in figure 3-1. The solid line represents the maneuver profile based on the guidance and navigation accelerometer reconstruction of the program and the dashed line shows the simulation from gimbal lock to impact.

Several simulations were made in order to determine the dispersion of the impact point caused by ascent engine thrusting during the time from gimbal lock to thrust decay (153 seconds). In these cases, attitude rates as high as 25 deg/sec in all axes were simulated. The dispersion in the impact points was no greater than 135 n. mi.

TABLE 3-I.- DEFINITION OF TRAJECTORY AND ORBITAL PARAMETERS

<u>Trajectory parameters</u>	<u>Definition</u>
Geodetic latitude	Spacecraft position measured positive north from the equator to the local vertical vector, deg
Longitude	Spacecraft position measured positive east from the Greenwich meridian to the local vertical vector, deg
Altitude	Perpendicular distance from the reference ellipsoid to the point of orbit intersect, ft
Space-fixed velocity	Magnitude of the inertial velocity vector referenced to the earth-centered, inertial reference coordinate system, ft/sec
Space-fixed flight-path angle	Flight-path angle measured positive upward from the geocentric local horizontal plane to the inertial velocity vector, deg
Space-fixed azimuth	Azimuth of the projection of the inertial velocity vector onto the local geocentric horizontal plane, measured positive eastward from north, deg
Apogee	Predicted maximum altitude above the oblate earth model, n. mi.
Perigee	Predicted minimum altitude above the oblate earth model, n. mi.
Period	Time required for spacecraft to complete 360 degrees of orbit rotation (perigee to perigee, for example), min
Inclination	Angle between the orbit plane and the equator, deg

TABLE 3-II.- LAUNCH PHASE PLANNED AND
ACTUAL TRAJECTORY PARAMETERS

Condition	Planned	Actual
S-IB Stage Inboard Engine Cutoff		
Time from range zero, hr:min:sec	00:02:19	00:02:19
Geodetic latitude, deg North	28.69	28.68
Longitude, deg West	80.03	80.03
Altitude, ft	192 979	194 228
Altitude, n. mi.	32	32
Space-fixed velocity, ft/sec	7578	7563
Space-fixed flight-path angle, deg	27.85	28.12
Space-fixed heading angle, deg E of N	75.71	75.78
S-IB Stage Outboard Engine Cutoff		
Time from range zero, hr:min:sec	00:02:22	00:02:22
Geodetic latitude, deg North	28.70	28.70
Longitude, deg West	79.98	79.98
Altitude, ft	203 675	206 014
Altitude, n. mi.	34	34
Space-fixed velocity, ft/sec	7771	7760
Space-fixed flight-path angle, deg	27.39	27.62
Space-fixed heading angle, deg E of N	75.64	75.71

TABLE 3-II.- LAUNCH PHASE PLANNED AND ACTUAL
TRAJECTORY PARAMETERS - Concluded

Condition	Planned	Actual
S-IVB Stage Engine Cutoff		
Time from range zero, hr:min:sec	00:09:58	00:09:53
Geodetic latitude, deg North	31.52	31.50
Longitude, deg West	62.64	62.57
Altitude, ft	535 400	536 166
Altitude, n. mi.	88	88
Space-fixed velocity, ft/sec	25 661	25 659
Space-fixed flight-path angle, deg	0.0	-0.01
Space-fixed heading angle, deg E of N	85.71	85.50
Insertion (S-IVB Stage Cutoff Plus 10 Seconds)		
Time from range zero, hr:min:sec	00:10:08	00:10:03
Geodetic latitude, deg North	31.57	31.56
Longitude, deg West	61.48	61.81
Altitude, ft	535 441	536 233
Altitude, n. mi.	88	88
Space-fixed velocity, ft/sec	25 684	25 684
Space-fixed flight-path angle, deg	0.01	0.0
Space-fixed heading angle, deg E of N	86.13	85.92

TABLE 3-III.- ORBITAL PHASE PLANNED AND
ACTUAL TRAJECTORY PARAMETERS

Condition	Planned	Actual
LM/S-IVB Stage Separation		
Time from range zero, hr:min:sec	00:54:06	00:53:56
Geodetic latitude, deg South	31.54	31.50
Longitude, deg East	106.81	106.04
Altitude, ft	733 098	728 707
Altitude, n. mi.	121	120
Space-fixed velocity, ft/sec	25 454	25 458
Space-fixed flight-path angle, deg	0.0	0.0
Space-fixed heading angle, deg E of N	94.11	94.58
Ignition of First Descent Engine Firing		
Time from range zero, hr:min:sec	03:59:54	03:59:42
Geodetic latitude, deg South	26.62	26.84
Longitude, deg East	103.12	102.52
Altitude, ft	706 396	704 041
Altitude, n. mi.	116	116
Space-fixed velocity, ft/sec	25 488	25 488
Space-fixed flight-path angle, deg	-0.18	-0.14
Space-fixed heading angle, deg E of N	72.03	72.34

TABLE 3-III.- ORBITAL PHASE PLANNED AND ACTUAL

TRAJECTORY PARAMETERS - Continued

Condition	Planned	Actual
Cutoff of First Descent Engine Firing		
Time from range zero, hr:min:sec	04:00:32	03:59:46
Geodetic latitude, deg South	25.80	26.76
Longitude, deg East	105.65	102.79
Altitude, ft	703 857	703 716
Altitude, n. mi.	116	116
Space-fixed velocity, ft/sec	25 622	25 490
Space-fixed flight-path angle, deg	-0.05	-0.14
Space-fixed heading angle, deg E of N	70.84	72.23
Ignition of Second Descent Engine Firing		
Time from range zero, hr:min:sec		06:10:42
Geodetic latitude, deg North		28.14
Longitude, deg West		115.95
Altitude, ft		570 883
Altitude, n. mi.		94
Space-fixed velocity, ft/sec		25 656
Space-fixed flight-path angle, deg		0.13
Space-fixed heading angle, deg E of N		105.39

TABLE 3-III.- ORBITAL PHASE PLANNED AND ACTUAL
TRAJECTORY PARAMETERS - Concluded

Condition	Planned	Actual
Cutoff of First Ascent Engine Firing		
Time from range zero, hr:min:sec		06:13:14
Geodetic latitude, deg North		24.91
Longitude, deg West		105.41
Altitude, ft		571 155
Altitude, n. mi.		94
Space-fixed velocity, ft/sec		26 319
Space-fixed flight-path angle, deg		-0.36
Space-fixed heading angle, deg E of N		110.09
Ignition of Second Ascent Engine Firing		
Time from range zero, hr:min:sec		07:44:13
Geodetic latitude, deg North		30.21
Longitude, deg West		150.75
Altitude, ft		699 611
Altitude, n. mi.		115
Space-fixed velocity, ft/sec		26 157
Space-fixed flight-path angle, deg		-1.51
Space-fixed heading angle, deg E of N		99.82

TABLE 3-IV.- MISSION PROGRAMMER SEQUENCES III AND V STATE VECTOR COMPARISON

Vector description and source	Time, hr:min:sec	Velocity, ft/sec	Flight-path angle, deg	Heading angle, deg	Latitude, deg	Longitude, deg	Altitude, n. mi.
First ascent engine firing on (abort stage)	06:12:14.7						
Accelerometer reconstructed		25 800	0.218	108.48	26.28	-109.49	94.6
Skin tracking (NORAD)		25 795	0.326	108.81	26.06	-109.32	93.9
Simulated		25 794	0.212	108.48	26.28	-109.48	94.8
First ascent engine firing off (thrust to zero)	06:13:14.7						
Accelerometer reconstructed		26 311	-0.366	110.06	24.90	-105.41	94.8
Best estimate trajectory (phase 3)		26 319	-0.359	110.09	24.91	-105.41	94.0
Simulated		26 321	-0.452	110.08	24.89	-105.37	94.6
Gimbal lock	07:47:29.9						
Accelerometer reconstructed		24 803	-1.77	105.55	27.16	-136.87	96.1
Simulated		24 792	-1.65	105.58	27.19	-137.00	96.6
Thrust decay	07:50:03.0						
Accelerometer reconstructed		24 965	-2.39	110.18	24.02	-126.78	72.8
Simulated		24 951	-2.27	110.23	24.04	-126.92	74.7
Entry (400 000 feet)							
Accelerometer reconstructed	07:50:41.6	25 016	-2.54	111.24	23.10	-124.31	65.8
Simulated	07:50:54.3	25 016	-2.46	111.62	22.80	-123.64	65.8
Impact							
Accelerometer					18.10	-112.85	
Simulated					17.22	-111.21	

TABLE 3-V.- NAVIGATION STATE VECTOR COMPARISONS

Vector description	Time, hr:min:sec	Inertial velocity, ft/sec	Flight-path angle, deg	Heading angle, deg	Latitude, deg	Longitude, deg	Altitude, n. mi.
Insertion	00:10:03.3						
Guidance computer		25 682	-0.049	85.08	31.81	-61.85	87.7
Best estimate trajectory (pre-separation)		25 686	0.006	85.91	31.56	-61.81	88.2
Real time computer complex (instrument unit)		25 685	-0.001	85.94	31.55	-61.80	88.1
Prior to first descent engine firing	03:15:28						
Guidance computer		25 669	0.087	107.47	27.39	-65.52	89.9
Best estimate trajectory (phase 1)		25 656	0.152	107.62	26.87	-66.25	92.3
Real time computer complex		25 656	0.152	107.62	26.87	-66.24	92.3
Navigation update vector	06:21:21						
Guidance computer		25 621	0.184	120.41	10.58	-74.89	96.0
Best estimate trajectory (phase 3)		26 184	1.420	120.05	9.98	-75.19	112.4
Real time computer complex ^a		26 213	1.340	120.07	9.94	-75.12	109.8

^aThis real time computer complex vector was the navigation update.

TABLE 3-VI.- ORBITAL ELEMENTS

Phase	Condition	Planned	Actual
Insertion	Apogee, n. mi.	123	120
	Perigee, n. mi.	88	88
	Period, min	88.45	88.39
	Inclination, deg	31.62	31.63
LM/S-IVB stage sep- aration	Apogee, n. mi.	121	120
	Perigee, n. mi.	97	90
	Period, min	88.58	88.43
	Inclination, deg	31.62	31.63
Completion of first descent engine firing	Apogee, n. mi.	174	120
	Perigee, n. mi.	116	92
	Period, min	89.95	88.47
	Inclination, deg	31.62	31.64
Completion of first ascent engine firing	Apogee, n. mi.		519
	Perigee, n. mi.		93
	Period, min		96.07
	Inclination, deg		31.48

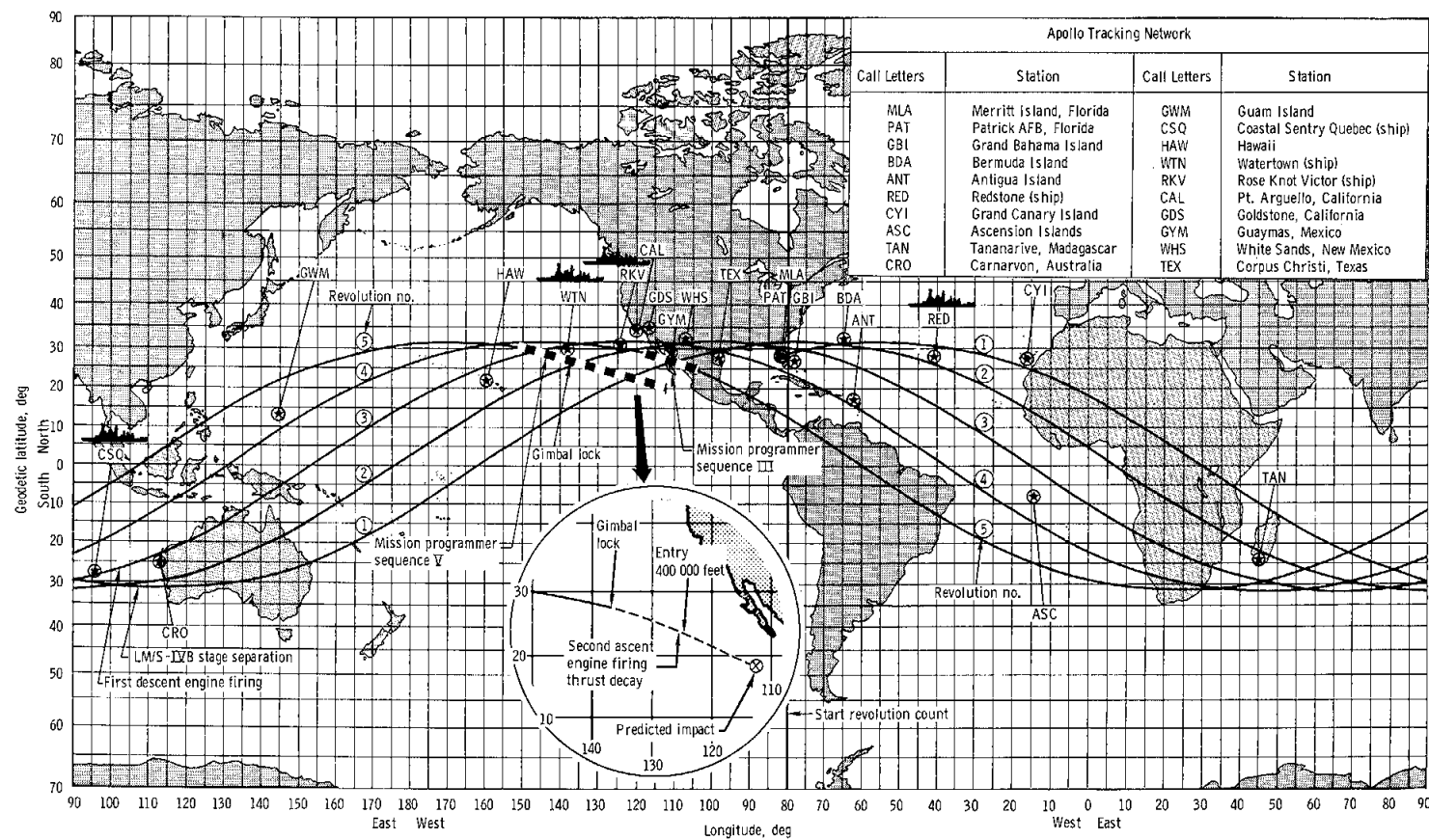
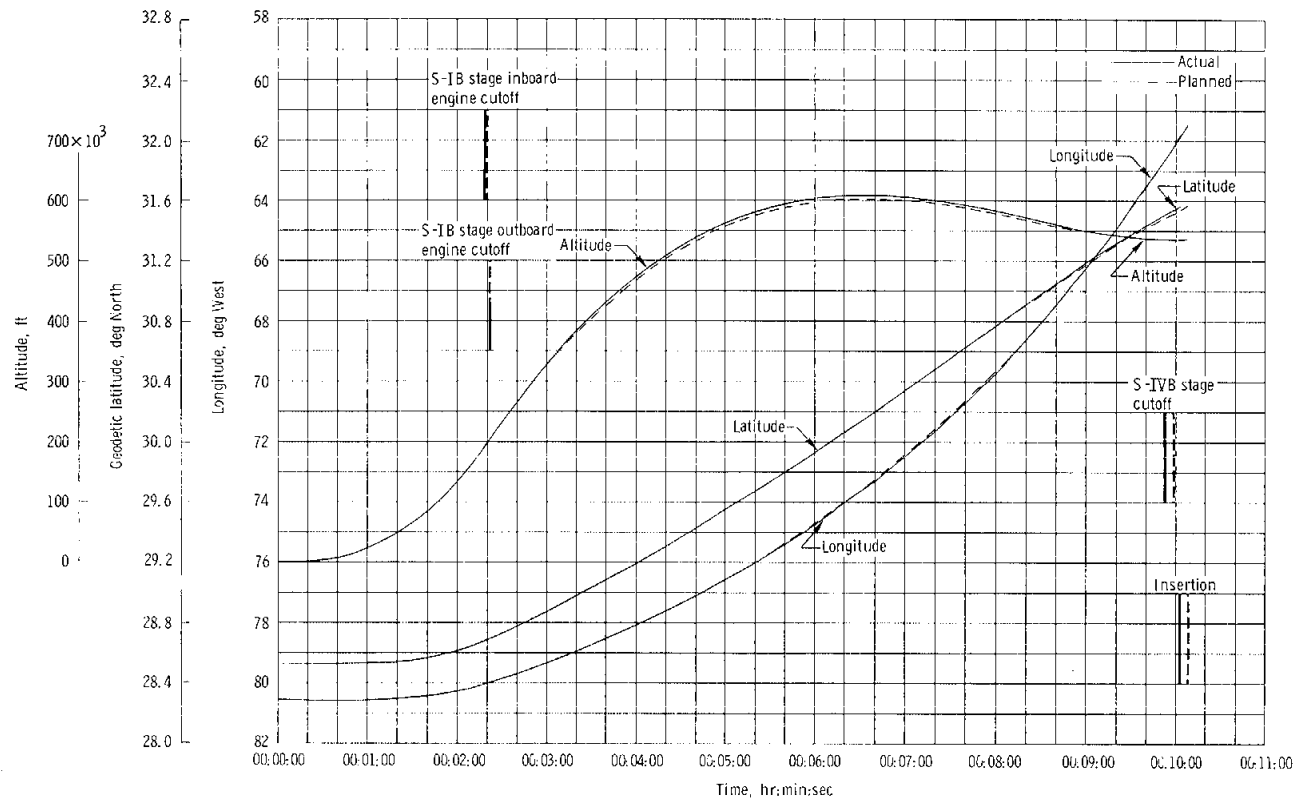
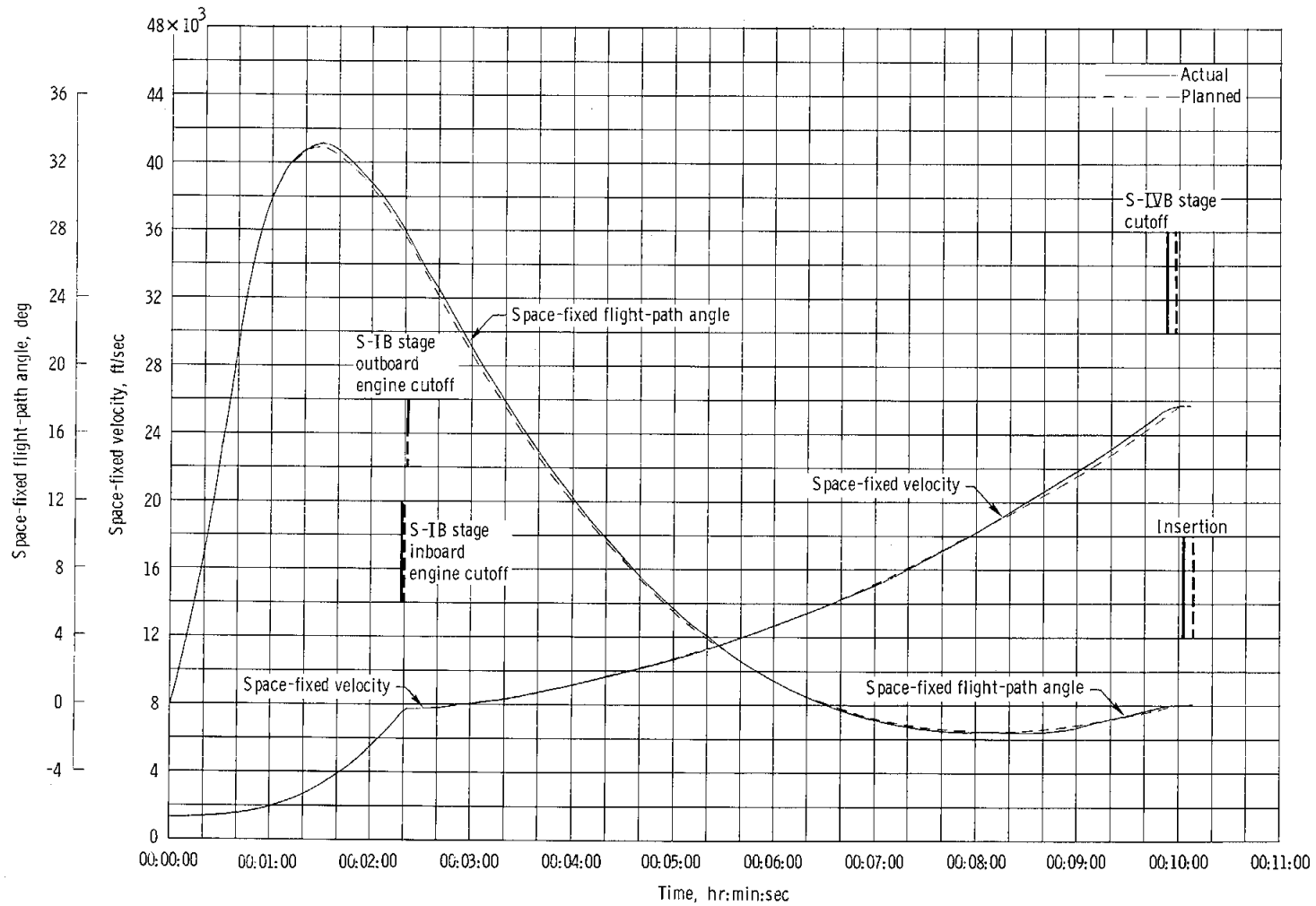


Figure 3-1. - Apollo 5 mission ground track.



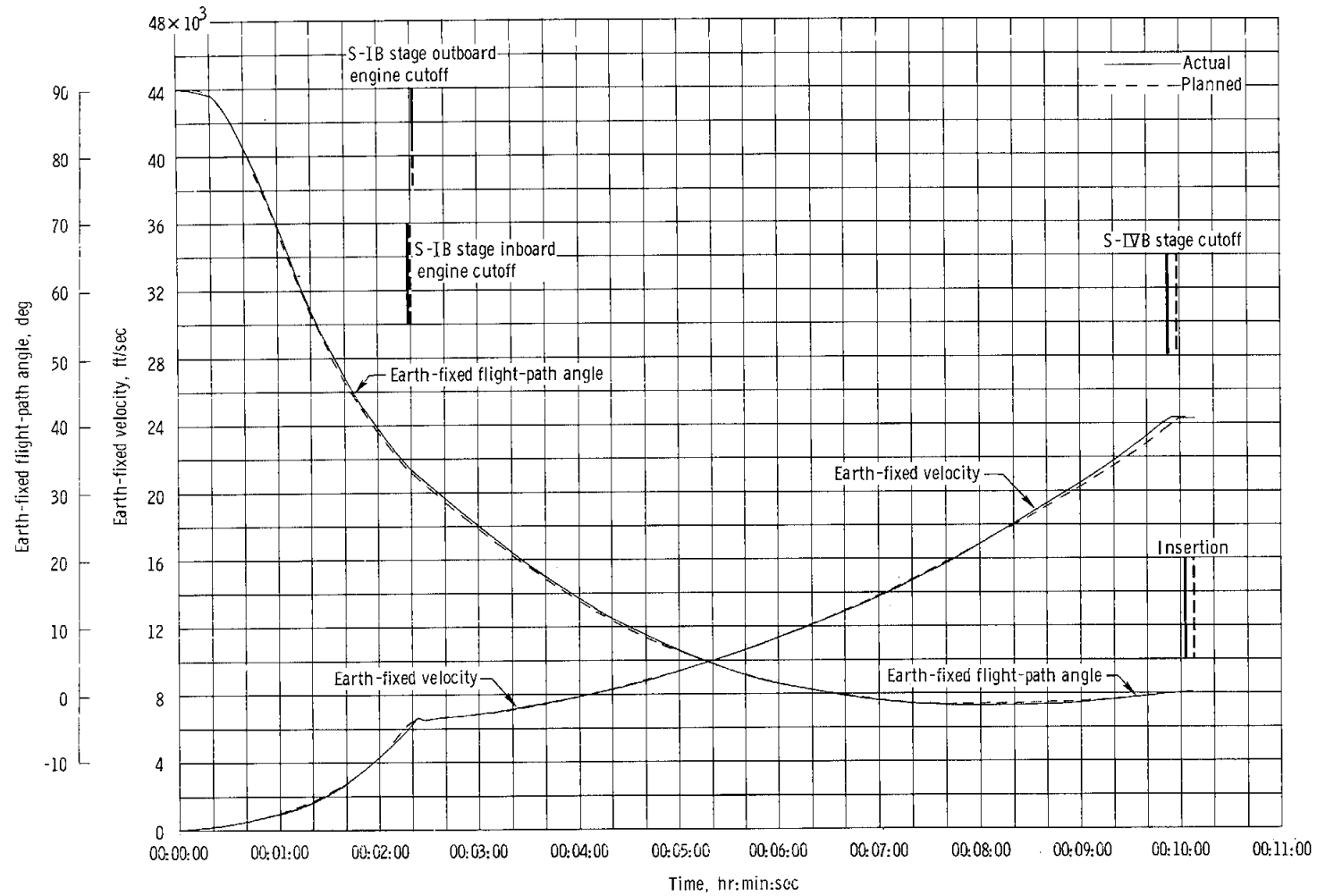
(a) Latitude, longitude, and altitude.

Figure 3-2. - Trajectory parameters during the launch phase.



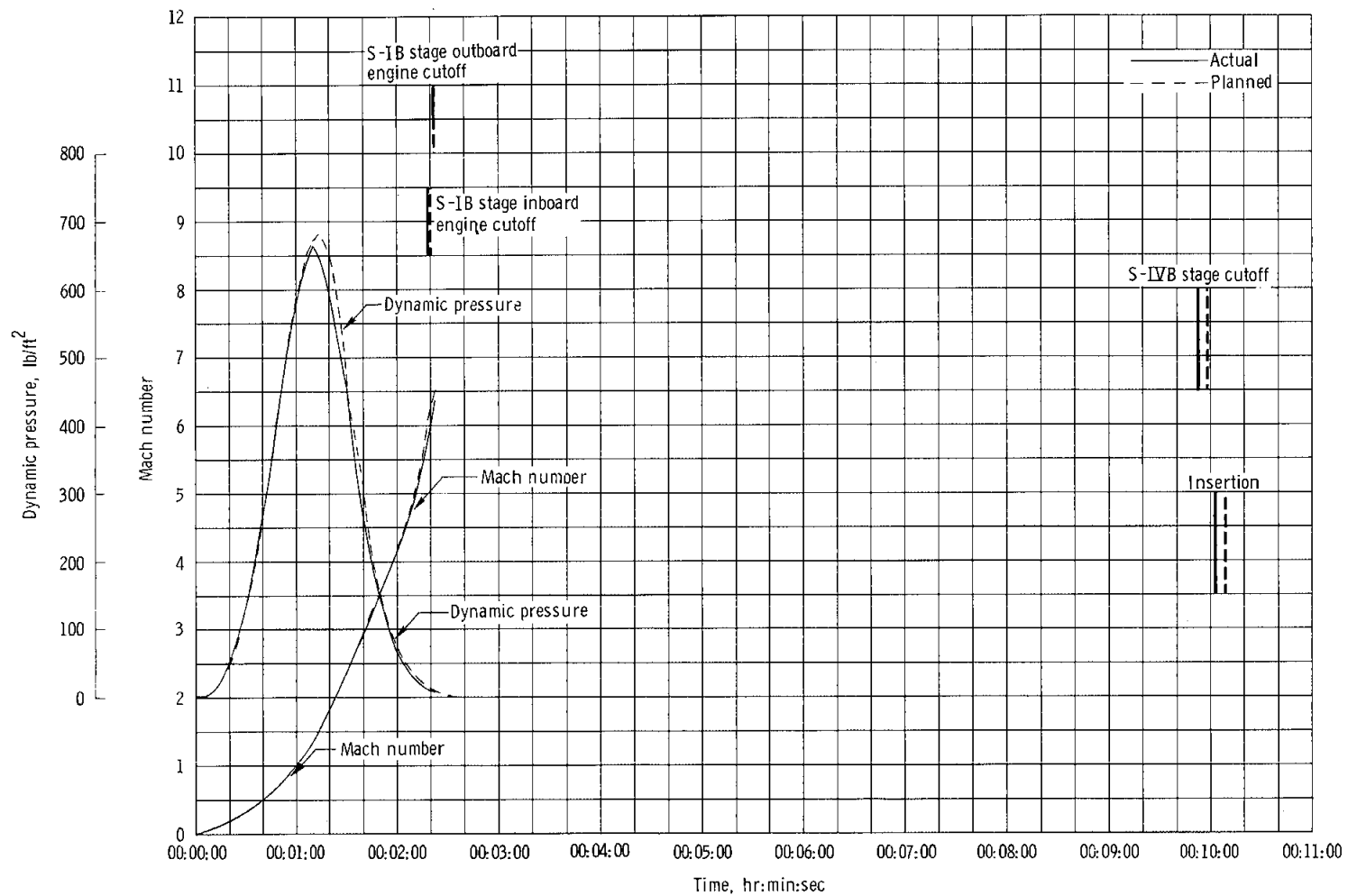
(b) Space-fixed flight-path angle and velocity.

Figure 3-2. - Continued.



(c) Earth-fixed flight-path angle and velocity.

Figure 3-2. -Continued.



(d) Mach number and dynamic pressure.

Figure 3-2. - Concluded.

NASA-S-68-1933

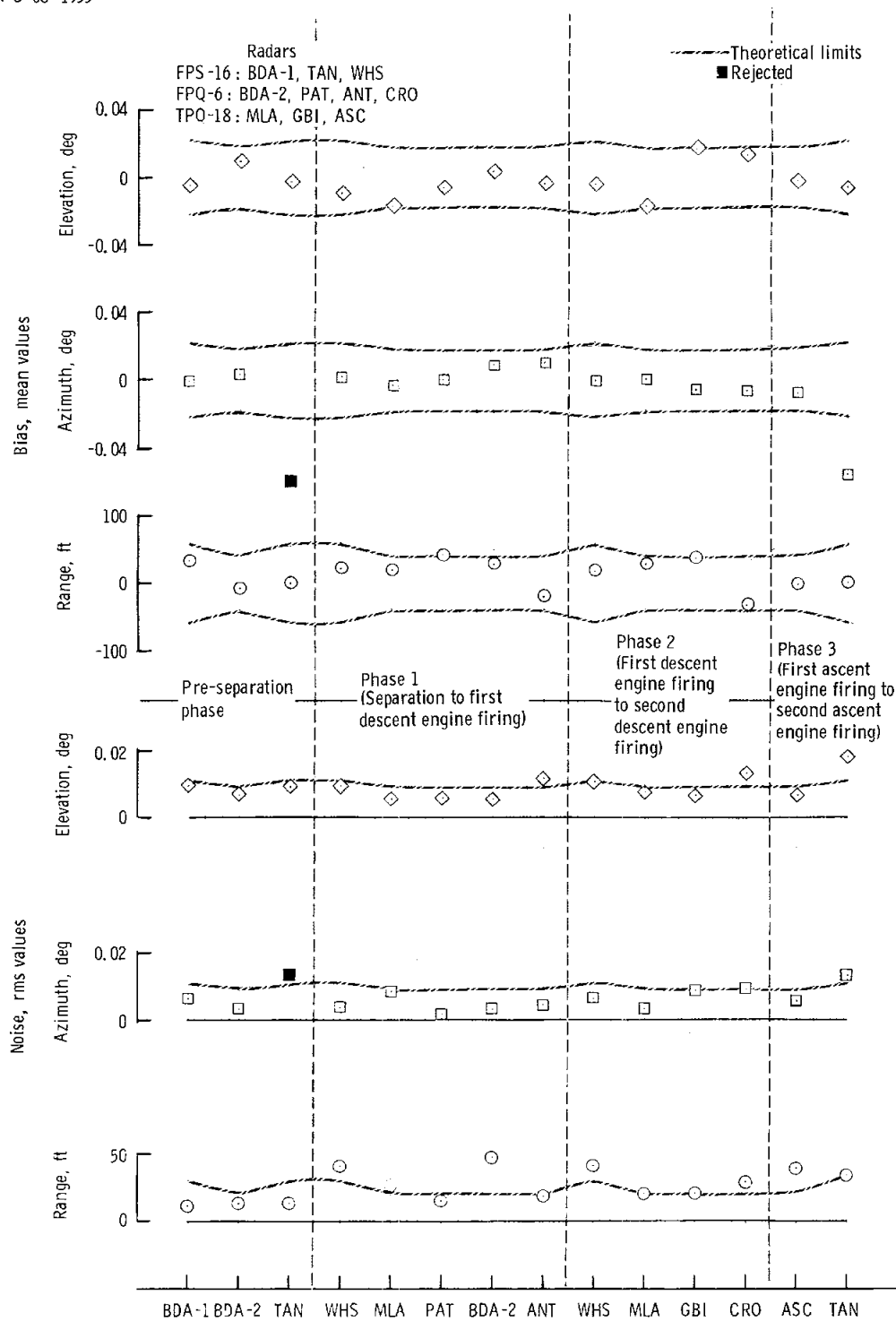


Figure 3-3. - Statistical summary of tracker residuals.

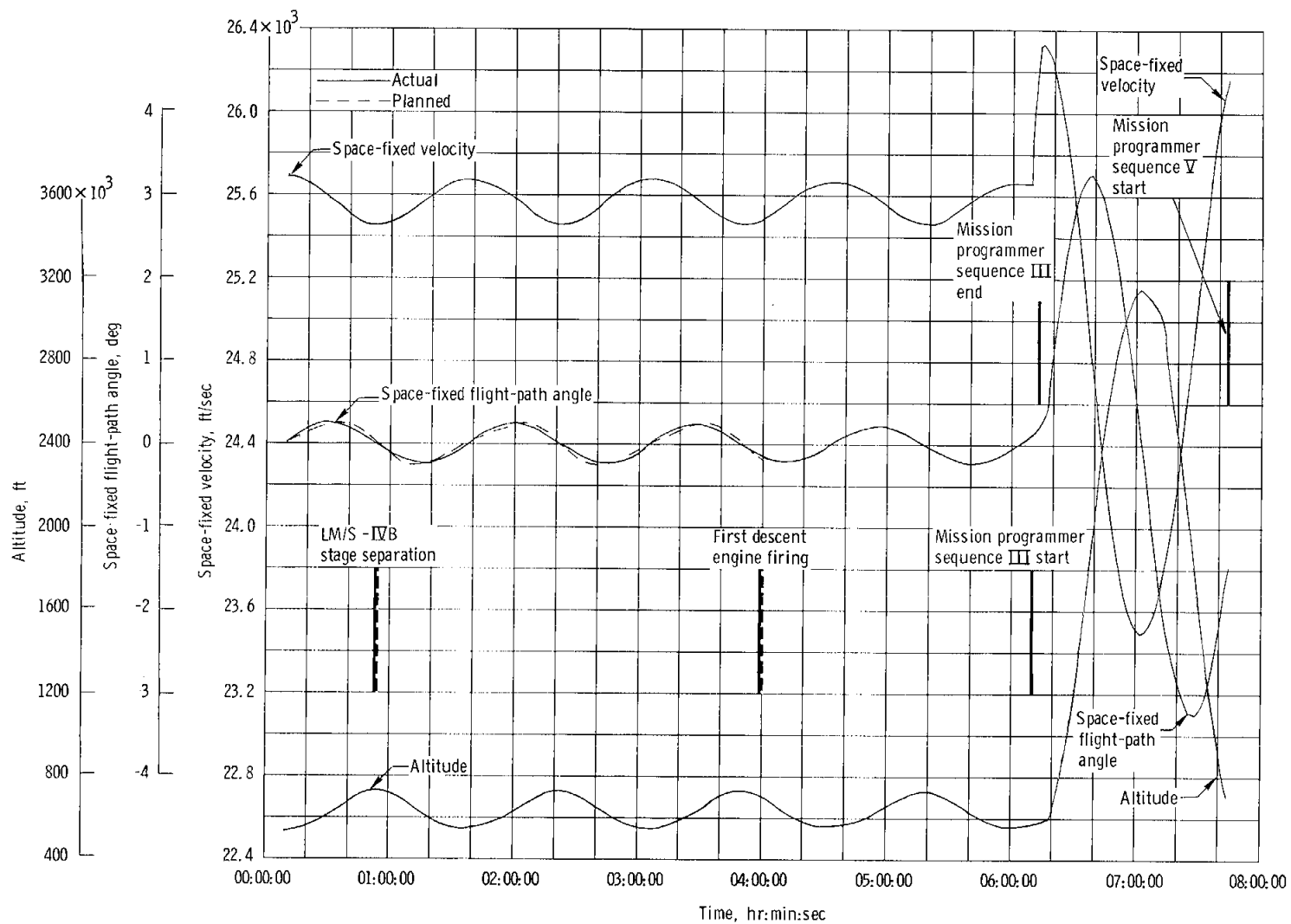


Figure 3-4. - Space-fixed velocity, flight-path angle, and altitude during the orbital phase.

NASA-S-68-1935

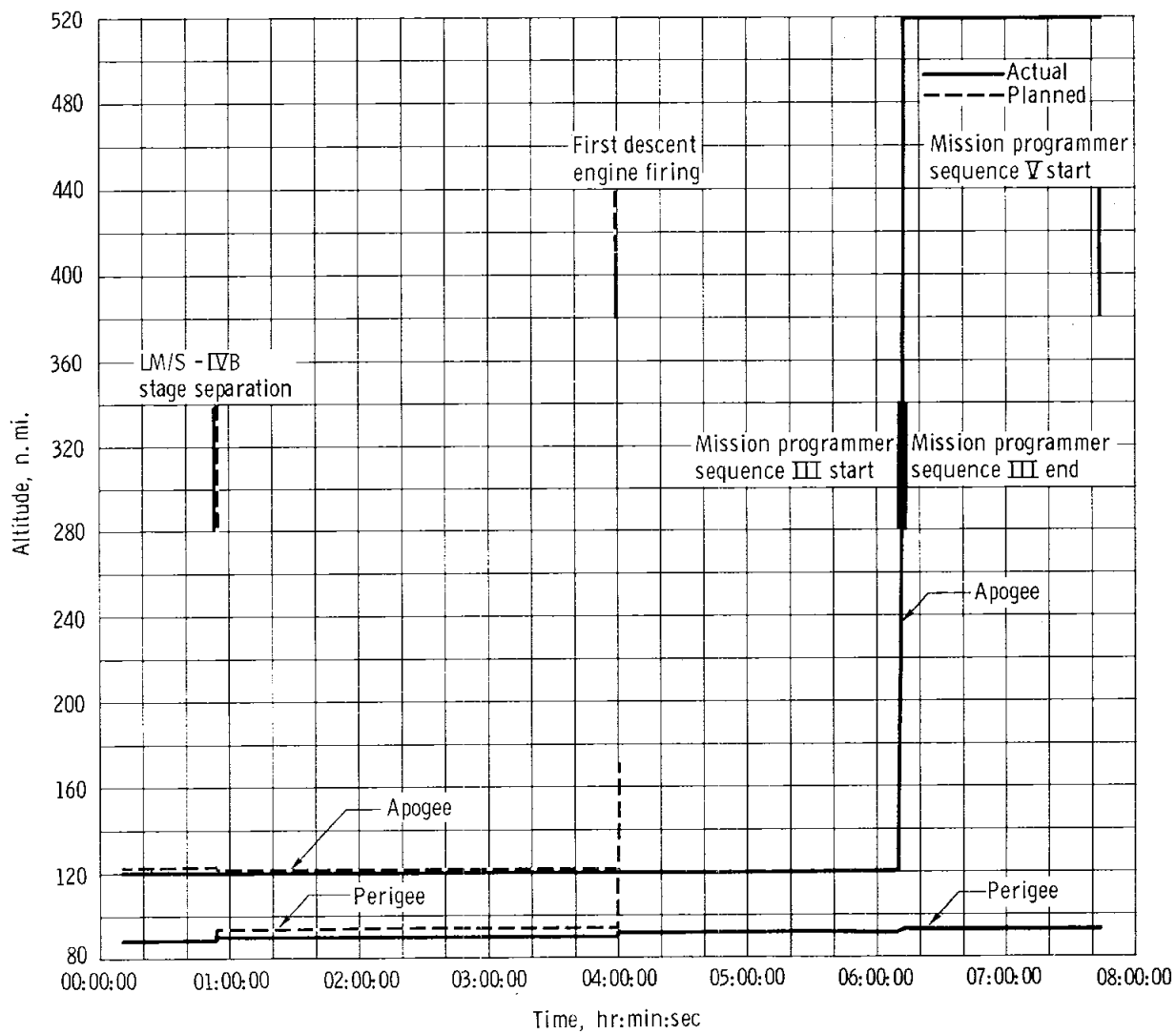
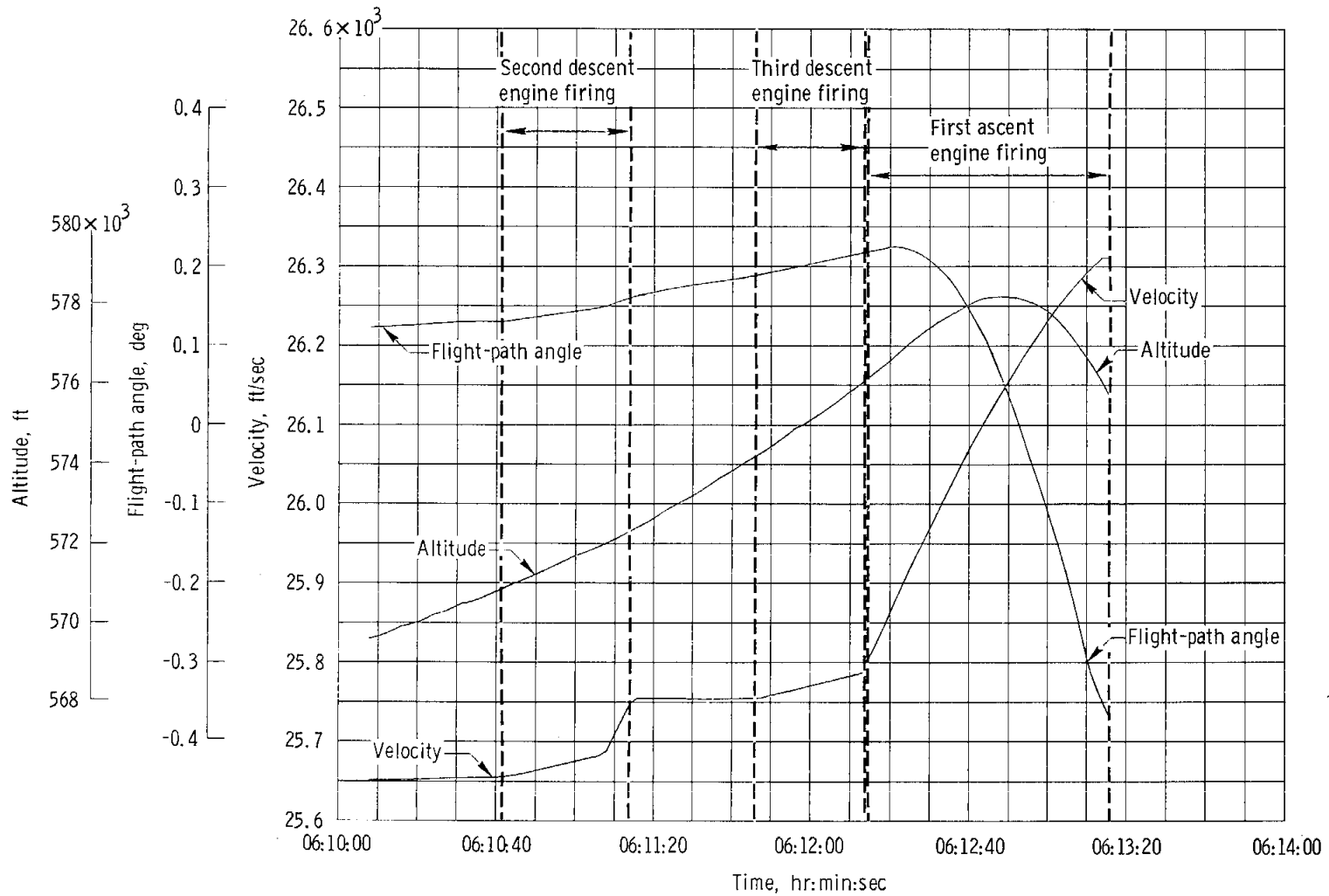
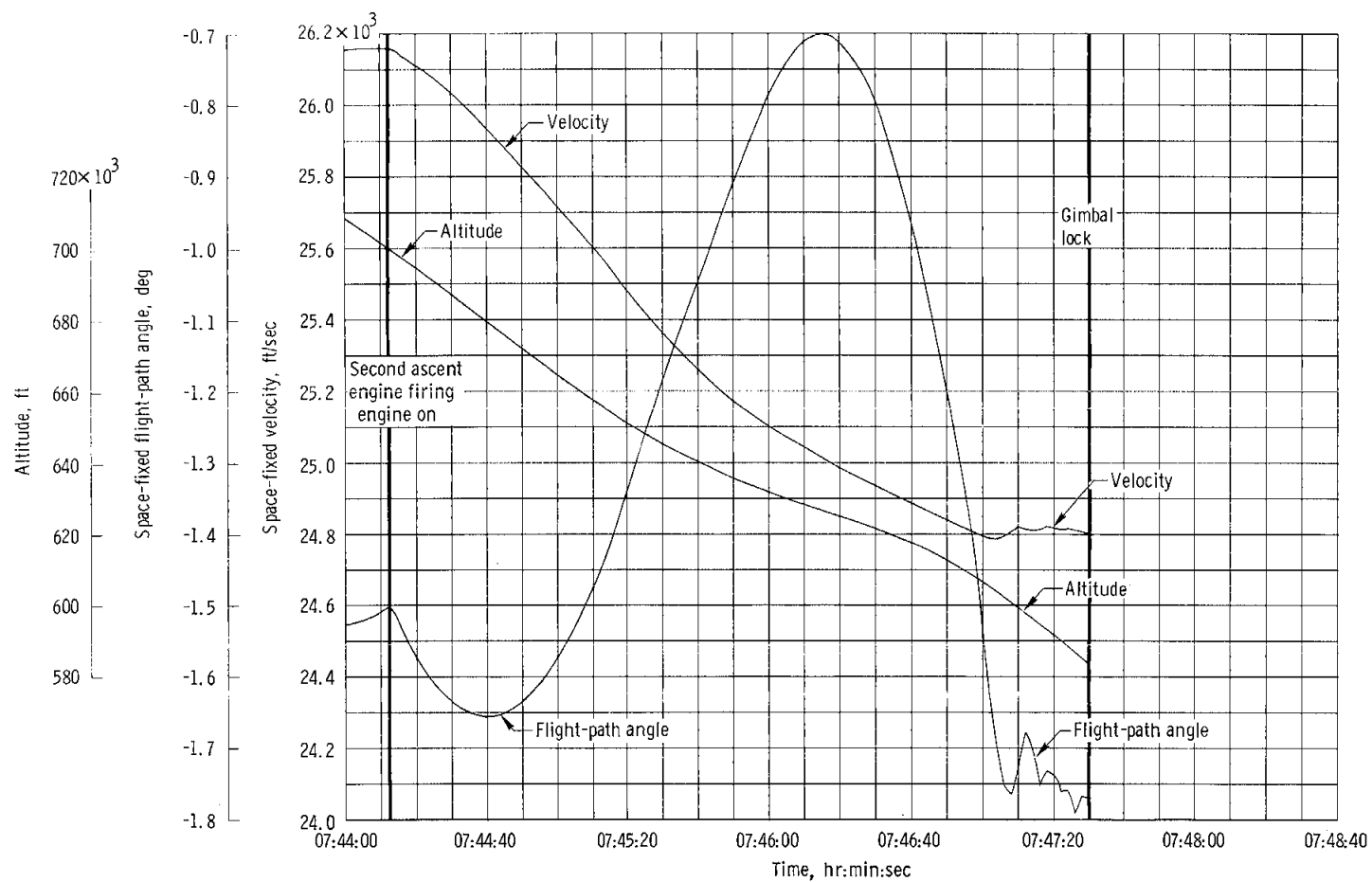


Figure 3-5. - Apogee and perigee altitude profile.



(a) Second and third descent engine firings, and first ascent engine firing.

Figure 3-6. - Space-fixed velocity, space-fixed flight-path angle, and altitude during maneuvers.



(b) Second ascent engine firing.

Figure 3-6, - Concluded.

4.0 LAUNCH VEHICLE PERFORMANCE SUMMARY

The launch vehicle, AS-204, satisfactorily placed the lunar module into orbit on January 22, 1968. All assigned mission objectives were met and no flight anomalies occurred affecting mission accomplishment. A detailed analysis of launch vehicle performance is contained in reference 3.

The launch vehicle rolled from 90 to 72 degrees east of north between 00:00:09.2 and 00:00:37.9. The programmed pitch attitude profile was accomplished between 00:00:09.2 and 00:02:15.3, at which time an essentially constant pitch attitude was maintained until the initiation of active guidance. Active guidance was initiated 16.0 seconds after separation of the S-IB/S-IVB stages. Shutdown of the S-IB stage engine occurred at 00:02:22.3 (0.1 second earlier than predicted). At S-IB stage engine cutoff, the actual trajectory parameters compared with nominal were 10.8 ft/sec low in space-fixed velocity, 0.40 n. mi. high in altitude, and 0.011 n. mi. less in range.

Separation of the S-IB/S-IVB stages occurred at 00:02:23.5, followed 1.4 seconds later by ignition of the S-IVB stage. All ullage rockets functioned as expected and were successfully jettisoned.

S-IVB stage engine cutoff occurred at 00:09:53.3 (5.1 seconds earlier than predicted). The nose cone/adaptor separation sequence was initiated 45.2 seconds after S-IVB stage engine cutoff and adaptor panel deployment was initiated at 00:19:53.5 (both events were 5.0 seconds earlier than predicted). The lunar module separation sequence was started at 00:53:55.2.

At S-IVB stage engine cutoff, the actual trajectory parameters compared with nominal were 2.3 ft/sec less in space-fixed velocity, 0.11 n. mi. high in altitude and 16.3 n. mi. greater in range.

All portions of the orbital safing experiment on the S-IVB stage were performed successfully, including propellant venting, propellant dump, and stage/engine pneumatic supply dump. The hydrogen start bottle was not scheduled to dump.

5.0 COMMAND AND SERVICE MODULE PERFORMANCE

(This section is not applicable.)

6.0 LUNAR MODULE PERFORMANCE

6.1 STRUCTURES

6.1.1 Loads

Adapter and lunar module loads and lunar module/adapter interaction loads were calculated for the critical design loading conditions; lift-off, S-IB midboost, and end of S-IB boost. Lunar module accelerations and plume impingement pressures during abort staging were examined. Comparisons with design and predicted values were made where appropriate.

Lateral loads during thrust buildup are caused by the steady drag load from ground winds and vehicle dynamic excitation from wind gusts, vortex shedding, and unsymmetric S-IB engine thrust buildup. These excitations result in a large constraining shear and moment at the base of the launch vehicle before release. The lateral loads after lift-off are caused primarily by the sudden removal of the constraining shear and moment at release. Typically, large axial dynamic oscillations result from the S-IB engine thrust buildup and the release of tension in the launch vehicle hold-down arms.

Before and during lift-off, the ground winds were light (4 to 5 knots) with almost no gusts. There was no evidence of vortex shedding and none was predicted at the observed wind speeds. Each pair of diametrically opposite S-IB outboard engines, the usual source of unsymmetric thrust buildup excitation, ignited almost simultaneously; therefore, the loads experienced at lift-off were low.

The winds aloft (fig. 6.1-1) during the boost phase were not severe, and the maximum calculated angle of attack due to winds was 1.92 degrees in the maximum dynamic pressure region.

The maximum axial acceleration and compressive loads were experienced immediately prior to S-IB inboard engines cutoff. The end-of-boost axial acceleration for this mission was 4.35g, very close to the nominal prediction of 4.38g, and well within the design value of 4.90g.

Adapter loads.— The adapter loads were calculated from the lunar module accelerometer data at lift-off and at the end of S-IB boost (figs. 6.1-2 and 6.1-3). These loads were well below the limit load capabilities and agree closely with the predicted loads.

Adapter loads during the maximum $q\alpha$ region of flight determined from the calculated angles of attack and actual lunar module acceleration were also well below limit capabilities. The adapter internal vent pressure (fig. 6.1-4) was determined from launch vehicle measurements located in the S-IVB stage forward skirt. Predicted pressures within the adapter (based on actual trajectory and measured ambient pressure) showed close agreement with actual pressures.

Lunar module loads.— Six linear accelerometers (three translational and three rotational) were mounted on the ascent stage 76 inches from the lunar module center of gravity (launch configuration). Figures 6.1-5 and 6.1-6 show accelerations measured by these accelerometers at lift-off and at S-IB shutdown, respectively. These two conditions represent the most severe low-frequency oscillations experienced during the flight.

Maximum lunar module load factors in the lateral and longitudinal directions are shown in table 6.1-I. The table shows that for all phases of the mission, the maximum measured load factors encountered were less than design. Close agreement is shown between predicted and measured values, within instrumentation accuracy.

Loads experienced during descent and ascent engine start-up are critical for the respective engine support structure. Strain gage instrumentation (GA2524S) on one of the descent engine upper support struts was used to obtain load data from lift-off to abort staging. This instrumentation was calibrated to measure axial force in the strut. Ignition of the descent stage engine at the 10-percent throttle setting caused only small load oscillations and the transition to full throttle was smooth. The maximum compressive force recorded was 3240 pounds during both firings at full throttle. The predicted value for these struts (based on a thrust of 9840 pounds at full throttle) is 3085 pounds compression.

The critical loads for the ascent engine support structure are a function of the engine start-up transient. The chamber pressures for the first and second ascent engine firings were 164 and 178 psia, respectively, as compared with the design value of 178 psia. The thrust rise times for both firings are shown in table 6.13-I in section 6.13. These times are longer than those used for design (0.013 second); consequently, the loads experienced were less severe than the design conditions.

Lunar module/adapter interaction loads.— The 16 outrigger struts were instrumented with strain gages to provide continuous load data. The lunar module/adapter interaction loads (fig. 6.1-7) were determined by summing the strut loads F_1 , F_2 , F_3 , and F_4 to obtain the reactions R_X , R_Y , and R_Z at each of the four adapter support points. A typical

outrigger strut load time history is shown in figure 6.1-8. The measured strut loads for the end of S-IB boost, which were the maximum loads experienced on any strut during this flight, are shown in table 6.1-II. A comparison of the measured, predicted, and design loads for the struts shows that in all cases, the measured loads were less than allowable loads. The predicted outrigger strut loads based on data from the six linear accelerometers agree well with the measured strut loads; this implies that the analytical model used for the design analysis was reasonably accurate. These predicted values were determined for inertia effects only. The apex-fitting reactions determined from the strut loads are shown in table 6.1-III, which is a comparison of the calculated and design interaction loads. All of the significant calculated loads were less than the design loads. Two of the calculated reaction loads slightly exceeded the design loads for the end of S-IB boost condition. However, the difference between the calculated and design loads for the -Y apex R_Y and R_Z reactions was within the accuracy of the instrumentation used for the measured loads. In any event, a greater design load does exist for another end-of-boost design condition.

Abort staging.- Abort staging pressure measurements on the ascent stage lower surface and the descent stage upper surface are shown in figures 6.1-9 and 6.1-10, respectively. Table 6.1-IV shows the peak pressures measured on the ascent and descent stage surfaces, with the design limit pressures and ground test results from White Sands included for comparison. The peak pressures measured during the flight were all lower than the design limit condition. The maximum measured pressure of 2.01 psia occurred on the +Y side of the ascent stage midsection base heat shield about 47 milliseconds after peak ascent engine chamber pressure. The descent stage pressures peaked from 10 to 50 milliseconds after peak ascent engine chamber pressure. The ascent stage base heat shield pressures peaked from 25 to 130 milliseconds after peak ascent engine chamber pressure (see section 6.17). Ground tests (ref. 4) showed that the peak heat shield pressure occurred 0 to 15 milliseconds after peak ascent engine chamber pressure. The design and ground test pressures are all for zero separation distance.

The following facts also indicate that no structural damage occurred to the ascent stage during the abort staging:

- a. The rate of cabin pressure decay remained constant.
- b. The pressure and temperature measurements (GA1133P and GA1113T) in the cavity between the ascent stage structure and the base heat shield remained constant.

6.1.2 Vibrations

The vehicle was instrumented with vibration accelerometers having the ranges and frequency responses shown in table 6.1-V. Additional instrumentation information is contained in section 13.2 and reference 4. An adequate analysis of the flight vibrations during the transient conditions associated with engine starts and shutdowns cannot be conducted because many of the vibration measurements were time-shared. As a result, only intermittent data were obtained: the time-shared channels provided 1.25 seconds of data during each period of 3.9 seconds, and the oscillations induced by engine starts and shutdowns decayed to very low levels in 3.9 seconds.

Examination of oscillographs for the launch and boost phases of the flight shows that the maximum vibration occurred at lift-off in response to launch vehicle noise. Lift-off vibrations were significant for a duration of approximately 8 seconds. The absence of significant vibrations during boost is attributed to the relatively clean aerodynamic configuration of the Apollo 5 nose cone and adapter. Power spectral density analyses of data recorded during lift-off were prepared for the following critical equipment areas:

- a. Ascent stage oxidizer tank bottom cover (X and Y axes)
- b. Ascent stage oxidizer tank support strut (Z axis)
- c. Descent stage oxidizer tank upper cover (X, Y, and Z axes)
- d. Landing radar antenna (normal to the plane of the antenna)
- e. Ascent engine support structure (sides 1, 2, and 3)
- f. Navigation base (inertial measurement unit) (roll, pitch, and yaw axes)
- g. Ascent stage aft equipment rack (X, Y, and Z axes)
- h. Ascent stage tunnel equipment area (1, 2, and 3)
- i. Descent engine thrust chamber (X, Y, and Z axes)

Most of the vibration levels measured in the 22 areas of the vehicle were below the current lunar module flight vibration criteria derived from the lunar module test article-3 (LTA-3) test data. However, data from 4 of the 22 exceed the current flight vibration criteria when compared as measured, or exceed the criteria when scaled to design limit levels. The factors of safety which were applied to the mission levels

to obtain design limit levels for the acceleration spectral densities were 1.3^2 for the equipment and 1.5^2 for the tanks. (The respective safety factors for the vibration amplitudes are 1.3 and 1.5.) In addition, the measured vibrations were scaled to the worst combination of Saturn V and Saturn IB levels to obtain maximum mission levels. This was accomplished by assuming a one-to-one relationship between sound pressure and vibration acceleration measured on the Apollo 4 and 5 missions. Of the four measurements, only two - the aft equipment rack and the landing radar antenna - exceed the current flight criteria by significant margins, and those only in narrow frequency bands. However, when compared on a root-mean-square basis (that is, square root of the area under the acceleration spectral density curve), none of the measured vibrations exceed the current flight vibration criteria.

Lunar module equipment qualification tests have been conducted to at least one of three sets of criteria, depending on when the equipment was procured. (1) Equipment procured prior to the end of 1966 (completion of LTA-3 testing) was tested to analytically derived vibration criteria. (2) Equipment procured between the end of 1966 and the end of 1967 was tested to vibration criteria derived from the LTA-3 test data. (3) After the end of 1967, an acceptance vibration test program was begun, and some equipment was acceptance-tested to higher vibration levels than used in the qualification tests. This equipment was given a delta qualification test to provide an adequate margin.

Comparisons made in the subsequent paragraphs will be to current flight vibration criteria (derived from LTA-3 test data) and to the actual levels to which the equipment was qualified.

Vibration of the navigation base (inertial measurement unit) approached the flight vibration criteria (LTA-3) as measured and exceeded the criteria when scaled to design limit conditions, as shown in figure 6.1-11. However, neither the measured nor the scaled vibrations exceeded the level to which the inertial measurement unit was subjected during qualification testing. No data are presented for the pitch-axis vibration because measurement GG6002D did not function properly.

Vibration response of the landing radar antenna exceeded the flight vibration criteria (LTA-3), as shown in figure 6.1-12. However, during acceptance vibration tests, the landing radar antenna was exposed to vibrations in excess of those measured in flight.

Figure 6.1-13 compares the response of the ascent stage oxidizer tank bottom cover to the flight vibration criteria (LTA-3). The criteria are exceeded at frequencies of 96 and 160 Hz. Vibrations at those frequencies are similar to those measured on the LTA-10R descent stage oxidizer tank and are considered to have no effect on the structural integrity of the tank and its support structure. During the tank qualification

test, a response at 150 Hz was also noted at the same measurement location. Since this response far exceeded the LM-1 response, no further testing is required.

Vibrations measured on the aft equipment rack exceeded the flight vibration criteria at a frequency of 210 Hz and, when scaled to design limit levels, also exceed the criteria at 40 Hz (fig. 6.1-14). Each component on the aft equipment rack was qualification-tested for the ascent and descent engine operation levels, which covered the 40 Hz peak. All but two of the components attached to the aft equipment rack had been tested to levels at 210 Hz (table 6.1-VI) which exceed the flight vibration criteria (LTA-3). Additional tests are not believed necessary for the two components (battery and digital uplink assembly) for the following reasons: First, the abort electronics assembly was not installed on LM-1. The absence of this mass would tend to result in higher vibration responses. Second, the affected components are mounted on different cold-rails than the one where the flight measurement was located. LTA-3 transmissibility data indicate attenuation at 210 Hz from the location of the flight measurement to the locations of the battery and the digital uplink assembly.

Orbit.- Vibrations were insignificant during steady-state descent and ascent engine firings. Figure 6.1-15 presents typical vibration data for the following four orbital flight conditions:

- a. Control, descent, and ascent engines not operating (instrumentation/telemetry noise floors)
- b. Third descent engine firing (start and 10 percent throttle)
- c. Third descent engine firing (full throttle), abort staging, and first ascent engine firing
- d. First ascent engine firing, including shutdown transients

Ascent engine ignitions produced a short-duration discrete frequency oscillation of approximately 55 Hz on the inertial measurement unit roll axis. Ignition for the second firing produced 1.5g on the roll axis. The ascent engine shutdown produced high frequency oscillations of the thrust chamber, but data in figure 6.1-15 indicate that these oscillations were not transmitted to equipment. Comparison of power spectral density analyses of inertial measurement unit and ascent stage aft equipment rack vibrations to lunar module criteria show that steady-state firings of the ascent and descent engines produced insignificant vibrations.

Low-frequency vibration.- No significant low-frequency vibrations (20 Hz or less) were observed during the mission.

TABLE 6.1-I.- LM MAXIMUM LOADING CONDITIONS

Flight condition	Load	Predicted	Measured	Design ^a
Lift-off				
Maximum lateral acceleration	Longitudinal load factor, g . . .	--	1.20	1.60
	Lateral load factor, g	0.25	0.20	0.65
Maximum longitudinal acceleration	Longitudinal load factor, g . . .	1.60	1.48	1.60
	Lateral load factor, g	--	0.03	0.65
Maximum q α	Longitudinal load factor, g . . .	2.00	2.00	2.00
	Lateral load factor, g	0.09	0.12	0.30
End of S-IB boost	Longitudinal load factor, g . . .	4.38	4.35	4.90
	Lateral load factor, g	0.10	0.07	0.10
Abort staging	Longitudinal load factor, g . . .	--	1.20	--
	Lateral load factor, g	--	Not detectable	--

^aDesign values are for Saturn V conditions.

TABLE 6.1-II.- LM OUTRIGGER LOADS AT END OF S-IB BOOST
(MAXIMUM AXIAL ACCELERATION)

Apex	Strut	Measured load, klb	Predicted load, klb	Allowable load, klb
+Y	1	-12.47	-14.27	-23.3
	2	17.01	16.39	21.0
	3	21.50	21.53	25.3
	4	-16.03	-16.45	-23.3
+Z	1	-13.16	-13.70	-23.3
	2	16.91	16.74	21.0
	3	17.84	17.07	21.0
	4	-12.64	-13.22	-23.3
-Y	1	-15.61	-16.25	-23.3
	2	21.36	21.51	25.3
	3	15.63	16.52	21.0
	4	-12.63	-14.14	-23.3
-Z	1	-12.18	-13.51	-23.3
	2	16.88	17.07	21.0
	3	18.01	16.70	21.0
	4	-13.12	-13.97	-23.3

TABLE 6.1-III.- LM/ADAPTER INTERACTION LOADS AT END OF
S-IB BOOST (MAXIMUM AXIAL ACCELERATION)

Apex	Reaction	Calculated load ^a , klb	Design load (70° F), klb
+Y	R _X	35.98	41.19
	R _Y	-2.70	-4.42
	R _Z	-0.37	-1.18
+Z	R _X	32.45	36.55
	R _Y	-0.66	-1.62
	R _Z	-2.44	-3.87
-Y	R _X	34.77	41.06
	R _Y	3.78	3.75
	R _Z	0.45	-0.43
-Z	R _X	32.53	36.72
	R _Y	-0.12	-0.88
	R _Z	2.05	-5.09

^aCalculated from measured loads in table 6.1-II.

TABLE 6.1-IV.- PEAK SURFACE PRESSURES AT STAGING

LM-1 measurement number (see figs. 6.1-9 and 6.1-10)		LM-1 peak pressure, psia ($P_c = 164$ psia)	Design limit pressure, psia ($P_c = 178$ psia)	PA-1 test data, Run 7A-007 ($P_c = 193$ psia)
Ascent stage base heat shield				
-Y	GB0801P	0.69	1.33	--
	GB0802P	0.28	1.49	--
	GB0803P	0.21	2.26	--
	GB0804P	0.82	2.02	--
	GB0806P	1.17	1.56	--
	GB0807P	1.31	2.90	2.20
	GB0808P	0.56	2.16	0.99
+Y	GB0809P	0.71	3.28	2.12
	GB0811P	0.29	1.08	--
	GB0812P	2.01	2.25	3.65
	GB0813P	1.5	2.45	--
	GB0814P	1.0	3.19	3.06
-Z	GB0815P	1.2	2.98	2.69
	GB0816P	0.4	0.66	0.86
	GB0622P	0.59	0.84	0.80
Descent stage upper stage				Run 7A-004 ($P_c = 166$ psia)
+Y	GB0901P	0.3	2.34	0.77
	GB0903P	0.8	2.34	1.64
	GB0904P	0.5	0.63	--
-Y	GB0902P	0.5	0.90	1.56
	GB0905P	0.6	1.51	0.64
	GB0907P	0.7	1.85	1.07

- NOTES: 1. P_c is ascent engine peak chamber pressure
2. LM-1 pressures are peak values and did not occur at the same time
3. Design pressures are based on 1/10-scale model data
4. Both design and PA-1 pressures shown are for zero separation distance
5. PA-1 data shown were obtained from approximately the same locations as LM-1 measurements
6. PA-1 tests simulating LM-1 were run at White Sands. Test run 7A-007 was used for ascent stage pressure comparison. Test run 7A-004 was the only run on which +Y descent stage surface pressures were obtained for peak engine chamber pressure conditions.

TABLE 6.1-V.- VIBRATION MEASUREMENTS

Number	Measurement description	Range, g	Frequency response, Hz	Time-shared
GA1501D	Vibration, ascent engine support structure, side 1	30	1000	Yes
GA1502D	Vibration, ascent engine support structure, side 2	30	1000	Yes
GA1503D	Vibration, ascent engine support structure, side 3	30	1000	Yes
GA1571D	Vibration, ascent engine oxidizer tank, X axis	10	160	No
GA1572D	Vibration, ascent engine oxidizer tank, Y axis	10	110	Yes
GA1573D	Vibration, ascent engine oxidizer tank, Z axis	10	110	Yes
GA2681D	Vibration, descent engine oxidizer tank, X axis	10	110	No
GA2682D	Vibration, descent engine oxidizer tank, Y axis	10	110	Yes
GA2683D	Vibration, descent engine oxidizer tank, Z axis	10	110	Yes
GA3601D	Vibration, ascent stage aft equipment bay, X axis	20	1000	Yes
GA3602D	Vibration, ascent stage aft equipment bay, Y axis	20	1000	Yes
GA3603D	Vibration, ascent stage aft equipment bay, Z axis	20	1000	Yes
GA3661D	Vibration 1, tunnel equipment area	30	2000	Yes
GA3662D	Vibration 2, tunnel equipment area	30	2000	Yes
GA3663D	Vibration 3, tunnel equipment area	30	2000	Yes
GG6001D	Vibration, navigation base, roll	2	2000	Yes
GG6002D	Vibration, navigation base, pitch	2	2000	Yes
GG6003D	Vibration, navigation base, yaw	2	2000	Yes
GN7559D	Vibration, landing radar antenna	10	110	Yes
GN7691D	Vibration, rendezvous radar dish antenna	10	110	Yes
GP2801D	Vibration, ascent engine thrust chamber, X axis	163	2000	No
GP2802D	Vibration, ascent engine thrust chamber, Y axis	35	2000	No
GP2803D	Vibration, ascent engine thrust chamber, Z axis	35	2000	No
GQ7301D	Vibration, descent engine thrust chamber, X axis	141	2000	No
GQ7302D	Vibration, descent engine thrust chamber, Y axis	141	2000	No
GQ7303D	Vibration, descent engine thrust chamber, Z axis	141	2000	No

TABLE 6.1-VI.- VIBRATION LEVELS TO WHICH EQUIPMENT MOUNTED ON THE
AFT EQUIPMENT RACK WAS TESTED AT 210 Hz

Component	Test level at 210 Hz, g^2/Hz
S-band power amplifier	0.075
S-band transceiver	0.075
VHF transceiver	0.075
Signal processor assembly	0.1
Digital up-link assembly	0.005
Caution and warning electronics assembly	0.075
Signal conditioning electronics assembly	0.067
Pulse code modulation and timing electronics assembly	0.075
Abort electronics assembly	0.075
Attitude and translation control assembly	0.075
Ascent stage battery	0.005
Electrical control	0.067
General-purpose inverter	0.075
Rendezvous radar electronics assembly	0.095

Note: IM-1 vibration data at 210 Hz scaled to the design limit level was $0.012 g^2/\text{Hz}$.

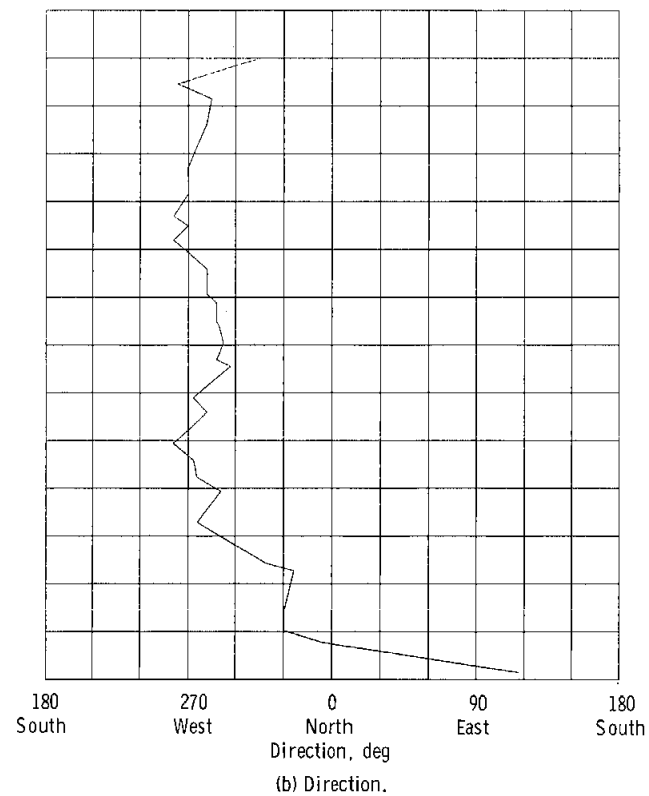
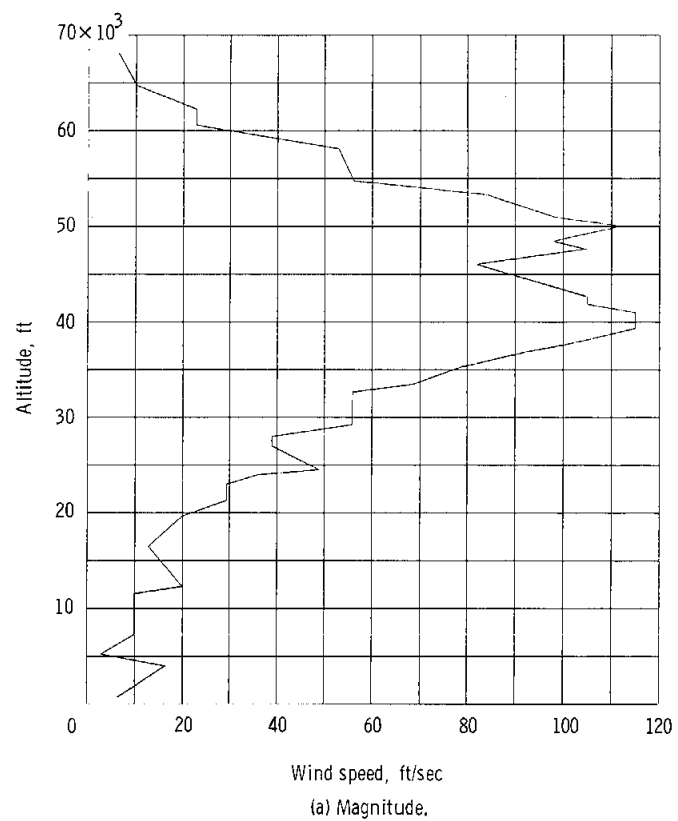


Figure 6.1-1. - Launch winds.

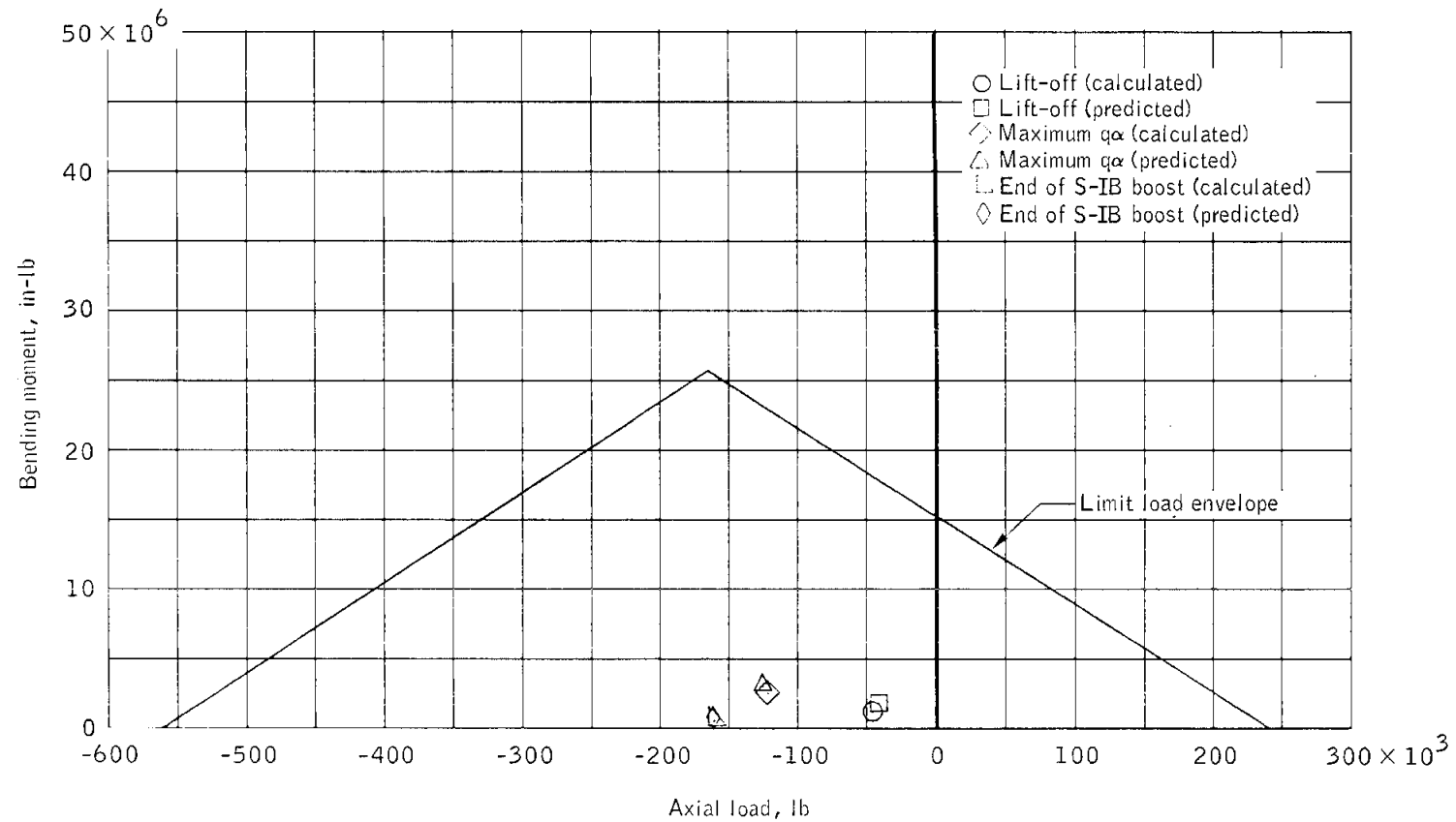


Figure 6.1-2.- Comparison of adapter body loads at the LM/adapter interface with limit design body load capabilities.

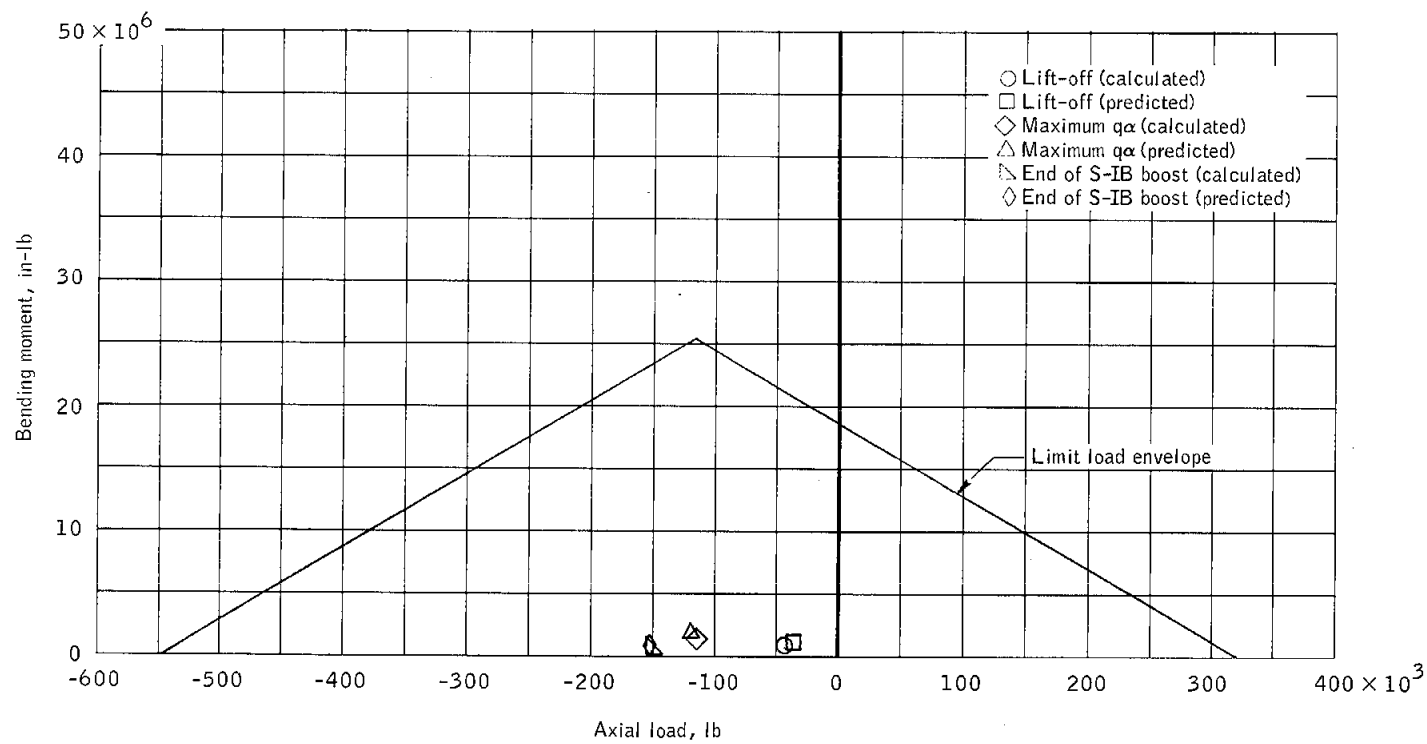


Figure 6.1-3.- Comparison of adapter body loads at the adapter/instrument unit interface with limit design body load capabilities.

NASA-S-68-1941

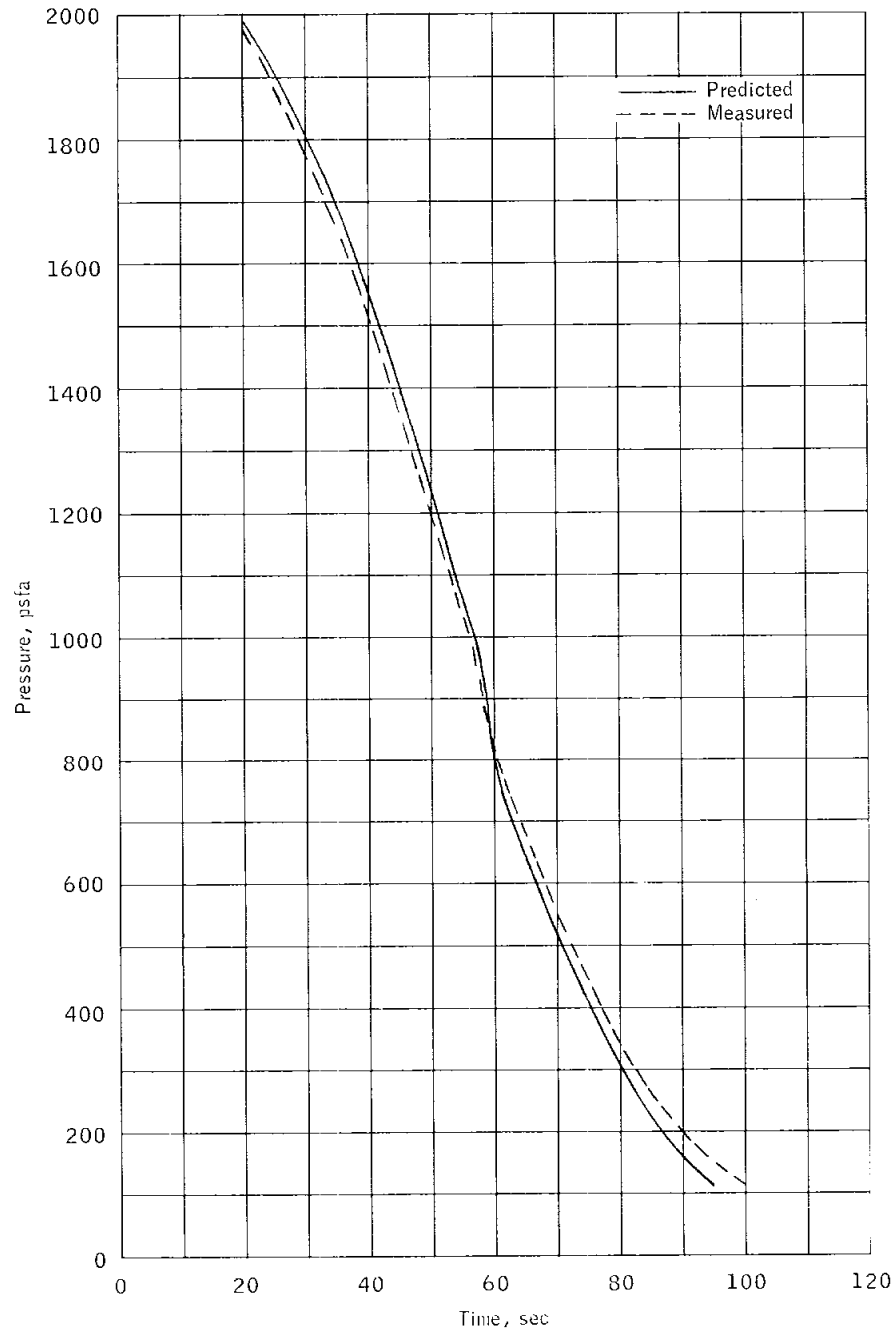
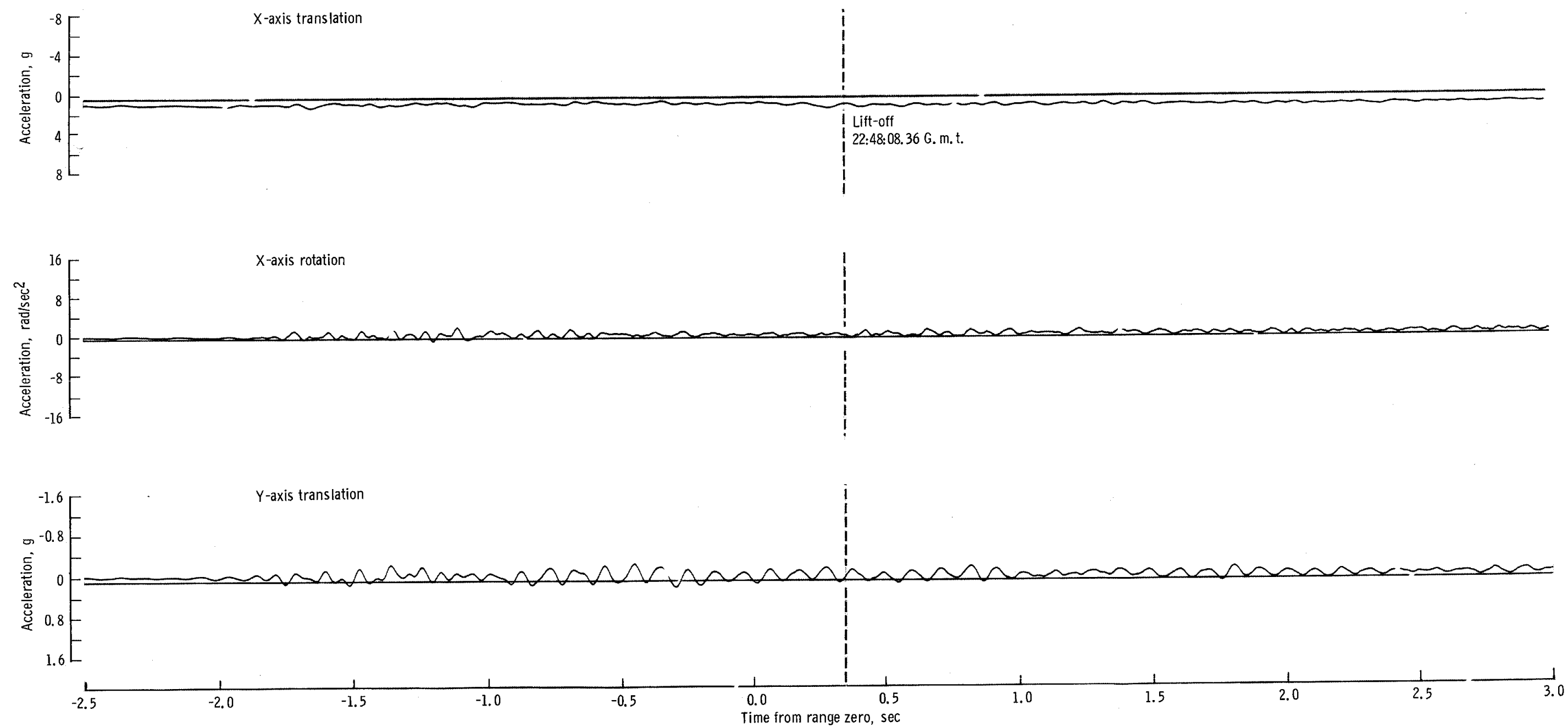


Figure 6.1-4.- Adapter vent pressure.

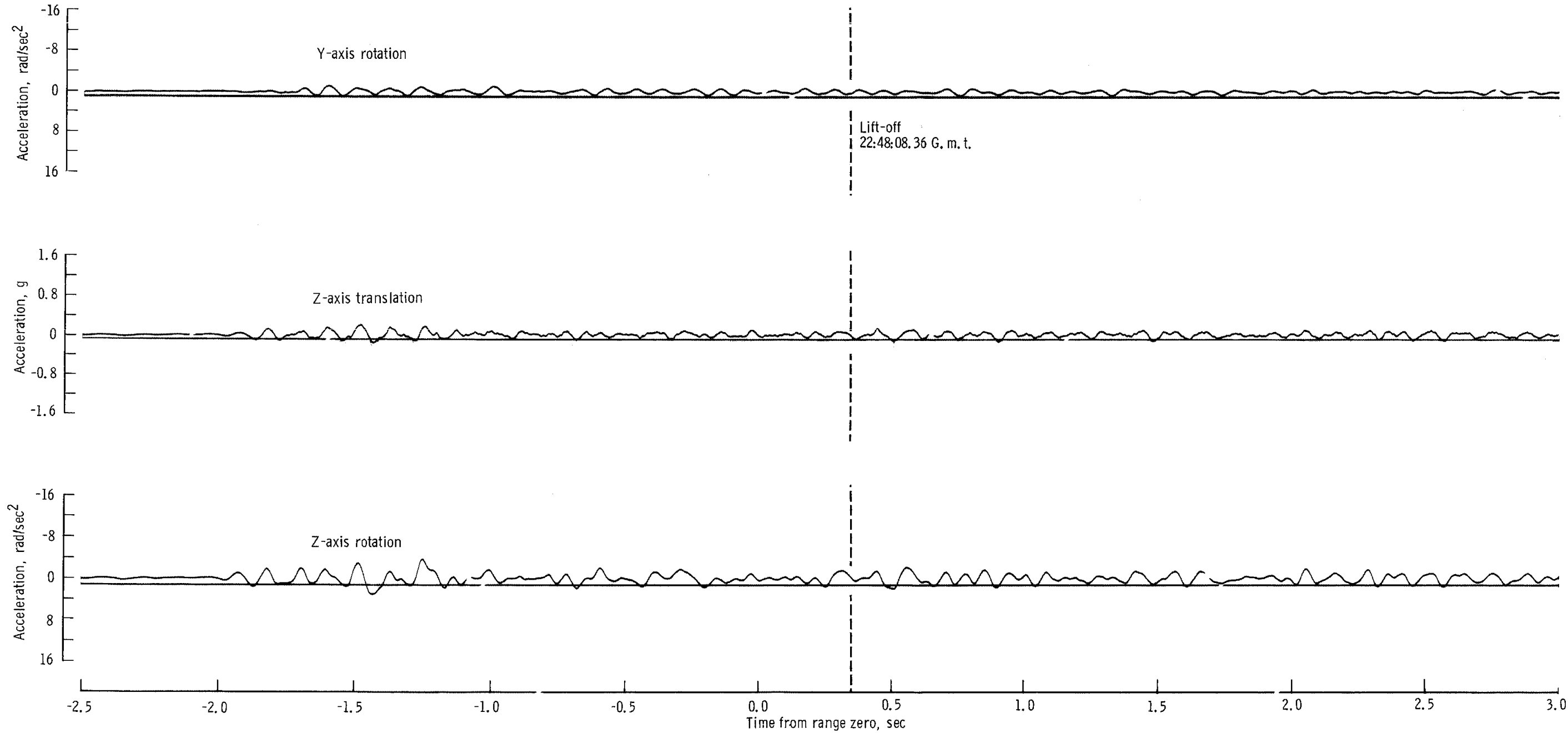
NASA-S-68-1942



(a) X-axis translation and rotation, and Y-axis translation.

Figure 6.1-5. - Lift-off accelerations.

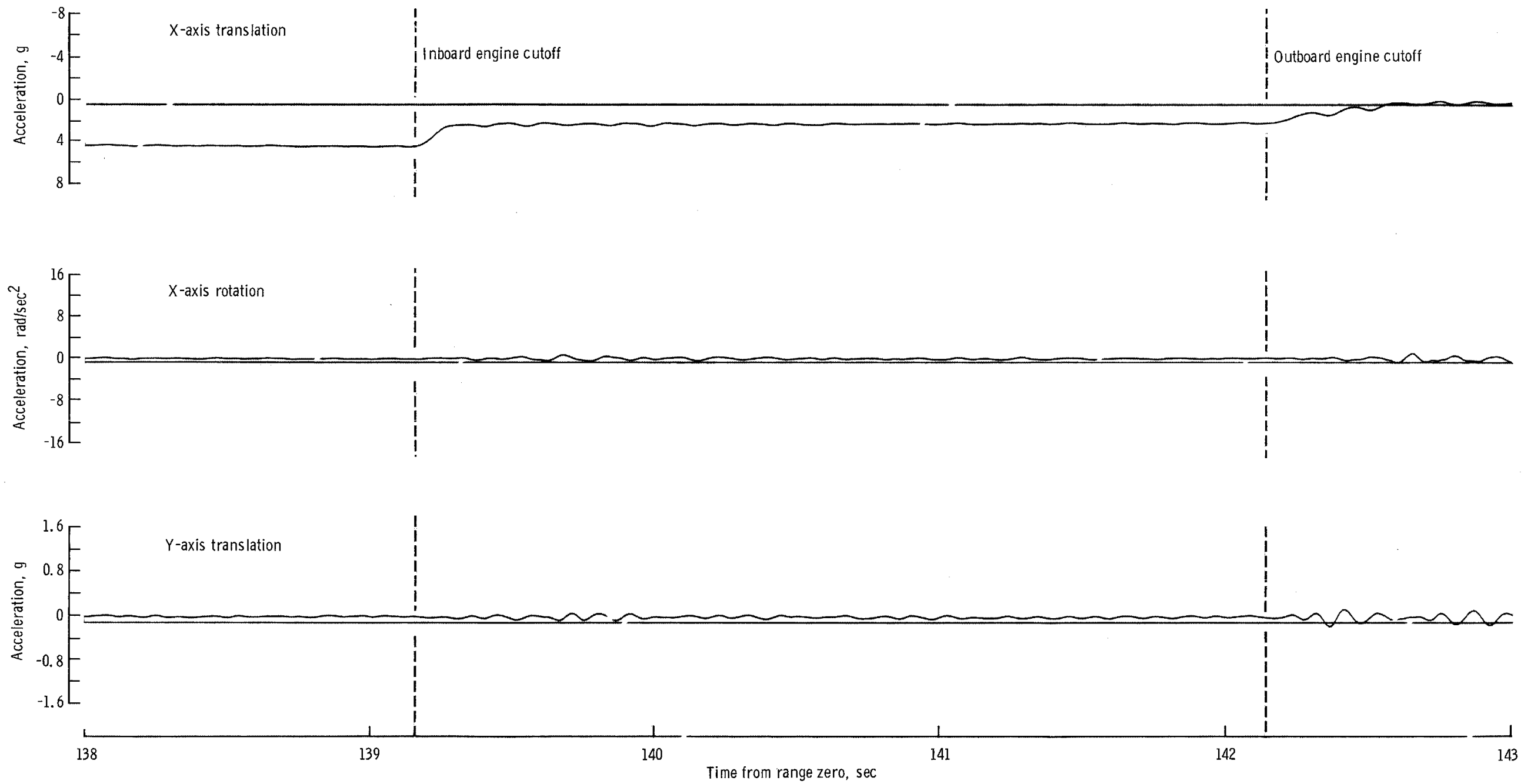
NASA-S-68- 1943



(b) Y-axis rotation, and Z-axis translation and rotation.

Figure 6.1-5. - Concluded.

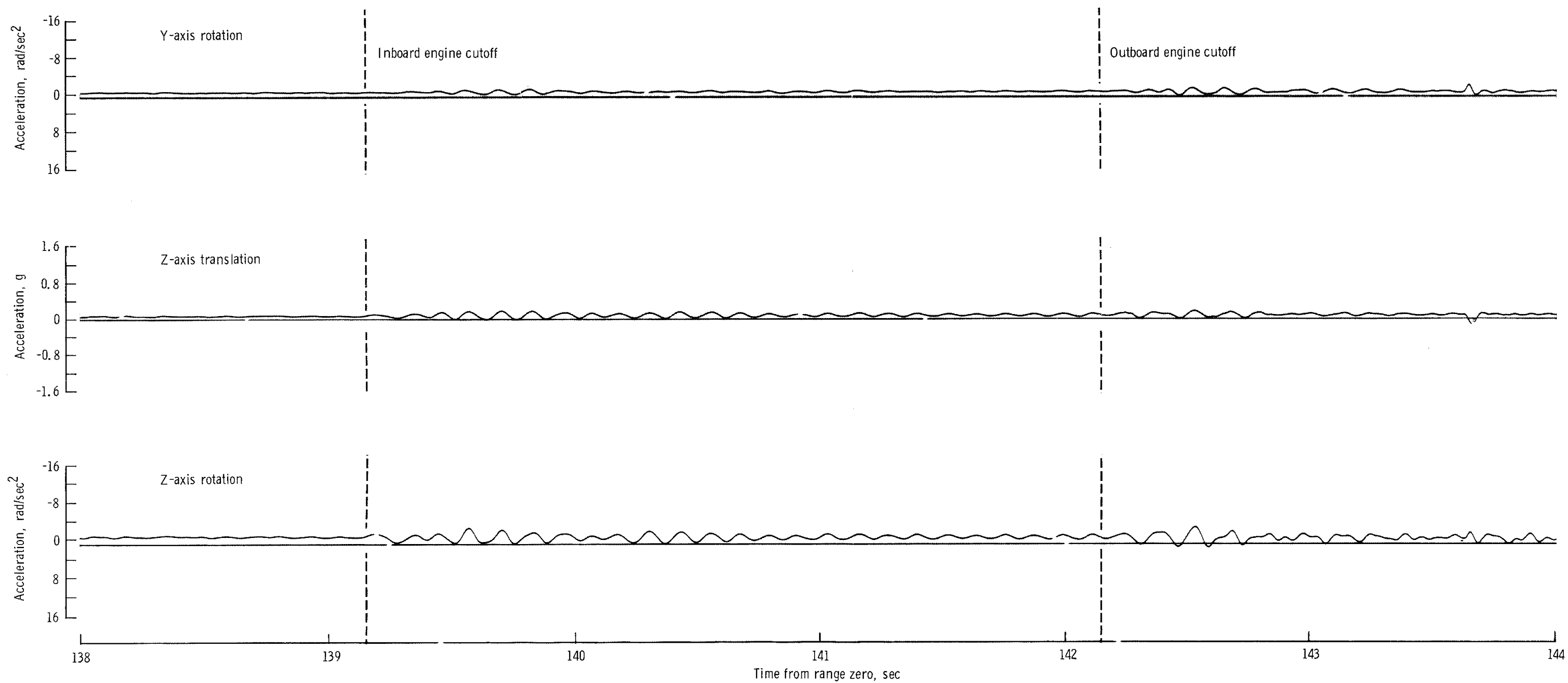
NASA-S-68-1944



(a) X-axis translation and rotation, and Y-axis translation.

Figure 6.1-6. - S-IB shutdown.

NASA-S-68-1945



(b) Y-axis rotation and Z-axis translation and rotation.

Figure 6.1-6. - Concluded.

NASA-S-68-1946

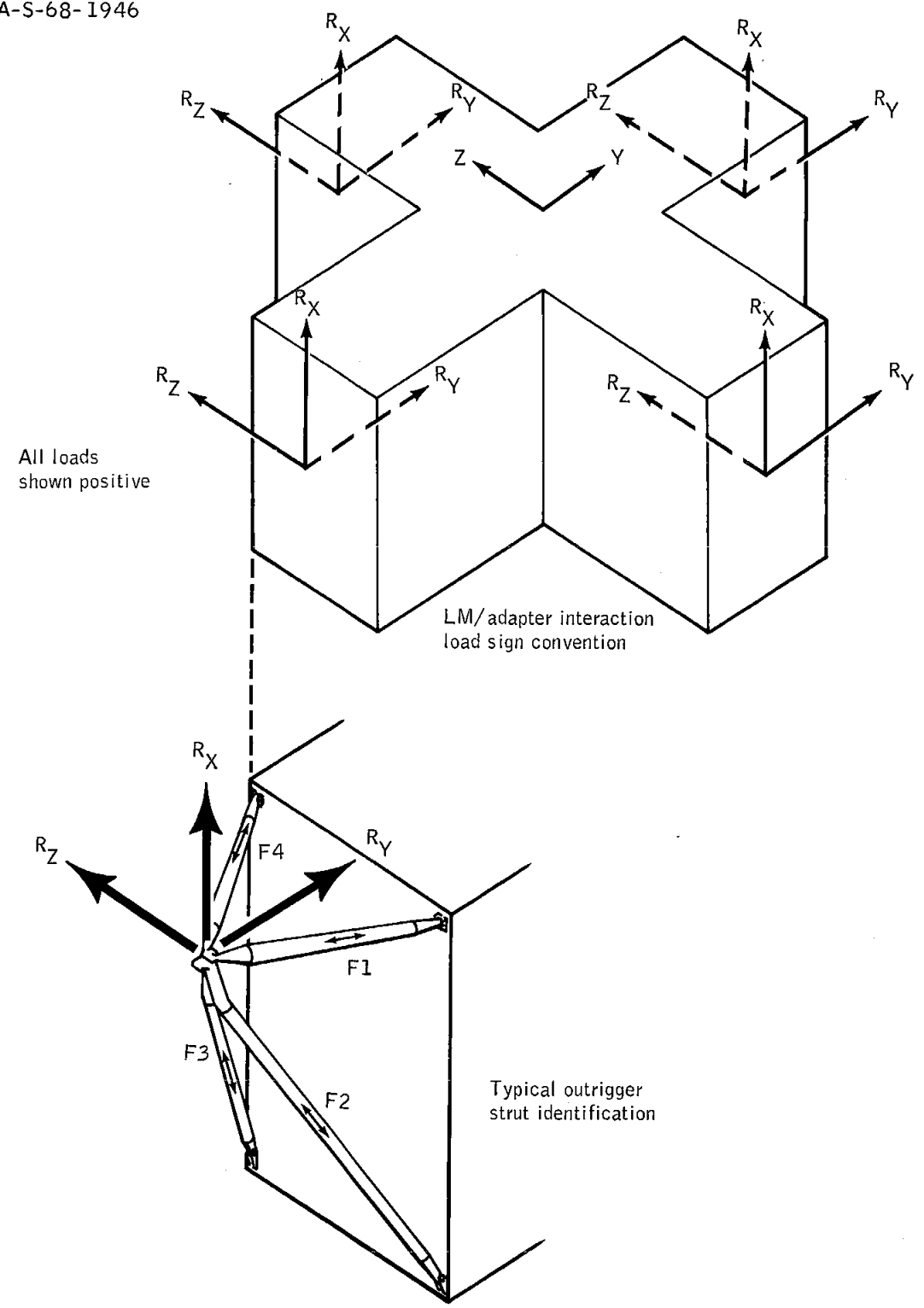


Figure 6.1-7.- LM/adaptor interaction loads sign convention and strut identification.

NASA-S-68- 1947

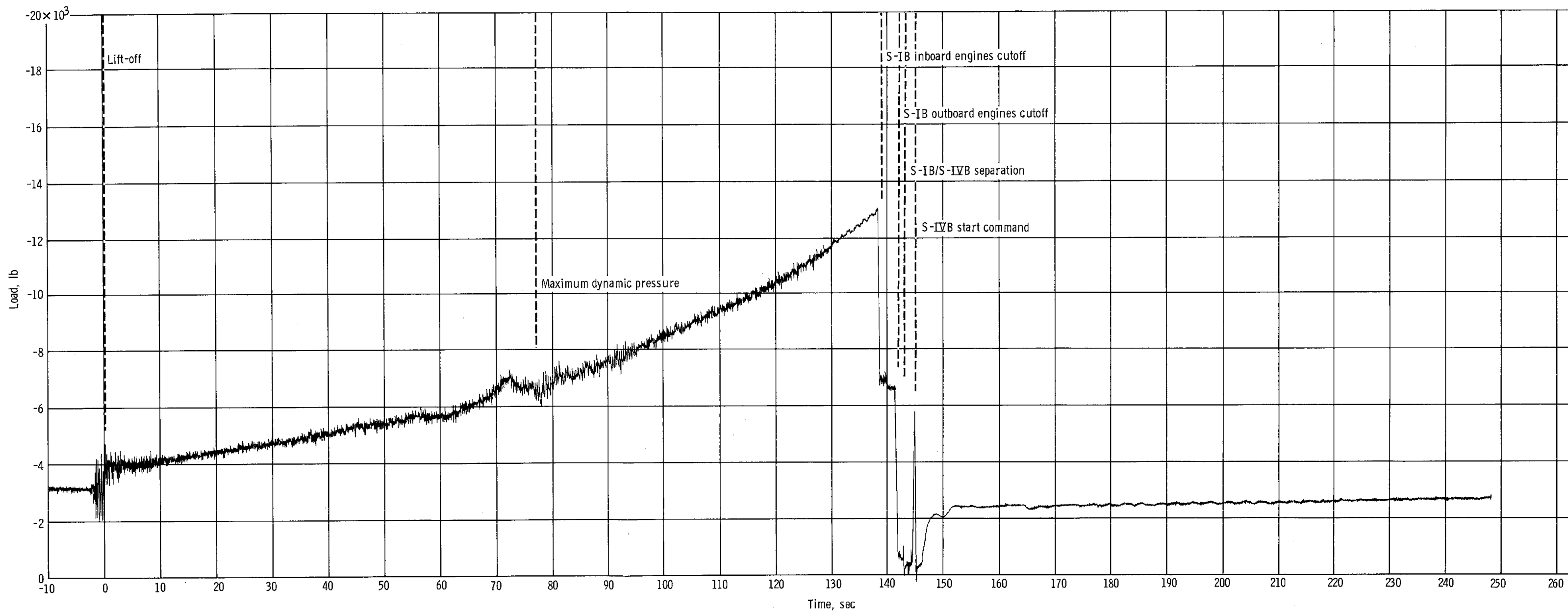


Figure 6.1-8. - Typical outrigger strut launch loads.

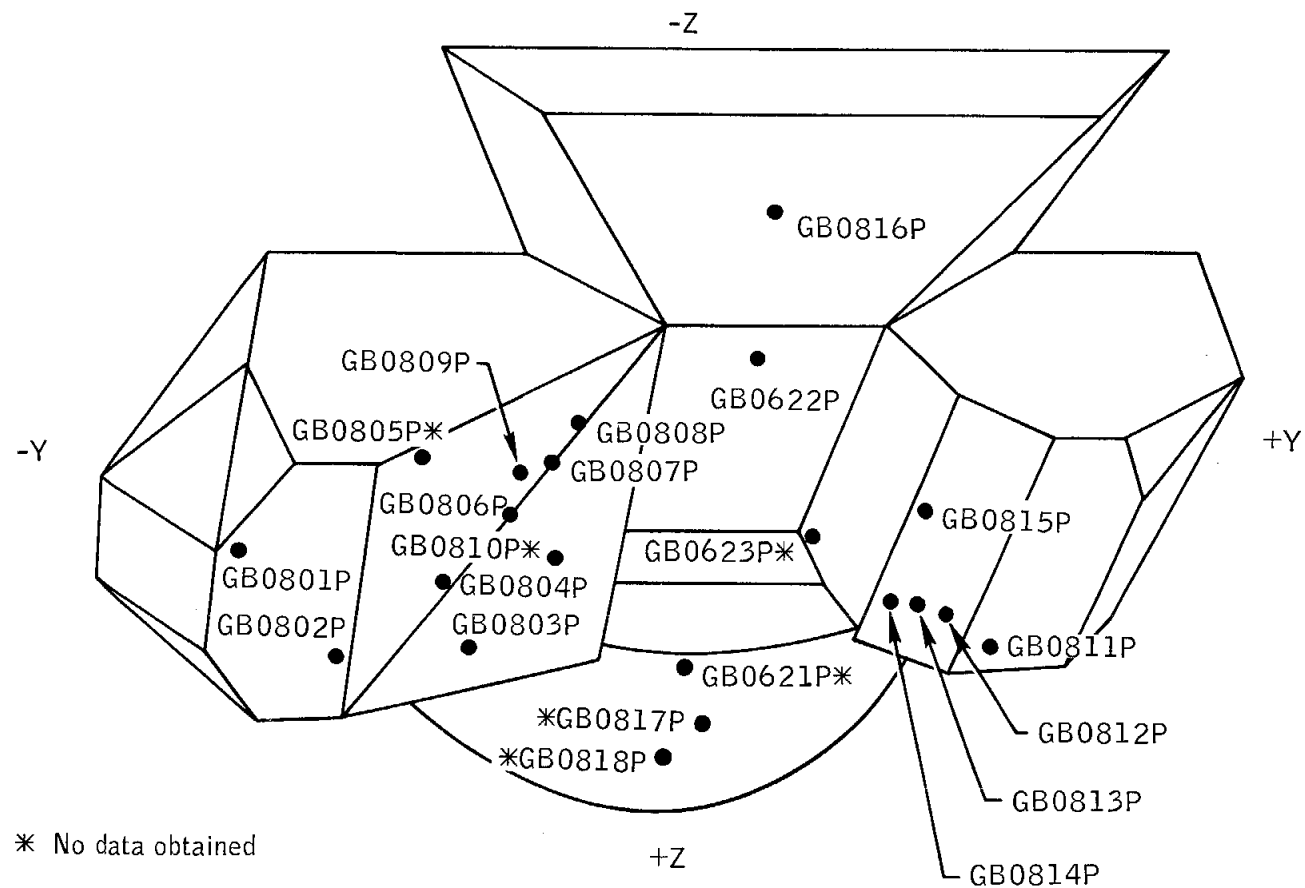
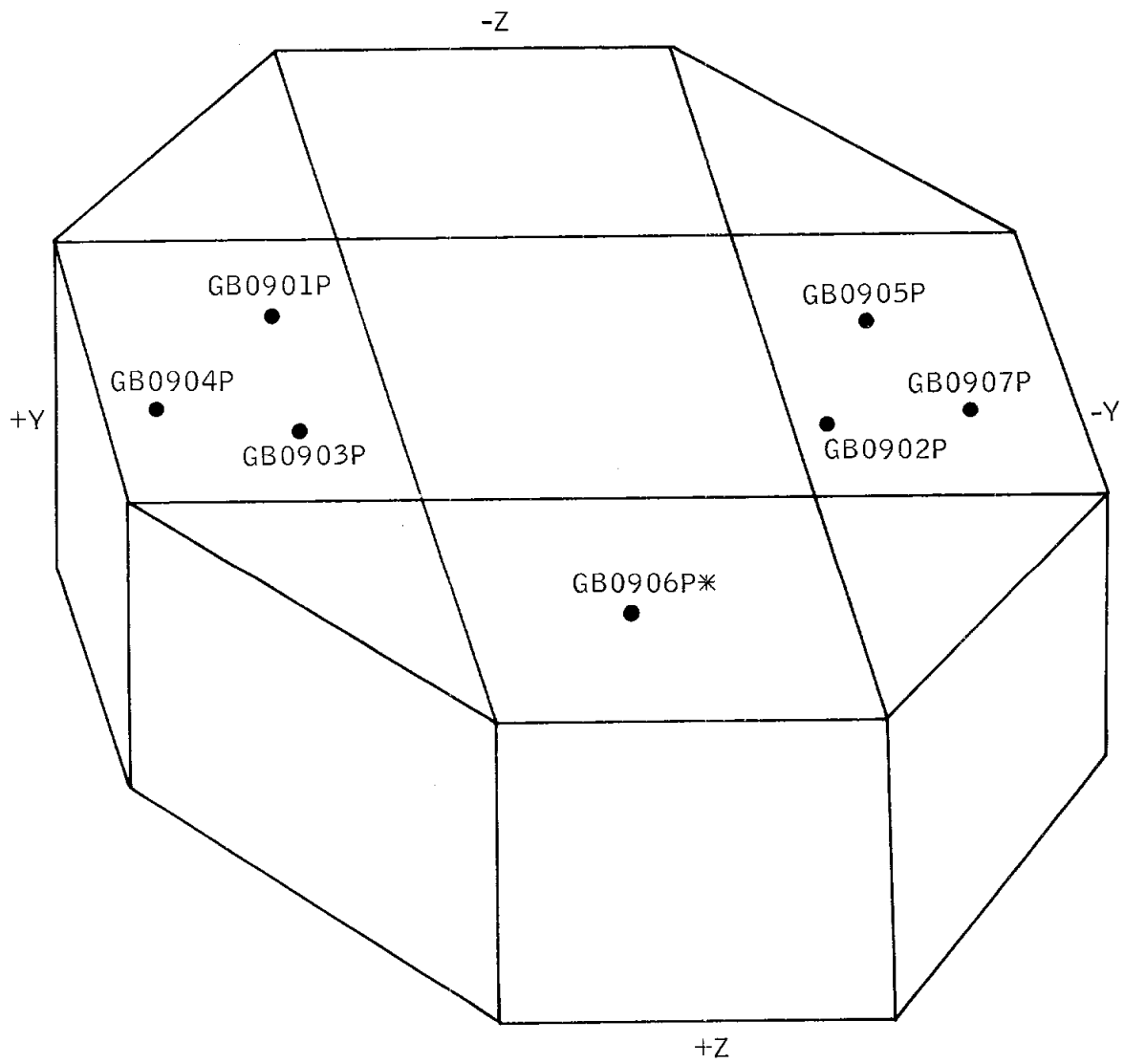


Figure 6.1-9.- Ascent stage base heat shield pressure measurement locations.

6.1-24

NASA-S-68-1949



* No data obtained

Figure 6.1-10.- Descent stage upper surface pressure measurement locations.

NASA-S-68-1950

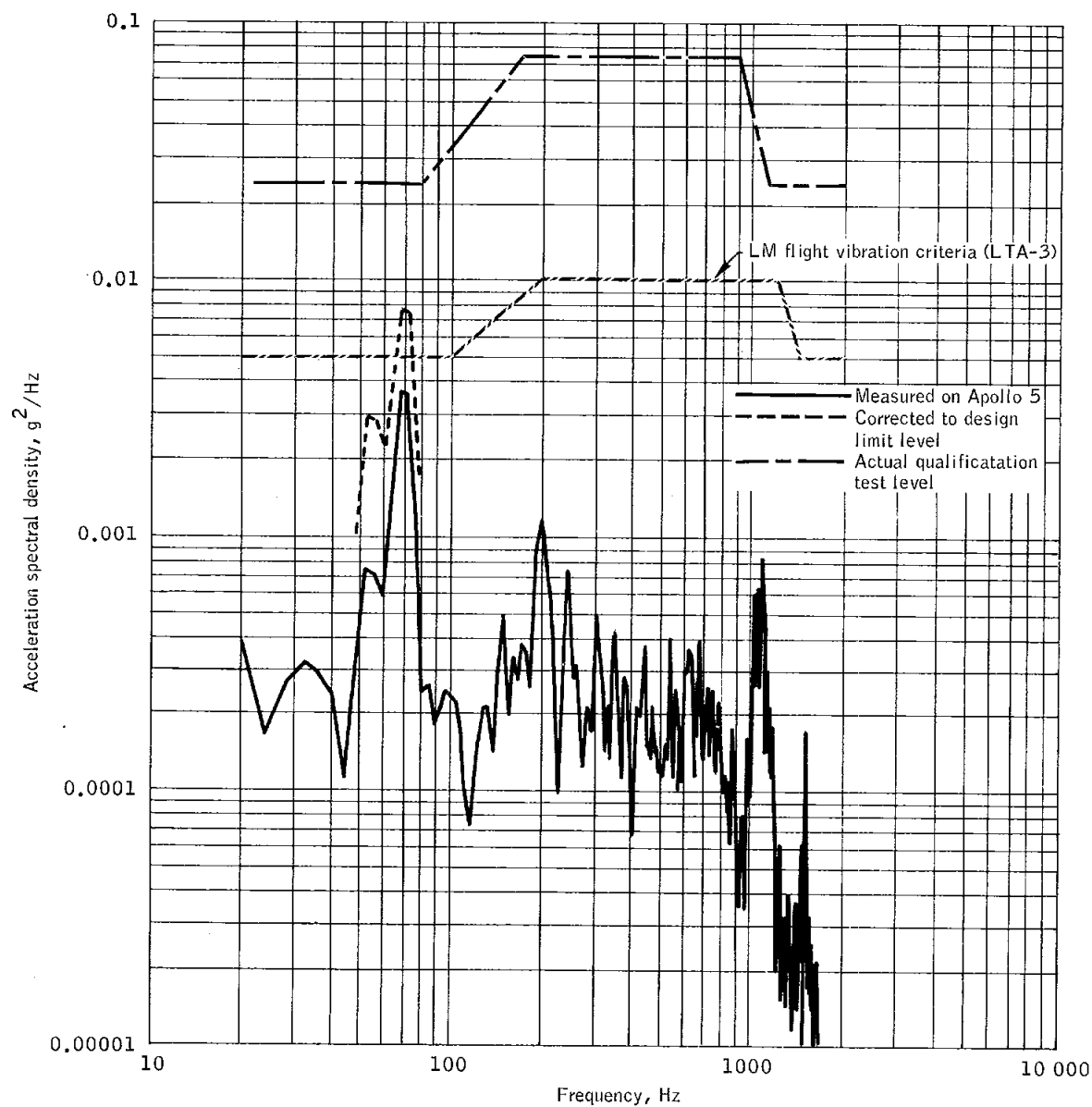


Figure 6.1-11.- Comparison of navigation base vibration response at lift-off to current flight vibration and actual qualification test levels.

NASA-S-68-1951

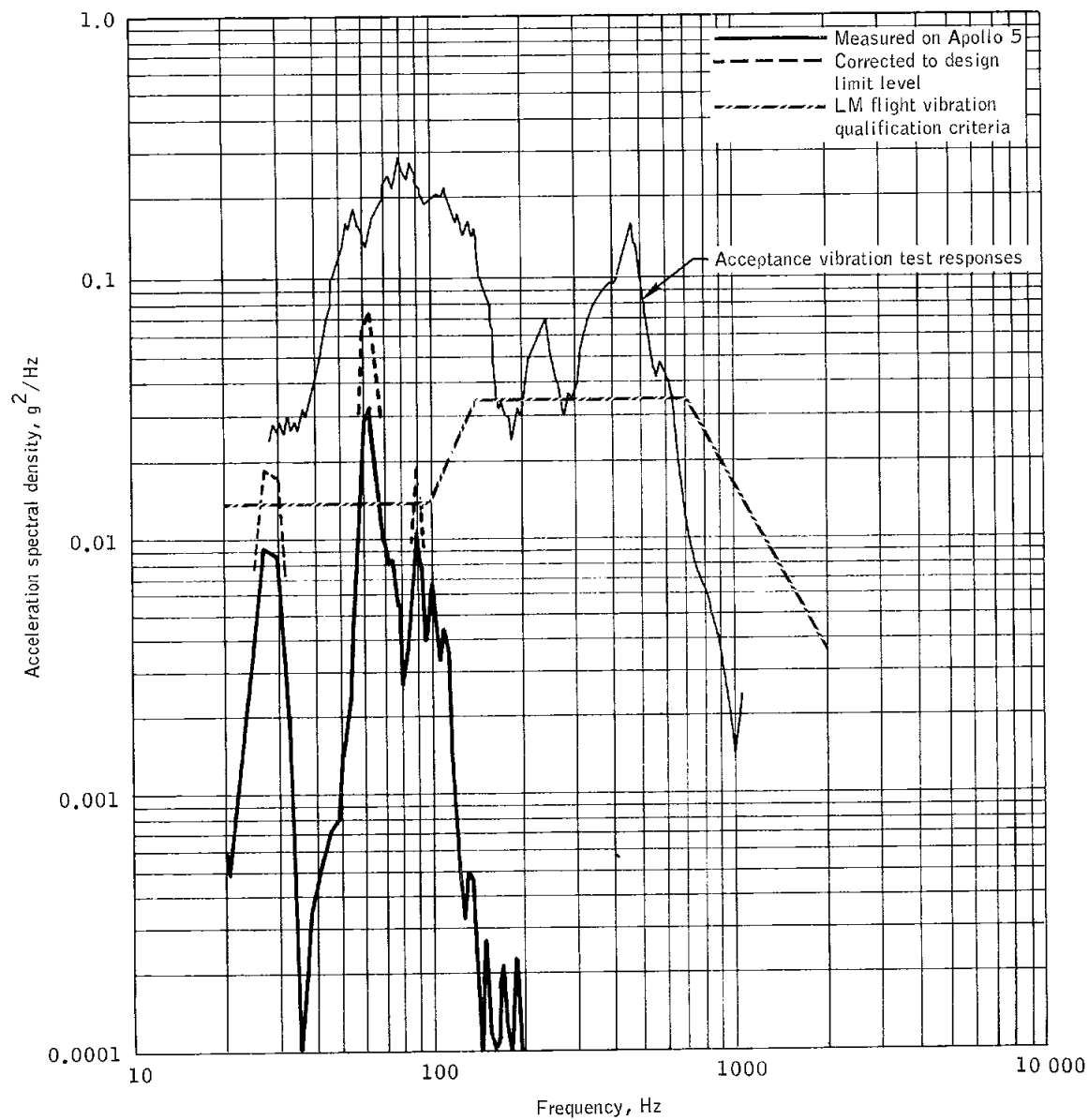


Figure 6.1-12.- Comparison of the landing radar antenna vibration response at lift-off to current flight vibration criteria and acceptance vibration test responses.

NASA-S-68- 1952

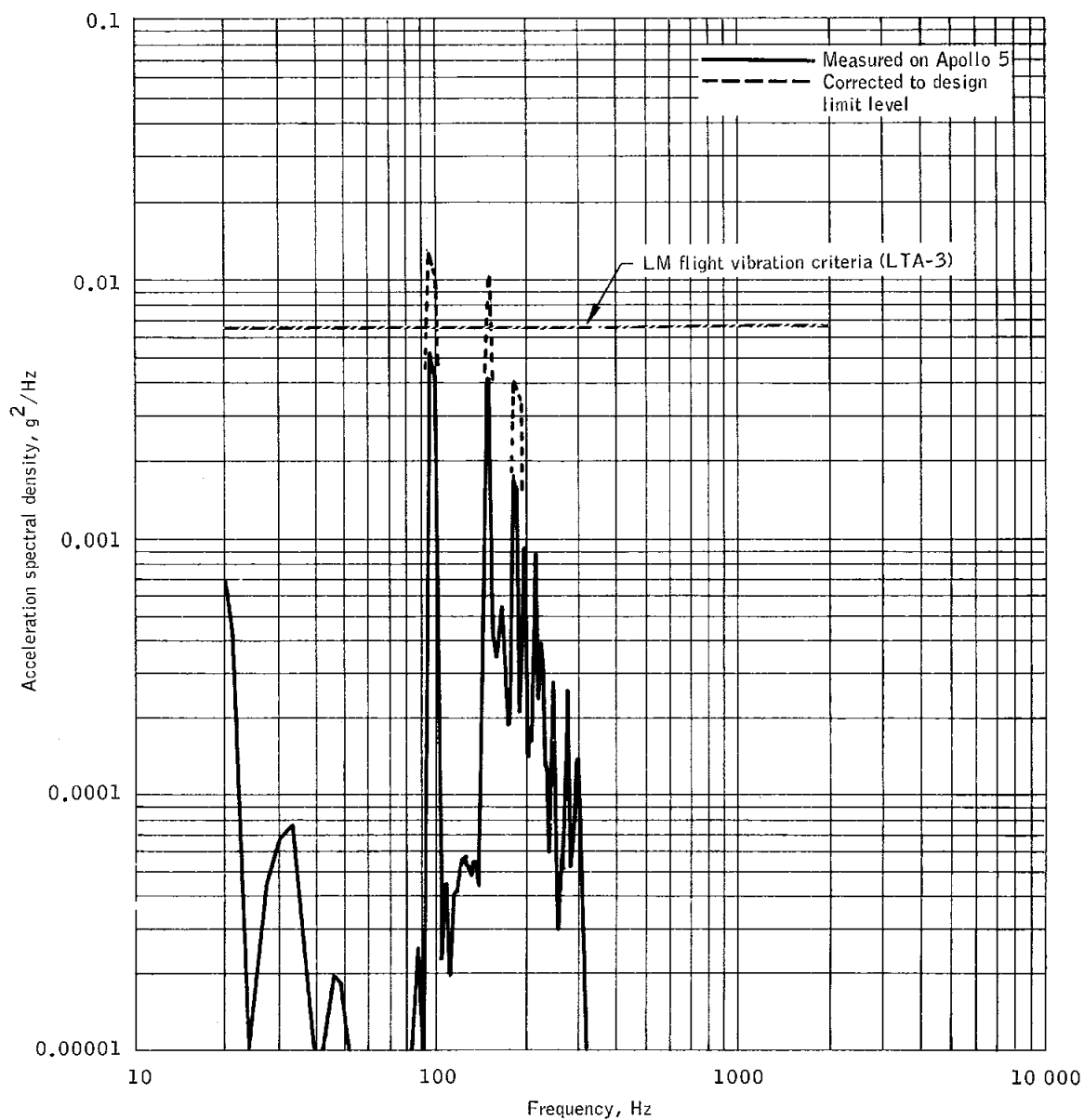


Figure 6.1-13.- Comparison of ascent stage oxidizer tank bottom cover vibration response at lift-off to current flight criteria.

NASA-S-68-1953

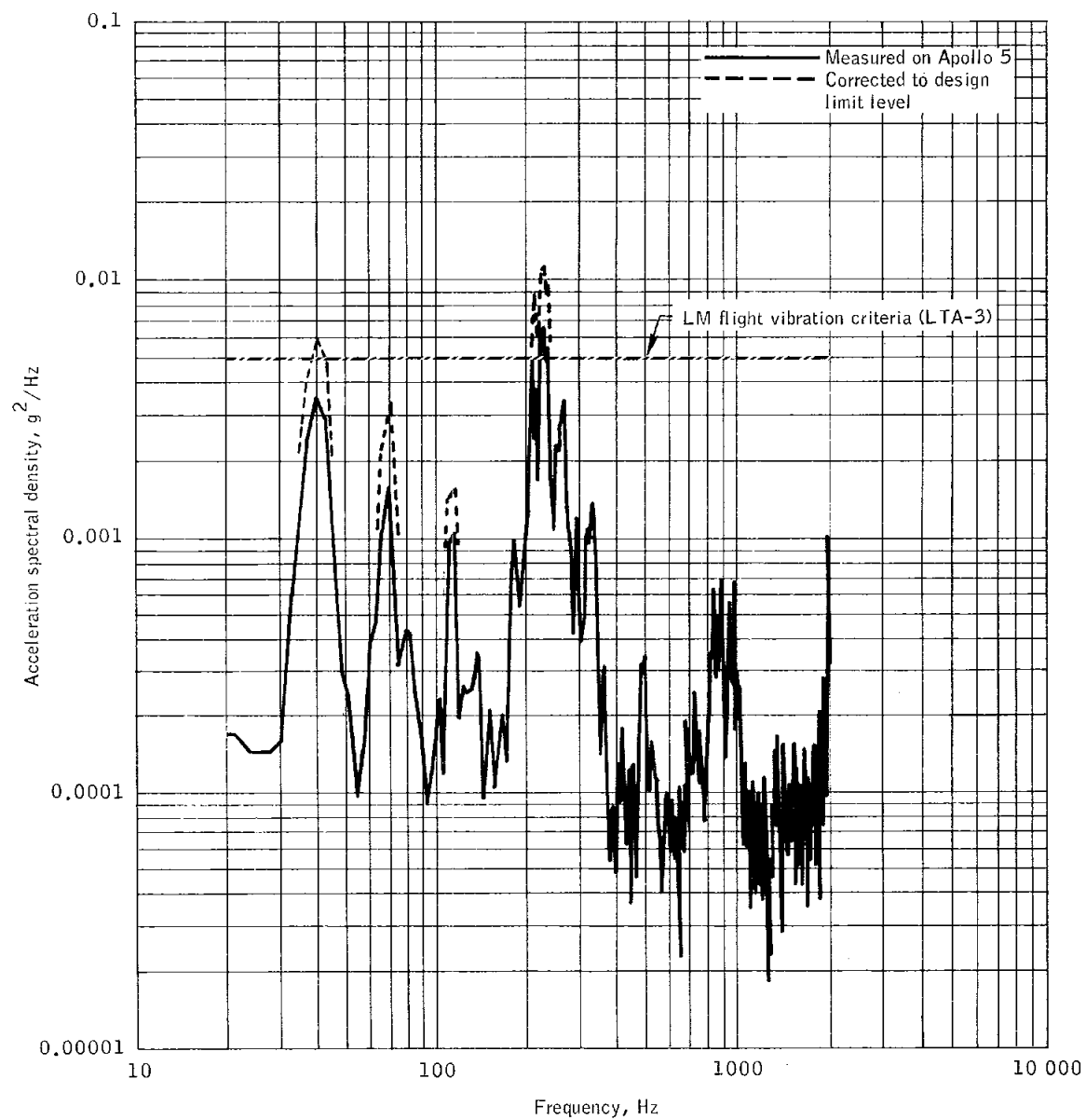
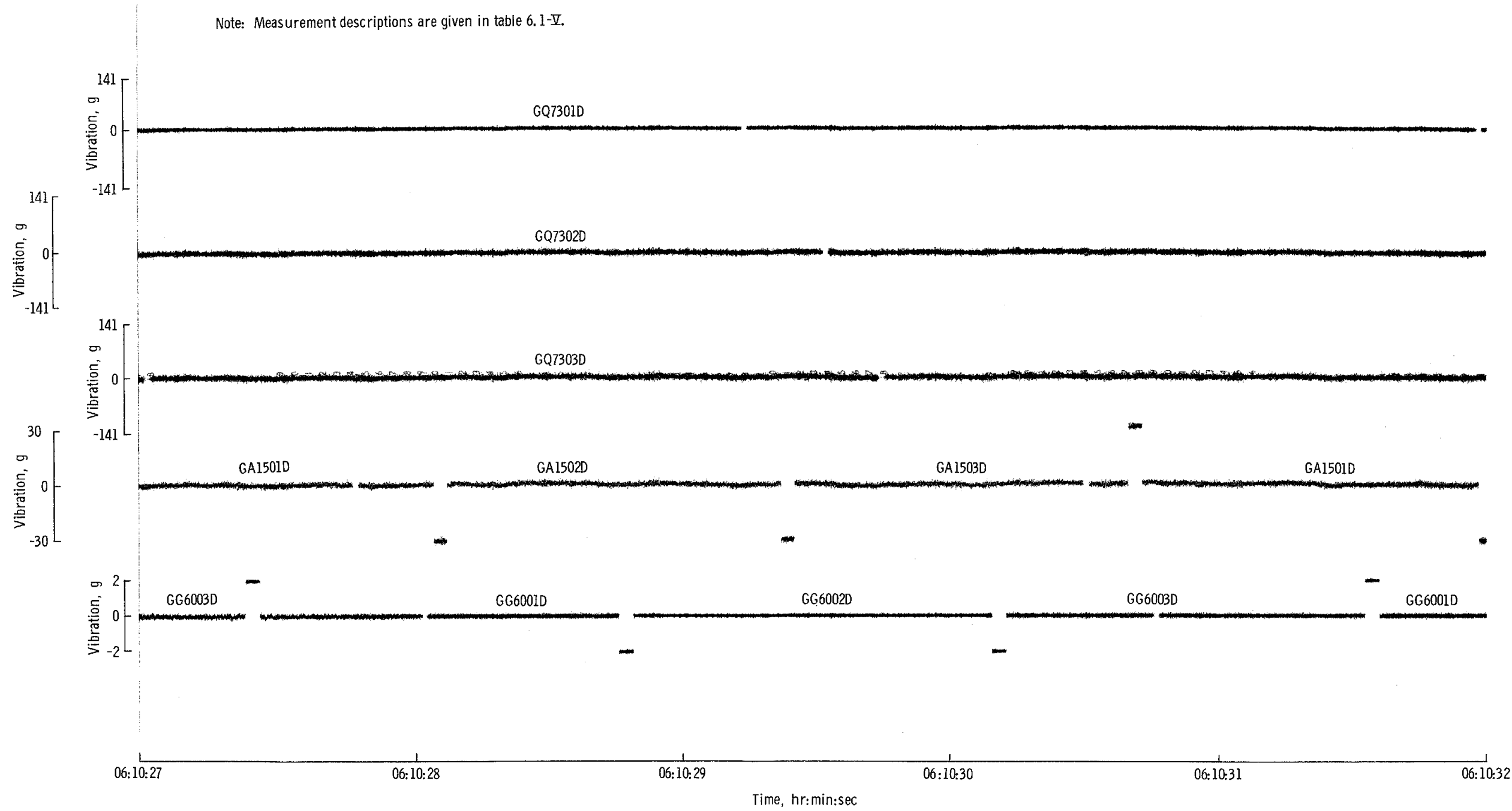


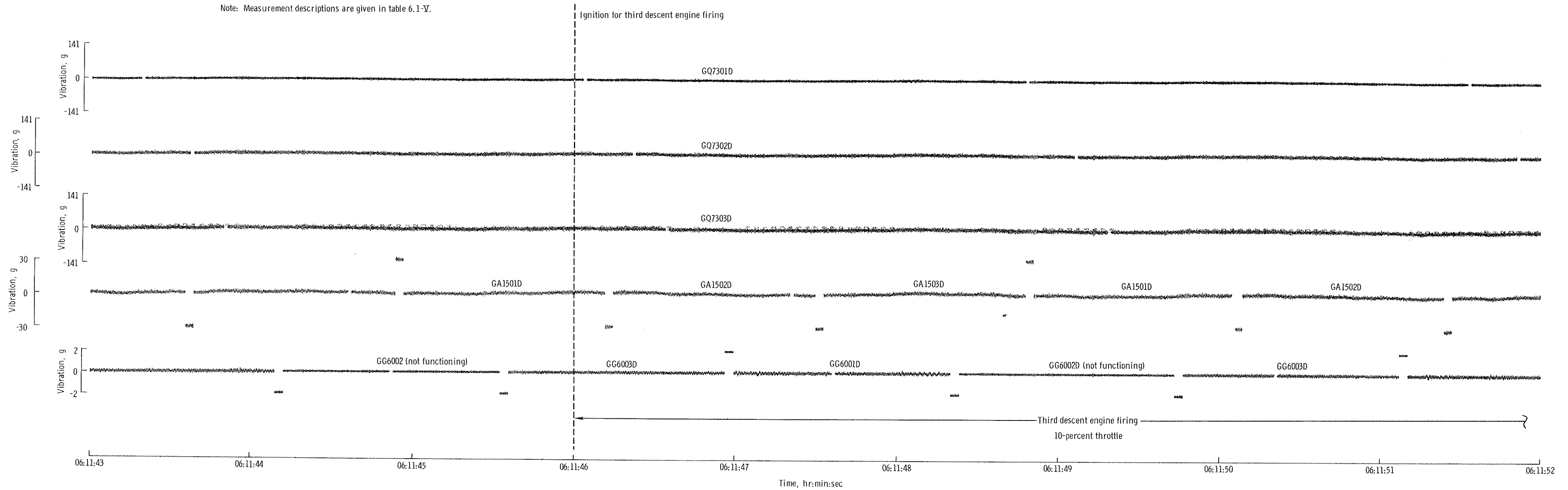
Figure 6.1-14.- Comparison of ascent stage aft equipment rack vibration response at lift-off to current flight vibration criteria.

NASA-S-68-1954



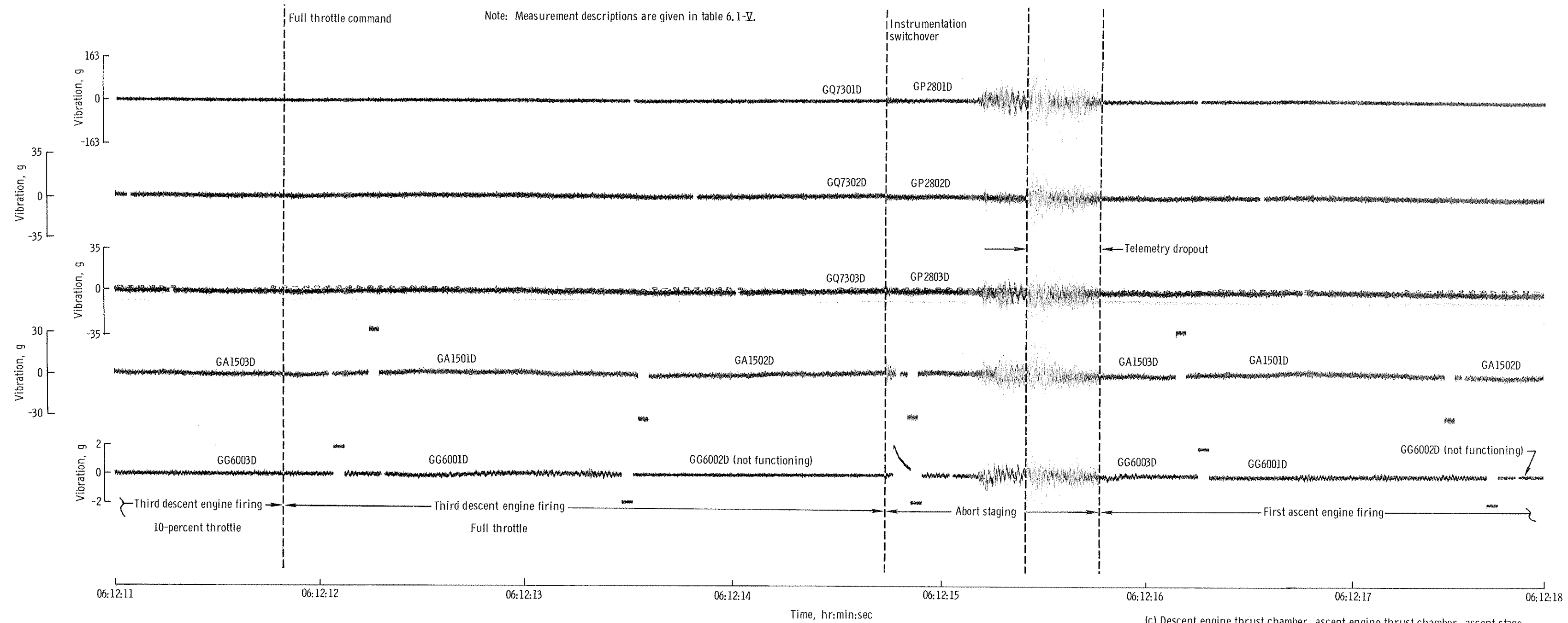
(a) Instrumentation/telemetry noise floor (engines not operating).
Figure 6.1-15. - Vibration measurements during mission programmer sequence III.

Note: Measurement descriptions are given in table 6.1-V.



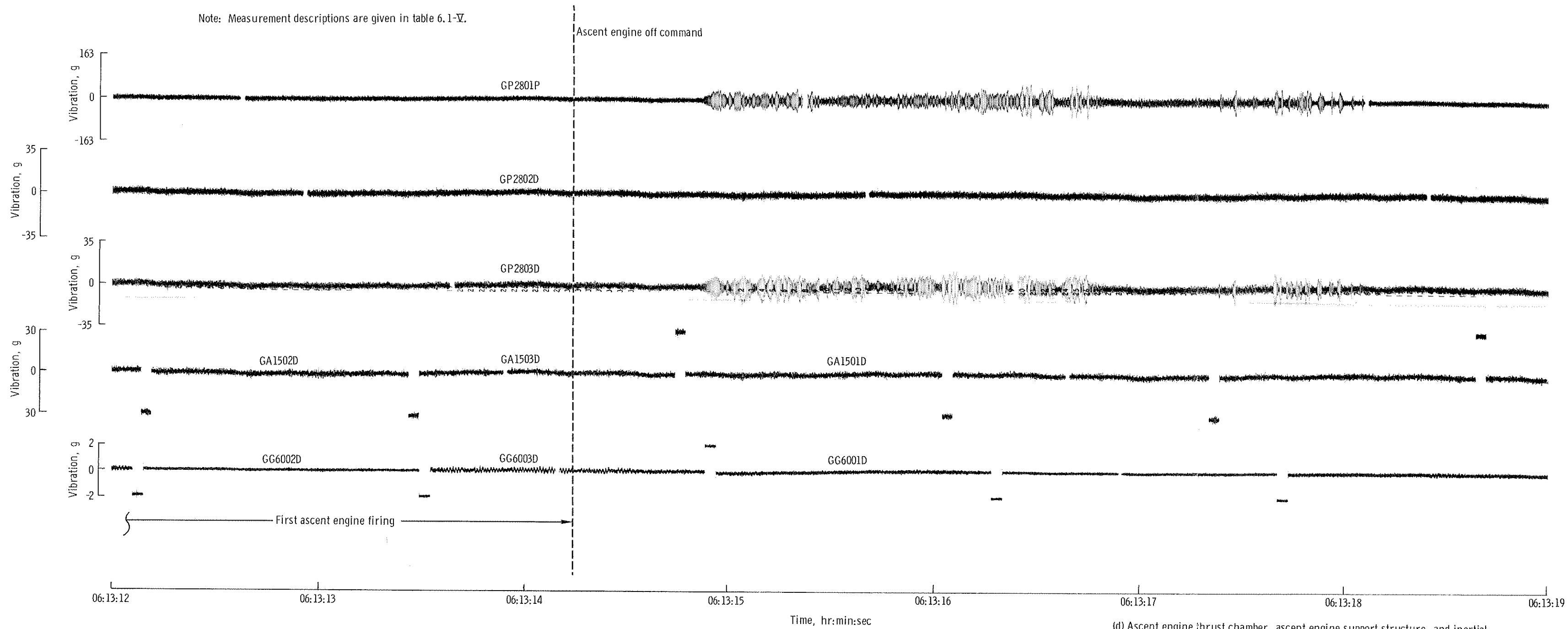
(b) Descent engine thrust chamber, ascent engine support structure, and inertial measurement unit during ignition and 10-percent throttle for third descent engine firing.

NASA-S-68- 1956



(c) Descent engine thrust chamber, ascent engine thrust chamber, ascent stage support structure, and inertial measurement unit during abort staging.

Figure 6.1-15. - Continued.



(d) Ascent engine thrust chamber, ascent engine support structure, and inertial measurement during shutdown of first ascent engine firing.

Figure 6.1-15. - Concluded.

6.2 THERMAL CONTROL

6.2.1 Launch Phase Thermal Response

Lunar module.- During the launch phase, all LM structural and thermal protection temperatures remained within 5° F of predicted values, based on 15 measurement locations for water and propellant tank temperatures and 47 locations for structural and thermal protection temperatures.

Adapter.- The thermal environment for the adapter during the boost phase was determined from the response of 12 thermocouples on the inner and outer skin of the adapter. The maximum recorded temperature was 185° F and occurred at 00:02:07 on the outer skin at longitudinal station X_A670, 7 degrees from the +Y axis. This peak temperature was considerably less than the design limit of 490° F.

No correlation was made between flight data and the analytical predictions for the adapter temperatures because the aerodynamic configuration was unique for this mission and because the temperature levels were well below design limits.

6.2.2 Control Engine Plume Impingement

The effect of the control engine plumes impinging the descent stage thermal protection during thrusting of down-firing engines was determined by the temperature sensors located as shown in figures 6.2-1 and 6.2-2. The predicted temperatures were higher than the actual temperatures during withdrawal of the lunar module from the adapter (fig. 6.2-3). This was attributed to the following conditions:

- a. The thermal mass of the sensor was not considered in the predictions.
- b. The predictions were based on a solar soak prior to plume impingement; this primarily affected internal temperatures.
- c. Sensor GB3023T (fig. 6.2-1) was covered by two layers of foil, and sensor GB3027T was covered by a layer of Kapton.

Tests were made to determine the effect of the thermocouple mass. The results showed that the effective Inconel skin thickness for the thermocouple was 5.5 mil. Temperature measurements from sensor GB3033T, which was attached to a 1.25-mil Inconel sheet, were compared with the postflight analysis data (fig. 6.2-3(a)), using the 5.5-mil effective

thickness, for the LM/S-IVB stage separation. The correlation is very good. Sensor GB3031T, also attached to Inconel foil, showed good correlation with postflight data (fig. 6.2-3(b)) during the LM/S-IVB stage separation.

Sensor GB3023T was covered by foil (fig. 6.2-1). Figure 6.2-3(c) compares the flight data with post-test analyses. One further assumption was made in this analysis. It was assumed that exhaust gases pressurized the space between the foil layers which covered the sensor. A pressure of 0.015 psi, equivalent to that behind the plume shock off the ascent stage tank bay, was assumed. The differences between the data and the analysis were within the accuracy of the instrumentation. Internal sensors, such as GB3021T and GB3022T, were not affected to the extent the surface sensors were, because they were located beneath insulation (figs. 6.2-1 and 6.2-2) and experienced slower heating rates.

Internal sensor GB3029T (fig. 6.2-3(d)) recorded approximately the same temperature response as outboard sensor GB3027T. This is not reasonable because the internal sensor was covered by an additional eight layers of Kapton.

The maximum temperatures recorded during +X translations for the second and third descent stage firings and during abort staging were as follows:

Sensor number	Maximum temperature, ° F	Time, hr:min:sec
GB3033	830	06:11:57
GB3023	630	06:10:54
GB3031	230	06:10:55
GB3025	85	06:12:00
GB3021	40	06:12:12

6.2.3 Descent Stage Heat Shield

The thermal measurement locations on the descent stage heat shield are shown in figure 6.2-4. The first descent engine firing was of insufficient duration and thrust level to affect the heat shield. The second descent engine firing resulted in nominal temperature rises of 40° F on the heat shield surface. Measurements located beneath the

insulation blanket showed no soak-back effects on the titanium structure. The data acquisition time for the third descent engine firing was insufficient to determine effects on the base heat shield. The descent engine cavity temperatures remained at a nominal 72° F until the measurement lines were severed at abort staging.

6.2.4 Abort Staging

Temperature data for the abort staging sequence were reviewed for the following areas: the descent stage blast deflector and top surface, and the ascent stage heat shield, ascent engine compartment, and cabin cover.

Blast deflector temperature measurements at the locations shown in figure 6.2-5 were lost at the time of the ascent engine firing. These temperatures remained at a nominal 70° F during the orbital portion of the mission. A temperature rise of 680° F was predicted for the 3.7-second separation period after engine firing, but no data were received. During the ground tests of ascent propulsion test article 1 (PA-1), the measurements at comparable locations were also lost.

Descent stage top surface sensors were located as shown in figure 6.2-5. All temperatures remained in the range of 60° F to 70° F throughout the mission until abort staging occurred. The temperature measured by GB0401T, located on the +Z deck, increased from 75° F to 200° F in 0.1 second at staging. The temperature then dropped to 140° F in 0.1 second. The temperature measured by GB0402T rose from 60° F to 110° F in 0.1 second. The temperature measured by GB0403T remained at 68° F throughout this period. These three sensors were attached to the outboard face of the tank bay upper aluminum decks facing the fiberglass cover. The fast temperature response recorded by sensors GB0401T and GB0402T was indicative of ascent engine exhaust gas impingement on the sensors which indicated a break in the fiberglass shield. The recorded temperatures are shown in figure 6.2-6.

Ascent stage heat shield thermocouples GB0302T, GB0303T, GB0304T, and GB0305T were lost at the time of engine firing. No instrumentation losses, such as those on the blast deflector, were experienced on the ascent stage during ground tests. Measurements GB0301T, GB0306T, and GB0307T continued to function and showed no response to ascent engine firing. The measurements were located on the inner face of the heat shield, which was covered with an insulation blanket (fig. 6.2-7) and were not expected to show any response. Temperature measurement GA1113T, located on the outer surface of the heat shield structure but beneath the insulation blanket, remained at a nominal 69° F. A rise in temperature would have indicated an insulation blanket failure.

Preflight predictions, made on a nominal 5-second engine firing, indicated that the ascent engine cover temperature would rise 10° F. The actual firing was 60 seconds and resulted in a rise from 57.5° F to 75° F on cover measurement GB0201T (fig. 6.2-8).

Ascent engine compartment temperatures GB0601T, GB0602T, and GB0603T (fig. 6.2-7) were affected by engine nozzle backface temperature, which reached 150° F. The measurements were located under an insulation blanket on H-film and Mylar and showed no response to the abort staging. Predictions, which assumed gaseous flow, showed a rise of 10° F for a 5-second firing; consequently, it is concluded that the backflow of hot gases did not occur.

6.2.5 Ascent Stage Structure

Ascent stage structural temperatures were obtained from three measurements (GB0203T, GB0204T, and GB0205T) located on the cabin floor and walls. Sensor GB0203T, located on the cabin floor, decreased 3° F during the 3-hour attitude hold and remained at a nominal 54° F until abort staging. The temperature then rose in a similar manner as the ascent engine cover measurement GB0201T, and reached 71° F at the time of the second ascent engine firing (fig. 6.2-8). The close thermal conduction relationship between the cover and cabin floor contributed to the similar responses. Measurements GB0204T and GB0205T, located on the cabin wall, decreased 14.5° F and 5° F, respectively, during the attitude hold (fig. 6.2-9). Although located on the walls, these measurements are close to the cabin roof and docking tunnel and are not considered indicative of total cabin wall temperatures. During the 3-hour attitude hold, the docking tunnel experienced a cold environment which, through conduction, influenced these sensors.

Ascent stage fuel and oxidizer tank measurements, GP0718T and GP1218T, varied only 3° F during the mission. These data are within 3° F of the preflight predictions.

Ascent stage helium tank temperature measurements, GP0201T and GP0202T, remained within 8° F of preflight predictions until the first ascent engine firing. A temperature drop of 28° F for sensor GP0201T and a drop of 18° F for sensor GP0202T were caused by helium gas expansion resulting from pressurization of the propellant tanks with the helium gas (fig. 6.2-10). The temperature then rose to 51° F prior to the second ascent engine firing. Measurements GP0201T and GP0202T dropped to -98° F and -90° F, respectively, again because of helium expansion, as was expected for the ascent engine firing to propellant depletion.

The reaction control system propellant tank temperature measurements GR2121T and GR2122T remained at a nominal 66° F throughout orbital flight. Reaction control system helium tank temperatures, GR1089T and GR1099T, remained at 60° F until the time of the second descent engine firing. At this time, these measurements dropped 20° F and 30° F, because of helium expansion.

Descent stage fuel tank temperature measurements, GQ3718T and GQ3719T, remained at 70° and 73° F, respectively. Oxidizer tank temperatures GQ4218T and GQ4219T remained at 71° F throughout the orbital flight.

Sensors GB3727T, GB3728T, and GB3729T were located on the S-band steerable antenna, and sensor GB3733T measured the VHF inflight antenna temperature. Figure 6.2-11 shows the cyclic data for measurements GB3728T and GB3729T. Minimum temperatures at the end of the 3-hour attitude hold were in the -28° to -35° F range. The cyclic variations (fig 6.2-11) were expected because of the environmental cycling during orbit. There was no evidence of control engine plume impingement.

The VHF inflight antenna temperature measurement GB3733T, received solar heating during the 3-hour attitude hold. The orbital temperature cycling is clearly shown in figure 6.2-12. There was no evidence of plume impingement indicated.

6.2.6 Second Ascent Engine Firing

Data were lost about 8 minutes after initiation of the second ascent engine firing. This did not allow sufficient time to assess engine firing effects on the ascent stage heat shield, engine compartment, or cover.

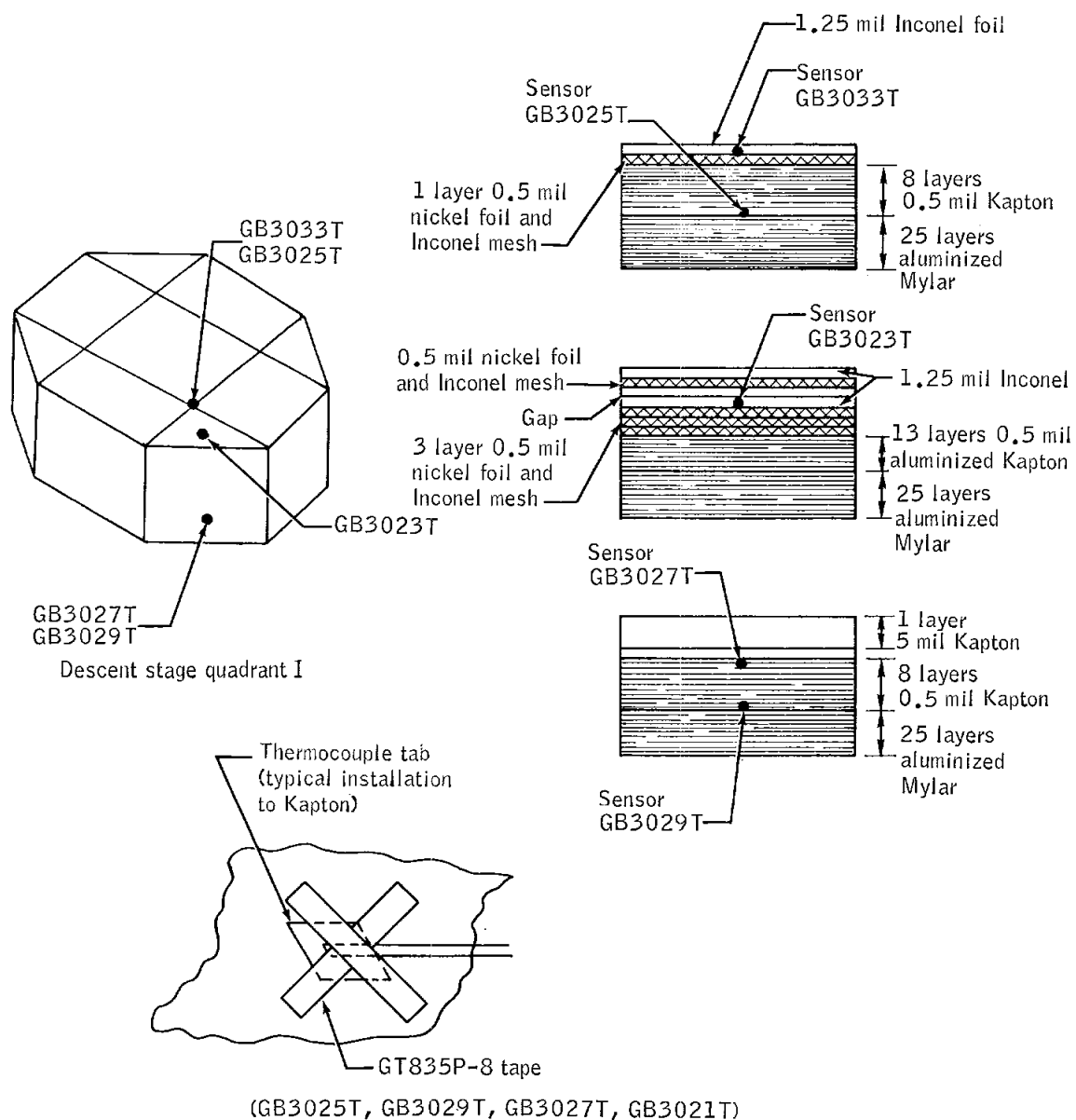
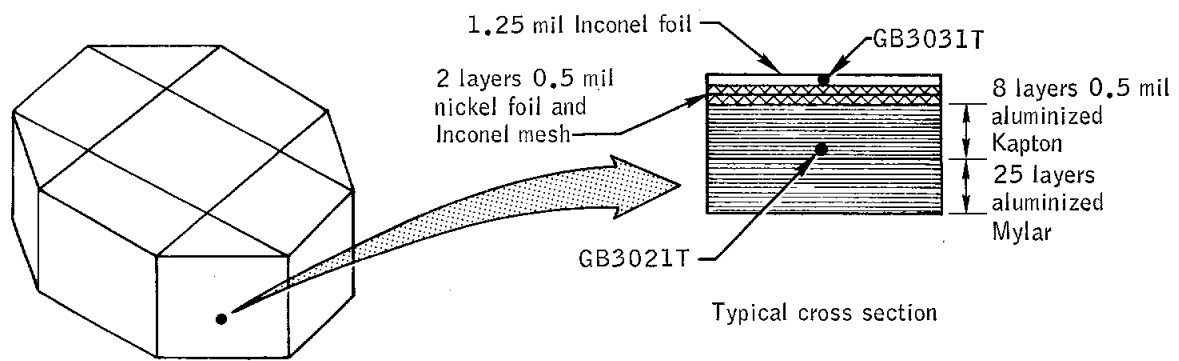


Figure 6.2-1.- Descent stage quadrant I control engine plume impingement sensor locations and configuration.

NASA-S-68-1959



Descent stage quadrant III

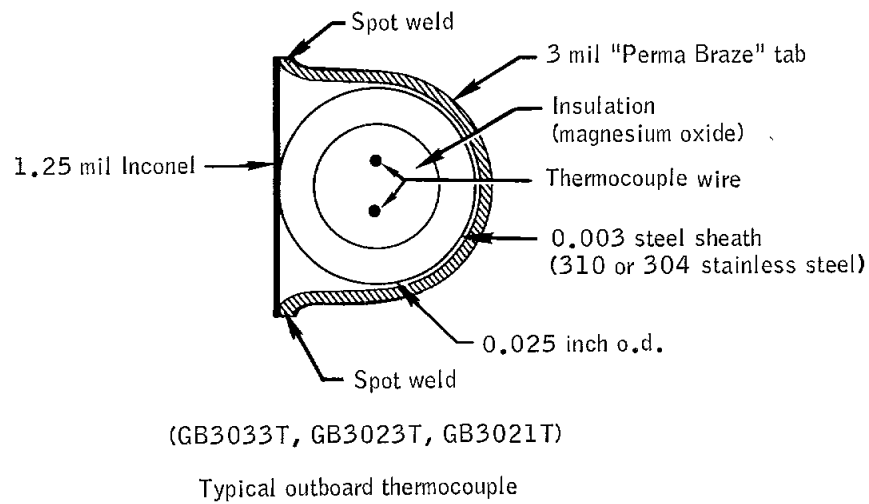
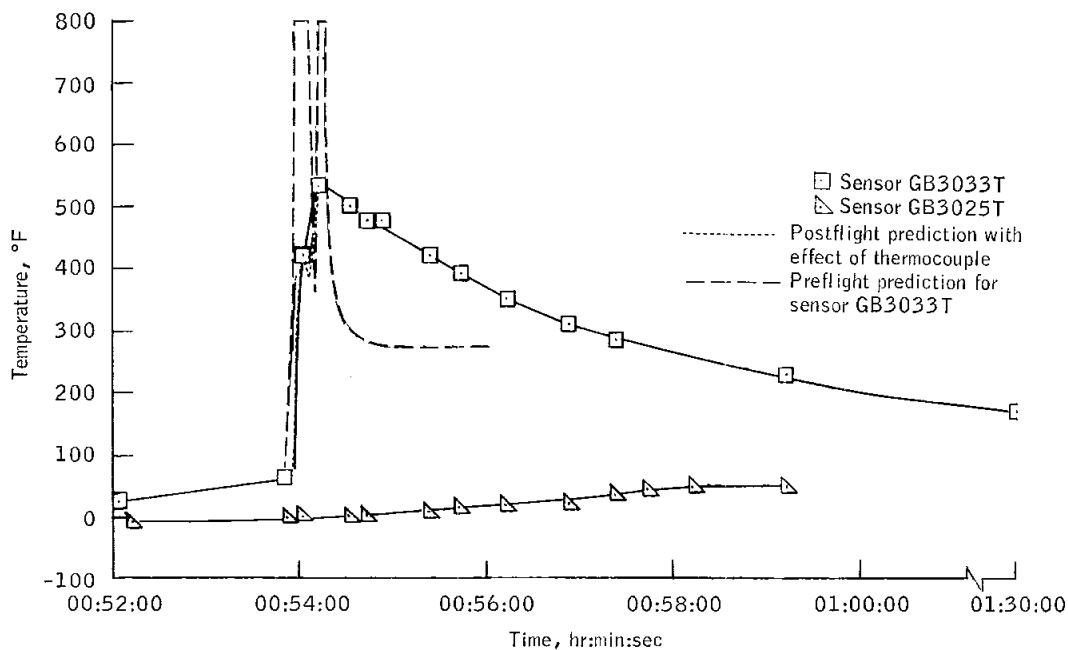
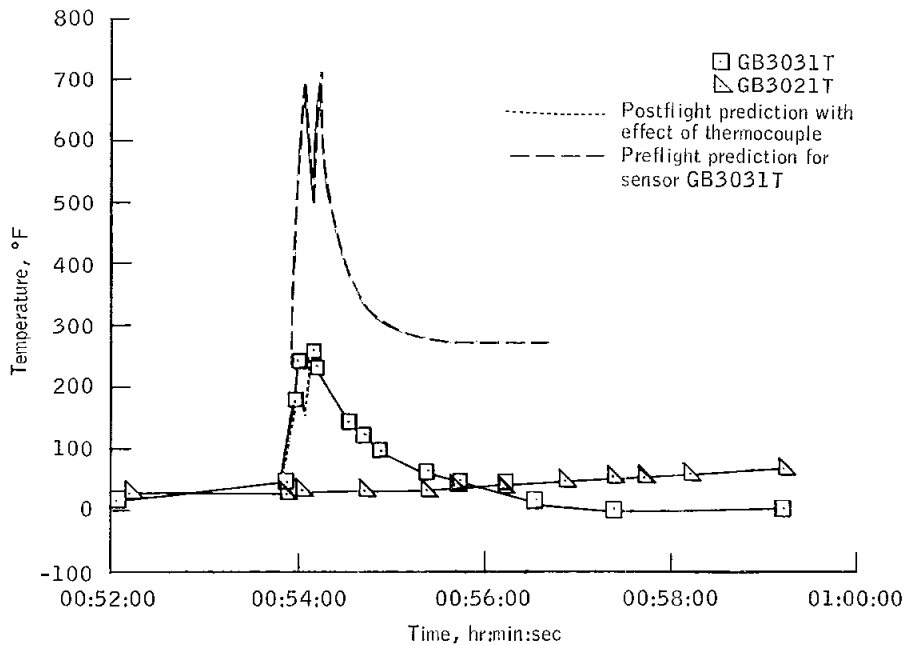


Figure 6.2-2.- Descent stage quadrant III control engine plume impingement sensor locations and installation.

NASA-S-68-1960

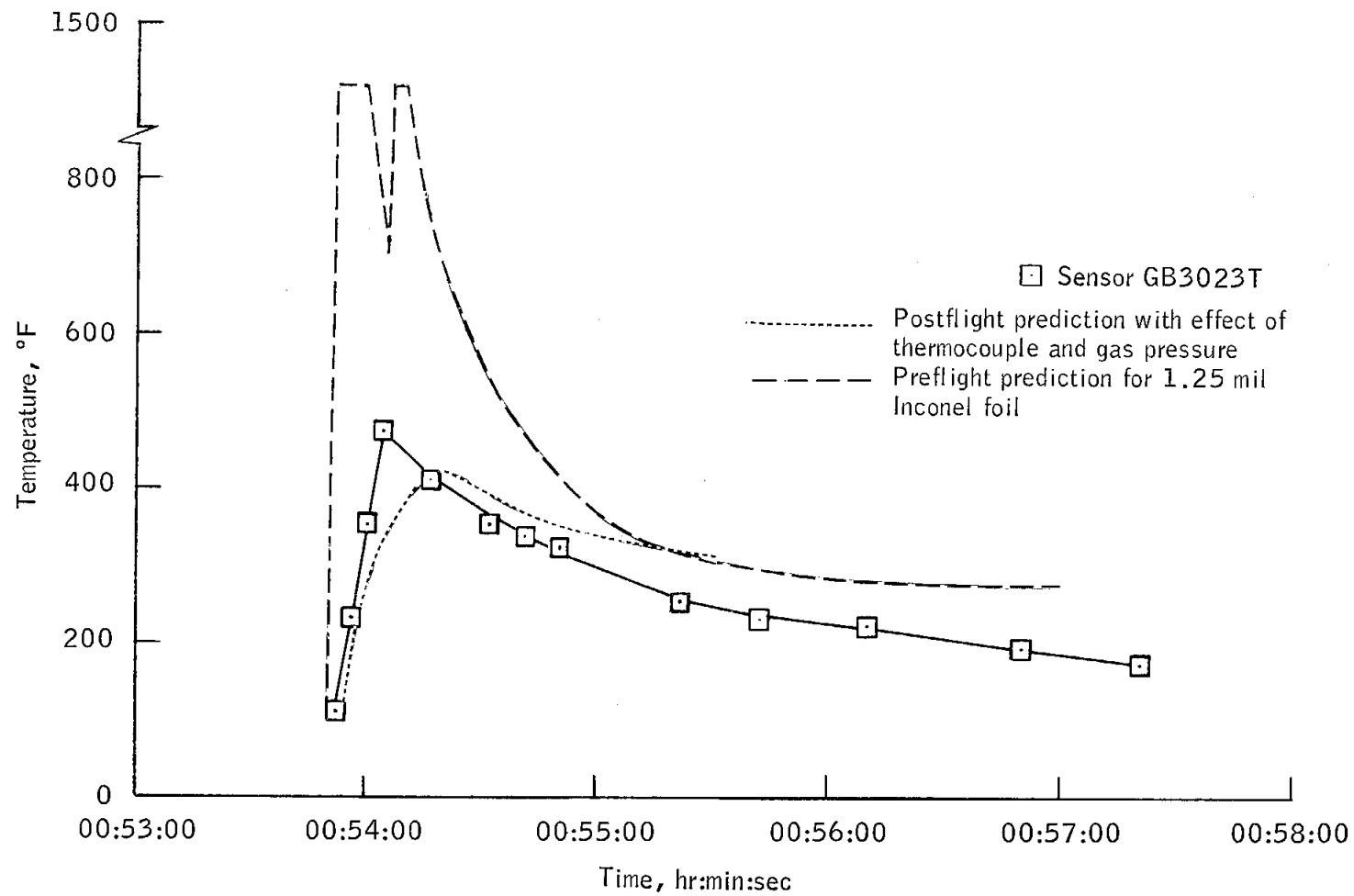


(a) Sensors GB3033T and GB3025T.



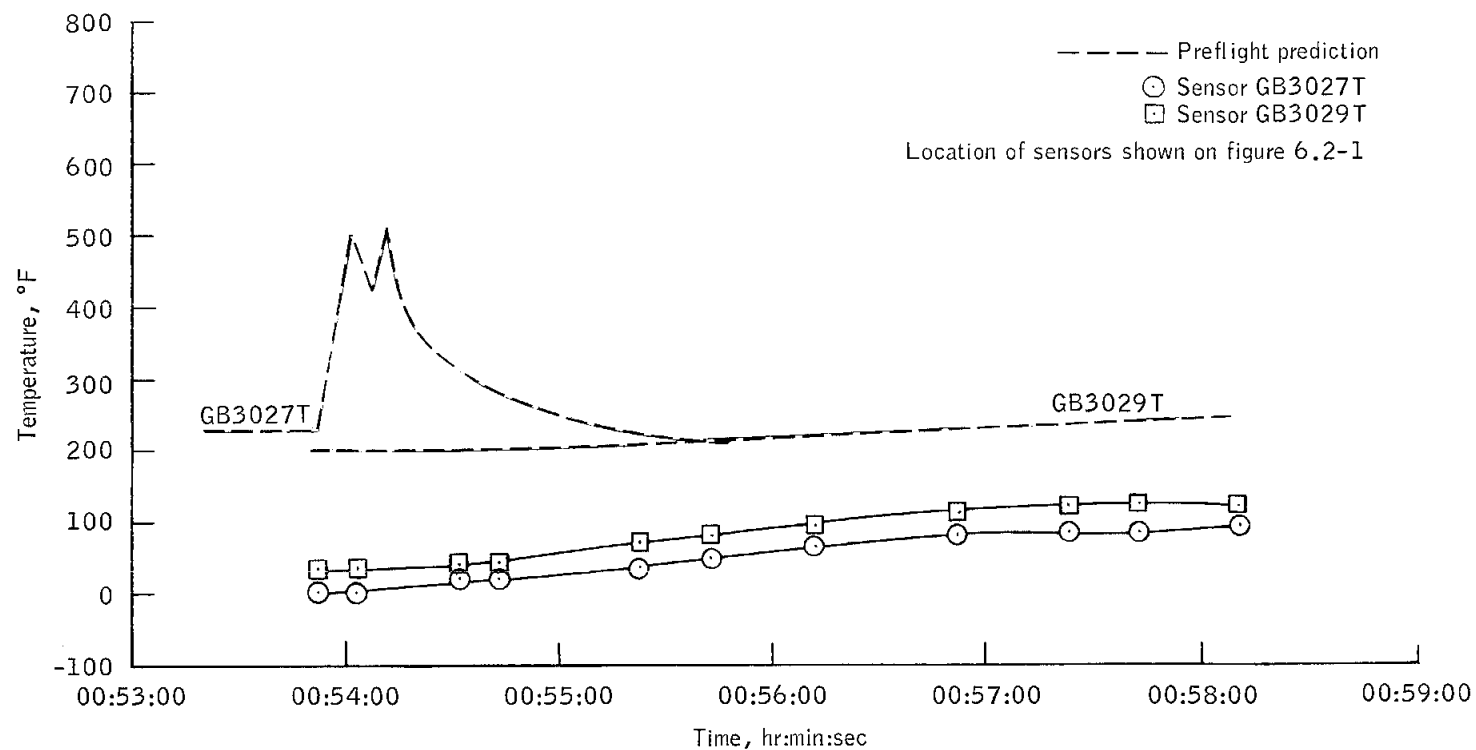
(b) Sensors GB3031T and GB3021T.

Figure 6.2-3.- Descent stage insulation blanket temperatures during LM/S-IVB stage separation.



(c) Sensor GB3023T.

Figure 6.2-3.- Continued.



(d) Sensors GB3027T and GB3029T.

Figure 6.2-3.- Concluded.

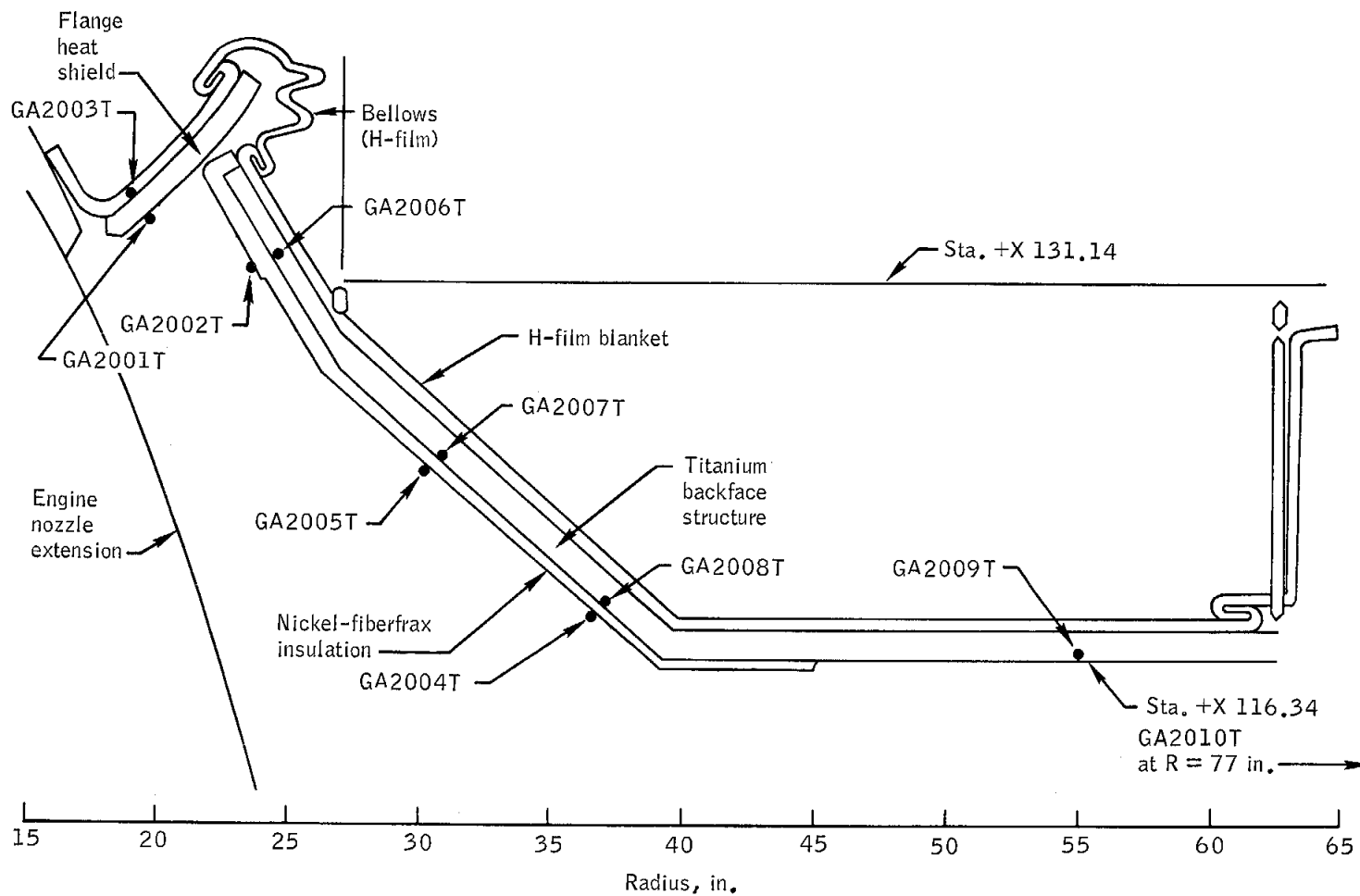


Figure 6.2-4.- Descent stage base heat shield sensor locations.

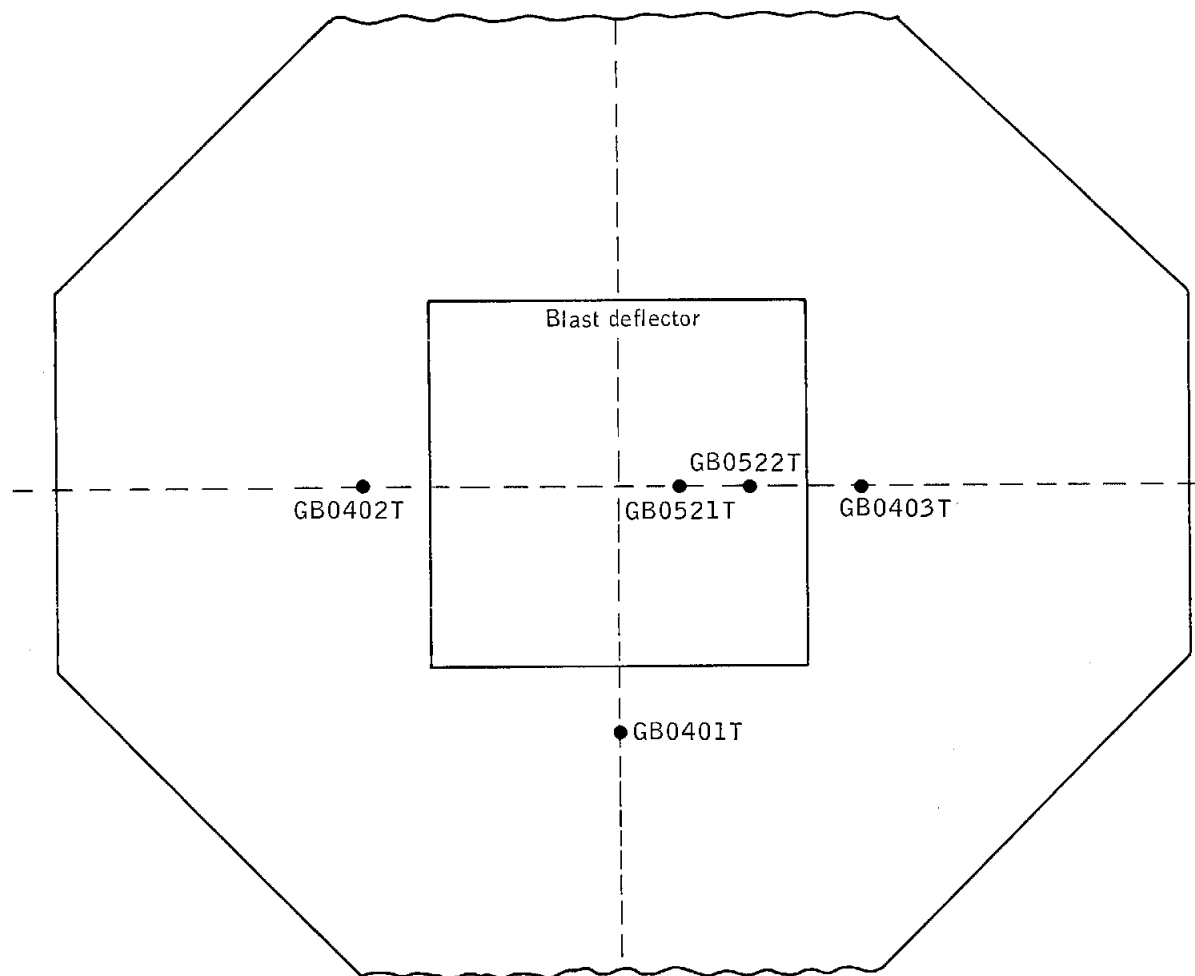


Figure 6.2-5.- Descent stage upper surface temperature instrumentation.

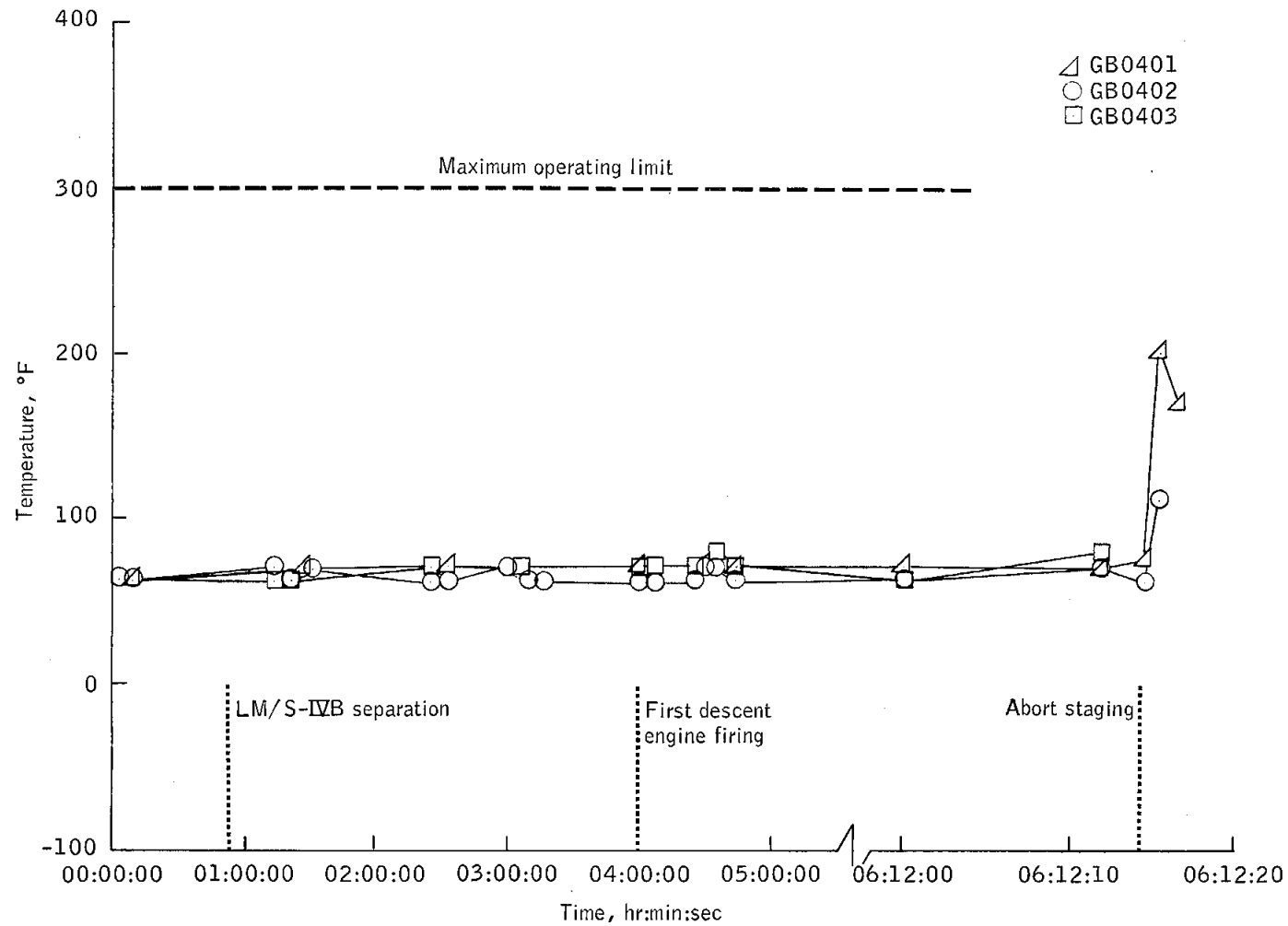


Figure 6.2-6.- Temperature measured on upper surface of descent stage.

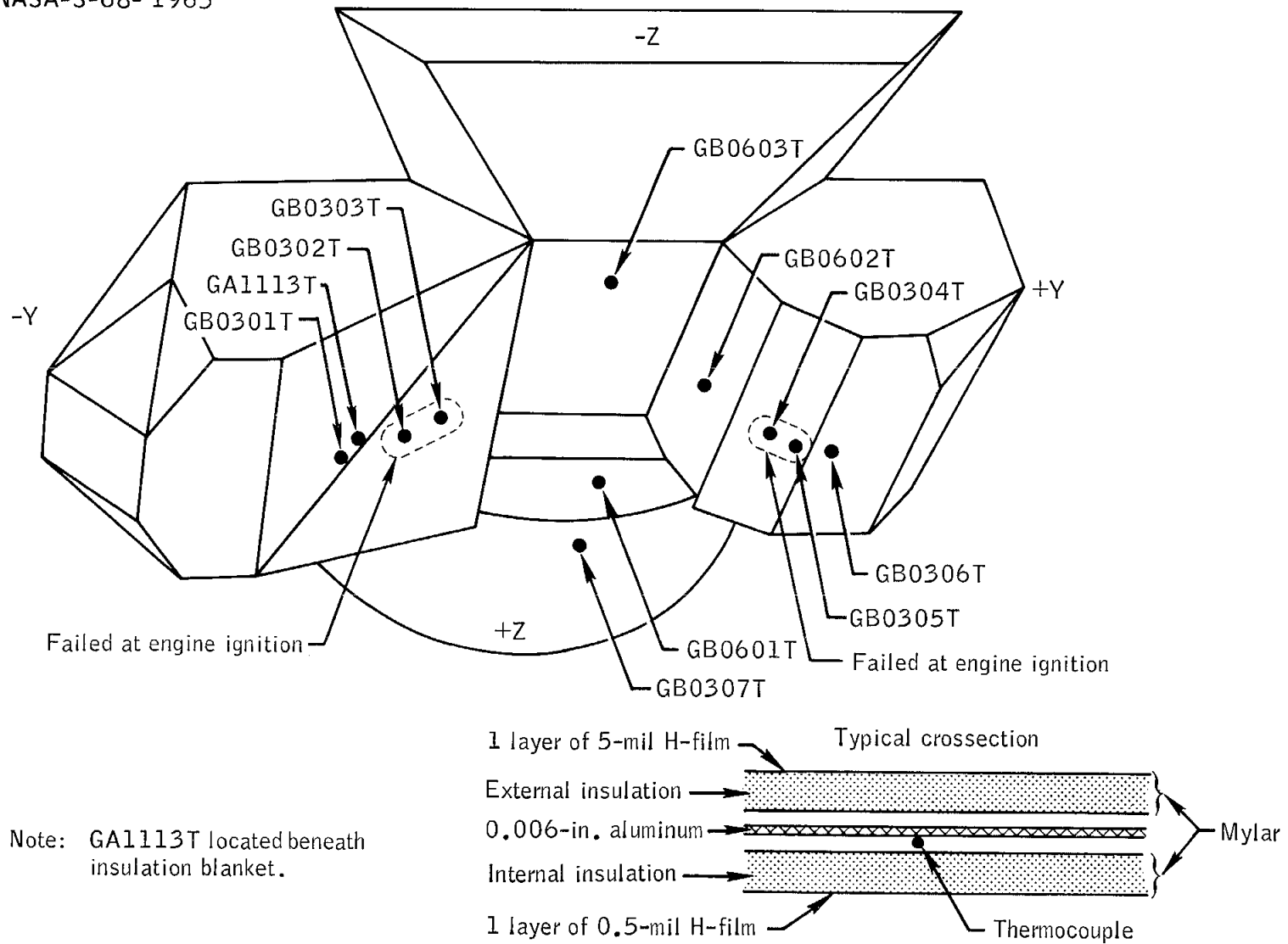


Figure 6.2-7.- Ascent stage heat shield sensor locations.

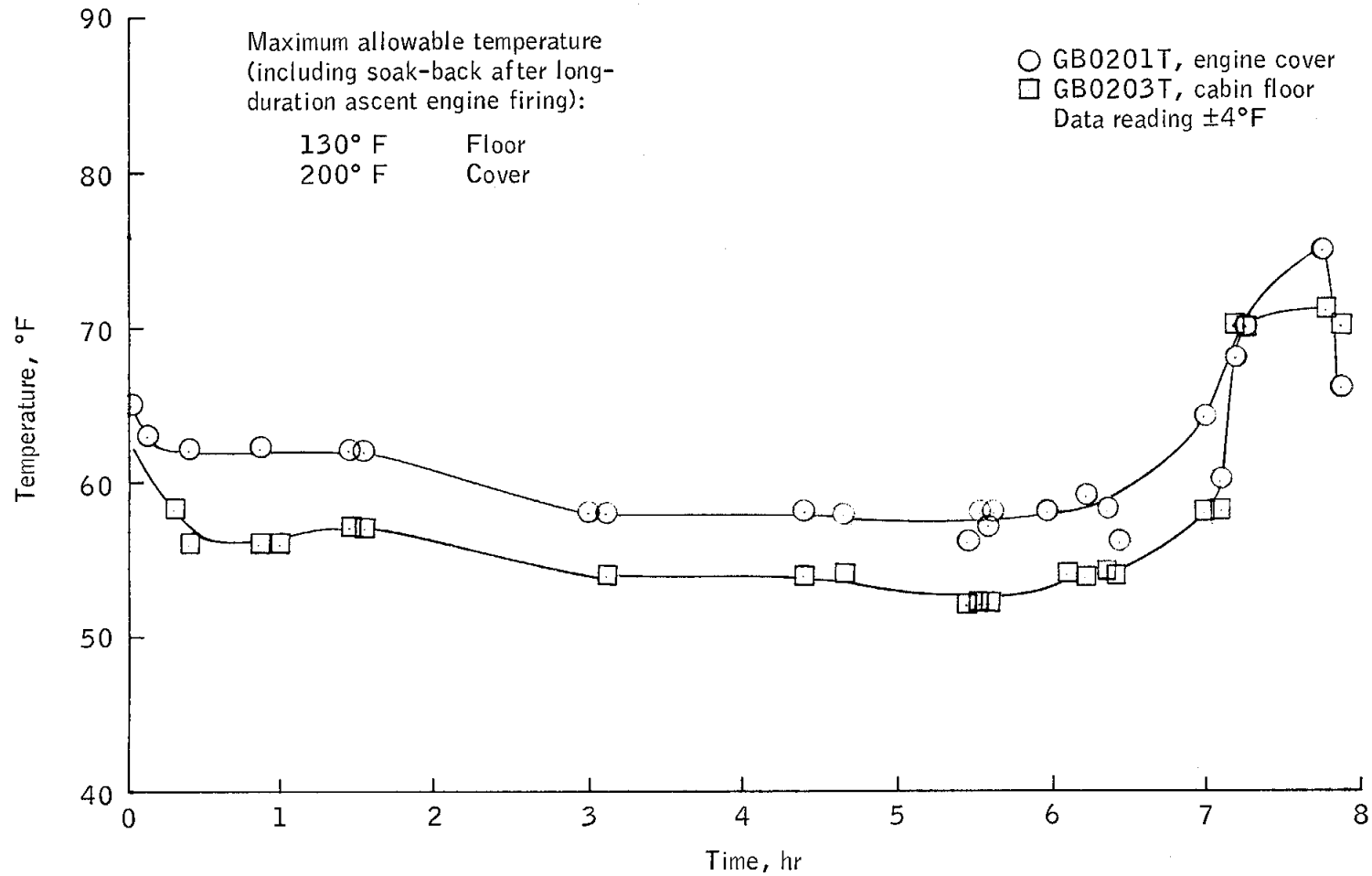


Figure 6.2-8.- Cabin floor and ascent engine cover temperatures.

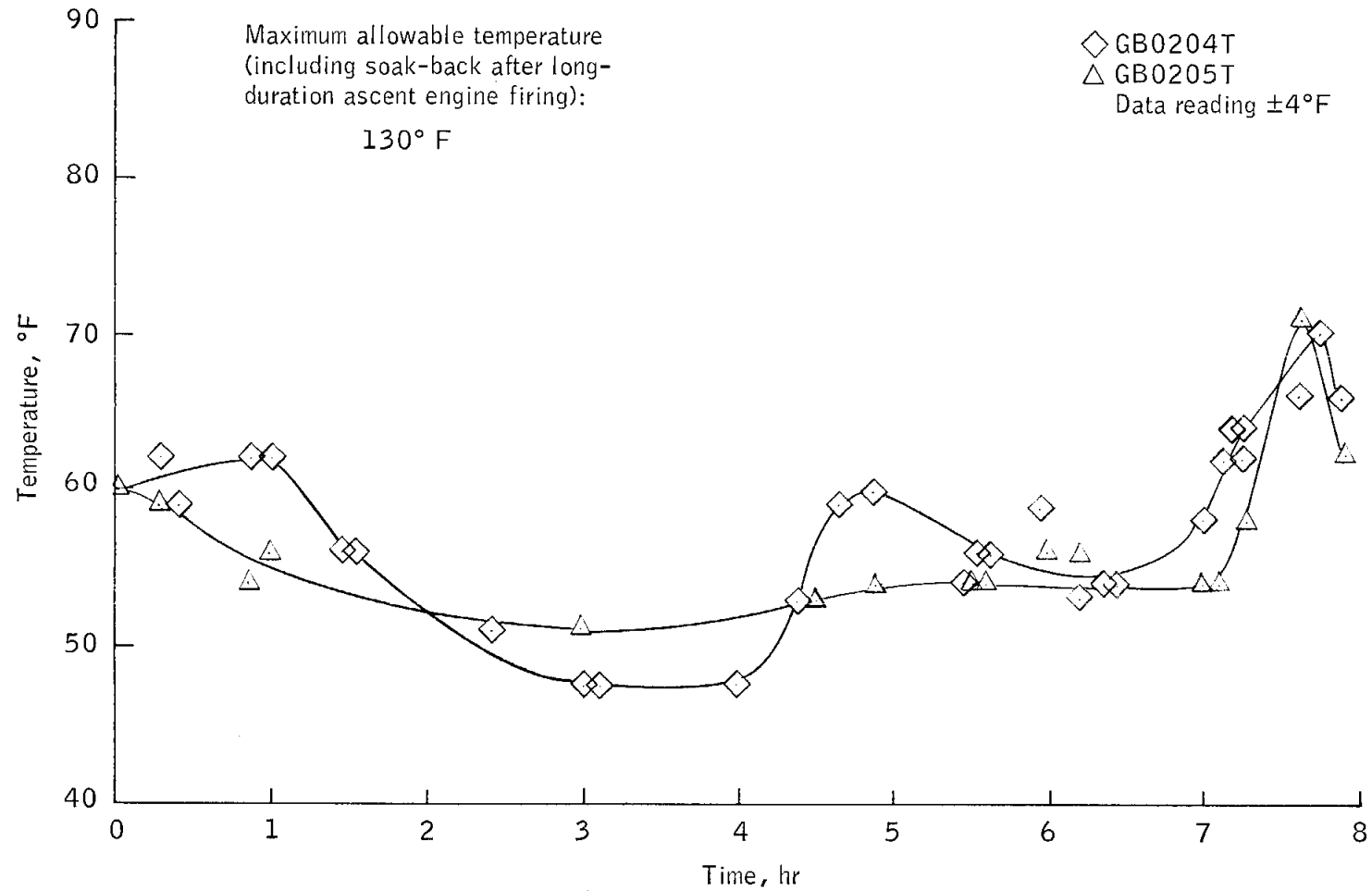


Figure 6.2-9.- Cabin wall temperatures.

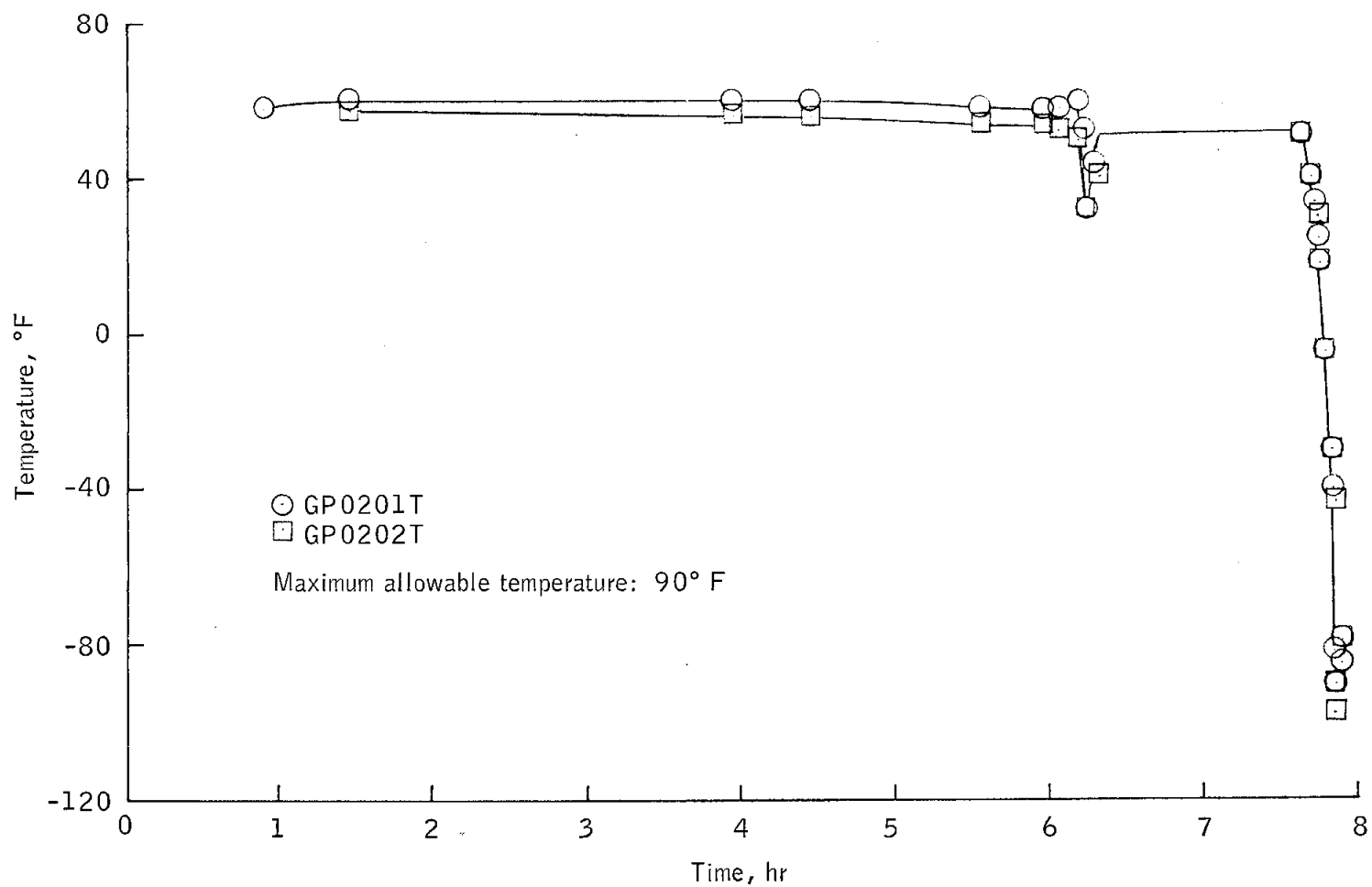


Figure 6.2-10.- Ascent stage helium tank temperatures.

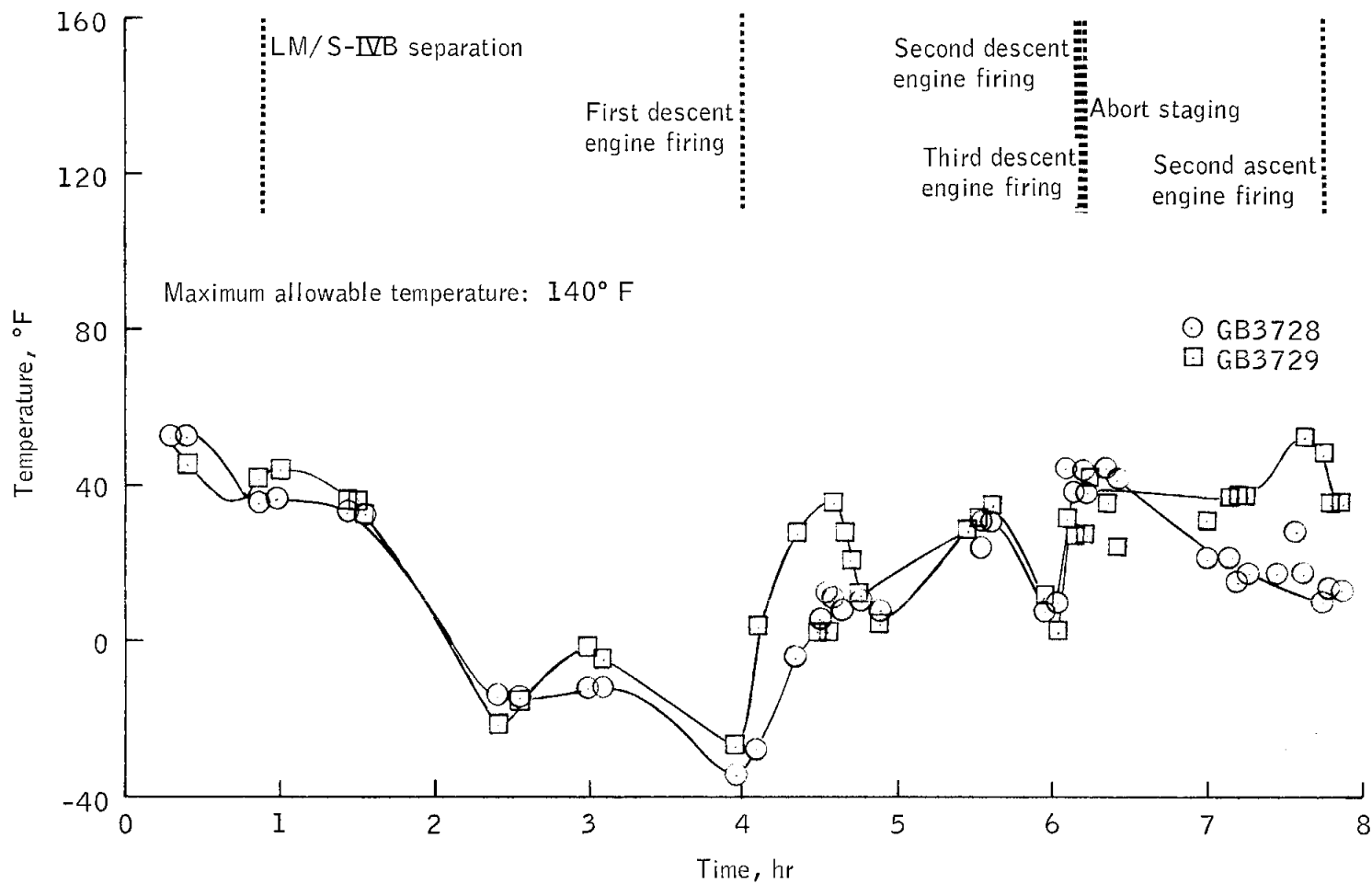


Figure 6.2-11.- Temperature of steerable S-band antenna.

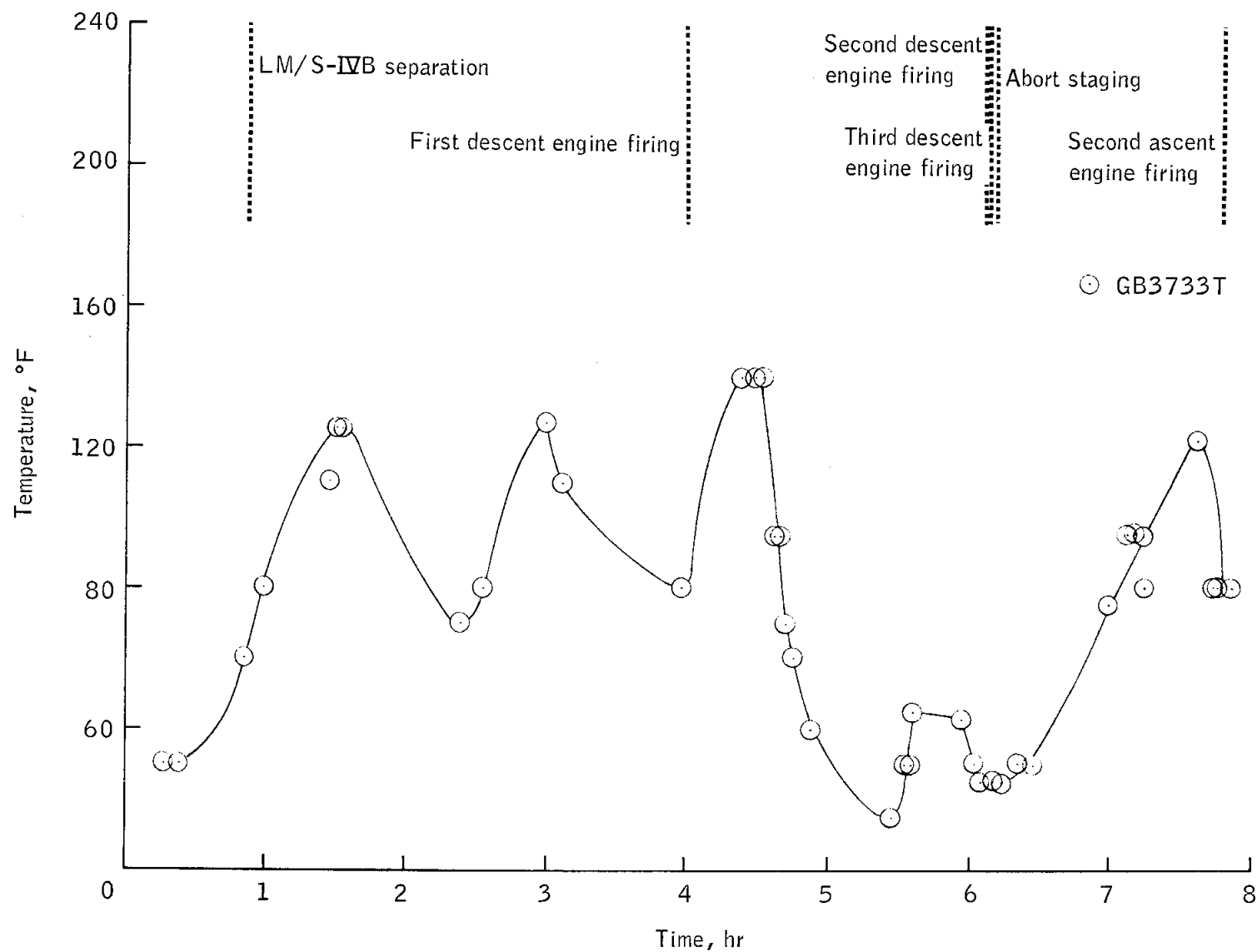


Figure 6.2-12.- Temperature of VHF inflight antenna.

6.3 LANDING GEAR

(This section is not applicable.)

6.4 PYROTECHNIC

There was no indication of malfunction of any pyrotechnic devices.
(See section 13.2 for locations of pyrotechnic devices.)

6.5 ELECTRICAL POWER

The characteristics of the dc and ac power were within expected limits throughout the mission. The dc and ac bus voltages and the total current during the mission are shown in figure 6.5-1. During the second ascent engine firing, the high control engine activity increased the total current to 87 amperes, decreasing the bus voltages to 28.8 volts.

The ac voltage remained between 117.6 and 118.1 volts at 400 Hz for a no-load condition. The ac voltage transients shown on figure 6.5-2 were associated with the inverter response to the load variations of the descent engine gimbal motor, the only load on the ac bus. These transient rms voltages corresponded to peak values of 145 to 188 volts and were within the specified peak transient limits of 90 to 225 volts.

Figure 6.5-3 shows the battery load sharing during mission programmer sequence III. One of the two ascent batteries was commanded "on" prior to abort staging, at which time this battery shared approximately 40 percent of the total load with the descent stage batteries. The ascent batteries were cooled to approximately 38° F before abort staging; the predicted temperature was 40° F. After abort staging, the ascent battery temperatures rose to approximately 49° F, as expected. The descent battery temperatures were controlled within a range of 55° F to 60° F by the coolant system as expected.

NASA-S-68-1966

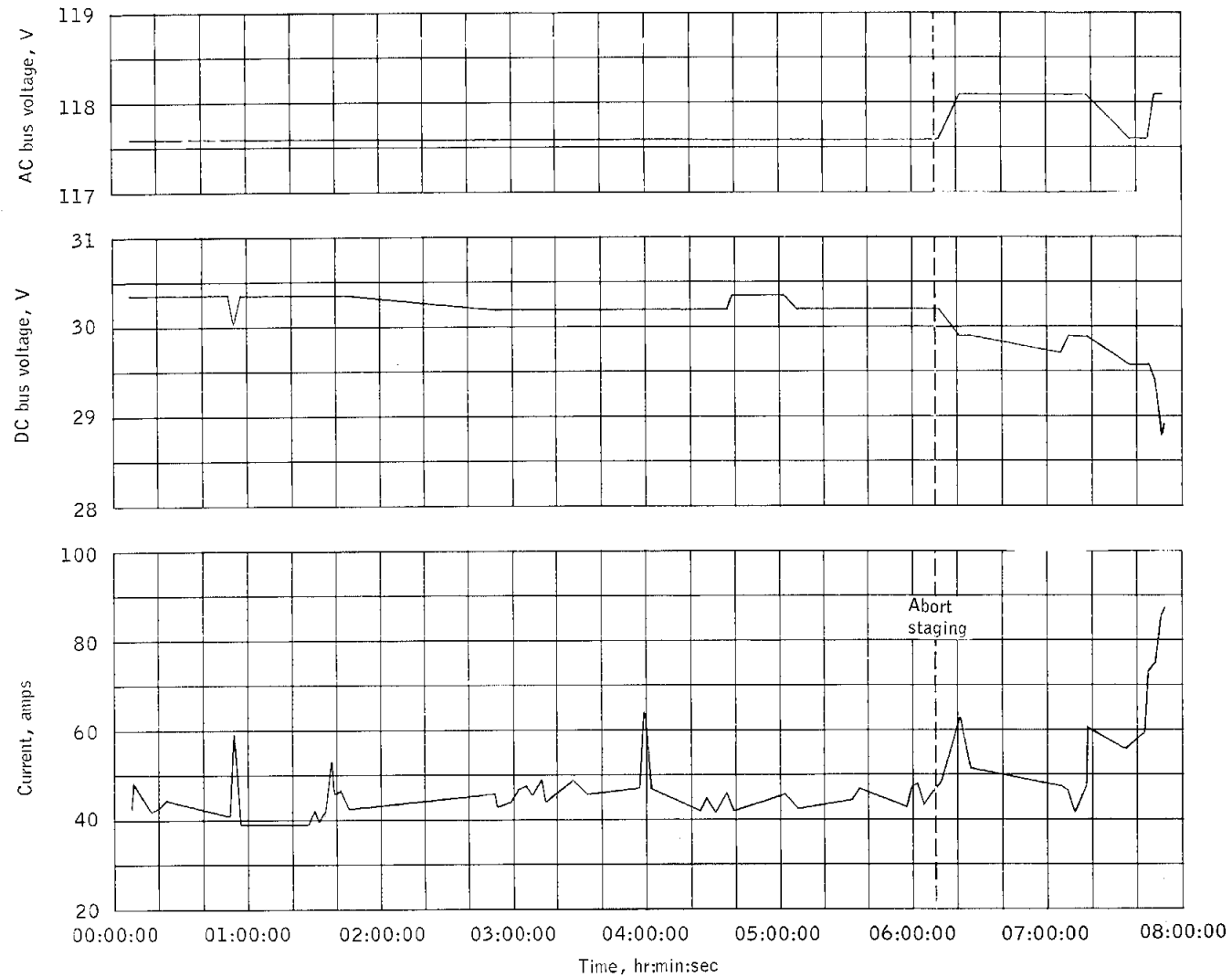


Figure 6.5-1.- Electrical power characteristics.

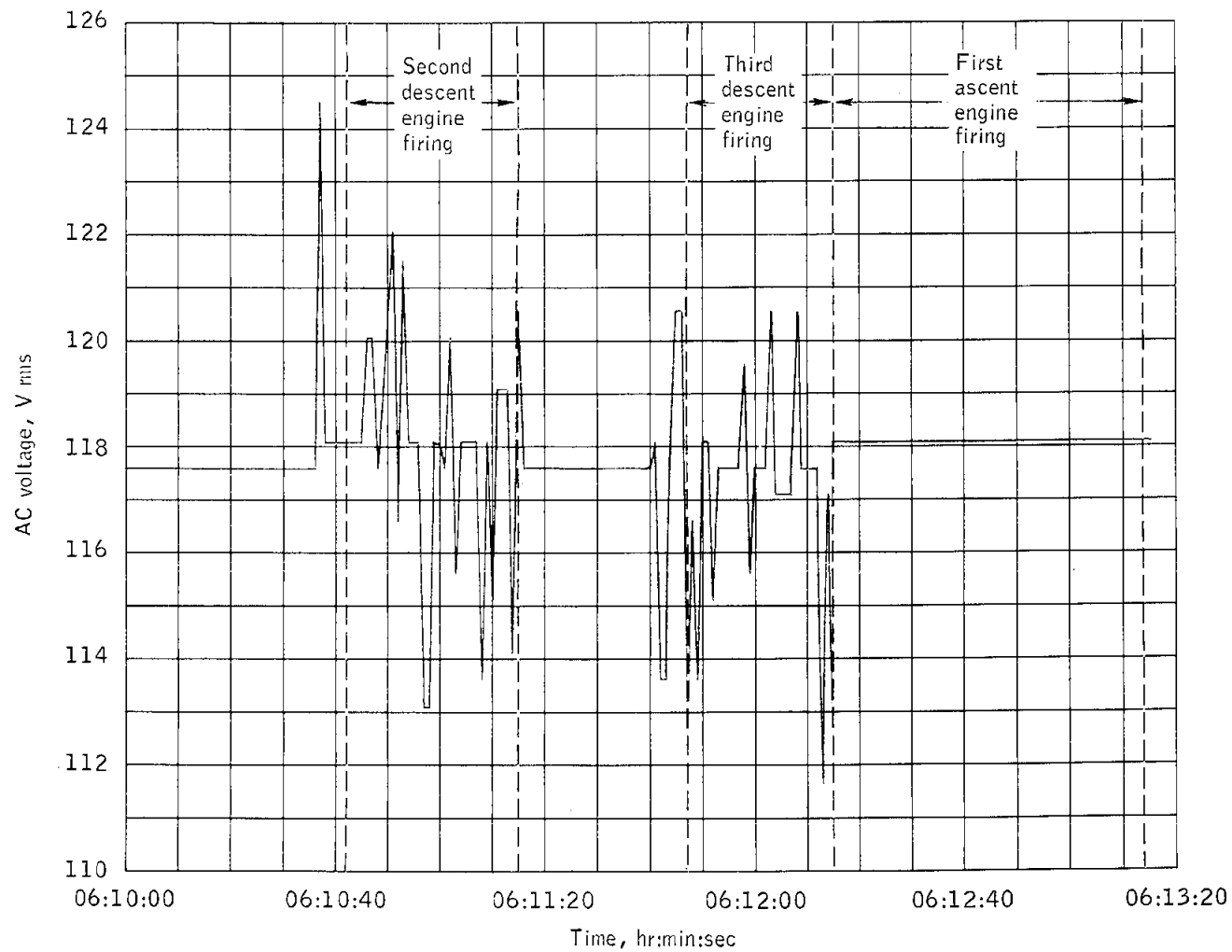


Figure 6.5-2.- AC voltage transients.

NASA-S-68-2100

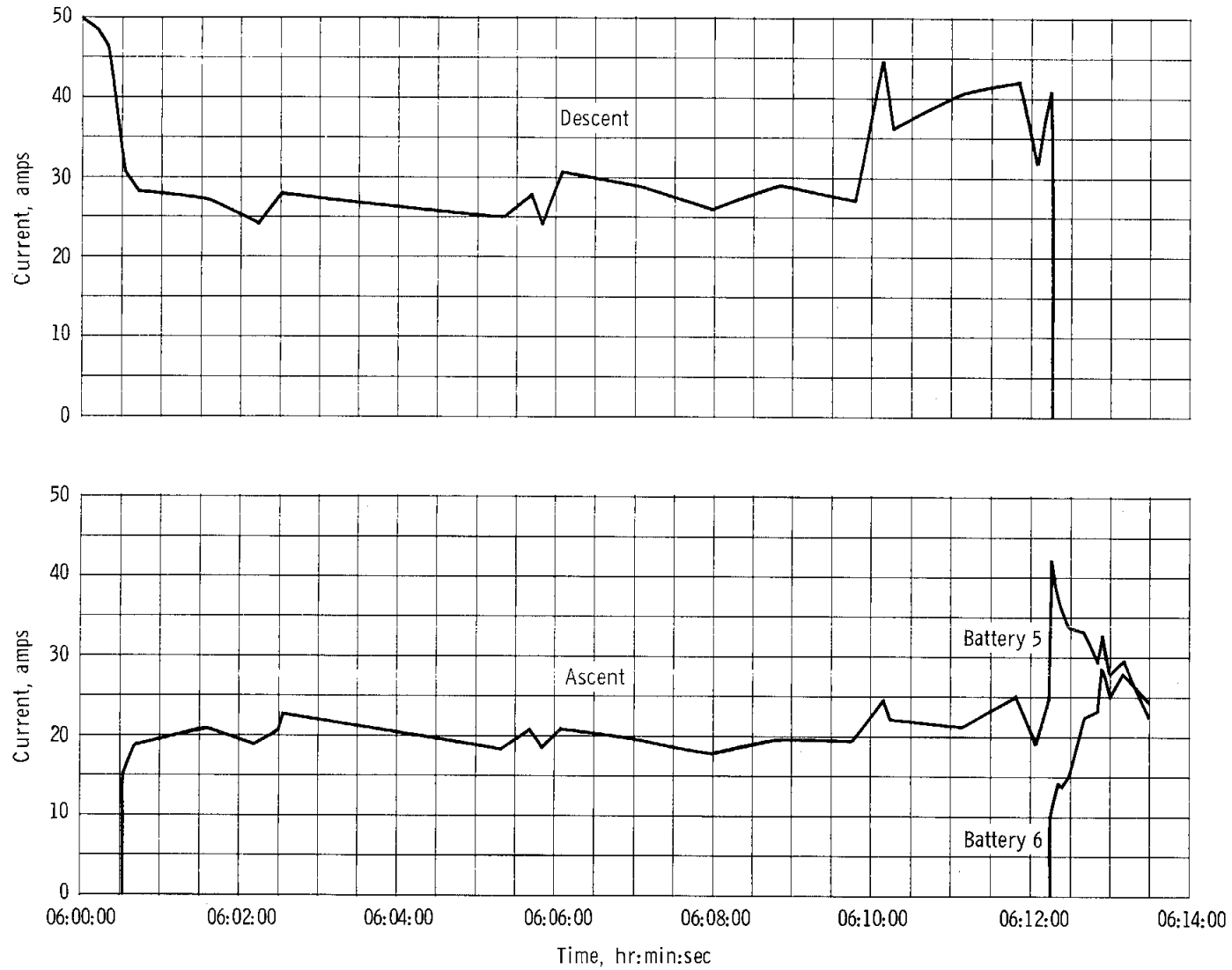


Figure 6.5-3. - Battery load sharing during mission programmer sequence III.

6.6 MISSION PROGRAMMER

The mission programmer performed all required functions throughout the mission. From lift-off until 06:10:00, the mission programmer was operated in the primary mode with the guidance computer in control. At 06:10:00, the backup mode was activated in which the mission programmer controlled all sequencing. Sequences III and V were utilized (tables 6.6-I and 6.6-II). Periodically through the mission, the ground command capability was utilized, and except for the periods of abnormal signal strength, performance was nominal (see section 6.8).

TABLE 6.6-I.- MISSION PROGRAMMER SEQUENCE III

Sequence elapsed time, min:sec	Functions	Function description	Remarks
00:00	Sequence start by ground command (programmer start); primary S-band on		Approximately 06:10:00
00:01	Master arm on	Pressurizes reaction control tanks if not already accomplished	Reaction control tanks were pressurized prior to this sequence
	Reaction control propellant valves open		
00:03	Reaction control pressurization valves open		
00:05	+X translation on		
00:10	Lunar module/adaptor separation arm Lunar module/adaptor separation fire		
00:15	+X translation off	Separates lunar module from the adaptor if not already accomplished	Lunar module was separated from the adaptor prior to this sequence
00:20	+X translation on		
00:21	Descent propellant quantity gage arm		
00:22	Descent propellant quantity gage on		
00:23	Descent engine arm		
00:25	+X translation off		
00:31	+X translation on		
	Manual throttle to 10 percent		
00:39	Descent engine start	First descent engine firing	Second descent engine firing accomplished by this sequence
00:44	+X translation off		
01:05	Manual throttle to 100 percent		
01:12	Descent engine shutdown		
01:14	Manual throttle to 30 percent		
01:35	Descent engine arm		
01:36	+X translation on		Accomplished by this sequence
	Manual throttle to 10 percent		

TABLE 6.6-I.- MISSION PROGRAMMER SEQUENCE III - Concluded

Sequence elapsed time, min:sec	Functions	Function description	Remarks
01:44	Descent engine start	Second descent engine firing	Third descent engine firing accomplished by this sequence
01:49	+X translation off		
02:10	Manual throttle to 100 percent		
02:11	Abort stage arm		
02:12	Abort stage fire	Abort staging and first ascent engine	Abort staging and first ascent engine firing accomplished by this sequence
SEQUENCE STOPPED AT THIS POINT BY GROUND COMMAND (ABORT GUIDANCE SELECT)			

TABLE 6.6-II.- MISSION PROGRAMMER SEQUENCE V

Sequence elapsed time, min:sec	Functions	Function description	Remarks
00:00	Sequence start by ground command (programmer start) Master arm on		Approximately 07:43:58
00:02	+X translation on		Accomplished by this sequence
00:07	Abort stage arm		
00:14	Abort stage fire Ascent engine arm Ascent engine start	First ascent engine firing	Second ascent engine firing accomplished by this sequence
00:19	+X translation off		
01:13	+X translation on		
01:14	Ascent engine shutdown		
01:24	Ascent engine start	Second ascent engine firing	Engine kept burning by ground command (engine on)
01:29	+X translation off		
01:33	Ascent/reaction-control propellant interconnect arm		
01:34	Ascent/reaction-control propellant interconnect A open Reaction control propellant A closed		
01:44	Ascent/reaction-control propellant interconnect B open Reaction control propellant B closed		
01:54	Reaction control crossfeed open		
02:43	Reaction control crossfeed closed		
02:44	Reaction control propellant A open Ascent/reaction-control propellant interconnect A closed		
02:54	Reaction control propellant B open Ascent/reaction-control propellant interconnect B closed Ascent propellant depletion		Thrust decay

6.7 INSTRUMENTATION

6.7.1 Development Flight Instrumentation

The performance of the development flight instrumentation and the associated major equipment items was satisfactory, with few exceptions. Satisfactory performance was obtained from 268 measurement sensors, except during abort staging when 11 measurements failed to provide data and four other staging measurements were questionable. In addition, three measurements (GN7691D, GG6002D, and GB0522T) were defective prior to launch, and four 0-35 psid propulsion measurements (GQ3666P, GQ4116P, GP0616P, and GP1116P) were expected to provide questionable data due to lack of inline pressure suppression devices to prevent transducer damage from pressure transients during engine startup and shutdown. (Suppression devices have been installed on LM-3 to prevent sensor damage.) Measurements GN7691D, GQ3666P, and GQ4116P operated partially during the flight, and some qualitative data were obtained.

Structural data obtained during the boost phase were satisfactory. Fifteen structural measurements were automatically switched out of the telemetry downlink at LM/S-IVB separation (00:53:55.5), and 18 other measurements were switched into the downlink. The 8.5-second inflight calibration sequence occurred at 00:54:17.6. The data channel containing engine chamber pressure measurement GR5039P had an 8 percent clipping at the lower level. This clipping did not affect the measurement reading when engine chamber pressure data were above 8 percent. The clipping was not observed during inflight calibration of the associated isolation amplifier and was probably caused by a sensing diaphragm restriction in one of the two thrust chamber pressure transducers.

Data obtained during the descent engine firings were satisfactory. At 06:12:14.7, during the abort staging sequence, 12 measurements were automatically switched out of the telemetry downlink, and replaced by 11 others.

The 15 measurements which failed to provide data or were questionable during abort staging are discussed in the following paragraphs.

The four interstage separation distance measurements (GB3102H through GB3105H) failed to function; no cause for these failures has been determined.

Five temperature measurements also failed during abort staging. The descent stage blast deflector measurement (GB0521T) failed coincident

with ignition for the first ascent engine firing; immediately thereafter, the ascent stage bottom surface measurements (GB0302T through GB0305T) also failed. The most likely cause of these failures was detachment of the thermocouple mounting tabs or breakage of the small thermocouple wires as a result of flexure of the heat shield material. Delicate mountings are inherent in high-response thermocouple installations; however, the installations on LM-3 will be improved.

Two of the 26 interstage pressure measurements (GB0817P and GB0818P) failed to provide data during abort staging. The response of these measurements to the relatively slow static pressure decay was considerably delayed from the other interstage pressure measurements, and their apparent failure to sense the rapid pressure rise during abort staging is attributed to an obstruction in the pressure tubing or transducer orifice.

Four other interstage pressure measurements (GB0621P, GB0623P, GB0805P, and GB0906P) were questionable because the data showed no measurable pressure rise. With the exception of measurement GB0621P, which was not telemetered during launch, these measurements responded properly to the atmospheric pressure decrease during the launch phase. No cause for the failure is apparent from analysis of the data and system configuration. One interstage pressure measurement (GB0814P) had an intermittent output signal throughout the flight; however, the measurement was valid during staging.

Twelve descent stage measurements (GB0521T, GB0522T, GB0401T through GB0403T, and GB0901P through GB0907P) were routed through a 4-foot, 2-inch ascent stage followup cable to provide descent stage data during abort staging. With the exception of GB0521T, GB0522T, and GB0906P previously discussed, the pressure measurements from the followup cable provided data through the period of maximum interstage dynamics until 06:12:15.6. At that time, these measurement channels indicated followup cable disconnect. Two of the three temperature measurements (GB0401T and GB0402T) provided data until 06:12:15.4, and the last valid data point for GB0403T occurred at 06:12:15.3. These temperature measurement readings were obscured by noise for the next 0.2 second; thereafter, their readings also indicated followup cable disconnect at 06:12:15.6.

Data obtained during the ascent engine firings and the remainder of the mission were satisfactory.

The qualitative characteristics of the transmitted end-to-end data varied with ground station acquisition and performance and is discussed in section 6.8.

6.7.2 Operational Instrumentation

The general operation of the 213 total operational PCM measurements (118 analog and 95 bilevel or digital) was good; however, two descent engine quantity gaging measurements were faulty prior to launch.

During the prelaunch period, propellant loading quantity gaging measurements GQ3604Q and GQ4104Q were not indicating correctly for the descent engine fuel and oxidizer no. 2 tanks. Tests have shown that the failure of an output transistor in the power converter of the quantity gaging system could cause an output voltage drop and loss of voltage regulation and could result in the improper readings noted during the prelaunch operations. The no. 1 quantity gaging system, which used a separate power supply, operated properly throughout the flight.

During the second and third descent engine firings, an out-of-phase indication was received from one of the two pairs of propellant shutoff valves (measurement GQ7498U). This problem has not been resolved, and further discussion is contained in section 6.12.

Data quality.- A special data quality sub-routine program operating on the initial phase-1 processing tape was used to obtain an accurate assessment of the PCM data quality, resulting in the percent of usable PCM data for each station pass. Such an assessment has been useful in the past to reveal poor data portions due to the loss of PCM synchronization, sub-par performance of individual Manned Space Flight Network (MSFN) stations, data processing errors, and other problems.

A tabulation of the stations by revolution for VHF or unified S-band links and the resulting percent usable PCM data from each is presented in table 6.7-I. For the TEL IV station during the revolution 3-4 pass, a usable PCM data quality of only 96.94 percent resulted, which was 1.90 percent lower than the launch phase data and more than 2 percent lower than the revolution 1-2, 2-3, and 4-5 passes. All passes (revolutions 1, 2, and 3) over the ship Coastal Sentry Quebec (CSQ) resulted in poor quality VHF PCM data being obtained. From table 6.7-I, it can be seen that usable data of 95.10, 89.55, and 90.52 percentages were obtained from the CSQ for revolutions 1, 2, and 3, respectively. Reasons for the poor data quality obtained from the TEL IV station during the revolution 3-4 pass and all passes over the CSQ are being investigated.

The usable S-band PCM data quality is generally comparable to the usable VHF PCM data quality for the same station pass. The usable VHF data quality for the Texas station during the revolution 2 pass was

6.7-4

99.68 percent while the usable S-band data quality was only 98.07 percent. This difference was probably caused by variations in the received S-band carrier power that was observed. The usable S-band data quality for the Hawaii station during revolution 3 pass was 94.60 percent while the usable VHF data quality was only 90.00 percent. The reason for this poor PCM data quality at this station is under investigation.

6.7.3 Calibration

Some bias adjustments were made to descent engine pressure measurements GQ6510, GQ4111, and GQ3501 for the postmission analysis of the propulsion system; GQ4111 and GQ3501 must read identically under static conditions and GQ6510 should read zero psia. The magnitude of these biases were within the end-to-end specification accuracy of the measurements involved. However, the calibrations used to reduce data for these measurements were derived from instrumentation component specifications.

6.7.4 Launch Vehicle Instrument Unit

The required LM/adaptor events data transmitted from the S-IVB instrument unit were satisfactory, except for the adaptor panel deployment monitor. The deployment event was transmitted through the instrument unit with other adaptor data. Indications were received from the relays which fire the pyrotechnics to separate the four panels. However, no indication was received from the four series-connected limit switches which monitor the deployment. The instrumentation was verified to be operating satisfactorily several times at the launch site. Other measurements show that the spacecraft separated from the S-IVB stage without any abnormal disturbances, thus indicating that the panels were, in fact, deployed. The panel deployment monitors were used for the first time on this flight and will not be installed for manned missions.

TABLE 6.7-I.- USABLE PULSE CODE MODULATED DATA

Station	Revolution	Percent usable data	
		VHF	S-band
TEL IV	1 (launch)	98.84	X
TEL IV	1-2	99.85	X
TEL IV	2-3	99.98	X
TEL IV	3-4	96.94	X
TEL IV	4-5	99.15	99.04
Canary Islands	1	99.73	X
Carnarvon	1	98.94	99.51
Carnarvon	3	99.47	X
Carnarvon	4	99.93	X
Coastal Sentry Quebec	1	95.10	X
Coastal Sentry Quebec	2	89.55	X
Coastal Sentry Quebec	3	90.52	X
Bermuda	2	100.00	X
Guaymas	4	99.72	X
Texas	2	99.68	98.07
Texas	3	99.05	X
Antigua	4	98.93	X
Antigua	5	98.68	X
Hawaii	3	90.00	94.60
Hawaii	4	99.06	X
Hawaii	5	99.24	X
Goldstone	4	X	99.17

X - not processed or not available.

6.8 COMMUNICATIONS

The communications system performance was evaluated by analysis of the lunar module (LM) communications system separately and the LM communications system and Manned Space Flight Network communications equipment as an integrated system. A diagram of communications capabilities during the mission is presented in figure 6.8-1.

Analysis of the mission data shows nominal performance of all communication channels except the UHF up-data channel.

The overall performance of the unified S-band RF system was satisfactory (table 6.8-1 and figs. 6.8-2 through 6.8-21) except for large variations in received carrier power.

The trajectory elements used for predictions were different from the actual spacecraft attitudes; therefore, the predicted data are not applicable. A comparison of received and predicted carrier power levels based on the final best estimate trajectory and actual spacecraft attitudes will be contained in supplement 3.

Computed bit error probabilities for the S-band and VHF pulse code modulation (PCM) telemetry channels for three station passes indicated good data reception during periods of adequate received signal powers.

Tests of the turned-around S-band up-voice and up-data subcarriers were conducted during four station passes. Signal-to-noise ratios were low during some periods; however, the uplink carrier power levels appeared adequate to support good up-voice and up-data communications.

Abrupt changes in the UHF received signal strength detected throughout the mission have been isolated to an intermittent failure in the flight hardware (see section 12.2).

6.8.1 LM Communications Performance

S-band.— The S-band equipment operation was satisfactory during the mission. Variations of the telemetered S-band transceiver RF power output data were caused by instrumentation noise, which existed prior to the flight.

The selected S-band receiver automatic gain control and static phase errors were nominal. The S-band power amplifier operated satisfactorily, although the telemetered measurement was inaccurate. The requirement for this measurement was waived prior to flight.

No degradation of transmitted power, from either the S-band transceiver or the power amplifier, was detected; therefore, breakdown caused by corona effects was not apparent.

Pulse code modulation telemetry.- Non-return-to-zero operational pulse code modulation telemetry data were transmitted satisfactorily through the VHF and S-band links.

Antenna temperatures.- Temperatures of the S-band steerable antenna, S-band omnidirectional antenna 1, and VHF inflight antenna 2 were within expected limits throughout the mission.

Development flight instrumentation communications.- Performance of the development flight instrumentation was nominal during the mission. Refer to section 6.7 for additional information concerning performance of this system.

6.8.2 LM/Network Communications System Performance

Unified S-band RF system.- The evaluation of the S-band RF system emphasized the periods of the mission associated with S-band transceiver and power amplifier activation, the descent and ascent engine firings, and the turned-around up-voice and up-data channel tests. A summary of the S-band RF system performance during these periods is presented in table 6.8-I and in figures 6.8-2 through 6.8-21. Analysis of the recorded data showed that large variations in received carrier power level occurred when look angles did not favor the active antenna. As soon as the final best estimate trajectory and actual spacecraft attitudes are made available, predicted and measured carrier power levels will be compared to determine whether the noted variation in received carrier power levels can be eliminated by optimum switching between the two lunar module antennas. Many of the procedural problems associated with the S-band communications during the Apollo 4 mission were not experienced during the Apollo 5 mission. Improvement was apparent in effecting station-to-station handovers of the S-band uplink.

Unified S-band ranging channel.- During prelaunch testing of the S-band equipment, the Merritt Island S-band site could not obtain correct range code acquisition when uplink signal combinations 4, 5, and 6 were utilized (table 6.8-II). Subsequent testing of production models of LM hardware showed that the problem was caused by insufficient range code power in the downlink spectrum and improper calibration procedure. The uplink modulation indices (table 6.8-II) were revised, and the sites were informed of procedures to be used if acquisition difficulties occurred.

Ranging capability existed throughout the mission. The LM transceiver was configured for range-code turn-around prior to launch and remained in this configuration throughout the mission. Also, each uplink signal combination that was utilized included range code modulation.

The range code acquisition sequences for 31 station passes were examined. The majority of the data reviewed showed good acquisition sequences. Typically, range code acquisition was initiated as soon as the exciter was locked to the synthesizer and the ranging receiver acquired lock; acquisition of range code was obtained approximately 5 seconds later. A typical ranging code acquisition sequence is shown in figure 6.8-22. Some of the sites had initial difficulty but obtained range code acquisition after adjusting an attenuator within the ranging receiver. This adjustment was determined to be necessary at the Merritt Island station prior to launch.

Unified S-band up-voice and up-data channels.- The configuration of the LM S-band transceiver is such that the up-voice and up-data subcarriers are turned around in the ranging channel and remodulated on the downlink carrier (fig. 6.8-23). Therefore, uplink signal combinations which include these subcarriers were transmitted, and the baseband modulation of the downlink carrier was recorded at selected sites. The performance of these channels was evaluated by measuring the postdetection or predetection signal-to-noise ratio of the turned-around up-voice modulation and by measuring the predetection signal-to-noise ratio of the turned-around up-data subcarrier. Since the measured data are dependent on the power levels of the received uplink and downlink carrier, the signal-to-noise ratio that would have been received at the LM would be better than the measured data indicate. The measured signal-to-noise ratios were related to the results of word intelligibility and up-data message acceptance tests performed at the Manned Spacecraft Center in an attempt to predict channel performance.

During the first orbital pass over the Texas, Merritt Island, and Bermuda stations, uplink combination 6 (table 6.8-II) was transmitted. Downlink coverage by the Merritt Island station was from 01:35:25 to 01:42:21. The Texas station transmitted the uplink S-band signal from 01:35:25 to 01:38:00, Merritt Island transmitted the signal from 01:38:08 to 01:41:00, and Bermuda transmitted the signal from 01:41:09 to 01:42:21. The predetection signal-to-noise ratio of the turned-around up-voice subcarrier did not fall below 10 dB during this downlink coverage by Merritt Island. The signal-to-noise ratio was consistent with a word intelligibility greater than 90 percent. Predetection signal-to-noise ratios of the 70-kHz subcarrier were also measured for the periods of Merritt Island coverage when Texas and Bermuda were transmitting the uplink S-band signal. The signal-to-noise ratio of the unmodulated 70-kHz subcarrier was greater than 12 dB during the pass (fig. 6.8-24). Based on command module communication system performance test results, this signal-to-noise ratio was above that required for up-data message acceptance.

The up-voice subcarrier transmitted by Guaymas (revolution 2) and by Merritt Island (revolution 2-3) was modulated by a 1-kHz tone. The variations in the measured signal-to-noise ratio varied from 0 to 22 dB (fig. 6.8-25), associated with variations in received downlink carrier power level (fig. 6.8-10). The received uplink power level measured was satisfactory during this pass, and the degraded signal-to-noise ratios were caused by variations in received downlink carrier power levels. The variations of measured signal-to-noise ratios (fig. 6.8-26) were time-associated with variations in received uplink and downlink carrier power level (figs. 6.8-11 and 6.8-12). Although variations in the received uplink carrier power level were observed, the received uplink carrier power level was consistent with satisfactory up-voice communications.

Unified S-band telemetry channel.— The unified S-band telemetry channel performance was evaluated by computing the probability of a bit error from the measured frame synchronization word error rate. The frame synchronization word error rate was determined by dividing the frame words in error during each 10-second interval of a pass by the number of frames observed.

Bit error probability calculations were performed for Carnarvon (revolution 1), Guaymas (revolution 4), and Hawaii (revolution 5). The results of these calculations are shown in figures 6.8-27, 6.8-28, and 6.8-29, respectively. The bit error probabilities for Carnarvon, revolution 1, do not correspond to the received downlink power levels (see figs. 6.8-2 and 6.8-27). However, the periods of poor telemetry channel performance are time-coincident with spikes observed on other data derived from the magnetic tape utilized in bit error probability computations. Therefore, the spikes may have caused the frame synchronization errors. During 12.3 percent of the pass, the bit error probabilities were below the limit of usable real-time data. However, station records provided data usable for postmission evaluation 99.51 percent of the pass (see section 6.7.2).

Bit error probability computations for the Guaymas coverage of revolution 4 are presented in figure 6.8-28. The degraded bit error probability coincident with abort staging was probably caused by the signal phase perturbations and the received carrier power level changes (fig. 6.8-17). The bit error probabilities were greater than the limit of usable real-time data throughout the pass.

The bit error probabilities shown in figure 6.8-29 were better than design goals for the periods when the received downlink carrier power level was adequate (see figure 6.8-21 for comparison). Exact time correlation of the bit error probabilities and the received carrier powers cannot be obtained because the error probabilities represent an average computed over a 10-second interval.

VHF RF communications.- The RF power output of the four development flight instrumentation VHF telemetry links was satisfactory throughout the flight. The qualitative characteristic of the end-to-end data varied because of RF transmission conditions at abort staging, periods of low look-angle elevations, uncontrolled vehicle attitudes, and noise susceptibility of the constant bandwidth telemetry link.

Telemetry dropout occurred at launch vehicle staging for 2 seconds beginning at 00:02:23.6 because of S-IB stage retrorocket plume attenuation. During LM/adaptor separation, data dropout occurred for 0.25 second. Figure 6.8-30 presents the received 237.8-MHz signal power level for the Guaymas coverage of the second and third descent engine firings, abort staging, and first ascent engine firing; a time history of the received 241.5-MHz signal power level during these events is presented in figure 6.8-31. As shown in this figure, four cyclic received power-level nulls (in addition to the transient at abort staging) were observed during the Texas pass. The cyclic nulls were common to all channels except the 230.9-MHz channel and are attributed to LM antenna patterns.

The multipath RF transmission problem due to low look angles was evident during the Hawaii station pass of the fifth revolution. Data quality received by the Rose Knot Victor during the second ascent engine firing was subjected to repetitive noise bursts because the vehicle was tumbling. The constant bandwidth link was susceptible to noise because of large data bandwidths and lower modulation indexes.

VHF PCM telemetry.- The probability of a bit error for the VHF PCM telemetry channel was computed utilizing the technique described previously. The results of these computations for Carnarvon (revolution 1), Guaymas (revolution 4), and Hawaii (revolution 5) are presented in figures 6.8-32, 6.8-33, and 6.8-34, respectively. As shown in figure 6.8-32, the bit error probability for the Carnarvon pass was satisfactory throughout the pass. Signal strength records show a recurrent spike appearing on all traces on that particular stripchart recording. The spikes which occur before, during, and after the presence of a signal are coincident with most of the degraded bit error probabilities. The distribution of these spikes indicates that spurious external signals were imposed on the magnetic tape at either the receiving or the playback station. The spikes appear to be affecting all data taken from this particular tape. A bit error probability greater than the design goal was experienced for a total of 80 seconds for Guaymas coverage of revolution 4. If the bit error probabilities associated with acquisition and loss of signal are discarded, there were no periods when the bit error probability was worse than the limit for usable real-time data.

The bit error probability for Hawaii coverage of revolution 5 (fig. 6.8-34) was better than the limit of usable real-time data throughout the pass.

S-band and VHF comparisons.- Data from Carnarvon (revolution 1) show that S-band and VHF PCM systems were both affected by spurious spikes. Data from Guaymas (revolution 4) indicate that the S-band telemetry had fewer synchronization word losses than did the VHF telemetry.

Data from Hawaii (revolution 5) indicate that the bit error probability for the S-band telemetry exceeded that for the VHF. The VHF system on the spacecraft used a pair of antennas with nearly spherical coverage, while the S-band system on the spacecraft used a single antenna providing only unidirectional coverage. This condition explains the difference in S-band and VHF performance at Hawaii.

These minor differences in bit error probability between the S-band and VHF systems were as expected for earth orbital missions.

UHF up-data channel.- Abrupt changes of about 34 dB in spacecraft received UHF signal strength were detected throughout the mission; a typical example is shown in figure 6.8-35. Corresponding changes did not occur in the ground received signal strength from the VHF data transmitters which shared the same two antennas through a diplexer. These abrupt changes in received power frequently caused the received command signal power to be below the message acceptance threshold. Consequently, command transmission had to be delayed or repeated.

The received signal power variations are consistent with an intermittent condition in either the digital command assembly RF stage, the coaxial cable assembly connecting the diplexer and digital command assembly, or the internal diplexer connections.

C-band system.- Operation of the C-band system is discussed in section 3.

TABLE 6.8-I.- S-BAND RF SYSTEM PERFORMANCE

Station	Revolution	Event	Time of two-way lock, hr:min:sec	Time of range receiver lock, hr:min:sec	Received carrier power presentation		Comments
					Uplink fig. no.	Downlink fig. no.	
Carnarvon	1	IM/S-IVB separation and primary S-band transceiver activation	00:53:53.6	00:54:23	-	6.8-2	Received uplink carrier power level was at transceiver automatic gain control saturation level for pass. Downlink carrier power level was good during pass
Texas	1	Secondary S-band transceiver and power amplifier activation	01:33:13	01:33:48	6.8-4	6.8-5	Primary S-band transceiver commanded "off" at 01:33:12 (see fig. 6.8-3). Secondary S-band transceiver and power amplifier combination commanded on at 01:33:29. Two-way lock reacquired at 01:33:34 and power amplifier warm-up cycle completed at 01:33:47. Handover from Guaymas to Texas required 9 seconds to complete. Abrupt change in received downlink carrier frequency caused Texas receivers to lose lock when handover from Guaymas was initiated (see fig. 6.8-3).
Merritt Island	1 - 2	Turn-around S-band up-voice and up-data tests	01:38:00	01:38:20	6.8-6	6.8-7	Single omnidirectional spacecraft antenna did not provide good coverage for complete pass. Spacecraft antenna nulls caused received uplink and downlink carrier power level variations from 01:39:00 to loss of signal.
Redstone	2	-	01:46:13	01:46:19	6.8-8	6.8-9	Some variations in received carrier power level because of inopportune spacecraft antenna patterns, but overall signal quality was good.
Guaymas	2	Turn-around S-band up-voice tests	03:06:02		-	6.8-10	Received downlink carrier power level variation observed from 03:05:10 to 03:07:00.
Merritt Island	2 - 3	Turn-around S-band up-voice tests	03:11:00		6.8-11	6.8-12	Abrupt changes (20 to 35 dB) in received downlink carrier power level during the pass. Abrupt changes caused by spacecraft antenna gain variations.
Carnarvon	3	First descent engine firing	03:57:50	03:58:34	6.8-13	6.8-14	Received uplink carrier power level would have supported good S-band communications. Received downlink carrier power levels were consistent with a good communications channel from 03:58:10 to 04:03:40. Downlink communications would have been intermittent from 04:03:40 to loss of signal.
Goldstone	4	Second and third descent engine firings and abort staging	-	-	-	6.8-15	Received carrier power variations observed during third descent engine firing and abort staging. Received carrier power level dropped off 7 dB at abort staging only; variation attributed to propulsion system activity.

TABLE 6.8-I.- S-BAND RF SYSTEM PERFORMANCE - Concluded

Station	Revolution	Event	Time of two-way lock, hr:min:sec	Time of range receiver lock, hr:min:sec	Received carrier power presentation		Comments
					Uplink, fig. no.	Downlink, fig. no.	
Guaymas	4	Second and third descent engine fir- ings, abort staging, and first ascent engine firing	06:08:28	06:08:51	6.8-16	6.8-17	Received uplink and downlink carrier power levels good during pass. A received downlink carrier power level drop of approxi- mately 13 dB observed at abort staging.
Texas	4	Third descent engine firing, abort staging, and first ascent engine firing	06:12:04		6.8-18	6.8-19	A drop in received uplink carrier power level of 9 dB detected at abort staging. Received uplink and downlink carrier power levels dropped sharply at 06:15:00. The abrupt drop caused Texas receiver to lose lock. Intermittent two-way lock was obtained between 06:15:18 and 06:17:10. Variations in received carrier power levels were caused by spacecraft antenna gain variations.
Hawaii	5	Second ascent engine firing	07:38:48	07:38:59	6.8-20	6.8-21	Received uplink and downlink carrier power level variations observed from acquisition of signal to 07:43:00. Downlink communications would have been intermittent until 07:43:00.

TABLE 6.8-II.- NETWORK/LM S-BAND TRANSMISSION COMBINATION SUMMARY

Combination	Information	Modulation technique	Subcarrier frequency, kHz	Initial carrier phase deviation, rad	Revised carrier phase deviation, rad
1	Carrier	Phase modulation (PM) on carrier	-	1.34	1.34
	Pseudo random noise ranging				
4	Carrier	PM on carrier	-	0.80	0.38
	Pseudo random noise ranging				
5	Voice	FM/PM	30	1.85	1.20
	Carrier				
6	Pseudo random noise ranging	PM on carrier	-	0.80	0.38
	Up-data	FM/PM	70	1.85	1.20
	Carrier	PM on carrier	-	0.50	0.44
	Pseudo random noise ranging				
	Voice	FM/PM	30	1.00	1.00
	Up-data	FM/PM	70	0.76	1.00

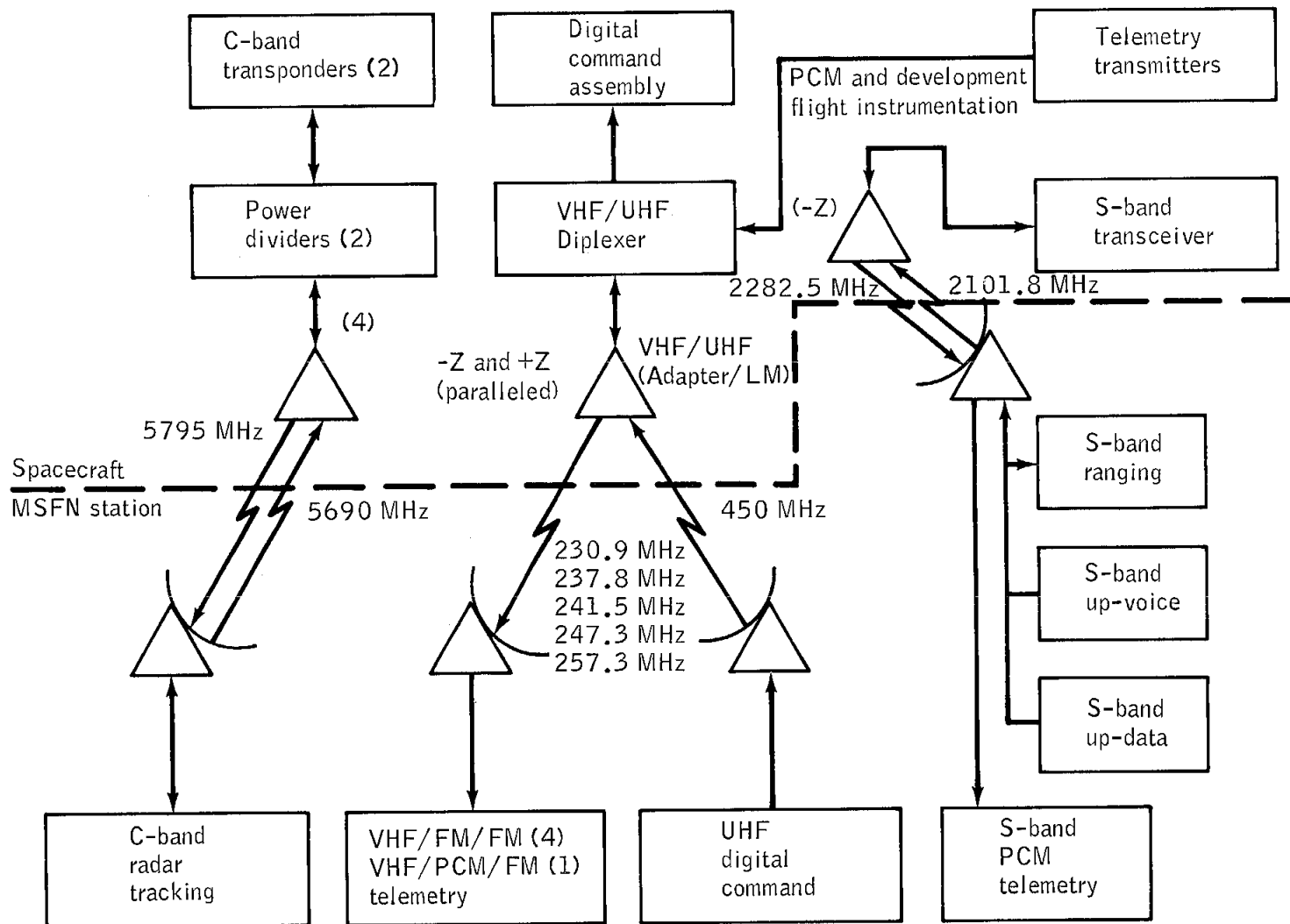


Figure 6.8-1.- Communication system configurations.

NASA-S-68-1969

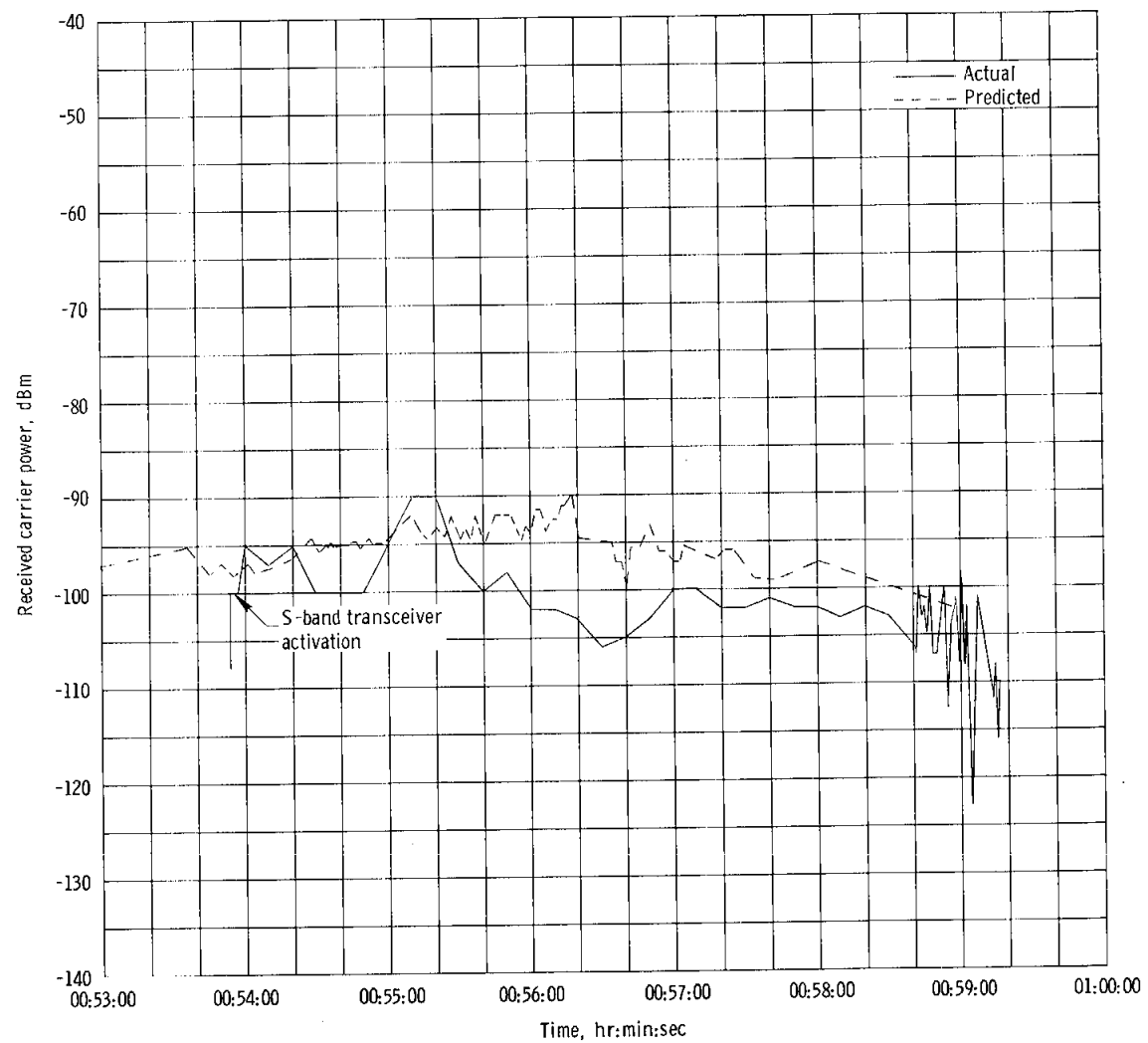


Figure 6.8-2. - Received unified S-band downlink carrier power, Carnarvon, revolution 1.

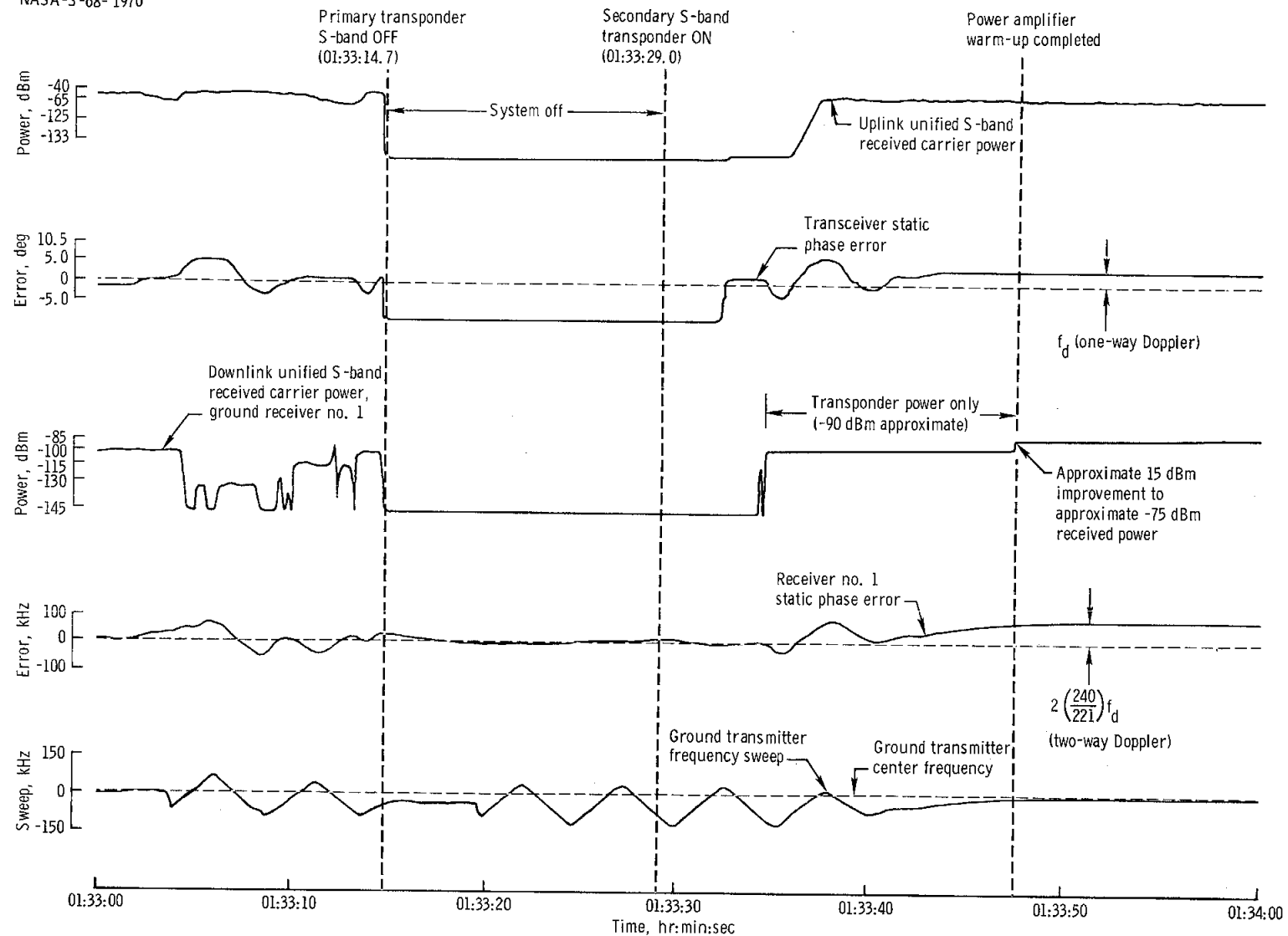


Figure 6.8-3. - Primary to secondary unified S-band system switchover, Texas, revolution 1.

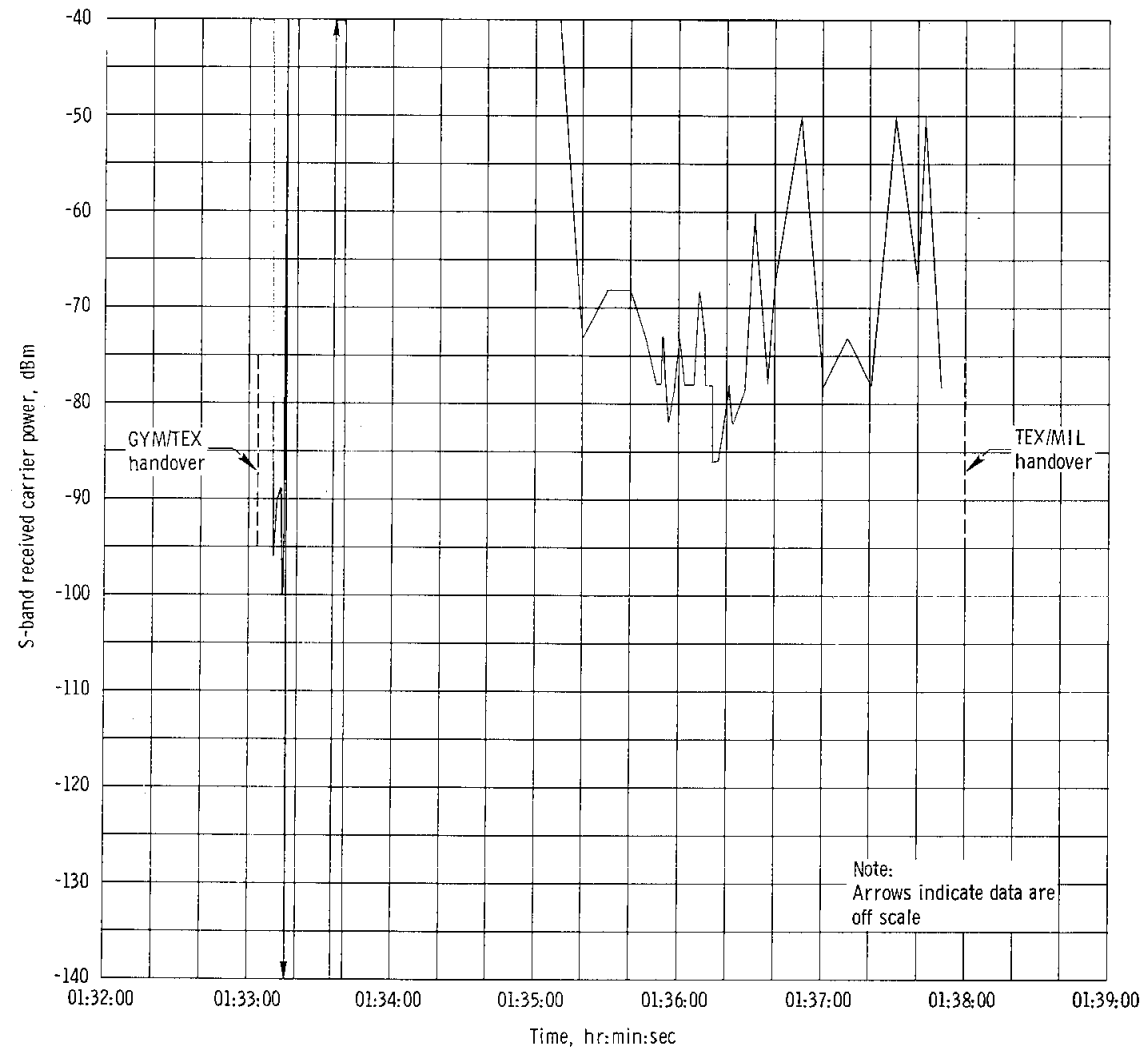


Figure 6.8-4. - Received unified S-band uplink carrier power, Texas, revolution 1.

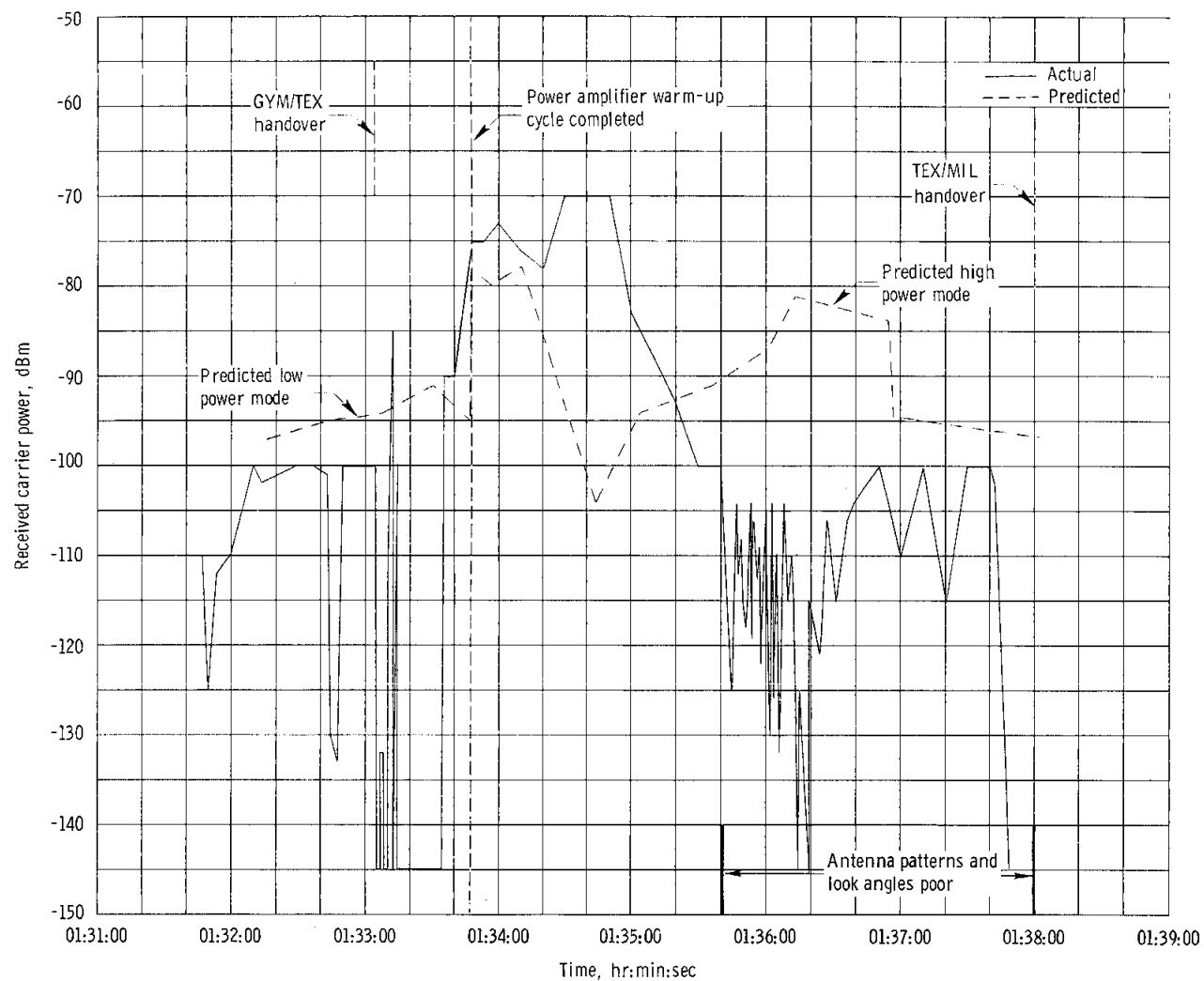


Figure 6.8-5. - Received unified S-band downlink carrier power, Texas, revolution 1.

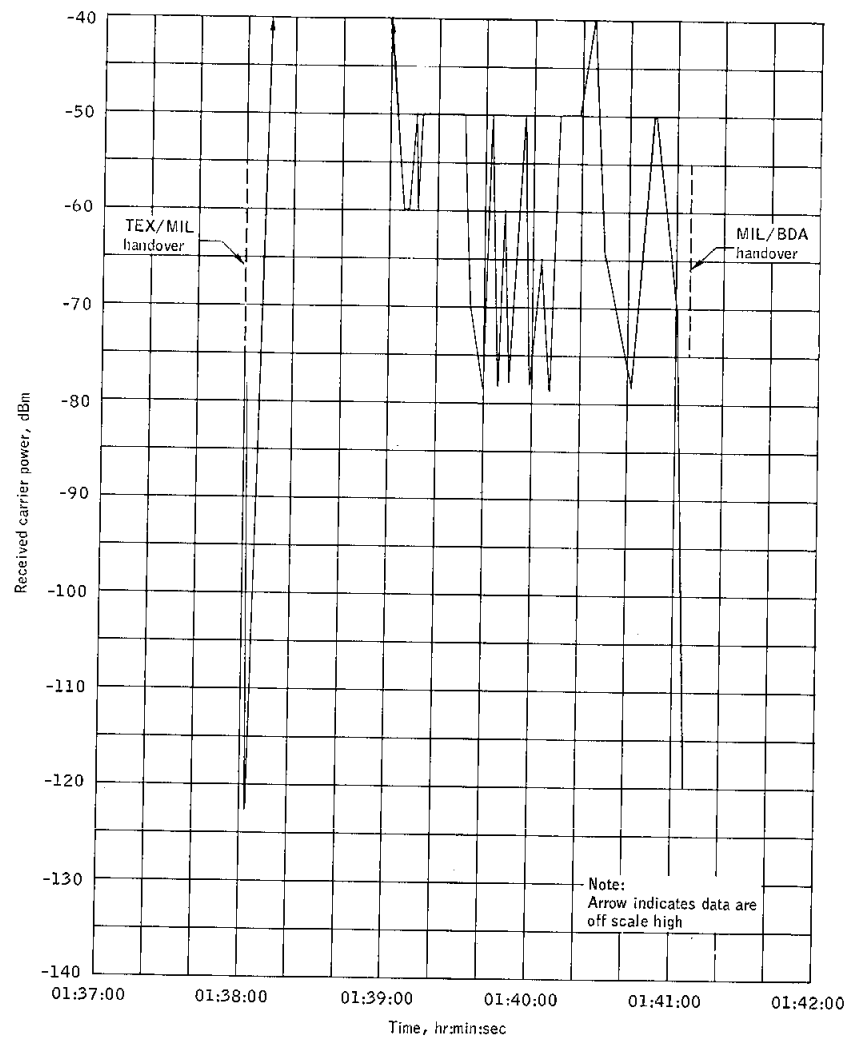


Figure 6.8-6.- Received unified S-band uplink carrier power, MILA, revolution 1-2.

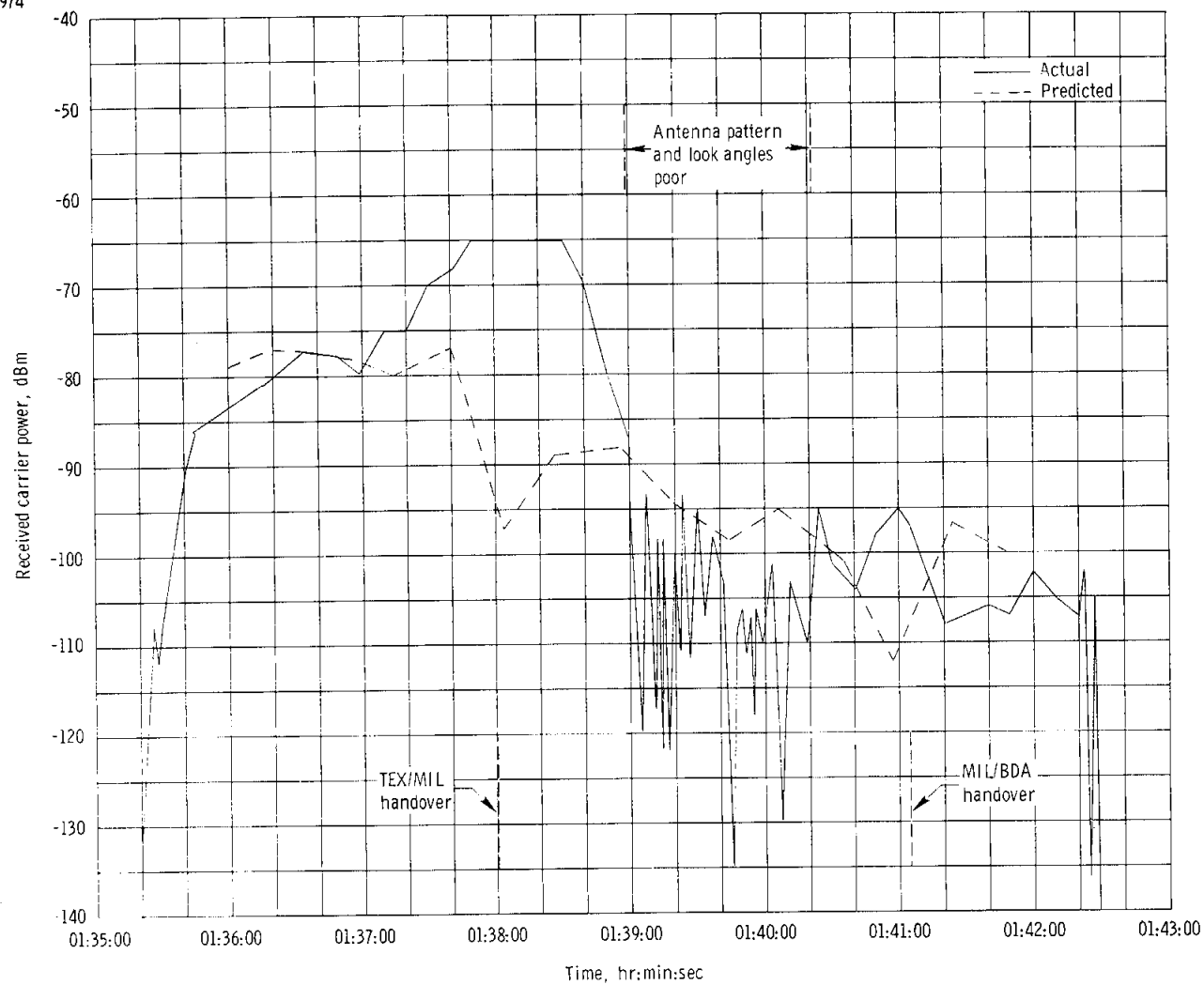


Figure 6.8-7. - Received unified S-band downlink carrier power, MILA, revolution 1-2.

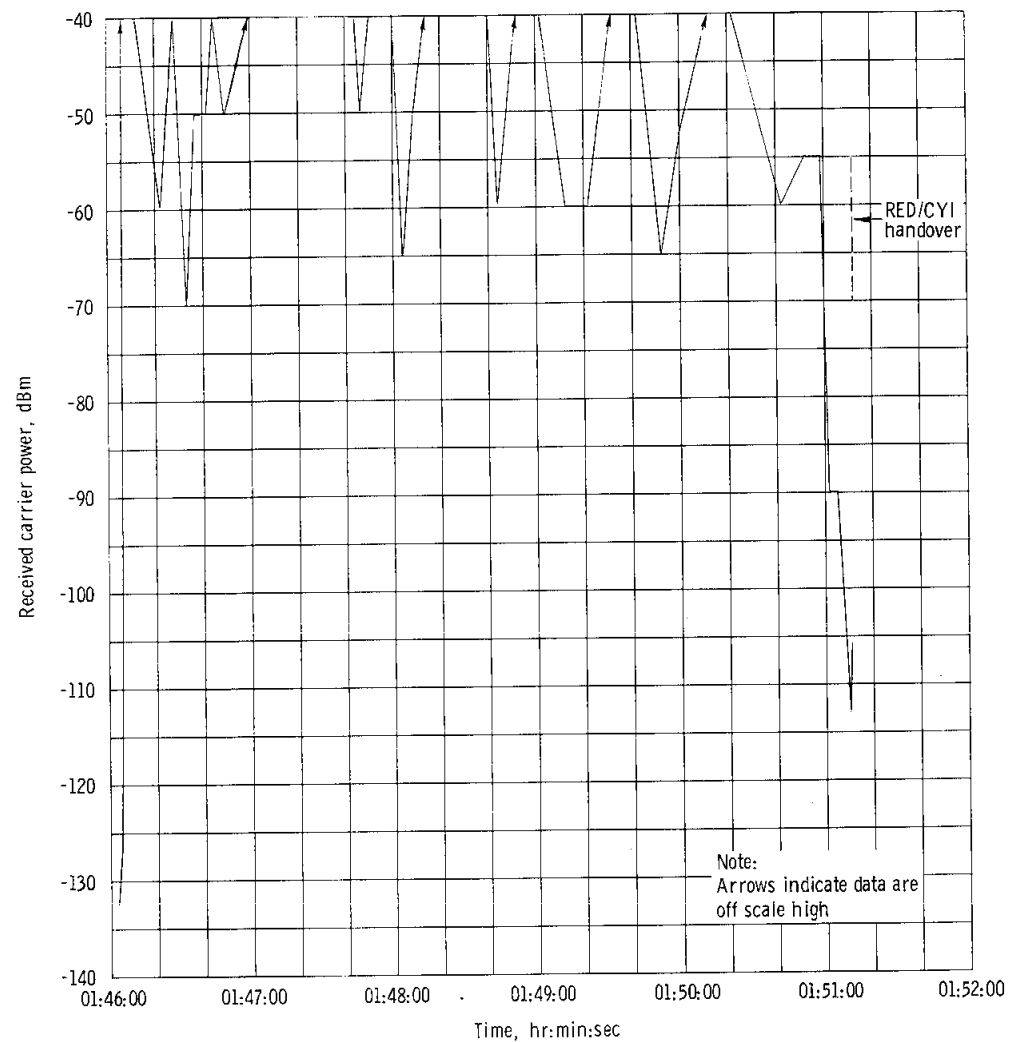


Figure 6.8-8. - Received unified S-band uplink carrier power, Redstone, revolution 2.

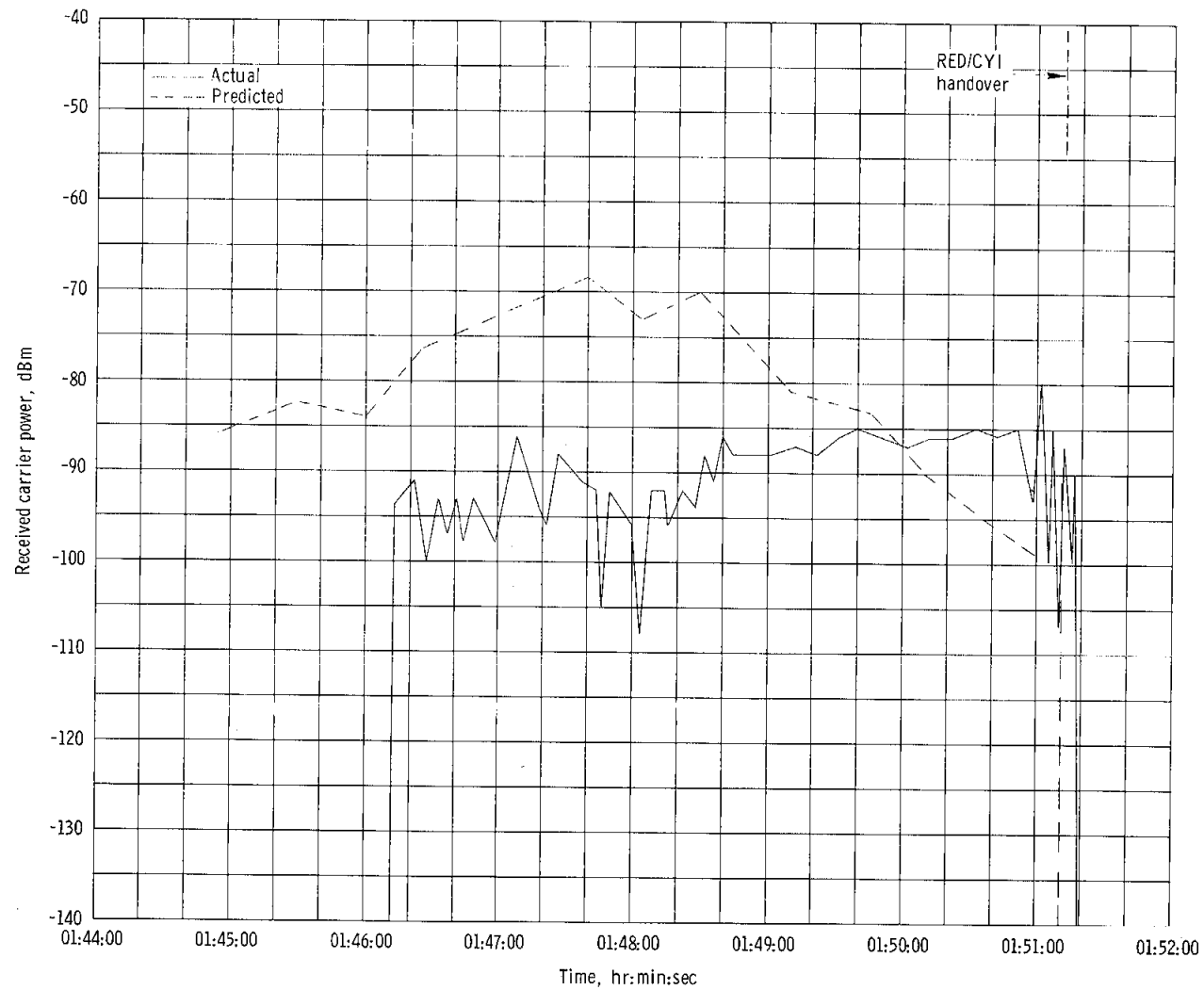


Figure 6.8-9. - Received unified S-band downlink carrier power, Redstone, revolution 2.

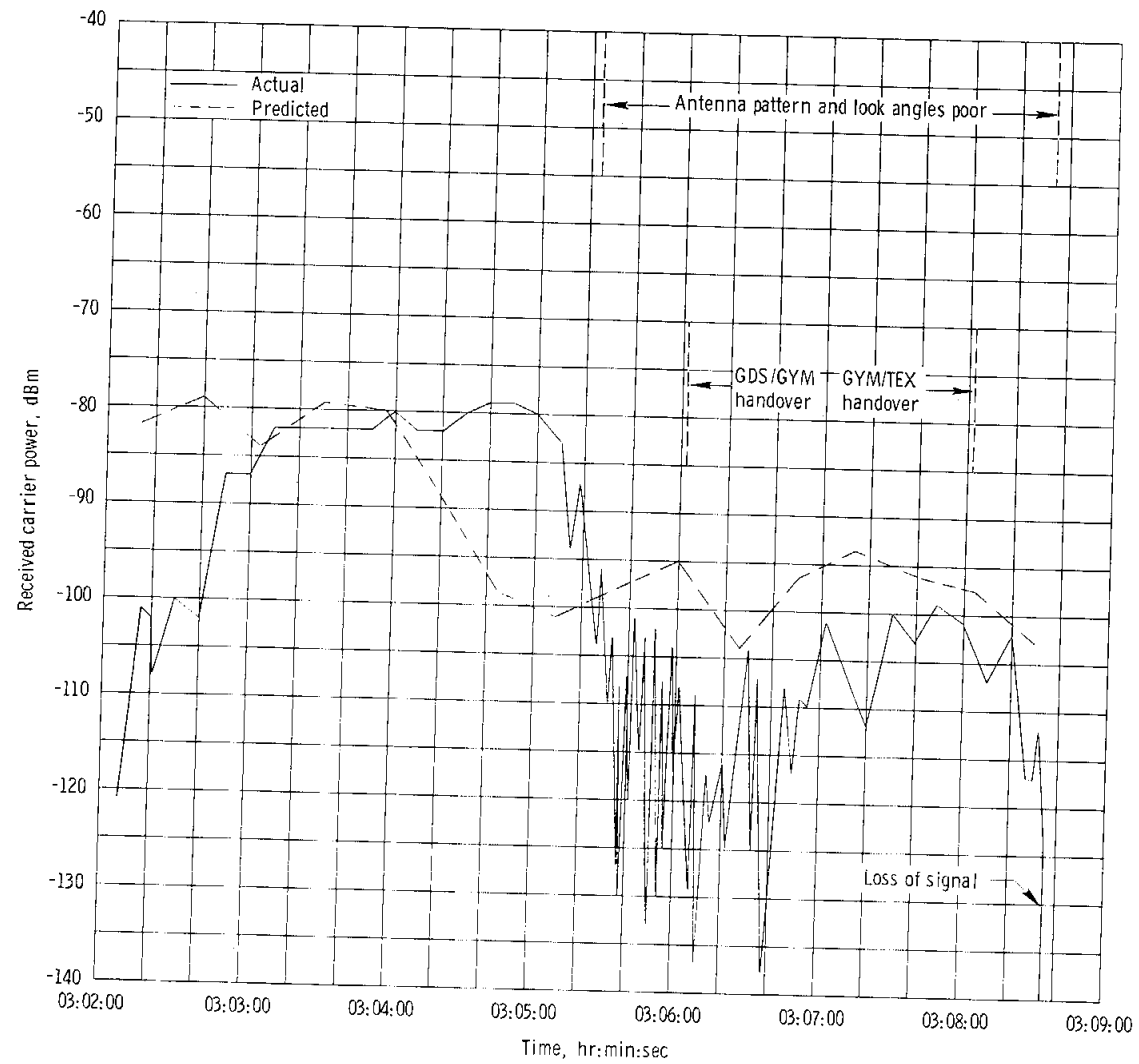


Figure 6.8-10. - Received unified S-band downlink carrier power, Guaymas, revolution 2.

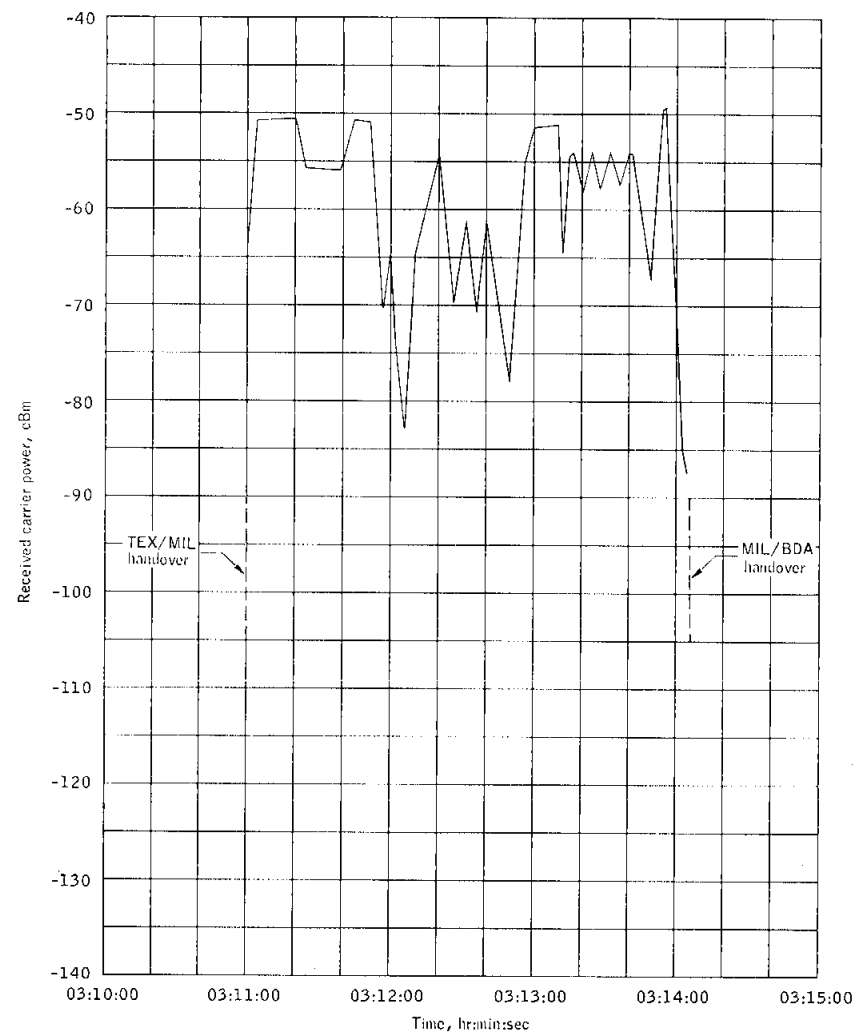


Figure 6.8-11.- Received unified S-band uplink carrier power, MILA, revolution 2-3.

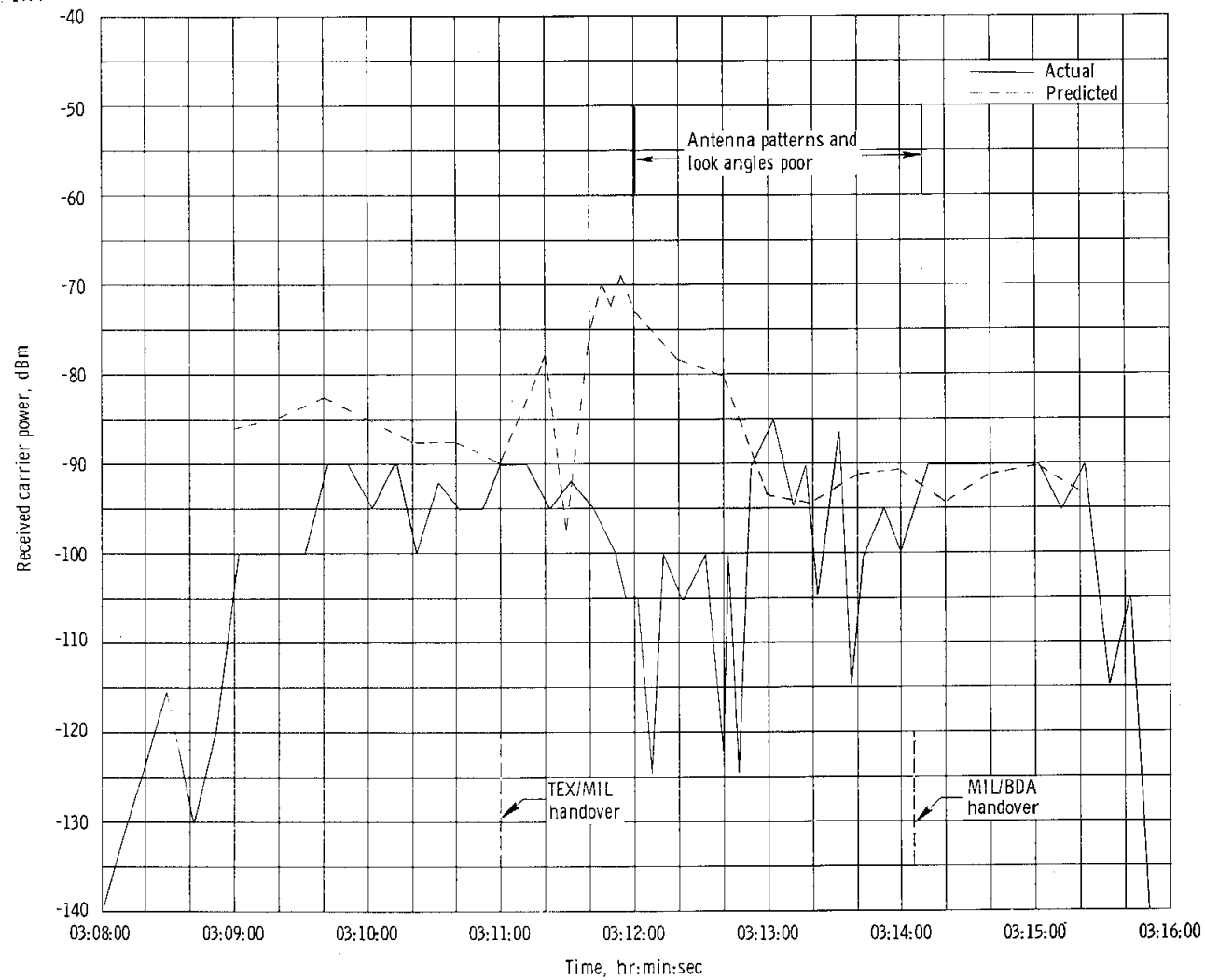


Figure 6.8-12. - Received unified S-band downlink carrier power, MILA, revolution 2-3.

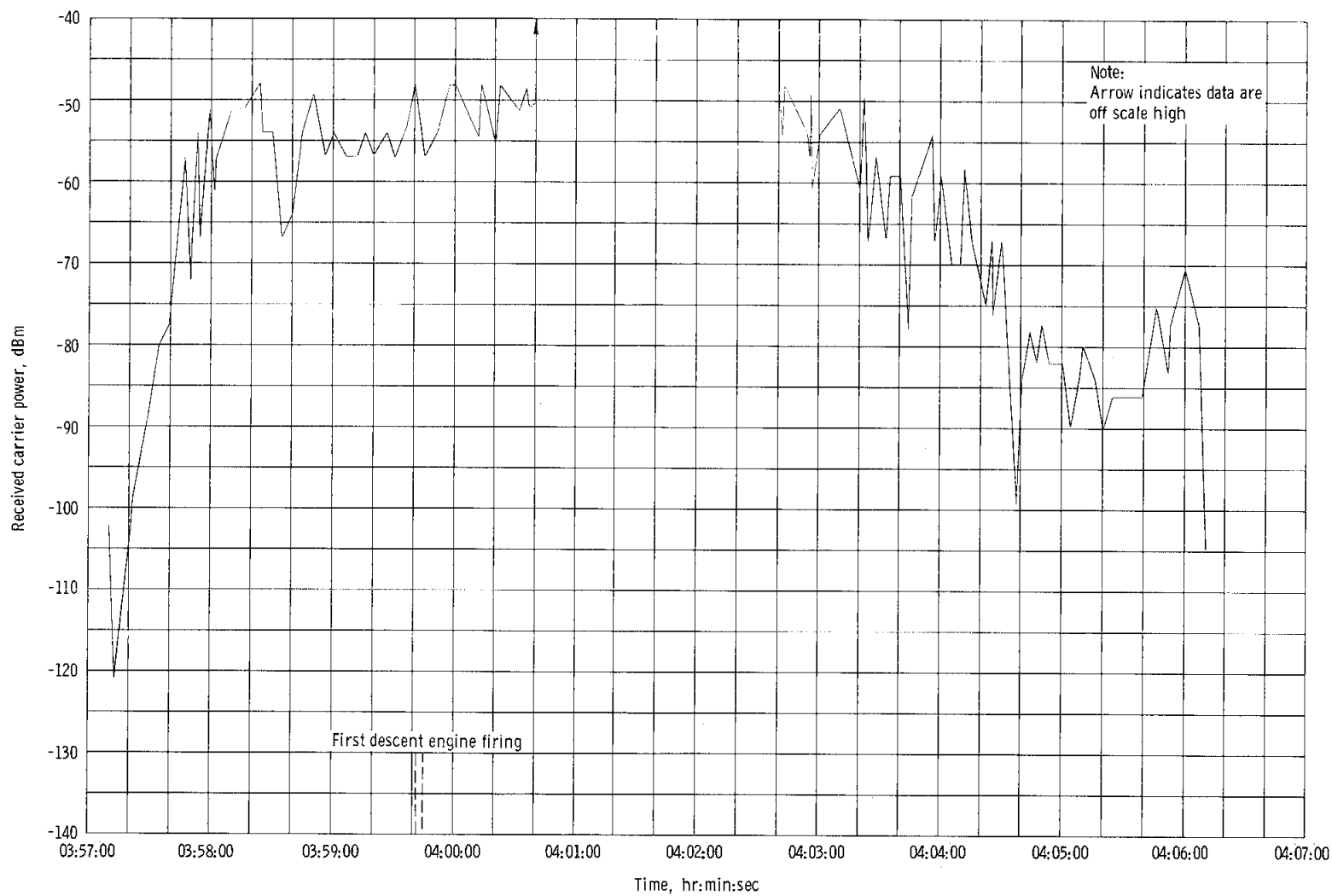


Figure 6.8-13. - Received unified S-band uplink carrier power, Carnarvon, revolution 3.

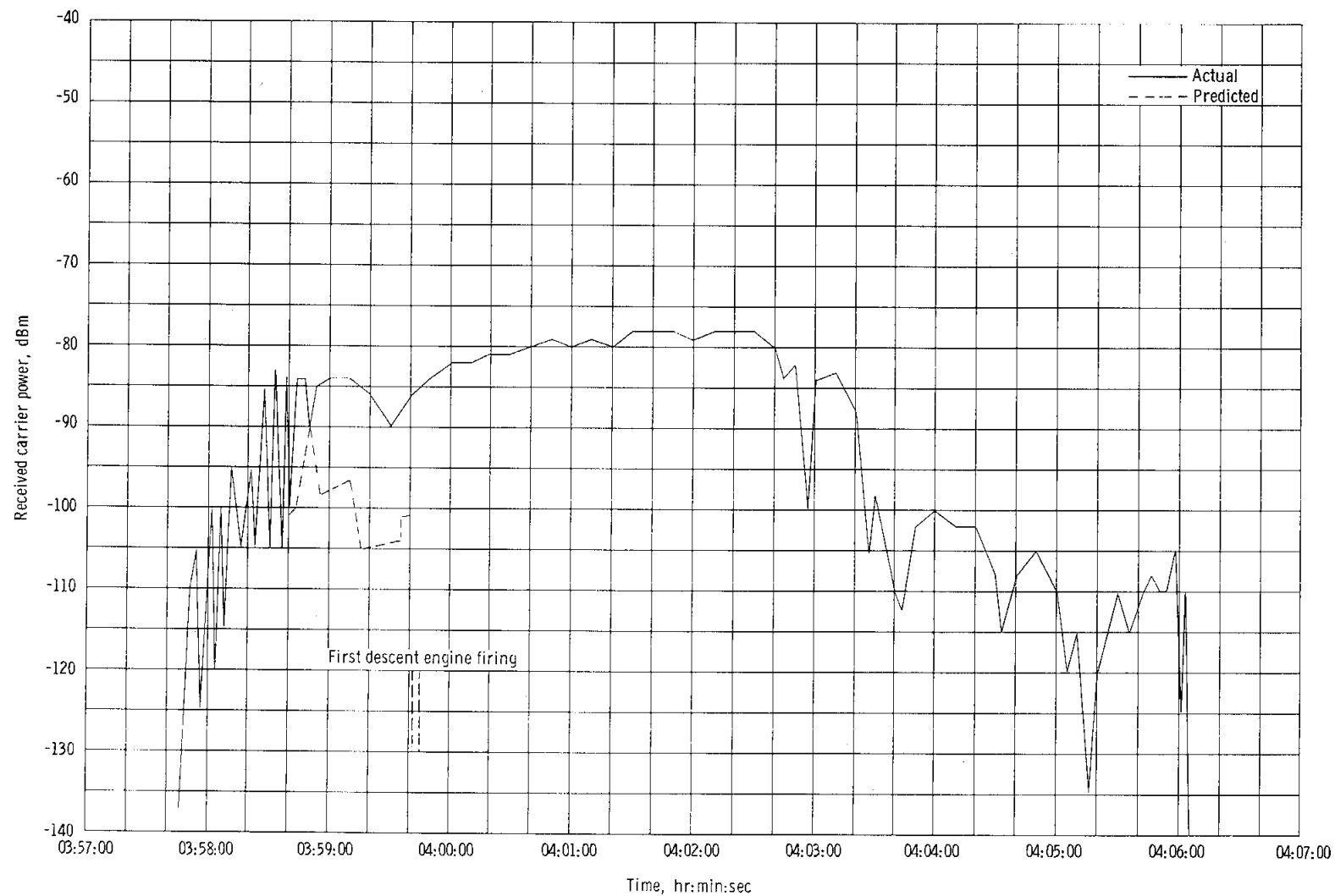


Figure 6.8-14. - Received unified S-band downlink carrier power, Carnarvon, revolution 3.

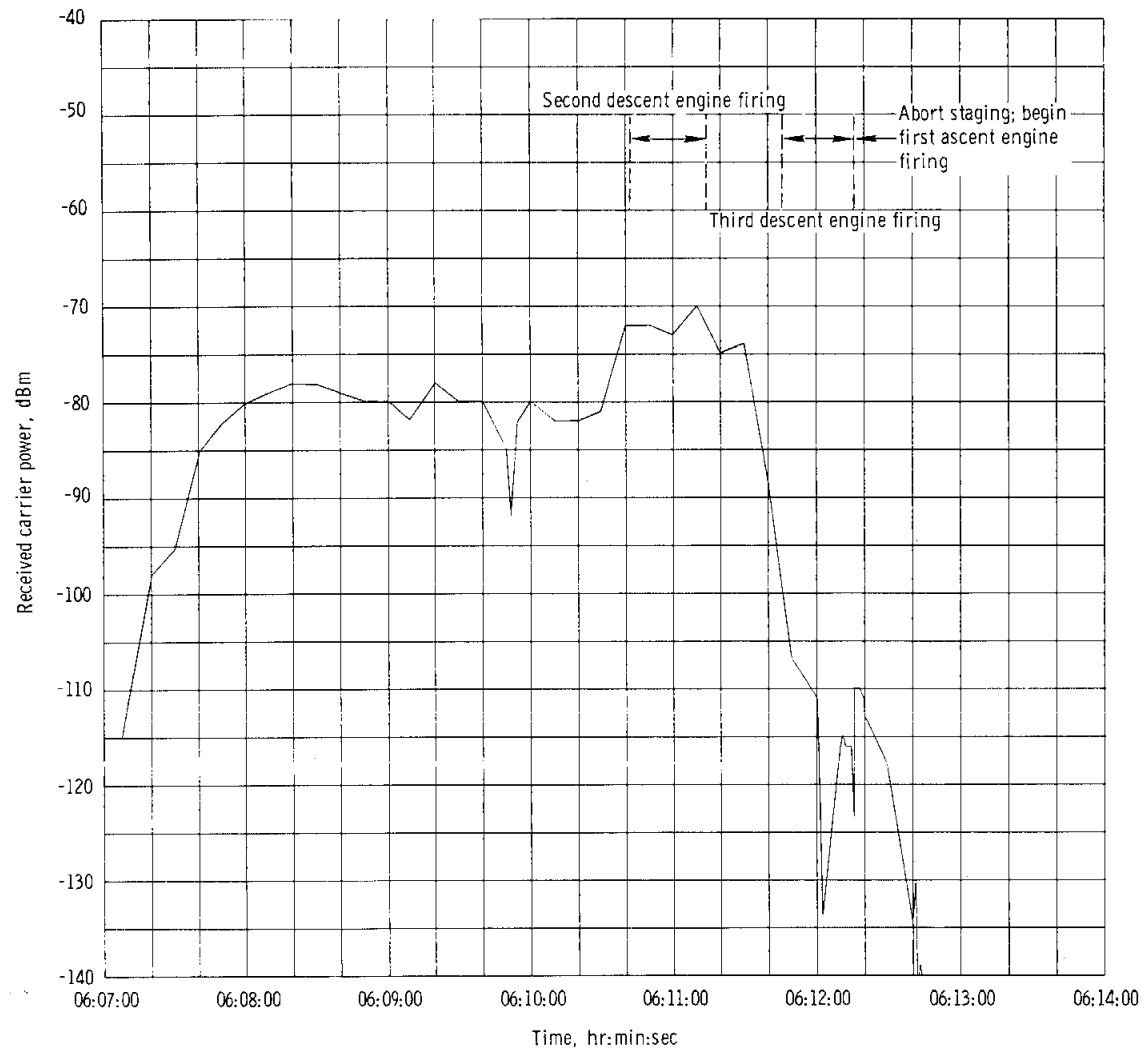


Figure 6. 8-15. - Received unified S-band downlink carrier power, Goldstone, revolution 4.

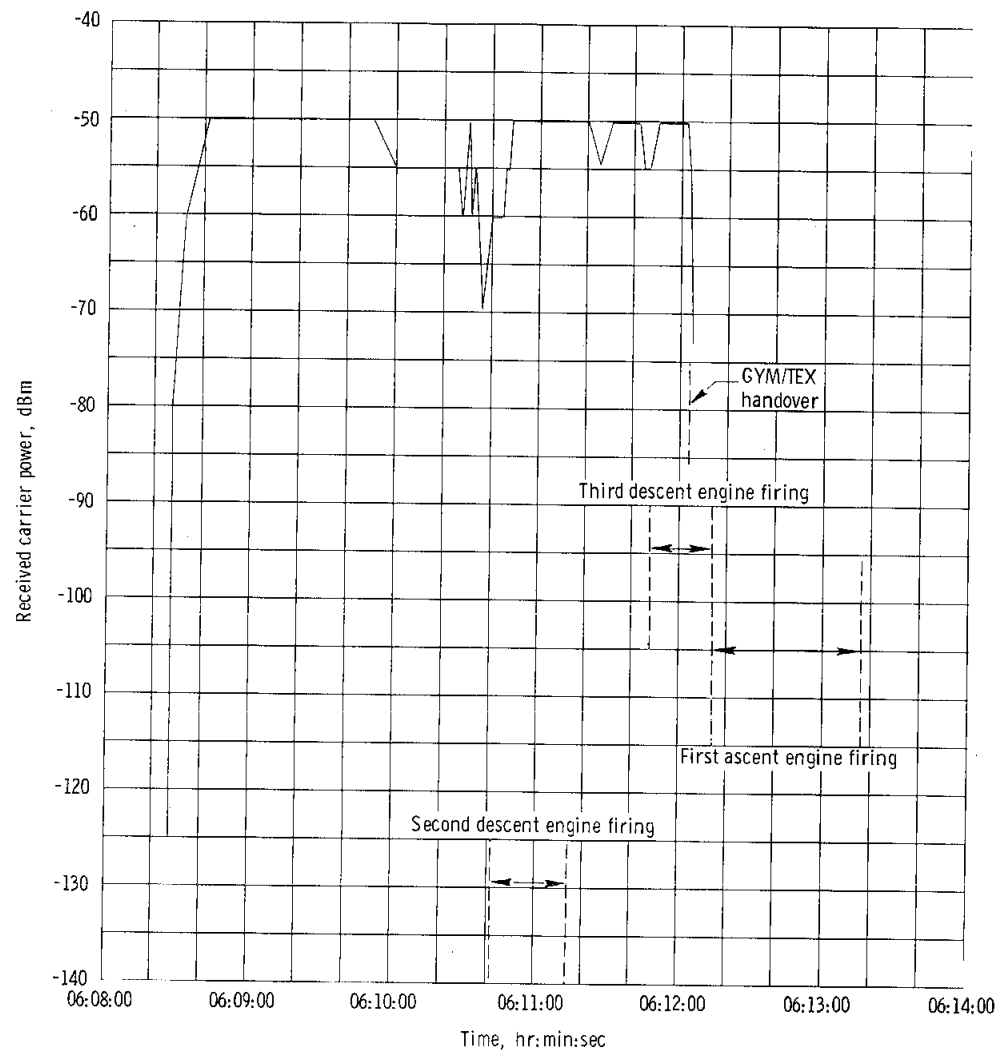


Figure 6.8-16. - Received unified S-band uplink carrier power, Guaymas, revolution 4.

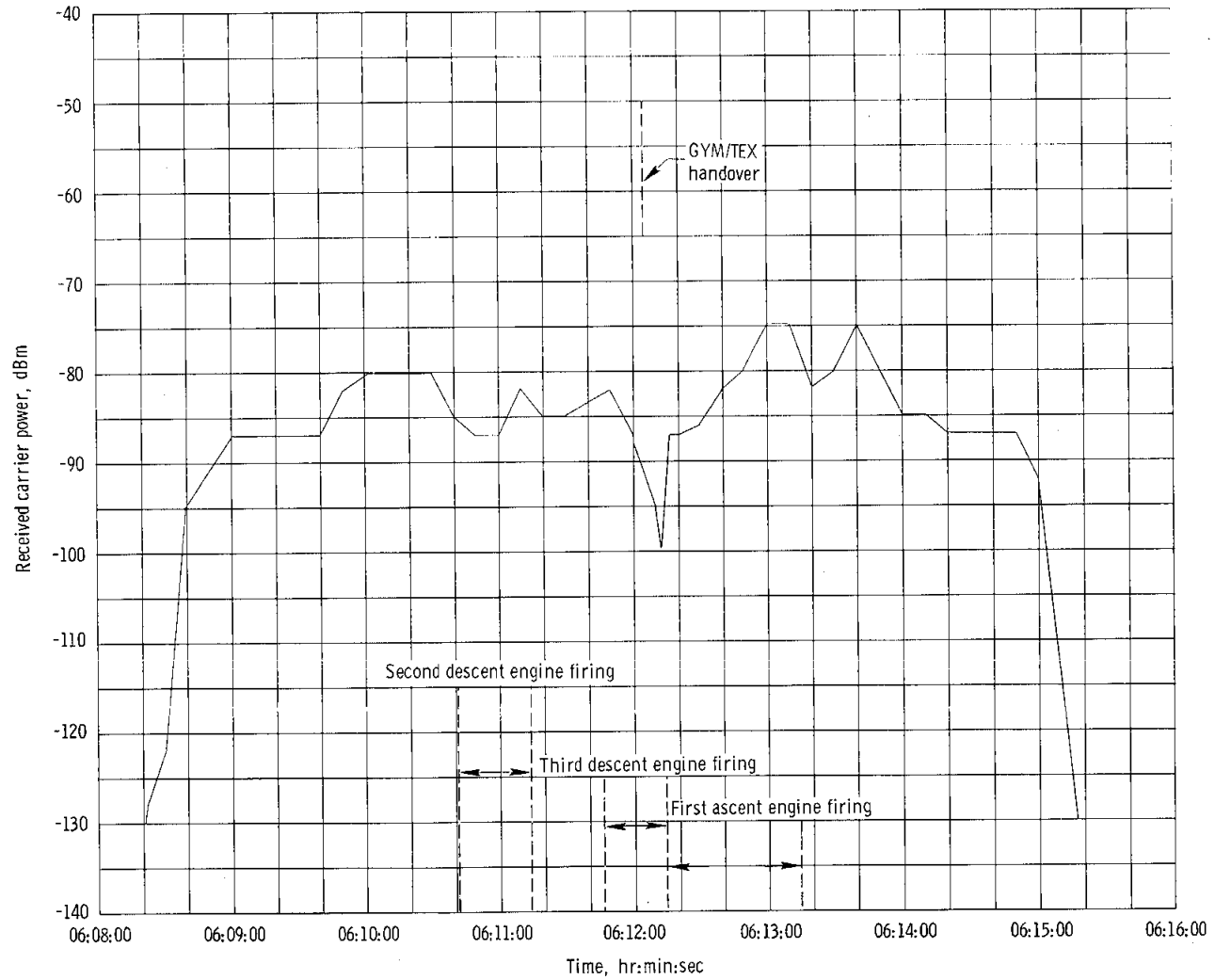


Figure 6.8-17. - Received unified S-band downlink carrier power, Guaymas, revolution 4.

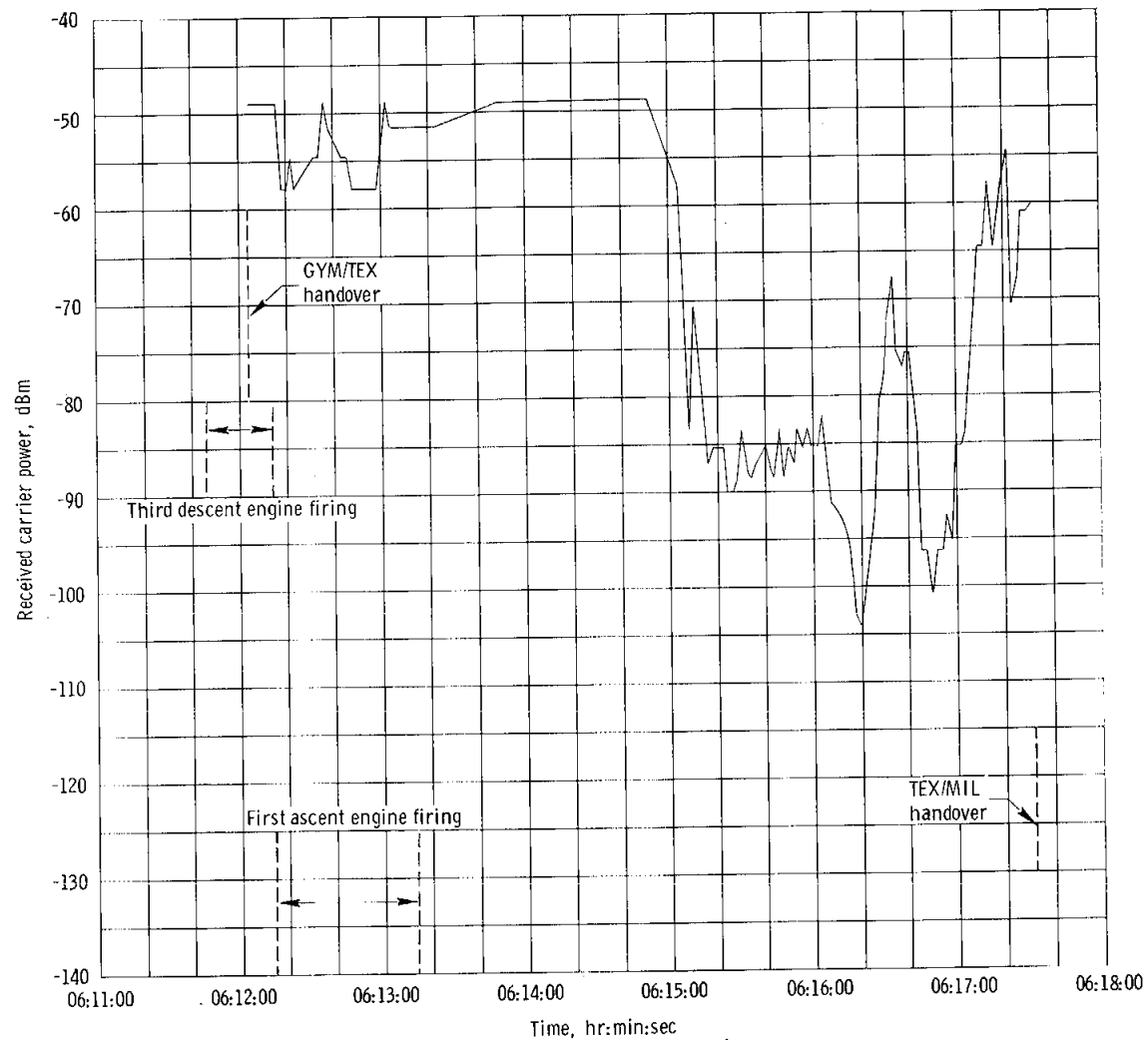


Figure 6.8-18. - Received unified S-band uplink carrier power, Texas, revolution 4.

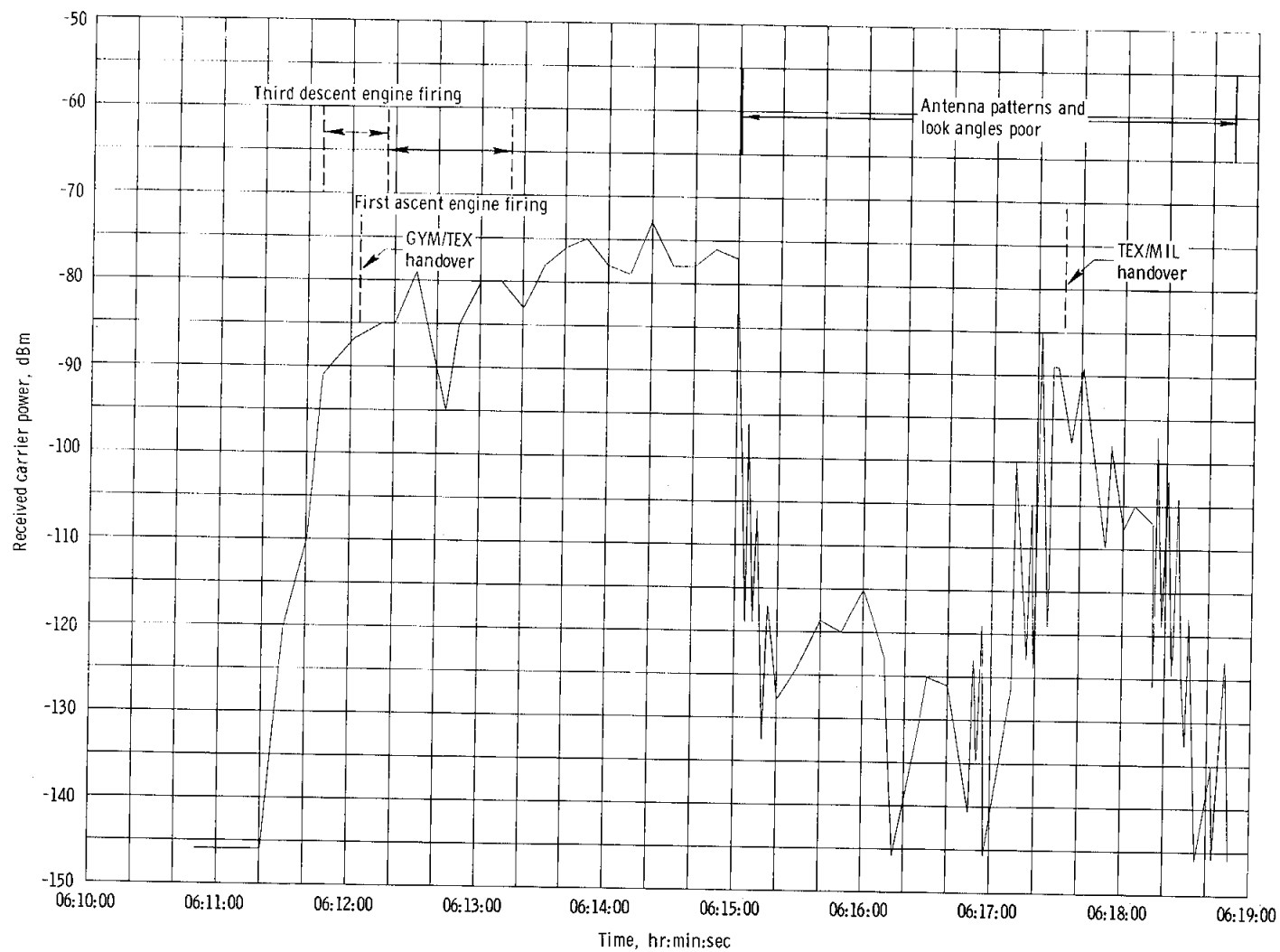


Figure 6.8-19. - Received unified S-band downlink carrier power, Texas, revolution 4.

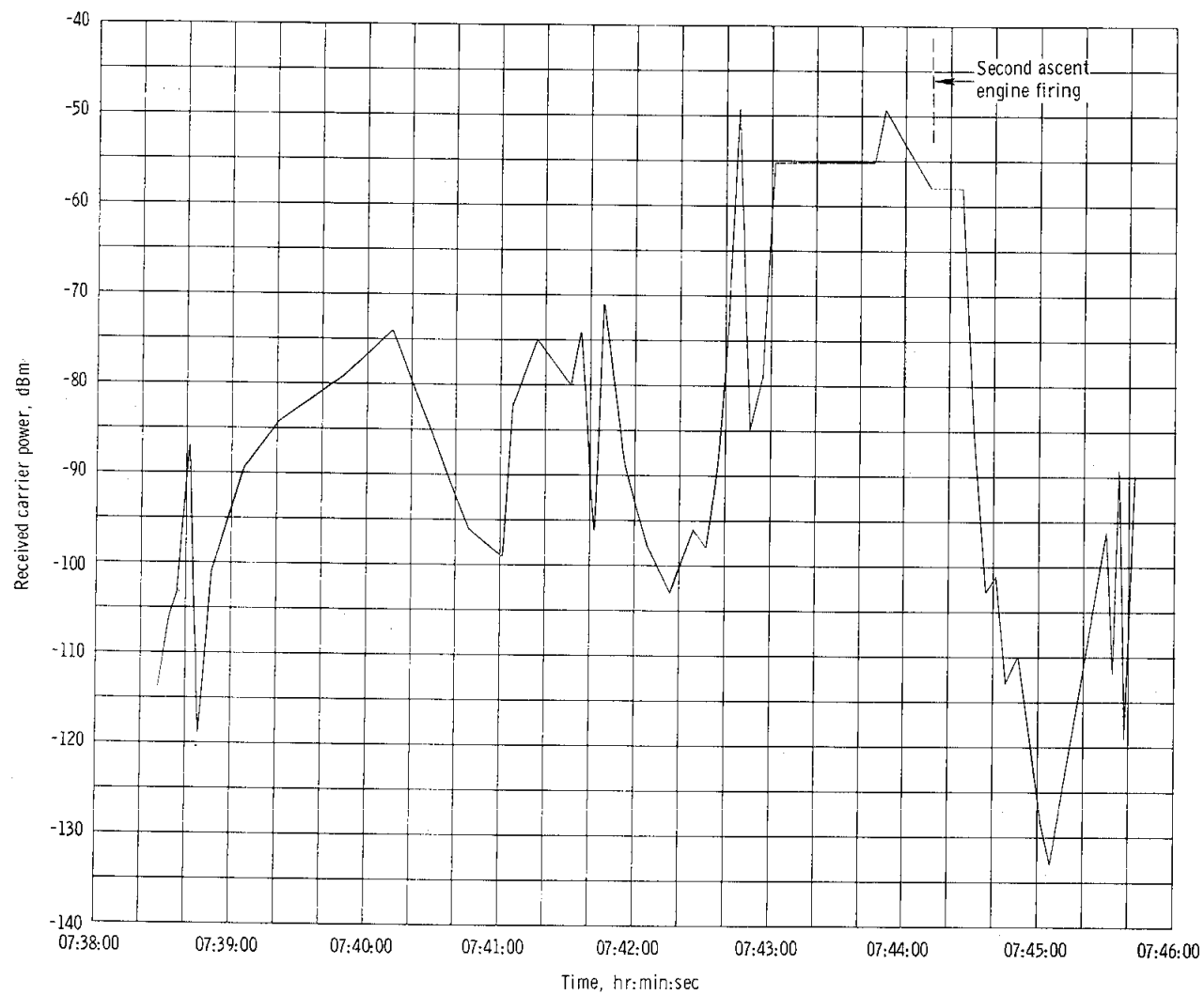


Figure 6.8-20. - Received unified S-band uplink carrier power, Hawaii, revolution 5.

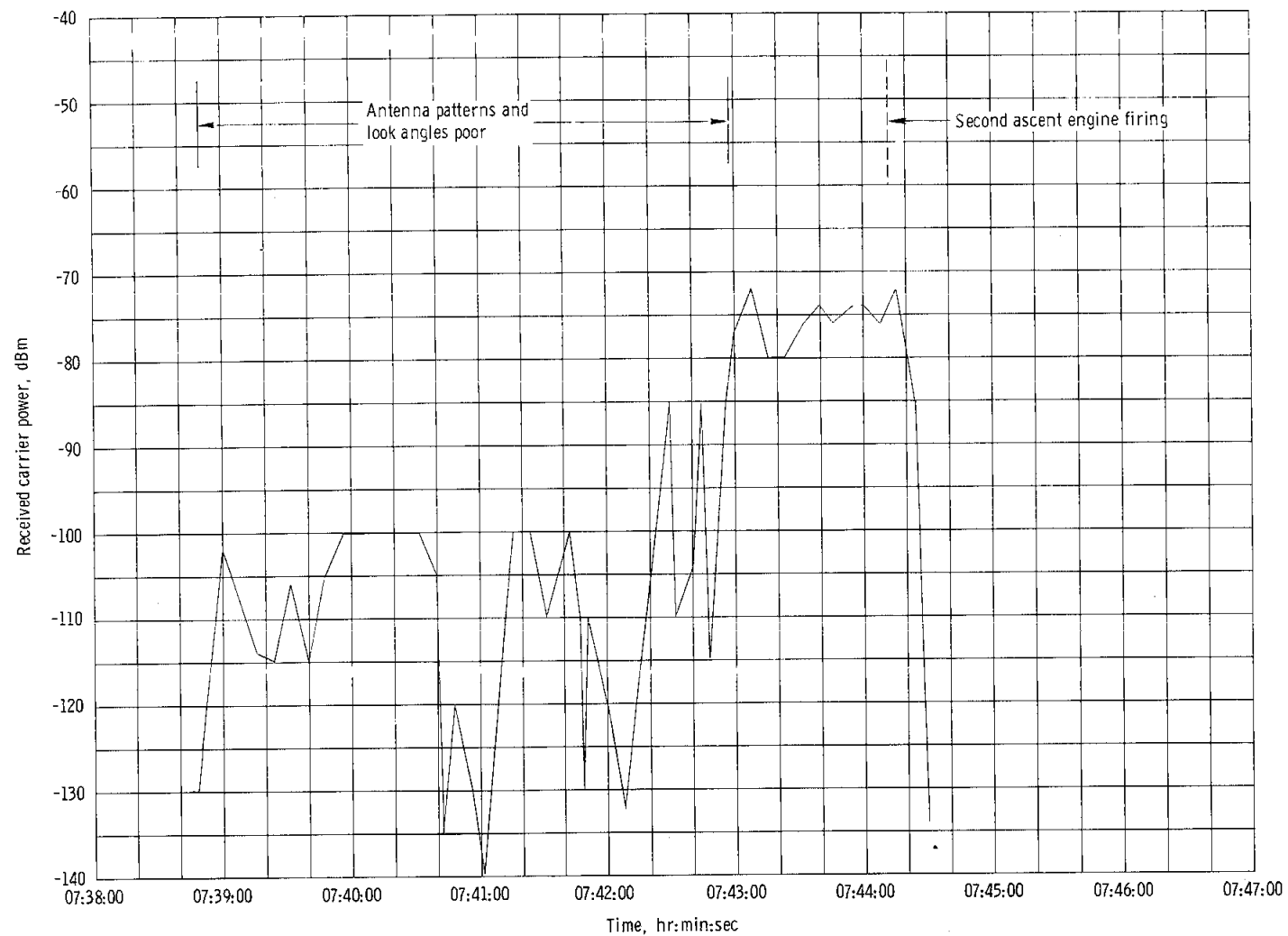


Figure 6.8-21. - Received unified S-band downlink carrier power, Hawaii, revolution 5.

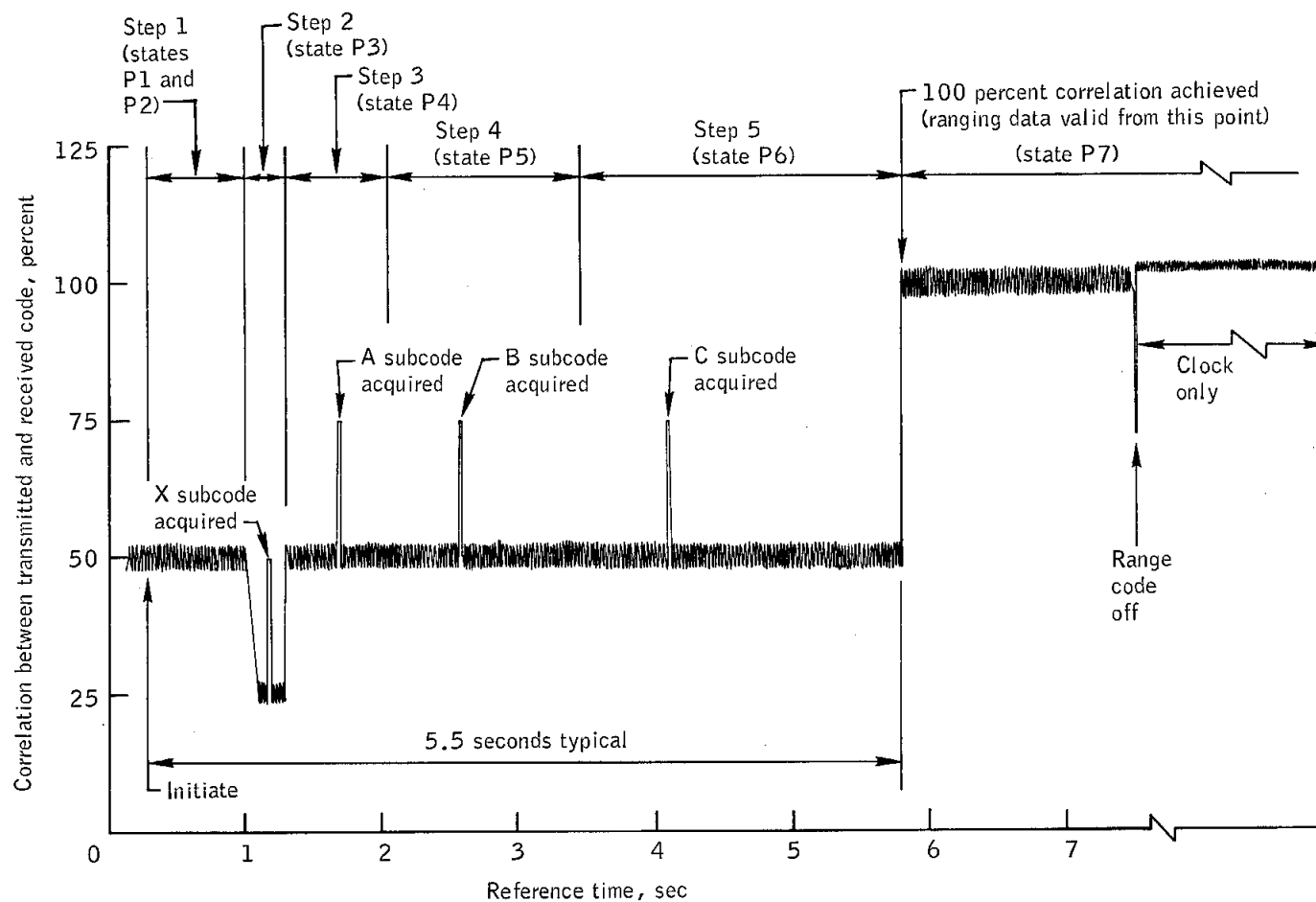
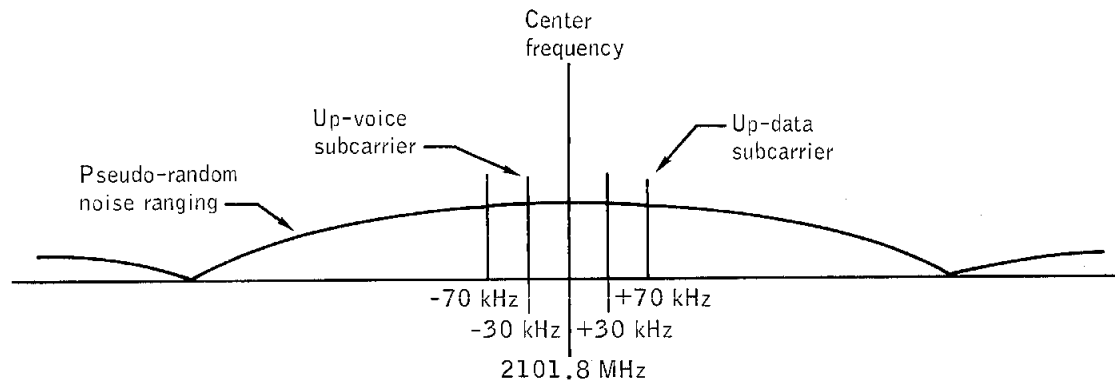
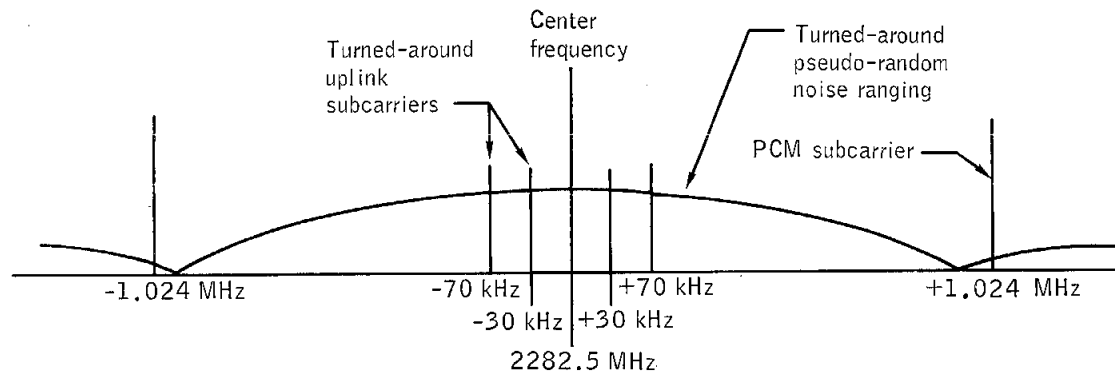


Figure 6.8-22.- Typical range code acquisition sequence (128 integrations per step).



(a) S-band uplink spectrum.



(b) S-band downlink spectrum.

Figure 6.8-23.- S-band RF spectrum.

NASA-S-68-1991

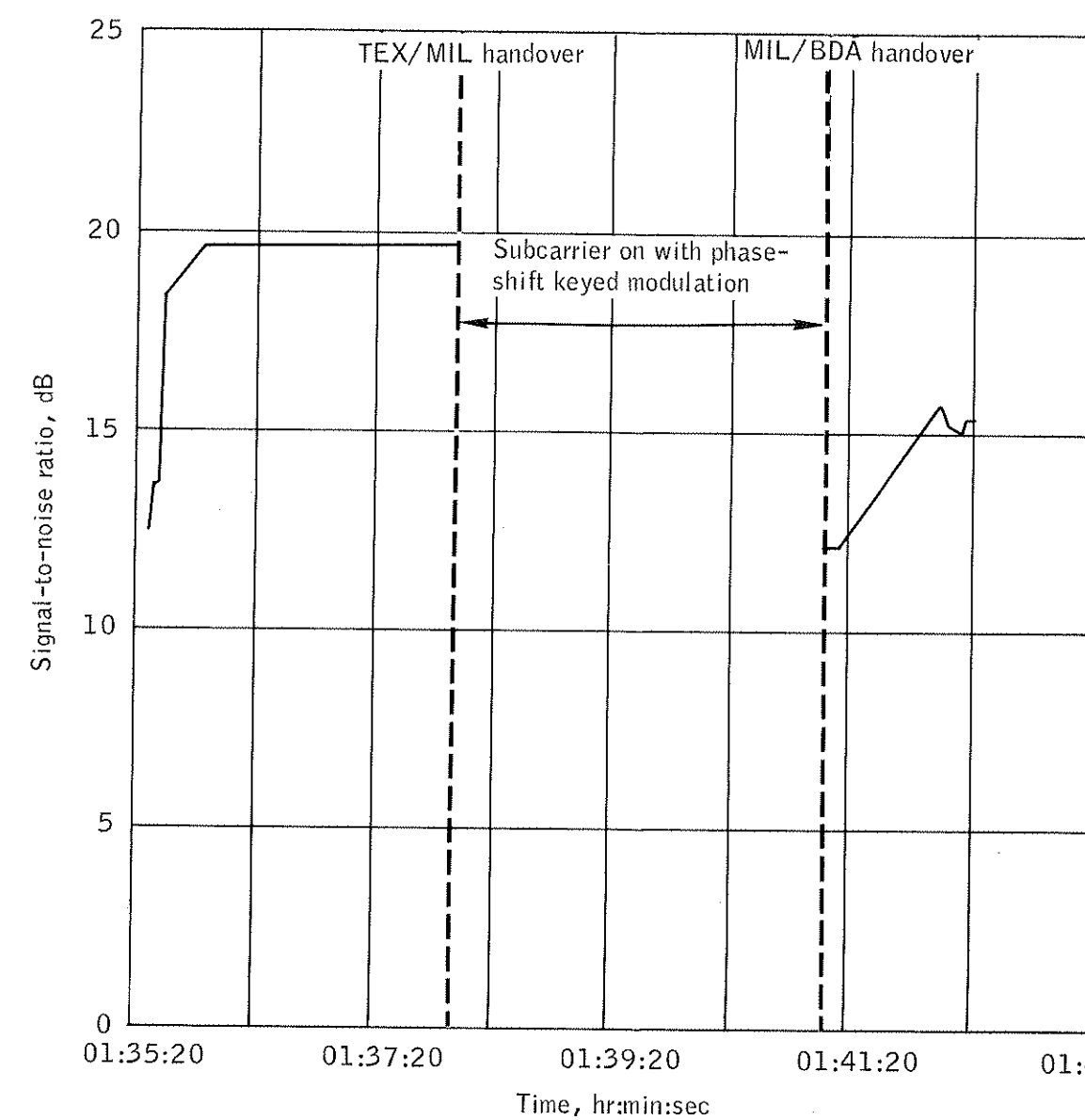


Figure 6.8-24.- Turned-around unified S-band up-data signal-to-noise ratio, MILA, revolution 1-2.

NASA-S-68-2092

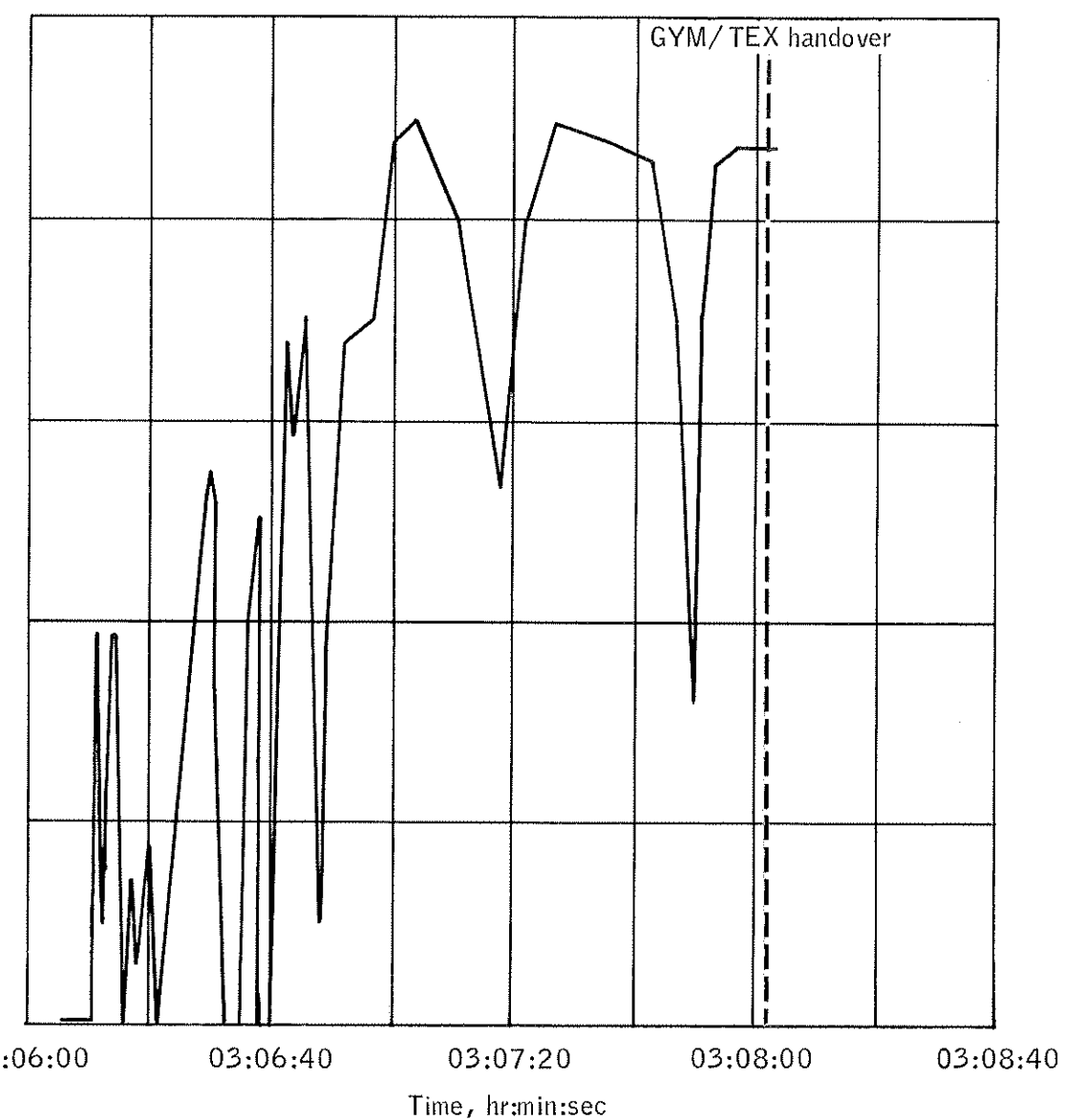


Figure 6.8-25.- Turned-around unified S-band up-voice signal-to-noise ratio, Guaymas, revolution 2.

NASA-S-68-2093

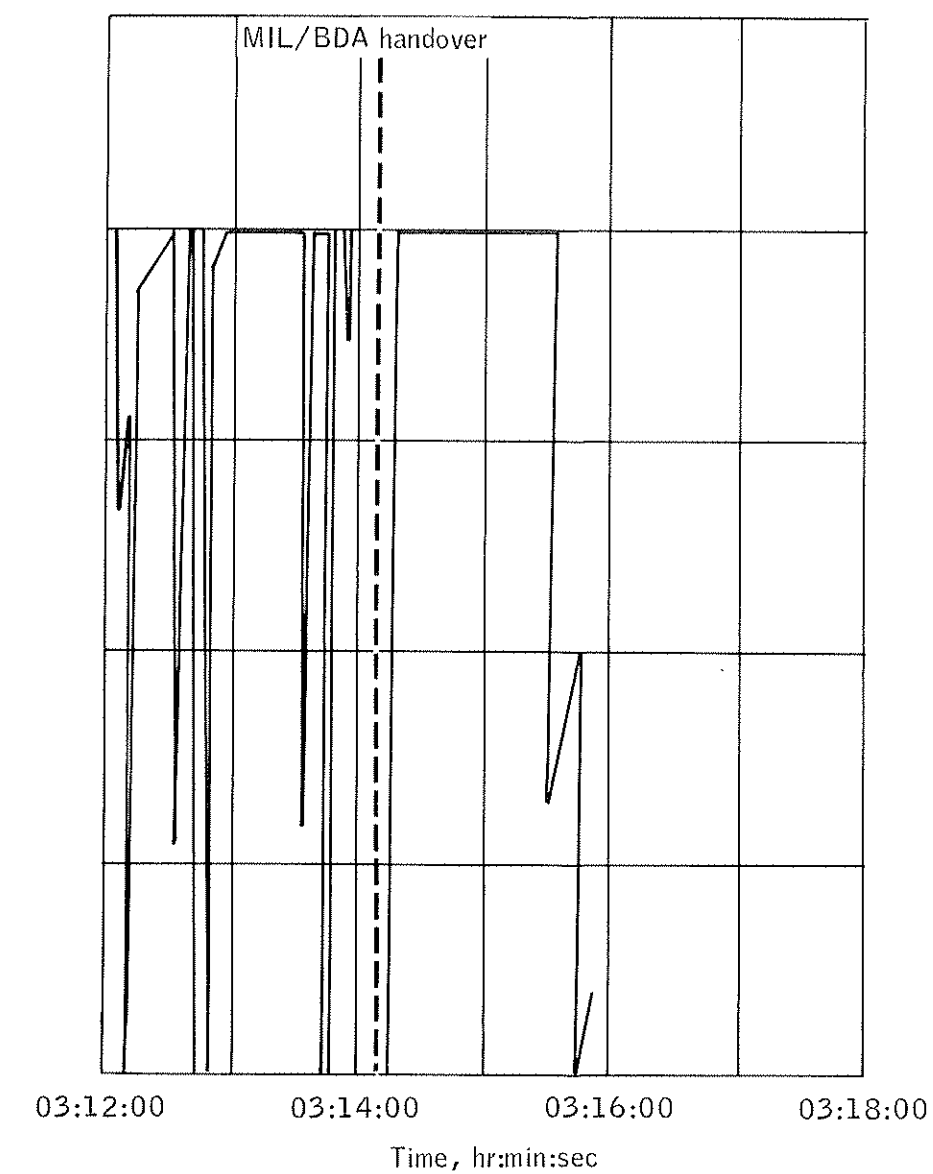


Figure 6.8-26.- Turned-around unified S-band up-voice signal-to-noise ratio, MILA, revolution 2-3.

NASA-S-68-1992

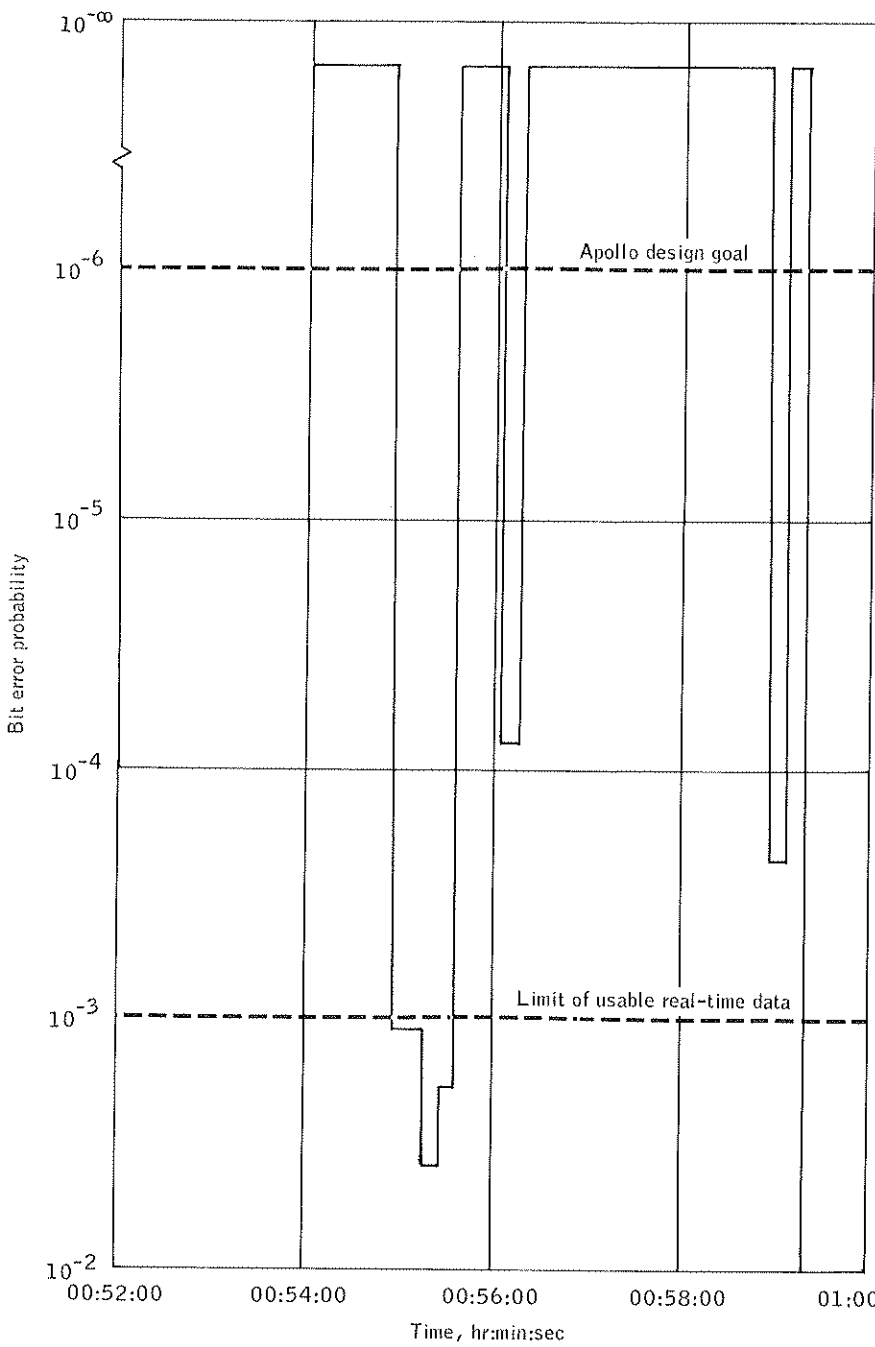


Figure 6.8-27.- Unified S-band PCM bit error probability, Carnarvon, revolution 1.

NASA-S-68-1993

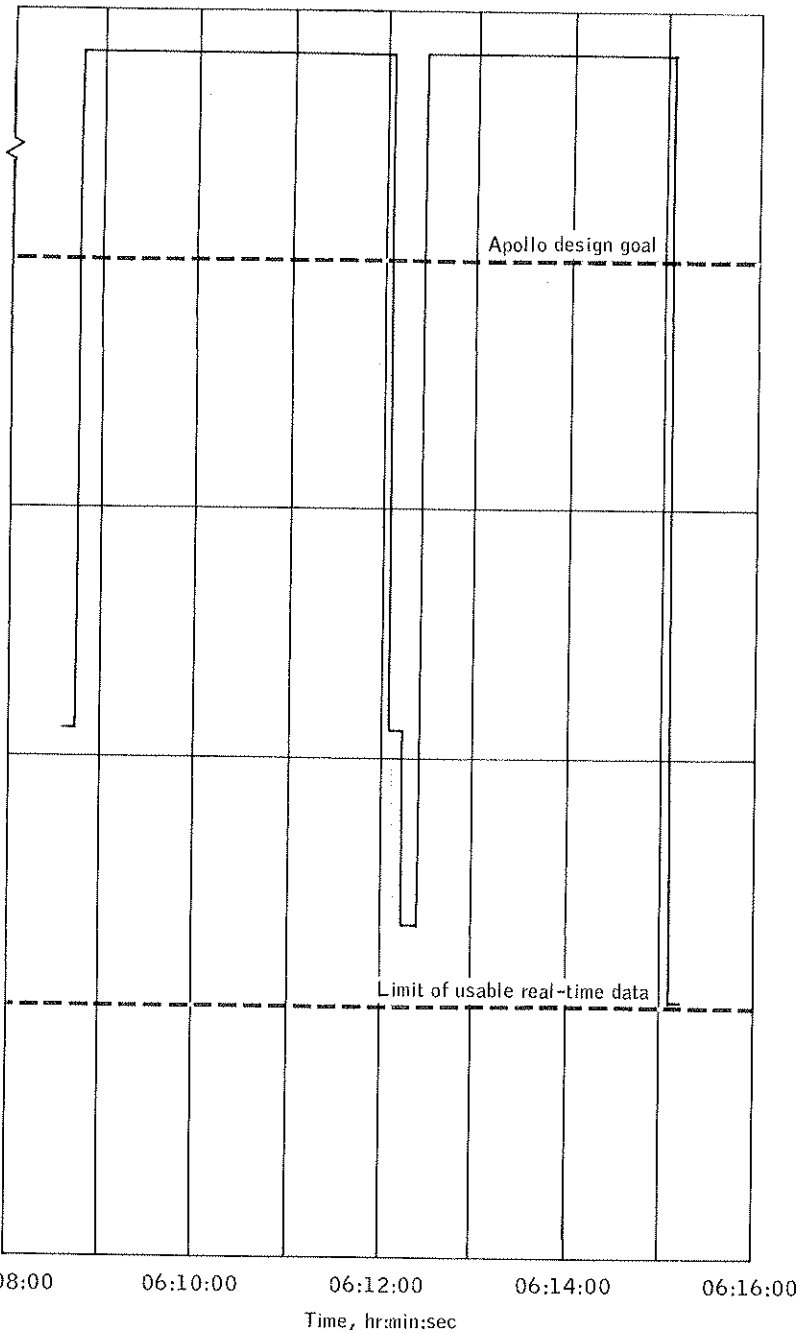


Figure 6.8-28.- Unified S-band bit error probability, Guaymas, revolution 4.

NASA-S-68-1994

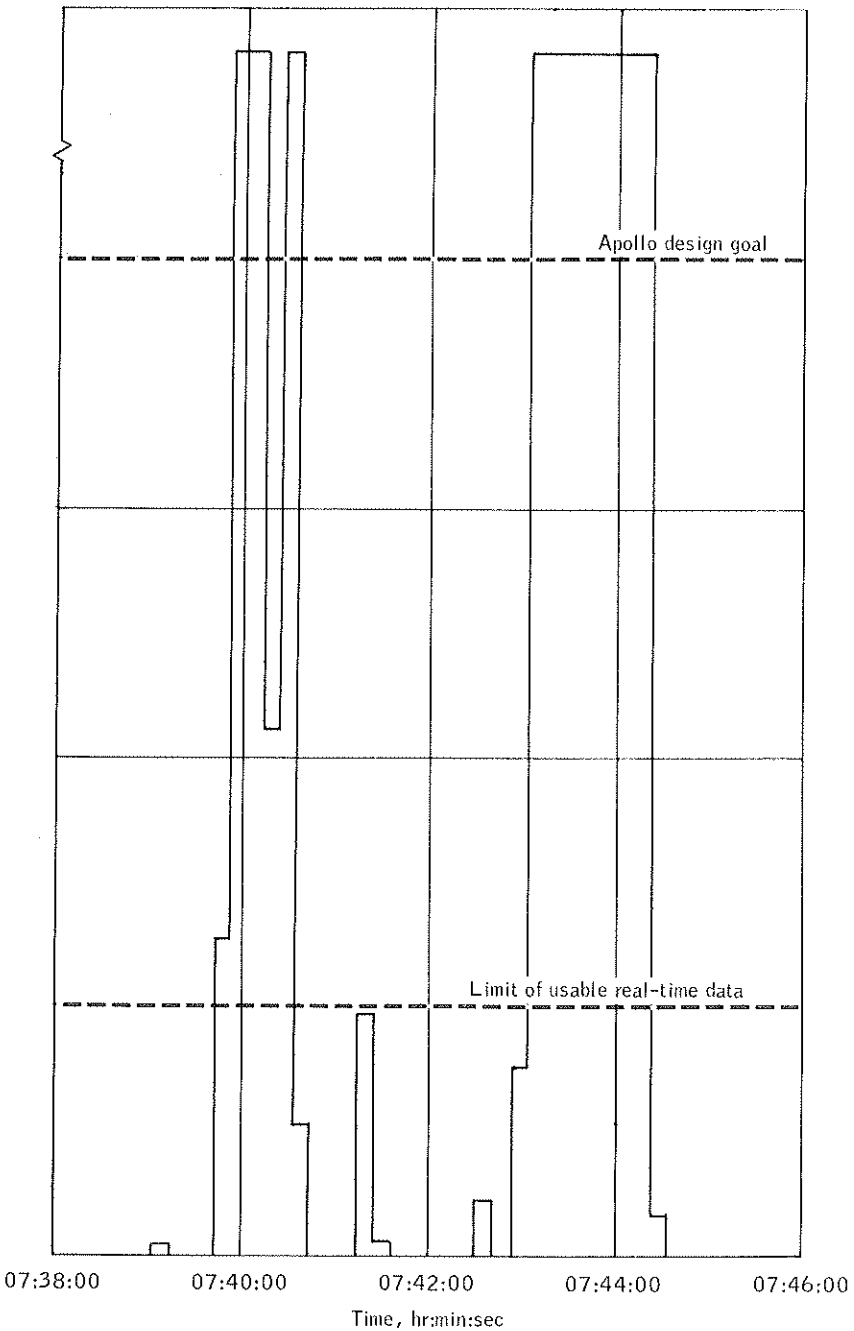


Figure 6.8-29.- Unified S-band PCM bit error probability, Hawaii, revolution 5.

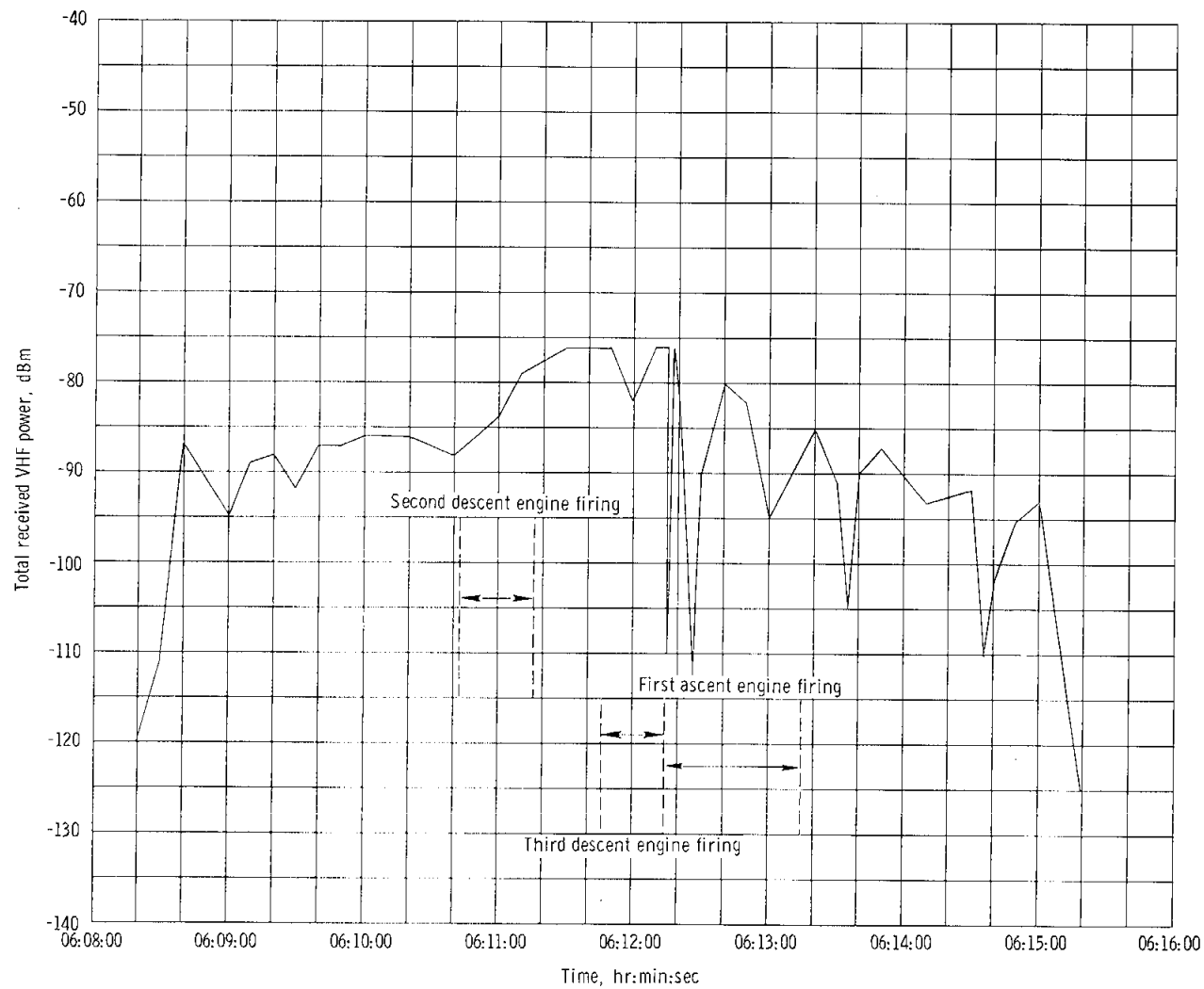


Figure 6.8-30. - Total received VHF power, Guaymas, revolution 4.

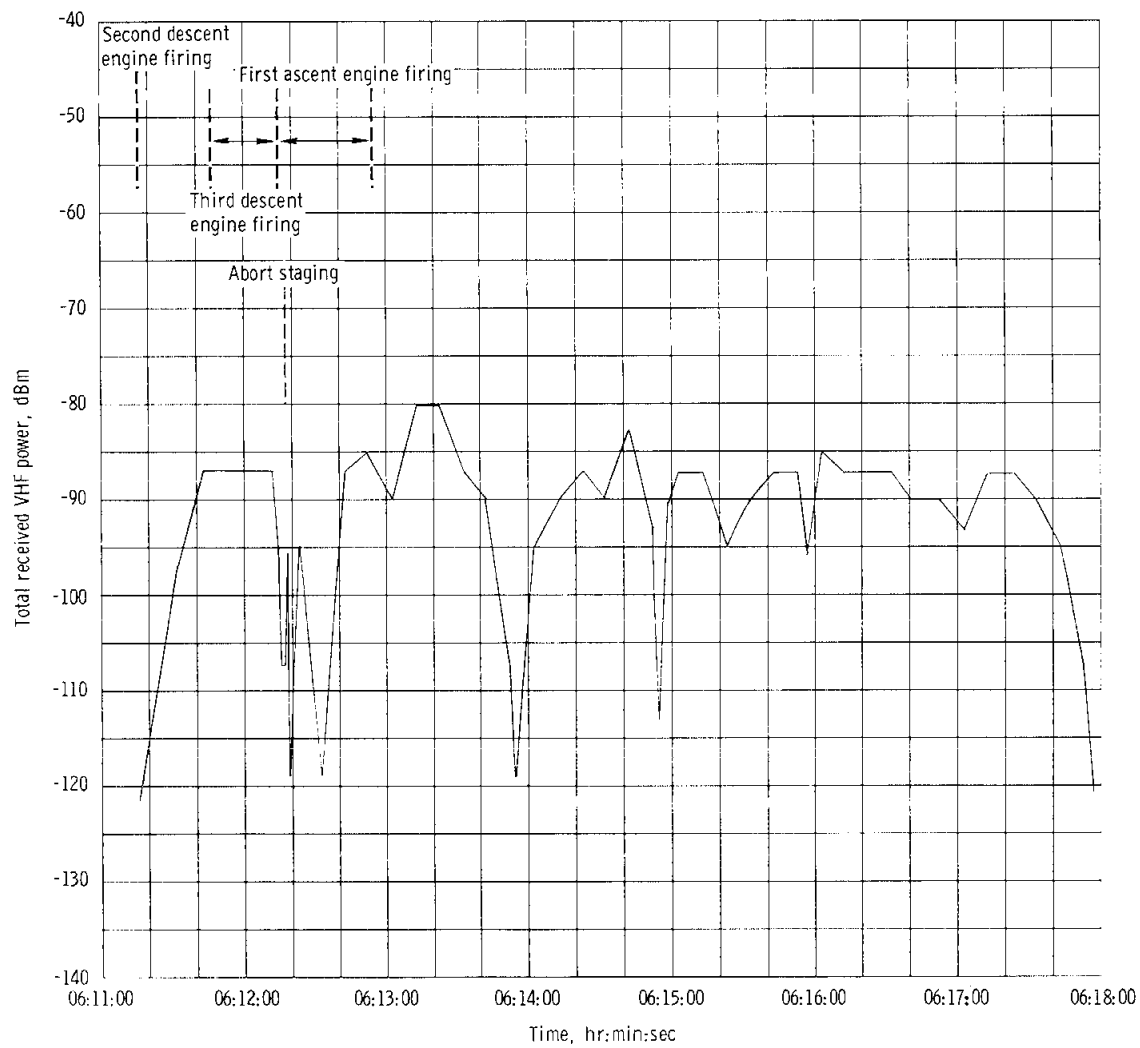


Figure 6.8-31. - Total received VHF power, Texas, revolution 4.

NASA-S-68-1997

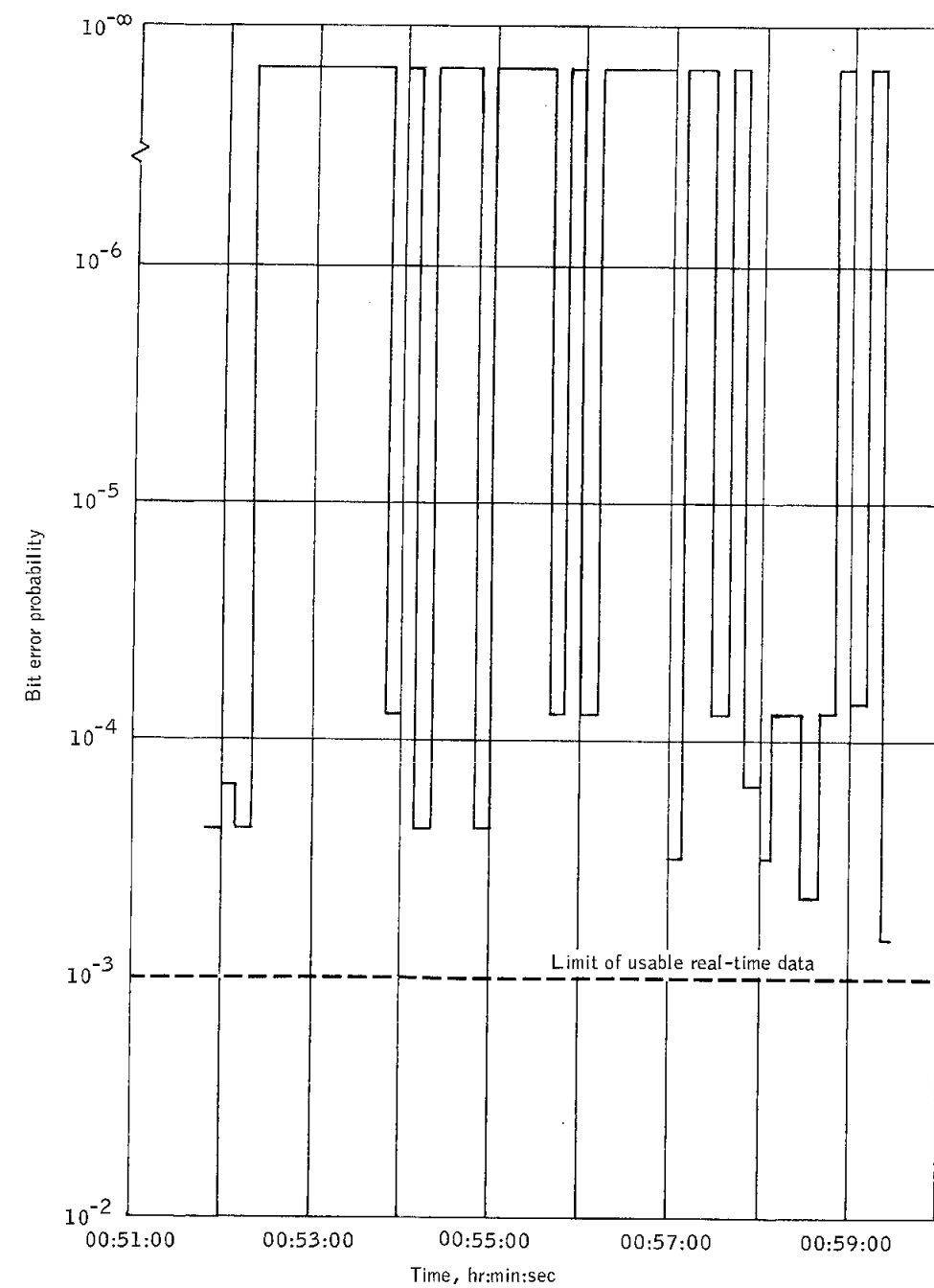


Figure 6.8-32.- VHF PCM bit error probability, Carnarvon, revolution 1.

NASA-S-68-1998

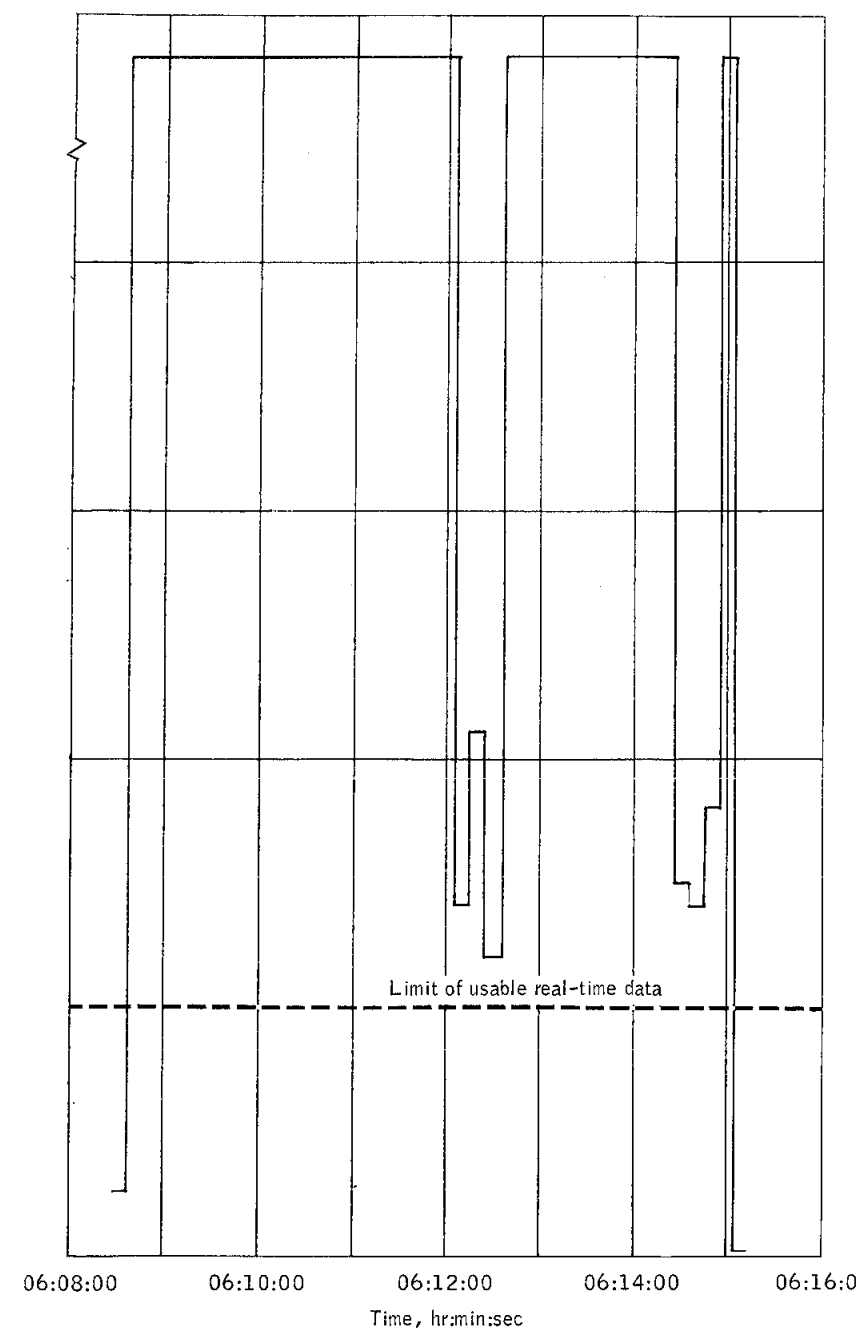


Figure 6.8-33.- VHF PCM bit error probability, Guaymas, revolution 4.

NASA-S-68-1999

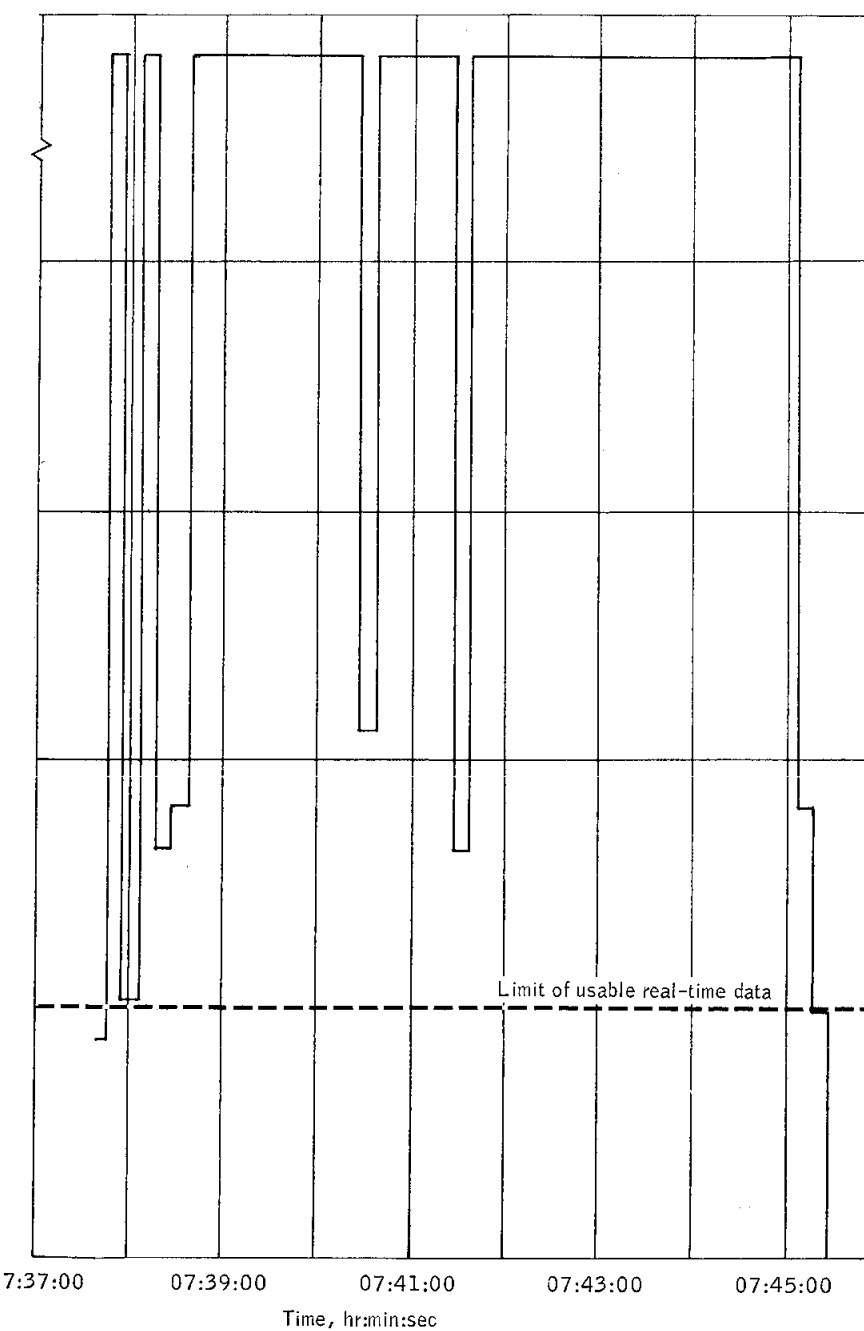


Figure 6.8-34.- VHF PCM bit error probability, Hawaii, revolution 5.

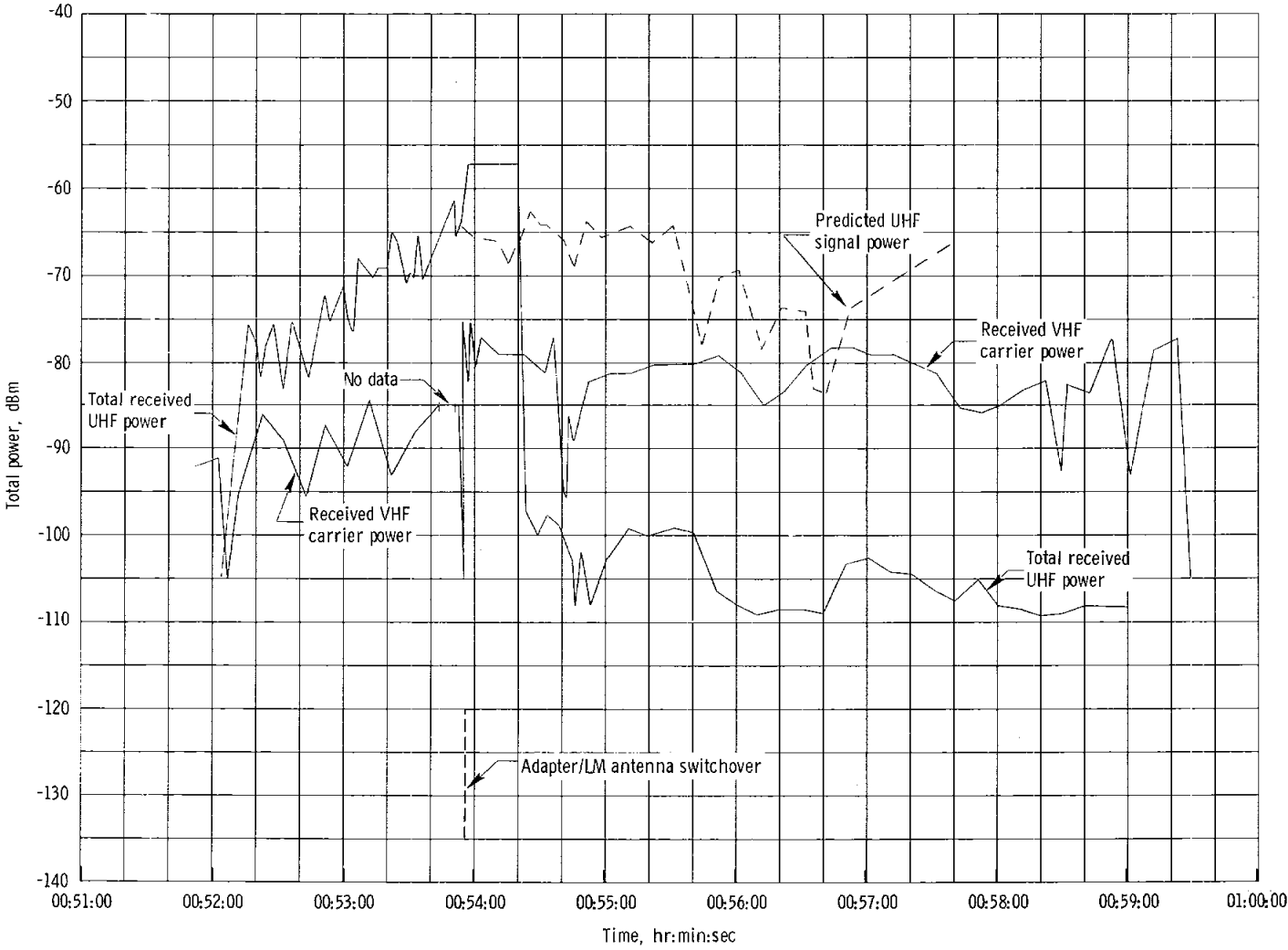


Figure 6.8-35. - Total received UHF and VHF power, Carnarvon, revolution 1.

6.9 RADAR

(This section is not applicable.)

6.10 GUIDANCE AND CONTROL

6.10.1 Summary

The primary guidance, navigation, and control system and the stabilization and control system functioned as designed throughout the mission. Navigation errors at insertion were commensurate with the system alignment errors existing at lift-off. LM/S-IVB stage separation, the maneuver to cold-soak attitude, the subsequent attitude hold, the maneuver to the attitude for the first descent engine firing and the initiation of the firing were all performed nominally by the primary system. The first descent engine firing was ended prematurely by the LM guidance computer because the descent engine thrust buildup did not meet the programmed velocity/time criteria. The subsequent attitude hold and ground commanded maneuver to the attitude for the second descent engine firing were also performed under primary system control. The second and third descent engine firings and the first ascent engine firing were performed by the stabilization and control system with mission programmer sequencing and were nominal for that system. Control was returned to the primary system after the first ascent engine firing, and an abnormal limit cycle occurred because the digital autopilot was configured for control of an unstaged vehicle. The second ascent engine firing was controlled by the stabilization and control system and the mission programmer with nominal results until control engine propellant depletion, when control authority was lost and the vehicle tumbled.

6.10.2 Integrated System Performance

Launch/S-IVB stage coast.- Prelaunch gyrocompassing was terminated and the inertial measurement unit was inertially fixed by the guidance computer at 00:00:00.86 when sensed acceleration exceeded 1.1g. The computer-determined lift-off was not noted on the ground; therefore, a backup command was sent at approximately 00:00:06. All guidance and control sequencing functions for this period were correct.

The body rate oscillations sensed in the spacecraft during launch remained less than ± 0.5 deg/sec. A comparison of spacecraft and launch vehicle gimbal angles for this phase indicates a maximum difference of 1.3 degrees during maximum dynamic pressure. The differences were within the uncertainties expected from initial misalignment, timing, and vehicle flexure. The guidance and control navigation errors at insertion, based on a comparison with the best estimate trajectory obtained using the S-IVB stage guidance system, are listed in table 6.10-I. Although the component errors are large, they are shown in section 6.10.3 to be caused primarily by prelaunch alignment errors purposely allowed to

meet a minimum perigee constraint for the second ascent engine firing. Total velocity at insertion agreed within 2 ft/sec. After sensing S-IVB stage shutdown, the guidance computer entered an idling mode until the programmed LM/S-IVB stage separation sequence was initiated.

LM/S-IVB stage separation.- The separation sequence of events controlled by the guidance computer is shown in figure 6.10-1. A +X translation began at 00:53:50.11. The best indication of physical separation was a telemetry noise transient at 00:53:55.24. This was substantiated by body rate and translational acceleration data. Figure 6.10-2 contains spacecraft dynamics for the separation. Rate transients were less than 0.2 deg/sec in all three axes, and attitude excursions were less than ± 1.2 degrees throughout the 20-second +X translation period. There was no indication of recontact between the two vehicles. The total velocity change during the separation sequence was 4.1 ft/sec. A detailed study of separation dynamics will be contained in supplement 6 to this report.

Cold-soak period.- Figure 6.10-2 also shows spacecraft dynamics and control engine firing commands during the maneuver to the cold-soak attitude. All parameters indicate nominal performance. Figure 6.10-3 compares the commanded gimbal angles with the actual gimbal angles during the maneuver. Nominal digital autopilot performance during the maneuver is indicated by the small difference between the actual and commanded values as shown in the figure. The divergence shown in the Z-axis prior to the maneuver was caused by residual rate in existence at the termination of the second +X translation when the attitude deadband was increased from ± 1 degree to ± 5 degrees.

After the attitude maneuver, the spacecraft entered a wide deadband attitude-hold period. Figure 6.10-4 contains a typical pattern of the control engine firing commands initiated by the digital autopilot. As shown by the occasional relatively long firings, an ideal minimum impulse limit cycle in pitch and roll did not occur. Figure 6.10-5 shows one pass through the pitch and roll body-rate/body-attitude phase plane and indicates unsymmetrical operation with the long firings occurring at each side of the attitude deadband. This phenomenon was experienced in pre-flight software verification runs and occurred whenever the pitch and roll attitude errors were phased such that large errors occurred in both axes simultaneously. The digital autopilots for LM-3 and subsequent spacecraft will incorporate logic to prevent this type of operation. Detailed analysis of limit cycle operation will be published in supplement 4.

First descent engine firing.- The maneuver to first firing attitude was calculated by the computer based on the onboard state vector and targeting parameters and was automatically performed under digital autopilot control. The maneuver dynamics are represented in figure 6.10-6,

and the gimbal angle comparisons are shown in figure 6.10-7. Performance was nominal.

All events leading up to and including the issuance of the "engine on" command by the computer were proper. However, the computer commanded the engine "off" 4.17 seconds later because the descent engine failed to meet the programmed velocity/time criteria. See section 12.2 for a more detailed discussion.

Coast between first and second descent engine firings.- The descent engine shutdown sequence initiated a wide deadband attitude-hold period controlled by the digital autopilot at the first firing attitude. The typical limit cycle was unsymmetrical but differed from that during the cold-soak period. The pitch and roll axes were uncoupled and all firings were near minimum impulse duration in all three axes. The asymmetry experienced is typical of that caused by an external disturbance torque.

The maneuver to the second descent engine firing attitude was initiated by a series of ground commands and was controlled by the digital autopilot (see figures 6.10-8 and 6.10-9). Response was nominal.

Second descent engine firing through abort staging.- The stabilization and control system was selected at 06:06:11.7 by ground command. Because the abort guidance system was not installed, the subsequent maneuvers were performed without closed-loop guidance or attitude control. Only rate damping was available with sequencing provided by the mission programmer.

Figures 6.10-10 and 6.10-11 contain time histories of pertinent parameters covering the following events.

- a. Three +X translations prior to the second descent engine firing
- b. Second descent engine firing, 10-percent throttle
- c. Second descent engine firing, full throttle
- d. One +X translation prior to the third descent engine firing
- e. Third descent engine firing, 10-percent throttle
- f. Third descent engine firing, full throttle
- g. Staging dynamics
- h. First ascent engine firing

Table 6.10-II contains selected performance characteristics extracted from figures 6.10-10 and 6.10-11.

The control engine duty cycle was higher in each case during the +X translations preceding the descent engine firings than it was after ignition, indicating that the disturbance torque due to center-of-gravity offset was greater than that due to thrust vector misalignment. Body rates remained close to the deadbands during all the firings with a substantial control margin. One second before the end of the second +X translation, the descent engine was armed, enabling the engine gimbal drive actuators to drive in response to the +X translation disturbance torque. Each time the actuators drove, the ac voltage fluctuated as shown in figure 6.10-10. This figure and table 6.10-II show that the direction of actuator motion reversed after ignition and indicate that the activity during the +X translation introduced an out-of-trim condition. The trimming action during the 10-percent-throttle period reduced the thrust-vector/center-of-gravity offset to an acceptable level before the increase to full throttle; consequently, the resulting disturbance torques were well within the control engine capability. It would be possible to exceed the available control authority at full throttle if a large thrust-vector/center-of-gravity offset was introduced during the +X translation, and an insufficient time at 10-percent throttle was allowed to trim the engine. Measures are being taken to prevent this problem from occurring on future missions.

Figure 6.10-12 is an expanded plot of spacecraft dynamics during the staging sequence. The only significant rate disturbances occurred simultaneously with the ascent engine peak chamber pressure. The rate disturbances of +7.7, +2.0, and -0.8 deg/sec in pitch, roll, and yaw, respectively, converged to deadband values of -0.8, -1.2, and -0.8 deg/sec within 2 seconds and remained within these values throughout the firing. The disturbances predicted from preflight simulations were -1.5 deg/sec in pitch and +3.5 deg/sec in roll. The significance of the simulation was that the rates experienced were of the same order of magnitude as the predictions.

The descent engine thrust during 10-percent throttle was 1221 pounds as determined from the inertial measurement unit accelerometers, which compares reasonably well with 1180 pounds as determined from the thrust chamber pressure. The ascent engine thrust was 3551 pounds based on the accelerometers and 3480 pounds based on the chamber pressure. Dynamics of the staging event are discussed in section 6.17.

Coast period between the first and second ascent engine firings.-
Mission programmer sequence III was interrupted after the ascent engine shutdown, and spacecraft attitude control was returned to the digital autopilot. High-rate limit cycle operation occurred immediately, causing excessive propellant usage. This abnormal performance occurred because the digital autopilot was still configured for control of an unstaged vehicle. The moments of inertia and predicted angular accelerations used by the digital autopilot to compute control engine "on" times are calculated based on the current value of vehicle mass contained in the

computer erasable memory. For this mission, the current value of mass (and, therefore, inertia and acceleration) was to be periodically updated during descent and ascent engine operation and automatically reinitialized at staging. Because of the premature shutdown of the first descent engine firing, the computer entered an idling mode and the mass update process did not occur during the second and third descent engine firings and the staging sequence. Therefore, the control engine "on" times computed by the digital autopilot for a given rate and attitude error were to correct an unstaged, fully loaded vehicle. The result was rapid oscillations of the vehicle as the digital autopilot overcontrolled in an attempt to keep attitudes within deadband limits. (See section 12.2 for further discussion.) The oscillations and resultant propellant usage have been reproduced in simulations.

Second ascent engine firing.- A time history of spacecraft dynamics for the second ascent engine firing is contained in figure 6.10-13. Immediately after switching from the primary to the backup system, the body rates converged to near zero in all axes and remained there until the start of +X translation. About 6.6 seconds after the start of the +X translation, a high-rate limit cycle began in the pitch axis and continued until engine start. This high-rate limit cycle was caused by nonlinearities in the pulse ratio modulation circuits in the stabilization and control system. The possibility of experiencing this type of operation during +X translation with a light, staged vehicle was predicted based on hybrid simulation runs. A design change to the pulse ratio modulation circuits has been approved which will prevent this phenomenon.

Rate damping during the ascent engine firing was nominal although the 4-up control engine had failed, and rates in all three axes held near the deadbands. A second +X translation (fig. 6.10-13) occurred 58.6 seconds after engine ignition. This was caused by the mission programmer sequence V, which included two ascent engine firings, each preceded by a +X translation. Because an engine start override ground command was sent after the first ignition, only one firing occurred. The second +X translation, therefore, occurred while the engine was on. Further, sequence V called for closing the propellant interconnect valves. The rates began to diverge and the vehicle began to tumble when the control propellant was depleted (see fig. 6.10-13). Rates in all axes periodically exceeded the rate gyro instrumentation saturation level of ± 25 deg/sec. Gimbal lock occurred at approximately 07:47:30, as verified by the gimbal lock alarm.

6.10.3 Primary Guidance, Navigation, and Control System Performance

The inertial measurement unit and associated electronics performed properly throughout the mission. Preflight test history for the inertial rate integrating gyros and the pulse integrating pendulous accelerometers

is contained in figure 6.10-14. The values used to compute inflight compensation and the compensation values are indicated on the figure. The affect of drift due to acceleration along the gyro output axis (ADOA), which is not compensated explicitly, was removed by correcting the null bias drift (NBD) and drift due to acceleration along the spin reference axis (ADSRA) terms. The compensation value for drift due to acceleration along the input axis (ADIA) was not corrected for ADOA because of the ADIA measurement uncertainty and the relative insignificance of the ADOA values.

The final series of prelaunch inertial measurement unit performance tests showed erratic behavior and large shifts in the ADIA X coefficient. Because of the uncertainties involved in measuring ADIA while the inertial measurement unit is installed in the spacecraft and because preflight dispersion analyses for this mission showed the minimum perigee constraint for the second ascent engine firing to be very sensitive to negative ADIA X errors, the compensation value chosen was close to the most negative excursion measured.

The prelaunch alignment orientation of the inertial measurement unit is shown in figure 6.10-15. The orientation was chosen, for this mission only, to avoid exceeding the 3.26g acceleration limit of the accelerometers during boost and to avoid the possibility of gimbal lock during the planned out-of-plane propulsion maneuvers. The inertial measurement unit will be powered-down during launch on subsequent missions. The maximum acceleration noted was approximately 3.11g in the Y axis at 00:02:18.8.

Figure 6.10-16 contains a comparison of velocity time histories during the launch phase computed by the primary guidance, navigation, and control system; by the S-IVB instrument-unit guidance system, and from the ground tracking network.

The instrument-unit and Glotrac data agreed within 1 ft/sec and, therefore, were used as the standard for this preliminary analysis. The guidance errors were larger than normally expected but are attributed largely to the inertial measurement unit misalignment at lift-off. The biased ADIA X compensation, which caused an effective drift, propagated through the prelaunch gyrocompassing loop into alignment errors in all three inertial measurement unit axes. The shape of the error propagation in all three axes is characteristic of a misalignment which causes the accelerometers to sense a disproportionate level of acceleration.

Table 6.10-III contains a preliminary set of error coefficients. The accelerometer bias errors shown are the average of three inflight bias measurements made during three quiescent coast periods with minimal control engine activity (see table 6.10-IV).

The residual velocity errors after compensating for the preliminary set of errors are contained in figure 6.10-16. It should be emphasized that the error coefficients shown are preliminary and subject to revision in the final inertial measurement unit analysis, which will be issued as supplement 5 to this report.

All inertial system temperatures and voltages remained within limits throughout the flight. The vibration levels measured at the navigation base are discussed in section 6.1.2.

The guidance computer performed as designed throughout the mission. Table 6.10-V lists the major modes used. All sequencing, including mission programmer commands, was as planned up to the premature descent engine shutdown and was nominal throughout the mission. No restarts were noted nor were any rejections of ground updates experienced.

6.10.4 Stabilization and Control System Performance

Performance of the stabilization and control system, consisting of the control electronics section, was nominal throughout the mission. The system gains and thresholds derivable from telemetry have been compared with preflight values. All values were correct within the calculation accuracy allowed by the telemetered data. Different time lags were noted for various pulse ratio modulator channels when two or more control engines were commanded on or off simultaneously. The lags were consistent throughout and were expected.

6.10-8

TABLE 6.10-I.- STATE VECTOR COMPARISON AT 00:10:00.86
IN LM-1 INERTIAL COORDINATE SYSTEM

Position	Spacecraft guidance	S-IVB/instrument unit best estimate trajectory
P _X , ft	15 294 214	15 260 716
P _Y , ft	14 185 672	14 248 462
P _Z , ft	4 948 702	4 887 572
Velocity		
V _X , ft/sec	-15 249.6	-15 370.1
V _Y , ft/sec	10 122.6	10 367.6
V _Z , ft/sec	18 015.3	17 774.4
V _{total} , ft/sec	25 682.0	25 683.8

TABLE 6.10-II.- PERFORMANCE CHARACTERISTICS DURING MISSION PROGRAMMER SEQUENCE III

Time, hr:min:sec	Event	Accumulated velocity change, ft/sec	Moment unbalance		Gimbal drive actuator			
			Pitch, ft-lb	Roll, ft-lb	Direction of motion	Pitch position, in.	Direction of motion	Roll position, in.
06:06:12	Select backup control path	0.0	-	-	N/A	-	N/A	-
06:10:07	+X translation on	0.0	+128	-108	N/A	0.103R	N/A	0.719R
06:10:18	+X translation off	2.9			N/A	0.103R	N/A	0.719R
06:10:22	+X translation on	2.9	+128	-108	N/A	0.103R	N/A	0.719R
06:10:27	+X translation off	4.4			Extend	0.040R	None	0.719R
06:10:33	+X translation on	4.4	+128	-108	Extend	0.040R	Extend	0.710R
06:10:42	Command 10 percent throttle	-	+115	-86	Extend	0.198E	None	0.672R
06:10:46	+X translation off	12.0	+48	+32	Retract	0.308E	None	0.672R
06:11:08	Command full throttle	38.0	-410	+250	Retract	0.055E	Retract	0.672R
06:11:15	Descent engine off	108.4			-	0.277R	-	0.909R
06:11:38	+X translation on	108.4	+145	-110	Extend	0.277R	Extend	0.909R
06:11:47	Command 10 percent throttle	-	+138	-109	Extend	0.055R	Extend	0.862R
06:11:51	+X translation off	111.4	-31	-10	Retract	0.087E	None	0.814R
06:12:13	Command full throttle	144.0	-340	-10	Retract	0.008E	Retract	0.813R
06:12:14	Descent engine off	160.0	-	-	-	0.150R	-	0.846R
06:12:15	Ascent engine on	168.0	-50	-203	N/A	-	N/A	-
06:13:14	Ascent engine off	855.0			-	-	-	-

R = retract
E = extend

TABLE 6.10-III.- PRELIMINARY INERTIAL MEASUREMENT UNIT

ERROR SOURCES

Error source	Magnitude	Specification	Comment
X bias, cm/sec ² . . .	-0.046	0.20	Derived from inflight bias measurement
Y bias, cm/sec ² . . .	-0.137	0.20	
Z bias, cm/sec ² . . .	-0.101	0.20	
YXMSL, arc sec . . .	10	20	Measured values from factory test
YZMSL, arc sec . . .	-4	20	
ZYMSL, arc sec . . .	-20	20	
X ADOA, mERU/g . . .	+2.3	N/A	Mean of preflight calibrations
Y ADOA, mERU/g . . .	+1.2	N/A	
Z ADOA, mERU/g . . .	+2.3	N/A	
X ADIA, mERU/g . . .	36.7	8	Approximately 30 mERU/g prelaunch offset

__MSL - accelerometer misalignment of the first axis toward the second

ADOA - drift due to acceleration along the output axis

ADIA - drift due to acceleration along the input axis

TABLE 6.10-IV.- INFLIGHT BIAS COMPUTATION

	X bias, cm/sec ²	Y bias, cm/sec ²	Z bias, cm/sec ²	Total time, sec
Carnarvon, passes 1, 2, and 3 (two revolutions)	0.094	0.358	0.019	10 994
Rose Knot Victor, passes 1 and 2 (one revolution)	0.093	-0.357	0.019	5 935
Merritt Island, passes 1/2 and 2/3 (one revolution)	0.095	-0.356	0.019	5 994
Mean	0.094	-0.357	0.019	
Compensation	0.140	-0.220	0.120	
Preflight mean	0.151	-0.258	0.120	
Bias error	-0.046	-0.137	-0.101	

TABLE 6.10-v.- LM-1 MAJOR MODE TIMELINE

Major mode	Program description	Program initiation time, hr:min:sec*
P-02	Prelaunch gyrocompassing	-00:02:09.1
P-04	Terminate gyrocompassing	-00:00:00.1
P-11	Pre launch escape tower jettison boost monitor	00:00:00.9
P-12	Post launch escape tower jettison boost monitor	00:02:38.9
P-13	Coast with S-IVB attached	00:09:56.9
P-00	Guidance computer idling	00:21:54.9
P-14	S-IVB/LM separation	00:49:52.6
P-00	Guidance computer idling	00:54:09.9
P-15	Cold-soak attitude maneuver	00:54:16.7
P-00	Guidance computer idling	00:56:46.7
P-27	Ground command update	No data
P-00	Guidance computer idling	01:35:36.9
P-27	Ground command update	01:37:35.9
P-00	Guidance computer idling	01:38:19.9
P-31	Pre descent engine first firing	01:55:03.7
P-41	Descent engine first firing	03:58:34.9
P-00	Guidance computer idling	03:59:46.9
P-27	Ground command update	05:34:07.9
P-00	Guidance computer idling	05:35:01.9
P-27	Ground command update	06:25:03.9
P-00	Guidance computer idling	06:25:59.9
P-27	Ground command update	07:11:30.9
P-00	Guidance computer idling	07:12:24.9
P-27	Ground command update	07:13:23.9
P-00	Guidance computer idling	07:14:06.9

*Program initiation times are not corrected for word position in the 2-second downlist.

NASA-S-68- 2001

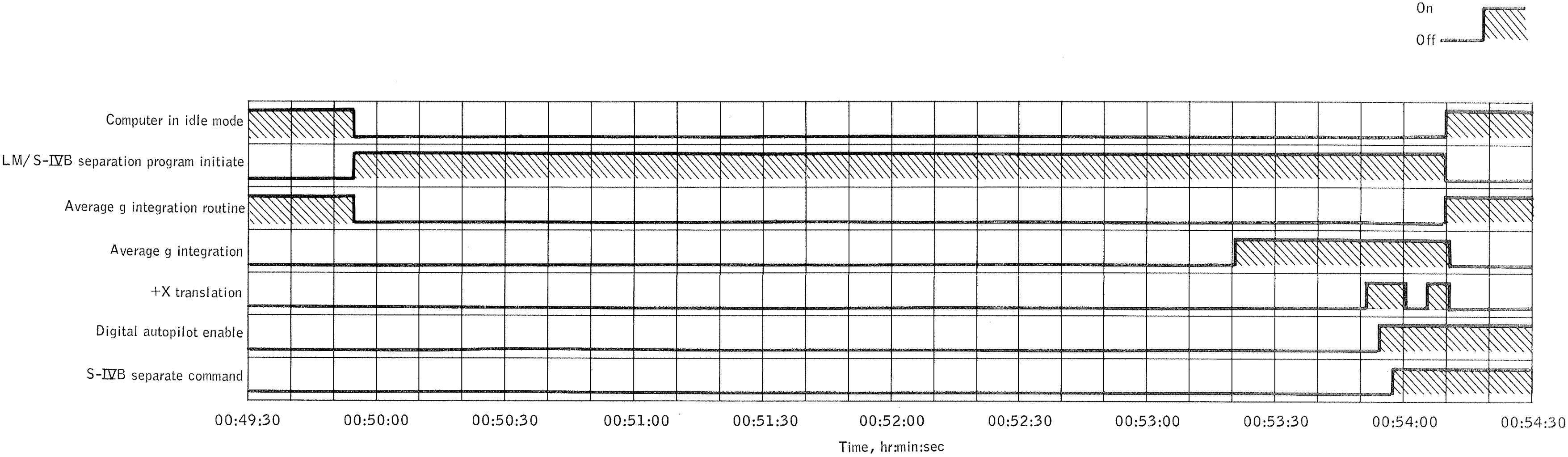


Figure 6.10-1.- LM/S-IVB stage separation sequence of events.

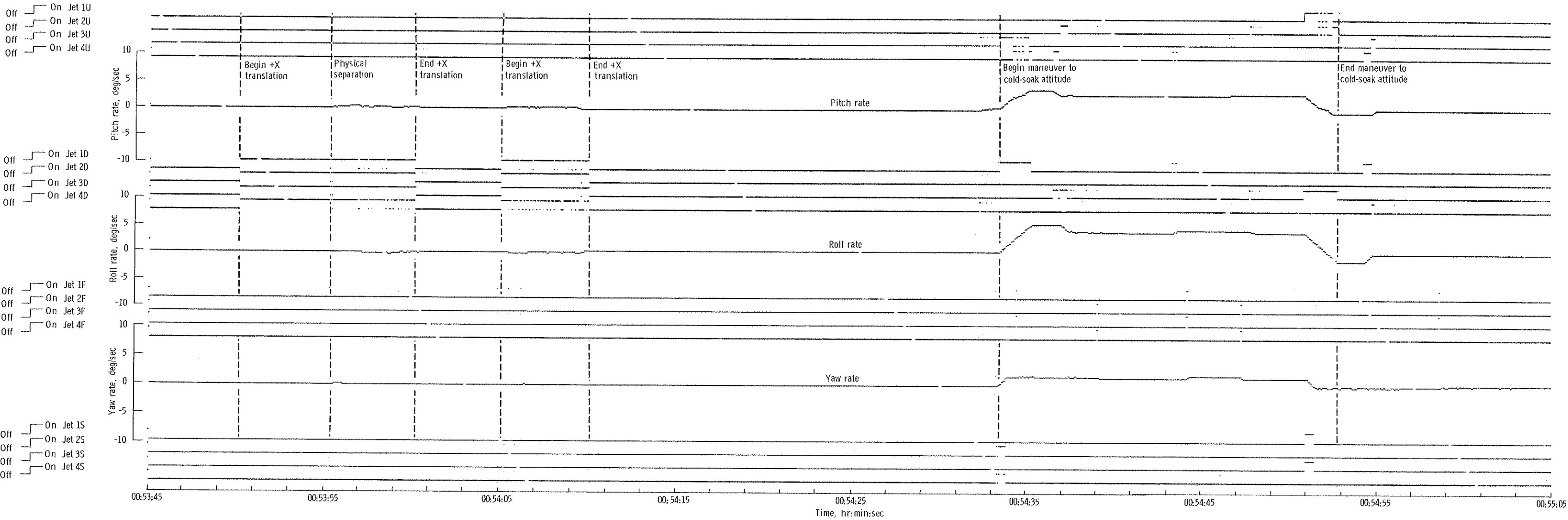


Figure 6.10-2. - Spacecraft dynamics - separation and maneuver to cold-soak attitude.

NASA-S-68-2003

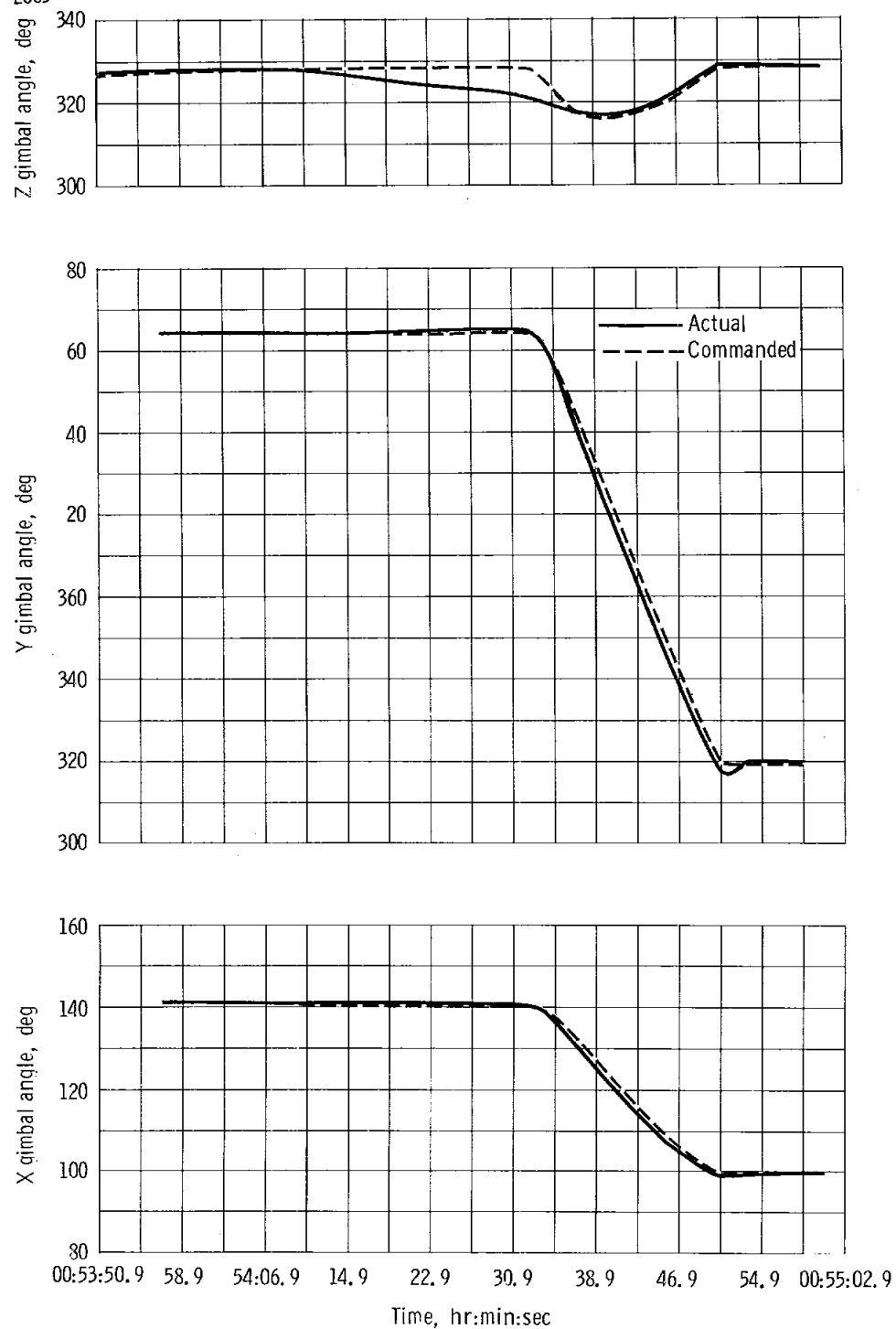


Figure 6.10-3. - Gimbal angle comparison - maneuver to cold-soak attitude.

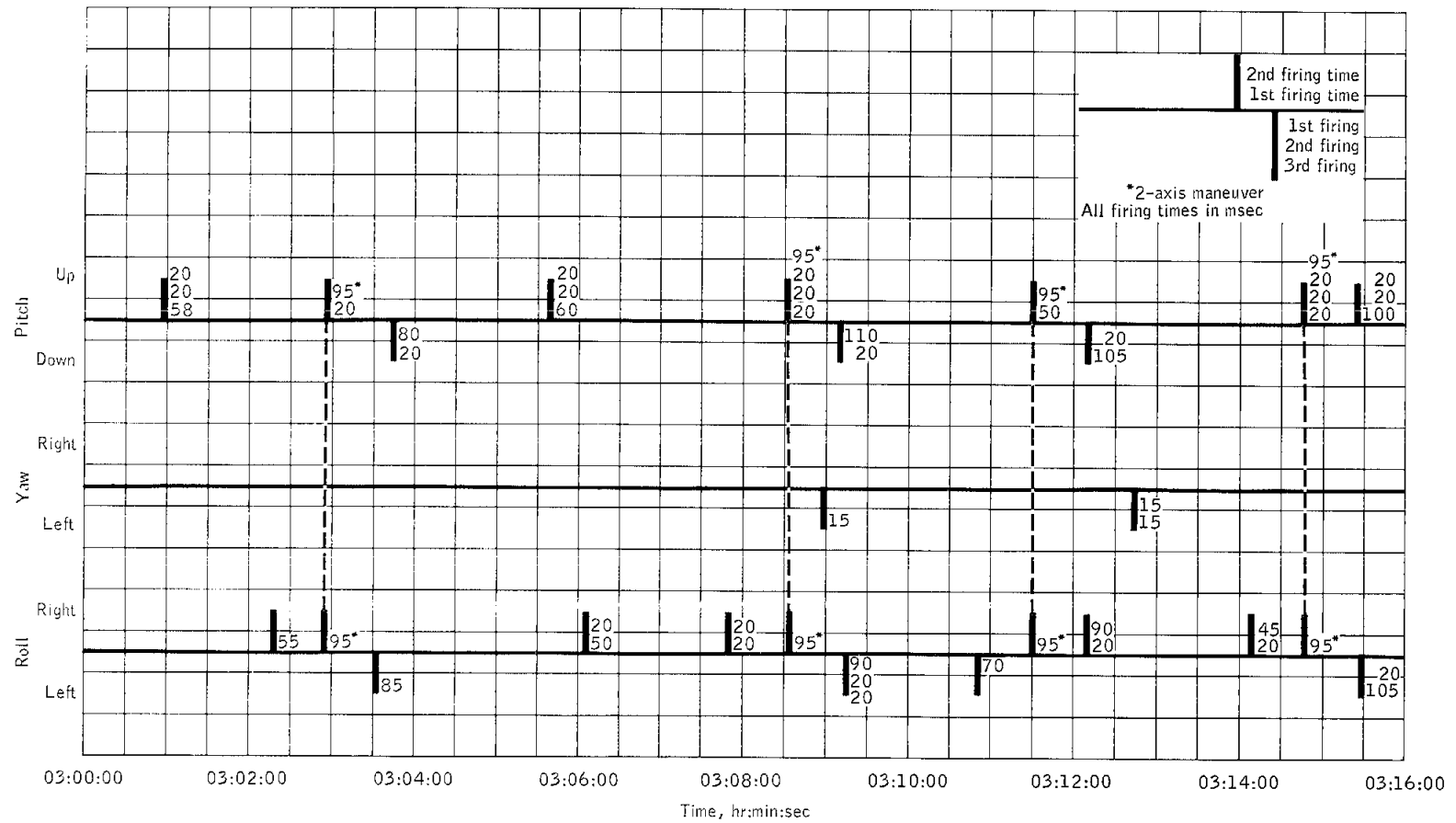


Figure 6.10-4.- Typical limit cycle during cold-soak attitude hold.

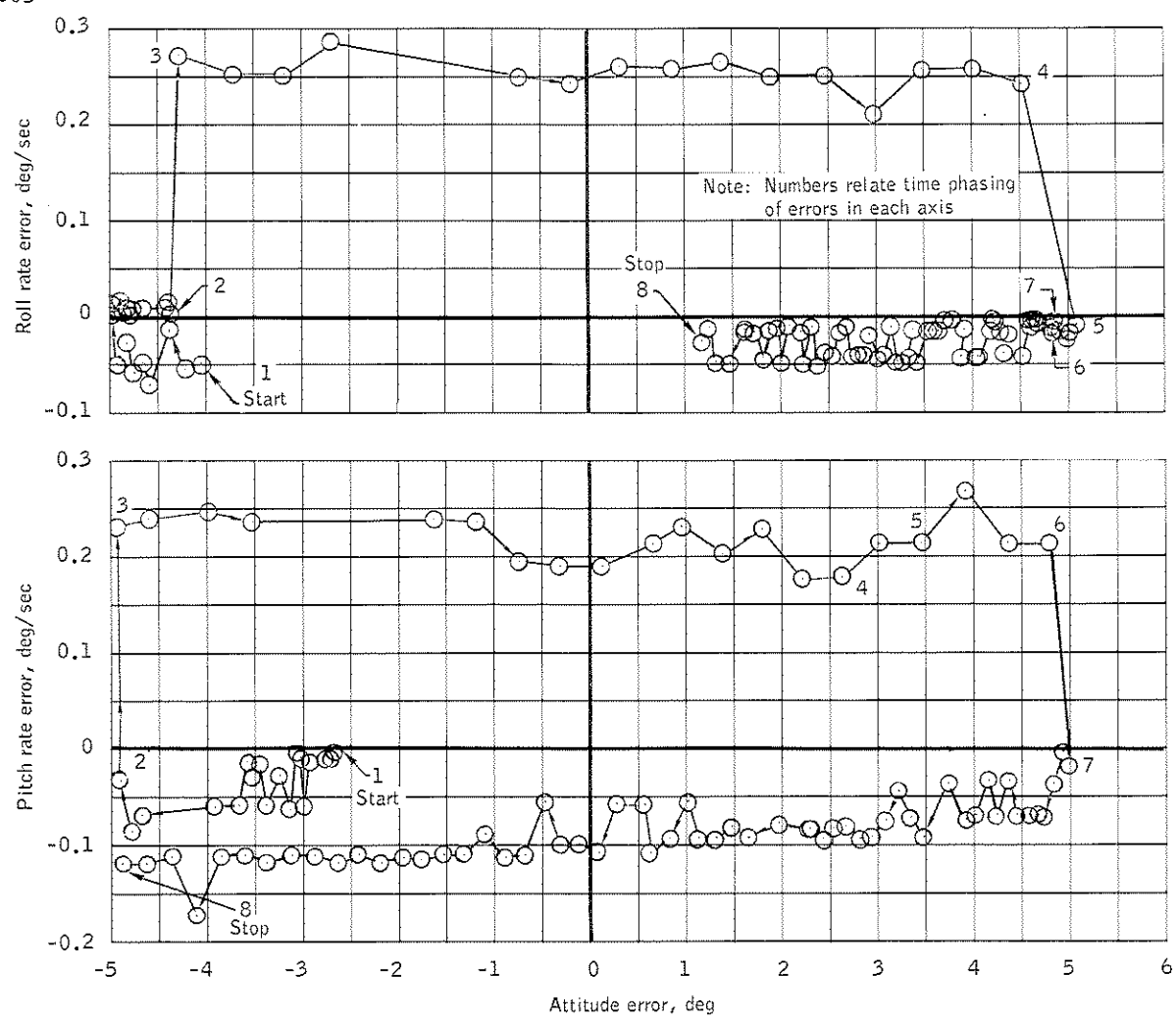


Figure 6.10-5.- Pitch and roll phase plane.

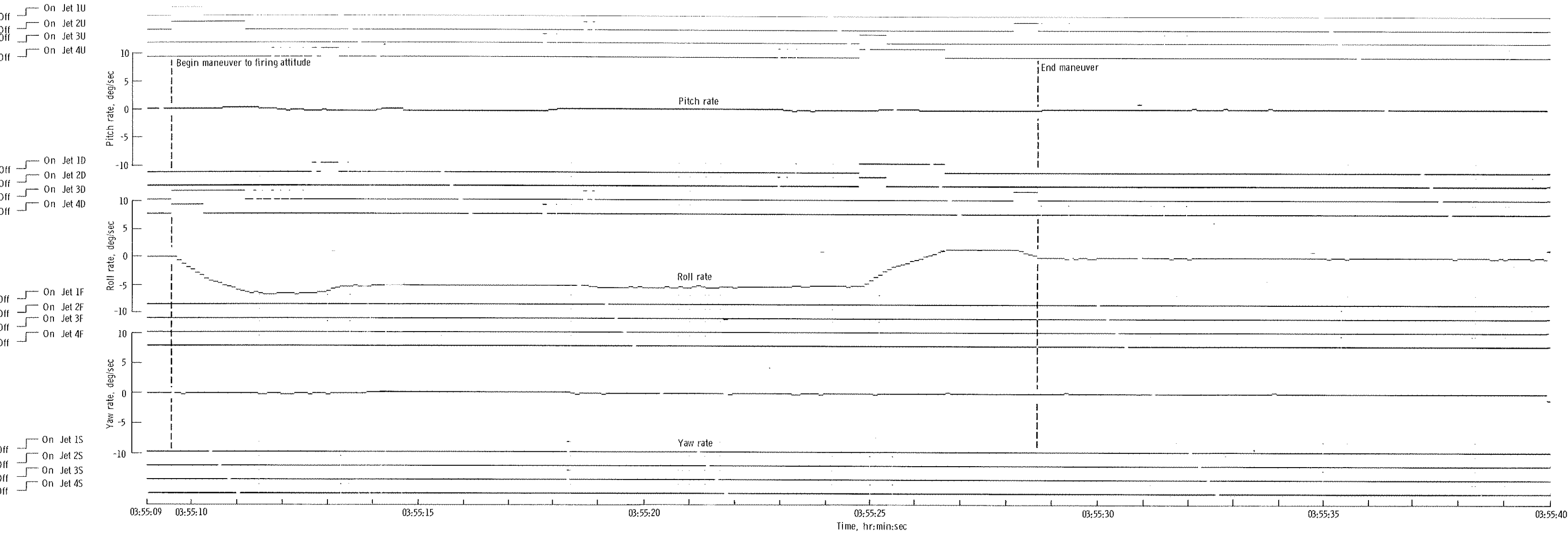


Figure 6.10-6. - Spacecraft dynamics - maneuver to attitude for first descent engine firing.

NASA-S-68- 2007

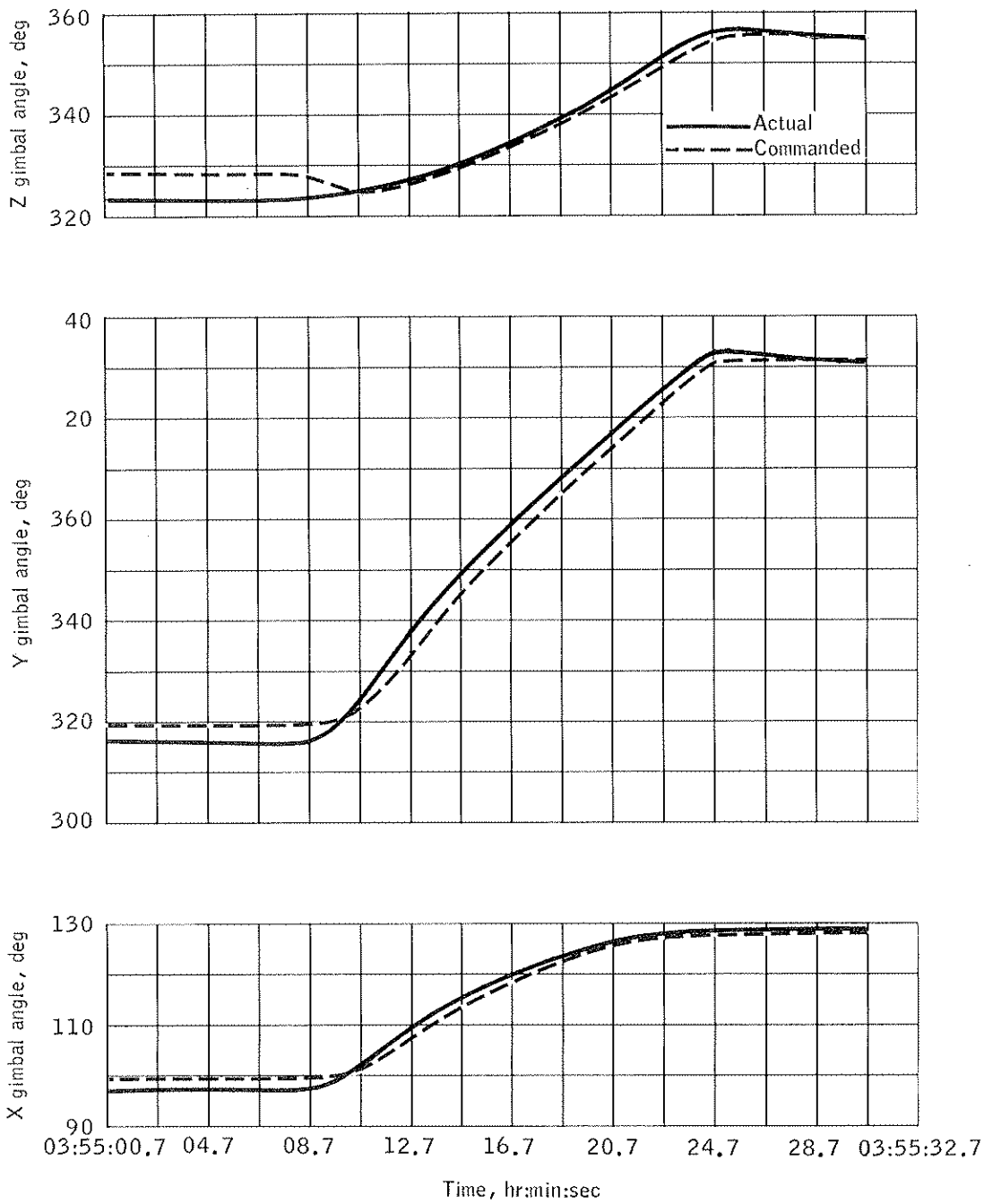


Figure 6.10-7.- Gimbal angle comparison - maneuver to attitude for first descent engine firing.

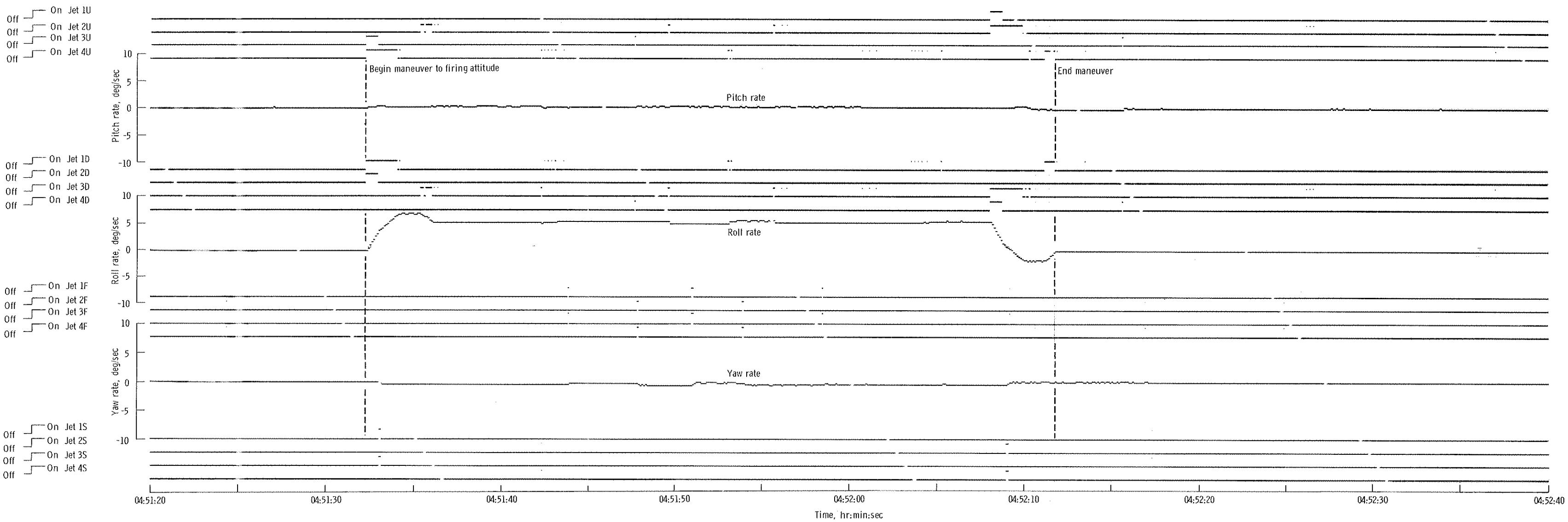


Figure 6.10-8. - Spacecraft dynamics - maneuver to attitude for second descent engine firing.

NASA-S-68-2009

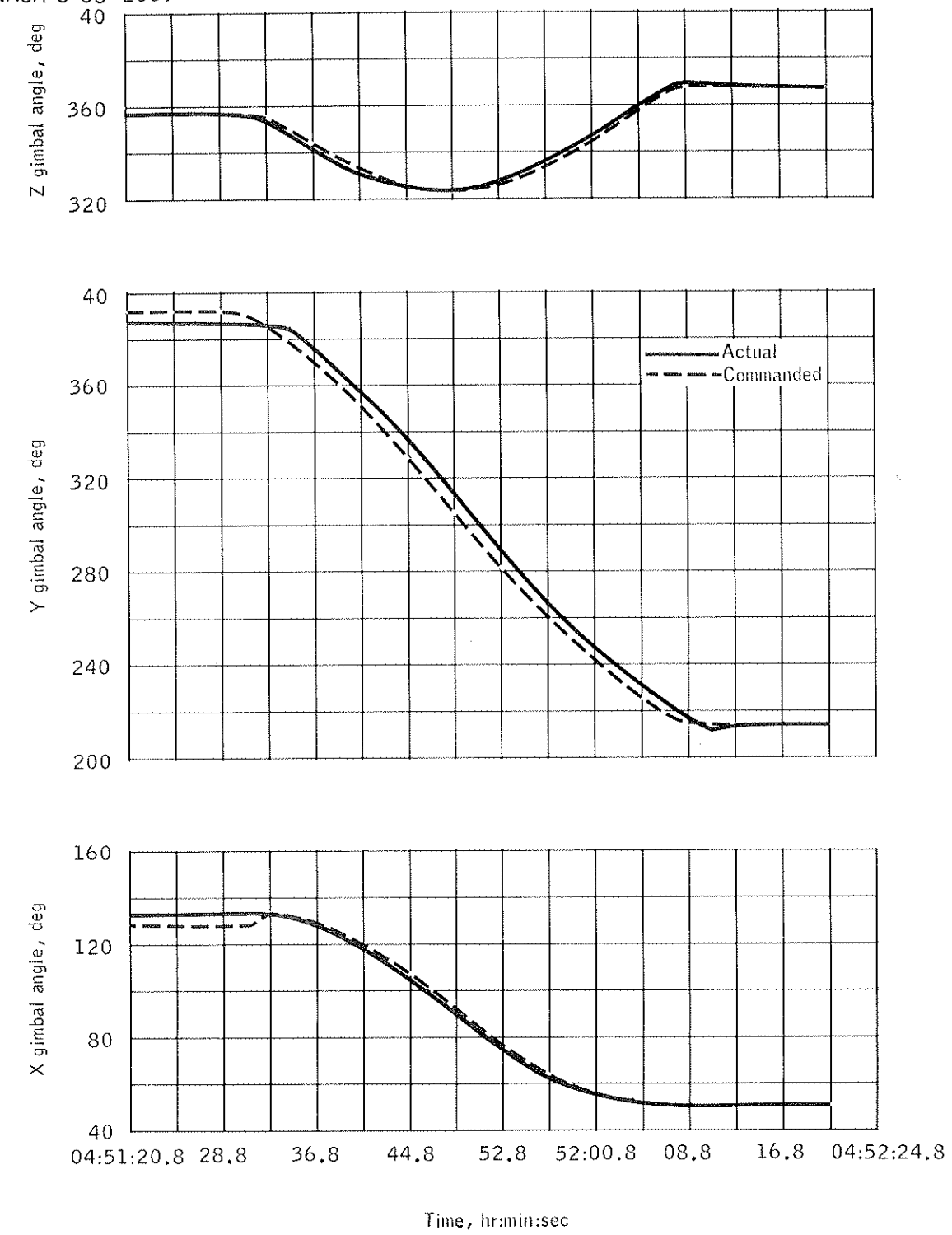


Figure 6.10-9.- Gimbal angle comparison - maneuver to attitude for second descent engine firing.

Off On Jet 1U
Off On Jet 2U
Off On Jet 3U
Off On Jet 4U

Off On Jet 1D
Off On Jet 2D
Off On Jet 3D
Off On Jet 4D

Off On Jet 1F
Off On Jet 2F
Off On Jet 3F
Off On Jet 4F

Off On Jet 1S
Off On Jet 2S
Off On Jet 3S
Off On Jet 4S

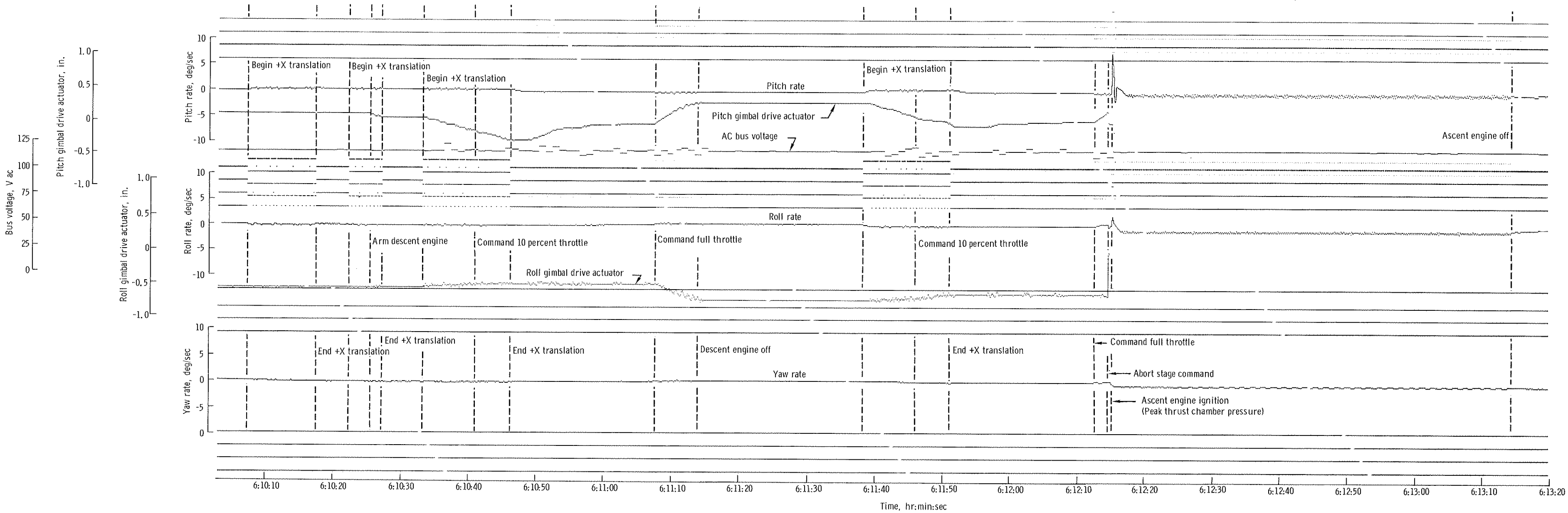


Figure 6.10-10. - Spacecraft dynamics - mission programmer sequence III.

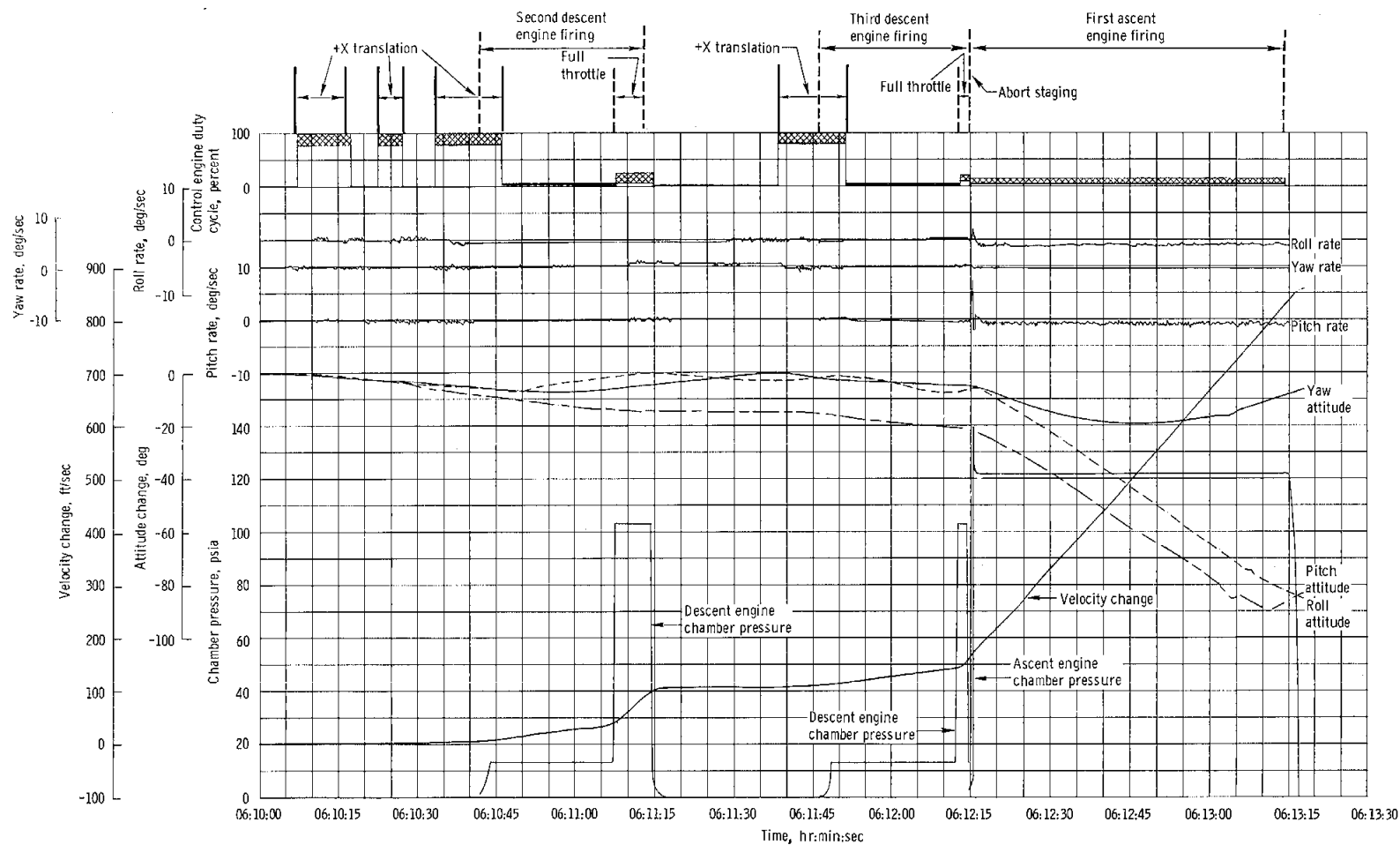


Figure 6, 10-11. - Mission programmer sequence III.

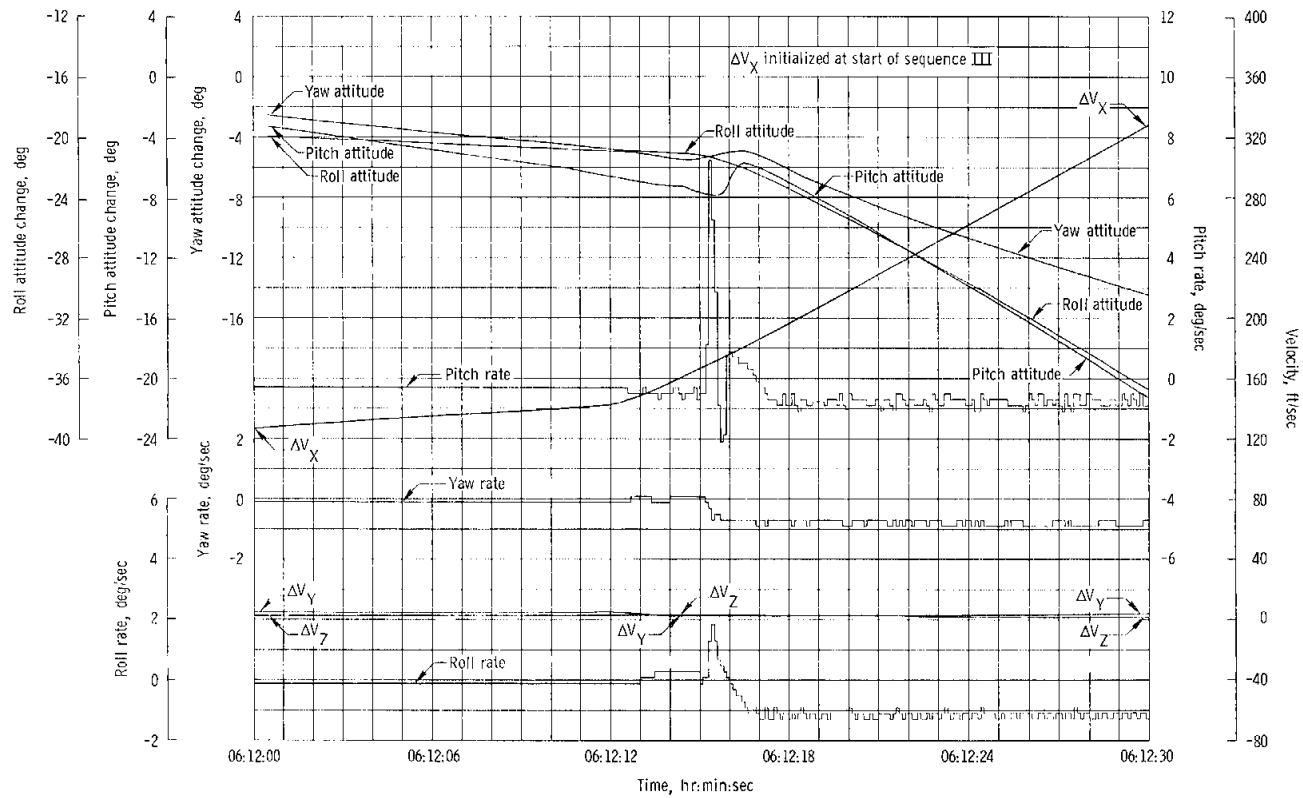
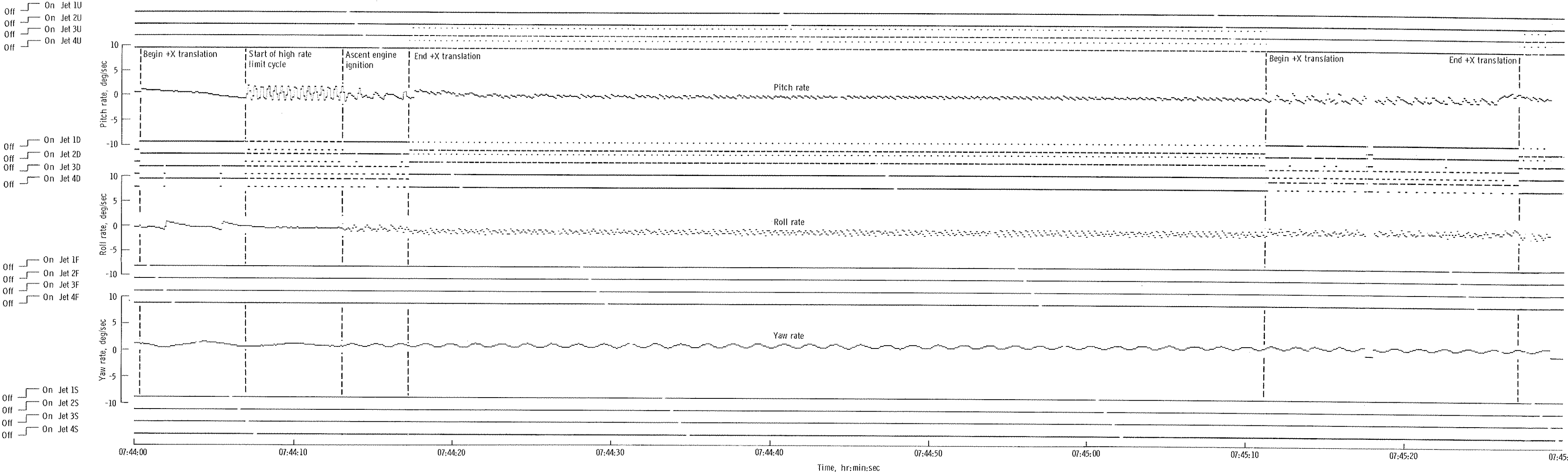


Figure 6.10-12 - Abort staging dynamics.



(a) Ignition and initial portion of firing, with rate control.

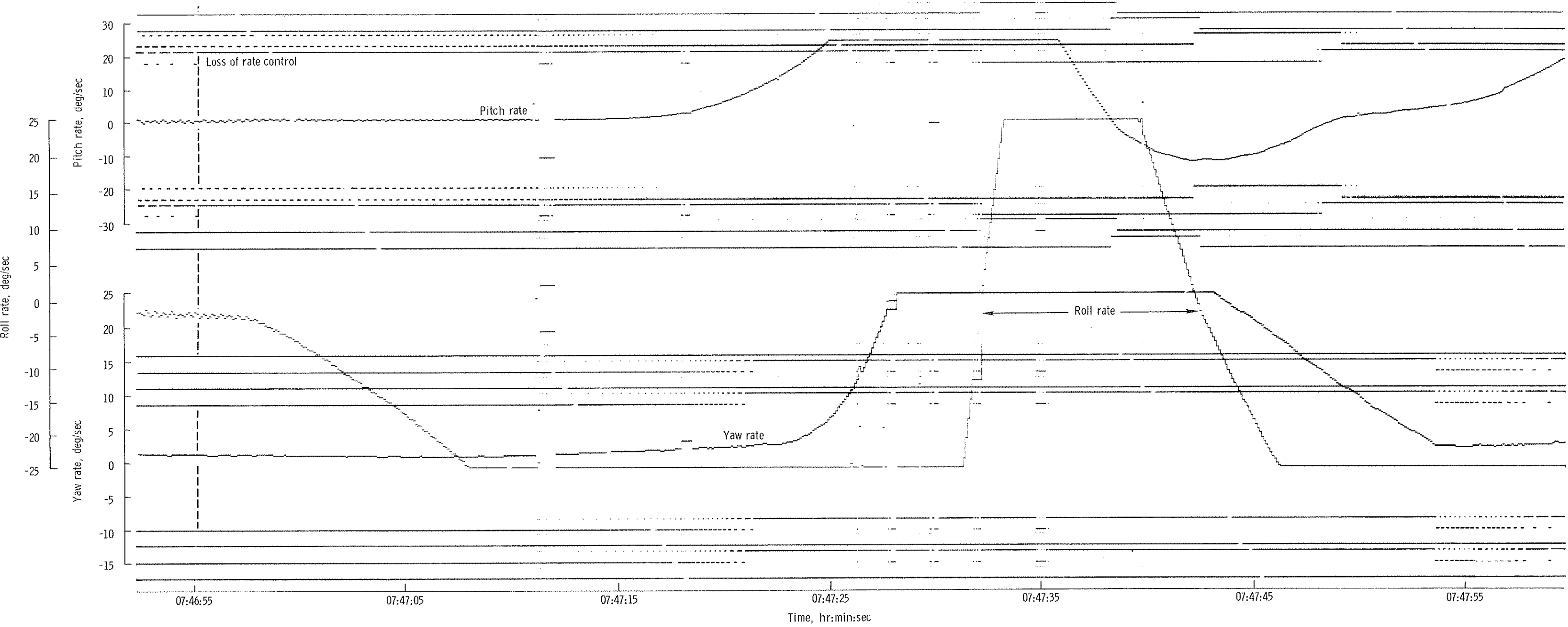
Figure 6.10-13. - Spacecraft dynamics - second ascent engine firing.

On Jet 1U
Off
On Jet 2U
Off
On Jet 3U
Off
On Jet 4U
Off

On Jet 1D
Off
On Jet 2D
Off
On Jet 3D
Off
On Jet 4D
Off

On Jet 1F
Off
On Jet 2F
Off
On Jet 3F
Off
On Jet 4F
Off

On Jet 1S
Off
On Jet 2S
Off
On Jet 3S
Off
On Jet 4S
Off



(b) Control propellant depletion.

Figure 6.10-13. - Concluded.

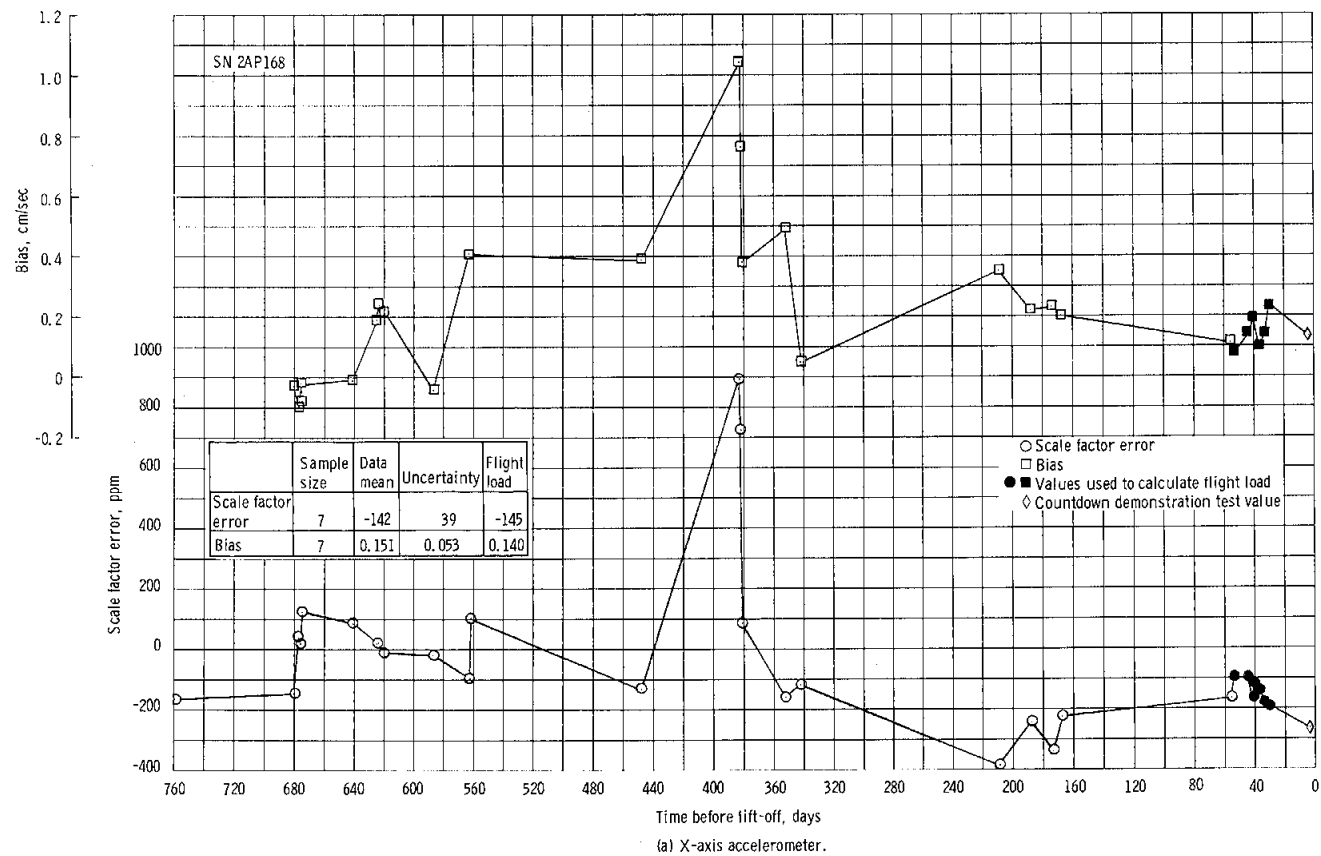


Figure 6.10-14. - Inertial measurement unit coefficient history.

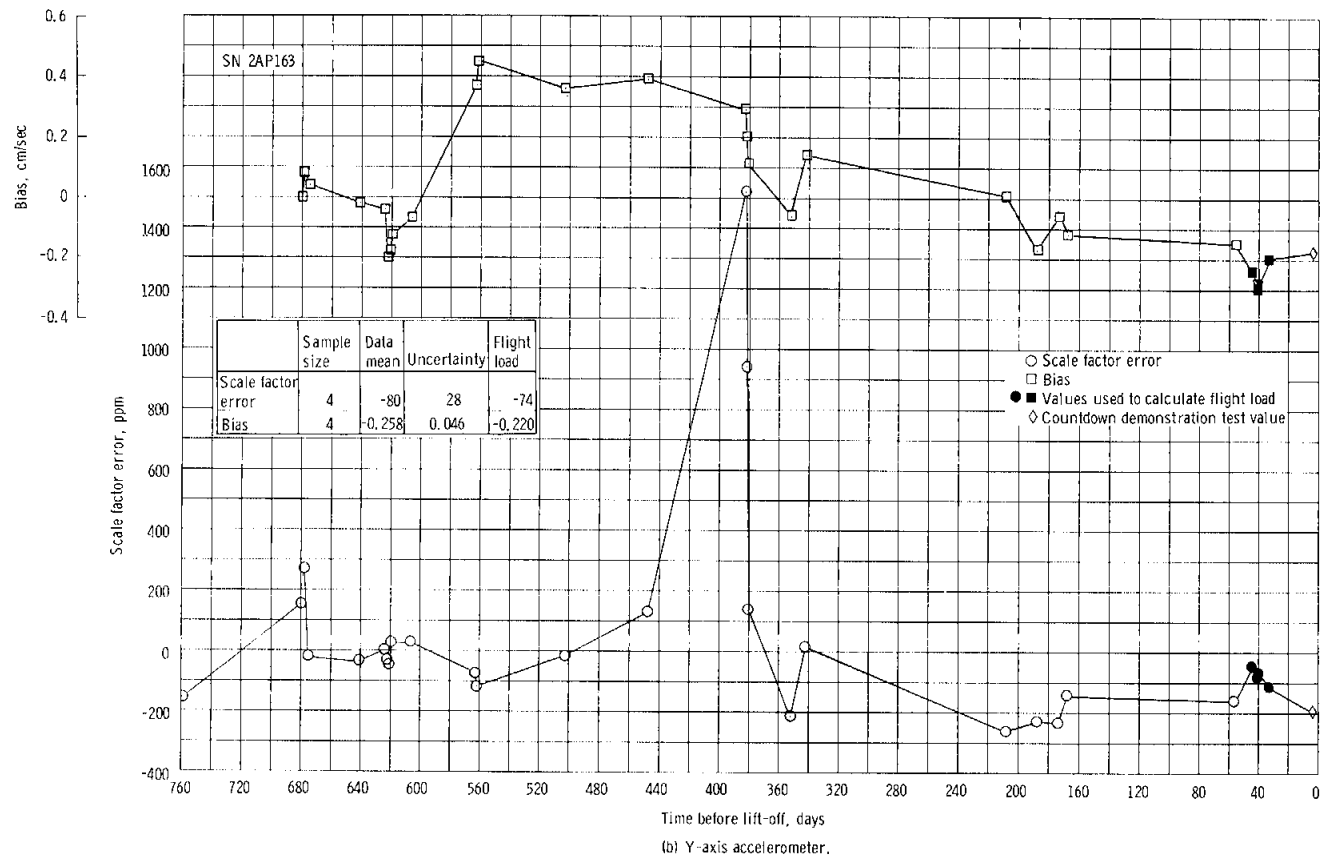
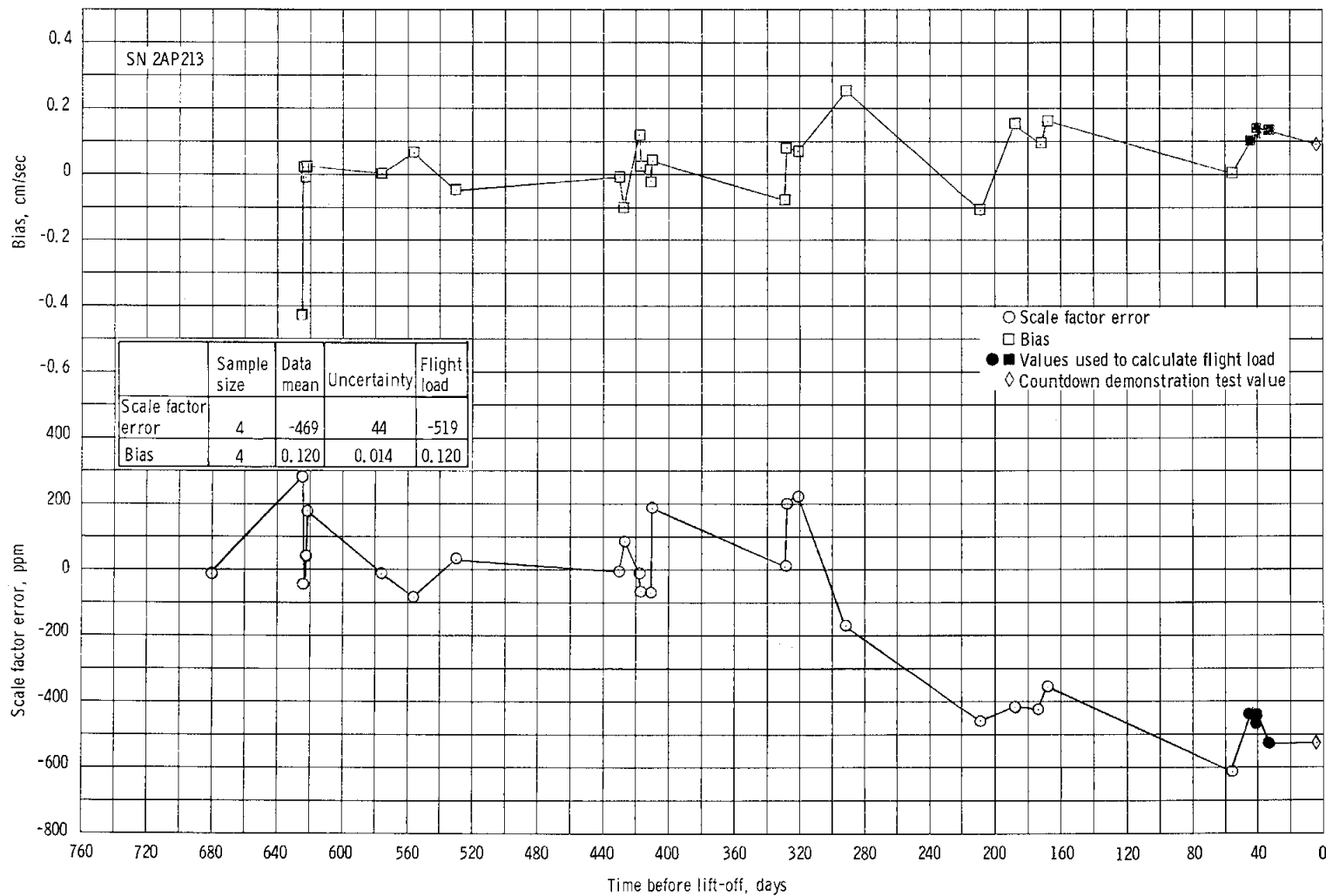


Figure 6.10-14. - Continued.



(c) Z-axis accelerometer.

Figure 6.10-14. - Continued.

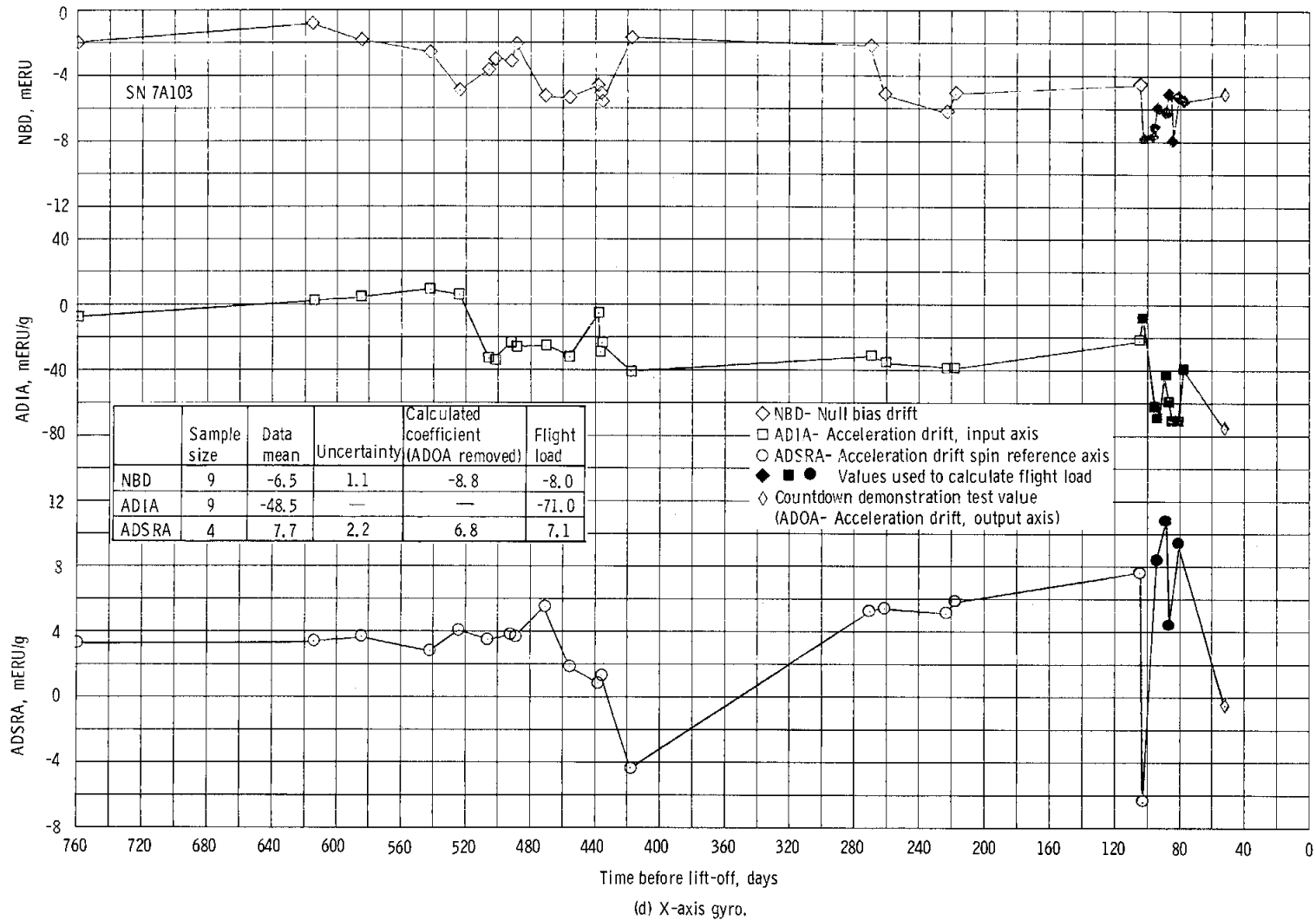


Figure 6.10-14. - Continued.

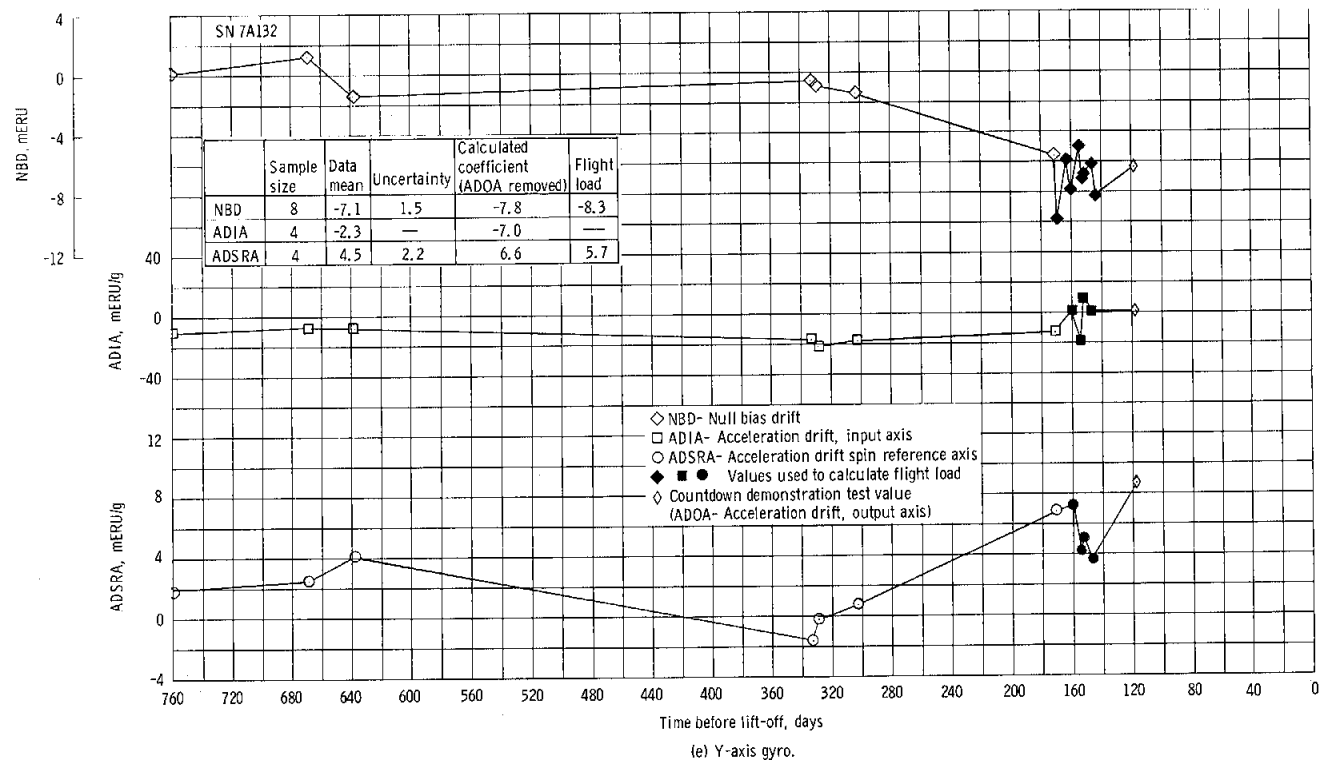


Figure 6.10-14. - Continued.

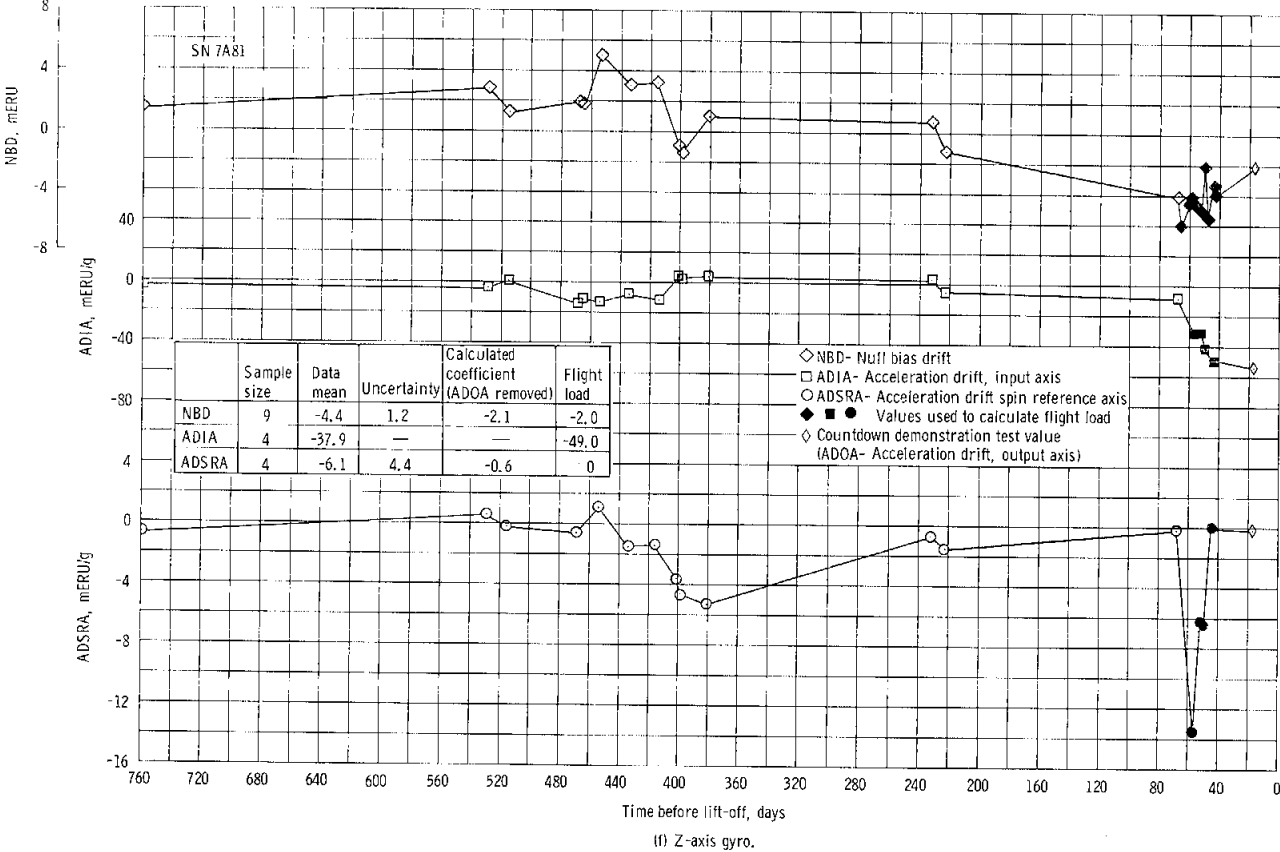
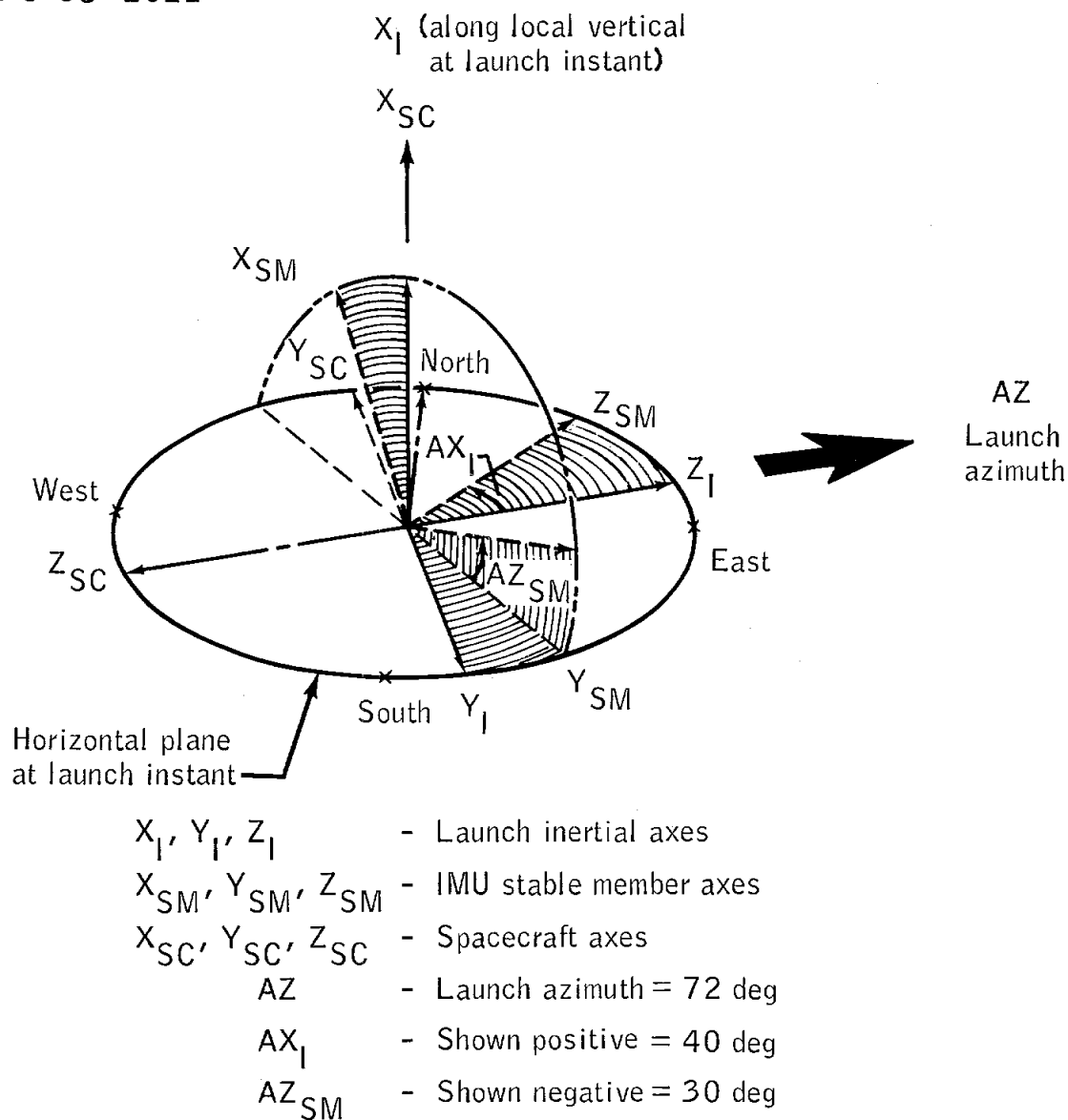


Figure 6.10-14. - Concluded.

NASA-S-68- 2021



Notes: Orientation angles for stable member are AX_I , AZ_{SM} . To align SM to the desired orientation, the SM axes are initially set colinear with launch inertial axes. The SM is then rotated about X_I through the angle, AX_I . Then it is rotated about Z_{SM} through the angle, AZ_{SM} .

Figure 6.10-15.- Inertial measurement unit prelaunch alignment orientation.

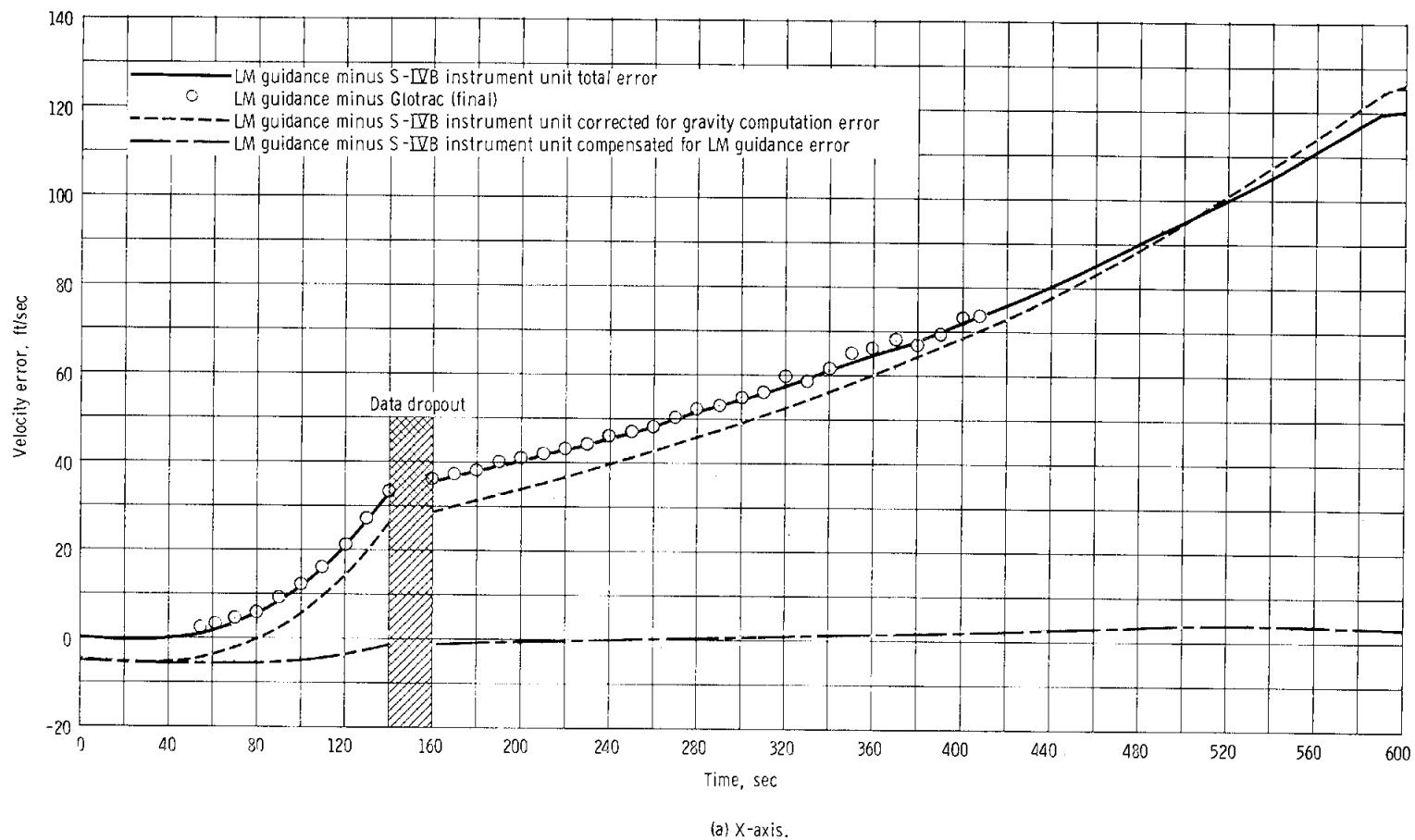
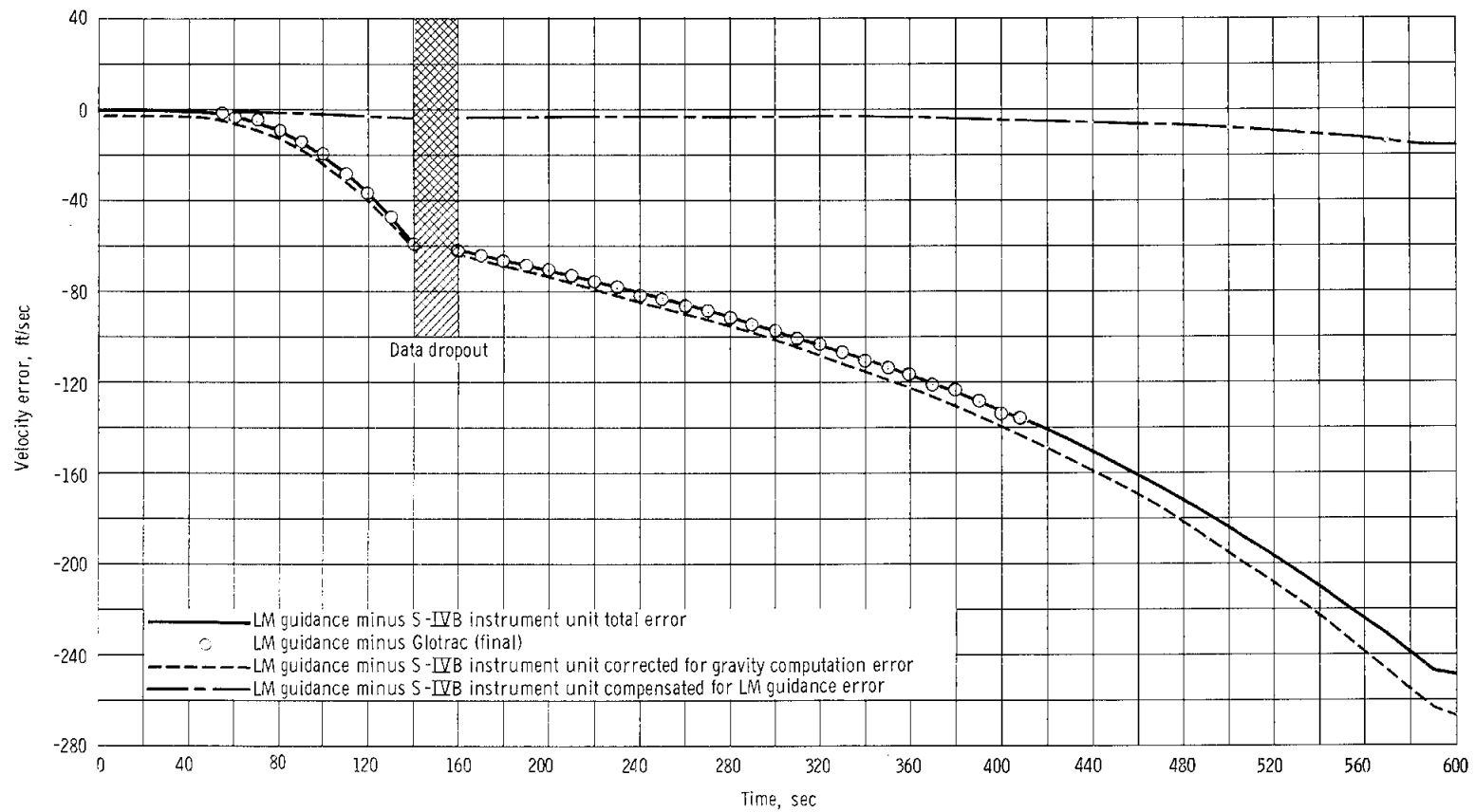
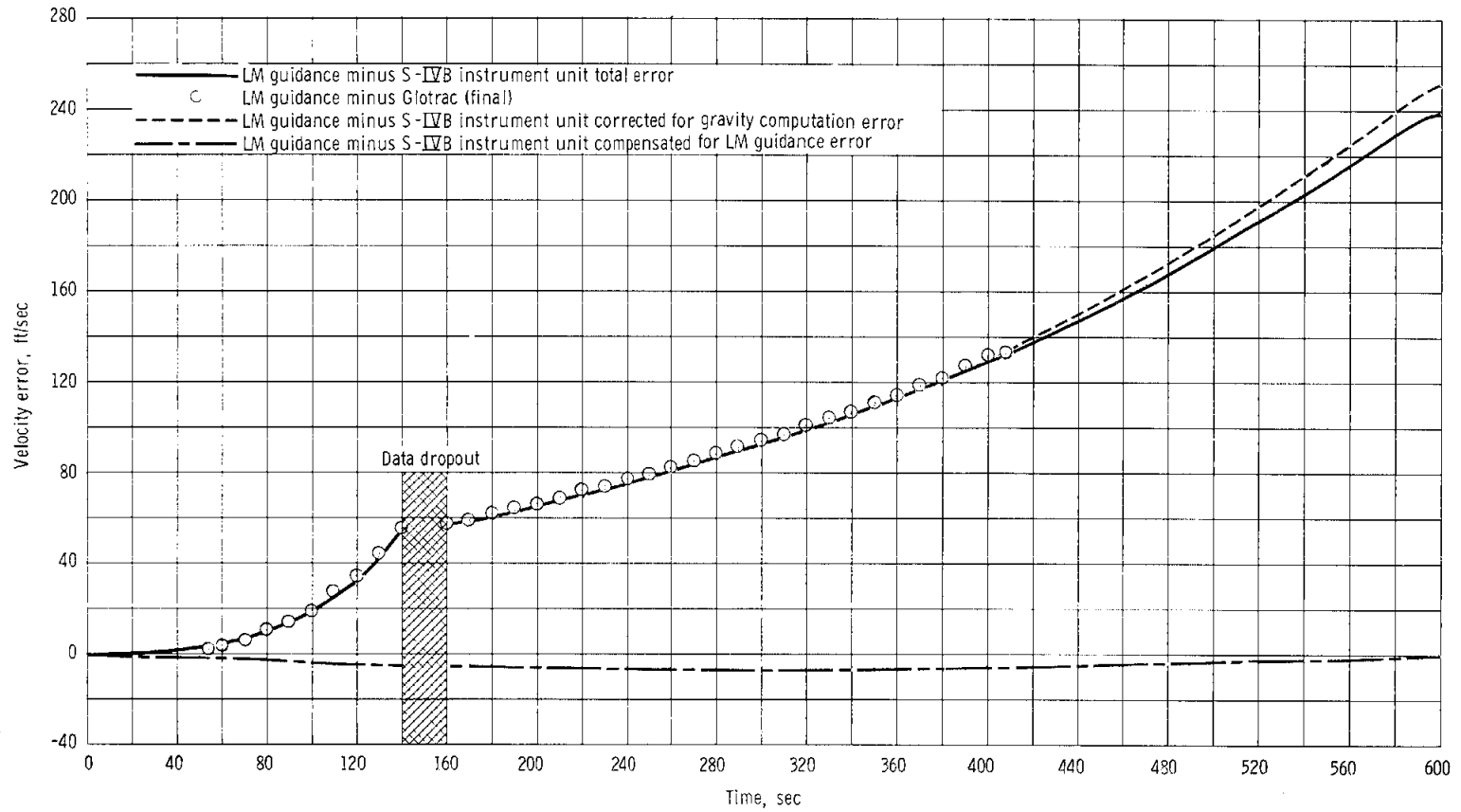


Figure 6.10-16. - Launch phase velocity comparisons.



(b) Y-axis.

Figure 6.10-16. - Continued.



(c) Z-axis.

Figure 6.10-16. - Concluded.

6.11 REACTION CONTROL SYSTEM

The reaction control system performance and operation were nominal until control of the spacecraft was switched to the guidance and control system after abort staging. At that time, the vehicle mass in the digital autopilot was configured for control of a two-stage, fully loaded vehicle, and the system was commanded to deliver propellant at a rate approximately 10 000 times greater than expected. This operational anomaly caused the reaction control system to operate in severe off-limit conditions, and resulted in failures in the system. Within 3.1 minutes, the A system propellant had been depleted to 27 percent, and that system was isolated to conserve propellant. The B system continued at a rapid duty cycle until propellant depletion 5 minutes later, at which time helium started leaking through the collapsed B system fuel bladder. Satisfactory vehicle rates were restored by the B system thrust reduction resulting from propellant depletion and by isolation of the A system propellant tanks, thereby compensating for the digital autopilot vehicle mass-constant error. While the B system was operating with two-phase oxidizer and helium-ingested fuel, engine 4-up failed. Just after the A system was reactivated, the main A oxidizer valve inadvertently closed. The ascent propellant interconnect valves were later opened, returning operation of the control engines to normal until the interconnect valves were closed. The depletion of all propellants during the last minutes of the second ascent engine firing allowed the spacecraft to tumble.

6.11.1 System Pressures and Temperatures

The helium pressurization system operated satisfactorily throughout the mission.

At 108 hours before launch, the two helium tanks were serviced with 1.05 pounds of helium, providing the preactivation conditions of 3099 psia at 74° F in tank A and 3168 psia at 73.2° F in tank B. A reversed differential pressure of 38 psi was applied across the check valves to increase the valve seating force and thereby prevent the flow of propellant vapors into the regulator where they could form corrosive residues. There was no evidence of external helium leakage.

Prior to launch, the propellant tanks were pressurized to 50 psia with helium, and the manifolds downstream of the main valves were evacuated. This manifold vacuum was maintained until system activation, with no evidence of leakage through the engines or main valves.

The activation sequence is shown in figure 6.11-1. The main valves were opened before the helium isolation valves to decrease activation dynamic pressures. After the helium isolation valves were opened, the

6.11-2

manifold pressures increased to a nominal 180 psia with no indication of pressure overshoots. Throughout the mission, the helium regulator maintained the regulator outlet pressure within specification limits of 183 ± 3 psia, even under abnormally high propellant usage rates.

The steady-state manifold pressures remained within specification limits prior to propellant depletion. The dynamic manifold pressure fluctuations for a single control engine firing were ± 30 psi and were as high as 170 psi above regulator pressure during the high duty cycling of the control engines. These pressure oscillations were consistent with those noted in the ground tests.

After the completion of the first ascent engine firing, attitude control was switched to primary guidance, which resulted in a high rate of reaction control propellant consumption (see section 6.10). The A system main valves were closed to conserve propellant. The high engine-firing rate caused the A system manifold pressures to rapidly decrease to zero (fig. 6.11-2). The B system manifold pressures remained nominal for 310 seconds; at that time, the fuel was depleted, and 24 seconds later, the oxidizer was depleted, as expected. The manifold pressure characteristics at that time are presented in figure 6.11-3. As shown in the figure, when the fuel pressure had decreased 50 psi, a helium leak through the bladder slowly restored the fuel manifold pressure to a nominal 180 psia. The decreased amplitude of the pressure fluctuations was caused by helium in the fuel manifold. Further evidence of bladder leakage is shown in figure 6.11-4. The helium pressure is shown to have continuously decreased after fuel depletion. When the main B valves were closed, the helium pressure remained essentially constant until the main valves were again opened, at which time helium pressure again decayed. The B system oxidizer manifold pressure decreased to 50 psia rather than to zero because the substantial decrease in engine activity at oxidizer depletion allowed oxidizer to remain within the manifold. The vapor pressure of the oxidizer at the temperature of the system heaters was 50 psia.

This manifold pressure condition remained essentially unchanged until the main A and B valves were reopened just prior to the second ascent engine firing. The small quantity of B system propellant trapped in the manifold and the reduced manifold pressures had been sufficient for control of the vehicle from B system propellant depletion until the main A valves were opened. The reopening of the main A valves provided an opportunity to evaluate an activation with 180 psia on the bladder and zero manifold pressure. Resulting hydraulic transients are shown in figure 6.11-5. No noticeable detrimental effect on the system was observed.

Opening of the crossfeed valves about 2 minutes after the main A valve was opened caused the B system fuel manifold pressure to increase

to 180 psia (fig. 6.11-6). However, the A system oxidizer manifold pressure decreased to 80 psia, and the B system oxidizer pressure increased to the same value. This resulted from the main A oxidizer valve inadvertently becoming unlatched and essentially closing at that time. Current had been continuously applied to the valve for almost an hour, supplying sufficient heat to vaporize the oxidizer in the valve. When the valve was opened, oxidizer vapor was trapped above the upper magnet. The vapor pressure forced the valve to unlatch when the downstream pressure decreased after the crossfeed valves were opened. Oxidizer leakage through the valve is indicated by the gradual oxidizer manifold pressure rise to 115 psia from 80 psia. The oxidizer manifold pressure again decreased to about 50 psia as engine firings reduced the manifold pressure to the oxidizer vapor pressure.

The interconnect valves were opened several minutes prior to the second ascent engine firing, and both oxidizer and fuel pressures increased to the 184-psia ascent engine propellant feed pressure. During the second ascent engine firing, the pressures dropped to 170 and 177 psia in the oxidizer and fuel manifolds, respectively. About 1 minute after the second ascent engine firing was initiated, the mission programmer automatically latched both main A valves in the closed position. About 3 minutes prior to ascent engine thrust decay, the mission programmer automatically closed the interconnect and crossfeed valves, and reopened the main A valves, as shown in figure 6.11-7. The A system oxidizer was depleted about 1.5 minutes after the A system interconnect valves were closed because of the inadvertent closure of the main A oxidizer valve. During this 1.5-minute interval, 64 pounds of oxidizer were cold-flowed through the engines, which were commanded on almost continually.

During the period of nominal operating conditions, the propellant tank temperatures varied between 61° and 67° F, but the cooling following control system propellant depletion caused the temperatures to range between 52° and 67° F. Fuel and oxidizer inlet temperatures were 65° to 75° F, depending upon engine activity. These values were satisfactory.

6.11.2 Propellant Utilization

The quantities of propellant serviced for this mission is shown in the following table:

System	Fuel (Aerozine 50)		Oxidizer (nitrogen tetroxide)	
	Quantity, lb	Time before launch, hr	Quantity, lb	Time before launch, hr
A	102.0 ± 1.6	319	203.4 ± 2.5	249
B	102.8 ± 1.6	306	203.4 ± 2.5	243

The propellant consumption was normal until spacecraft control was switched from the backup to the primary control system at 06:14:05.2, resulting in an extremely high propellant consumption rate (70 lb/min).

The propellant expended by the control engines throughout the mission is shown in figure 6.11-8. At separation, the quantity of propellant expended by the A system, as calculated by the propellant quantity measuring device, was about 4 percent higher than had been predicted. The B system showed essentially the same usage as predicted. The propellant usage was also calculated by a set of equations permitting consideration of additional variables not considered by the measuring device. The two calculated quantities differed as a result of different inputs such as tank volume, propellant loads, and instrumentation variances. Overshoots in expended propellants were a result of temperature stabilization lag.

The B system fuel depletion occurred at 06:21:56, followed by oxidizer depletion 24 seconds later. This indicates an average mixture ratio of 1.94 compared with 1.99 usable, indicating good propellant utilization. The expected average ratio was 1.98. The B system consumed 287 pounds of propellant (100 percent of that usable).

The A system fuel depletion occurred at 07:46:42, followed 84 seconds later by the depletion of the remaining 64 pounds of oxidizer. Fuel depletion preceded oxidizer depletion by such a comparatively long time because the main oxidizer valve closed without command at 07:12:24 and was not reopened until 07:46:42. For this reason, no attempt was made to determine A system mixture ratio for the flight. The A system consumed 273 pounds of propellant (95 percent of that nominally available).

At the time of A system propellant depletion, helium tank A pressure had decreased by 1478 psi. Depletion of propellant in the B system corresponded to a helium tank pressure decrease of 1571 psi, both corrected to 70° F. This difference of about 100 psi is equivalent to approximately 15 to 20 pounds less propellant being consumed by the A system and can be related to the 4-percent initial bias. The bias was probably caused by less propellant than expected having been loaded in the A system and by accrued system volume tolerances. Because of the fuel bladder leak, the B system helium tank pressure eventually dropped from the value of 1360 psia (70° F) at propellant depletion to 1157 psia (70° F).

The performance of the propellant quantity measuring devices is shown in figure 6.11-9. The convergence of the A and B system propellant remaining at approximately 6 hours is due to greater usage by the B system engines (see section 6.10). The estimated steady-state accuracy of the measuring devices was ±5 percent.

Specific quantities of ascent fuel and oxidizer consumed by the reaction control system during these periods are listed in table 6.11-I. Reaction control system fuel used by the A system between the start of the second ascent engine firing and the main A valve closure was 1.4 pounds. The amount consumed by the B system was 1.3 pounds.

6.11.3 Control Engine Performance

Control engine performance values were within expected limits for the various existing operating conditions except for the 4-up engine failure.

The first control engine firings were normal, as shown in figure 6.11-10. The small pressure oscillations noted at startup are attributed to small quantities of helium passing through the injector. Entrained helium was expected to separate from the propellants during the initial flash-off period as the propellants were exposed to the manifold vacuum. The chamber pressure of all four engines was a nominal 97 psia.

When the manifold pressures were nominal, typical engine ignition delays ranged between 8 and 11 milliseconds, measured from engine "on" indication to the first rise in chamber pressure. The times from engine "on" indication until the chamber pressure reached 70 percent of nominal ranged between 16 and 29 milliseconds, which is within the specification requirement of 30 milliseconds. Shutdown specifications were also satisfied.

The effect of manifold line lengths on ignition transients is shown in figure 6.11-11. Engine 4-up was about three times closer to its propellant tanks than engine 4-down. Manifold inlet pressures at the engines located near the propellant tanks recovered from the pressure drop at valve opening about 5 milliseconds sooner than engines on the opposite side of the vehicle, thereby decreasing the ignition transient buildup time. The difference in rise time appreciably affected the total impulse of minimum impulse firings.

Maximum chamber pressures during the 15-millisecond pulses usually varied between 50 and 100 psia. Chamber pressures on longer pulses were between 96 and 100 psia as expected.

During multiengine operation, the effects of manifold pressure dynamics were evident in chamber pressure. An engine firing at steady-state level would frequently experience a momentary pressure drop as much as 30 psi for several milliseconds when an engine in the same system was commanded "on"; the manifold pressure surges associated with valve closure produced the momentary chamber pressure increases. This was expected and agreed with the results of ground tests.

The chamber pressure for B system engines decreased to about 80 psia when the fuel manifold pressure dropped to 130 psia at fuel depletion. After helium began to leak through the bladder, the manifold pressure rose to the nominal 180 psia; engine chamber pressure also returned to normal. At oxidizer depletion some 24 seconds after fuel depletion when the manifold pressures dropped to 50 psia, engine chamber pressures dropped to about 40 psia (see fig. 6.11-12). Performance was quite varied from this time until the ascent propellant interconnect valves were opened. Shortly after the oxidizer was depleted and before the helium leakage in the fuel manifold was purged through the engines, the engine chamber pressures were about 40 psia. The combustion instability (± 10 psi) of 300 Hz (characteristic of two-phase flow) also occurred at this time (fig. 6.11-12). Two-phase flow could be expected because the oxidizer manifold pressure was equivalent to the vapor pressure of the oxidizer. Later, as helium from the fuel manifold passed through the engine, chamber pressure showed a sharp drop to about 10 psia until the bubble was purged; the chamber pressure then returned to 40 psia. Several minutes later, the chamber pressure of those engines which were frequently fired was only about 10 psia, with occasional increases to 40 psia. The 10-psia value was indicative of oxidizer cold-flow; 40 psia indicated combustion.

Continued operation of the B system at these manifold pressures is believed to have precipitated the failure of up-firing engine 4 sometime during the 15-minute period between the Ascension and the Coastal Sentry Quebec stations during revolution 5. Engine 4-up produced no detectable chamber pressure during the Coastal Sentry Quebec pass nor during the remainder of the mission. Ground tests have shown that similar operation enhances formation of explosive compounds which accumulate within the combustion chamber, even in the vacuum environment. Detonation of these residues have ruptured combustion chambers. Detonation characteristics with the 3-down engine were noted during this time, indicating compound formation (fig. 6.11-13).

After the main A valves were reopened, the A system was commanded to fire only about 8 pulses of 15 milliseconds duration until the cross-feed valves were opened. The first two pulses usually exhibited less than nominal chamber pressure, but by the third pulse, all A system engines were indicating nominal chamber pressure. After the crossfeed valves opened, B system engines required about 10 pulses before chamber pressures above 10 psia were produced. This delay occurred while the helium was being purged from the manifold. The chamber pressures of engines in both systems were equal, but because the oxidizer pressure remained between 50 and 115 psia until the ascent propellant interconnect valves were opened, engine performance varied between 30 and 70 percent of nominal. When the interconnect valves were opened and manifold pressures had returned to normal, engine thrust (except for 4-up) returned to normal. Because of a mass error in the guidance computer, the engines

again were commanded to fire a very heavy duty cycle until vehicle control was switched from primary guidance to the backup control path. The characteristic instability indicative of gas ingestion occurred twice during this period but existed for only about 100 milliseconds. When the second ascent engine firing began, the reaction control system fuel and oxidizer manifold pressures dropped approximately 6 and 12 psi, respectively. Engine chamber pressures were nominal during the interconnect operation with the ascent engine firing. At this time, the effect of the slightly lower inlet pressures should have decreased the chamber pressure by about 2 percent; however, the resolution of the data was not adequate to provide confirmation.

Cluster temperatures.- The temperature variations of the four clusters are presented in figure 6.11-14. The engine heaters maintained the cluster temperatures above the minimum of 120° F throughout the cold-soak periods. There was no evidence that a heater which had failed before launch on engine 2-down resulted in any serious degradation of the thermal control of cluster 2. Temperatures on clusters 1 and 3 exceeded the 190° F upper red-line limit because of the heating rate associated with the high firing rate experienced after the first ascent engine firing, as well as during the second ascent engine firing. The high control engine activity just prior to the second ascent engine firing was partially the cause of the high cluster temperatures. However, the maximum preflight predicted cluster temperature for the second ascent engine firing was 188° F, which is probably low, since the contractor's preflight analyses predicted lower cluster temperatures for the LM/S-IVB separation maneuver than actually occurred. In addition, since the cluster temperature sensors were installed near the down-firing engines, the measurements were more sensitive to the activity of these engines than to the total activity of all the engines on the cluster. The predictions, however, had shown a lesser dependence on the activity of the down-firing engines. Therefore, there is a high probability that the 190° F upper red-line cluster temperature limit will be exceeded on future flights. This situation requires re-evaluation of both the upper red-line temperature limit and the cluster temperature mathematical model.

Figure 6.11-14 shows four areas of heat soakback caused by engine activity. Because of the lack of data after separation and after the first descent engine firing, the actual peak temperature was not known but was estimated to have been 180° F, as compared with a prediction of 160° F.

Normal temperature rises were experienced during the mission programmer sequence III until control was switched from the backup control path to primary guidance at 06:14:05, which resulted in the abnormally high duty cycles. The subsequent temperature increases on clusters 1 and 3 occurred when the heat from the high engine usage rate was conducted to the clusters, causing the temperatures of clusters 1 and 3 to

exceed the upper instrumentation limit of 200° F. Clusters 2 and 4 were cooler because the down-firing engines in these clusters were A system engines, which were isolated at 06:17:12 when the main valves were closed, allowing the injectors to be cooled somewhat from subsequent valve actuations as the residual propellants in the lines were vented. Cluster 1 temperature, the highest of the four, probably reached at least 230° F. However, no degradation in engine performance was evident.

Following a normal cooldown, the temperatures again increased from the control activity associated with the firing activity at the time of the second ascent engine firing. Cluster 1 temperature again exceeded the 200° F upper instrumentation limit. Cluster 3 temperature reached 191° F, exceeding the upper red-line temperature limit. However, cluster 4 temperature never exceeded 145° F, even though the 4-down engine injector temperature exceeded 200° F. This is the only time during the mission when the cluster temperature did not follow the down-firing engine injector temperature. This low temperature was the result of propellant cold-flow through the failed 4-up engine. The cooldown of clusters 2, 3, and 4 were notably more accelerated than had been experienced earlier. This was a consequence of the expulsion of the 64 pounds of oxidizer from the A system engines because of the inadvertent closure of the main A oxidizer valve when the crossfeed valves were opened.

Injector temperatures.- A summary of the instrumented injector head temperatures during the flight is presented in table 6.11-II. The recorded injector head temperatures ranged from a minimum of 84° F for engine 2-down to a maximum of 322° F for engine 1-down. Both the minimum and maximum recorded temperatures occurred on engines which, at the time, had no propellant available to them. The minimum injector temperature of 84° F occurred on engine 2-down after the main A valves had been closed during the period of high control engine firing activity and the residual A system propellants had been vented through the engines. The lowest injector temperature measured during the periods when the engines were supplied with propellants was 132° F on engine 3-up (06:11:22) during pulsing operation between the second and third descent engine firings. Therefore, the engine heaters, under normal operating conditions, maintained the instrumented engine injectors above 130° F throughout the mission.

The maximum injector temperature of 322° F was recorded on engine 1-down after A system propellant was expended during the high activity following abort staging, and again after the interconnect valves had been closed near the end of the second ascent engine firing. In both cases, the maximum temperature was achieved through heat soakback from the hot combustion chamber after severe engine firing. The engine throat will normally attain a temperature of approximately 2200° F during continuous operation. If the engine had been restarted following these

high activity periods, the injector temperature would have rapidly dropped below 300° F because of the regenerative cooling effect of the propellant within the injector.

Typical temperature histories of the instrumented control engine injector heads during LM/S-IVB stage separation, the second and third descent engine firings, and the first and second ascent engine firings are presented in figures 6.11-15 through 6.11-18.

Figure 6.11-15 shows the typical thermal response of the instrumented 1-down and 1-forward injectors and cluster 1 for the separation maneuver. Also included in the figures are the predicted responses for the cluster and the down-firing engine injector. These curves are typical for a maneuver of this type (hence, the first descent engine firing), for which the primary engine activity is the +X translation using the down-firing engines. The cluster temperature was much more responsive to the increasing down-firing engine injector temperature than the predicted curves show, despite the close agreement between the actual and predicted injector temperature curves.

Figures 6.11-16 and 6.11-17 show the temperature histories of clusters 1 and 2 and their instrumented injector heads from the second descent engine firing through the first ascent engine firing. The temperature histories of clusters 3 and 4 were similar to those of clusters 1 and 2, respectively, in that similar thermal characteristics existed but with somewhat smaller temperature excursions. The similarity existed because clusters 1 and 3 have vertical down-firing engines on the B system, while clusters 2 and 4 have vertical down-firing engines on the A system. The difference between clusters 1 and 2 is a consequence of the deactivation of the A system (06:17:11) during the period of high activity. Prior to this time, all clusters were operated in a similar manner. The minimum and maximum injector head temperatures were recorded during this phase of the mission.

Figure 6.11-18 shows thermal responses of cluster 1 and its instrumented injector heads during the second ascent engine firing. Cluster 1 was the only cluster which responded thermally in a normal manner during this mission phase. The A system engines of clusters 2 and 3 were extensively cooled by the residual oxidizer coldflow after the interconnects were closed. Approximately 64 pounds of residual oxidizer remained in the A system because of the inadvertent closure of the main A oxidizer valve when the crossfeed valve was opened. Cluster 4 temperatures were also reduced as a consequence of propellant cold-flow through engine 4-up. Figure 6.11-19 shows the temperature differences between clusters 3 and 4. Both clusters received comparable engine firing duty cycles (calculated over 10-second intervals for fig. 6.11-19) and hence should have experienced comparable temperature rises until the interconnect valves were closed. The fact that cluster 4 was substantially cooler indicates that engine 4-up was coldflowing propellant.

TABLE 6.11-I.- ASCENT PROPELLANT USED BY THE REACTION CONTROL ENGINES

Event	Time, hr:min:sec	Oxidizer, lb		Fuel, lb		Propellant, lb		Total, lb	
		A	B	A	B	A	B		
A interconnect valves opened	07:40:59	}	65.5	66.3	32.5	32.9	98.0	99.2	197.2
Second ascent engine start	07:44:13		2.8	2.6	-	-	2.8	2.6	5.4
Main A valves closed	07:45:33		7.8	8.0	3.8	4.0	11.6	12.0	23.6
Crossfeed and A interconnect valves closed, main A valves opened	07:46:43		-	2.8	-	1.4	-	4.2	4.2
B interconnect valves closed	07:46:53								
Total			76.1	79.7	36.3	38.3	112.4	118.0	230.4

6.11-10

TABLE 6.11-II.- REACTION CONTROL ENGINE INJECTOR TEMPERATURES

Phase	Time, hr:min:sec		Engine injector head temperature, °F													
			1-down		1-forward		2-down		2-up		3-up		4-down		4-forward	
	From	To	Min.	Max.	Min.	Max.	Min.	Max.	Min.	Max.	Min.	Max.	Min.	Max.	Min.	Max.
Separation and cold-soak	00:52:00	01:46:00	147	225	142	171	138	225	138	161	142	171	147	225	138	156
First descent engine firing	03:54:22	04:28:42	142	225	142	161	142	215	142	171	142	165	134	205	134	161
Second and third descent engine firings and first ascent engine firing	06:10:00	06:25:52	142	322	138	200	137 ^a ₈₄	220	137	306	132 ^a ₁₃₀	176	142 ^a ₉₃	218	138	220
Second ascent engine firing	07:38:42	07:52:02	134	322	142	195	142 ^b ₁₂₅	205	142	249	142	239	134 ^b ₁₃₀	217	134 ^c ₁₀₃	156

^aTemperatures achieved after venting A system propellants through engines.
^bTemperatures achieved after cold-flowing A system residual oxidizer through engines.
^cThis temperature achieved from heat transfer to engine 4-up, through which propellant coldflowed throughout the second ascent engine firing, and from venting B system propellants.

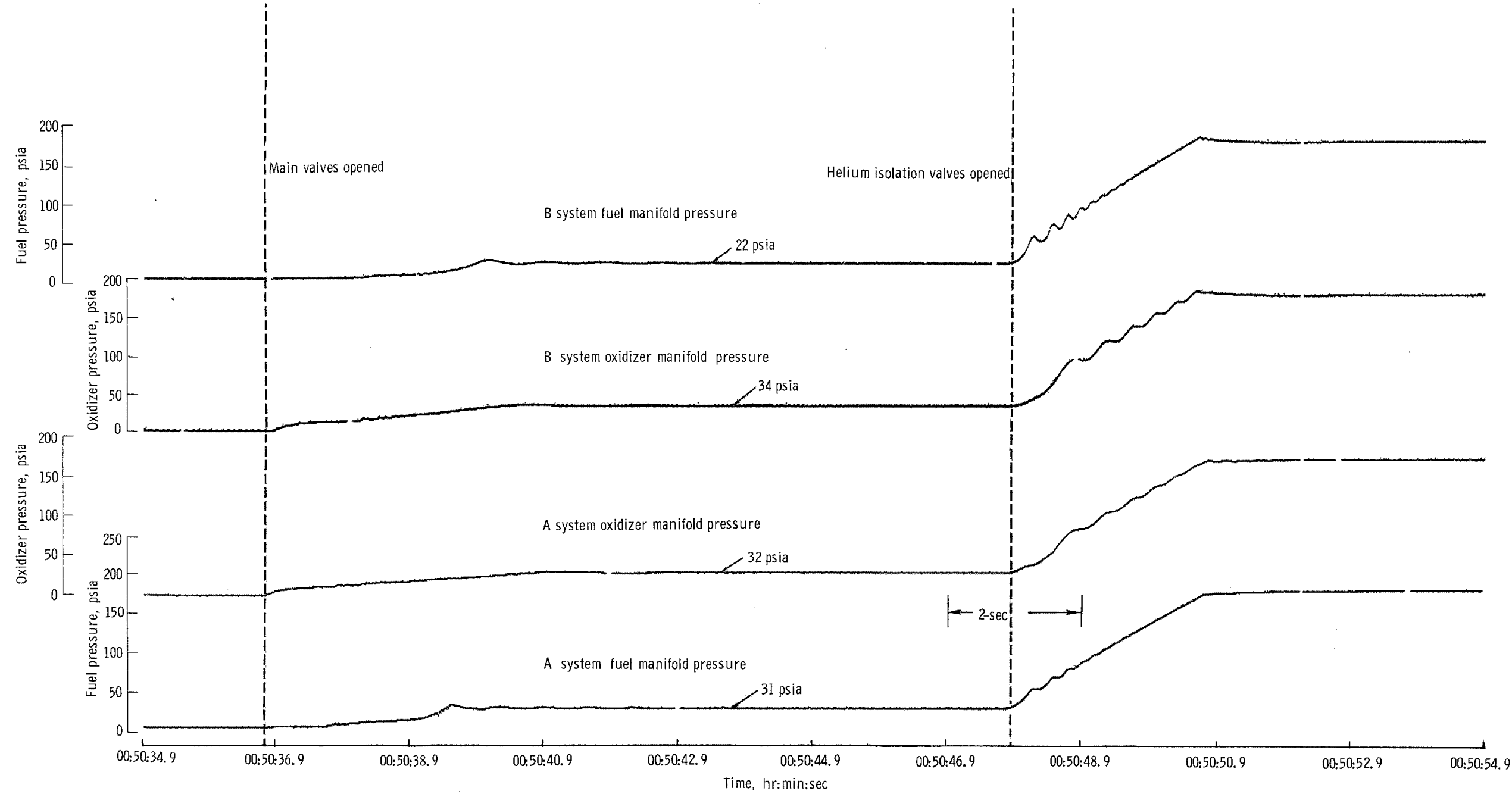


Figure 6.11-1. - Manifold pressures during system activation sequence.

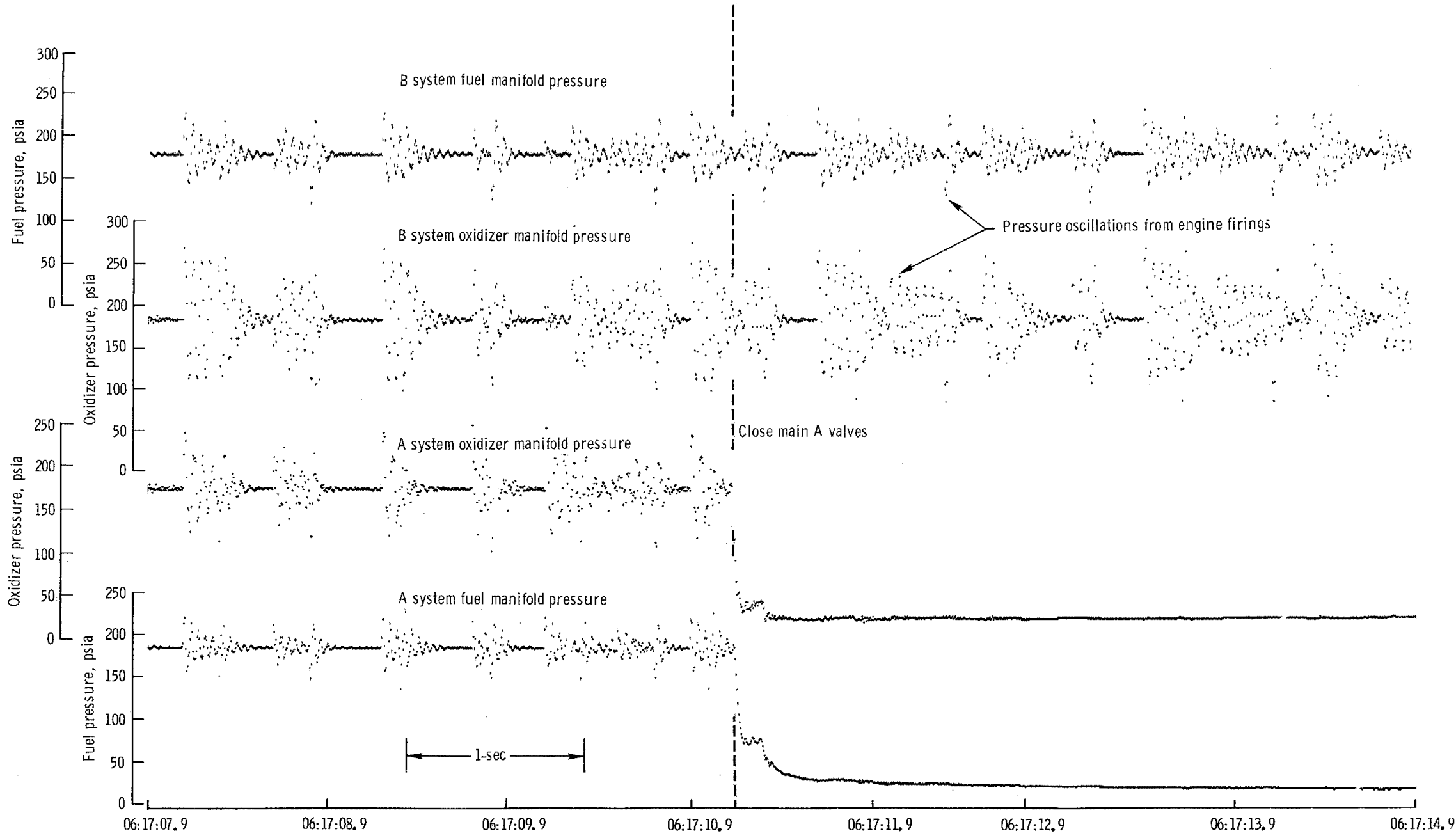


Figure 6.11-2. - Manifold pressures at main A closure.

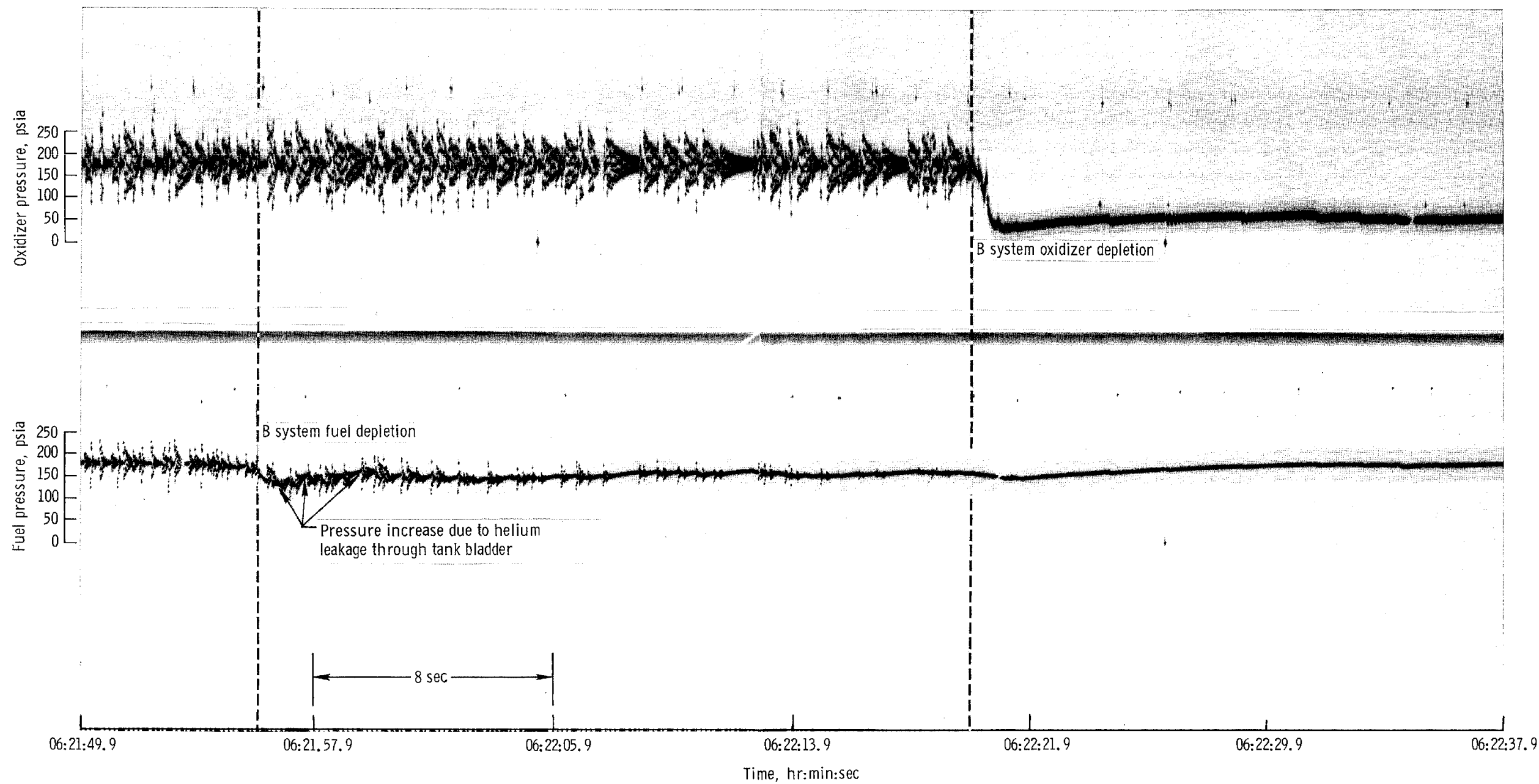


Figure 6.11-3. - B system manifold pressures at propellant depletion.

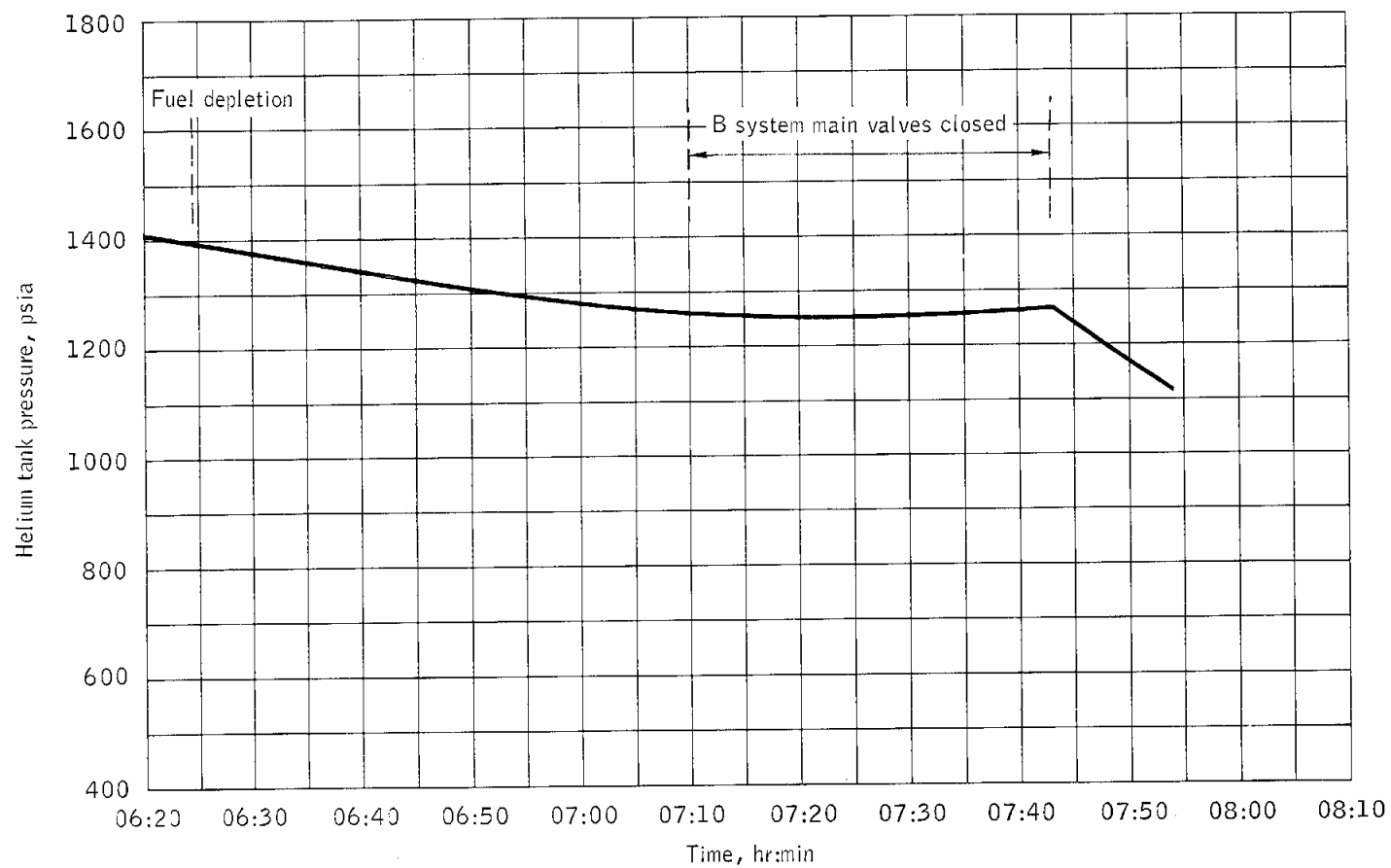


Figure 6.11-4.- Helium B tank pressure (corrected to 70°F) during period of propellant depletion.

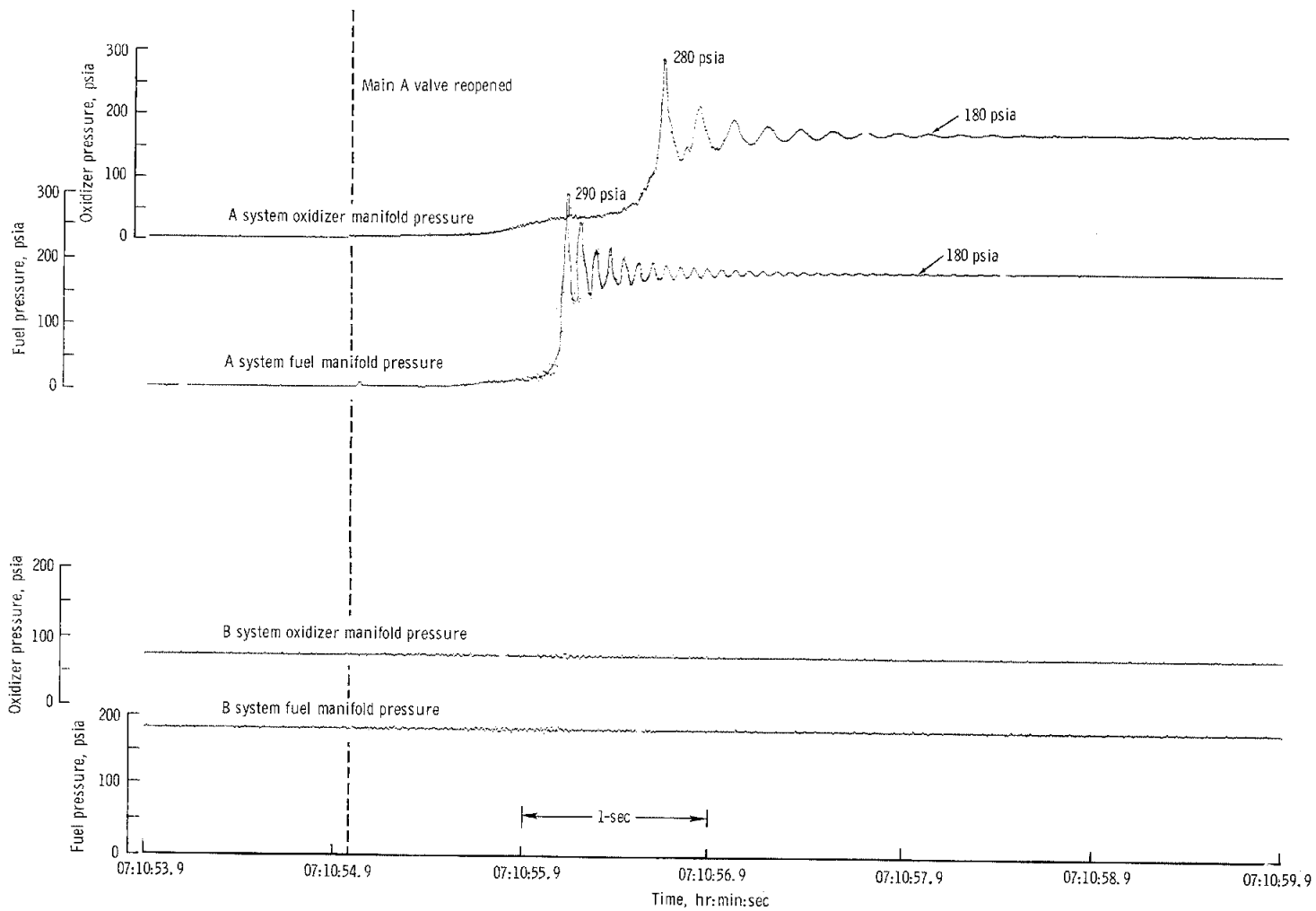


Figure 6.11-5. - Manifold pressures during A system reactivation.

68-2030

Both sides

NASA-S-68-2030

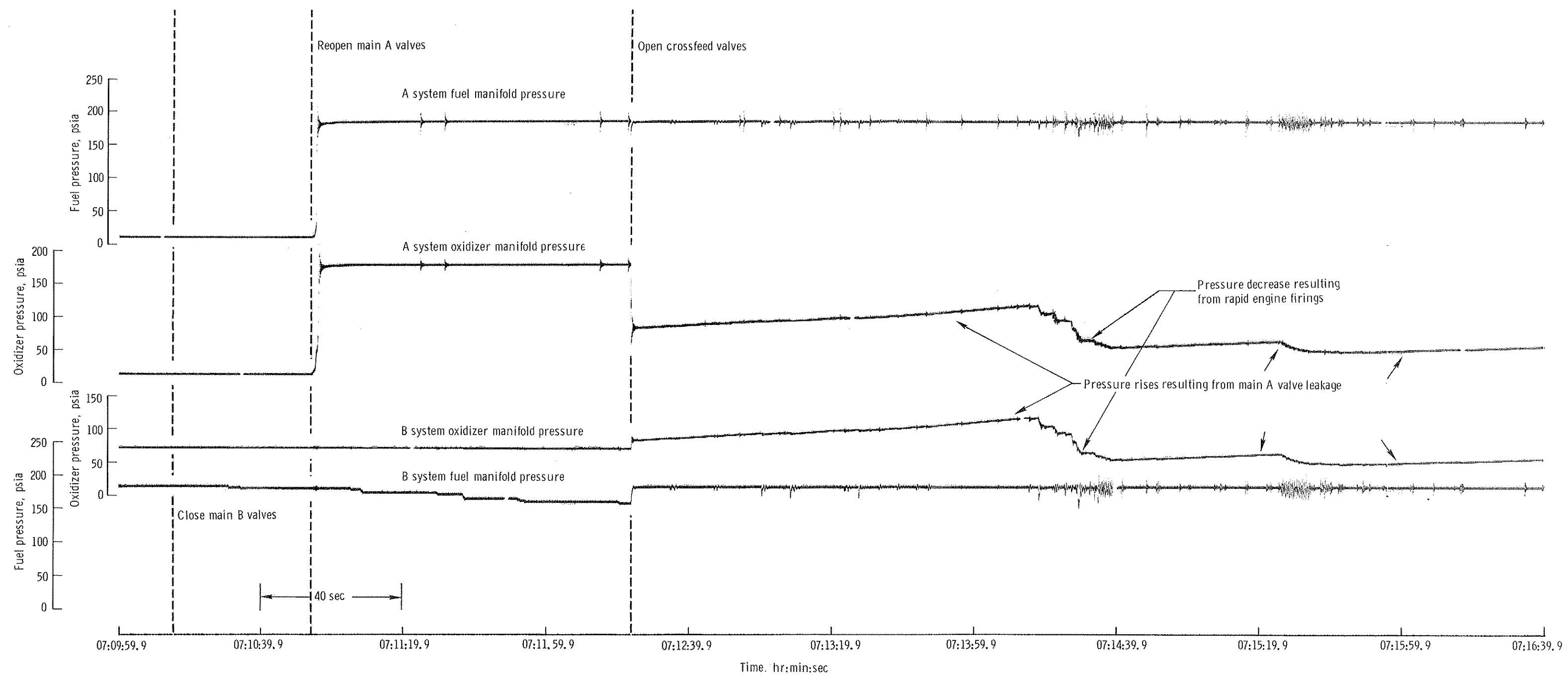


Figure 6.11-6. - Manifold pressures during period of A system reactivation and crossfeed valve opening.

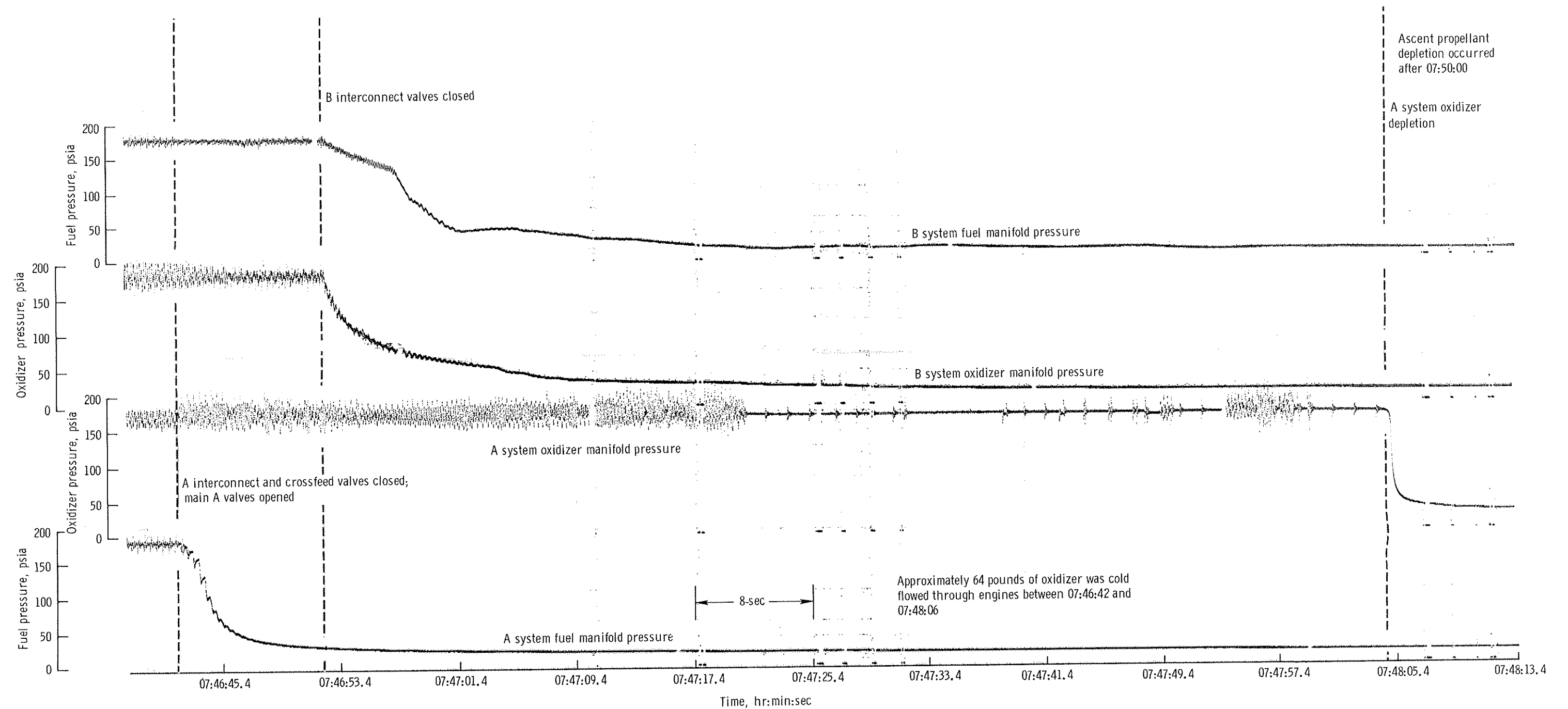


Figure 6.11-7. - Manifold pressures after interconnect valves closure.

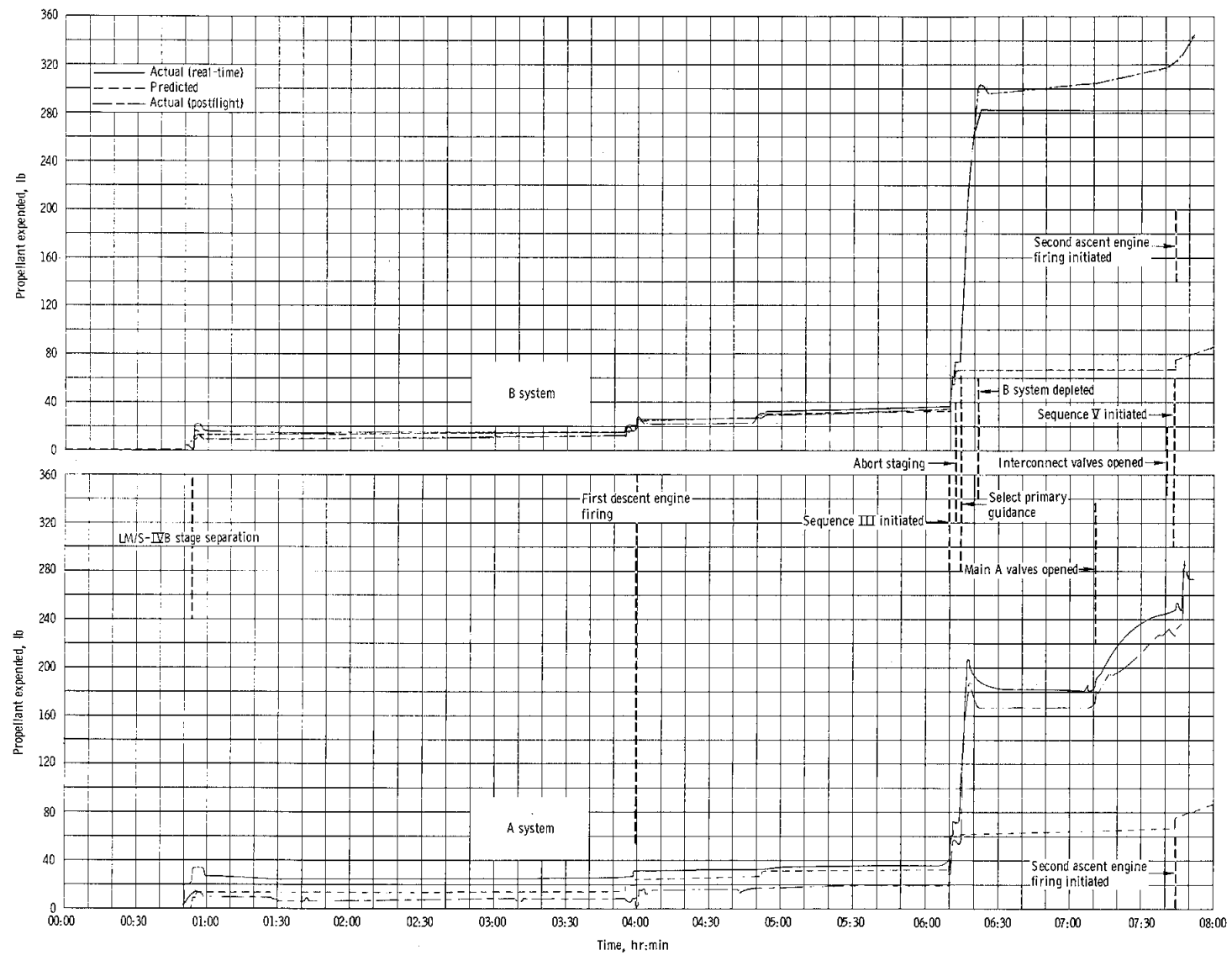


Figure 6.11-8. - Propellant expended.

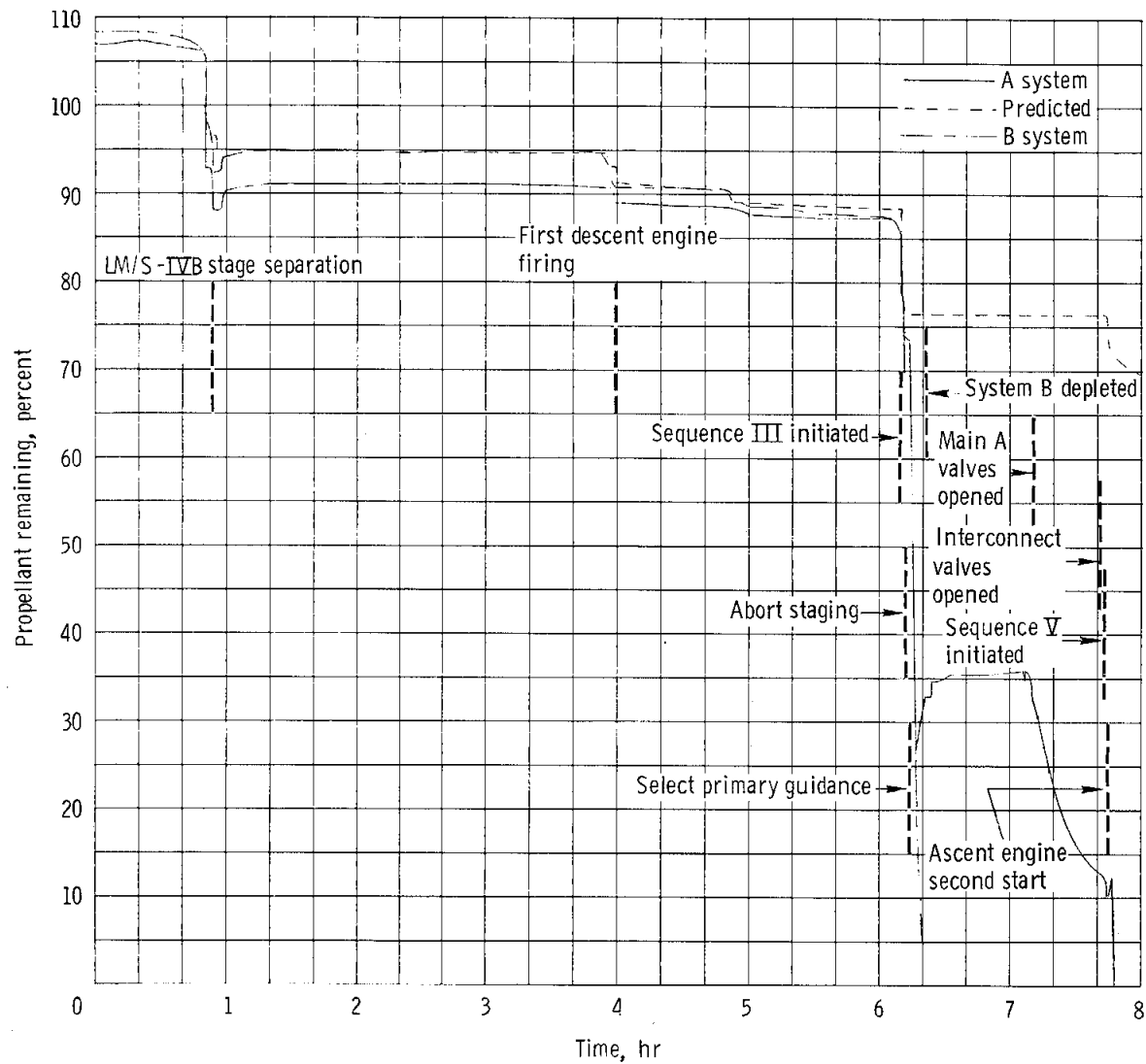


Figure 6.11-9. - Performance of propellant quantity measuring device.

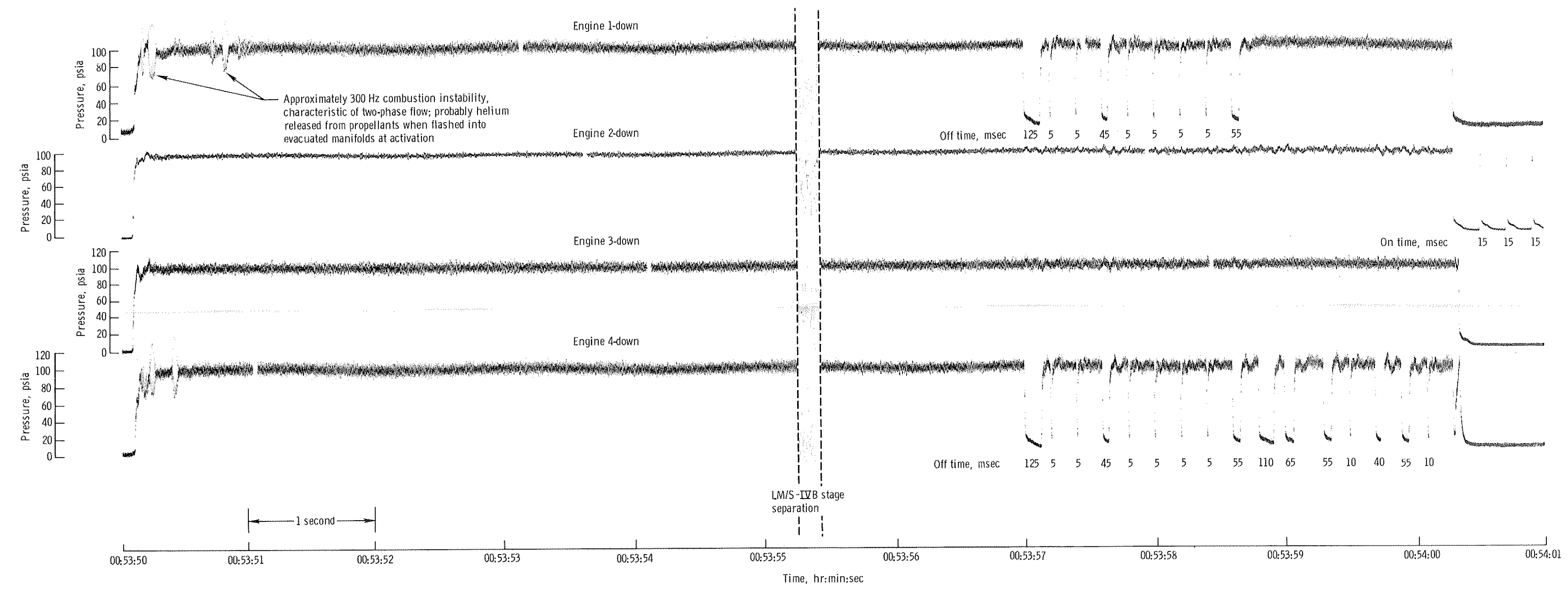


Figure 6.11-10. - Engine chamber pressures during first firings (separation sequence).

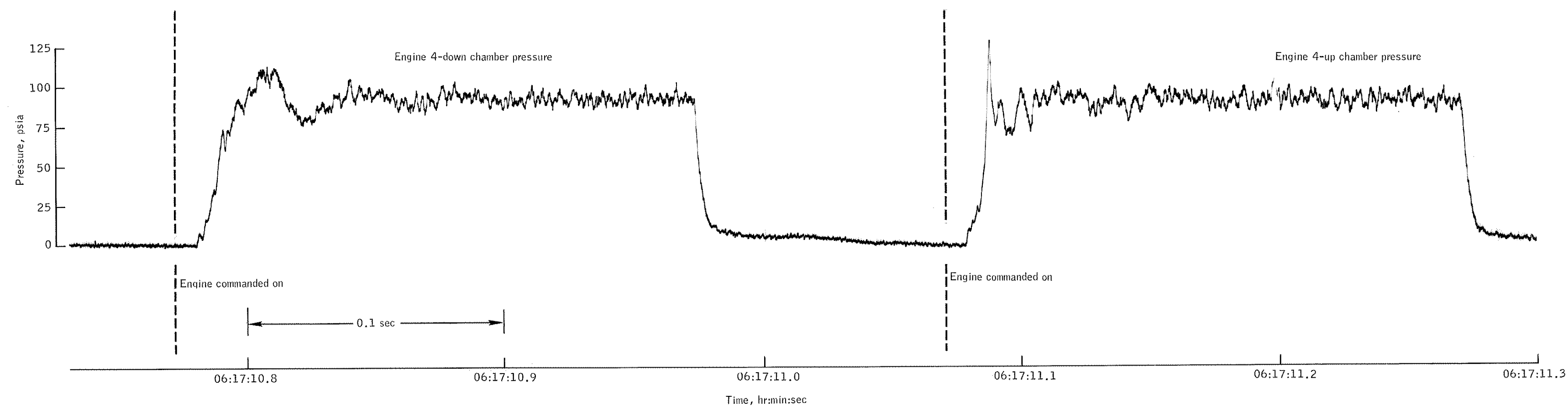


Figure 6.11-11.- Chamber pressure of engines 4-down and 4-up during high propellant usage following first ascent engine firing.

NASA-S-68-2036

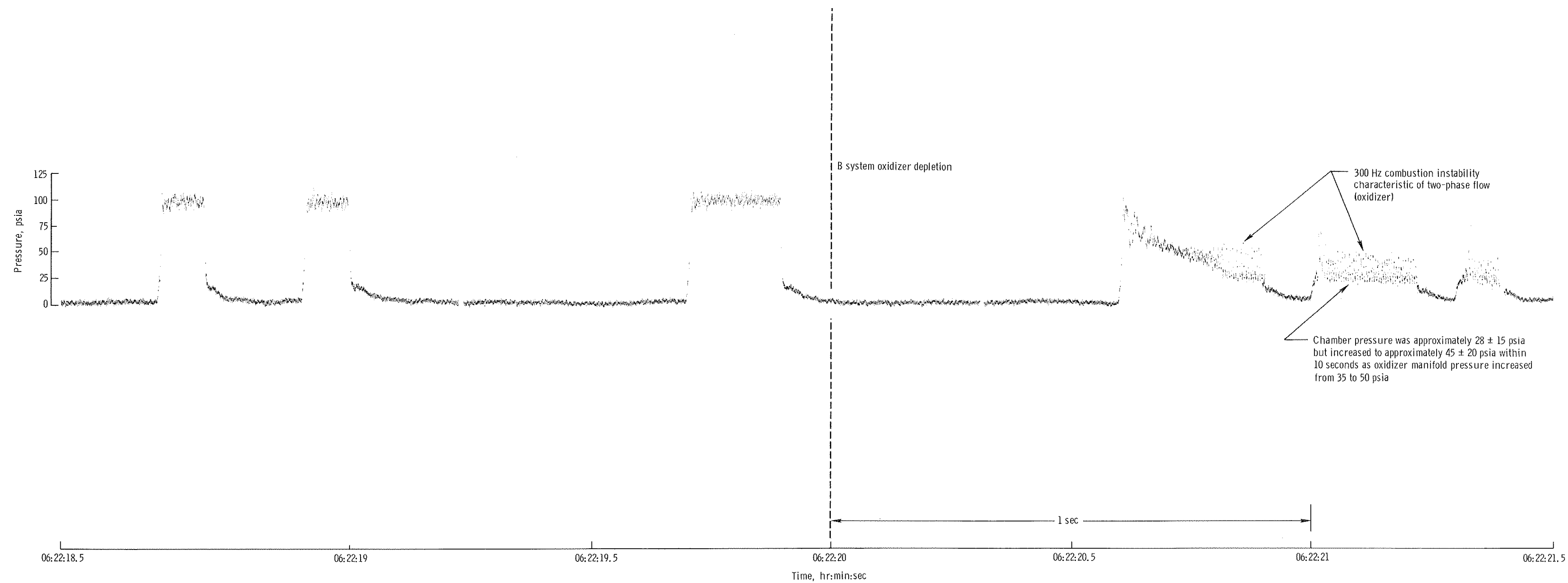


Figure 6.11-12. - Engine 4-up chamber pressure at B system oxidizer depletion.

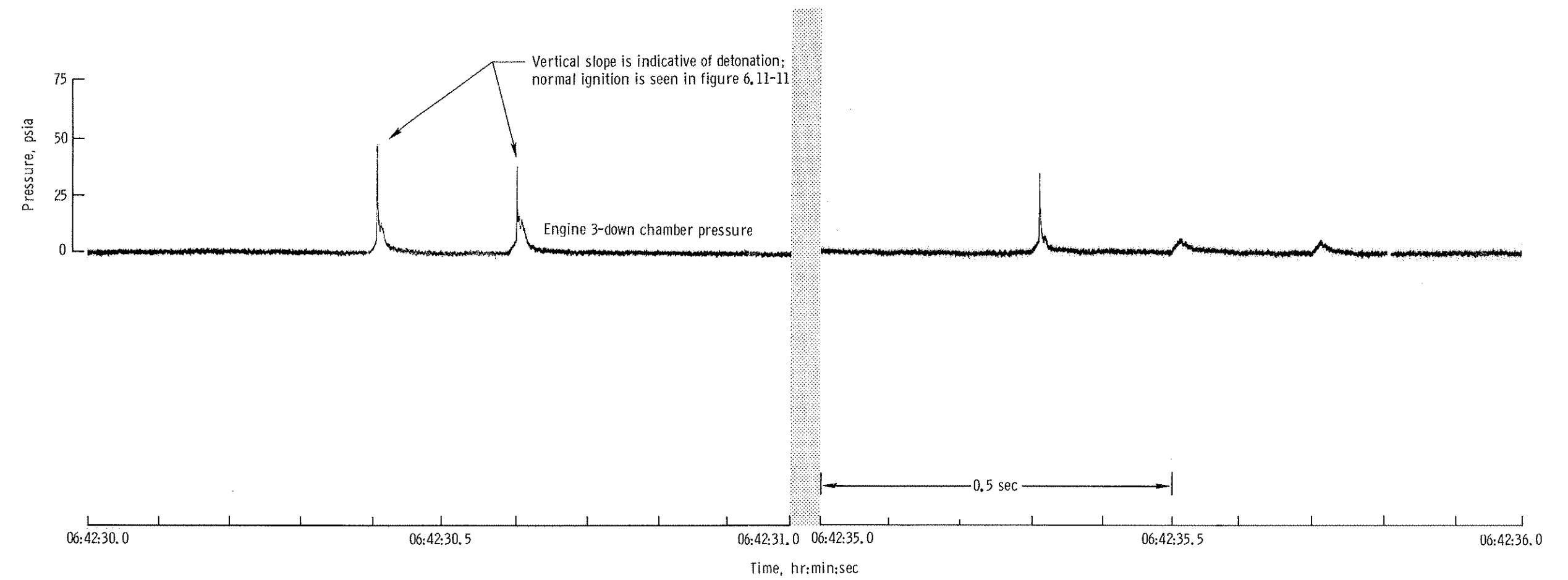


Figure 6.11-13. - Ignition pressure spike (detonation) in engine 3-down during operation with two-phase oxidizer at 50 psia manifold pressure and with helium in fuel manifold.

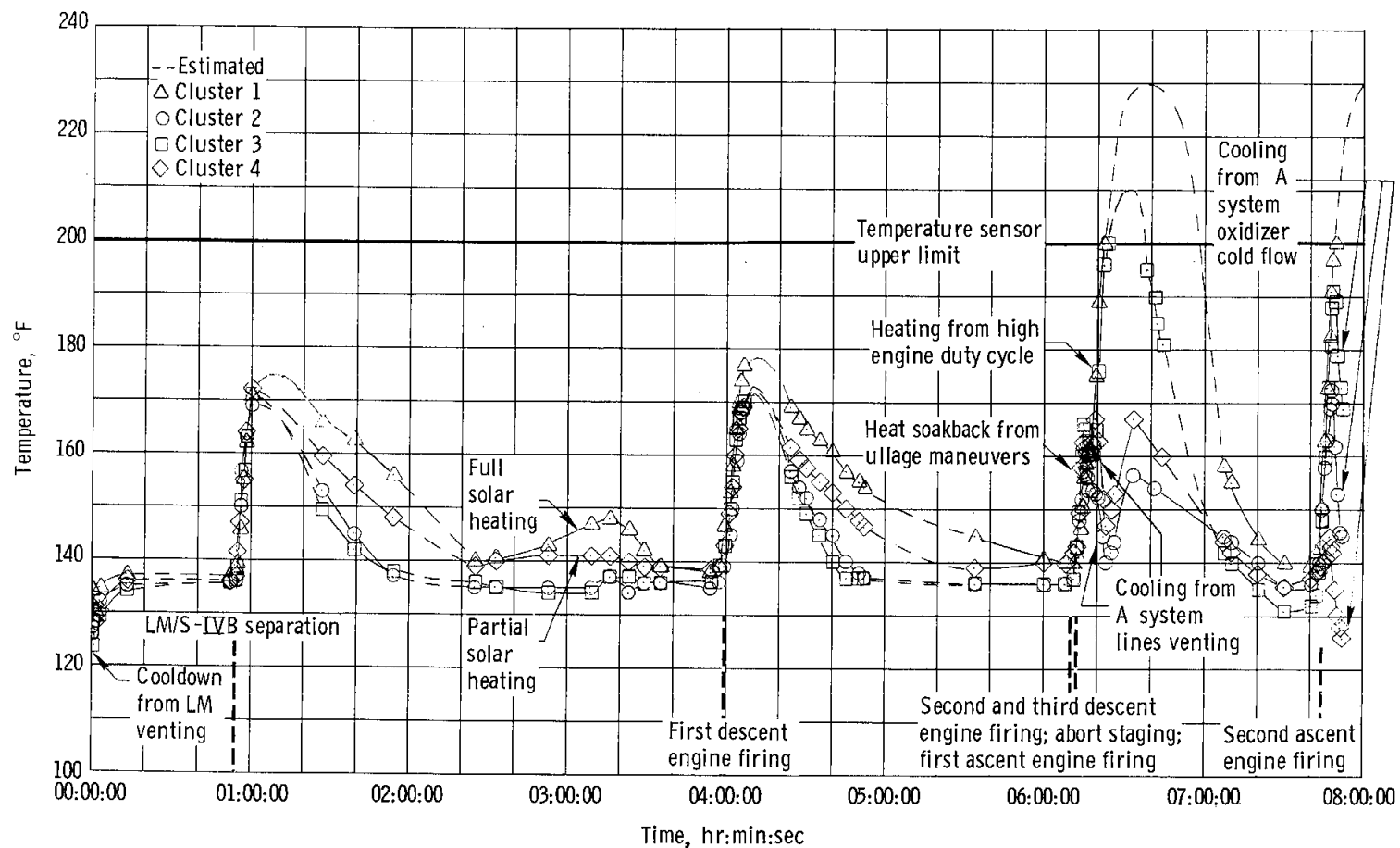


Figure 6.11-14. - Cluster temperatures during the mission.

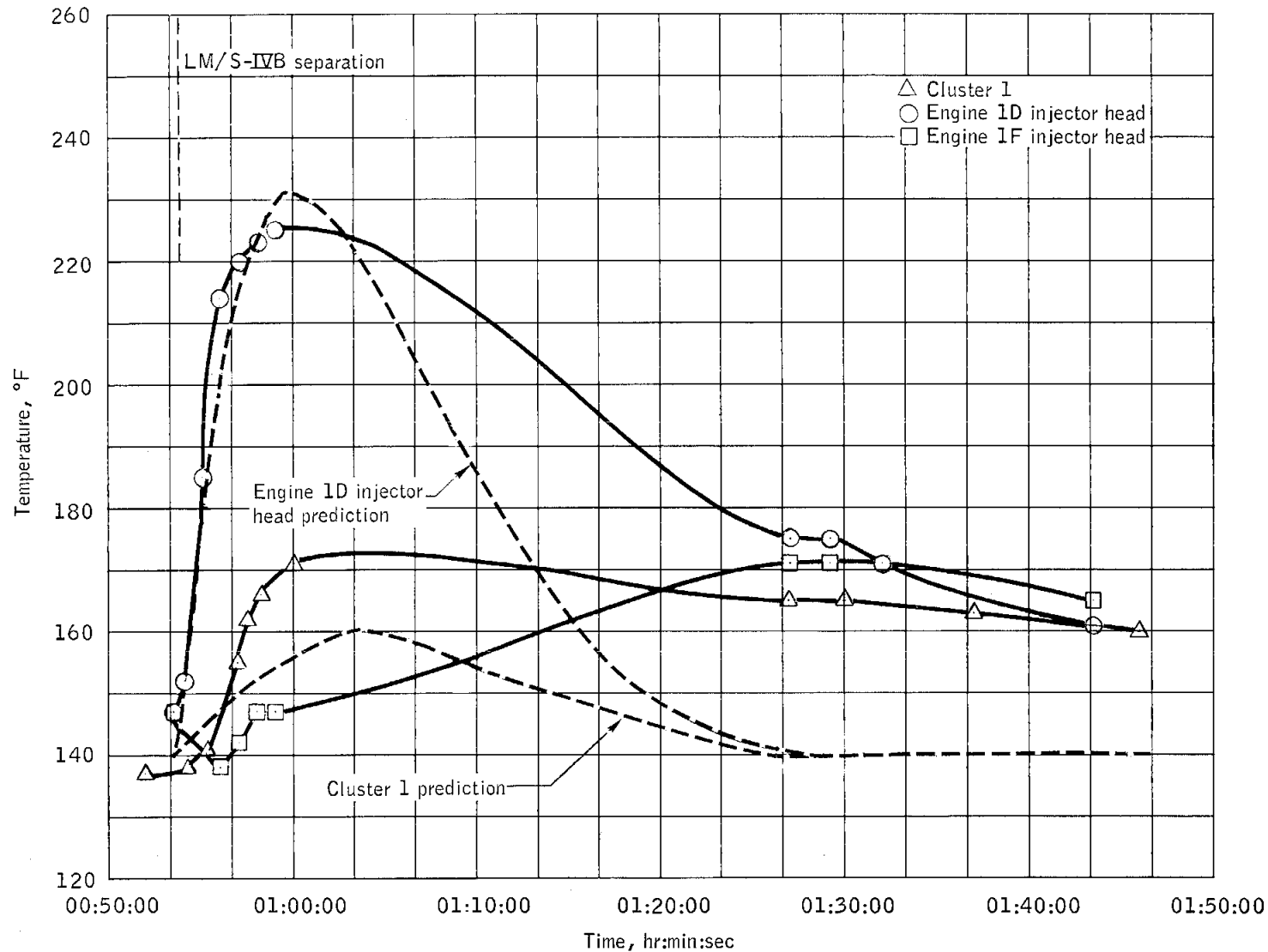


Figure 6.11-15.- Cluster 1 and engines 1-down and 1-forward injector head temperatures at LM/S-IVB stage separation.

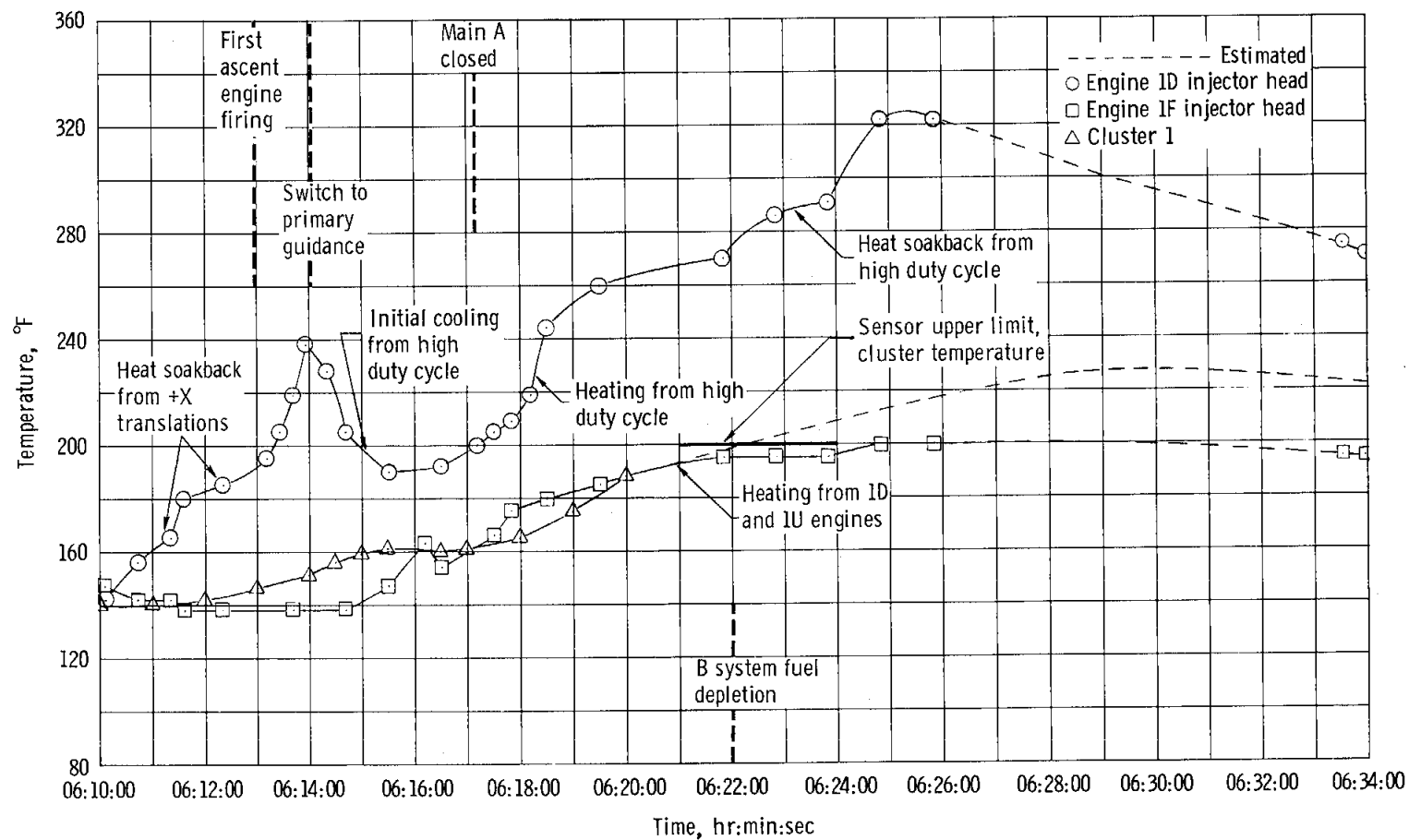


Figure 6.11-16. - Cluster 1 and engines 1-down and 1-forward injector head temperatures during mission programmer sequence III.

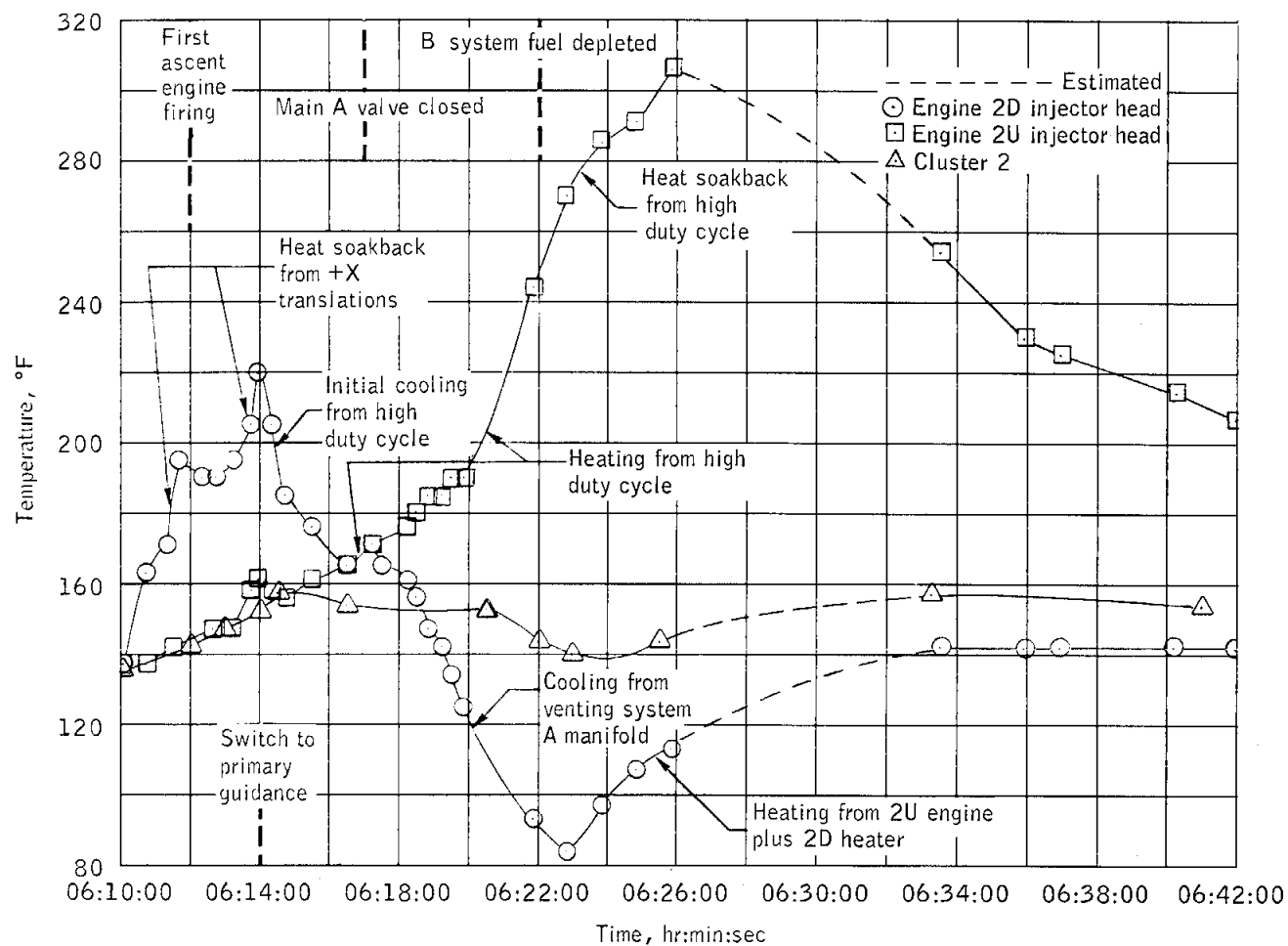


Figure 6.11-17.- Cluster 2 and engines 2-down and 2-up injector head temperatures during mission programmer sequence III.

NASA-S-68-2042

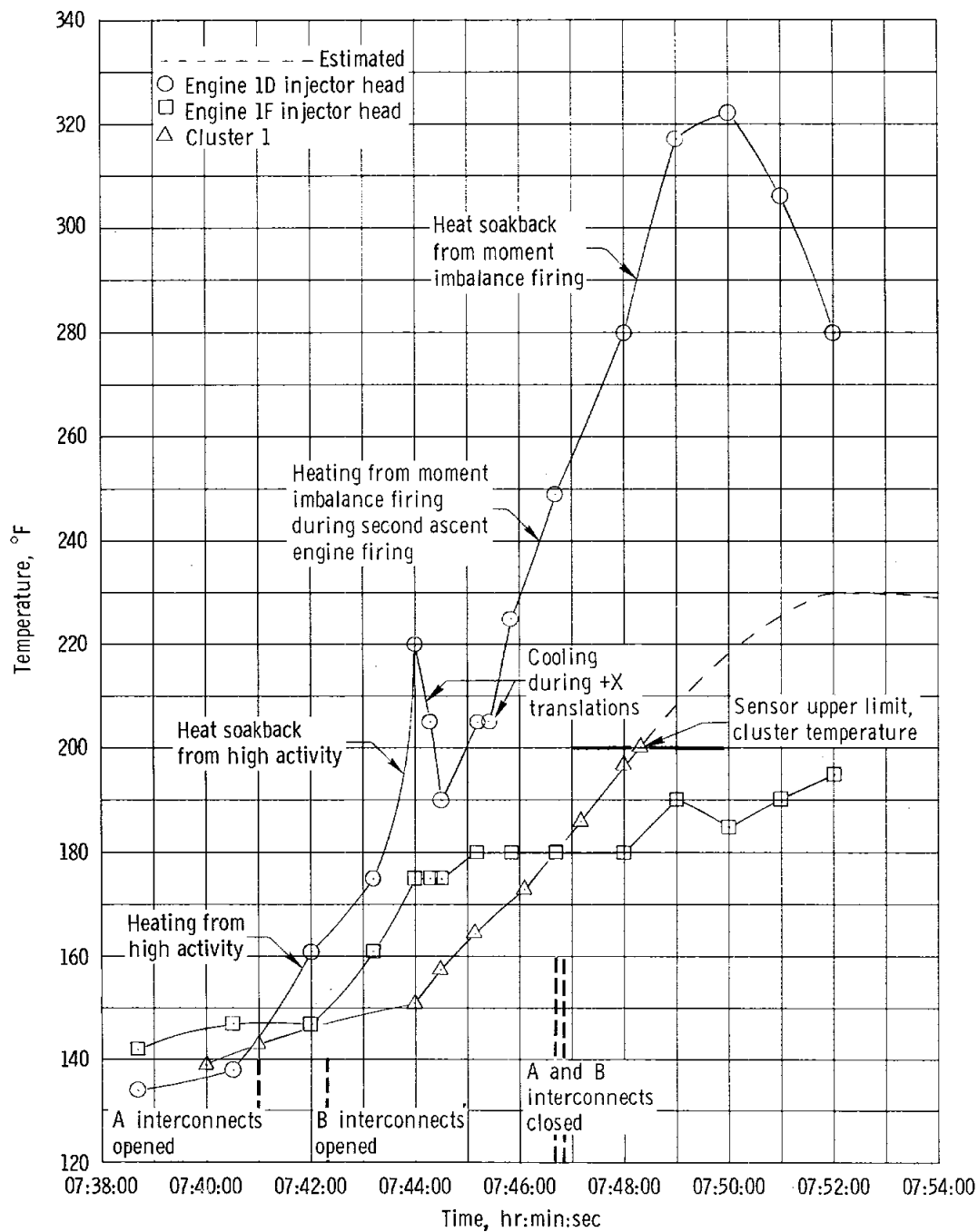


Figure 6.11-18. - Cluster 1 and engines 1-down and 1-forward injector head temperatures during second ascent engine firing.

NASA-S-68-2043

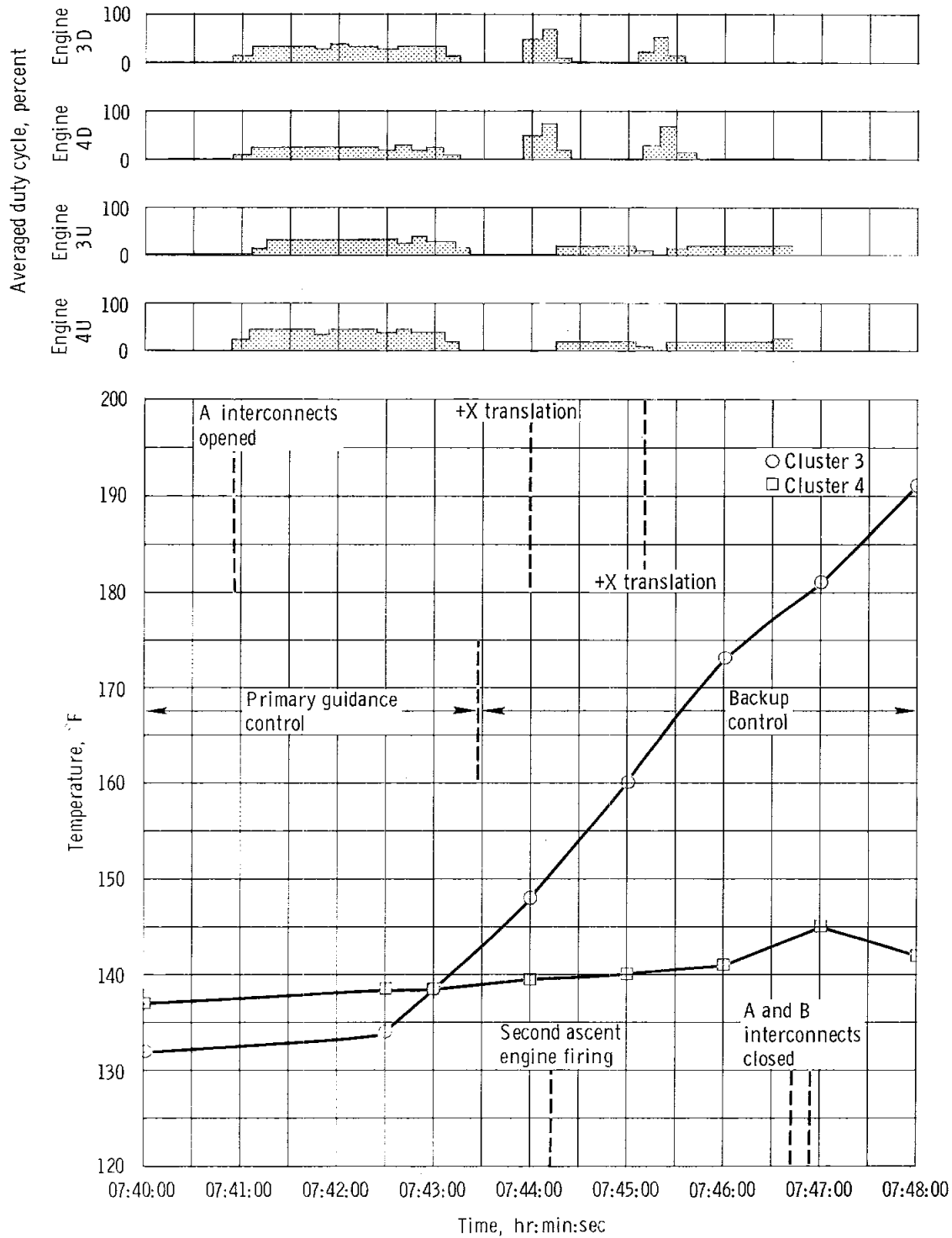


Figure 6.11-19. - Comparison of thermal response of clusters 3 and 4 to control engine activity during second ascent engine firing.

6.12 DESCENT PROPULSION

The first planned descent engine firing was shut down after 4.17 seconds by the guidance computer. Alternate mission C, which included two descent engine burns, was then implemented. Each of these firings began with 26 seconds at 10-percent throttle, followed by 7 seconds at full throttle during the first firing and 2 seconds at full throttle during the second firing. The original mission plan required approximately 782 seconds of engine firing time, which included various throttling activities, and 374 seconds at full throttle. The descent propulsion system appeared to operate satisfactorily to the extent exercised; however, the firing times were not of sufficient duration to permit an accurate determination of the performance of the descent engine or supercritical helium pressurization system.

6.12.1 Start Characteristics

Figure 6.12-1 shows the variations in chamber pressure for the three descent engine starts. A nominal start curve, obtained from tests under normal regulated pressures of 242 psia, is also shown for comparison. The regulated tank pressures for the second and third firings were about 242 psia and show close agreement with the nominal curve. The quicker start noted for the third firing may have resulted from the fuel injector manifold still being partially primed because of the short 32-second coast period. At the start of the first firing, oxidizer and fuel tank pressures were essentially as planned, approximately 127 and 132 psia, respectively. About 1.3 seconds after the "engine on" command, the helium pressurization isolation valves were opened and the tank pressures started to increase. This pressurization activation delay was designed into the system to prevent fuel freezing in the heat exchanger. The pressures were still increasing at the time the computer issued an "engine off" command. The engine was shut down because the impulse required by the computer was not obtained; the computer required 1440 lb-sec impulse over a 2-second interval. The engine had obtained a total of only 1075 lb-sec at the time of cutoff. From the figure, it is evident that nearly all the 1075 lb-sec impulse was accumulated in the last 2-second interval. The engine-delivered impulse before shutdown was as expected for the existing start conditions.

Figure 6.12-1 shows the results of a special test conducted at the White Sands Test Facility after the mission. This test utilized similar initial conditions except that tank pressurization was initiated 0.9 second after the "engine on" command. The resulting initial thrust level, corresponding to the 10-percent throttle setting, was somewhat lower. This initial thrust level varies from engine to engine.

6.12.2 Transient Characteristics

The transient characteristics for the second and third firings, along with the corresponding ground test and specification values, are shown in table 6.12-I. Because the steady-state thrust was not achieved during the first firing, the shutdown impulse was not computed. For the second firing, the shutdown impulse at cutoff was 1727 lb-sec from "engine off" initiate to 10-percent thrust. The time to 10-percent thrust from "engine off" was 0.26 second as compared with the specification value of 0.25 second. All other data show the engine transient characteristics to be satisfactory. The oscillations of chamber pressure were essentially nonexistent during 10-percent throttle operation, and only insignificant oscillations were present during full throttle operation (fig. 6.12-2).

6.12.3 Engine Throttle Response

During the second and third firings, mission programmer sequence III commanded the descent engine from the 10-percent throttle to full throttle at a constant rate. Throttle response of the engine was within the 1.0-second allowable time. Figure 6.12-2 shows chamber pressure and injector actuator position during the transition to full throttle for the second firing. The engine reached the full thrust level 0.40 second after the command was initiated for the second firing and 0.46 second for the third firing. The chamber pressure was within 5 psia of the full chamber pressure in 0.34 second after the command for the second firing and in 0.4 second for the third firing as compared with acceptance test time of 0.35 second.

The plateau experienced at approximately 70-percent thrust is assumed to be associated with the engine changing from a cavitating to a non-cavitating propellant flow and is characteristic of this engine. This plateau of approximately 70 milliseconds, however, exceeds the 10 milliseconds normally experienced in acceptance testing. There was also a simultaneous pressure increase in the oxidizer and fuel engine interface pressures. The surge in the interface pressures at the time of the plateau had not been noted during ground tests; however, the ground data will be further reduced to determine whether these surges were present. The cause of the plateau phenomenon will be investigated by additional ground testing.

6.12.4 Steady-State Characteristics

The chamber pressure characteristics during the second firing are shown in figure 6.12-3. Characteristics during the third firing were

essentially the same. The following table presents some of the parameters within the engine feed system.

Event	Helium regulator outlet pressure, psia	Engine oxidizer interface pressure, psia	Engine fuel interface pressure, psia	Thrust chamber pressure, psia
Corrected Flight Data for Second Firing				
Before ignition	241.9	241.9	241.9	0
Ten-percent throttle	239.5	239.5	239.5	12.6
Full throttle	239.5	220.5	216.0	102.8
Corrected Flight Data for Third Firing				
Before ignition	241.9	241.9	241.9	0
Ten-percent throttle	239.5	239.5	239.5	12.6
Full throttle	-	-	-	-

No analysis of the flight data was made to determine the steady-state performance parameters because the short duration engine firings provided insufficient duration of acceleration data at full throttle and low propellant usage. The steady-state pressure parameters at 10-percent throttle and at full throttle were comparable to ground test results.

6.12.5 Shutoff Valve Phasing

The configuration of the propellant shutoff valves is shown in figure 6.12-4. During the second and third firings, while throttling from 10-percent to full thrust, an out-of-phase indication was received from one of the two pairs of actuators which control the eight propellant shutoff valves. The indication remained until the end of each of these firings.

Each of the four shutoff valve actuators (A, B, C, and D) controlled one fuel and one oxidizer shutoff valve. The actuators were instrumented in two pairs, so that an indication was received if actuators A and B or C and D were not in the same position (open or closed). During the second and third firings, the received signal indicated that either A or B actuator was not fully open. This indication slightly lagged the thrust plateau and the momentary increase in the oxidizer and fuel interface pressure as noted under section 6.12.3. The occurrence was nearly identical on the second and third firings. At present, no conclusions can be drawn as to whether there is any connection between the pressure transients and the valve out-of-phase indication. Further evaluation and special ground tests will be conducted in an attempt to resolve the problem.

6.12.6 Propellant Quantity Gaging

The flight data show that the quantity gaging system was not indicating correctly for the number 2 fuel and oxidizer tanks; however, this condition was known prior to flight. A failure investigation has attributed the effect to a faulty transistor within the gaging system. The descent engine firing time was not sufficient to permit a full assessment of system accuracy.

6.12.7 Supercritical Helium Pressurization

Because of the short duration of the engine firings and the lack of long-duration full-throttle data, it is not possible to evaluate the performance of the supercritical helium pressurization system. Figure 6.12-5 presents the flight data for the first descent engine firing and also data from a simulation performed at White Sands Test Facility.

As shown in the figure, the supercritical helium tank pressure decay resulted from the higher than normal helium flow rate required to pressurize the ullage in the tanks to the normal operating level. The increased decay indicated by the White Sands simulation data was the result of a larger ullage volume than was present during flight, and this caused a greater pressure drop. The White Sands simulation was also not shut down at 4 seconds but continued at 10-percent throttle level.

Figures 6.12-6 and 6.12-7 show flight data and predicted pressures from a computer program simulation for the second and third firings, respectively. The figures indicate that the measured tank pressure was less than had been predicted by the ground simulation computer program. The computer simulation accuracy is not known for short firings because empirically derived coefficients from ground test data were used in the

formulations. As a result, it is not possible to determine whether the apparent low pressure obtained during the flight was actually below normal. Figure 6.12-8 shows the flight data during the coast period between the first and second firings. The figure indicates that the steady-state pressure rise was as predicted (approximately 10 psia per hour).

Table 6.12-II shows the performance of the helium/helium and helium/fuel heat exchangers. Although the pressure profiles do not exactly follow the predictions (figs. 6.12-5 through 6.12-8), the maximum and minimum temperatures recorded at various stations were well within specification limits.

TABLE 6.12-I.- DESCENT ENGINE TRANSIENT CHARACTERISTICS

6.12-6

	Start - "engine on" to 90-percent thrust		Shutdown - "engine off" to 10-percent thrust	
	Impulse, lb-sec	Time, sec	Impulse, lb-sec	Time, sec
Second firing	894	2.66	1727	0.26
Third firing	574	2.13	1820	0.25
Engine 1026 acceptance tests at sea level, 10-percent throttle start	-	2.60	-	-
	-	2.42	-	-
Engine 1026 acceptance tests at above 100K feet, 15-percent throttle start	982	1.31	-	-
	1041	1.36	-	-
Specification limits	-	4.0	-	0.25

TABLE 6.12-II.- SUPERCRITICAL HELIUM HEAT EXCHANGER PERFORMANCE

Measurement	Specification value	First firing	Second firing	Third firing
Temperature, helium/helium heat exchanger outlet, °R	>260	^a 273	^a 343	^a 347
Temperature, helium/fuel heat exchanger outlet, °R	>400	^a 468	^a 473	^a 475
Temperature, engine interface, fuel, °F	(b)	71.4	62.0	63.7
Temperature, fuel tank no. 1, fuel bulk, °F	(b)	70.5	70.5	70.5
Temperature, fuel tank no. 2, fuel bulk, °F	(b)	70.5	72.0	72.0

^aMinimum observed value during time period.

^bSpecification constrains difference between fuel tank temperature and fuel engine interface temperature to be no less than 5° F.

NASA-S-68- 2044

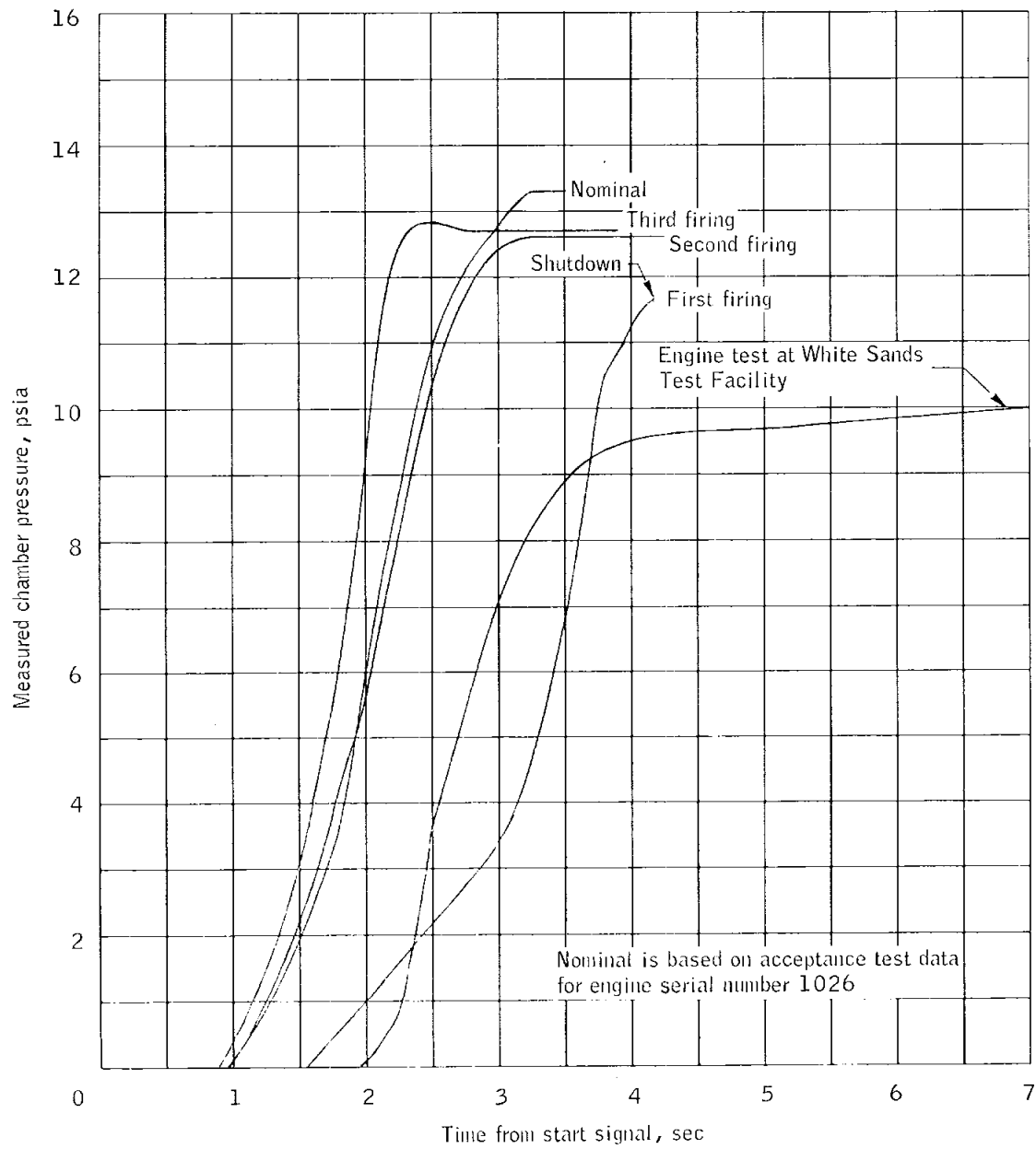


Figure 6.12-1.- Chamber pressure during start sequence of descent engine firings.

NASA-S-68- 2045

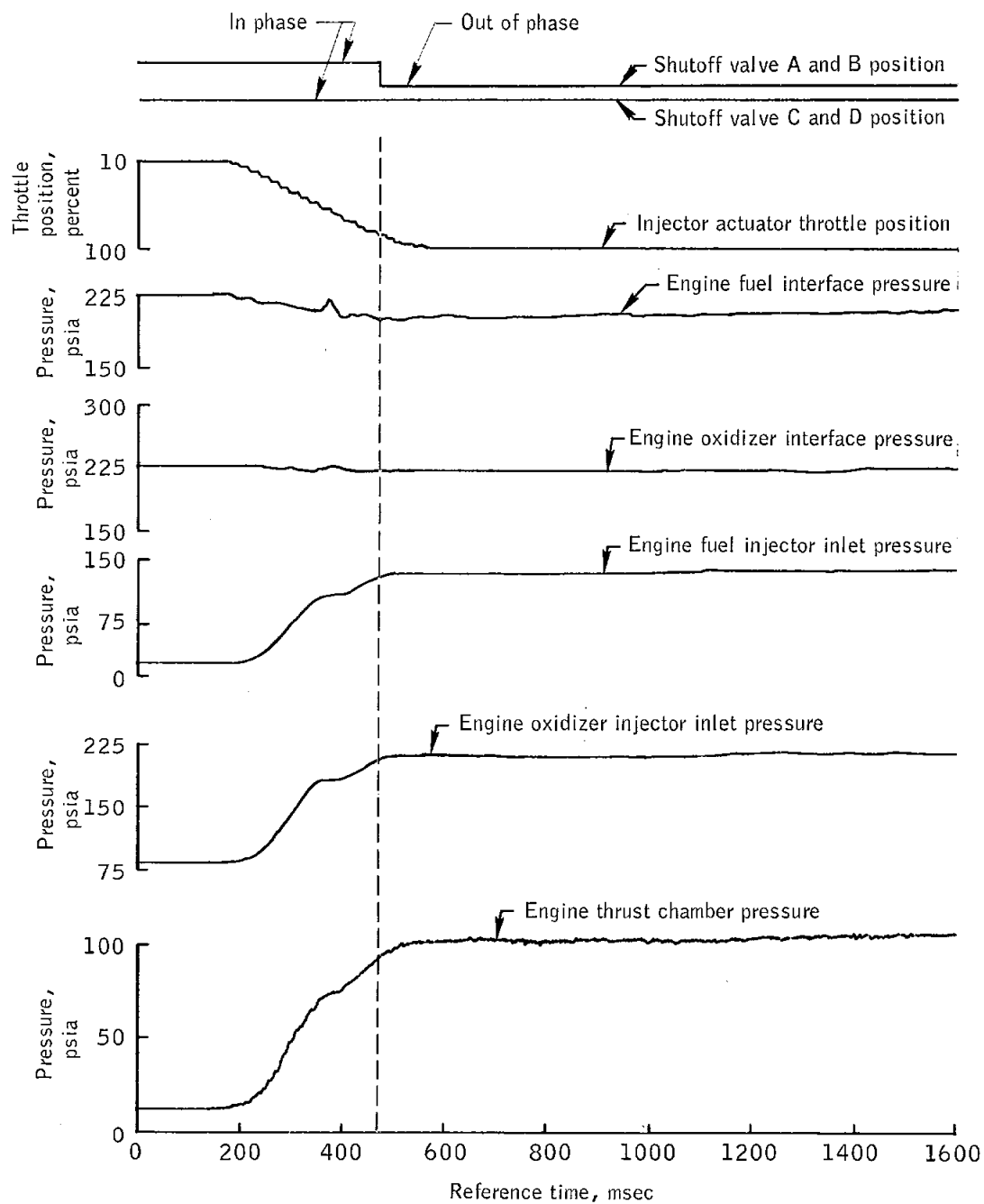


Figure 6.12-2.- Descent propulsion parameters during transition from 10-percent throttle to full throttle (typical of second and third firings).

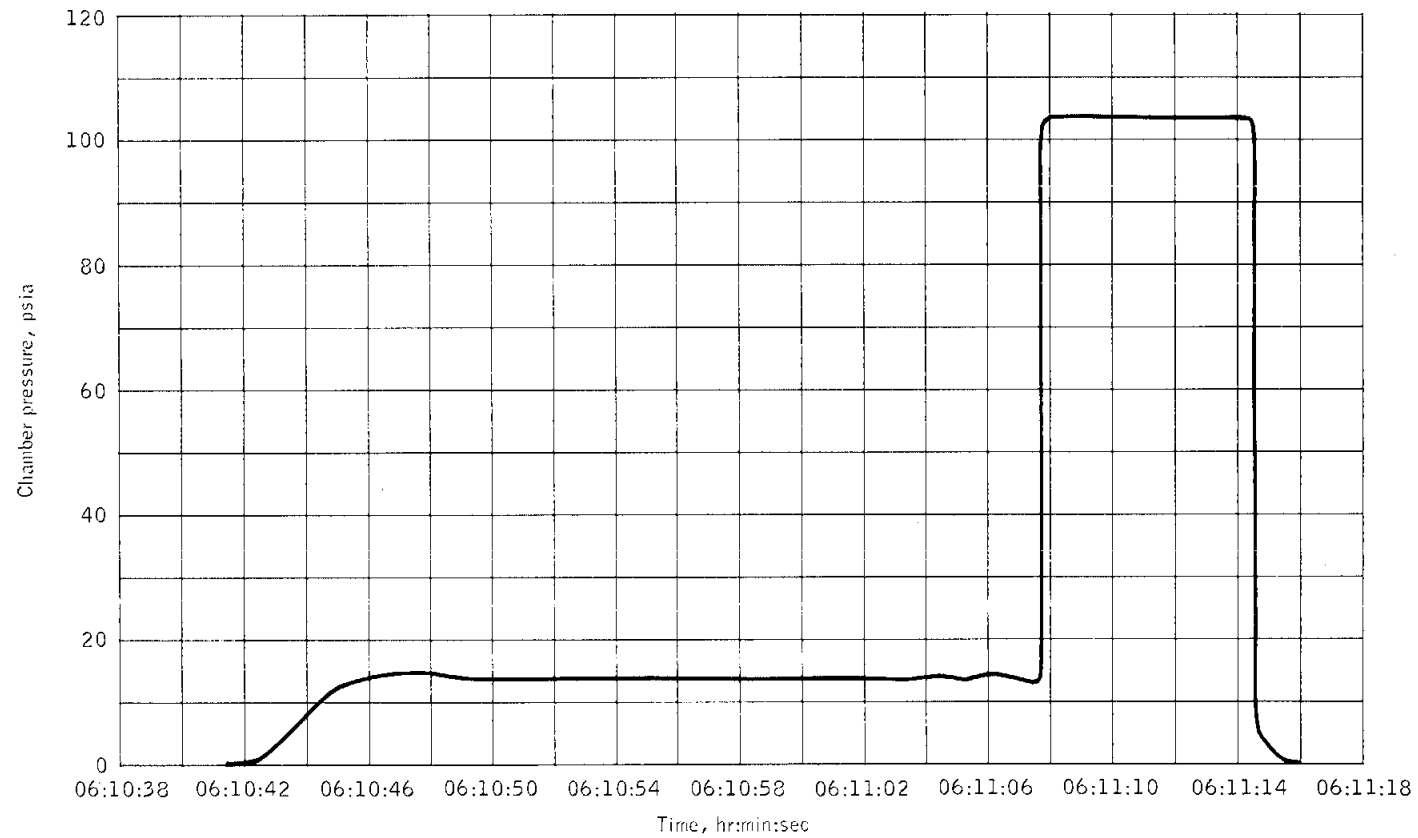


Figure 6.12-3.- Chamber pressure during second descent engine firing.

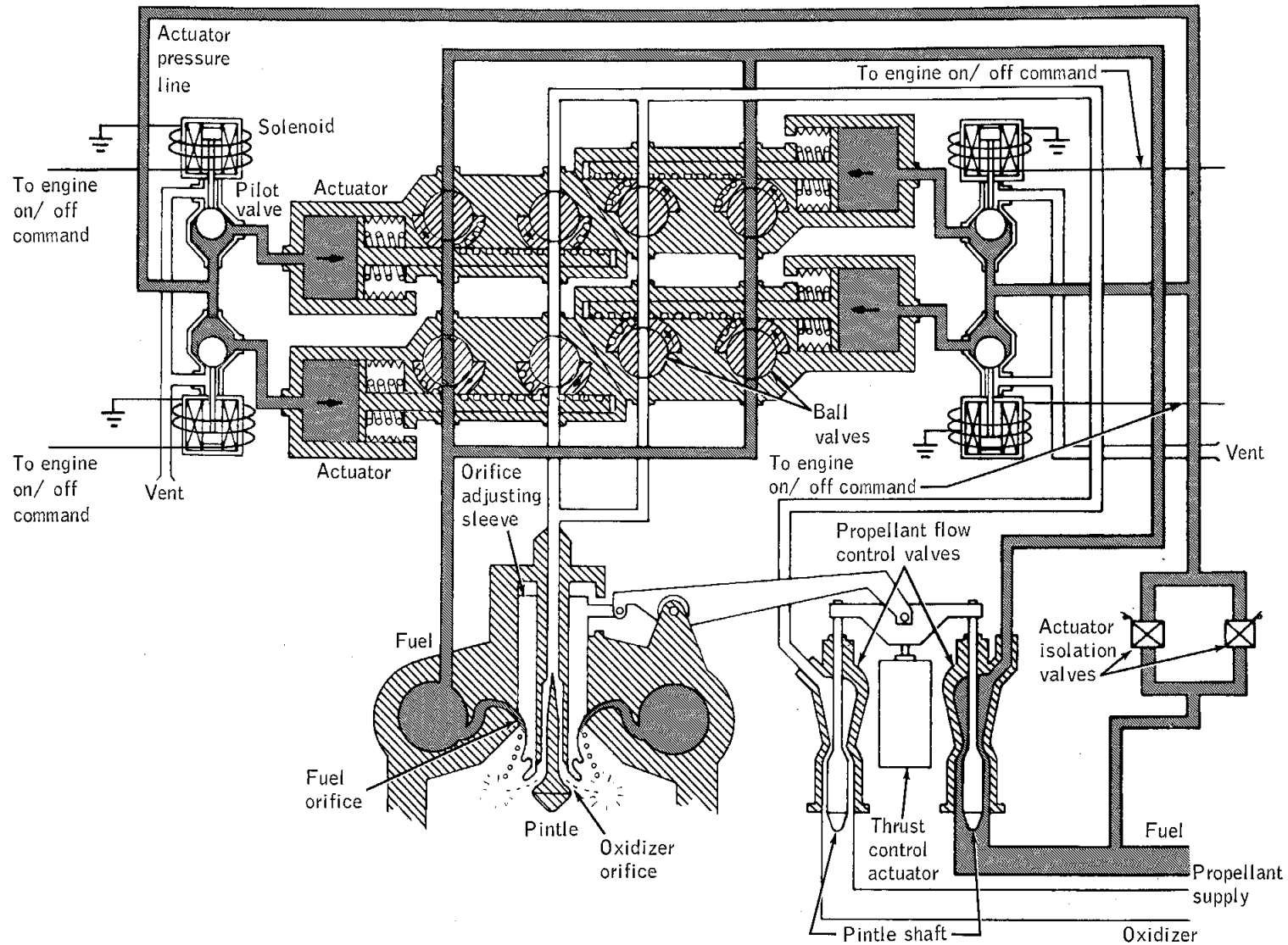


Figure 6.12-4.- Descent engine schematic.

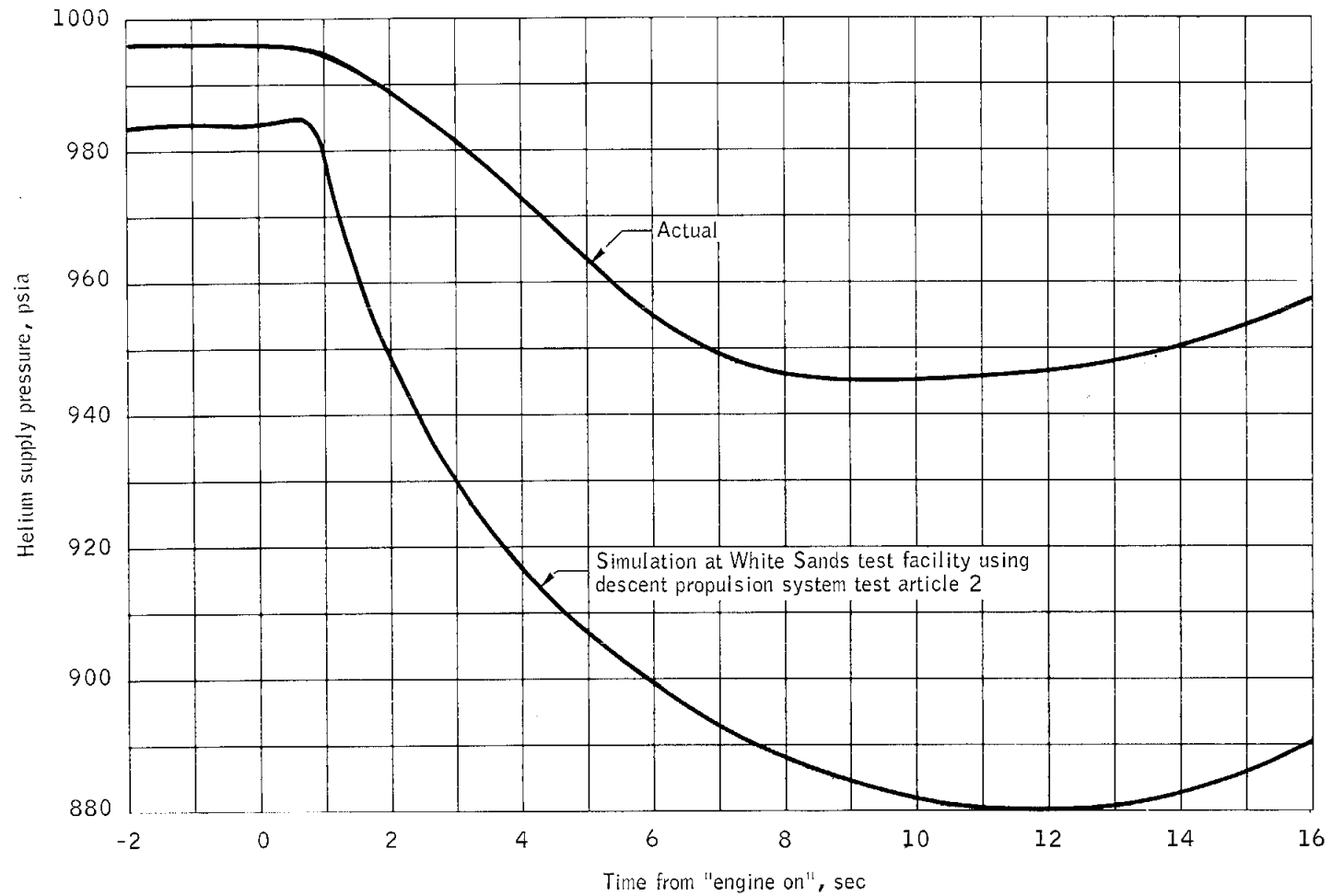


Figure 6.12-5.- Supercritical helium supply pressure during first descent engine firing.

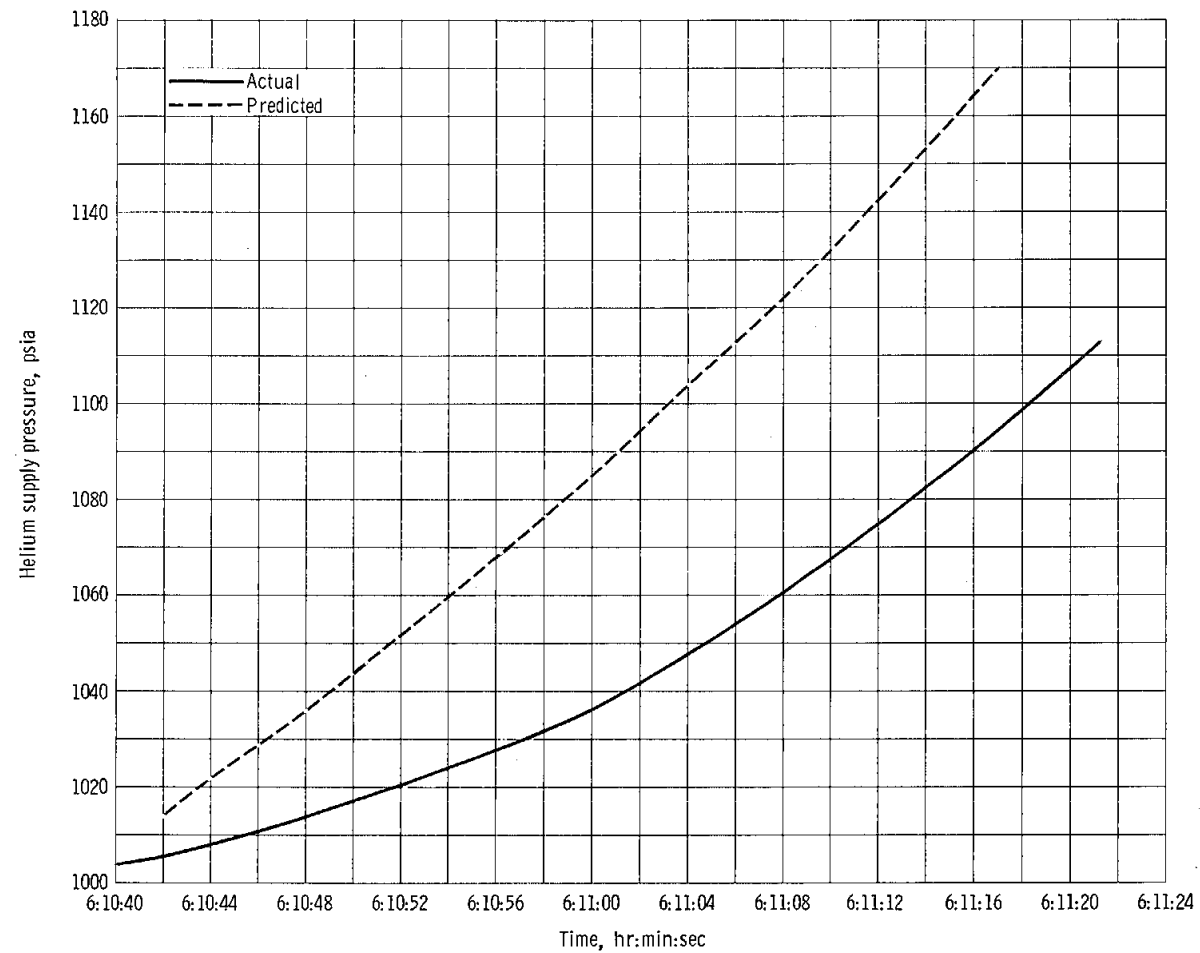


Figure 6.12-6. - Supercritical helium supply pressure during second descent engine firing.

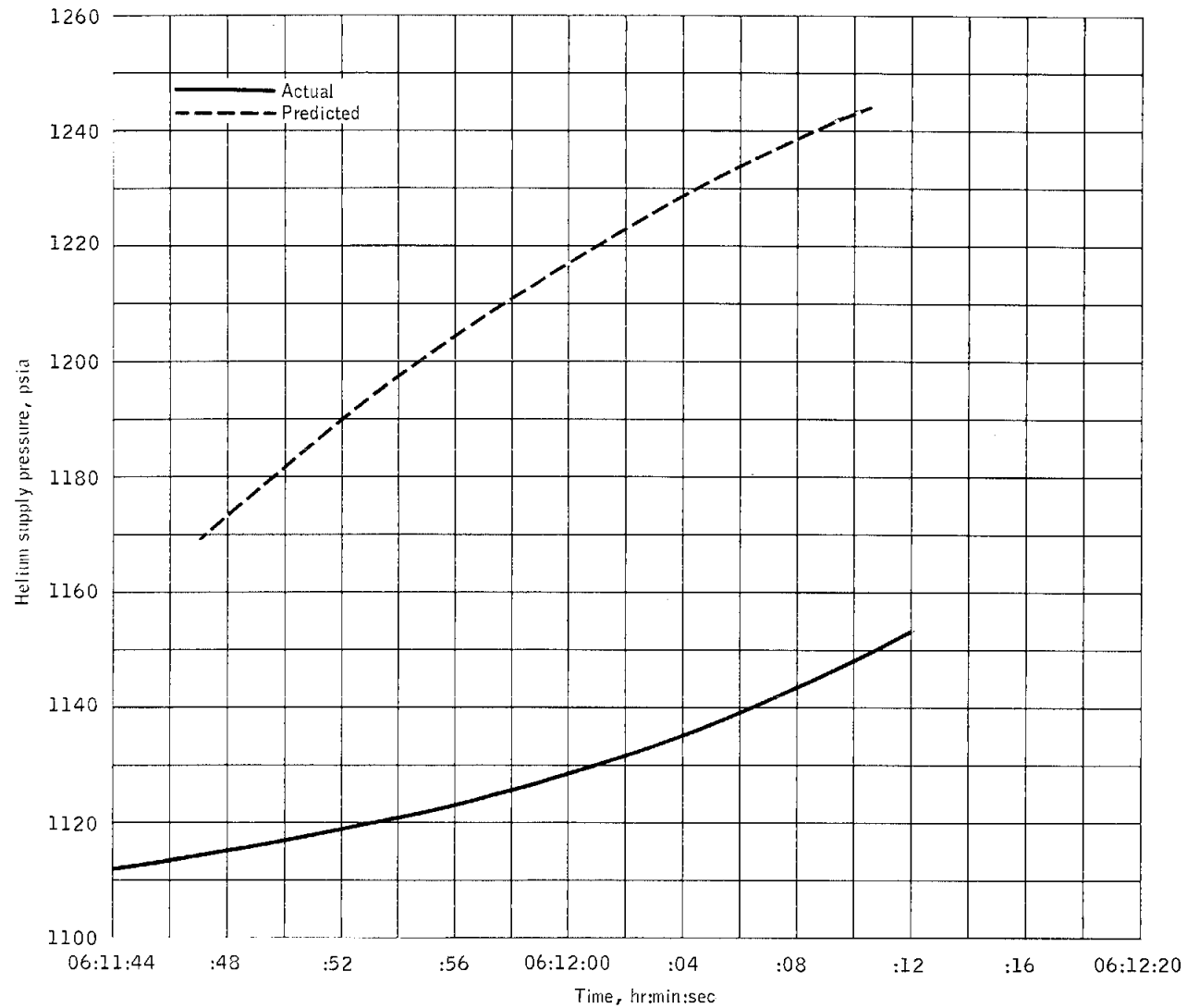


Figure 6.12-7.- Supercritical helium supply pressure during third descent engine firing.

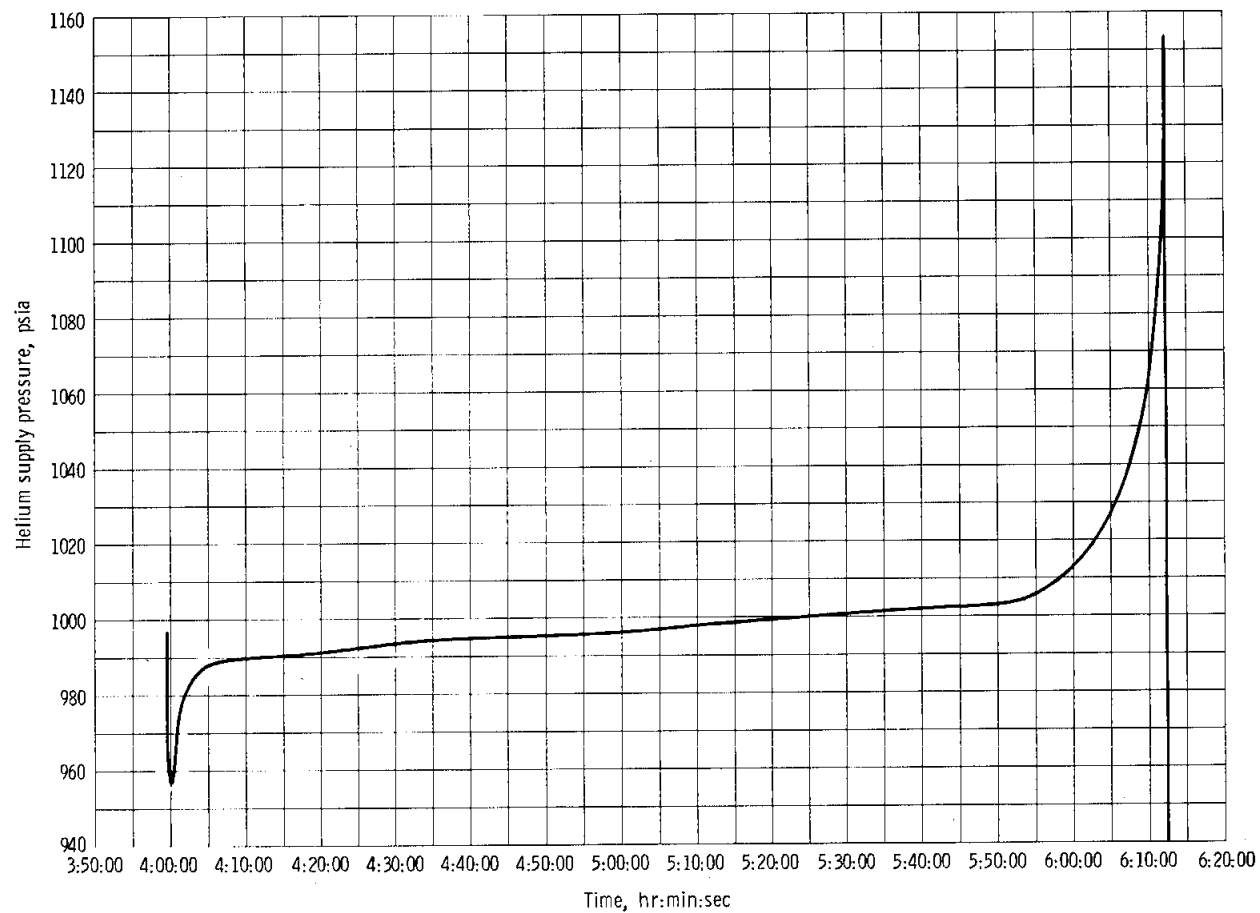


Figure 6.12-8. - Supercritical helium supply pressure during coast period between second and third firings.

6.13 ASCENT PROPULSION

The alternate mission plan selected resulted in two ascent engine firings. The first firing was initiated at 06:12:14.7, and the engine was commanded "off" 60 seconds later.

Propellant interconnect valves A and B were opened at 07:40:59 and 07:42:17, respectively. A 17-second +X translation with the control engines was initiated at 07:44:00.3, and the ascent engine was commanded "on" at 07:44:12.7 for a final firing to propellant depletion. Interconnect valves A and B were closed at 07:46:43 and 07:46:53, respectively. Thrust decay occurred at 07:50:01, approximately 40 seconds earlier than predicted.

6.13.1 Propellant Loading

The propellant tanks were serviced with 3170 pounds of oxidizer and 1993 pounds of fuel leaving an ullage volume of 0.5 ft³ per tank at 90° F. The propellant sample analysis showed the oxidizer density to be 90.22 lb/ft³ at 67.7° F and ambient pressure and the fuel density to be 56.40 lb/ft³ at 71.4° F and ambient pressure.

6.13.2 Steady-State Performance

The performance of the ascent engine has not yet been verified to have been within the expected accuracy; however, the engine pressure measurements and the vehicle velocities obtained indicate that the ascent engine performance was within the nominal predicted tolerances. Chamber pressure during the two firings is shown in figure 6.13-1.

The oxidizer and fuel propellant tank low-level sensors were uncovered at 07:49:59.7 and 07:50:00.7, respectively, during the second firing. Under nominal operating conditions, the low-level sensors are uncovered when approximately 10 seconds of usable propellant remain in the tanks; however, thrust decay began at 07:50:01.5. The timing of these events indicates that propellant slosh resulting from high vehicle attitude rates caused the propellant tank outlet ports to be uncovered. An oxidizer-depletion shutdown had been expected. However, when the propellant in the feed lines (sufficient for approximately 1 second of nominal operation) was depleted, as indicated by the engine interface pressures, helium was ingested into the oxidizer and fuel lines almost simultaneously, causing thrust decay.

The total ascent engine firing time for the mission was about 40 seconds less than predicted. At least 20 seconds of this time discrepancy can be attributed to higher-than-expected propellant usage by the control

engines through the propellant interconnect valves. As indicated by the "on" time between low-level sensor uncoverings and thrust decay, an additional 10 seconds of normally usable propellant was in the tanks at thrust decay but was unavailable due to the sloshing and high vehicle rates. The 10-second propellant discrepancy could be easily attributed to any combination of the following: (1) greater propellant residuals due to high vehicle attitude rates, (2) higher than estimated control engine usage of ascent engine propellants, and (3) ascent engine performance lower than predicted, but within the predicted nominal tolerance. The lack of acceleration data after gimbal lock may prevent accurate determination of the engine performance parameters.

6.13.3 Chamber Pressure Oscillations

An analysis of the start and shutdown transients was performed to determine the transient total impulses and response times. The results of this analysis are summarized in table 6.13-I. Engine acceptance test data and specification requirements, as well as the average of the LM-1 type ascent engines, were used to provide a better interpretation of the flight data.

There were several significant differences in conditions prior to the two engine starts. The first firing was an abort staging start with the propellant tanks in the prelaunch pressurized conditions of 10⁴ psia in the oxidizer tank and 128 psia in the fuel tank. In the abort start mode, the pressurization system squib valves are initiated approximately 1.4 seconds before the "engine on" command. Due to the low initial tank pressures, this delay was insufficient to allow propellant tank pressures to reach normal operating pressure. At the time of the first "engine on" command, the propellant tank pressures were approximately 169 psia instead of the nominal 184 to 203 psia. In comparison, the propellant tank pressures were approximately 185 psia prior to the second engine firing.

Another difference in the two starts was that the fuel line between the two parallel engine actuator isolation solenoid valves and the four engine actuator solenoid pilot valves was dry prior to the first start. The time required to fill this line causes the first start to be slower than subsequent engine starts.

The data presented in table 6.13-I provide a comparison of the engine start transients. The time from the "engine on" command until the engine reached 90 percent of rated thrust was 0.47 (± 0.01) second on the first start and 0.27 (± 0.01) second on the second start. The slower engine start transient on the first firing may be attributed, at least in part, to the lower tank pressures and the dry fuel actuation line.

The start transient and the beginning of steady-state operation showed high amplitude chamber pressure oscillations on both the first and second engine starts (fig. 6.13-2). The 400-Hz oscillations which occurred immediately after the start transient overshoot were characteristic of this engine during ground testing and were expected on this flight. The oscillations appear to be a form of low-frequency instability caused by the coupling of the combustion process with the resonant frequency of the engine feed system. Ground tests have indicated that helium gas dissolved or entrained in the fuel tends to induce coupled instability.

The magnitude of the measured 400-Hz chamber pressure oscillations immediately following "engine on" was 90 to 100 psia peak-to-peak, and the oscillations were approximately the same magnitude during both firings. Ground tests with both flight and ground instrumentation have indicated that the flight instrumentation may possibly amplify the magnitude of the indicated chamber pressure oscillation by a factor of approximately 2. The oscillations on the second firing lasted approximately 190 milliseconds. The full duration of the oscillation on the first firing is not known because telemetry was lost 150 milliseconds after the oscillation started. At that time, there was no indication that the oscillation was damping; however, when telemetry was reacquired 310 milliseconds later, the oscillation had been damped. The chamber pressure overshoot on the second start was approximately 20 psi higher than that on the first start, as can be seen from figure 6.13-1. The peak of the chamber pressure oscillation was greater than the peak overshoot during the first start and was approximately equal to the peak overshoot on the second start.

During the entire steady-state operation of both firings, 400-Hz chamber pressure oscillations occurred intermittently, as shown in figure 6.13-2. The chamber pressure oscillation, after the initial oscillation, ranged between 2 and 10 psia peak-to-peak. The oscillations appeared slightly more severe on the second firing, with the 400-Hz oscillations increasing to 25 psia peak-to-peak for approximately 200 milliseconds at 19 and 23 seconds into the firing, as shown in figure 6.13-2. During the remainder of the steady-state operation, for which data are available, the oscillations generally did not exceed 10 psia peak-to-peak until shortly before the thrust decay.

Approximately 15 seconds before thrust decay, the 400-Hz oscillations increased to 60 psia peak-to-peak in both chamber pressure and fuel injector manifold pressure, as shown in figure 6.13-2. The first period of sustained high magnitude oscillation lasted for approximately 4 seconds, at which time the magnitude decreased to 10 psia peak-to-peak, which had been observed all through the firing. Between 6.5 and 5.5 seconds before thrust decay, the oscillation again increased to 60 psia peak-to-peak, and then damped again until 4.5 seconds before thrust decay.

The high magnitude 400-Hz oscillations resumed approximately 4.5 seconds before thrust decay, then damped when the chamber pressure began to drop sharply because of helium ingestion.

The final portion of the thrust decay appeared smooth, with no spikes or other detrimental effects apparent after the damping of the 400-Hz oscillations and the rapid chamber pressure decay. The most detrimental effect of the helium ingestion appears to be the excitation of the high magnitude 400-Hz oscillations. Ground tests have indicated that the entrainment of helium in the fuel tends to excite 400-Hz oscillations. The oscillations may therefore be an indication of pressurant gas entrainment due to vortexing or slosh caused by the high vehicle attitude rates experienced during this portion of the mission.

The engine valve position indicators showed that the engine valves started to close at 07:51:25.8 (85 seconds after the thrust decay) but were not completely closed when the telemetry signal was lost by the ground station at 07:52:23. System pressures and temperatures indicate that some blockage of fluid flow occurred between the propellant tanks and the engine after the initial thrust decay. This blockage was most likely caused by small amounts of propellant frozen by cold helium that was ingested into the feed lines. Although it was not a normal depletion shutdown, no hazardous or detrimental effects were apparent after the initial thrust decay.

6.13.4 Propellant Pressurization

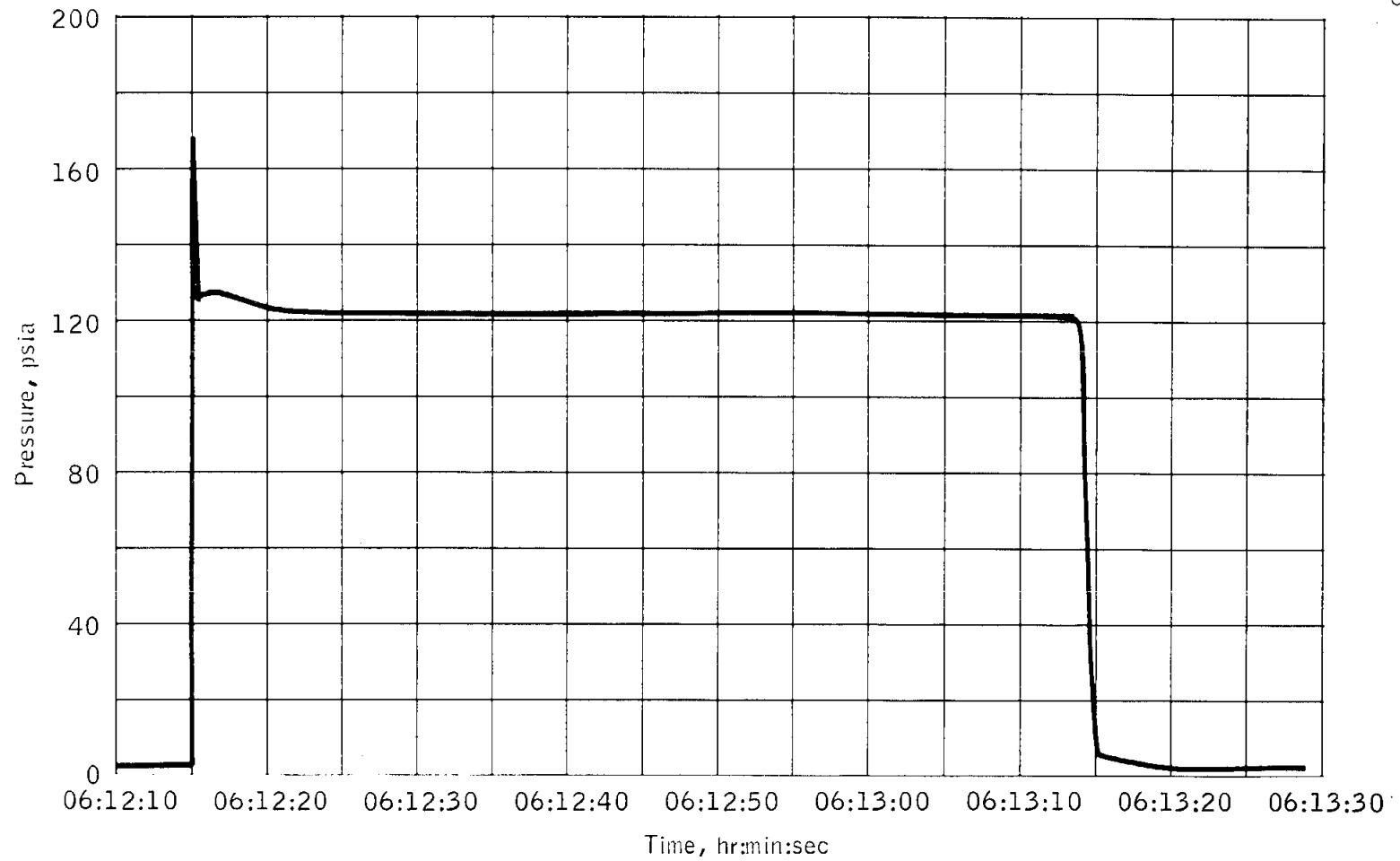
The ascent and descent propellant tanks experienced pressure drops from the time of prepressurization at the launch site (approximately 110 hours prior to launch) to the time of final pressurization in flight (approximately 4 hours after launch). The ascent oxidizer tank experienced the largest pressure decay. This pressure decay was initially believed to be the result of an oxidizer leak. However, subsequent analyses have shown that all of the experienced pressure decays could be attributed to helium diffusion into the liquid propellants.

The flight data indicate nominal propellant pressurization during the mission. Calculated helium usage during the second firing agrees with analytical predictions.

Helium flow occurred during the coast between the first and second firings amounting to approximately 2.5 percent of the total helium loaded. This helium flow is evidently the result of opening the propellant interconnect valves. During this time, the control engines used approximately 200 pounds of propellant from the ascent tanks. The amount of helium flow during the coast would be sufficient, in normal system operation, to expel approximately 180 pounds of propellant.

TABLE 6.13-I.- ASCENT ENGINE TRANSIENT ANALYSIS SUMMARY

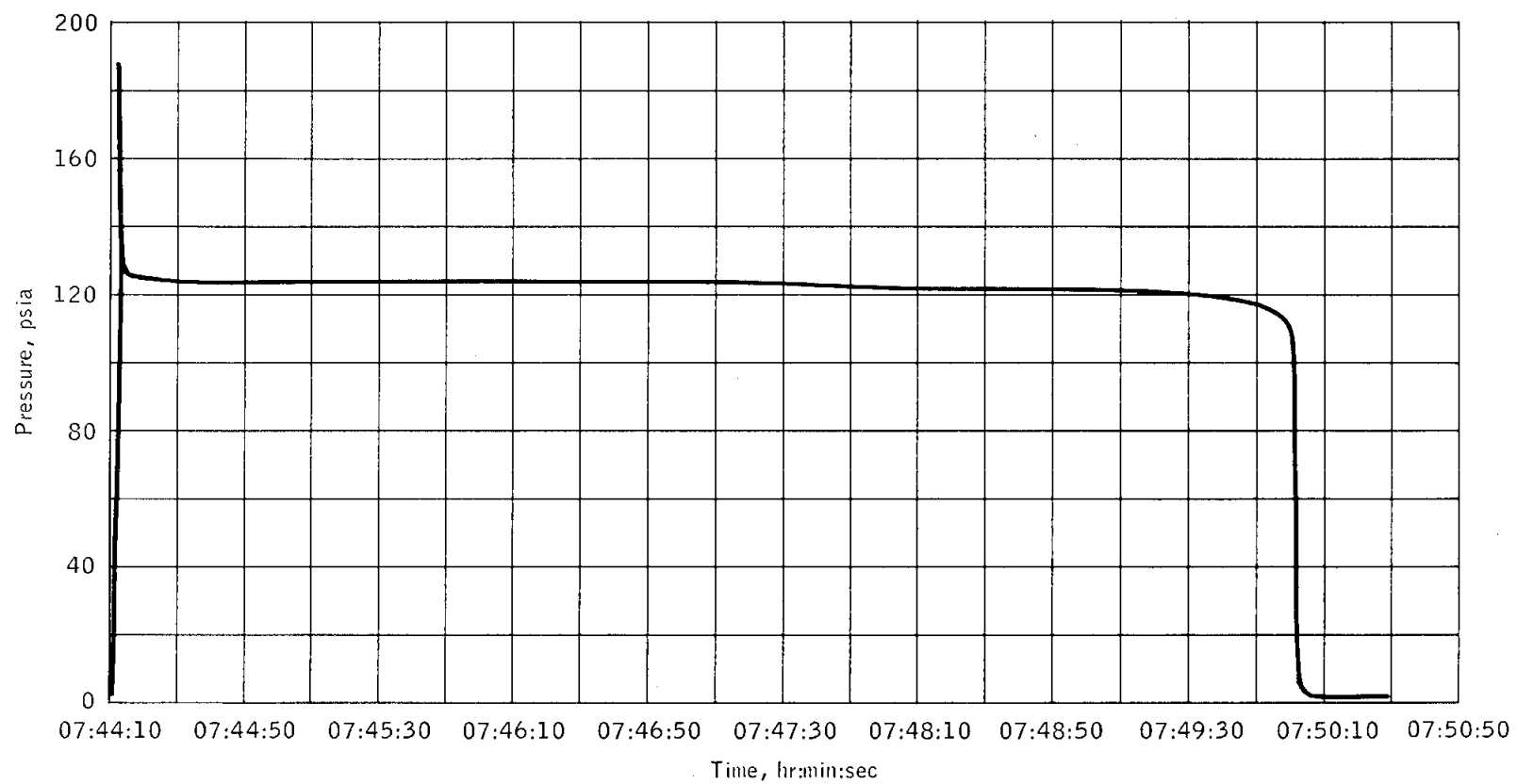
Condition	Specification value	First firing	Second firing	Engine acceptance test	Average of LM-1 type engines
Start transient total impulse from engine start signal to 90-percent steady-state thrust, lb-sec	---	57.0	65.5	57.8	62.0
Time from engine start signal to initial thrust rise, sec	---	0.26 ± 0.01	0.15 ± 0.01	0.285 ± 0.005	0.264 ± 0.058
Time from engine start signal to 90-percent steady state thrust, sec	0.400 maximum	0.47 ± 0.01	0.27 ± 0.01	0.351 ± 0.016	0.355 ± 0.032
Engine run-to-run start repeatability, lb-sec	± 35	± 8.5		± 0.4	± 19.0
Shutdown transient total impulse from engine shutdown signal to 10-percent steady-state thrust, lb-sec	---	257.2	---	429.4	429.0
Time from engine shutdown signal to 10-percent steady-state thrust, sec	0.200 maximum	$0.22 \begin{smallmatrix} +0.0 \\ -0.02 \end{smallmatrix}$	---	0.285 ± 0.030	0.312 ± 0.121
Engine run-to-run shutdown repeatability, lb-sec	± 75	---		± 15	± 101
Shutdown transient total impulse from engine shutdown signal to zero thrust, lb-sec	---	428.2	---	---	---
Time from engine shutdown signal to zero thrust, sec	---	3.0	---	---	---



(a) First firing.

Figure 6.13-1.- Chamber pressure during ascent engine firings.

NASA-S-68- 2053



(b) Second firing.

Figure 6.13-1.- Concluded.

NASA-S-68-2054

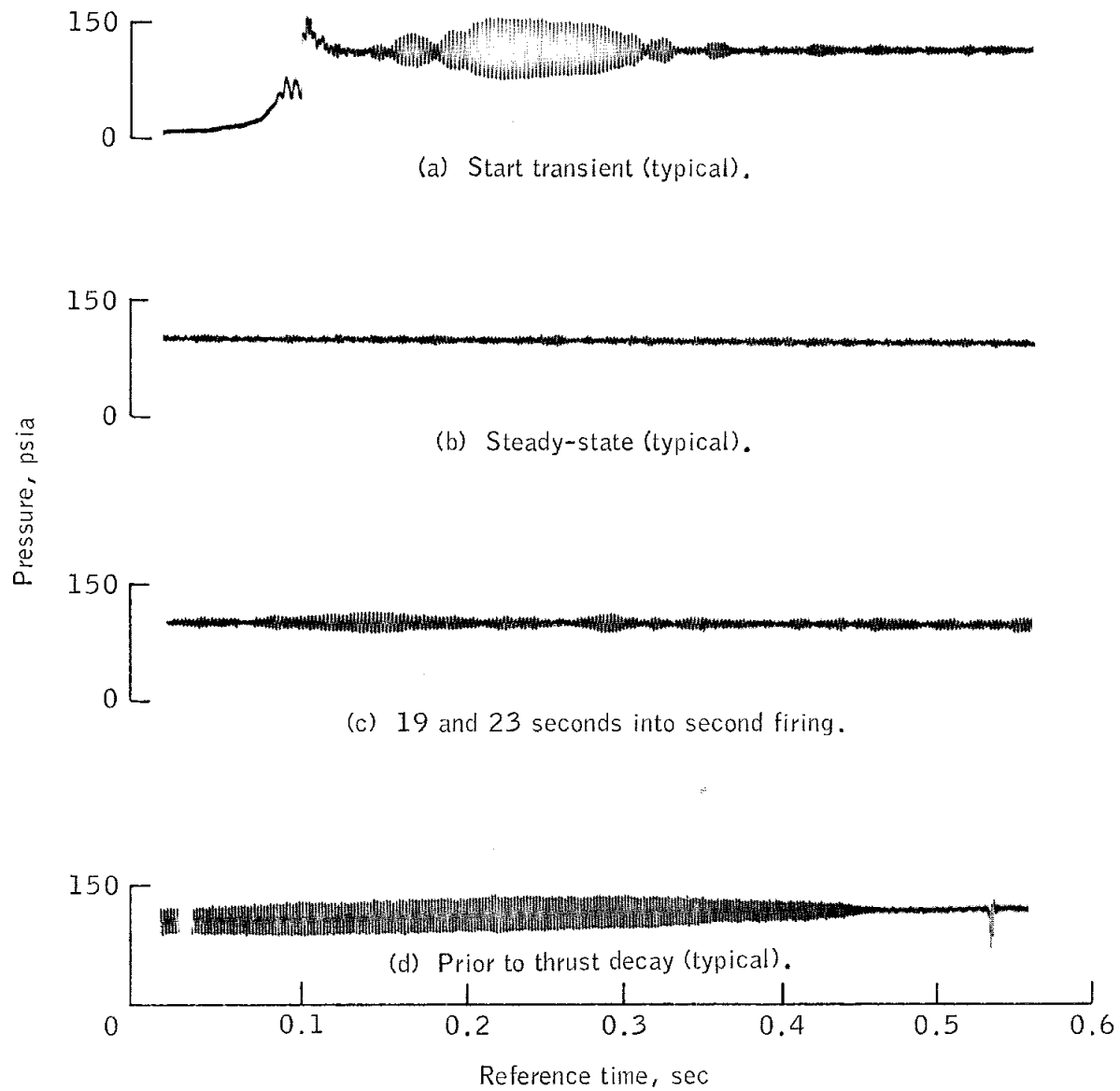


Figure 6.13-2.- Ascent engine chamber pressure oscillations.

6.14 CREW STATION

(This section is not applicable.)

6.15 ENVIRONMENTAL CONTROL

The environmental control system performed satisfactorily throughout the mission. The water/glycol coolant loop temperatures and pressure, and the water usage rate were within preflight-predicted values.

6.15.1 Cabin Pressure

Figure 6.15-1 shows the cabin pressure and the cabin relief valves internal pressures for the first 30 minutes of the flight. Preflight ground tests revealed the two cabin pressure relief valves would open at slightly different cabin-to ambient pressure differentials; the forward hatch relief valve at 5.7 psid and the upper hatch relief valve at 5.5 psid. About 47 seconds after lift-off, the upper hatch relief valve started to relieve cabin pressure. One second later, the forward hatch relief valve cracked momentarily then shut because the cabin-to-ambient pressure differential across the valve was no longer great enough to cause the valve to open. The upper hatch relief valve continued to relieve pressure until the cabin was sealed-off at 5.6 psia after 00:02:13. Eighteen minutes later, the internal pressure of the upper hatch valve was equal to cabin pressure, verifying the valve had closed. The internal pressure of each valve remained slightly above cabin pressure (within 0.3 psia) for the rest of the flight. Each relief valve operated normally. The requirement that one valve relieve cabin pressure was demonstrated.

Figure 6.15-2 shows the cabin pressure decay for the mission, which did not remain constant. The calculated equivalent flow area increased from 0.0014 to 0.0044 square inch at 03:27:00, when the vehicle was in a quiescent state and had just passed through the dark side of the orbit. The internal pressure of each cabin pressure relief valve was slightly above cabin pressure, verifying that the valves did not open. At about 04:38:00, the flow area began to decrease to 0.0026 square inch.

After launch, the upper cabin wall temperatures near the tunnel decreased from 60° to 52° F by 03:10:00. The upper wall temperatures then slowly increased to about 63° F by the end of the mission. The temperature of the cabin floor remained at about 56° F during most of the mission but increased to about 76° F during the last revolution (see section 6.2.5).

The allowable leakage established prior to flight was based on a leak rate that would maintain a cabin pressure above the mission minimum requirement of 1 psia for the second ascent engine firing. This leak rate was greater than will be allowed for a manned vehicle. There is no known cause for the leak rate changes shown in figure 6.15-2.

6.15.2 Water System

The water system operated satisfactorily during the flight. After the two water tanks were serviced, a slow water quantity decay was noted in tank 2, caused by either a water or a gas leak. A visual inspection before launch showed no evidence of water, indicating that the leak was on the gas side of the tank. At launch, the tank 2 quantity measurement indicated 88 percent due to a tank pressure decrease from about 47.2 to 35 psia. Consequently, all the water was supplied from tank 1 until about 00:50:00, when the pressure in the two tanks equalized. The water usage from each tank was then about equal for the remainder of the mission.

Water flow was initiated to the sublimator by opening the primary water solenoid valve at about 3 minutes 15 seconds. The differential pressure across the water flow control regulator stabilized at 0.58 psid then gradually increased to 0.7 ± 0.05 psid after about 30 minutes, where it remained for most of the flight. Water pressure at the inlet to the sublimator was constant throughout the mission at 5.63 ± 0.05 psia, which included a 0.28 psia prelaunch correction.

The sublimator inlet water temperature was 60° F at launch. When proper water flow to the sublimator was achieved after orbital insertion, the temperature approached the water tank outlet temperature of about 64° F. The temperature then slowly decreased to about 57° F as the sublimator operation and the heat transport section stabilized. The water tank outlet temperatures remained essentially constant throughout the flight.

6.15.3 Heat Transport Section

The coolant pump package pressures remained within predicted values throughout the flight. After insertion, the discharge pressure stabilized at 38.2 ± 0.3 psia until abort staging when it increased to 39 ± 0.3 psia due to loss of the descent stage battery coldplates. An increase of 0.8 psia occurred during staging and the second ascent engine firing and was caused by vehicle acceleration.

The pump package differential pressure was constant at 34 psid after the first hour and increased slightly to 34.2 psid at abort staging. The fluctuation during the first portion of the flight was due to increases in viscosity and density caused by a decrease in the temperature of the coolant. This pressure rise indicated a normal average coolant flow of 410 lb/hr before abort staging and 395 lb/hr after staging.

Sublimator temperature control.- Figure 6.15-3 shows the actual and predicted water/glycol coolant temperatures at the pump inlet, which is a direct indication of sublimator performance. The temperature increased from about 49° F at launch to about 56° F prior to starting water flow at 3 minutes 15 seconds. A delay in effective cooling was caused by the acceleration of the S-IVB stage preventing full water flow from reaching the sublimator until engine cutoff. Once proper water flow was attained, the coolant temperature decreased rapidly, then slowly stabilized at 42° F. The sublimator performance was completely satisfactory throughout the mission.

The water/glycol coolant temperature at the pump inlet was within predicted values during the mission. The decrease at abort staging was caused by loss of the descent battery heat load located between the sublimator and pump inlet. The slow rise after staging was caused by the increased heat load from the ascent batteries as they warmed up after being turned on.

The temperature fluctuations (38° to 54° F) during prelaunch were caused by a mixture of nitrogen pressurization gas with the freon used for vehicle cooling. Injection of the nitrogen was caused by a malfunction in the ground support equipment.

6.15-4

NASA-S-68- 2055

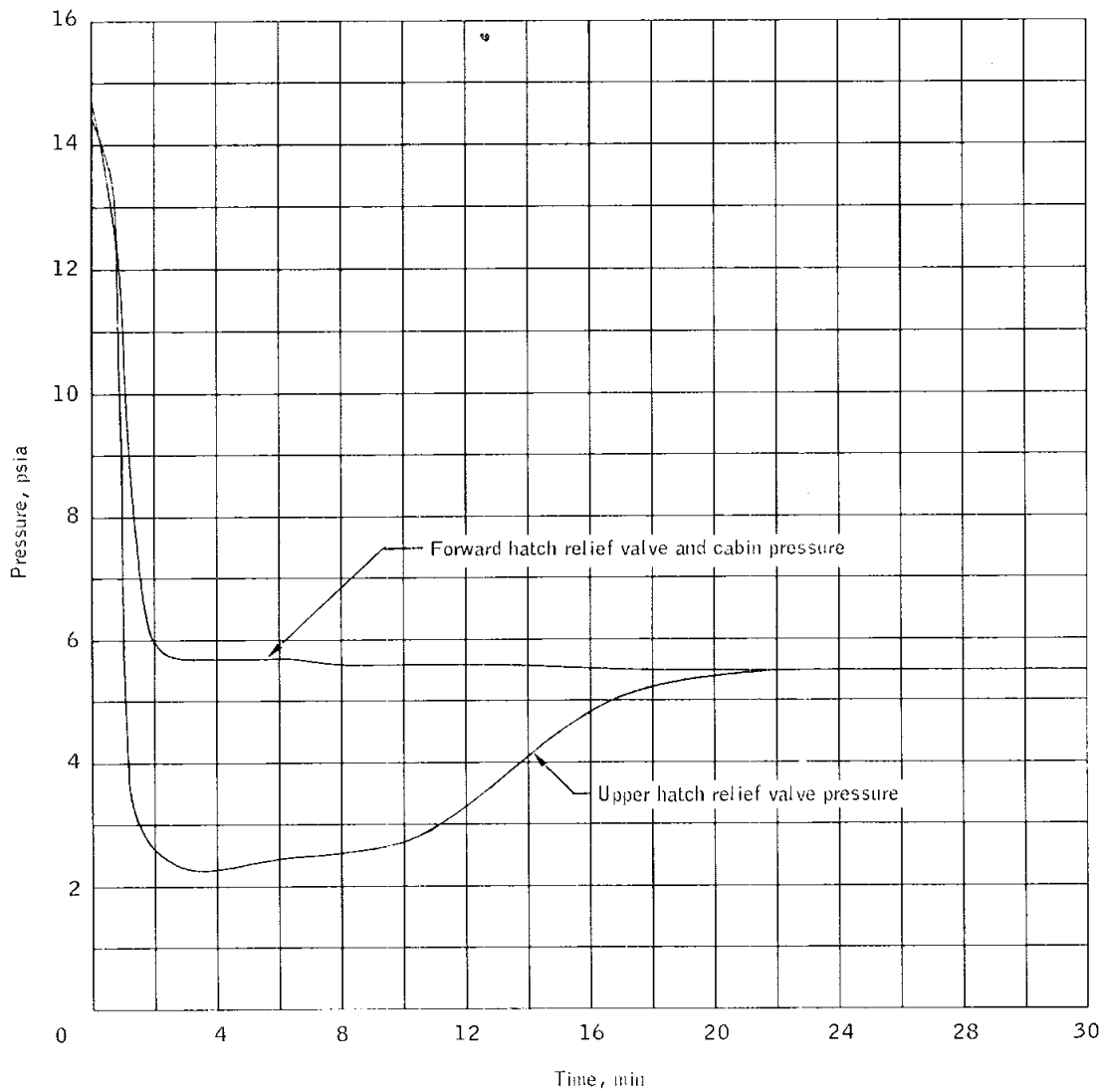


Figure 6.15-1.- Pressure of cabin and internal pressure of cabin pressure relief valves.

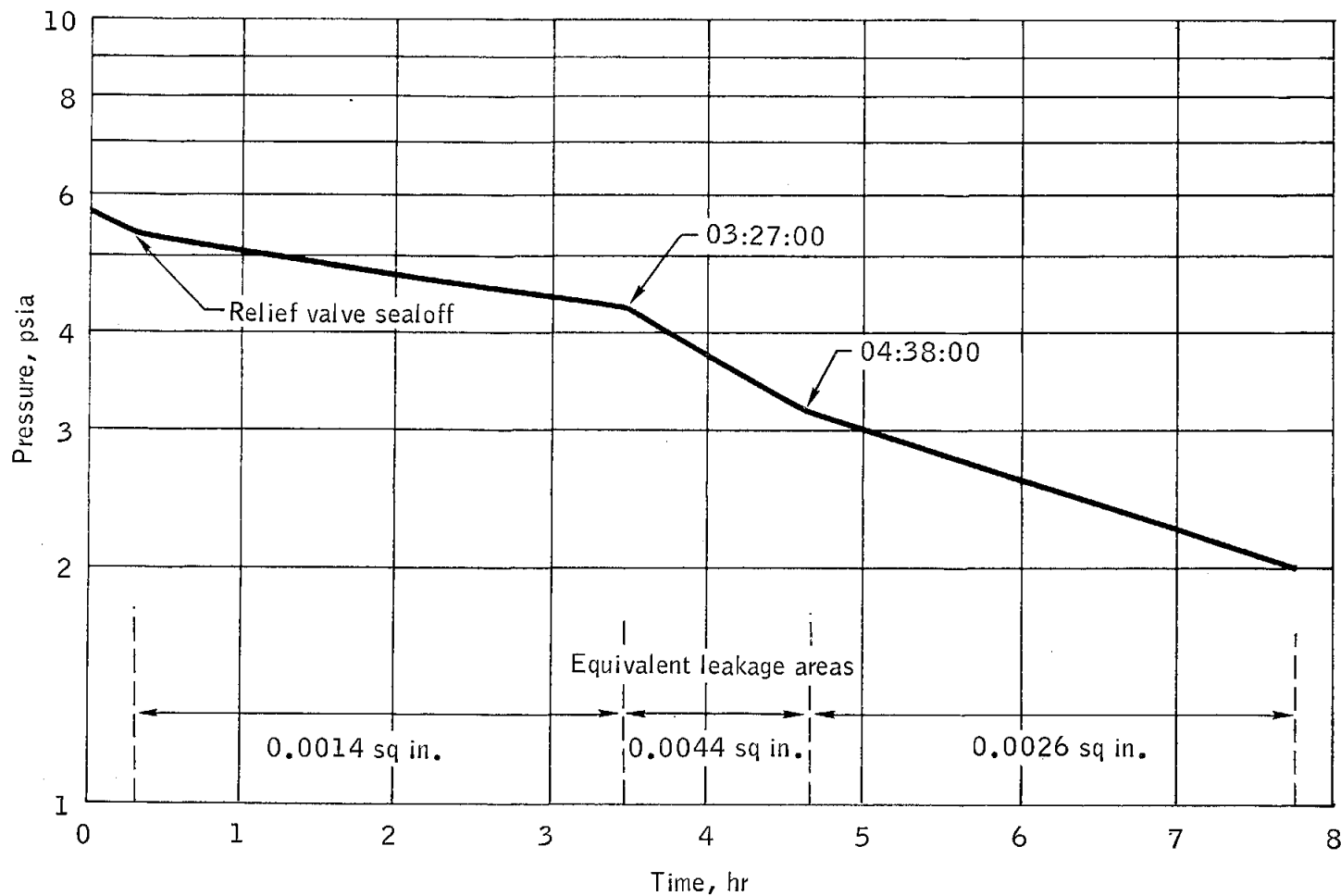


Figure 6.15-2.- Cabin pressure profile.

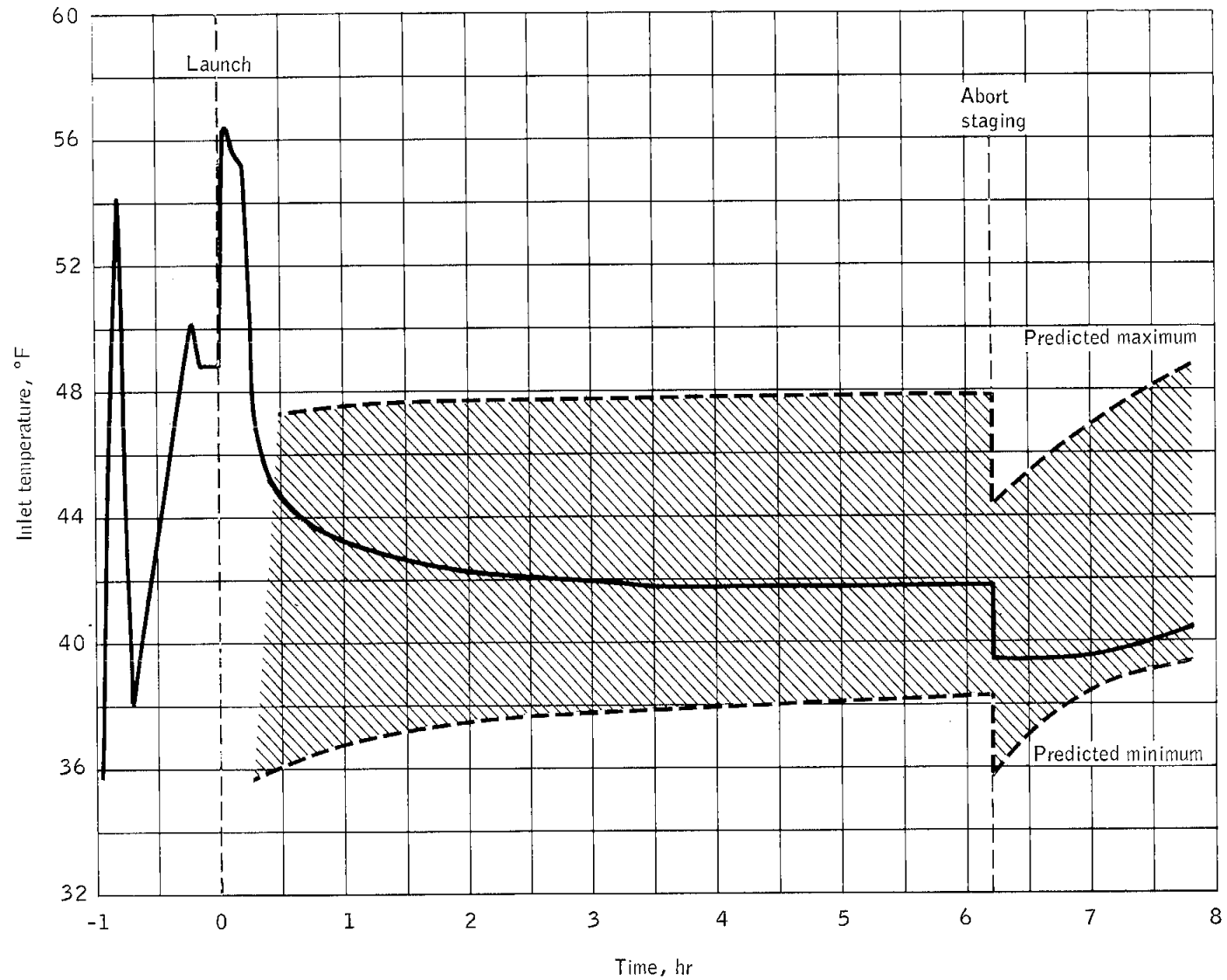


Figure 6.15-3.- Water/glycol pump inlet temperature.

6.16 CONSUMABLES

The quantities of consumables loaded are shown in table 6.16-I. The quantity of water remaining in the ascent stage tanks 1 and 2 throughout the mission is shown in figure 6.16-1. The difference between the actual and predicted consumption is consistent with the difference in predicted and actual electrical power used.

The total usable prelaunch power was 1400 amp-hr in the descent batteries and 492 amp-hr in the ascent batteries. The actual power usage during the mission was 264 amp-hr in the descent batteries and 91 amp-hr in the ascent batteries. The predicted and actual power usage is shown in figure 6.16-2. The difference between predicted and actual can be attributed to power variations within specific components compared with predicted values. The higher usage of ascent power was caused by activity of the control engines.

Based on a nominal propellant flow rate of 11.43 lb/sec, about 87 percent of the ascent propellant remained after the first ascent engine firing. Figure 6.16-3 shows the actual propellant usage. For the second ascent engine firing, propellant depletion shutdown should have occurred about 40 seconds later than the thrust decay occurred, based on the nominal flow rate. Usage of ascent propellant by the control engine system through the interconnects and propellant nonavailability caused by the tumbling of the spacecraft contributed to the early shutdown. The only quantity gaging device for the ascent system propellants was the low-level sensor which was uncovered early because of the spacecraft tumbling.

Only 2.7 percent of the total descent engine propellants were used for the three descent engine firings. (See fig. 6.16-4.) The calculated consumption for the actual mission profile, as based on nominal performance data, agrees with the actual consumption within the accuracy of the propellant quantity gaging device.

Figure 6.16-5 presents the control engine consumable history (see section 6.11 for further details).

TABLE 6.16-I.- CONSUMABLES

	Fuel	Oxidizer
Ascent propulsion propellant		
Total loaded, lb	1993	3 170
Total usable, lb	1932	3 091
Ullage volume, cu ft	0.5 per tank at 90° F	
Descent propulsion propellant		
Total loaded, lb	6957	10 948
Total usable, lb	6710	10 736
Ullage volume, cu ft	0.5 per tank at 90° F	
Reaction control propellant		
Loaded, system A, lb	102.0	203.4
Loaded, system B, lb	102.8	203.4
Total loaded, lb	204.8	406.8
Minimum usable, lb	189.0	360.8
Ascent stage water		
Loaded, tank 1, lb	42.5	
Loaded, tank 2, lb	42.5	
Total loaded, lb	85.0	
Total usable, lb	80.0	

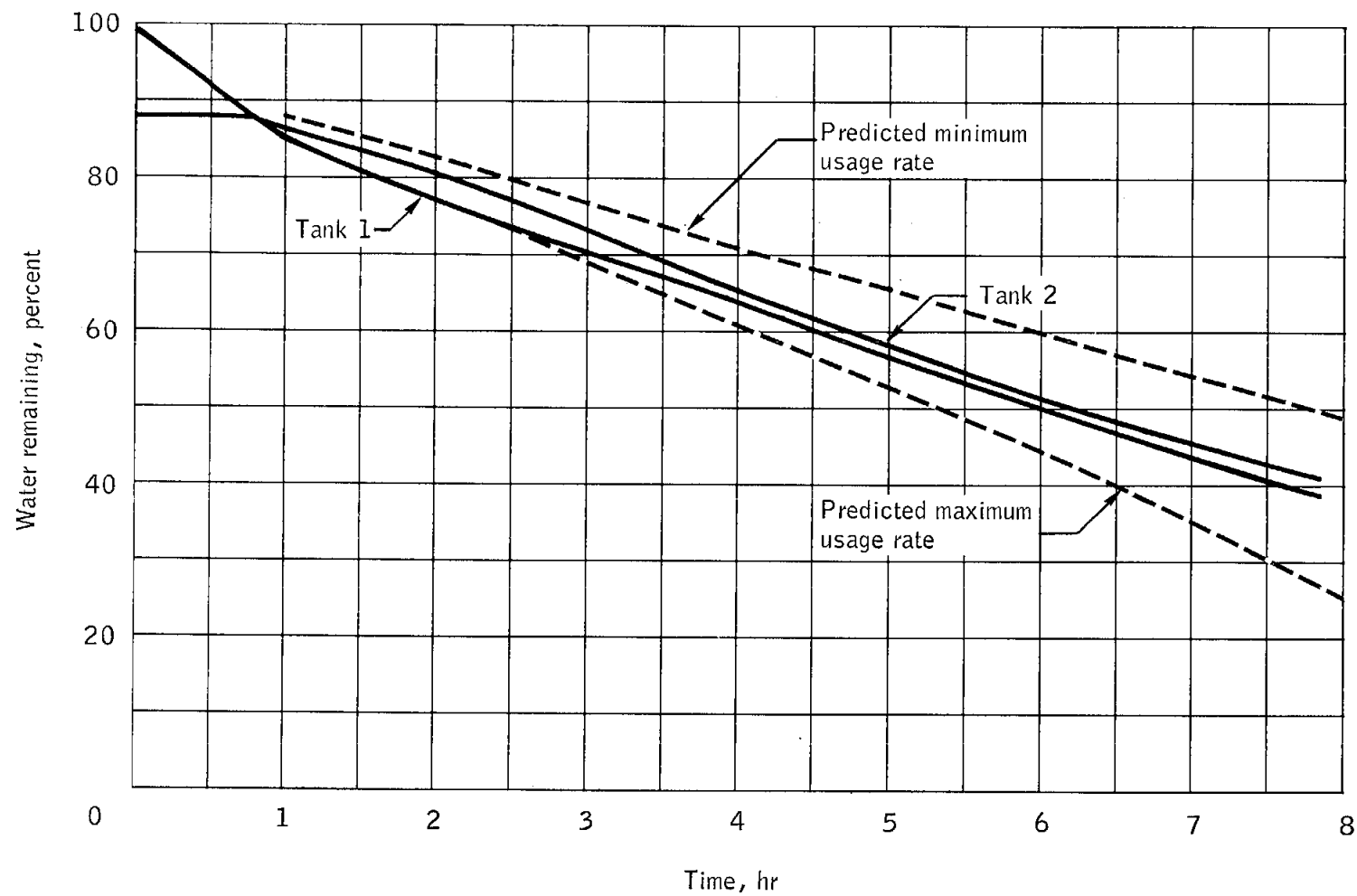


Figure 6.16-1.- Water usage.

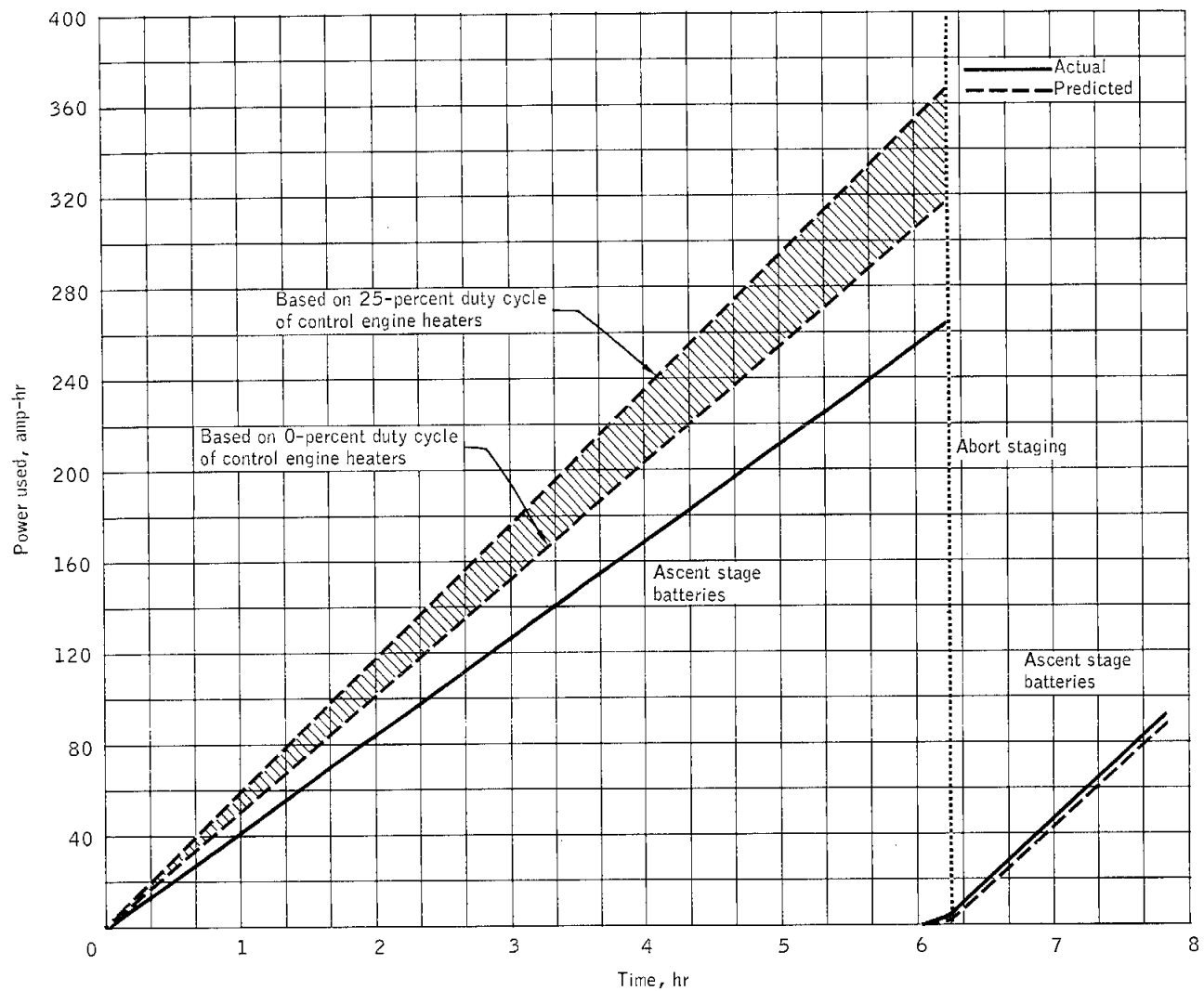


Figure 6.16-2.- Electrical power consumption.

NASA-S-68-2102

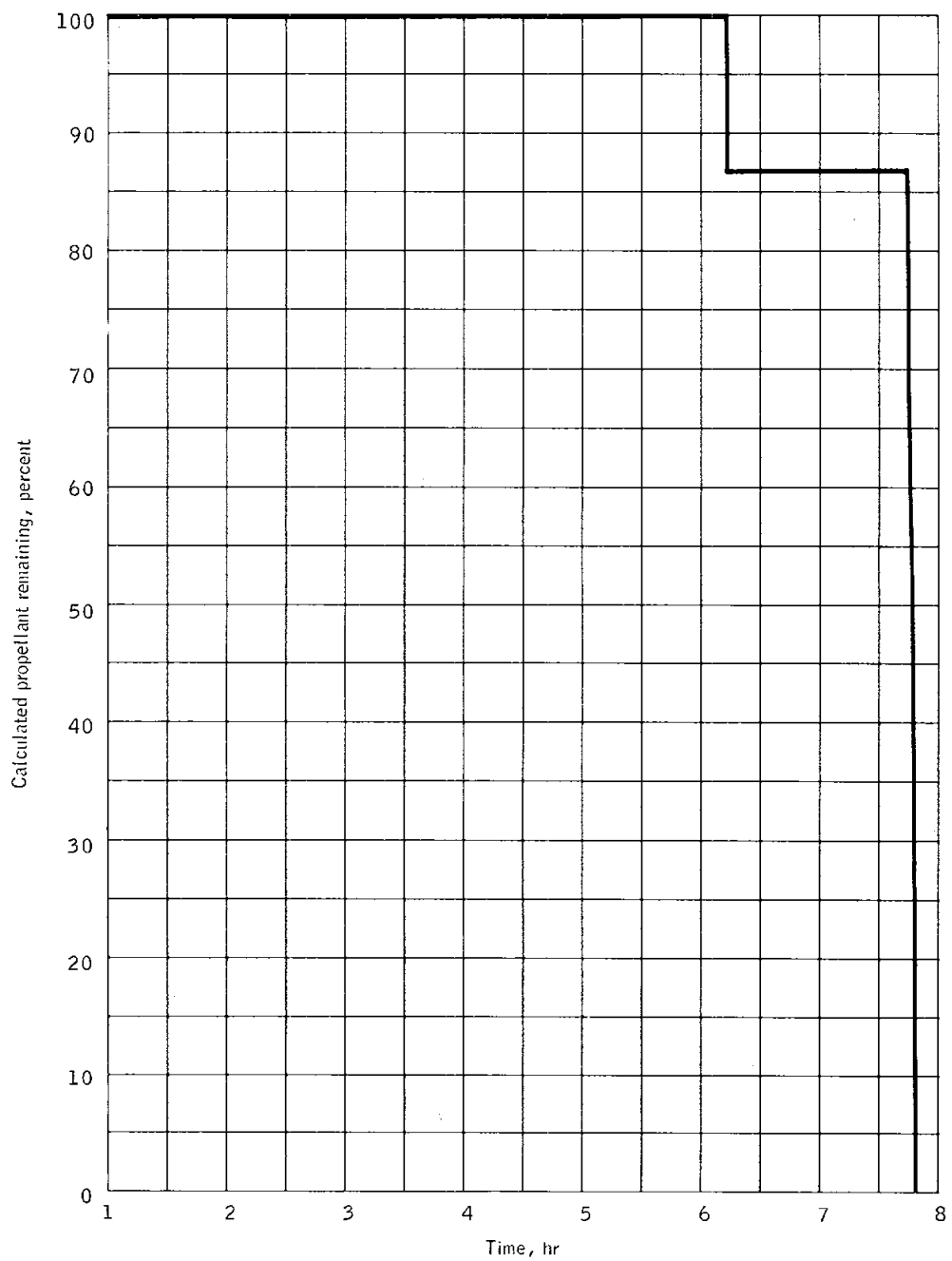


Figure 6.16-3.- Ascent engine propellant usage.

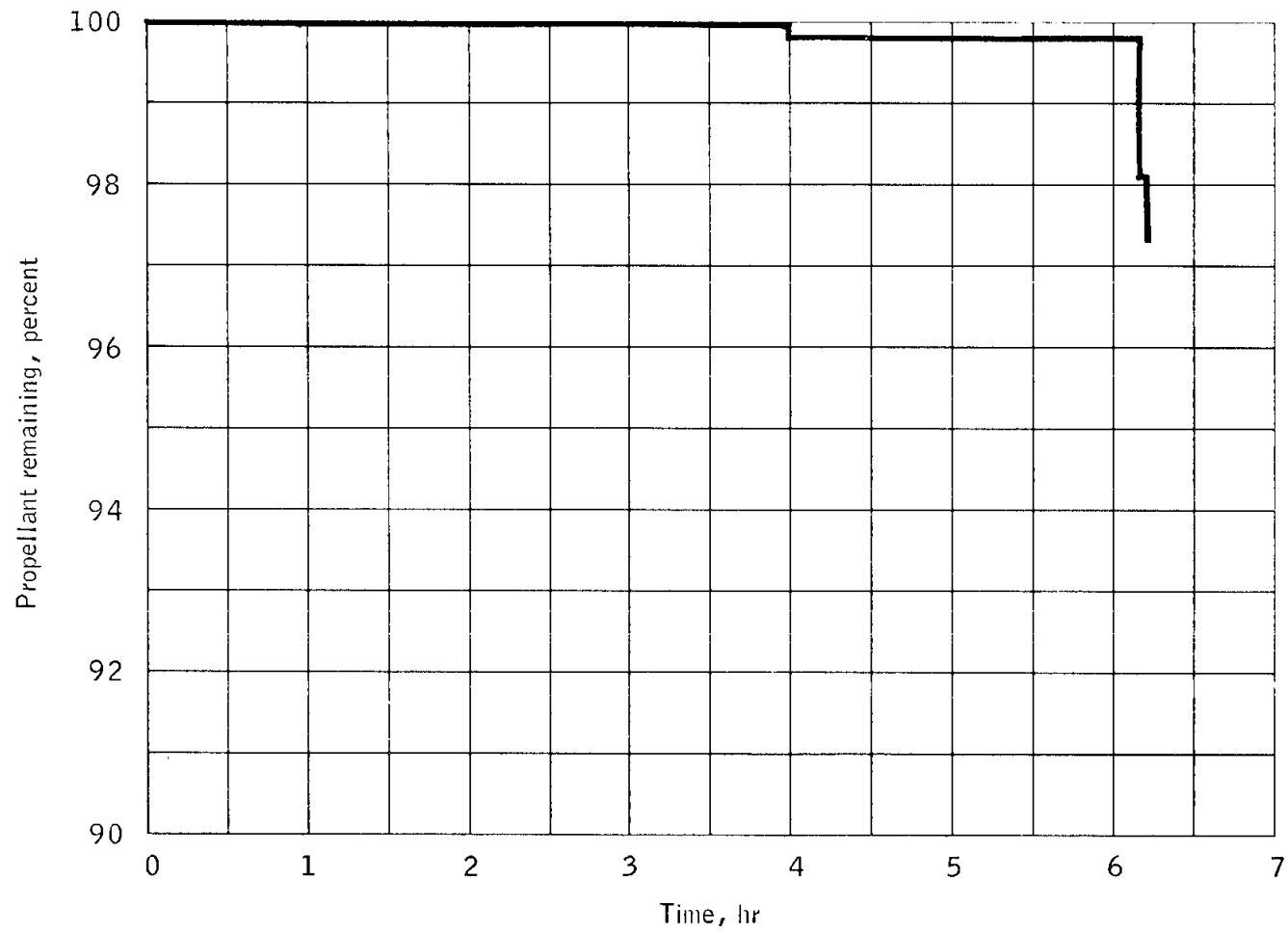


Figure 6.16-4.- Descent engine propellant usage.

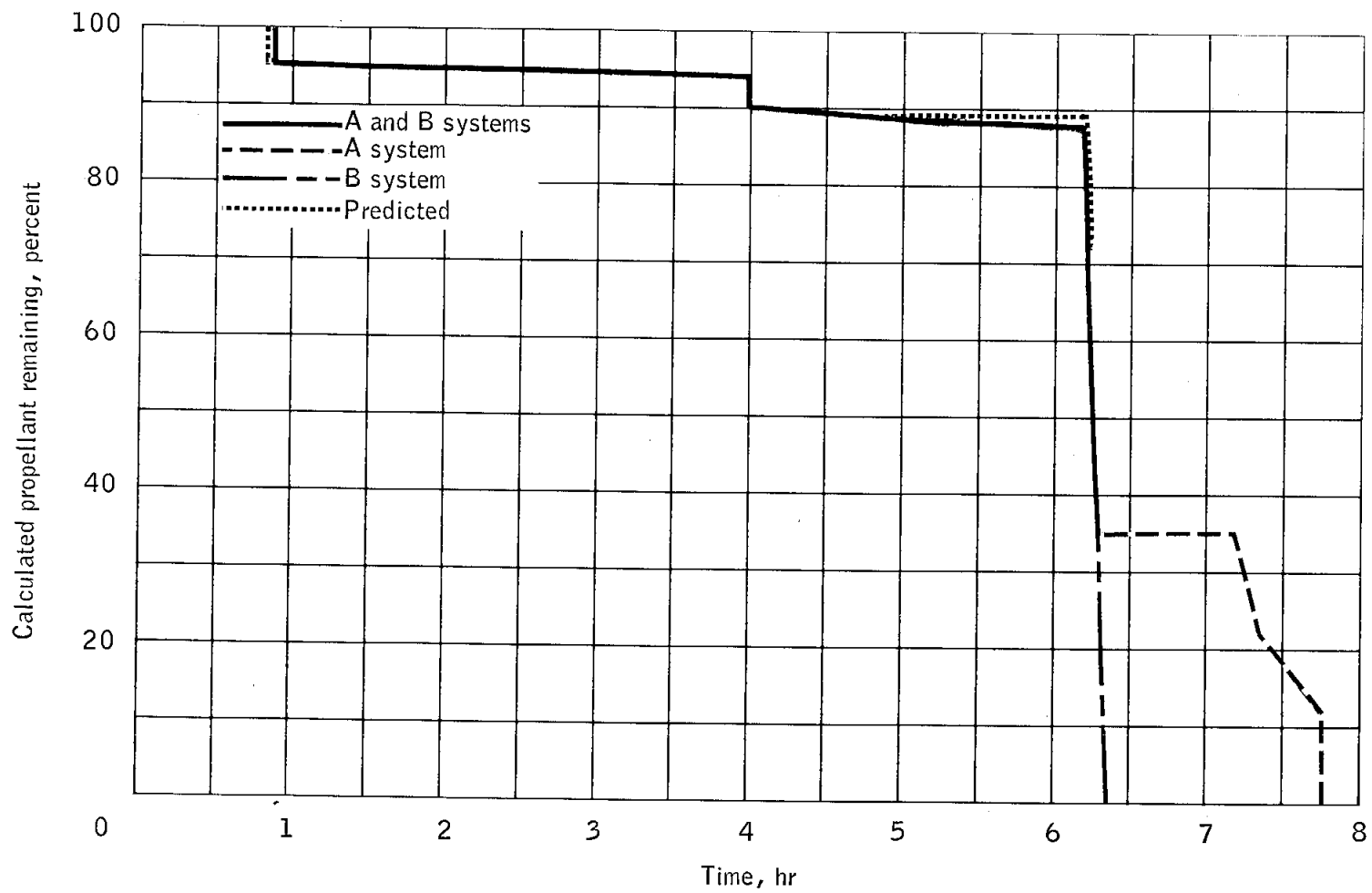


Figure 6.16-5.- Reaction control propellant usage.

6.17 ABORT STAGING

Abort staging was successfully accomplished and all systems operation and performance throughout the staging event were satisfactory. The abort sequence was initiated and controlled by the stabilization and control system and mission programmer sequence III, with modifications as detailed in section 6.6. Only rate damping was provided when the stabilization and control system was used. After switchover to primary guidance prior to the second ascent engine firing, all rates were near null, and the spacecraft gimbal angles were 50.7, 213.6, and 8.2 degrees in yaw, pitch, and roll, respectively.

Figure 6.17-1 shows the parameters associated with the staging event and certain mission programmer events. The abort stage "fire" and engine "on" were instrumented events. The other events shown in figure 6.17-1 were derived from the logic times-of-sequence system in figure 6.17-2. The event times for the two instrumented events are known within 20 milliseconds and were within allowable limits. Other event times were within specification, as demonstrated by the proper functional responses.

The descent engine was shut down at 06:12:14.3, and as the chamber pressure decayed to about 5 psia, the instrumentation channel was switched to the ascent engine chamber pressure as shown by the logic sequence. Figure 6.17-1 shows the overlap of ascent engine chamber pressure rise and the descent engine tailoff and was determined by extrapolating the descent chamber pressure to zero, based on the tailoff characteristics obtained from the second descent engine firing. The staging bolts were severed during the thrusting overlap period of the descent and ascent engines, 30 milliseconds after ascent engine "on." No disturbances were sensed by angular rates for this event. The ascent engine chamber pressure rose sharply to the start transient peak. At that instant, the change in pitch rates showed a disturbance torque that was trimmed out by the control engines. This disturbance torque is discussed in more detail in section 6.10. The resulting angular rate in pitch and roll was damped within 1 second to within the deadband limits. The rates (fig. 6.17-1) indicate that only a single disturbance occurred which was at the point of peak chamber pressure. No recontact of the two stages was indicated at any time.

The highest pressure transients on the ascent stage bottom surface and the descent stage upper surface are shown in figure 6.17-1. These peak pressures were within design limits (see section 6.1 for further discussion). The peaks occurred at least 25 milliseconds after the peak of ascent engine chamber pressure. At this time, based on guidance platform accelerations, the stages were estimated to be less than half a foot apart and separating at a rate of 11.0 ft/sec².

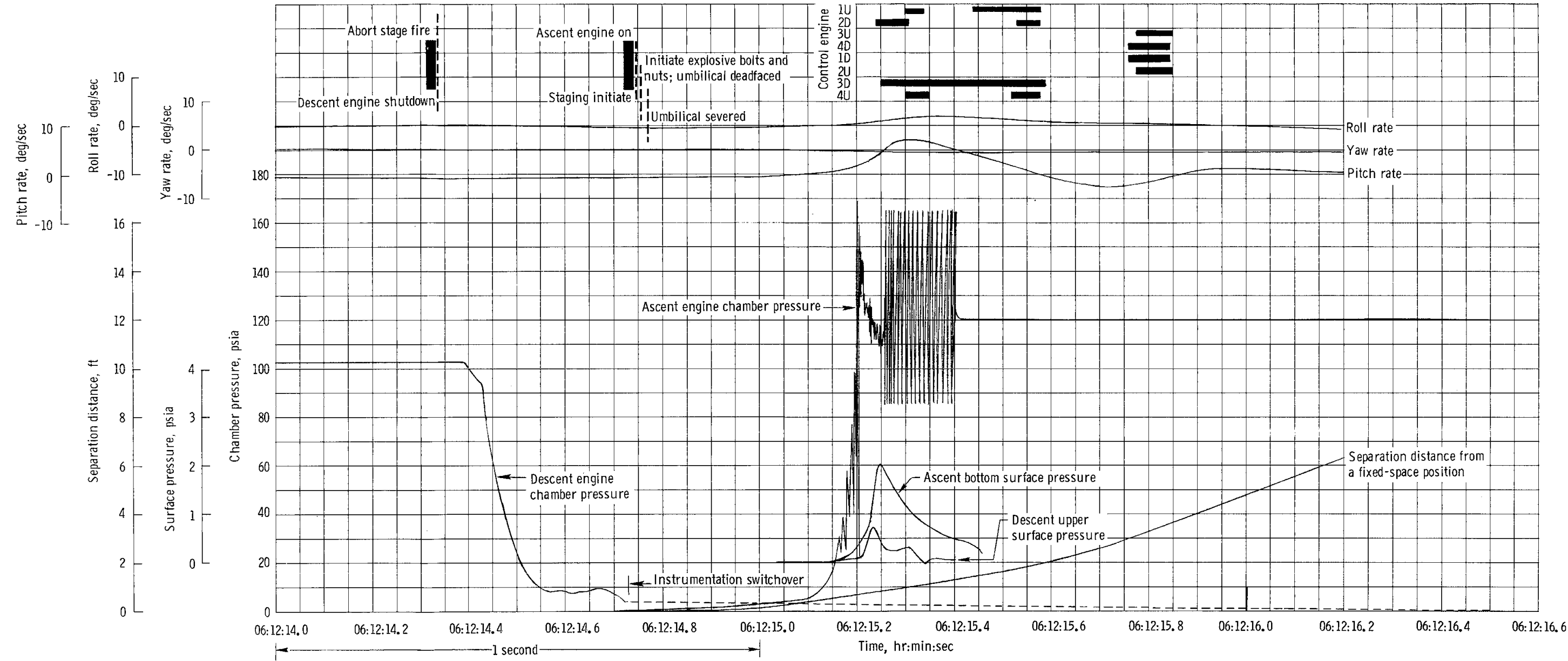


Figure 6.17-1. - Abort staging characteristics.

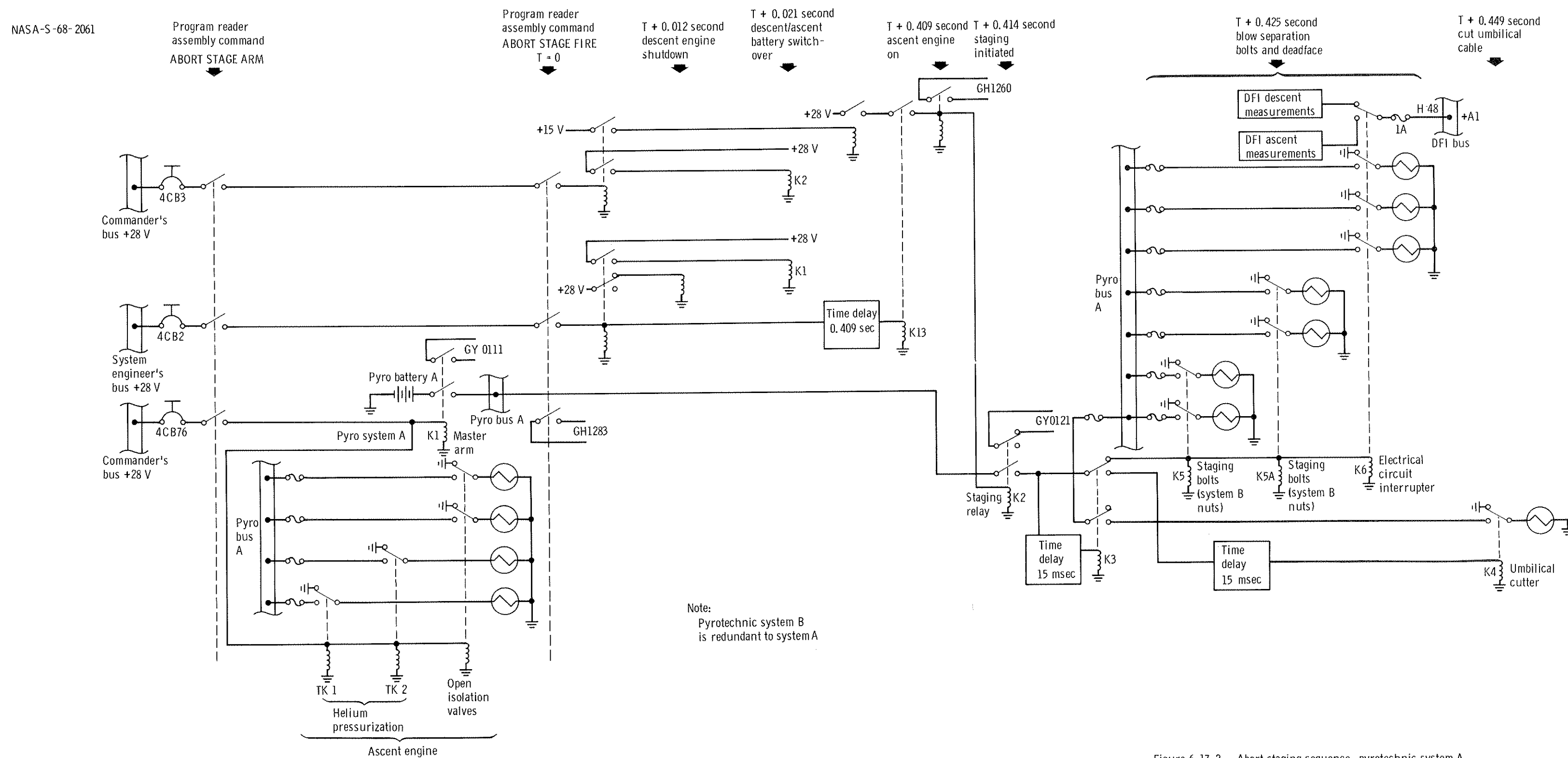


Figure 6.17-2 - Abort staging sequence, pyrotechnic system A.

7.0 FLIGHT CREW

(This section is not applicable.)

8.0 BIOMEDICAL EVALUATION

(This section is not applicable.)

9.0 MISSION SUPPORT PERFORMANCE

This section of the report is based upon real-time observations, unless otherwise noted, and may not agree with the final analysis of the data in other sections of the report.

9.1 FLIGHT CONTROL

9.1.1 Prelaunch Operations

The Mission Control Center-Houston began flight control support of the terminal countdown at T minus 10 hours 30 minutes on January 22, 1968. Lunar Module-1 (LM-1) cabin closeout had been performed during the countdown demonstration test at 20:50:00 G.m.t. on January 18, 1968. Command support of the LM-1 and launch vehicle by the Mission Control Center was nominal.

The Redstone telemetry computer was declared no-go at approximately T minus 3 hours 30 minutes and remained so until 05:42:00 after lift-off. Procedures were developed for the launch phase to permit commands to be transmitted without the use of the telemetry computer and to use local site printouts for command validation. The redstone telemetry and command processing had been documented as mandatory for launch; however, the Flight Director decided to continue to countdown. The command computer was utilized for command support during the launch phase and for telemetry support during revolutions 2 and 3.

The terminal count progressed as scheduled until T minus 3 hours 30 minutes when attempts were made to increase the freon flow to drop the glycol temperature from the 55° F level to the desired lift-off temperature of approximately 35° F. In so doing, freon flow appeared to be completely lost and the glycol temperature rose as high as 65° F. A hold was called at T minus 2 hours 30 minutes while efforts were made to correct this problem. The problem was traced to the ground support equipment freon supply and resulted in insufficient freon being available to extend the count until the desired termination time, if a high freon flow was constantly maintained. The areas of concern were the effect of elevated temperature on water boiler start-up, the effect on the temperature profile prior to water boiler start-up, and whether equipment degradation might result from operating at elevated temperatures. It was determined that water boiler start-up would not be jeopardized by a glycol temperature of 55° F at lift-off, although all efforts should be made to maintain the temperature below the maximum red-line value of 45° F. Freon control was eventually regained, and although several variations in the

glycol temperature occurred, stabilization was maintained at less than 55° F. Glycol temperature at lift-off was 48.5° F.

The LM was placed on internal electrical power at T minus 42 minutes. Variations greater than 15 amperes occurred during prelaunch, and the current was near the maximum observed level at lift-off (55 amperes). The inertial measurement unit, with a stabilized glycol temperature of 55° F, had a 17-percent heater duty cycle during prelaunch operations. When the spacecraft was cooled for flight, this heater duty cycle rose to 27 percent and ranged between 27 and 19 percent for the rest of the mission. At lift-off, 96 amp-hr had been consumed in addition to the 200 amp-hr (50 amp-hr per battery) that had been predischarged.

9.1.2 Powered Flight

Lift-off occurred at 22:48:09 G.m.t. The space vehicle was in a nominal configuration at lift-off. Data delays prevented the Guidance Officer from observing the automatic spacecraft guidance reference release. As a result, the 5 and ENTER commands were transmitted as a back-up at 00:00:06 and 00:00:07, respectively. The LM cabin pressure began relieving at approximately 00:00:53. Approximately 60 seconds after lift-off, the Guidance Officer detected a lunar module guidance computer navigation error in crossrange. However, the actual trajectory was nominal in that plane. This divergence existed throughout both stages of powered flight and was expected because of the prelaunch platform alignment errors. The total LM battery currents gradually increased from an average of 43 amperes to a maximum of 65 amperes at 00:02:00. The current usage then slowly decreased to an average of 43 amperes. The rise was attributed to the near-simultaneous actuation of the reaction control heaters. The S-IB stage inboard and outboard engine cutoffs occurred at approximately 00:02:00, and staging was confirmed by the trajectory.

The S-IVB stage ignition occurred at 00:02:25, followed by activation of the propellant utilization system at 00:02:31. The thrust chamber pressure for the S-IVB stage engine indicated a high nominal value from 00:02:31 until engine mixture ratio cutback occurred at approximately 00:07:48. An attitude error of up to 4 degrees in yaw was indicated throughout the S-IVB stage firing. This could have been the result of a thrust vector misalignment, because the vehicle end conditions were nominal. S-IVB engine cutoff occurred at approximately 00:09:53; the velocity cutoff was normal. The LM cabin pressure had stabilized at 5.5 psia by 00:02:30. The crossrange navigation error first experienced during the S-IB stage powered flight had reached a 400 ft/sec value at insertion. Based on data from the Bermuda station, the orbit at insertion was 87.6 by 119.5 n. mi.

9.1.3 Orbital Flight

First revolution.- Venting of the S-IVB stage was nominal after cut-off with a slightly greater rate of oxidizer ullage decay than had been expected. The nose cone was jettisoned at 00:10:38. Attitude control after jettison was nominal; rates and errors were held to dead-band limits. A nominal pitchover to a posigrade earth rate attitude was initiated and proper attitude and rates were achieved. The measurement for the environmental control gaseous nitrogen sphere indicated an off-nominal pressure decay attributed to a system leak. As the mission progressed, the pressure decay rate was observed to decrease and ultimately the pressure followed closely the minimum predicted value for the system.

The Canary Island station acquired telemetry from both the launch vehicle and the LM at 00:16:59. Deployment of the adapter panels was not observed at the programmed time. The Booster Systems Engineer sent the adapter deploy command at about 00:21:11. Command verification was received, but no telemetry confirmation of the event was received. Subsequent tape playback and readout verified that the adapter deploy relays A and B were closed, and the panel deploy monitor indication was not present. The Coastal Sentry Quebec confirmed that both panel deploy relays A and B had actuated but without a deploy indication. Based on the two out of three indications, the Flight Director elected to permit the separation sequence to proceed.

The Coastal Sentry Quebec had intermittent telemetry which was caused, in part, by radio frequency interference from the ship's ground communications equipment. To alleviate the problem the teletype B-channel power was reduced during acquisition. At 00:50:01, the Coastal Sentry Quebec reported that the counters were disabled and that the intermittent synchronization problem still existed. Separation was confirmed at 00:50:23:00. The reaction control pressurization sequence was nominal.

Carnarvon acquired telemetry at 00:51:47. The separation sequence was nominal, with LM/adapter separation occurring at 00:53:54. Rates were low, with little activity by the reaction control engines. A data dropout of about 2 seconds occurred as expected at the time of separation. The primary S-band system operating in the low power mode came on as programmed. Prior to activation of the reaction control system, the propellant quantities were showing a bias between the two systems; A system was approximately 93 percent, B system was approximately 98 percent at Carnarvon acquisition. Usage was nominal during separation. The maneuver to the cold-soak attitude was nominal. The final attitudes were pitch 319.7 degrees, roll 328.5 degrees, and yaw 99.4 degrees and agreed with those planned.

The Rose Knot Victor acquired the LM at approximately 01:28:16. The UHF received-signal strength fluctuated around -65 dBm. It should be

noted that throughout the mission, the Rose Knot Victor was the only Manned Space Flight Network station with consistently good telemetry and command capability. During this pass, all clocks were synchronized. The Rose Knot Victor also reported reception of intermittent data from the S-IVB stage.

At approximately 01:29:00, the Guaymas station acquired LM data, and systems operation was satisfactory. Glycol temperature was 42.6 degrees. The UHF received-signal strength dropped to about -95 to -100 dBm at 1 minute before loss of signal by the Rose Knot Victor.

The Mission Control Center transmitted the primary S-band OFF command at 01:33:12. The secondary S-band ON command was transmitted at 01:33:28. Secondary S-band data (high power mode) were of good quality throughout the remainder of the mission. Command sequence to close the reaction control propellant crossfeed valves was initiated at 01:34:17. At completion of the command, there was a crossfeed valve OPEN indication which had not been observed prior to that time but was probably caused by power being on the valve coils. The Guidance Officer started the crossfeed valve CLOSE reset command sequence from the Texas station at 01:36:01 and the proper telemetry confirmation was received. During the pass over the United States, the control cluster 1 temperature (156° F) was about 18° F higher than that of clusters 2 and 3 (137° and 138° F, respectively) and 8° F higher than that of cluster 4 (148° F). This difference was believed to have been caused by exposure to the sun. Water, electrical, and reaction control propellant usage had been near nominal through the end of revolution 1. Operation of the guidance computer had been satisfactory.

The S-IVB stage had been following a nominal time line through the end of the first revolution. The only apparent anomalies were the leak in the environmental control gaseous nitrogen sphere, the poor telemetry received, and the fuel ullage pressure indicating zero. The zero fuel ullage pressure was caused by more fuel being vaporized and vented than had been expected. The prediction of the lifetime of the gaseous nitrogen supply was extended to 05:30:00.

Second revolution. - The Bermuda station acquired data at approximately 01:41:00. The S-IVB stage was satisfactory for the passivation experiment and automatic enabling occurred over Bermuda.

The Redstone tracking ship, which had a telemetry computer that had been faulting since early in the countdown, had acquisition at approximately 01:46:40. The UHF signal strength was again marginal. An evaluation was made of the available data in an attempt to predict the command coverage of the firings.

Carnarvon reported acquisition of the LM telemetry at 02:24:23 and command handover from the Coastal Sentry Quebec was completed at 02:24:56. At 02:25:10, it was reported from the Mission Control Center that the S-IVB stage was satisfactory. The liquid hydrogen ullage pressure was considerably lower than expected. At 02:26:19, Carnarvon reported that the launch vehicle was showing flight control computer burn mode ON which indicates start of passivation. The oxidizer dump began 1 second later. At 02:27:41, Carnarvon reported burn mode OFF. The oxidizer dump was terminated at 02:28:27, and 10 seconds later, the fuel dump started. At 02:29:04, Carnarvon reported that the oxidizer ullage pressure had not relieved as much as expected, and the fuel dump was terminated at 02:31:27. Nominal fuel and oxidizer venting was reported at 02:31:51. At loss of signal, the fuel ullage pressure was about zero psia. Attitudes were nominal and steady during passivation.

At 02:48:25, approximately 3 minutes early, Hawaii reported acquisition of signal, but the Mission Control Center was unable to synchronize on the data. It was not determined whether this was actual acquisition of the signal due to multipath or whether it was radio frequency interference. Actual Hawaii acquisition of signal occurred at 02:51:00. The S-IVB stage cold helium dump was initiated at 02:52:38 and the dump sequence was nominal.

During the pass over the Redstone, Canary Island, Carnarvon, and Hawaii stations, the guidance system status was checked.

The Rose Knot Victor reported the initial UHF received-signal strength as -105 dBm. The guidance computer time was reported as lagging 1 second with variations to 10 seconds; however, no such indication was noted by any other site.

The handover from the Rose Knot Victor to the Texas station was completed at 03:05:45. UHF signal strength was poor. The scheduled self-test of the digital command assembly was postponed until after the predicted time of signal strength improvement, immediately prior to the initiation of mission programmer sequence V.

Command handover from Texas to Merritt Island was accomplished at 03:09:12. At 03:12:58, the UHF received signal strength was sufficient to transmit the digital code assembly self-test command which cued the program reader assembly. The compare pulse was received at 03:14:40.

Near the time of Merritt Island loss of signal, the Mission Control Center reported that the S-IVB stage oxidizer vent valve had not closed. The oxidizer vent valve CLOSE command was transmitted twice at 03:15:05. It appeared, however, that command had been handed over to Antigua and that Antigua had not yet acquired the signal. After the mission, it was reported that the telemetry discrete had dropped out properly.

Third revolution.- The Ascension Communications Officer reported that part of the problem with poor telemetry reception by the Coastal Sentry Quebec was caused by the outgoing teletype traffic; permission was granted to terminate the summary message channel. The Coastal Sentry Quebec had acquisition at 03:54:24 and immediately reported that the remote site data processor was out-of-commission. This would prevent confirmation of guidance computer program, phase, and display and keyboard data. However, driven events and analog data could still be monitored.

Based on the prefiring events reported from the Coastal Sentry Quebec, it was confirmed that the guidance computer had entered mission phase 9 at the nominal time of 03:55:04 and the predicted time of ignition for the first descent engine firing was 03:59:40. Normal operation of the vent valves on the S-IVB stage was confirmed.

Carnarvon acquired data at 03:57:58; however, command handover was delayed, as planned, until after the first descent engine firing ARM signal at 03:58:42. The firing attitudes of pitch 31.8 degrees and roll 355.6 degrees were close to predicted. Descent engine ignition occurred at 03:59:40.6, based on the Carnarvon strip chart recorders. At 03:59:57, immediately after reporting 10 percent throttle, Carnarvon reported a primary, guidance, and navigation CAUTION indication, which was later changed to a program CAUTION, and program 00. The engine was commanded OFF at 03:59:44.8 by the guidance computer. Carnarvon was directed to make the Mission Control Center prime for command at 04:00:30.

The UHF received-signal strength was -99 dBm when the prime relay reset command was transmitted unsuccessfully at 04:01:18 and again at 04:01:39. At 04:02:19, the prime relay reset command was transmitted and was accepted; the descent engine ARM discrete was removed. Transmission of the command sequence Verb 15-Noun 50, to enable display of the error codes, was started at 04:03:34 and completed at 04:04:26. The error codes received were 1405, DELTA V MONITOR ALARM, and 315, FORGETIT. These codes indicated that the guidance computer had commanded shutdown of the engine because of failure to sense adequate acceleration.

After engine shutdown, the actual orbit was 100 by 119 n. mi. At 04:06:50, the Mission Control Center reported that there were no system problems that would affect vehicle lifetime. The Flight Dynamics Officer recommended waiting until the next revolution before starting an alternate mission. Figure 9.1-1 shows the subsequent real-time logic. The two prime alternates for this type failure were C and L. There were targets for L at the Hawaii station, if they had been required for execution during this pass over the United States. However, they were based on prelaunch nominal data with no descent engine firing and may not have been valid. If used, a manual abort staging sequence would have been required.

The Flight Director concurred in these recommendations. He further requested an evaluation of the possibility of retargeting for another attempt at performing the planned firing for the next pass over the Coastal Sentry Quebec and Carnarvon. This possibility had been previously rejected because of the limited coverage available from those sites during revolution 4.

After Carnarvon loss-of-signal, command plans for the pass over Hawaii and the continental United States were started. The only commands required for Hawaii were the guidance and control error reset command, and the selecting of the mission programmer sequence III for alternate mission C. To insure the vehicle was in a safe condition, the prime relay reset command was to be left in the guidance computer until just prior to going into an alternate mission. At this time the cause of the descent engine shutdown was still unknown.

Alternate mission L was not desirable because it could not be re-targeted to avoid a manual abort staging sequence. The maximum descent engine firing time available would have been 60 seconds. This did not satisfy the requirement for a long descent engine firing. Further, if the manual abort staging sequence were not effective, the descent propellants would be depleted while the vehicle was below the minimum perigee limit. Because there had been severe commanding problems, attempting alternate L with a manual abort staging sequence would jeopardize not only the abort staging test, but also the ascent engine firing to depletion and the reaction control/ascent feed test.

After Hawaii loss-of-signal during revolution 3, the Guidance Officer indicated that the attitude for mission programmer sequence III would be retrograde and recommended using the guidance and control system to establish an optimum attitude during the pass over the continental United States. The command sequence started at 04:41:47 and ended at 04:51:30. The LM went to the commanded attitude of pitch 213.6 degrees, roll 7.8 degrees, and yaw 50.9 degrees. As a result of these commands, the digital autopilot went to minimum deadband and remained there.

The active part of the S-IVB mission ended with the ambient helium dump during the pass over the continental United States.

Fourth revolution.— Prior to signal acquisition by the Coastal Sentry Quebec it had been determined that the modified alternate mission C was the preferred alternate. Based on vehicle attitudes (+X antenna down), the Rose Knot Victor was predicted to be in the correct position for maximum command capability. The mission phase and timer uplink for mission phase 13 was started at Carnarvon, and the uplink was completed at 05:35:01.

The abort guidance select command was selected as the mode for interrupting, because if cuing of another sequence were required this command would have to be transmitted anyway. If failures should prevent continuing the mission for another revolution, the sequence could be resumed by sending the mission programmer start command.

It was recommended that mission programmer sequence III not be terminated after the first ascent engine firing. This was a deviation from the alternate mission C. The reason for the deviation was that the guidance and control system was still good, and if the mission programmer could be interrupted prior to reaching the ascent engine propellant depletion firing, this firing could be performed under guidance control the next revolution. If the sequence could not be interrupted, the ascent engine propellant firing-to-depletion coverage would be marginal. It was also recommended that initiation time be 06:10:00, and that the sequence be terminated no later than 06:13:32. The latter time was approximately 7 seconds prior to getting into the +X translation for the ascent engine firing to propellant depletion.

At Hawaii, during revolution 4, the pre-sequence commands were sent for mission programmer sequence III. Signal strength was very poor at first, and rejects were received from the vehicle for the first two attempts at transmitting the prime relay OFF command. Signal strength improved and the third transmission, at 05:59:37, was accepted. Battery 5 was commanded ON at 06:00:28 as a precautionary measure against switching failure during staging. At that time, battery 5 assumed about 45 percent of the load. Batteries for the explosive devices were commanded on line at 06:00:46.

The Rose Knot Victor commanded the LM to the abort guidance mode at 06:05:34 and commanded mission programmer start at 06:10:00; the sequence proceeded normally. The Mission Control Center was monitoring the sequence through the Goldstone and Guaymas stations. Rates were low, and the sequence continued normally. The abort staging sequence occurred at about 06:12:14. The resultant orbit, based on White Sands data, was 93.4 by 526 n. mi.

After the cutoff of the first descent engine firing, it was decided not to continue with the ascent engine propellant depletion firing part of the sequence. The vehicle had approached within about 8 degrees of gimbal lock but had returned to a nominal condition. The abort guidance select command was sent to stop the sequence before any further commands were executed by the mission programmer. The first command was transmitted at 06:13:40, and a second command was initiated 1 second later; both commands were accepted. The primary guidance select command and the prime relay reset command were sent at 06:14:03 and 06:14:15, respectively. Shortly afterward, an extremely high reaction control propellant usage rate was reported, but was believed to be the result of

the primary guidance control with the digital autopilot using the full vehicle mass for its control engine command calculations. This had been discussed before the mission and was expected but not to the extent observed. The Guidance Officer prepared mass update loads, but these were not available for immediate transmission because the mass values required would have been a function of the vehicle state and how far sequence III had progressed.

Two indications believed to be anomalous were noted during sequence III. First, during the time the descent engine was armed, the inverter voltage oscillated between 113 and 124.5 V ac. No gimbal-drive-actuator fail indications nor other effects were noted as a result of this fluctuating voltage. Second, at staging, battery 5 carried 86 percent of the load for about 30 seconds. For the next 5 minutes, both battery currents sought stabilization levels. This was believed to have resulted from battery 5 being warmer, battery 6 having a higher charge, and a high total current load because of control engine activity, although the number of variables involved prevents any definite conclusions. Thereafter, both batteries shared the load equally. [Editor's note: Both of these indications were, in fact, normal.]

A review of the command histories from mission programmer sequence III showed that the abort guidance select command had not been sent prior to the start of the +X translation for the second ascent engine firing. If this is correct, there would have been some 36 seconds of +X translation, which would have accounted for some of the high reaction control usage of propellants. Reaction control usage had been as expected until the time the primary guidance mode was selected.

The guidance computer had been updated with the proper attitude for the mission programmer controlled engine firings and an erasable memory update was sent to reenable the proper computer routine, if further guidance computer controlled firings were to be accomplished. This was started at 06:16:47, and completed by 06:17:43.

In order to conserve some attitude hold capability, rather than depleting both systems, the reaction control main A valve was closed at 06:17:09, trapping approximately 34 percent of the propellant. At 06:23:20, it was reported that B system propellants were being depleted and a recommendation was made that the abort guidance system mode be used to conserve the propellants. This request was vetoed to preclude the possibility of a gimbal lock condition, which would have prevented the use of the guidance and control system for the ascent engine firing-to-propellant-depletion sequence.

A navigation update load, based on data after engine cutoff, was started from the Merritt Island station at 06:24:47, and was completed through the Antigua station at 06:25:58. A verification was received,

but loss-of-signal occurred prior to the guidance computer telemetry verification that the load had been accepted; this was confirmed later at Carnarvon.

Fifth revolution.-- At 06:28:10, the network was advised that either mission programmer sequence V or guidance computer mission phase 13 would be followed. The starting point for either would be Hawaii and the propellant depletion firing would not be completed until the Rose Knot Victor acquired the signal. A 1-minute gap between Hawaii and the Rose Knot Victor would be covered by the Watertown, which was being used on an engineering evaluation basis; the Watertown had been recording data during the previous passes.

At this time (06:28:10), the mass update, target update, and a timer update for mission phase 13 was still required, and an update to lengthen the guidance computer acceleration sample period was highly desirable. The exact cause of the descent engine shutdown was still unresolved, and if the vehicle were unable to complete the maneuver as planned because of a similar problem, there would be little range coverage left for subsequent attempts. Further, attitude control would be lost when the reaction control B system propellants were depleted; consequently, it was decided to open the A system and the control engine crossfeeds as soon as possible after the mass update was completed. Tracking data confirmed a 91 by 532 n. mi. orbit, indicating a fairly long pass at Carnarvon. However, the time available for all the updates was marginal.

The Coastal Sentry Quebec acquired broken telemetry at 07:10:30 and telemetry for that pass remained fairly poor. Part of the problem was apparently caused by a failure of a pulse code modulation power supply at the station. This prevented the Coastal Sentry Quebec from cuing mission programmer sequence V as planned.

The first command transmitted from Carnarvon was reaction control main A valve closed reset at 07:08:06. Uplink of the mass update (EMU 1, load 3701) was started at 07:08:50 and was completed by 07:09:41. The following commands for the reaction control main shutoff valves were completed by 07:10:57: main B closed, main B closed reset, main A open, and main A open reset. The next activity at Carnarvon was to get the reaction control crossfeed valves opened. The first command, prime relay off, was sent at 07:11:07, and the crossfeed open commands were uplinked at 07:11:20. The sequence was completed by 07:12:22. The reset commands were started at 07:13:05 and completed at 07:14:05. After the crossfeed valves were opened, an uplink (EMU 2, load 3801) was initiated to increase the sampling period for the delta V monitor routine and to get the digital autopilot into maximum deadband. However, the data were not accepted with the load messages because of intermittent drops in UHF received-signal strength. An attempt was made to send the load through the display and keyboard commands. The load was still not completed when the signal was lost.

During the load attempt to the erasable memory unit, high control engine activity and occasional high rates were observed. Also, the reaction control oxidizer pressures were low, and it was recommended that the ascent feed valves be opened prior to executing any firing sequence. The mass update previously transmitted did not restore normal digital autopilot operation, because the design of the system is such that the current mass is ignored until the guidance computer is in an average g routine.

Hawaii acquired the signal at 07:38:00, and the UHF received-signal strength was good. The command sequence to open the ascent feed valves was started at 07:38:31 and completed at 07:42:14. Immediately after the ascent feed valves were opened, the Guidance Officer sent the cue for mission programmer sequence V, and the compare pulse was received at approximately 07:42:38. At 07:42:57, the reaction control main B valve open command was transmitted to trap as much propellant as possible, in the event the sequence could not be stopped before the ascent feed valves were closed. The following command sequence started the mission programmer firing.

Guidance select abort guidance 07:43:07

Mission programmer start (not 07:43:19 Delay in sending second
accepted) command to verify not
accepted.

Mission programmer start 07:43:54
(accepted)

Engine start 07:44:15 First command accepted.
07:44:18
07:44:21

The firing was normal and attitudes were steady. At the time the ascent feed and reaction control valves were confirmed to be in the normal configuration for the ascent feed test, the abort guidance select command was transmitted. However, Hawaii had loss of signal and the command was approximately 12 seconds too late. If the first mission programmer start command had been accepted, confirmation could have been made in time.

The Rose Knot Victor acquired a signal at 07:46:48. Twelve seconds later, the last ascent feed valve closed. The firing continued with good attitude stability until approximately 07:47:45. At that time rates started going off scale high and low in all axes. The Rose Knot Victor maintained solid telemetry until loss of signal. The firing continued until depletion, but the time of depletion could not be determined in

real time. The Rose Knot Victor received approximately 5 pulse code modulation counts on the chamber pressure measurement after ascent engine cutoff.

Communications coverage during the sequence was good. This sequence was nominal except that after reaction control propellant depletion, eight control engines remained on electrically. This resulted in the total current increasing to 81 amperes.

The vehicle structure apparently held during the entire firing. Cabin pressure was reported as 52 PCM counts at loss of signal at the Rose Knot Victor. Two commands were transmitted in the blind from the Texas station in an attempt to put the vehicle in a usable condition for the postmission test plan.

After an apparent C-band loss of signal during the maneuver, all sites were instructed to go to a skin-track mode. There was no C-band acquisition after the completion of the maneuver. Maximum elevation angle during Guaymas pass was approximately 1 degree. Only two tracking sites, Pretoria and Hawaii, would be able to track during the next several revolutions. The extended mission team then assumed shift duties; however, they were unable to acquire the spacecraft. The effort continued until approximately 11:00:00 G.m.t.

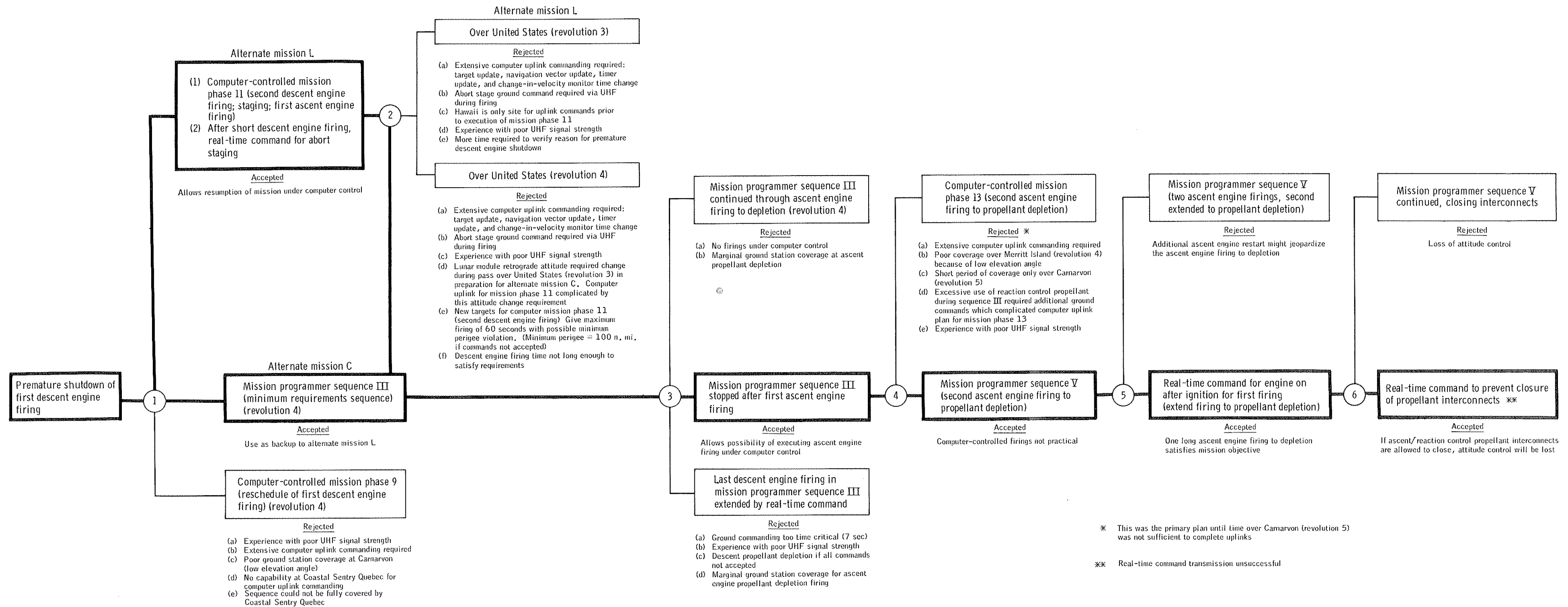


Figure 9.1-1. - Real-time decision logic.

9.2 NETWORK PERFORMANCE

Support from the NASA and Department of Defense network stations was satisfactory. Minor problems were experienced with commands, telemetry, and radar acquisition. No mission impact resulted from any of the problems, and no mission capabilities were lost.

9.2.1 Telemetry

The telemetry computer on the Redstone network ship faulted during the countdown period and was out of service for the mission. A post-mission inspection revealed that a wiring error occurred during incorporation of a modification. The Ascension station did not acquire during the third revolution because an erroneous acquisition message was transmitted from the Mission Control Center in Houston. At the start of the third revolution, the playback bit at Carnarvon station was set erroneously and resulted in a loss of about 5 seconds of data. Data from the Guam station during the fourth revolution were not received at the Mission Control Center. The problem was traced to an operator error in patching the communications line terminal at Goddard Space Flight Center.

9.2.2 Tracking

The Canary Island station had a range bias of 2000 yards during the first revolution. The problem was caused by a drifting fine-range adjustment, which was corrected before the second revolution. During the first revolution, data from the White Sands station were not accepted at the Mission Control Center because of a tagging error by Goddard. During the second revolution, the California and White Sands stations tracked an antenna side-lobe signal because of erroneous acquisition messages from the Mission Control Center. The California station could not support the mission during the third revolution because a malfunction in the computer affected the high-speed data.

9.2.3 Command

During a command interface test at the Goldstone station, a load/clear-load (2507) input was attempted; however, the output was a UHF up-link request for command and service module navigation update (0001). The problem was caused by simultaneous inputs to the program request module and the manual entry device. Procedures have been changed to preclude the problem in the future.

During the countdown period, an erroneous computer load was sent to the Carnarvon station. After switching to the standby central processor (B-system), load control indications showed a load transferred to Carnarvon. An attempt was made to clear the output buffer by clearing load 4563, the last load sent to Carnarvon, but no action resulted. The problem was finally corrected by clearing the previous load (2509) in the output buffer and load 4563 was subsequently transferred. It was concluded that the standby computer processor had dropped the input during the time the validation was received from Carnarvon for load 2509; as a result, load 4563 was stacked behind it. The problem is under investigation.

9.2.4 Mission Control Center Central Processors

The output of the polynomial buffer terminal was interrupted 14 times on the standby system and 11 times on the online system. These interrupts were manually cleared, and the buffer terminals were reinitialized within 10 seconds after each occurrence. The buffer terminals have been subsequently modified so that each has an individual input/output channel to interface with the central processors.

The central processor guard faulted once at T minus 9 minutes and at three additional times during the mission. No data were lost except that at 04:41:00 data from the Pretoria station were not routed to the real-time computer complex. However, the rotary system permitted all message traffic to overflow to other teletype machines. The problem is under investigation.

9.2.5 Miscellaneous Problems

During the countdown period, the Goddard central processors faulted six times within approximately 40 minutes. Hardware problems were discovered in the A-system. A software problem associated with a collective message header was also found, but the procedure was changed to eliminate use of this message header. The computers were returned to service before launch.

During the countdown period, computer faults occurred at the Texas, Hawaii, and Carnarvon stations. A fault also occurred at the Canary Island station when the Mission Control Center transmitted a load (GMTLO) after loss-of-signal at Canary Island. Canary Island was trying to transmit a low-speed summary message at that time. In addition, during receipt of the GMTLO load, the Mission Control Center executed an S-IVB history request, and both computers started cycling (went into a loop). The problems are under investigation.

9-16

At approximately 00:18:00, a fuse was blown in the B master instrumentation timing equipment. One computer had to be restarted and two computers had to be switched.

9.3 RECOVERY OPERATIONS

(This section is not applicable.)

10.0 EXPERIMENTS

(This section is not applicable.)

11.0 CONCLUSIONS

The analysis of the mission data has resulted in the following conclusions:

1. The overall performance of the lunar module was good, and based on the results of the LM-1 flight, the lunar module is acceptable for manned orbital flight.
2. All system operations and vehicle dynamics associated with the abort staging sequence were satisfactory for manned operation.
3. The start, steady-state, throttling, and shutdown characteristics of the descent propulsion system were satisfactory for the engine firings that were performed.
4. The thermal aspects of supercritical helium pressurization system could not be adequately evaluated due to the short duration of the three descent engine firings.
5. The ascent propulsion system exhibited operational characteristics similar to those noted during ground testing, and the overall performance of the system was satisfactory.
6. The temperature limits on the control engine clusters were exceeded with no detrimental effects on system operation.
7. The excessive use of reaction control propellants was caused by the failure to update the guidance computer to reflect the staged-vehicle mass constants. As a result of the high usage, reaction control propellants were depleted. Continued operation was outside the design limits and precipitated three failures.
8. The premature shutdown of the first descent engine firing demonstrated a lack of complete systems coordination.
9. Loads experienced during the mission were within design limits of the structure.
10. The vibration analysis indicated that the lunar module can satisfactorily withstand vibrations which are expected during launch on a Saturn V.
11. The guidance and control systems operated as designed, proving their capability for withstanding the launch and space environments. The digital autopilot capability for attitude and +X translation control was adequately demonstrated. The stabilization and control system maintained

11-2

proper rate control through the descent and ascent engine firings and the abort staging sequence.

12. The water/glycol coolant system maintained equipment at proper temperature levels. The coolant system temperature was controlled by the sublimator, verifying its startup capability and heat rejection capacity.

12.0 ANOMALY SUMMARY

Analyses of the Apollo 5 mission results have disclosed seven anomalies and several instrumentation failures. Of the seven anomalies, one occurred during the countdown, and six during the mission. The anomalies are discussed in the following sections.

An additional problem was previously reported as an anomaly: The pressures in the ascent and descent propellant tanks decreased from the time of prepressurization at the launch site (110 hours prior to launch) to the time of final pressurization in flight (4 hours after launch). The ascent oxidizer tank pressure showed the largest decay. The pressure decay was initially believed to be the result of an oxidizer leak. However, subsequent analyses have shown that all of the pressure decays can be attributed to helium absorption into the liquid propellants.

12.1 ERRATIC FREON COOLING DURING COUNTDOWN

Statement - Coolant temperatures, which were controlled with the freon supply ground support equipment, were erratic during the countdown.

Discussion - The water/glycol coolant of the heat transport system of the lunar module (LM) was cooled prior to launch by two freon boilers in the environmental control system. The freon was supplied to the boilers from two freon bottle racks, which were part of the ground support equipment.

Shortly after freon flow was increased to begin the chilldown of the heat transport system, the freon delivery pressure to the LM dropped, and the heat transport system coolant temperature began to increase, indicating loss of freon cooling. Consequently, a hold was called at T minus 2.5 hours, and rack 1 was manually shut off. Satisfactory conditions were established with rack 2, and the count was resumed at T minus 2.5 hours (about 3:15 p.m.).

At approximately T minus 50 minutes (at which time rack 1 showed a weight loss equivalent to two bottles of freon), coolant temperatures again increased. Attempts to increase flow rate by further opening the freon flow control valve failed to produce any cooling. By lowering the freon flow rate, the erratic operation of the system ceased but at a higher vehicle coolant temperature. The LM coolant temperature upper limits for launch were changed, and the temperature was maintained within the prescribed limits.

Examination of the freon racks the morning following launch revealed the following:

- a. All bottles in rack 2 were about one-half full.
- b. Two bottles in rack 1 were empty, even though rack 1 was shut off at T minus 2.5 hours. All other bottles in rack 1 were full.
- c. The standpipes in two of the full bottles in rack 1 had dropped out of the cap block and were resting on the bottom of the bottle.

The temperature problem encountered at T minus 3.5 hours can be explained by item c. With the standpipe unattached, a direct nitrogen flow path into the freon manifold was opened. When the nitrogen pressure was increased to begin high freon flow to the vehicle, sufficient nitrogen mixed with the freon to degrade heat absorption in the freon boilers.

The two empty bottles in rack 1 may have inadvertently been left open when the rack was isolated during the hold at T minus 2.5 hours. If this was the case, at the time these two bottles emptied, a nitrogen flow path was opened; the freon was again mixed with nitrogen, resulting in coolant temperature fluctuations.

Conclusion - The analysis has shown that the reduced cooling capacity by the freon supply was caused by nitrogen pressurization gas mixing with the freon. Two factors contributed to the gas mixing: broken standpipes in two of freon bottles, and depletion of freon in two other bottles.

Freon ground support equipment for prelaunch cooling is not to be used for manned lunar modules.

12.2 PREMATURE SHUTDOWN OF FIRST DESCENT ENGINE BURN

Statement - The first descent propulsion maneuver, which was controlled by the primary guidance, navigation, and control system, was scheduled to last approximately 38 seconds. The primary guidance system commanded the "engine on" as planned at 03:41:39, but 4.17 seconds later, the guidance system issued an "engine off" discrete with an accompanying alarm, indicating that the thrust/time criteria programmed in the LM guidance computer were not met.

Discussion - At the time of "engine on" minus 30 seconds, the guidance system started recording sensed velocity changes from the inertial measurement unit pulse-integrating pendulous accelerometers. The descent engine thrust monitor was programmed to turn off the engine if any

three consecutive 2-second accelerometer samples taken after commanded "engine on" indicated an accumulated velocity of less than 45 cm/sec each. Because of phasing established at "engine on" minus 30 seconds, the first accelerometer sample utilized by the thrust monitor was taken within 0.01 second after commanded "engine on" and therefore represented only velocity accumulation due to the control engine +X translation. The +X translation ended 0.5 second after commanded "engine on"; therefore, the second sample, taken at "engine on" plus 2 seconds, represented a combination of velocity accrued from the control engines and from the start of the descent engine firing. The third sample, taken at "engine on" plus 4 seconds, was the first that represented descent engine velocity accumulation only. Because none of the three samples met the 45 cm/sec minimum criteria programmed in the guidance computer, the engine was commanded off.

The helium which was used to pressurize the propellant tanks after activation was stored supercritically in a cryogenic storage vessel. The vessel was isolated by the three explosive valves which were fired automatically by the pyrotechnic system 1.3 ± 0.3 seconds after the "engine on" command was given. Therefore, the firing was begun with less than normal propellant tank pressures, causing a slower thrust buildup.

Conclusion - All data indicate that the guidance system and the descent engine functioned as designed. The slower than normal thrust buildup, caused by the start at less than full tank pressure, resulted in failure of the engine to meet the thrust/time criteria programmed in the guidance computer.

All logic and circuits that could issue any engine cutoff or inhibit any engine start will be evaluated to determine which should be eliminated or altered and which should be retained within the software.

12.3 ABRUPT CHANGE IN CABIN PRESSURE LEAK RATE

Statement - At 03:27:00, the equivalent cabin pressure leak area abruptly increased from 0.0014 to 0.0044 square inch. After 71 minutes, the leak area decreased to approximately 0.0026 square inch.

Discussion - The characteristics of the cabin pressure decay from cabin seal-off until 03:27:00 indicated that a constant leak area existed during this period. At 03:27:00, the leak area abruptly changed. Calculations show that the change in rate was equivalent to a change in area from 0.0014 to 0.0044 square inch. The leak area then decreased 71 minutes later to a value equivalent to about 0.0026 square inch and remained constant to the end of the mission.

Conclusion - At the time the leak area first changed, the vehicle was in a quiescent state, and the available data provide no indication as to the cause of the change.

The minimum cabin pressure requirement was maintained to the end of the mission.

12.4 OUT-OF-PHASE INDICATION FROM DESCENT ENGINE

PROPELLANT SHUTOFF VALVES

Statement - During the transition from 10-percent throttle to full throttle on the second and third descent engine firings, an out-of-phase indication was received from one of the two pairs of actuators which control the eight propellant shutoff valves. The indication remained until the end of both firings.

Discussion - There were four shutoff valve actuators (A, B, C, and D), each of which controlled a fuel and an oxidizer shutoff valve. The actuators were instrumented in two pairs, so that an indication was received if actuators A and B or C and D were not in the same position (open or closed). During the transition from 10-percent throttle to full throttle on the second and third descent engine firings, the signal received indicated that either A or B had closed. The indication slightly lagged an inflection point in the pressure/time curves for oxidizer and fuel injection pressures and chamber pressure. In addition, almost simultaneously, pressure rises were noted in the oxidizer and fuel engine-inlet pressures. The phenomenon was nearly identical on both firings.

Conclusion - At present, no conclusions can be drawn as to whether there is any connection between the pressure transients and the valve out-of-phase indication. Ground tests will be made in an effort to determine the cause of this anomaly.

12.5 ABRUPT CHANGES IN RECEIVED UHF SIGNAL STRENGTH

Statement - Abrupt changes were detected in received UHF signal strength in the spacecraft throughout the Apollo 5 mission.

Discussion - Abrupt changes in spacecraft-received UHF signal strength of about 30 to 40 dB in the command-link data were detected throughout the Apollo 5 mission. Corresponding changes did not occur in the ground-received signal strength from the VHF data transmitters, which shared the same two antennas through a diplexer. The abrupt

changes in received power frequently caused the received command signal power to be below the message acceptance threshold. Consequently, command transmission had to be delayed or repeated.

Conclusion - The results of the data analysis isolate the fault of the intermittent operation to the flight hardware. Specifically, the fault can be isolated either to the RF stage of the digital command assembly or to the coaxial cable assembly connecting the diplexer and the digital command assembly.

12.6 EXCESSIVE CONTROL ENGINE PROPELLANT USAGE

Statement - Abnormally high thruster activity and excessive control engine propellant usage began immediately after primary guidance was selected by command at 06:14:03.

Discussion - Since staging occurred with the vehicle in the backup guidance mode, the digital autopilot, which is part of the primary guidance system, did not sense vehicle mass change that occurred at staging. Consequently, when guidance was returned to the primary mode, thruster "on" time for attitude corrections was calculated by the autopilot using incorrect inertia constants. The result was rapid oscillations of the vehicle about all axes as the guidance system overcontrolled in an attempt to keep attitudes within the deadband limits. Control propellant usage increased to an unacceptable rate, and ground controllers isolated the A system with 30-percent propellants remaining. The propellants in B system were depleted within 5 minutes, which precipitated the following four undesirable secondary effects.

12.6.1 Discrepant Manifold Pressure Indications

Statement - Following the propellant depletion in B system, the oxidizer manifold pressure decreased from 180 psia to 50 psia with no apparent decrease in the fuel pressure.

Discussion - Based on serviced quantities of the propellants in B system and normal mixture ratios during thrusting, the fuel should have been depleted first. Data showed that the fuel manifold pressure did, in fact, begin to decay first, but very rapidly increased again. Because it happened so rapidly, it was not evident until data were available for the precise time of incidence.

An oxidizer manifold pressure of 50 psia was indicated after oxidizer depletion in the B system. At the existing temperature, 50 psia was the vapor pressure of the oxidizer; therefore, a two-phase oxidizer condition was present in the manifold. Because of the low duty cycling of the control engines during this time interval, sufficient liquid remained in the manifold to sustain the 50-psia pressure until the A system was turned on and the crossfeed opened.

Conclusion - The fuel depleted first and the fuel bladder collapsed. Fuel depletion was obscured by the effects of bladder leakage and the manifold pressure sensor sensing helium pressure.

12.6.2 Inadvertent Closure of Oxidizer Shutoff Valve

Statement - When the control system crossfeed was opened, the A system oxidizer manifold pressure decreased and the B system pressure increased.

Discussion - Subsequent to B system propellant depletion, the A system main valves were commanded open. The crossfeed valves between the A and B systems were then opened, and the A system oxidizer manifold pressure immediately decreased to 90 psia and B system pressure increased to 90 psia. The oxidizer manifold pressure varied between 50 and 115 psia dependent on the engine duty cycle.

An unlatched valve moved to a null position would not be positively locked open or closed. This type condition would essentially isolate the tank but still allow some leakage into the manifold, which would explain why the manifold pressure varied from 50 psia (the vapor pressure) and 115 psia, depending on the thruster duty cycle.

Conclusion - The abnormal oxidizer line pressures have been attributed to an inadvertent unlatching of the A system oxidizer shutoff valve from the open position. A test is planned to determine the effects of valve operation with the pressure and temperature conditions found at the shutoff valve during the Apollo 5 mission.

12.6.3 Thrust Chamber Failure

Statement - Over Carnarvon during the fifth revolution, vehicle rates about the pitch and roll axes and the lack of detectable chamber pressure indicated a failure of the 4-up engine.

Discussion - The up-firing engine in cluster 4 was last observed to be operating over Ascension during the fifth revolution. Ground tests have been conducted with manifold pressure conditions similar to those which existed in the B system between Ascension and Carnarvon (pressures less than 100 psia with a gas/liquid state); in some of the ground tests, explosive mixtures were produced within the engine chambers.

Conclusion - The 4-up engine chamber apparently ruptured during the fifth revolution.

12.6.4 High Cluster Temperatures

Statement - Temperatures on clusters 1 and 3 exceeded the 190° F upper red-line limit.

Discussion - The temperature increases on clusters 1 and 3 occurred when the heat from the engines experiencing high duty cycle was conducted back to the clusters. The temperatures exceeded the upper instrumentation limit of 200° F. Because the cluster temperatures sensors were installed near the down-firing engines, these measurements were sensitive to the activity of those engines and not of the clusters in general. Clusters 2 and 4 were cooler because the down-firing engines in these clusters were A system engines, which were isolated shortly before the main valves were closed. This allowed the injectors to be cooled somewhat from subsequent valve actuations as the residual propellants in the lines were vented. Cluster 1 temperature, the highest of the four, probably reached at least 230° F. However, no degradation in engine performance was evident.

Conclusion - The high cluster temperatures are not considered an anomaly since they were caused by the increased control engine activity and would be expected to be high under these circumstances.

12.7 FAILURE OF DESCENT STAGE FIBERGLASS

THERMAL SHIELD

Statement - Two temperature sensors on the upper surface of the descent stage facing the fiberglass covering the upper surface of the descent stage showed abrupt temperature rises at abort staging.

Discussion - The temperature measured by GB0401T, located on the +Z deck, increased from 75° to 200° F in 0.1 second at staging. The temperature then dropped to 140° F in 0.1 second. The temperature measured by GB 0402T rose from 60° to 110° F in 0.1 second. The

temperature measured by GB0403T remained at 68° F throughout this period. These three sensors were attached to the outboard face of the tank bay upper aluminum decks facing the fiberglass cover. The fast temperature response recorded by sensors GB0401T and GB0402T was indicative of ascent engine exhaust gas impingement on the sensors. The fiberglass shield was 0.080-inch thick at the center and reduced to 0.050 around the periphery of the shield.

Conclusion - One possible explanation for the abrupt rise in these temperatures would be for a break or opening to exist in the fiberglass shield. A further investigation of this anomaly is in progress at the time of report publication.

12.8 INSTRUMENTATION DISCREPANCIES

12.8.1 Adapter Panel Deployment

Statement - No adapter panel deployment indication was received from the event monitor.

Discussion - The adapter panel deployment event was transmitted through the Saturn instrument unit with other adapter data. Indications were received from the relays which fire the pyrotechnics to separate the four panels. However, no indication was received from the four series-connected limit switches which monitor the physical deployment. The instrumentation was checked several times at the launch site and operated satisfactorily. The panel deploy indication instrumentation was flown for the first time on this flight. The system is not used on manned flights.

Other measurements show that the spacecraft separated from the S-IVB stage without any abnormal disturbances, indicating that the panels were, in fact, deployed.

Conclusion - A number of causes could explain the lack of deploy indication; no exact cause can be isolated.

12.8.2 Separation Distance Monitors

Statement - The four separation distance monitors did not function during abort staging.

Discussion - The separation distance sensors mounted on the ascent stage, measured up to 4 feet of distance between the ascent and descent stages.

Conclusion - A number of factors could explain the lack of separation distance indication; no cause can be isolated.

12.8.3 Pressure and Temperature Sensors

Statement - During the abort staging sequence, one of the two descent engine blast deflector temperature measurements and four of the seven ascent stage bottom surface temperature measurements failed. This is discussed in further detail in section 6.2. Six interstage pressure measurements did not show any detectable pressure increase.

Discussion - All five thermocouples were spot-welded to the skins. This method of attachment, required for high thermal response, makes the thermocouples susceptible to detachment caused by vibration, panel flexure, temperature conditions, or accidental jarring of the thermocouple wires.

Six of the 26 interstage pressure measurements showed no detectable increase in pressure at staging. Five of the six had been monitored on telemetry during the launch phase, and all five showed proper response to the change in static pressure. There were no components common to the six measurements.

Conclusion - A number of causes could explain the lack of pressure and temperature indications; however, no exact cause can be isolated.

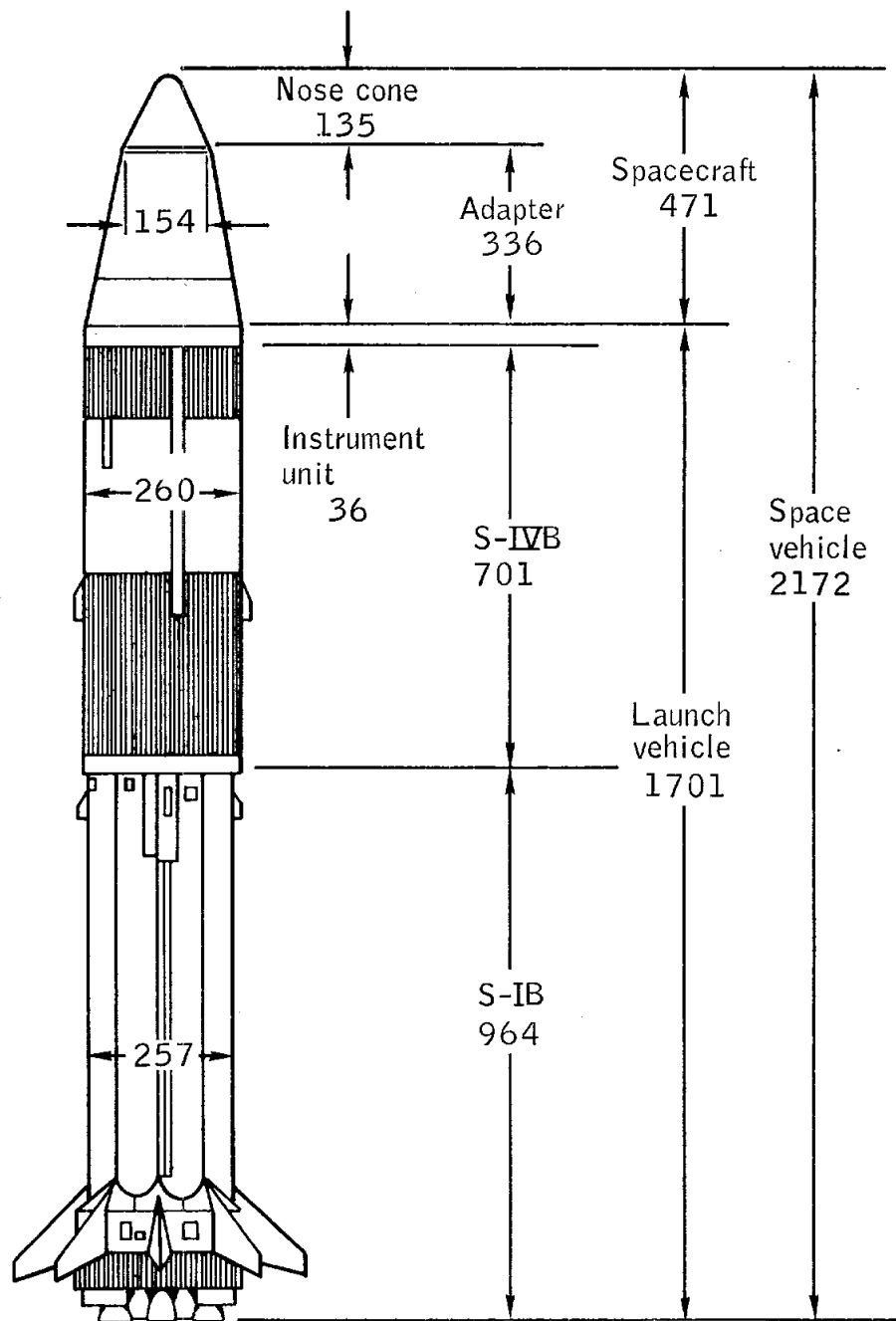
12.8.4 Vibration Measurement

Statement - The rendezvous radar antenna vibration measurement located on structure adjacent to the rendezvous radar antenna operated intermittently during engine firings.

Conclusion - The characteristics of the data indicate an intermittent failure in the transducer signal wires.

13.0 VEHICLE AND SYSTEMS DESCRIPTION

The space vehicle (fig. 13.0-1) for the Apollo 5 mission consisted of an Apollo lunar module (LM-1), a spacecraft/lunar module adapter (SLA 7), a nose cone, and a Saturn S-IB launch vehicle (AS-204). The combined space vehicle was approximately 181 feet long.



All dimensions are in inches

Figure 13.0-1.- Apollo 5 space vehicle.

13.1 COMMAND AND SERVICE MODULES

(This section is not applicable.)

13.2 LUNAR MODULE

The lunar module (LM) is designed to land two men on the lunar surface and return them to a lunar orbit where the LM will rendezvous and dock with the command and service modules. The LM is composed of the ascent stage and the descent stage (figs. 13.2-1 and 13.2-2). The first flight configuration lunar module (LM-1) was flown on the Apollo 5 mission. LM-1 was significantly different from subsequent lunar modules. Many of the differences resulted from the Apollo 5 mission being an unmanned flight. The following systems were aboard the LM-1 and were operational for this mission:

- a. Environmental control (partial)
- b. Electrical power
- c. Reaction control
- d. Ascent propulsion
- e. Communications
- f. Operational instrumentation
- g. Development flight instrumentation
- h. Primary guidance, navigation, and control
- i. Stabilization and control
- j. Pyrotechnics
- k. Controls and displays (partial)
- l. Descent propulsion

The following significant equipment was added to LM-1 for the Apollo 5 mission:

- a. LM mission programmer
- b. Development flight instrumentation telemetry
- c. C-band transponder

- d. Two freon boilers
- e. Scimitar antenna

The following were inoperative on LM-1:

- a. Oxygen supply and cabin pressure control section of the environmental control system
- b. Atmosphere revitalization section of the environmental control system
- c. Secondary coolant loop of the heat transport section
- d. VHF inflight antennas
- e. S-band steerable antenna
- f. Rendezvous radar antenna
- g. Landing radar antenna
- h. S-band omnidirectional antenna (+Z axis only)
- i. Selected cabin displays
- j. Alignment optical telescope.

The following equipment was deleted from LM-1:

- a. Landing point designator
- b. VHF transceivers
- c. Landing gear
- d. Crew provisions
- e. Tracking lights
- f. Abort guidance system
- g. Rendezvous radar electronics
- h. Landing radar electronics
- i. Two attitude controller assemblies

- j. Two thrust translation controller assemblies
- k. Descent stage oxygen tank
- l. Windows (replaced with aluminum plates).

The significant differences listed in the previous paragraphs are discussed in more detail under the applicable system description in this section.

13.2.1 Structures

The mass properties of LM-1 at earth launch and at separation of the ascent and descent stages are listed in section 13.5. The overall LM dimensions are shown in figure 13.2-3.

Ascent stage.— The ascent stage structure (figs. 13.2-4 through 13.2.6) consisted of a crew compartment, midsection, aft equipment bay, tanks, and equipment mountings. The primary and secondary structures did not include changes for weight reduction but otherwise was identical to the basic LM design.

Crew compartment: The crew compartment structural shell was cylindrical and of semimonocoque construction, composed of aluminum alloy chem-milled skins and machined longerons. The shell was supported by formed Z sheet metal rings riveted to the structural skin, forming a structure 92 inches in diameter.

The front face assembly (fig. 13.2-4) incorporated openings in the structure for two triangular windows and the egress/ingress hatch. The LM-1 windows were replaced with aluminum plates. Two structural beams extending up the forward side of the front face assembly supported the structural loads applied to the cabin and were attached to additional beam structure extending across the top of the cylindrical crew compartment.

Midsection: The midsection structure consisted of a ring-stiffened semimonocoque shell of construction similar to that of the crew compartment.

The lower deck of the midsection at station +X233.500 provided the structural support for the ascent engine. The upper deck at station +X294.643 provided the structural support for the docking tunnel and docking hatch.

The ascent engine propellant storage tanks were attached to the +Z27 and -Z27 bulkheads.

Two canted beam assemblies secured to the bottom of the lower deck and to the +Z27 and -Z27 bulkheads formed the ascent engine compartment. The engine support members were bolted to the lower deck.

Aft equipment bay: The main supporting structure of the aft equipment bay (fig. 13.2-6) consisted of tubular truss members fastened to the -Z27 bulkhead. The vertical box beams of the equipment rack assembly contained integral coldplates for cooling electronic equipment.

Thermal shield support: The aluminized Mylar thermal blankets, formed into various sizes and shapes, were secured to standoffs on the outer surface of the structure. In the midsection and aft equipment bay areas where the thermal shield could not be attached directly to the primary structure, an aluminum tubular framework was installed. The thermal shield was attached to this framework by standoffs similar to those in the crew compartment.

The base heat shield protected the entire bottom of the ascent stage from the staging pressures and temperatures.

Descent stage.- The descent stage primary structure (figs. 13.2-7 and 13.2-8) was constructed of aluminum alloy, chem-milled webs, extruded and milled stiffeners, and capstrips. The main structures consisted of two pairs of parallel beams arranged in a cruciform, with structural upper and lower decks. The ends of the beams were closed off by bulkheads. The outrigger truss assemblies, consisting of aluminum alloy tubing, were attached at the ends of each pair of beams.

The five compartments formed by the descent stage main beam assemblies housed the major components of the descent propulsion system. The center compartment housed the descent engine, and compartments in the X and Y beam housed the oxidizer and the fuel tanks, respectively.

13.2.2 Thermal Control

Thermal control was provided by a passive system consisting of propellants, structures, insulation, and thermal control coatings. Thermal control of the electronic equipment was provided by coldplates, which were part of the environmental control system.

The large thermal mass of the propellants and structures was enclosed by multilayer radiation superinsulation to reduce the heat loss to the space environment. This superinsulation was basically a composite of 25 layers of 0.15-mil aluminized Mylar sheets encapsulated with 0.5-mil aluminized Kapton (H-film) sheets. A maximum of up to thirteen layers of 0.5-mil aluminized Kapton was added to the 25-layer superinsulation depending on the applicable heating rates in areas exposed to

impingement by the control engine plume. Thermal shielding was located outboard from the insulation on both stages and provided protection from micrometeoroids and additional protection from control engine plume impingement.

The ascent stage thermal shielding consisted of aluminum panels varying in thickness from 0.004 to 0.032 inch, depending on the calculated local heating rates for impingement. The descent stage thermal shielding consisted of localized panels made up of alternate layers of nickel foil and Inconel mesh (separator) and an outer sheet of 1.25-mil Inconel all external to the basic 25 layer blanket and 0.5-mil aluminized Kapton layers. These panels provided a high-temperature radiative barrier, whereas the aluminum panels on the ascent stage absorbed the heat for maximum engine firing conditions. Thermal control coatings were painted on the exterior of the thermal shielding and on externally exposed structure to maintain vehicle temperatures.

Thermal protection was also provided on the exterior bottom side of the ascent stage and the upper exterior surface of the descent stage for protection from ascent engine firing during stage separation. This protection consisted of the 25-layer radiation superinsulation and several outboard layers of 0.5-mil aluminized Kapton plus one outer layer of 5-mil aluminized Kapton.

The base heat shield thermally insulated the bottom of the descent stage from engine plume radiation. This insulation was a composite of alternate layers of nickel foil and Fiberfrax.

13.2.3 Pyrotechnics

The components of the pyrotechnic system and their locations are shown in figure 13.2-9. The two independent systems, A and B, were mutually redundant. Each system consisted of the following:

- a. Four explosive bolts and four explosive nuts to separate the ascent from the descent stage
- b. Three circuit interrupters for deadfacing electrical circuits prior to staging
- c. An umbilical guillotine for severing the ascent/descent stage umbilical
- d. Thirteen fully redundant pyrotechnic valves for pressurizing the ascent, descent, and reaction control propellants. The control power for the A system was from the Commander's bus and the B system was connected to System Engineer's bus. Firing power for the pyrotechnic devices was supplied by a separate pyrotechnic battery for each system.

13.2.4 Electrical Power

The electrical power system consisted of the following units:

- a. Four silver-zinc primary descent batteries (400 amp-hr, 28 V dc)
- b. Two silver-zinc primary ascent batteries (300 amp-hr, 28 V dc)
- c. Two descent electrical control assemblies
- d. Two ascent electrical control assemblies
- e. Relay junction box
- f. Deadface relay
- g. Control panel
- h. Two circuit breaker panels
- i. Two 115 V, 400 Hz inverters, 350 V-amps.

The basic ac power distribution system is shown in figure 13.2-10.
The basic dc power distribution system is shown in figure 13.2-11.

Descent batteries.- Four descent batteries supplied power to the LM dc buses. The initially high voltage characteristics of a fully charged battery required a tap at the output of 17 cells and a tap at the output of 20 cells to maintain the bus voltage within specification limits, depending on the discharge state of the batteries. Each LM-1 descent battery was pre-discharged 50 amp-hr in order to utilize the high voltage tap without the danger of excessive voltages.

Ascent batteries.- Two ascent batteries supplied power to the dc buses, after they were sequenced ON at staging.

Descent electrical control assembly.- The two descent electrical control assemblies provided electrical protection and control of descent batteries. A current-sensing system within the control assemblies would have automatically disconnected a descent battery in the event of an over-current between 200 and 2000 amperes. An indication of reverse current between 6 and 10 amperes also would have been provided by the current sensing devices through pulse code modulation data.

Control circuits within the electrical control assembly normally would provide a selection of either the 20-cell or 17-cell taps of each descent battery to the distribution system. For LM-1 both the high and

low voltage-select contacts were tied together and connected to only the high-voltage battery tap. Instrumentation for measuring battery current and voltages was included in the descent electrical control assemblies.

Ascent electrical control assembly.- Two ascent electrical control assemblies provided electrical protection and control of each ascent battery identical to those described for the descent electrical control assemblies. In addition, two contactors allowed selection of each battery to feed either or both of the dc buses. With the batteries selected in the normal position (see control assemblies 3 and 4 on figure 13.2-11) overcurrent protection would be provided. In figure 13.2-11, battery 5 is shown commanded to the backup position.

Relay junction box.- External/internal power control was located within the relay junction box. This junction box (in conjunction with the deadface relay) deadfaced the main power cables between the ascent and descent stages, as shown in figure 13.2-11.

The launch umbilical tower latching relay, which was controlled from the ground support equipment, connected ground power to the LM electrical loads when the lunar module batteries were not in use.

DC buses.- The two dc buses (Commander's and Systems Engineer's) were connected electrically by the crosstie wire system, through the crosstie circuit breakers (fig. 13.2-11). The five circuit breakers which were slugged, are as follows:

4CB17	}	Battery feed tie
4CB18		
4CB25		
4CB26		
4CB179		IM mission programmer

AC power.- The 400-Hz 117 V ac power was supplied from one of two solid-state inverters (fig. 13.2-10). Both inverters were supplied with dc power through the mission programmer from the Commander's bus.

13.2.5 Instrumentation

Operational instrumentation.- The operational instrumentation system (fig. 13.2-12) consisted of sensors, a signal conditioning electronics assembly, a caution and warning electronics assembly, and a pulse code modulation and timing electronics assembly.

Electrical output signals from some instrumentation sensors were conditioned to the proper voltage and impedance levels within the signal conditioning electronics assembly. Other signals which were preconditioned and were not processed by the signal conditioning electronics assembly, together with event information in the form of bi-level inputs, were routed to the pulse code modulation and timing electronics assembly. Signals from critical parameters were also routed to the logic elements of the caution and warning electronics assembly, which in turn controlled displays and warning lights.

The pulse code modulation and timing electronics assembly sampled the incoming analog and bi-level information according to a pre-programmed matrix. The individual sampling rates were determined by the frequency response of the parameter being measured and intelligence desired. The analog to digital converter translated the signal voltages into eight-bit words which gave a resolution of one part in 254. Bi-level inputs such as an "on" and an "off" event were converted to a bit state (one or zero) in the digital multiplexer section of the pulse code modulation and timing electronics assembly. Eight events can be represented in an eight-bit word.

Each frame contained 128 eight-bit words and 50 frames of pulse code modulation data were transmitted per second. Synchronization and timing signals to other spacecraft systems and a serial time code for mission elapsed time was also generated within the pulse code modulation and timing electronics assembly.

The words representing the converted analog signals, event functions, and time were stored in the output registers and were read-out serially into the bit stream. This bit stream modulated both S-band and VHF telemetry transmitters providing the measurement link to the ground stations.

The design of the LM-1 operational instrumentation was similar to the design of the system for the manned vehicles. If the caution and warning assembly monitoring the control engines sensed an electrically failed "on," the system would have automatically isolated propellants going to the failed control engine and a second control engine which obtained its propellants from the same propellant lines. On a manned vehicle, the caution and warning system would merely illuminate a light in the cabin and the flight crew would be required to take corrective action. The caution and warning system also provided discrete status information for failures within the control electronics system. The data storage electronics assembly (voice recorder) was not installed on LM-1.

Development flight instrumentation.— The development flight instrumentation supplemented the operational instrumentation in certain areas for validating systems design. The basic components and their operational

relationships are shown in figures 13.2-13, 13.2-14, and 13.2-15. A list of all measurements is contained in table 13.2-I.

Six development flight instrumentation measurements were commutated into the operational pulse code modulation system. Eight operational measurements were transmitted both by the FM/FM link and the operational pulse code modulation.

Three mission measurement periods existed: from lift-off to LM/S-IVB separation, from LM/S-IVB separation to ascent/descent stage separation, and from stage separation to end of mission. A different set of measurements was activated during these periods by means of automatic inflight switching.

The FM composite outputs from modulation packages were routed to 10-watt VHF FM transmitters as shown. A fifth VHF transmitter was used to transmit the operational pulse code modulation signals simultaneously with pulse code modulation signals on S-band. The RF transmitter outputs were routed to the UHF/VHF scimitar antenna (fig. 13.2-14). Launch phase measurement signals were transmitted through two scimitar antennas mounted on the adapter. At LM/S-IVB stage separation, the signals were switched to the LM-mounted scimitar antennas.

Two parallel C-band transponders allowed real-time measurements of vehicle azimuth, elevation, and slant range to be made by ground radar stations. A dual pulse-code interrogation signal (5690 MHz) from ground radar triggered a single-pulse reply (5765 MHz) from the 500-watt transponder. Each transponder drove two cavity-backed helix antennas through a power divider. The interrogation signal was also received by these antennas and was isolated from the transmitter by means of a ferromagnetic diplexer located within the transponder.

13.2.6 Communications

Radio frequency communications were provided between LM-1 and the Manned Space Flight Network by the LM communication system, the development flight instrumentation, and the UHF command receiver system.

The development flight instrumentation, described in section 13.2.5, consisted of instrumentation equipment, VHF transmission equipment, and C-band tracking equipment. This system provided prime tracking data and the flight qualification data required for lunar mission preparation.

The UHF command system received signals in a modulated serial digital format for ground control of selected systems. The receiver, or digital command assembly, was part of the lunar module mission programmer and is described in section 13.2.7.

The communications system included all S-band and signal processing equipment necessary to verify compatibility with the network stations with respect to tracking and ranging data, RF uplink (with simulated up-voice and up-data), and the transmission of PCM data.

Tracking and ranging.- The S-band transponder, providing a ranging and tracking backup to the C-band system, received coded pseudo-random-noise signals from the network stations in the selected phase-locked-loop receiver. These signals were routed to the selected pulse modulation transmitter for in-phase-coherence retransmission back to the stations. The retransmitted signal received by the stations was compared with the originally transmitted signal, and range was determined by the time required for the signal to travel from the stations to the lunar module and return. Once the range had been established accurately by the pseudo-random-noise code, the code was discontinued and the range was updated continually by a technique employing the Doppler frequency shift caused by lunar module velocity rates. The phase-locked-loop in the lunar module receiver insured the accuracy of the Doppler tracking signal by comparing the phase of the received signal with the phase of a local oscillator and then altering the local oscillator frequency to bring it in phase with the received signal.

RF uplinks.- The S-band up-voice function was simulated by modulating the 30-kHz subcarrier with a 1-kHz tone. The uplink data function, planned for use on LM-4 and subsequent vehicles, was simulated by an unmodulated 70-kHz subcarrier. The uplink signals were transmitted by the network stations to the lunar module, turned around in the ranging channel, and modulated onto the downlink S-band carrier transmitted from the lunar module to the station.

Pulse code modulation data.- Operational pulse code modulation telemetry data were transmitted to the network stations through both the S-band and development flight instrumentation communications, with the development flight instrumentation being the prime mode (see section 13.2.5).

Major component functional description.- The following communications equipment is shown in figure 13.2-16:

- a. RF electronic equipment (S-band transponder and power amplifier)
- b. Signal processing equipment
- c. Antenna equipment.

The S-band transponder assembly consisted of two identical phase-locked receivers, two phase modulators with drivers and multiplier chains, and a frequency modulator. The nominal power output was 0.75 watt. The

operating frequencies of the S-band equipment were 2282.5 MHz (transmit) and 2101.8 MHz (receive). A power amplifier increased the S-band transmitted output to 14.8 watts. The amplifier consisted of a primary and secondary amplifitron with associated power supplies and an input and an output isolator.

The circuit breaker for the primary power amplifier power supply remained open during the LM-1 mission. This provided a low-power primary mode and a high-power secondary mode. During the portion of the mission when the primary mode was selected, the power amplifier was used in the feed-through mode, resulting in an insertion loss of 3.2 dB, maximum. When the secondary system was selected, 28 V dc was supplied to the secondary power supply. The transmitter output was supplied to the power amplifier input and was amplified through the secondary power amplifier. The diplexer, connected directly to the output of the power amplifier, permitted duplex transmission and reception using one antenna.

Signal processor assembly: The signal processor assembly was the common acquisition and distribution point for all data received and transmitted by the communications system. The signal processor assembly consisted of an audio center at each flight crew member position and a pre-modulation processor. The premodulation processor accepted pulse code modulation data and timing from the instrumentation system and provided proper signal modulation, mixing, and switching to insure signal processing in accordance with the selected mode of operation.

The data were routed to a bi-phase-modulator where the phase of the telemetry subcarrier frequency was controlled. Each logic-level change of the pulse code modulation data changed the bi-phase-modulator output by 180 degrees. The bi-phase-modulator output was supplied to the mixing network where it was combined with other signals processed in the pre-modulation processor.

Two 512-kHz clock signals were provided by the instrumentation system to the communication system. The 1.024-MHz telemetry subcarrier was generated from a 512-kHz square wave (reference signal) from the PCM section of the pulse code modulation timing electronics assembly. This 512-kHz square wave was routed to a frequency doubler with a 1.024-MHz sine wave output, phase-referenced to the pulse code modulation non-return-to-zero data which modulated the 1.024-MHz subcarrier. The bi-phase-modulator output reflected the change in logic-level by a 180-degree change in subcarrier phase. The modulated subcarrier was routed through a 1.024-MHz band-pass filter to the mixing network.

Antenna equipment: The communications system antenna equipment consisted of two S-band inflight antennas, an S-band steerable antenna, and two VHF inflight antennas.

The S-band inflight antennas were omnidirectional, one located on the forward section and one located on the aft section of the LM. The antennas were right-hand circularly polarized radiators that collectively covered 90 percent of the sphere with a gain of -3 dB at the nominal S-band frequencies. The aft inflight antenna was used during the mission.

The S-band steerable antenna was a 26-inch diameter parabolic reflector with a point source feed consisting of a pair of cross-sleeved dipoles over a ground plane. This antenna was installed but not used for LM-1.

The VHF inflight antennas were not used on LM-1.

13.2.7 Guidance and Control

The guidance and control system provided attitude control, guidance, and navigation capabilities for the lunar module. The system consisted of the following:

- a. Primary guidance, navigation, and control system
- b. Stabilization and control system
- c. Lunar module mission programmer

Two means of spacecraft control were provided (fig. 13.2-17): a primary guidance and control path, which provided attitude control, and a backup path, which provided angular rate control. The primary path used the sensing and computing components of the primary guidance system with the control electronics section of the stabilization and control system and the mission programmer. The backup control path comprised the stabilization and control system and the mission programmer. The backup path was to be used in the event the mission could not be completed using the primary guidance system. The mission control capability of the backup path consisted of fixed sequences of system function commands pre-stored on tape.

Primary guidance, navigation, and control system.— The primary guidance system consisted of an inertial system and a computer. When used in conjunction with certain other systems, the primary guidance system could perform the following functions:

- a. Establish an inertial reference
- b. Provide prelaunch alignment of the inertial measurement unit by a computer-controlled gyrocompassing program

c. Provide a means of calculating position and velocity of the spacecraft

d. Generate and issue attitude control and thrust commands to maintain the spacecraft on a satisfactory trajectory.

The inertial system consisted of the following components:

- a. Inertial measurement unit
- b. Pulse torque assembly
- c. Electronic coupling data unit
- d. Power servo assembly

Three pulse-integrating pendulous accelerometers were mounted on the stable member along orthogonal axes. Prior to launch, the stable member was aligned in azimuth by means of a gyrocompassing routine and in a desired orientation with respect to launch accelerations. The stable member was fixed with respect to inertial space at launch. During the mission a change in the spacecraft position about the stable member was sensed by resolvers mounted on the gimbal axes. These angular measurements (gimbal angles) were transmitted to the guidance computer where they were compared with the desired spacecraft attitude. Attitude error signals generated by comparing actual attitude to desired attitude were transmitted to the attitude and translation control assembly for attitude corrections. The logic in this assembly determined attitude correction required by the control engines of the descent engine gimbal assembly as appropriate for the flight phase. Acceleration of the spacecraft was sensed by the accelerometers which supplied incremental velocity pulses to the computer.

The computer was used for primary guidance, navigation, and control system data processing and computations and performed the following major functions:

a. Calculated steering signals and generated engine on-off and throttling commands, descent engine gimbaling commands, and control engine jet commands to control spacecraft attitude and maintain a required trajectory

b. Positioned the stable member in the inertial measurement unit to a coordinate system defined by internal computer programs for launch and maintained this attitude reference during flight

c. Served as a primary guidance failure detection monitor and as a status and performance monitor for critical systems.

To accomplish these functions the computer accepted as major inputs:

- a. Inertial measurement unit gimbal angle increments from the electronic coupling data unit
- b. Velocity increments from the accelerometers
- c. Vehicle status from the control electronics system
- d. Real-time commands from the digital command assembly.

Stabilization and control system.-- The stabilization and control system consisted of the following assemblies of the control electronics section:

- a. Attitude and translation control assembly
- b. Descent engine control assembly
- c. Rate gyro assembly
- d. Gimbal drive actuators

The control electronics section was designed to use the 16 reaction control engines to control the vehicle about all vehicle axes. The control electronics section could operate in both the primary guidance control path and the backup control path. When operating in the primary guidance path, the control electronics logic implemented the control signals originating from the guidance computer as follows:

- a. Converted control engine commands to the required electrical power to operate the control engine solenoid valves
- b. Converted on-off commands to the descent engine gimbal drive actuator to required electrical power
- c. Routed on-off commands to the descent engine
- d. Routed throttle commands to the descent engine.

The rate gyro assembly measured the spacecraft rates. When operating in the backup control path, the control electronics section provided rate damping for vehicle stabilization.

Mission programmer.- The mission programmer executed the functions normally performed by the flight crew and was composed of the following components:

- a. A program reader assembly which stored a contingency sequence of commands
- b. A digital command assembly that provided the uplink capability from the ground stations to the guidance computer, the program assembly, or certain relays in the program coupler assembly
- c. The program coupler assembly which provided the interface for commands from the guidance computer, program reader assembly, digital command assembly, and the lunar module systems
- d. A power distribution assembly that provided the 28 V power distribution and current protection for the mission programmer components.

The mission programmer provided the following capabilities:

- a. Open-loop sequencing of system functions upon command from the guidance computer or digital command assembly
- b. A sequence of commands to lunar module systems by the program reader assembly upon command from the digital command assembly.

The mission programmer had three modes of operation: primary, backup, and ground command. In the primary mode, the lunar module system functions were controlled by the guidance computer; in the backup mode, by the program reader assembly; and in the ground command mode, by digital commands from the ground network stations. The ground command capability could also be used during the primary mode of operation to provide the data inputs to the guidance computer to initiate system functions. The capability to select alternate sequences during the backup mode was also provided by the ground command capability.

13.2.8 Reaction Control

The reaction control system (fig. 13.2-18) was composed of two parallel, independent systems, A system and B system. Each system contained identical components with the associated valves and plumbing necessary to deliver and control the propellants to the control engines. Normally both systems were operated together. The arrangement of the engines was such that rotational control in all axes was provided when the systems were isolated.

All helium pressurization components, propellant tanks, main shut-off valves, and propellant-servicing quick-disconnect couplings were arranged into an independent module for each system. Sixteen identical engine assemblies, arranged in clusters of four, were mounted on four outriggers equally spaced around the ascent stage.

When a system was activated, squib-actuated isolation valves were opened and allowed high pressure helium from the helium tank to pressurize the propellant tanks. The A system and the B system each contained an oxidizer tank with 206-pound capacity, and a fuel tank with 103-pound capacity. The propellants used were nitrogen tetroxide (oxidizer) and Aerozine 50 (fuel).

Normally open solenoid propellant main valves, located just downstream of the propellant tanks in each system, were capable of isolating the tanks of either system in case of an upstream malfunction or depletion of propellants. These valves were operated in pairs (fuel and oxidizer) for each system by prime commands from the guidance computer, commands from the mission programmer, or real-time commands from the ground.

Normally closed solenoid valves, in a crossfeed arrangement, allowed the fuel and oxidizer manifolds of the A system to be interconnected with the respective manifolds of the B system. In addition, normally closed valves interconnected the respective fuel and oxidizer manifolds of the ascent propellant system with the reaction control system propellant manifolds. These valves normally would be opened to supply the ascent stage propellants to the reaction control manifolds during ascent engine firing. The control engine feed lines contained isolation valves which could isolate the propellants from a malfunctioning control engine.

The 100-pound thrust engines were radiation cooled. The cluster assembly and the cluster support struts were covered by a thermal shield to maintain passive temperature control for the propellant lines. Two redundant resistance wire heaters were attached to each engine to maintain engine temperatures within the safe operating range.

13.2.9 Descent Propulsion

The descent propulsion system (fig. 13.2-19) consisted of a liquid-propellant rocket engine, two fuel tanks, two oxidizer tanks, and the associated propellant pressurization and feed components. The engine was throttleable between thrust levels of 1050 and 10 500 pounds. The engine was mounted in the center compartment of the descent stage through a gimbal ring arrangement which allowed gimbaling within ± 6 degrees to provide trim in pitch and roll.

The propellant tanks were pressurized by helium stored supercritically in a cryogenic vessel. Squib valves isolated the supercritical helium supply until the initial engine start. After activation of the valves, the supercritical helium passed through the first loop of a two-pass fuel/helium heat exchanger located in the engine fuel feed line. The warmed helium was routed back through a heat exchanger inside the cryogenic vessel where heat was transferred to the supercritical helium remaining in the vessel, thereby maintaining the pressure. The helium was then routed through the second loop of the fuel/helium heat exchanger before passing to a regulator which reduced the pressure to a suitable level, approximately 235 psi, for introducing into the tanks.

A second squib valve was fired 1.3 seconds after engine start. This delay provided time for the fuel to circulate through the heat exchangers and prevent fuel freezing by establishing fuel flow prior to helium flow. A pressure relief valve in each helium supply line prevented tank over-pressurization; a burst disk upstream of each relief valve prevented helium leakage during normal operation. Each pair of oxidizer tanks and each pair of fuel tanks was manifolded into a common discharge line. Total propellant capacity was 17 800 pounds. The propellant tanks were interconnected by a double crossfeed piping arrangement (fig. 13.2-19) to maintain positive pressure balance across the helium and the propellant portions of the tanks. A capacitance-type quantity gaging system provided propellant quantity information during thrusting.

The descent engine (fig. 13.2-19) used hypergolic propellants consisting of a 50-50 fuel mixture of hydrazine (N_2H_4) and unsymmetrical dimethylhydrazine (UDMH), with nitrogen tetroxide (N_2O_4) as the oxidizer. Engine controls, mounted integral to the injector end, included a gimbal ring, a variable-area injector, flow control and shutoff valves, and a throttle actuator. The thrust chamber consisted of a composite ablative-cooled nozzle (area ratio 16:1) and a crushable radiation-cooled nozzle extension (area ratio 49:1). The ablative components were encased in a titanium shell and jacketed in a stainless-steel-foil/glass-wool-composite thermal blanket.

The fuel and oxidizer were piped directly into the flow control valves and then into a series-parallel ball valve assembly controlled by four actuators. After engine start had energized the solenoid operated pilot valves, fuel was introduced into the valve actuators and caused the ball valves to open, allowing propellant flow to the injector. For engine shutdown, the solenoid-operated pilot valves were de-energized, the spring-loaded actuators closed the ball valves, and residual fuel from the actuator cavities was vented overboard.

The mechanical throttling scheme utilized variable-area, cavitating-venturi, flow-control valves mechanically linked to a variable-area injector as shown in figure 13.2-19. This scheme permitted separation of the propellant flow control and propellant injection functions so that each could be optimized without compromising the other. Two separate flow-control valves metered the fuel and oxidizer simultaneously. The throttling was controlled by an electrical linear servo actuator powered by three redundant dc motors. Throttling between 10 and 60 percent was achieved through hydraulic decoupling; movement of the pintle would reduce the venturi exit pressure to the vapor pressure of the propellant, inducing cavitation. The valves then functioned as cavitating venturis, and downstream pressure fluctuations did not affect the flowrates.

The injector consisted of a faceplate and fuel manifold assembly with a coaxial feed tube and a movable metering sleeve. Oxidizer entered through the center tube and exited between a fixed pintle and the bottom edge of the sleeve. Fuel was introduced into an outer race, and the fuel aperture was an annular opening between the side contour and the injector face. As the metering sleeve moved, both propellant apertures changed in area and maintained close-to-optimum injection conditions at any thrust level.

13.2.10 Ascent Propulsion

The ascent propulsion system (fig. 13.2-20) consisted of a restartable pressure-fed liquid propellant rocket engine and a propellant and pressurization storage system. The ascent engine was fixed-mounted and developed a constant thrust of 3500 pounds. The engine used hypergolic propellants consisting of a 50-50 fuel mixture of hydrazine (N_2H_4) and unsymmetrical dimethylhydrazine (UDMH), with nitrogen tetroxide (N_2O_4) as the oxidizer. Figure 13.2-20 shows the primary engine components that controlled propellant flow to the engine which consisted of an injector, two trim orifices, four electromechanical flow control actuators, and eight propellant shutoff valves. The valve package assembly, similar to the descent, consisted of eight shutoff valves, which were series-parallel redundant, in both the fuel and oxidizer feed lines. Each fuel-oxidizer pair was simultaneously opened or closed on a common crankshaft by a hydraulic actuator that used fuel as the actuating medium.

The engine consisted of a structural shell with mounts and ablative material in the thrust chamber and in the nozzle extension for cooling. The ablative material for the combustion chamber and nozzle throat, to the region where the expansion ratio was 4.67, was a refrasil phenolic backed with an insulator of asbestos phenolic. The nozzle utilized asbestos phenolic for ablative material for the extension from the regions of expansion ratio of 4.6 to 45.6. The combustion chamber and nozzle extension were bonded together and wrapped with fiberglass for structural

support. The combustion chamber and throat were encased in an aluminum alloy casing, which served primarily as a mounting surface for engine components.

The injector assembly consisted of propellant inlet lines, a fuel torus manifold, an oxidizer manifold, and an injector orifice plate assembly. The injector assembly was a fixed orifice type with a baffle for damping any induced combustion disturbances. The injector assembly face was divided into three combustion zones: the primary, the barrier, and the baffle. The primary zone employed impinging triplets (two fuel and one oxidizer) which were spaced in concentric radial rings on the injector assembly face. The barrier zone utilized fuel-on-oxidizer impinging doublets, which operated off-ratio (fuel-rich) to provide a barrier of low-temperature gases near the ablative chamber wall. The baffle zone (1.25 inches downstream from the injector face) utilized impinging doublets (fuel-on-oxidizer) placed in radial position relative to the injector face.

There were two titanium storage tanks for the ascent engine, one for oxidizer and one for fuel. The tanks were spherical and had a combined capacity of approximately 5000 pounds of propellant. Each tank was equipped with a helium diffuser at the inlet to provide even pressurization at the helium/propellant interface. A series of vanes were arranged at the tank outlet of each tank. These devices allowed unrestricted propellant flow from the tank to the engine under normal pressurization but would not allow reverse flow of propellant from the outlet line back into the tank under zero g conditions or even at the maximum negative g-load expected. The propellant tanks did not have a quantity gaging system but did have low-level sensors to monitor propellant quantities when propellants were depleted to a level equivalent to approximately 10 seconds of burn time.

The outflow from each tank was divided into two paths. The main path passed through a trim orifice and a filter to the engine shutoff valve. The other path led to normally closed solenoid valves interconnecting the ascent and reaction control propellant systems. Opening these valves would permit the use of ascent propellants by the control engines.

The gaseous helium that was used for pressurization of the propellant feed system was stored in two tanks at approximately 3500 psi and ambient temperature. A normally closed squib valve in the line immediately downstream of each storage tank isolated the helium supply until the initial ascent engine start.

Each parallel helium flow path contained a filter to trap any debris resulting from squib valve actuation. After the filter, each helium flow path contained a normally open latching solenoid valve and two pressure regulators or reducers. The upstream regulators in each flow path were set to a slightly lower pressure than the downstream regulators, and the two series regulators in the primary flow path were set to a slightly lower pressure than their corresponding regulators in the redundant flow path. The pressure settings of the four regulators varied from 172 psi to 194 psi with the primary-path controlling regulator set at approximately 184 psi. In normal operation, the upstream regulator in the primary flow path was the controlling element. Downstream of the pressure reducers, the helium flow paths were manifolded together and then divided into two separate tank pressurization paths, each having a quadruple check valve.

13.2-11 Environmental Control

The function of the environmental control system was to provide active thermal control for the electrical/electronic components. The major components consisted of the ascent oxygen tanks, the primary coolant circuit with heat rejection from one sublimator, water supplied from the ascent water tanks, and a cabin pressure relief valve (fig. 13.2-22).

During prelaunch, two freon boilers maintained thermal control in the water/glycol (65 percent water, 35 percent glycol) circuit. In flight, cooling of the water/glycol was provided by the water sublimator. Three minutes after launch, the mission programmer commanded a solenoid valve open which initiated water flow to the sublimator. During normal flight operation, the glycol temperature from the sublimator should range from 32° to 45° F.

The design of the water pressure regulators and ascent oxygen tanks was modified from the manned configuration. During sublimator operation, water flowed from both ascent water tanks through the primary water pressure regulators to the sublimator. The redundant water pressure regulator could have been selected through the mission programmer. The two ascent oxygen tanks provided a reference of about 4.0 psia to the water pressure regulators.

The capability to select either of two glycol pumps had been deleted from the mission programmer, and to preclude loss of cooling in the event of a single glycol pump failure, both pumps were operating.

13-24

The lunar module cabin was at atmospheric pressure, or slightly above, prior to launch. During the launch phase, the cabin pressure relief valve opened and allowed cabin pressure to bleed to 5.6 psia (nominal). After the relief valve closed, the cabin pressure continued to decay as a function of cabin leak rate.

TABLE 13.2-I.- LX-1 INSTRUMENTATION PARAMETERS

(a) Operational Instrumentation.

Electrical power subsystem

GC0071V AC bus voltage, V rms
 GC0155F AC bus frequency, Hz
 GC0201V Battery 1 voltage, V dc
 GC0202V Battery 2 voltage, V dc
 GC0203V Battery 3 voltage, V dc
 GC0204V Battery 4 voltage, V dc
 GC0205V Battery 5 voltage, V dc
 GC0206V Battery 6 voltage, V dc
 GC0301V Commander's bus voltage, V dc
 GC0302V System Engineer's bus voltage, V dc
 GC1201C Battery 1 current, A
 GC1202C Battery 2 current, A
 GC1203C Battery 3 current, A
 GC1204C Battery 4 current, A
 GC1205C Battery 5 current, A
 GC1206C Battery 6 current, A
 GC4361X Battery 1 high tap, off/on
 GC4362X Battery 1 low tap, off/on
 GC4363X Battery 2 high tap, off/on
 GC4364X Battery 2 low tap, off/on
 GC4365X Battery 3 high tap, off/on
 GC4366X Battery 3 low tap, off/on
 GC4367X Battery 4 high tap, off/on
 GC4368X Battery 4 low tap, off/on
 GC4369X Battery 5, Commander's bus, off/on
 GC4371X Battery 5, System Engineer's bus, off/on
 GC4372X Battery 6, System Engineer's bus, off/on
 GC9961U Battery 1 malfunction
 GC9963J Battery 3 malfunction
 GC9964U Battery 4 malfunction
 GC9965U Battery 5 malfunction
 GC9966U Battery 6 malfunction

Environmental control system

GF2021P Primary glycol pump differential pressure, psid
 GF2041X Low glycol level
 GF3571P Cabin pressure, psia
 GF3582P Ascent oxygen tank 1 pressure, psia
 GF3583P Ascent oxygen tank 2 pressure, psia
 GF3591P Upper hatch relief valve pressure, psia
 GF4101P Primary water regulator differential pressure, psid
 GF4511T Primary water boiler water temperature, °F
 GF4541T Suit water boiler inlet temperature, °F
 GF4582Q Ascent water tank 1 quantity, %
 GF4583Q Ascent water tank 2 quantity, %
 GF9997U Glycol pump pressure, psia
 GF9998U Glycol temperature, °F

Guidance and navigation

GG0301X FGKCS downlink data
 GG1040V 130 V dc pulse torque reference, V dc
 GG1110V 2.5 V dc telemetry bias, V dc
 GG1201V IMU 28 V ac 800 Hz, V rms
 GG1331V Rate gyro 28 V supply 3.2 kHz, V rms
 GG1513X IMU standby/off
 GG1523X LGO operate
 GG2001V X PIPA output in phase, V rms
 GG2021V Y PIPA output in phase, V rms
 GG2041V Z PIPA output in phase, V rms
 GG2107V Inner gimbal servo error in phase, V rms
 GG2110C Inner gimbal torque motor current, A
 GG2112V Inner gimbal resolver output sine, V rms
 GG2113V Inner gimbal resolver output cosine, V rms
 GG2121V Inner gimbal 1X resolver sine expanded, V rms
 GG2137V Middle gimbal servo error in phase, V rms
 GG2140C Middle gimbal torque motor current, A
 GG2142V Middle gimbal resolver output sine, V rms
 GG2143V Middle gimbal resolver output cosine, V rms
 GG2151V Middle gimbal 1X resolver sine expanded, V rms
 GG2167V Outer gimbal servo error in phase, V rms
 GG2170C Outer gimbal torque motor current, A
 GG2172V Outer gimbal resolver output sine, V rms
 GG2173V Outer gimbal resolver output cosine, V rms
 GG2181V Outer gimbal 1X resolver sine expanded, V rms
 GG2219V Pitch attitude error, V rms
 GG2249V Yaw attitude error, V rms
 GG2279V Roll attitude error, V rms

Guidance and navigation - concluded

GG2300T PIPA temperature, °F
 GG2301T Rate gyro temperature, °F
 GG6020T PIPA calibration module temperature, °F
 GG9001X LGO warning
 GG9002X Inertial sensing system warning
 GG9003X FGKCS warning

Stabilization and control

GH1204X Throttle out of descent
 GH1214X RCS AUTO on command
 GH1217X RCS AUTO off command
 GH1230X APF arm command
 GH1240V X translation command, V dc
 GH1247V Yaw error command, V dc
 GH1248V Pitch error command, V dc
 GH1249V Roll error command, V dc
 GH1260X APF on
 GH1283X Abort stage commanded
 GH1286X Engine fire override
 GH1301X DPF on
 GH1311V Manual thrust command, V dc
 GH1313V Pitch GDA position, V rms
 GH1314V Roll GDA position, V rms
 GH1323X Pitch trim fail
 GH1330X Roll trim fail
 GH1331V Automatic thrust command, V dc
 GH1345X DPF arm (DECA output)
 GH1413V Jet driver 4 up output
 GH1419V Jet driver 4 down output
 GH1420V Jet driver 4 forward output
 GH1421V Jet driver 4 side output
 GH1422V Jet driver 3 up output
 GH1423V Jet driver 3 down output
 GH1424V Jet driver 3 aft output
 GH1425V Jet driver 3 side output
 GH1426V Jet driver 2 up output
 GH1427V Jet driver 2 down output
 GH1428V Jet driver 2 aft output
 GH1429V Jet driver 2 side output
 GH1430V Jet driver 1 up output
 GH1431V Jet driver 1 down output
 GH1432V Jet driver 1 forward output
 GH1433V Jet driver 1 side output
 GH1461V Rate gyro assembly yaw rate, V rms
 GH1462V Rate gyro assembly pitch rate, V rms
 GH1463V Rate gyro assembly roll rate, V rms
 GH1603X Deadband select
 GH1608X AUTO control mode
 GH1609X Attitude hold
 GH1621X AG3 select
 GH1896X Unbalanced couples

Instrumentation

GL0300C Frame synchronization and identification
 GL3302C Format identification
 GL0401V 95% calibration, V dc
 GL0402V 15% calibration, V dc
 GL0501W Mission elapsed time
 GL1026X Control electronics ac power failure
 GL1027X Control electronics dc power failure
 GL1054X Caution and warning power failure
 GL1221X DPF calibration on
 GL1222X LX/SLA separator

Ascent propulsion subsystem

GP0301P Helium tank 1 pressure, psia
 GP0302P Helium tank 2 pressure, psia
 GP0303P Helium regulator pressure, psia
 GP0201T Helium tank 1 temperature, °F
 GP0202T Helium tank 2 temperature, °F
 GP0318X Helium sol valve 1 closed
 GP0718T Fuel temperature, °F
 GP0908X Fuel low
 GP1218T Oxidizer temperature, °F
 GP1408X Oxidizer low
 GP1501P Fuel pressure, psia
 GP1503P Oxidizer, psia
 GP201CP Thrust chamber pressure, psia
 GP2997U Propellant valves delta position

Descent propulsion subsystem

GQ3301P Helium regulator pressure, psia
 GQ3305X Helium tank 1 closed
 GQ3301X Helium tank 2 opened

*Loading number formats are shown on page 13-29.

TABLE 13.2-I.- LM-1 INSTRUMENTATION PARAMETERS - Continued

(a) Operational Instrumentation - Concluded

Descent propulsion subsystem - concluded

GR3439F Helium pressure, psia
GR3603Q Fuel tank 1 quantity, %
GR3604Q Fuel tank 2 quantity, %
GR3611P Fuel pressure, psia
GR3718T Fuel tank 1 temperature, °F
GR3719T Fuel tank 2 temperature, °F
GR4103Q Oxidizer tank 1 quantity, %
GR4104Q Oxidizer tank 2 quantity, %
GR4111P Oxidizer pressure, psia
GR4218T Oxidizer tank 1 temperature, °F
GR4219T Oxidizer tank 2 temperature, °F
GR4455X Propellant low
GR4510P Thrust chamber pressure, psia
GR4603R Variable injector actuator position, %
GR4746U Propellant valves delta position
GR4749U Propellant valves delta position

*1002069-15H+007
1028005-15H+109
1027037-15H+106
1024069-15H+095
1002005-15H
1031037-15H
1043037-15H+170
1035037-15H+138
1005101-15H+020
1001101-15H
1009101-15H
1038096C15E
1020101-15H+080
1050037-15H+196
1038098C15E
1038098C15E

Reaction control subsystem

GR1085Q System A propellant quantity, %
GR1090T System A helium tank surface temperature, °F
GR1095Q System B propellant quantity, %
GR1099T System B helium tank surface temperature, °F
GR1101P System A helium pressure, psia
GR1107T System B helium pressure, psia
GR1201P System A regulator pressure, psia
GR1207P System B regulator pressure, psia
GR2124U System A fuel temperature, °F
GR2125T System B fuel temperature, °F
GR2201P System A fuel manifold pressure, psia
GR2202P System B fuel manifold pressure, psia
GR3201P System A oxidizer manifold pressure, psia
GR3202P System B oxidizer manifold pressure, psia
GR6001T Quad 4 temperature, °F
GR6002T Quad 3 temperature, °F

*1039101-15H
1035069-15H+139
1031101-15H
1040069-15H+159
1033037-15H+130
1033005-15H+129
1030005-15H+117
1036069-15H+113
1018037-15H+070
1022037-15H+078
1004069-15H+015
1004101-15H+016
1006069-15H+023
1010101-15H+040
1003005-15H+009
1010005-15H+037

Reaction control subsystem - concluded

GR6003T Quad 2 temperature, °F
GR6004T Quad 1 temperature, °F
GR6009J RCS main A closed
GR6100J RCS main B closed
GR6111U Ascent feed A open
GR6121U Ascent feed B open
GR6123U Crossfeed open
GR6661U 4A isolation valve closed
GR6662U 4E isolation valve closed
GR6663U 3A isolation valve closed
GR6664U 3B isolation valve closed
GR6665U 2A isolation valve closed
GR6666U 2B isolation valve closed
GR6667U 1A isolation valve closed
GR6668U 1B isolation valve closed

*1022005-15H+095
1023005-15H+089
1013098F15E+122
1013098E15E+122
1013098D15E+122
1013098C15E+122
1013098B15E+122
1048098H15E
1048098G15E
1048098F15E
1048098E15E
1048098D15E
1048098C15E
1048098B15E
1048098A15E

Communications subsystem

GT0444X DCA uplink verify word
GT0619V UHF signal strength, dBm
GT0902B S-band state phrasing error, deg
GT0903E S-band transmitter RF power, W
GT0904V S-band receiver signal, V dc

*5101097-15D
1001037-15H
1101066-15H
1050101-15H+200
1101067-15H

Stabilization and control (LM-1)

GW5151V FRA compare
GW5153V FRA clock on

*6101088H15E
1103100H15E

Pyrotechnic subsystem

GY0303X Abort commands
GY0111X Emergency detection arm A on
GY0112X Emergency detection arm B on
GY0121X Staging relay A fire
GY0122X Staging relay B fire

*1014096E15E+123
1014096G15E+123
1014096F15E+123
1014096E15E+123
1014096D15E+123
1014096C15E+123

(b) Development Flight Instrumentation

Structures

GA00531 Z landing rig 1 temperature, °F
GA00534 Z landing rig 2 temperature, °F
GA00534 Z landing apex 1 temperature, °F
GA0201T Descent engine cavity temperature 1, °F
GA0202T Descent engine cavity temperature 2, °F
GA0203T Descent engine cavity temperature 3, °F
GA0204T Descent engine cavity temperature 4, °F
GA0601B Beam boost strut 1 +Z, klb
GA0602B Beam boost strut 2 +Z, klb
GA0603B Beam boost strut 3 +Z, klb
GA0604B Beam boost strut 4 +Z, klb
GA0605B Beam boost strut 1 -Z, klb
GA0606B Beam boost strut 2 -Z, klb
GA0607B Beam boost strut 3 -Z, klb
GA0608B Beam boost strut 4 -Z, klb
GA0609B Beam boost strut 1 +Y, klb
GA0610B Beam boost strut 2 +Y, klb
GA0611B Beam boost strut 3 +Y, klb
GA0612B Beam boost strut 4 +Y, klb
GA0613B Beam boost strut 1 -Y, klb
GA0614B Beam boost strut 2 -Y, klb
GA0615B Beam boost strut 3 -Y, klb
GA0616B Beam boost strut 4 -Y, klb
GA1113T Ascent stage heat shield top temperature, °F
GA1113F Ascent stage heat shield top pressure, psia
GA1501D Ascent engine support vibration 1, g
GA1502D Ascent engine support vibration 2, g
GA1503D Ascent engine support vibration 3, g
GA1571E APS oxygen tank vibration X, g
GA1572E APS oxygen tank vibration Y, g
GA1573D APS oxygen tank vibration Z, g
GA2001T Descent stage heat shield temperature 1, °F
GA2002T Descent stage heat shield temperature 2, °F
GA2003T Descent stage heat shield temperature 3, °F
GA2004T Descent stage heat shield temperature 4, °F
GA2005T Descent stage heat shield temperature 5, °F

*D-EXX-05
C-14X-17
C-14X-14
C-14X-20
C-14X-21
C-14X-23
C-14X-24
C-05X/1
C-06X/1
C-09X/1
C-07X/1
C-05X/1
D-06X/1
D-07X/1
D-08X/1
D-09X/1
D-10X/1
C-05X/1
C-06X/1
C-07X/1
C-08X/1
C-09X/1
C-08X/1
C-14X-26
D-EXX-27
A-100-01
A-100-02
A-100-03
E-12X
C-11X-02
D-11X-02
C-14X-43
D-EXX-18
C-14X-30
D-EXX-79
C-14X-27

Structures - concluded

GA2006T Descent stage heat shield temperature 6, °F
GA2007T Descent stage heat shield temperature 7, °F
GA2008T Descent stage heat shield temperature 8, °F
GA2009T Descent stage heat shield temperature 9, °F
GA2010T Descent stage heat shield temperature 10, °F
GA2524S Descent engine support strut 4, klb
GA2681D DPS oxygen tank 1 vibration X, g
GA2682D DPS oxygen tank 1 vibration Y, g
GA2683D DPS oxygen tank 1 vibration Z, g
GA3001A X-axis acceleration 1, g
GA3002A X-axis acceleration 2, rad/sec/sec
GA3003A Y-axis acceleration 1, g
GA3004A Y-axis acceleration 2, rad/sec/sec
GA3005A Z-axis acceleration 1, g
GA3006A Z-axis acceleration 2, rad/sec/sec
GA3601D Aft equipment bay vibration X, g
GA3602D Aft equipment bay vibration Y, g
GA3603D Aft equipment bay vibration Z, g
GA3601D Tunnel equipment area vibration 1, g
GA3602D Tunnel equipment area vibration 2, g
GA3603D Tunnel equipment area vibration 3, g

*C-14X-33
C-14X-35
C-14X-36
C-14X-38
E-15X/1,2
E-11X
C-11X-03
C-11X-03
C-10X
C-15X
D-10X/2,3
D-15X
D-08X/2,3
E-14X
A-02C-01
A-02C-02
A-02C-03
A-03C-01
A-03C-02
A-03C-03

Thermodynamics

GB0201T Ascent engine cone temperature 1, °F
GB0203T Cabin tunnel temperature, °F
GB0204T Cabin skin temperature 1, °F
GB0205T Cabin skin temperature 2, °F
GB0301T Ascent stage bottom surface temperature 1, °F
GB0302T Ascent stage bottom surface temperature 2, °F
GB0303T Ascent stage bottom surface temperature 3, °F
GB0304T Ascent stage bottom surface temperature 4, °F
GB0305T Ascent stage bottom surface temperature 5, °F

*C-14X-44
C-14X-47
D-EXX-69
C-14X-50
D-EXX-19
D-EXX-21
D-EXX-23
D-EXX-25
D-EXX-26

*Loading number formats are shown on page 13-29.

TABLE 13.2-I.- LM-1 INSTRUMENTATION PARAMETERS - Continued

(b) Development Flight Instrumentation - Continued

Thermodynamics - continued

GB0306T	Ascent stage bottom surface temperature 6, °F	*D-EXX-28
GB0307T	Ascent stage bottom surface temperature 7, °F	D-EXX-30
GB0401T	Descent stage top surface temperature 1, °F	D-EXX-36
GB0402T	Descent stage top surface temperature 2, °F	D-EXX-34
GB0403T	Descent stage top surface temperature 3, °F	D-EXX-32
GB0521T	Descent stage blast deflector temperature 1, °F	D-EXX-40
GB0522T	Descent stage blast deflector temperature 2, °F	D-EXX-42
GB0601T	Ascent engine compartment temperature 1, °F	D-EXX-46
GB0602T	Ascent engine compartment temperature 2, °F	D-EXX-48
GB0603T	Ascent engine compartment temperature 3, °F	D-EXX-50
GB0621P	Ascent engine compartment pressure 1, psia	C-06X/2,3
GB0622P	Ascent engine compartment pressure 2, psia	C-04X
GB0623P	Ascent engine compartment pressure 3, psia	C-03X
GB0801P	Ascent stage bottom surface pressure 1, psia	E-06X/2,3
GB0802P	Ascent stage bottom surface pressure 2, psia	D-07X/2,3
GB0803P	Ascent stage bottom surface pressure 3, psia	D-02X
GB0804P	Ascent stage bottom surface pressure 4, psia	D-03X
GB0805P	Ascent stage bottom surface pressure 5, psia	E-03X
GB0806P	Ascent stage bottom surface pressure 6, psia	C-02X
GB0807P	Ascent stage bottom surface pressure 7, psia	C-05X/2,3
GB0808P	Ascent stage bottom surface pressure 8, psia	C-06X/2,3
GB0809P	Ascent stage bottom surface pressure 9, psia	C-07X/2,3
GB0811P	Ascent stage bottom surface pressure 11, psia	D-04X
GB0812P	Ascent stage bottom surface pressure 12, psia	D-05X/2,3
GB0813P	Ascent stage bottom surface pressure 13, psia	C-EXX-13345576
GB0814P	Ascent stage bottom surface pressure 14, psia	C-EXX-14355677
GB0815P	Ascent stage bottom surface pressure 15, psia	C-EXX-15365778
GB0816P	Ascent stage bottom surface pressure 16, psia	C-EXX-16375879
GB0817P	Ascent stage bottom surface pressure 17, psia	C-EXX-17385980
GB0818P	Ascent stage bottom surface pressure 18, psia	C-EXX-18396081
GB0901P	Descent stage top surface pressure 1, psia	C-EXX-19406182
GB0902P	Descent stage top surface pressure 2, psia	C-EXX-20416283
GB0903P	Descent stage top surface pressure 3, psia	C-EXX-21426384
GB0904P	Descent stage top surface pressure 4, psia	C-EXX-22436485
GB0905P	Descent stage top surface pressure 5, psia	C-EXX-23446586
GB0906P	Descent stage top surface pressure 6, psia	C-EXX-24456687
GB0907P	Descent stage top surface pressure 7, psia	C-EXX-25466788
GB0908P	Descent stage top surface pressure 8, psia	C-EXX-26476889
GB0909P	Descent stage top surface pressure 9, psia	C-EXX-27486990
GB0910P	Descent stage top surface pressure 10, psia	C-EXX-28497091
GB0911P	Descent stage top surface pressure 11, psia	C-EXX-29507192
GB0912P	Descent stage top surface pressure 12, psia	C-EXX-30517293
GB0913P	Descent stage top surface pressure 13, psia	C-EXX-31527394
GB0914P	Descent stage top surface pressure 14, psia	C-EXX-32537495
GB0915P	Descent stage top surface pressure 15, psia	C-EXX-33547596
GB0916P	Descent stage top surface pressure 16, psia	C-EXX-34557697
GB0917P	Descent stage top surface pressure 17, psia	C-EXX-35567798
GB0918P	Descent stage top surface pressure 18, psia	C-EXX-36577899
GB0919P	Descent stage top surface pressure 19, psia	C-EXX-37587900
GB0920P	Descent stage top surface pressure 20, psia	C-EXX-38598001
GB0921P	Descent stage top surface pressure 21, psia	C-EXX-39608102
GB0922P	Descent stage top surface pressure 22, psia	C-EXX-40618203
GB0923P	Descent stage top surface pressure 23, psia	C-EXX-41628304
GB0924P	Descent stage top surface pressure 24, psia	C-EXX-42638405
GB0925P	Descent stage top surface pressure 25, psia	C-EXX-43648506
GB0926P	Descent stage top surface pressure 26, psia	C-EXX-44658607
GB0927P	Descent stage top surface pressure 27, psia	C-EXX-45668708
GB0928P	Descent stage top surface pressure 28, psia	C-EXX-46678809
GB0929P	Descent stage top surface pressure 29, psia	C-EXX-47688910
GB0930P	Descent stage top surface pressure 30, psia	C-EXX-48699011
GB0931P	Descent stage top surface pressure 31, psia	C-EXX-49709112
GB0932P	Descent stage top surface pressure 32, psia	C-EXX-50719213
GB0933P	Descent stage top surface pressure 33, psia	C-EXX-51729314
GB0934P	Descent stage top surface pressure 34, psia	C-EXX-52739415
GB0935P	Descent stage top surface pressure 35, psia	C-EXX-53749516
GB0936P	Descent stage top surface pressure 36, psia	C-EXX-54759617
GB0937P	Descent stage top surface pressure 37, psia	C-EXX-55769718
GB0938P	Descent stage top surface pressure 38, psia	C-EXX-56779819
GB0939P	Descent stage top surface pressure 39, psia	C-EXX-57789920
GB0940P	Descent stage top surface pressure 40, psia	C-EXX-58790021
GB0941P	Descent stage top surface pressure 41, psia	C-EXX-59800122
GB0942P	Descent stage top surface pressure 42, psia	C-EXX-60810223
GB0943P	Descent stage top surface pressure 43, psia	C-EXX-61820324
GB0944P	Descent stage top surface pressure 44, psia	C-EXX-62830425
GB0945P	Descent stage top surface pressure 45, psia	C-EXX-63840526
GB0946P	Descent stage top surface pressure 46, psia	C-EXX-64850627
GB0947P	Descent stage top surface pressure 47, psia	C-EXX-65860728
GB0948P	Descent stage top surface pressure 48, psia	C-EXX-66870829
GB0949P	Descent stage top surface pressure 49, psia	C-EXX-67880930
GB0950P	Descent stage top surface pressure 50, psia	C-EXX-68891031
GB0951P	Descent stage top surface pressure 51, psia	C-EXX-69901132
GB0952P	Descent stage top surface pressure 52, psia	C-EXX-70911233
GB0953P	Descent stage top surface pressure 53, psia	C-EXX-71921334
GB0954P	Descent stage top surface pressure 54, psia	C-EXX-72931435
GB0955P	Descent stage top surface pressure 55, psia	C-EXX-73941536
GB0956P	Descent stage top surface pressure 56, psia	C-EXX-74951637
GB0957P	Descent stage top surface pressure 57, psia	C-EXX-75961738
GB0958P	Descent stage top surface pressure 58, psia	C-EXX-76971839
GB0959P	Descent stage top surface pressure 59, psia	C-EXX-77981940
GB0960P	Descent stage top surface pressure 60, psia	C-EXX-78992041
GB0961P	Descent stage top surface pressure 61, psia	C-EXX-79002142
GB0962P	Descent stage top surface pressure 62, psia	C-EXX-80012243
GB0963P	Descent stage top surface pressure 63, psia	C-EXX-81022344
GB0964P	Descent stage top surface pressure 64, psia	C-EXX-82032445
GB0965P	Descent stage top surface pressure 65, psia	C-EXX-83042546
GB0966P	Descent stage top surface pressure 66, psia	C-EXX-84052647
GB0967P	Descent stage top surface pressure 67, psia	C-EXX-85062748
GB0968P	Descent stage top surface pressure 68, psia	C-EXX-86072849
GB0969P	Descent stage top surface pressure 69, psia	C-EXX-87082950
GB0970P	Descent stage top surface pressure 70, psia	C-EXX-88093051
GB0971P	Descent stage top surface pressure 71, psia	C-EXX-89103152
GB0972P	Descent stage top surface pressure 72, psia	C-EXX-90113253
GB0973P	Descent stage top surface pressure 73, psia	C-EXX-91123354
GB0974P	Descent stage top surface pressure 74, psia	C-EXX-92133455
GB0975P	Descent stage top surface pressure 75, psia	C-EXX-93143556
GB0976P	Descent stage top surface pressure 76, psia	C-EXX-94153657
GB0977P	Descent stage top surface pressure 77, psia	C-EXX-95163758
GB0978P	Descent stage top surface pressure 78, psia	C-EXX-96173859
GB0979P	Descent stage top surface pressure 79, psia	C-EXX-97183960
GB0980P	Descent stage top surface pressure 80, psia	C-EXX-98194061
GB0981P	Descent stage top surface pressure 81, psia	C-EXX-99204162
GB0982P	Descent stage top surface pressure 82, psia	C-EXX-00214263
GB0983P	Descent stage top surface pressure 83, psia	C-EXX-01224364
GB0984P	Descent stage top surface pressure 84, psia	C-EXX-02234465
GB0985P	Descent stage top surface pressure 85, psia	C-EXX-03244566
GB0986P	Descent stage top surface pressure 86, psia	C-EXX-04254667
GB0987P	Descent stage top surface pressure 87, psia	C-EXX-05264768
GB0988P	Descent stage top surface pressure 88, psia	C-EXX-06274869
GB0989P	Descent stage top surface pressure 89, psia	C-EXX-07284970
GB0990P	Descent stage top surface pressure 90, psia	C-EXX-08295071
GB0991P	Descent stage top surface pressure 91, psia	C-EXX-09305172
GB0992P	Descent stage top surface pressure 92, psia	C-EXX-10315273
GB0993P	Descent stage top surface pressure 93, psia	C-EXX-11325374
GB0994P	Descent stage top surface pressure 94, psia	C-EXX-12335475
GB0995P	Descent stage top surface pressure 95, psia	C-EXX-13345576
GB0996P	Descent stage top surface pressure 96, psia	C-EXX-14355677
GB0997P	Descent stage top surface pressure 97, psia	C-EXX-15365778
GB0998P	Descent stage top surface pressure 98, psia	C-EXX-16375879
GB0999P	Descent stage top surface pressure 99, psia	C-EXX-17385980
GB1000P	Descent stage top surface pressure 100, psia	C-EXX-18396081

Thermodynamics - concluded

GB3035T	Aft equipment bay skin temperature, °F	*C-14X-25
GB3036T	Descent stage -2 panel skin temperature, °F	C-14X-66
GB3102H	Interstage separation distance monitor 1, ft	C-EXX-09305172
GB3103H	Interstage separation distance monitor 2, ft	C-EXX-10315273
GB3104H	Interstage separation distance monitor 3, ft	C-EXX-11325374
GB3105H	Interstage separation distance monitor 4, ft	C-EXX-12335475
GB3727T	Antenna support boom temperature 1, °F	C-14X-57
GB3728T	Steerable S-band antenna temperature 2, °F	D-EXX-87
GB3729T	Steerable S-band antenna temperature 3, °F	D-EXX-80
GB3730T	S-band omni antenna temperature, °F	C-14X-60
GB3733T	VHF inflight antenna temperature, °F	D-EXX-76
GB6001T	Electronics package cold plates temperature 1, °F	C-14X-63
GB6002T	Electronics package cold plates temperature 2, °F	D-EXX-82

Electrical power subsystem

GC3501T	Battery 1 temperature, °F	*C-14X-03
GC3502T	Battery 2 temperature, °F	C-14X-04
GC3503T	Battery 3 temperature, °F	C-14X-07
GC3504T	Battery 4 temperature, °F	C-14X-10
GC3505T	Battery 5 temperature, °F	C-14X-13
GC3506T	Battery 6 temperature, °F	C-14X-16

Environmental control subsystem

GF2521T	Primary water boiler glycol temperature, °F	*D-EXX-85
GF2621T	Cabin heat exchanger glycol inlet temperature, °F	C-14X-69
GF2721T	Regenerative heat exchanger glycol outlet temperature, °F	C-14X-73
GF2821T	Regenerative heat exchanger glycol inlet temperature, °F	C-14X-82
GF2921T	Cabin heat exchanger glycol outlet temperature, °F	D-EXX-52
GF4102P	Redundant water regulators (AR3) differential pressure, psid	E-EXX-71
GF4561T	Descent water tank outlet temperature, °F	C-14X-75
GF4562T	Ascent water tank 1 outlet temperature, °F	D-EXX-54
GF4563T	Ascent water tank 2 outlet temperature, °F	E-EXX-10
GF9996U	Glycol pump rate select, krpm	E-EXX-10

Guidance and navigation

GG1111V	DFI telemetry bias voltage, V dc	*E-EXX-07
GG2220V	Inner gimbal CDU fine error, V rms	C-EXX-27
GG2250V	Middle gimbal CDU fine error, V rms	C-EXX-29
GG2280V	Outer gimbal CDU fine error, V rms	E-EXX-09
GG2303X	IMU blower off/on	E-EXX-11
GG3311V	Radar shaft CDU fine, V rms	E-EXX-28
GG3321V	Radar trunnion CDU fine, V rms	E-EXX-87
GG6001D	Navigation base roll vibration, g	A-05C-01
GG6002D	Navigation base pitch vibration, g	A-05C-02
GG6003D	Navigation base yaw vibration, g	A-05C-03

Stabilization and control

GH1450V	Pitch trim error, V dc	*D-EXX-70
GH1452V	Roll trim error, V dc	D-EXX-71

Instrumentation

GI0236X	50-pps start signal	*C-14X-58
GI0237X	2-kpps bit synchronization signal	C-14X-59
GI0238X	50-pps stop signal	C-14X-61
GI0241Y	1200-pps synchronization signal	C-14X-46
GI0242Y	50-pps stop signal	C-14X-49
GI0251U	Timing electronics synchronization no-go/go	C-14X-62
GI0832X	LGC serial data to PCMTEA	C-14X-65

Guidance and navigation (radars)

GR7559D	Landing radar antenna vibration, g	*D-11X-01
GR7564T	Landing radar antenna temperature, °F	C-14X-55
GR7565T	Landing radar antenna temperature, °F	C-14X-56
GR7691D	Rendezvous radar antenna dish vibration, g	D-11X-01
GR7721T	Rendezvous radar antenna temperature 3, °F	D-EXX-75
GR7722T	Rendezvous radar antenna temperature 2, °F	C-14X-52

*Loading number formats are shown on page 13-29.

TABLE 13.2-I.- LM-1 INSTRUMENTATION PARAMETERS - Concluded

(b) Development Flight Instrumentation - Concluded

Ascent propulsion subsystem

3P0019F	Regulator 1 inlet pressure, psia	*E-1CX/3
3P0020F	Regulator 2 inlet pressure, psia	E-04X/3
3P0025F	Helium regulator pressure, psia	C-12X/3
3P0501F	Fuel tank ullage pressure, psia	E-EXX-72
3P0616F	Fuel tank/engine differential pressure, psia	E-EXX-24
GP1001F	Oxygen tank ullage pressure, psia	E-EXX-12
GP1004F	Oxygen relief valve pressure, psia	E-EXX-25
GP1116F	Oxygen tank/engine differential pressure, psia	E-EXX-26
GP1501F	Fuel pressure, psia	C-13X/3
GP1503F	Oxidizer pressure, psia	D-13X/3
GP2001F	Fuel injector pressure, psia	E-13X/3
GP2016F	Thrust chamber pressure, psia	E-16X/3
GP2701F	Thrust chamber wall temperature 1, °F	D-EXX-51
GP2702F	Thrust chamber wall temperature 2, °F	D-EXX-52
GP2703F	Thrust chamber wall temperature 3, °F	D-EXX-53
GP2704F	Thrust chamber wall temperature 4, °F	D-EXX-57
GP2706F	Injector surface temperature, °F	D-EXX-55
GP2801F	Thrust chamber vibration X, g	A-04C/3
GP2802F	Thrust chamber vibration Y, g rms	A-06C/3
GP2803F	Thrust chamber vibration Z, g rms	A-09C/3

Descent propulsion subsystem

GQ3009F	Regulator 1 inlet pressure, psia	*E-10X/1,2
GQ3010F	Regulator 2 inlet pressure, psia	E-04X/1,2
GQ3018F	Helium regulator pressure, psia	C-12X/1,2
GQ3451F	Helium temperature, °F	D-EXX-60
GQ3452F	Helium heat exchanger inlet temperature, °F	D-EXX-03
GQ3453F	Helium heat exchanger outlet temperature, °F	D-EXX-04
GQ3463F	Fuel heat exchanger outlet temperature, °F	E-EXX-06
GQ3476F	Helium tank temperature, °F	D-EXX-08
GQ3501F	Fuel tank 1 ullage pressure, psia	E-EXX-33
GQ3502F	Fuel relief valve pressure, psia	E-EXX-34
GQ3611F	Fuel pressure, psia	C-13X/1,2
GQ3666F	Fuel tank 2/engine differential pressure, psia	E-EXX-35
GQ3611F	Fuel temperature, °F	D-EXX-67
GQ4001F	Oxidizer tank 1 ullage pressure, psia	E-EXX-14
GQ4005F	Oxidizer relief valve inlet pressure, psia	E-EXX-41
GQ4111F	Oxidizer pressure, psia	D-13X/1,2
GQ4116F	Oxidizer tank 1/engine differential pressure, psia	E-EXX-36
GQ4311F	Oxidizer temperature, °F	D-EXX-66
GQ6501F	Fuel injector pressure, psia	E-13X/1,2
GQ6506F	Oxidizer injector pressure, psia	E-14X/1,2
GQ6510F	Thrust chamber pressure, psia	E-16X/1,2
GQ7206F	Injector surface temperature, °F	D-EXX-15
GQ7211F	Descent engine heat shield temperature 1, °F	D-EXX-63
GQ7212F	Descent engine heat shield temperature 2, °F	D-EXX-64
GQ7213F	Descent engine heat shield temperature 3, °F	D-EXX-65
GQ7214F	Descent engine heat shield temperature 4, °F	D-EXX-73
GQ7301F	Thrust chamber vibration X, g rms	A-04C/1,2
GQ7302F	Thrust chamber vibration Y, g rms	A-06C/1,2
GQ7303F	Thrust chamber vibration Z, g rms	A-09C/1,2

Reaction control subsystem

GR4322F	4B fuel injector surface temperature, °F	*C-14X-79
GR4323F	3A fuel injector surface temperature, °F	D-EXX-61
GR4325F	2B fuel injector surface temperature, °F	D-EXX-17
GR4327F	1A fuel injector surface temperature, °F	D-EXX-62
GR4424F	3B oxidizer injector surface temperature, °F	C-14X-72
GR4435F	33 oxidizer valve temperature, °F	C-14X-87
GR4441F	4D fuel injector surface temperature, °F	C-14X-73
GR4448F	1D fuel injector surface temperature, °F	C-14X-88
GR457CT	4D injector head temperature, °F	D-EXX-56
GR4571F	1F injector head temperature, °F	D-EXX-58
GR4577F	2U injector head temperature, °F	D-EXX-77
GR4578F	2D injector head temperature, °F	D-EXX-81
GR4582F	1D injector head temperature, °F	D-EXX-78
GR4583F	1F injector head temperature, °F	D-EXX-74
GR5012F	4B fuel inlet pressure, psia	C-EXX-66
GR5013F	3A fuel inlet pressure, psia	C-EXX-63
GR5014F	3B fuel inlet pressure, psia	E-EXX-29
GR5015F	2A fuel inlet pressure, psia	E-09X/2,3
GR5016F	2B fuel inlet pressure, psia	C-EXX-26
GR5017F	1A fuel inlet pressure, psia	C-EXX-28
GR5018F	1B fuel inlet pressure, psia	D-09X/2,3
GR5019F	4A oxidizer inlet pressure, psia	D-EXX-30
GR5020F	4B oxidizer inlet pressure, psia	D-EXX-31
GR5021F	3A oxidizer inlet pressure, psia	E-EXX-32
GR5022F	3B oxidizer inlet pressure, psia	C-EXX-46
GR5023F	2A oxidizer inlet pressure, psia	E-15X/3
GR5024F	2B oxidizer inlet pressure, psia	D-EXX-51
GR5025F	1A oxidizer inlet pressure, psia	E-34X-52
GR5026F	1B oxidizer inlet pressure, psia	C-09X/2,3
GR5031F	4C thrust chamber pressure, psia	A-06C
GR5032F	4D thrust chamber pressure, psia	A-06C
GR5033F	4F thrust chamber pressure, psia	D-16X/2,3
GR5034F	4S thrust chamber pressure, psia	E-06X/2,3
GR5035F	3C thrust chamber pressure, psia	A-01C
GR5036F	3D thrust chamber pressure, psia	A-01C
GR5037F	3F thrust chamber pressure, psia	D-16X/2,3
GR5038F	3S thrust chamber pressure, psia	E-07X/2,3
GR5039F	2C thrust chamber pressure, psia	D-12X
GR5040F	2D thrust chamber pressure, psia	D-12X
GR5041F	2F thrust chamber pressure, psia	C-16X/2,3
GR5042F	2S thrust chamber pressure, psia	E-07X/2,3
GR5043F	1J thrust chamber pressure, psia	A-07C
GR5044F	1D thrust chamber pressure, psia	A-07C
GR5045F	1F thrust chamber pressure, psia	C-16X/2,3
GR5046F	1S thrust chamber pressure, psia	E-06X/2,3

Communications

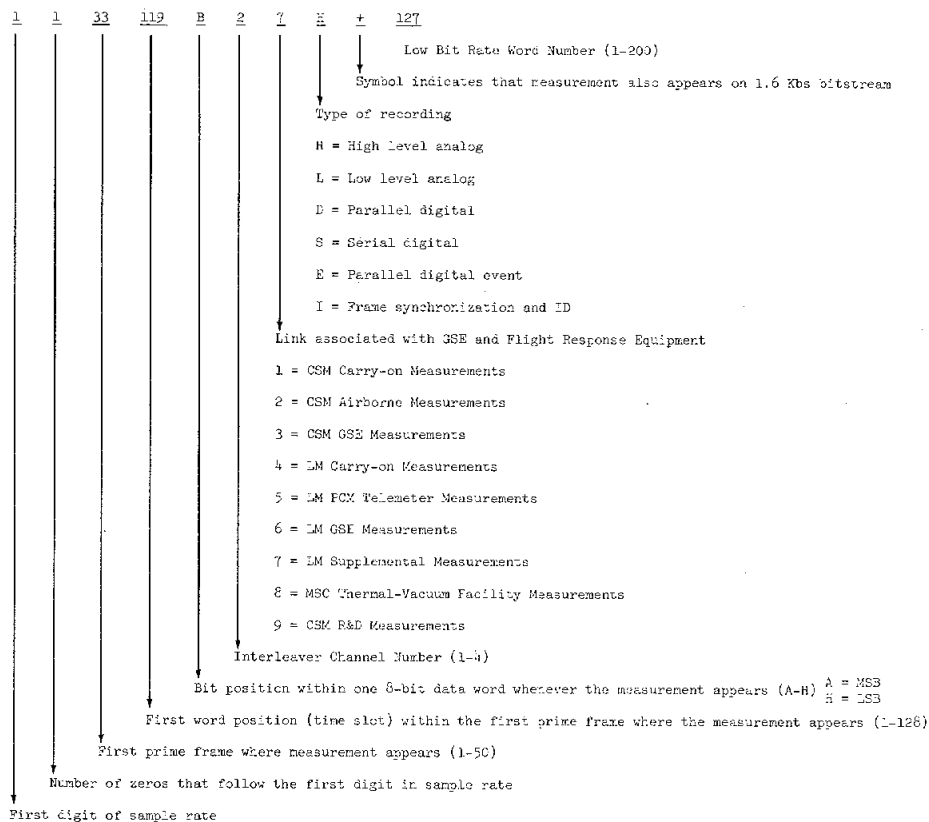
GT0224C	S-band power amplifier 1, mA	*E-EXX-34
GT0225C	S-band power amplifier 2, mA	E-EXX-33

*Loading number formats are shown on page 13-29.

LOADING NUMBER FORMATS

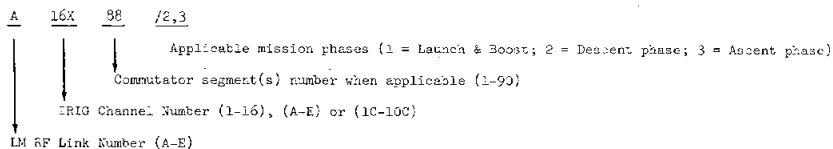
(a) Operational Instrumentation

Example: 1133119B27H+127



(b) Development Flight Instrumentation

Example: A-16X-88/2,3



NASA-S-68-2065

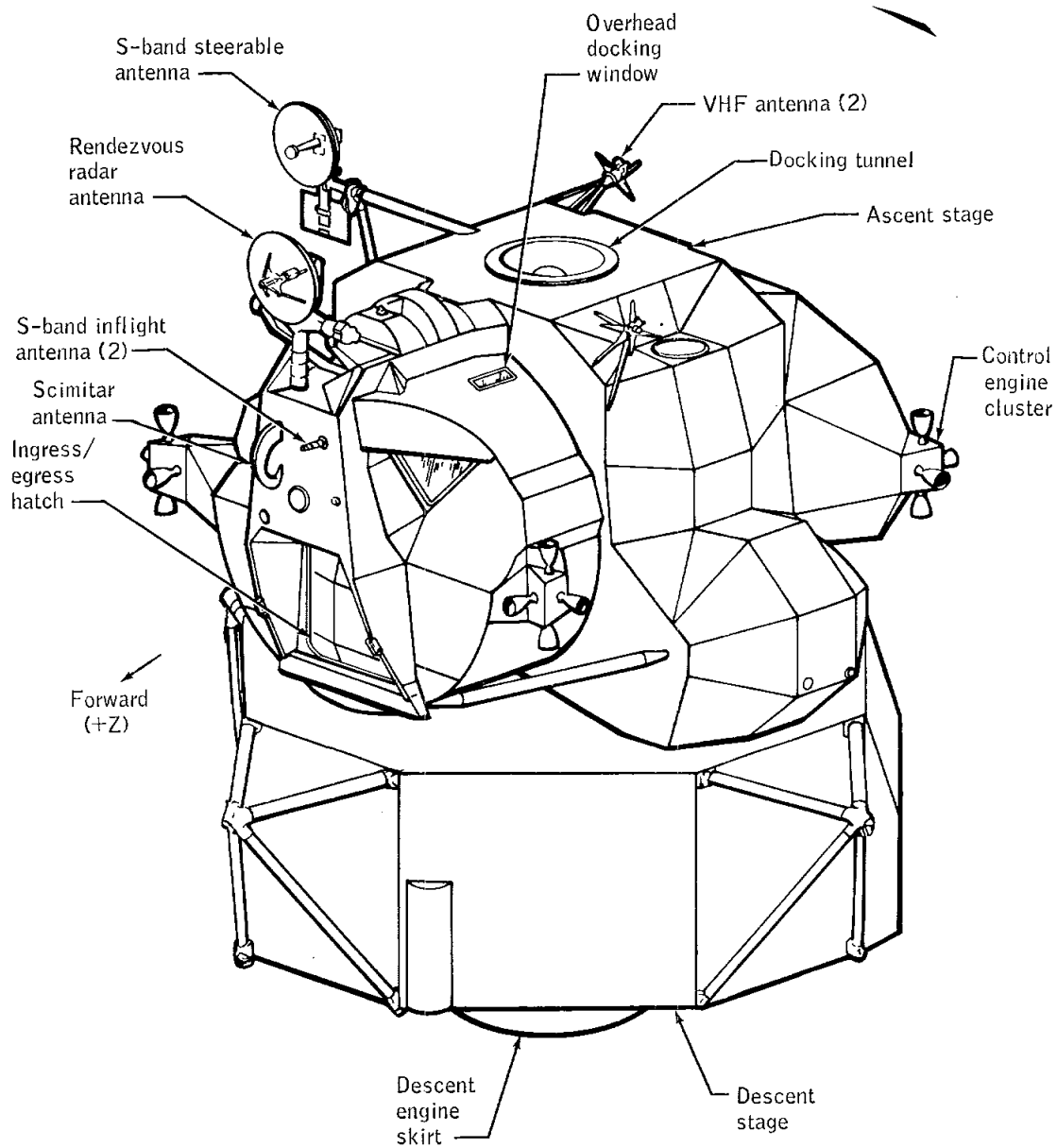


Figure 13.2-1.- Lunar module configuration.

NASA-S-68-2066

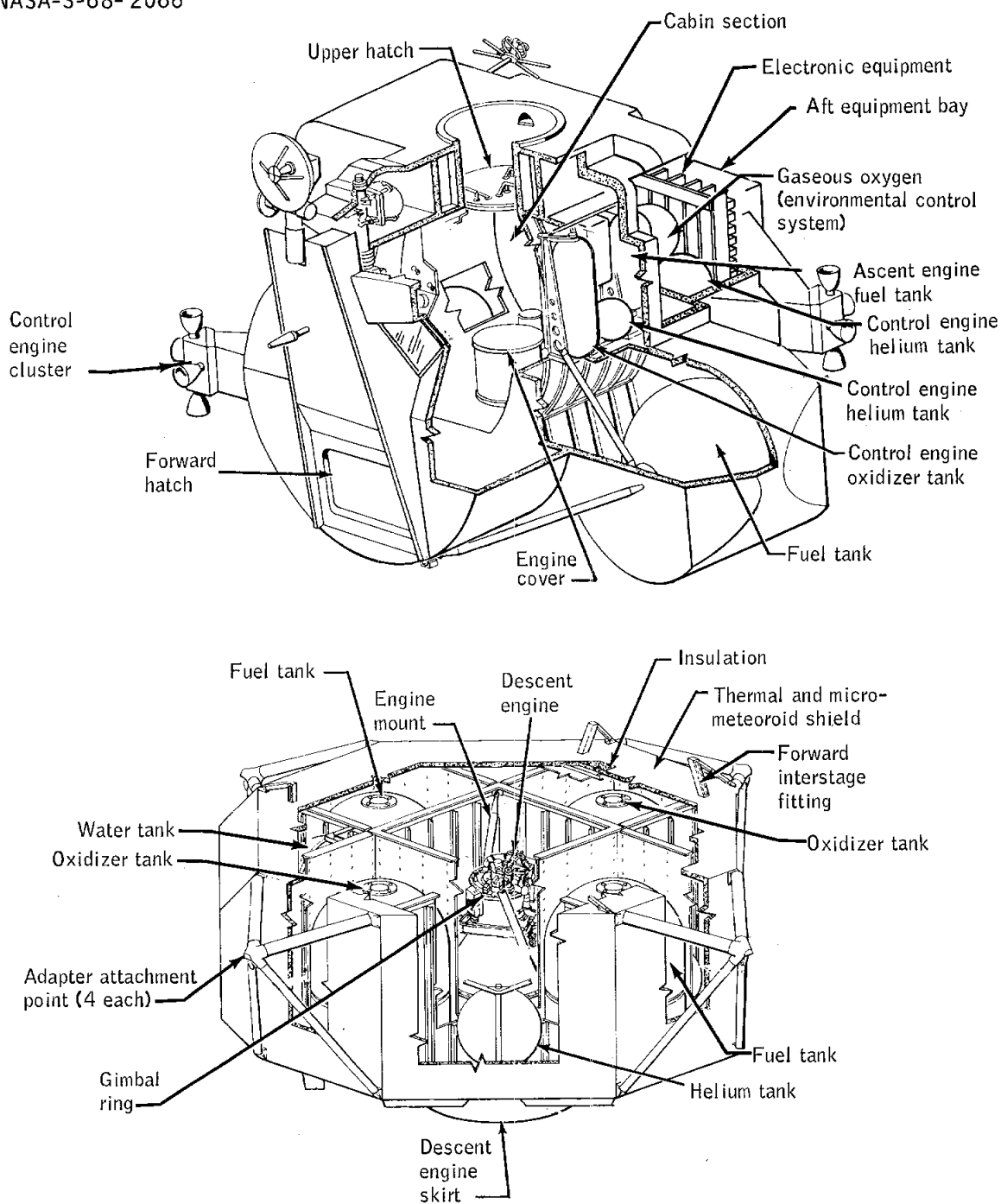


Figure 13.2-2.- Ascent and descent stages of LM-1.-

NASA-S-68- 2067

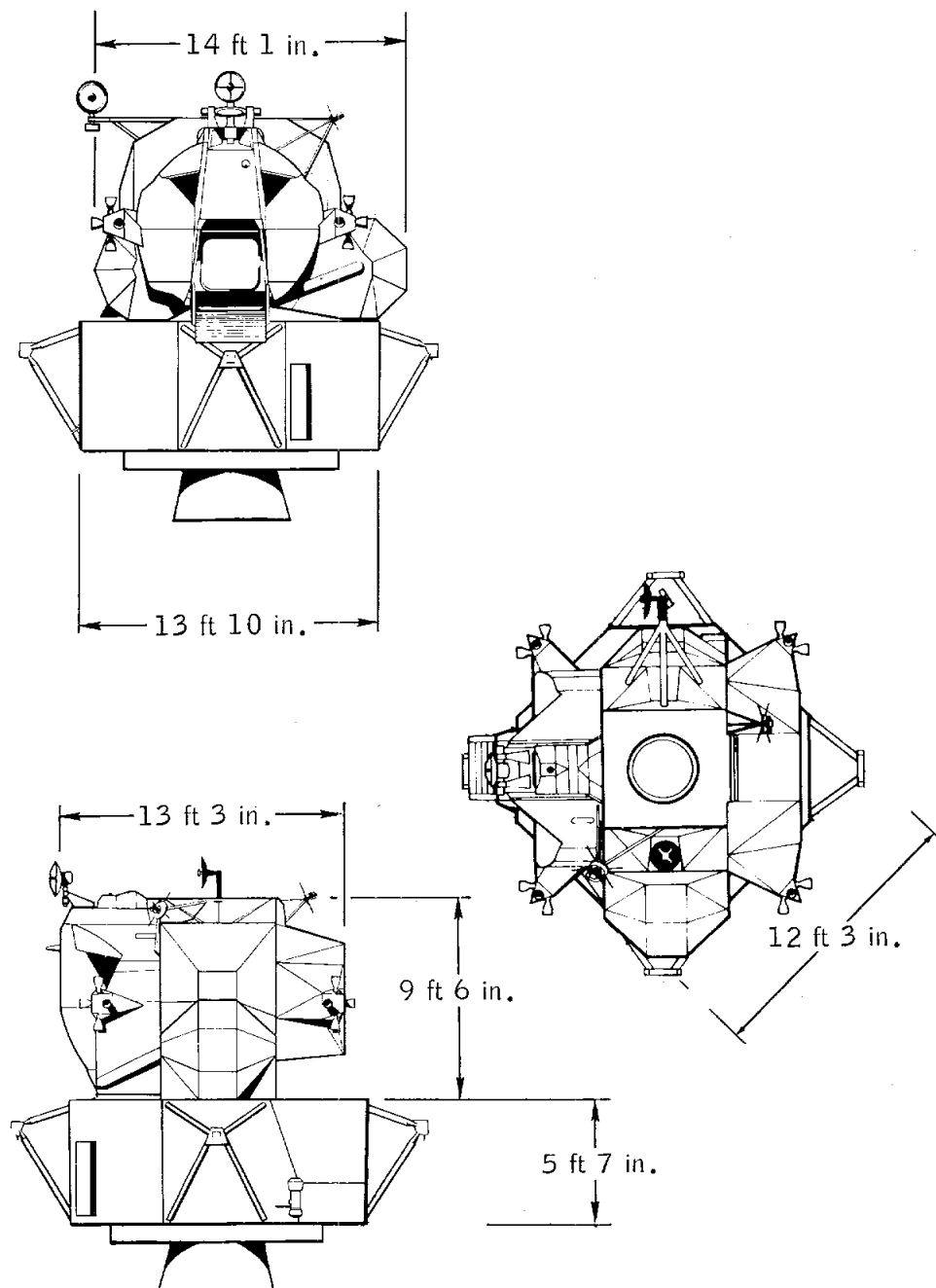


Figure 13.2-3.- Dimensions of lunar module.

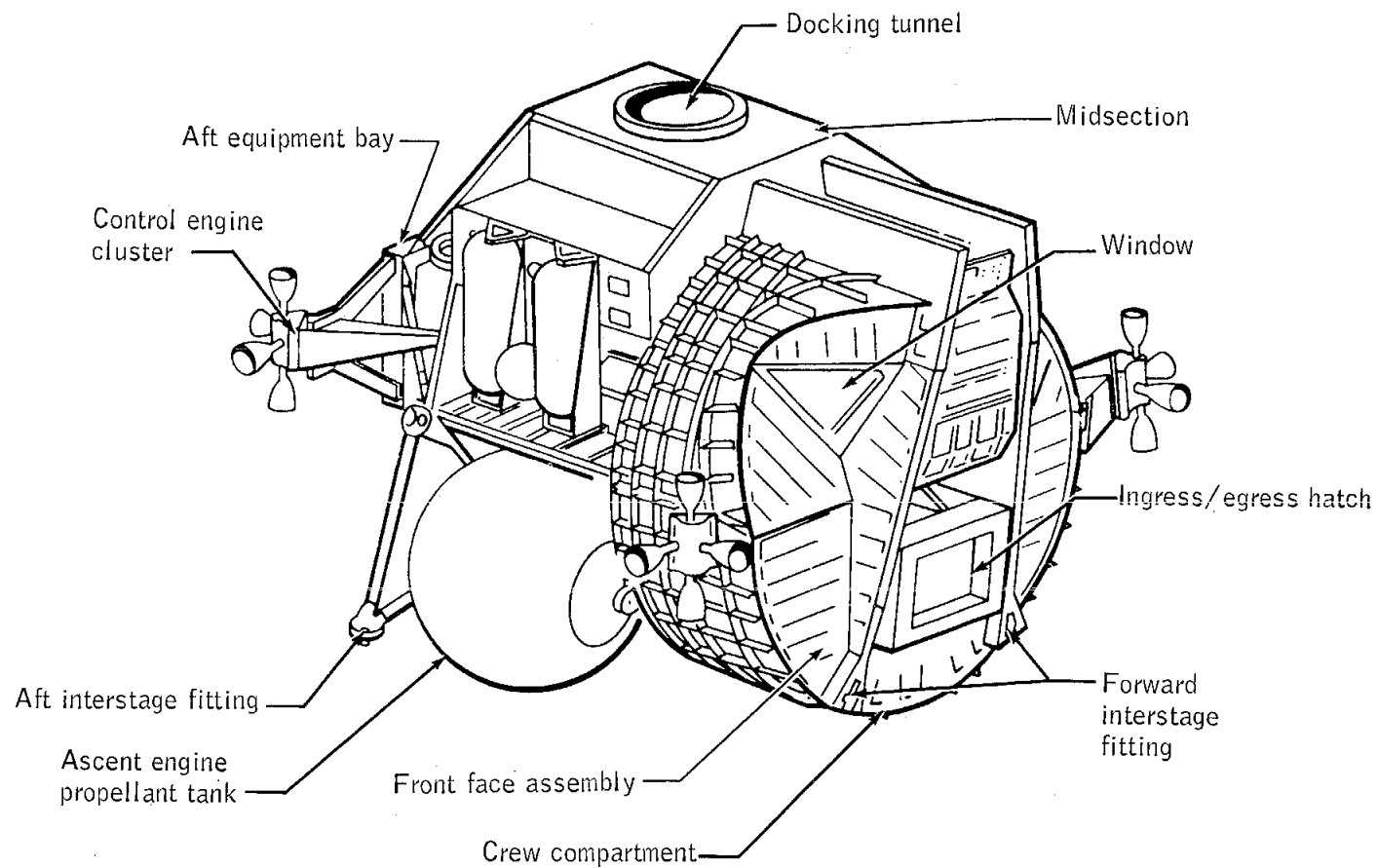


Figure 13.2-4.- LM ascent stage structure.

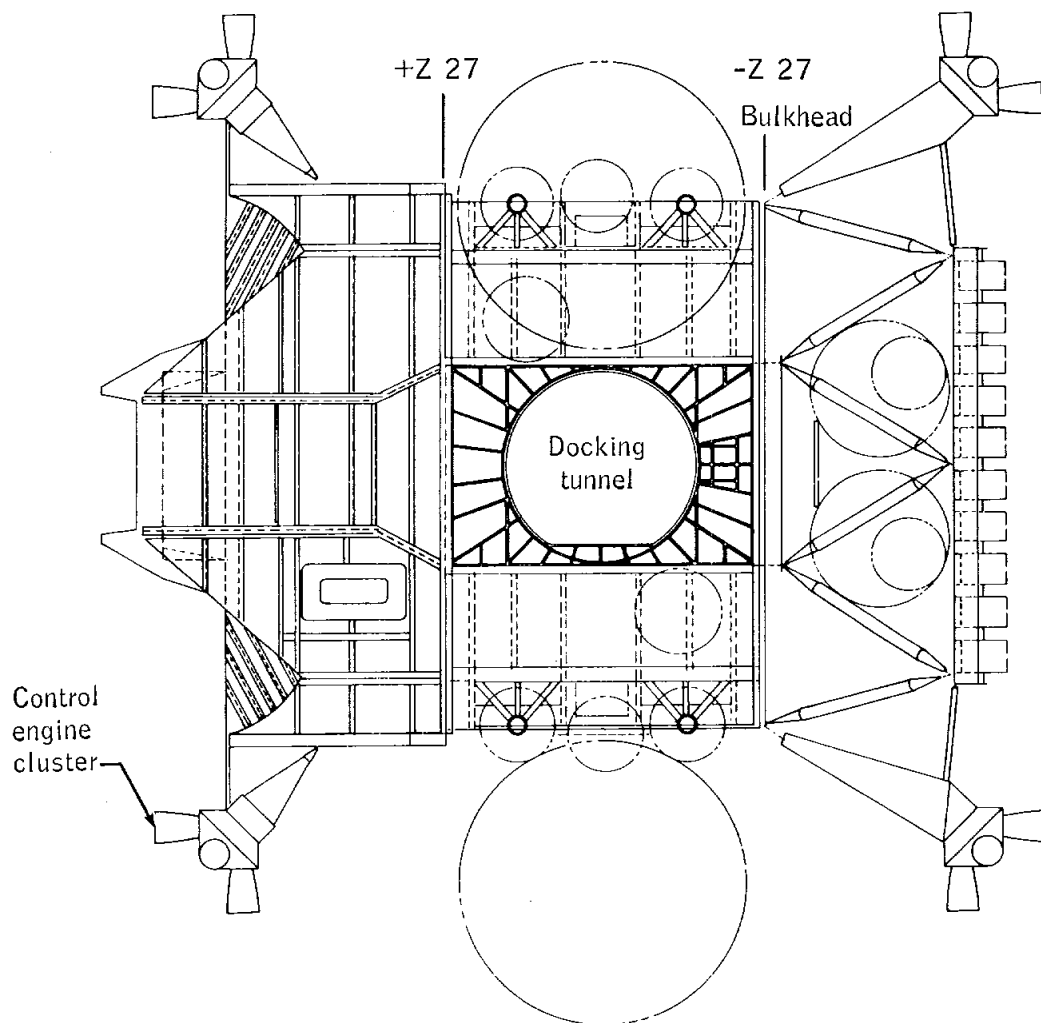


Figure 13.2-5.- LM ascent stage structure (top view).

NASA-S-68-2070

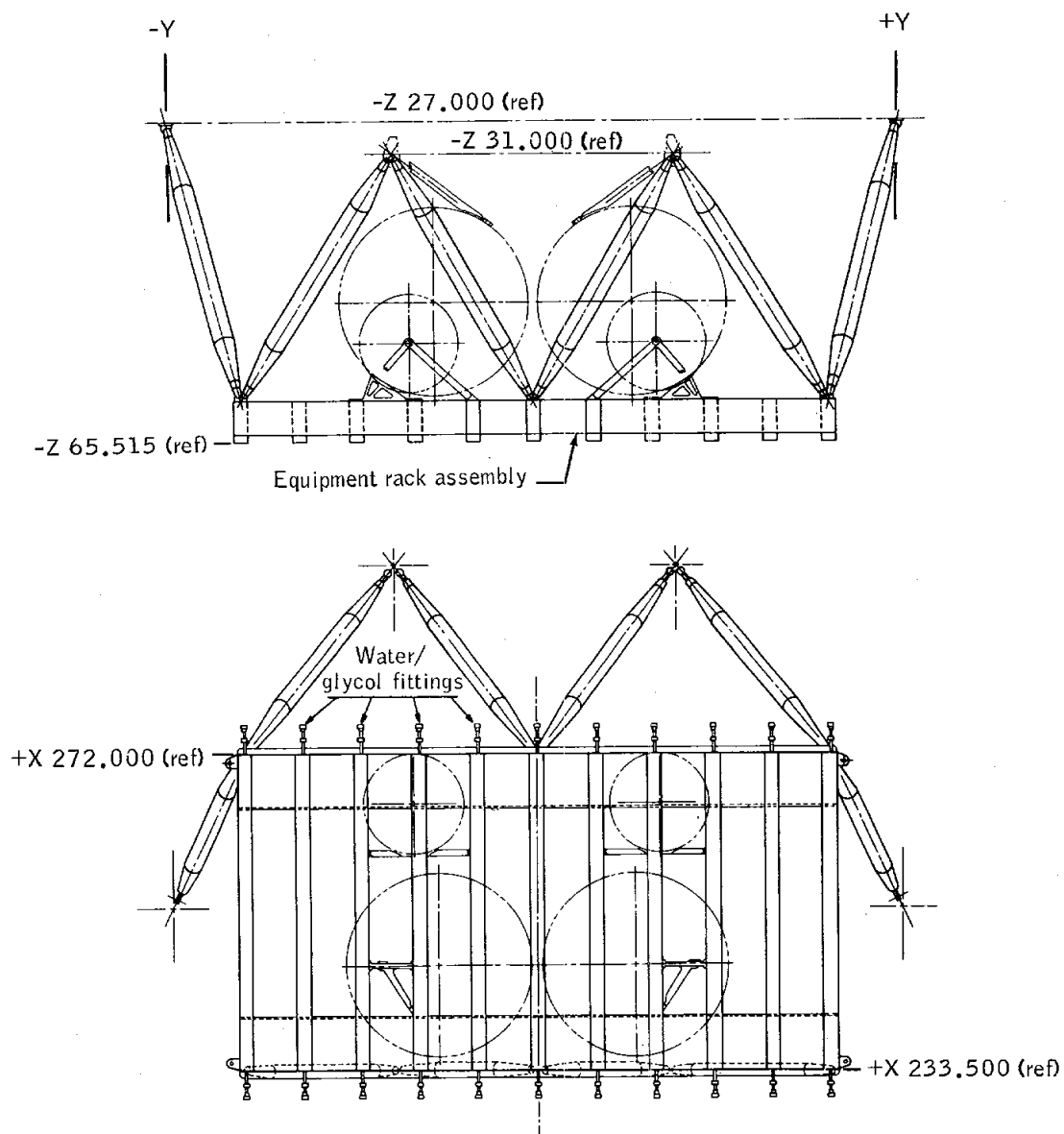


Figure 13.2-6.- Aft equipment bay structure.

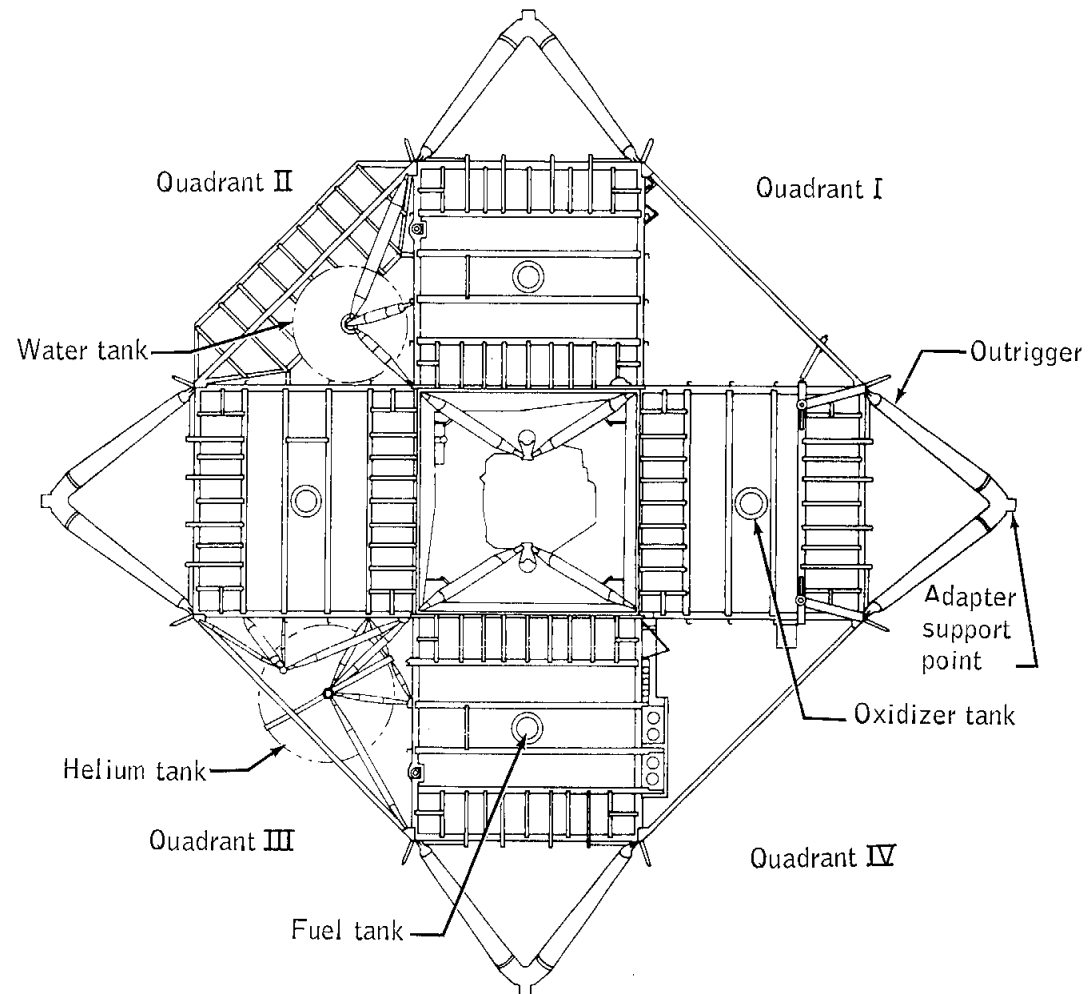


Figure 13.2-7.- Descent stage structure (top view).

NASA-S-68-2072

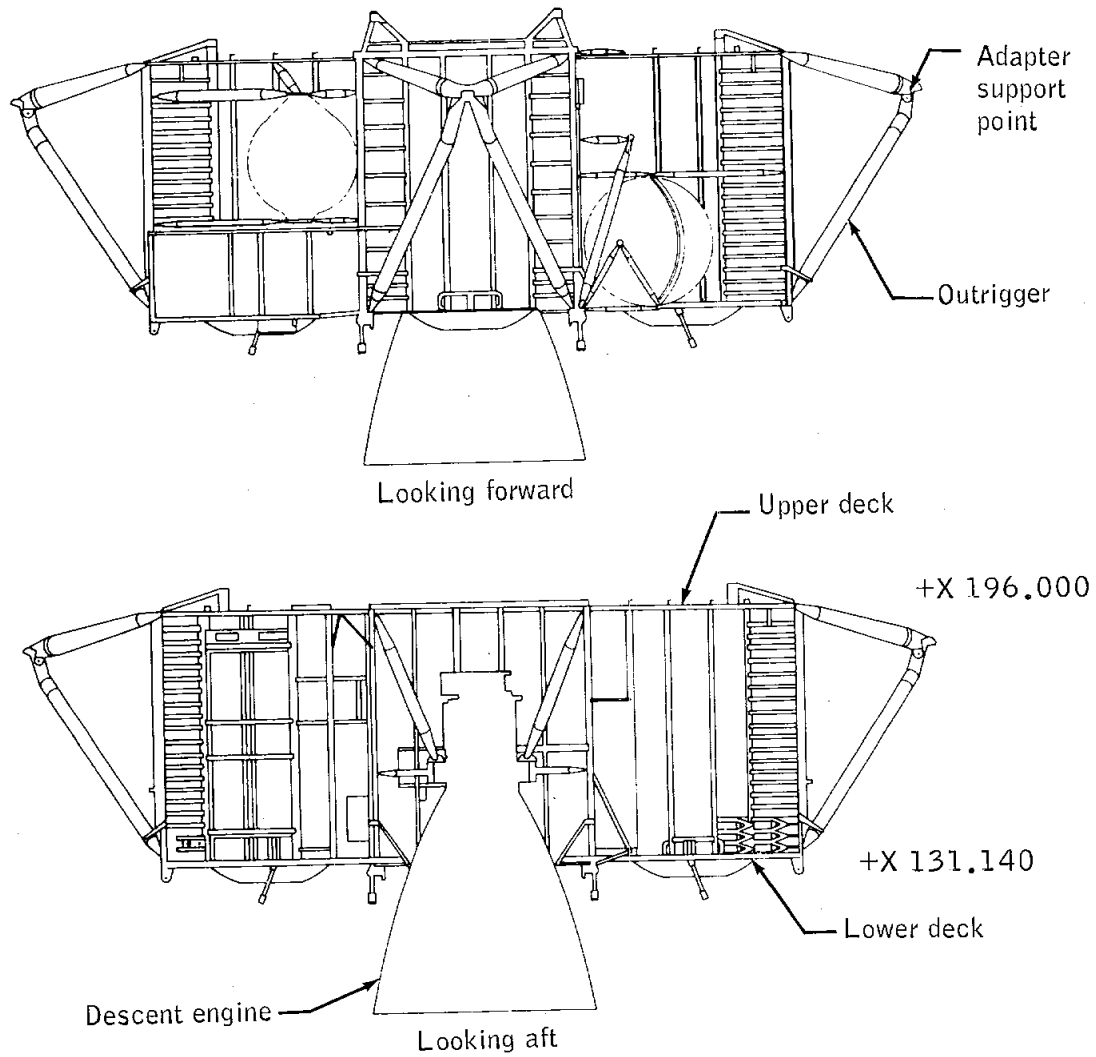


Figure 13.2-8.- Descent stage structure (side views).

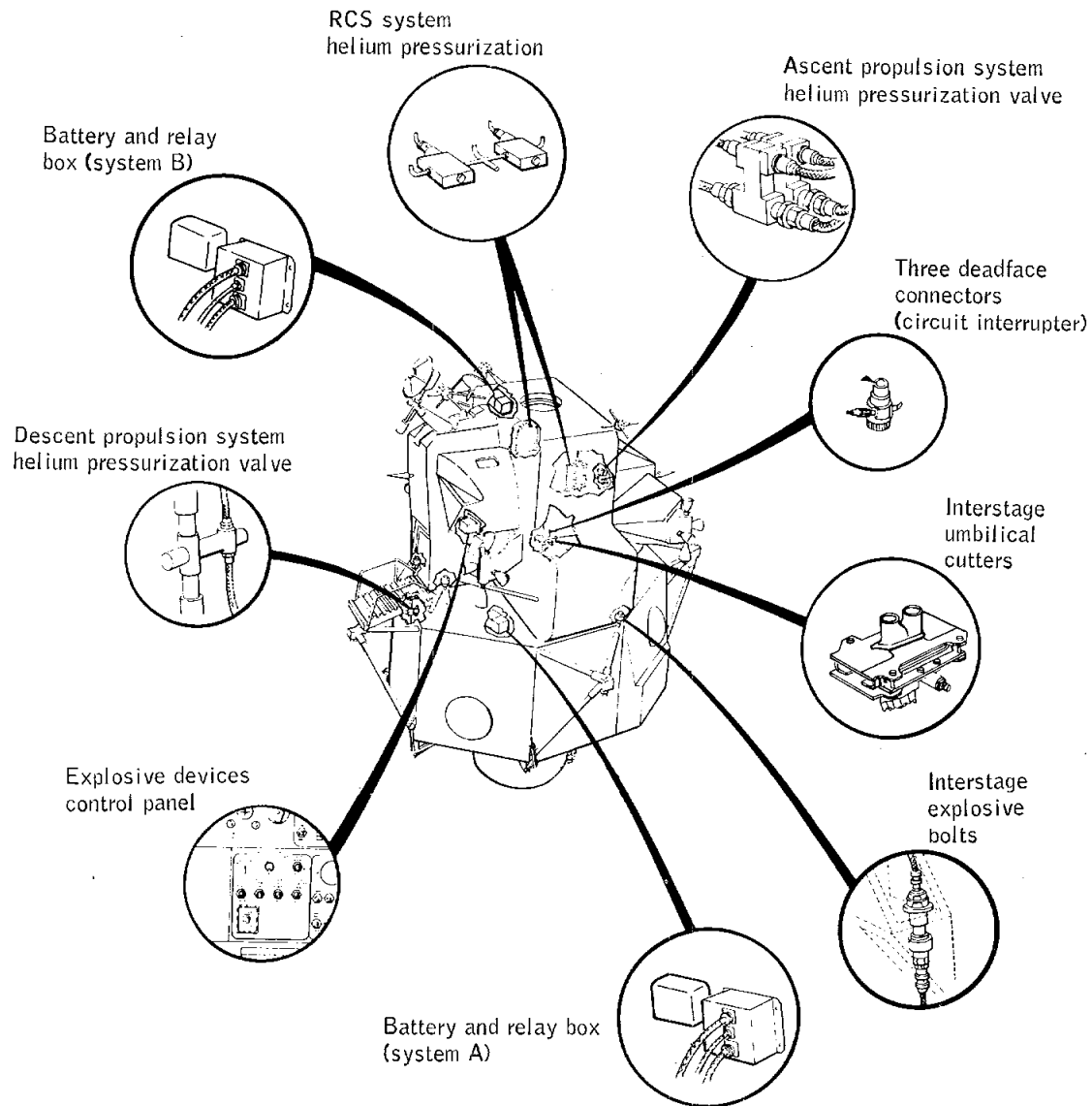


Figure 13.2-9.- Locations of explosive devices.

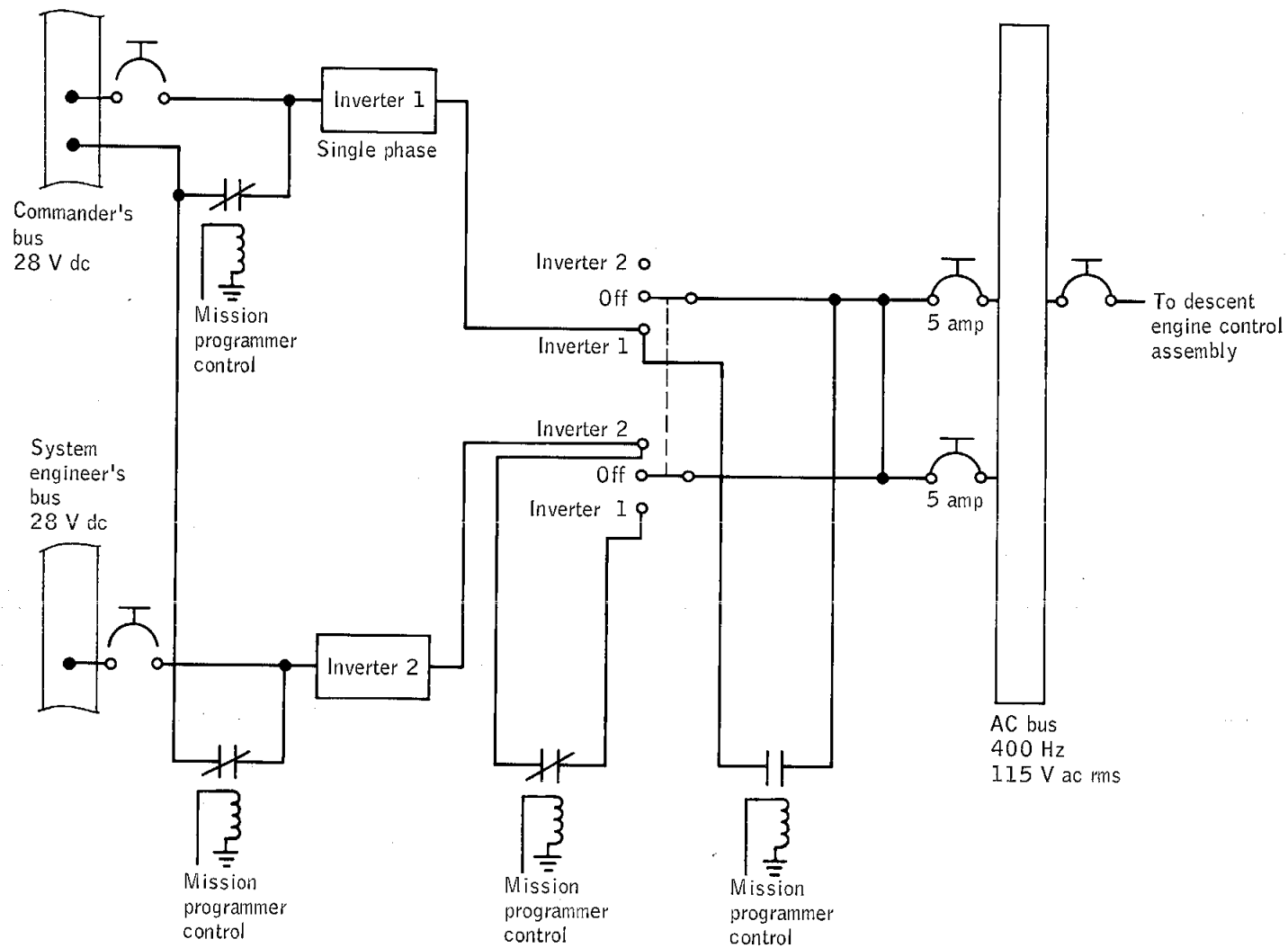


Figure 13.2-10.- AC power system (contact positions shown are as-flown).

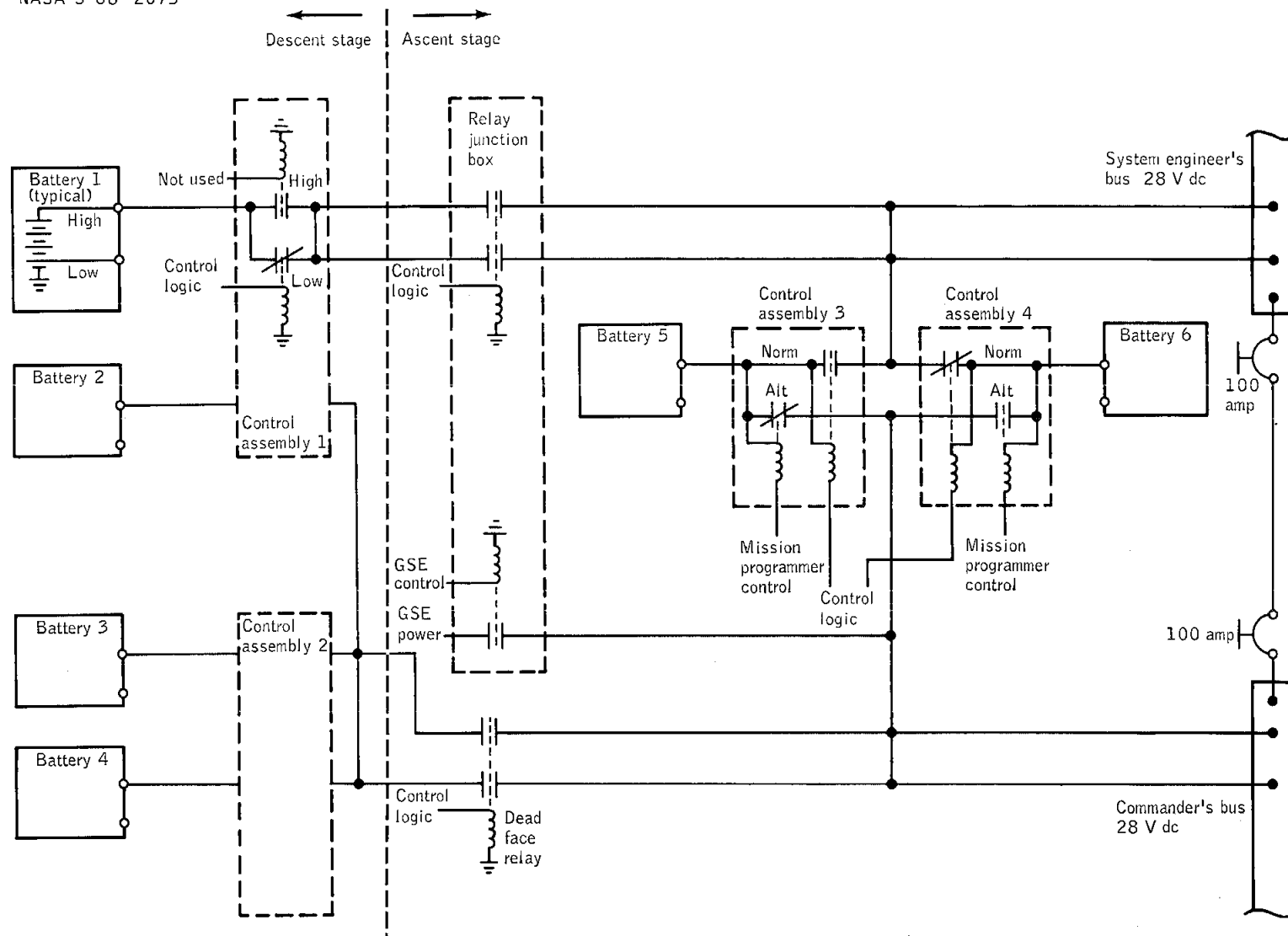


Figure 13.2-11.- DC power system (contacts shown in as-flown configuration).

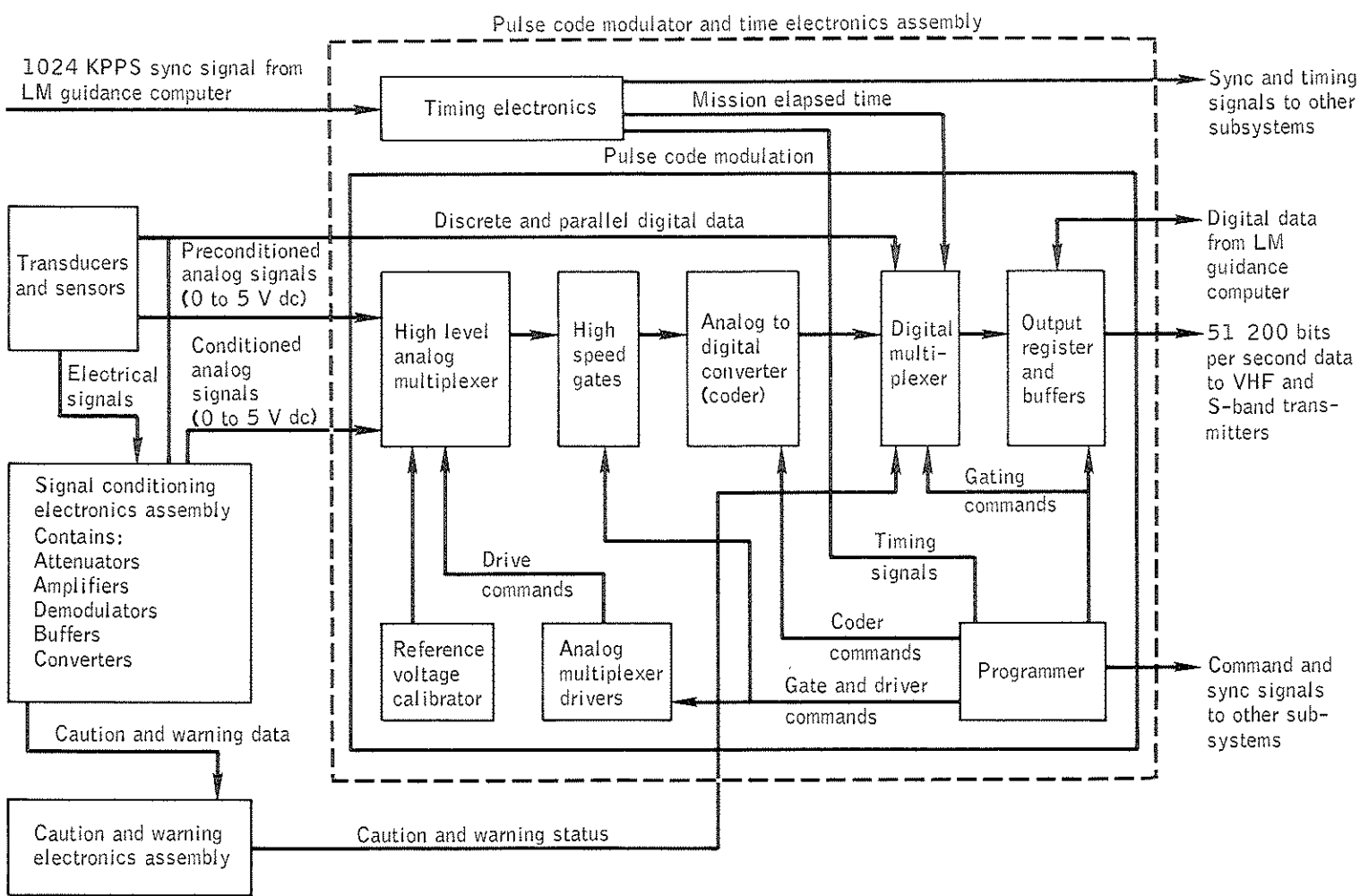


Figure 13.2-12.- Operational instrumentation functional block diagram.

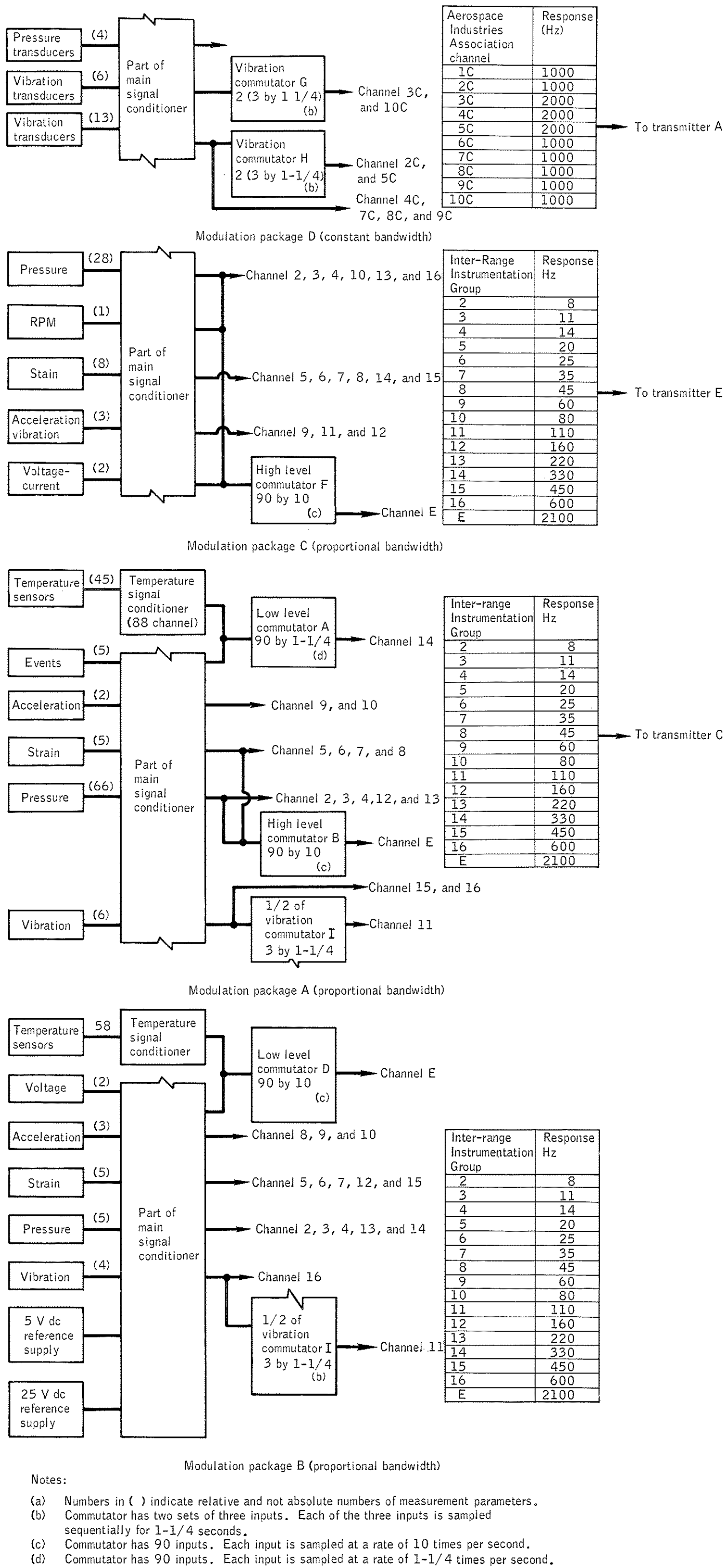


Figure 13.2-13.- Development flight instrumentation data conditioning and processing system.

NASA-S-68-2079

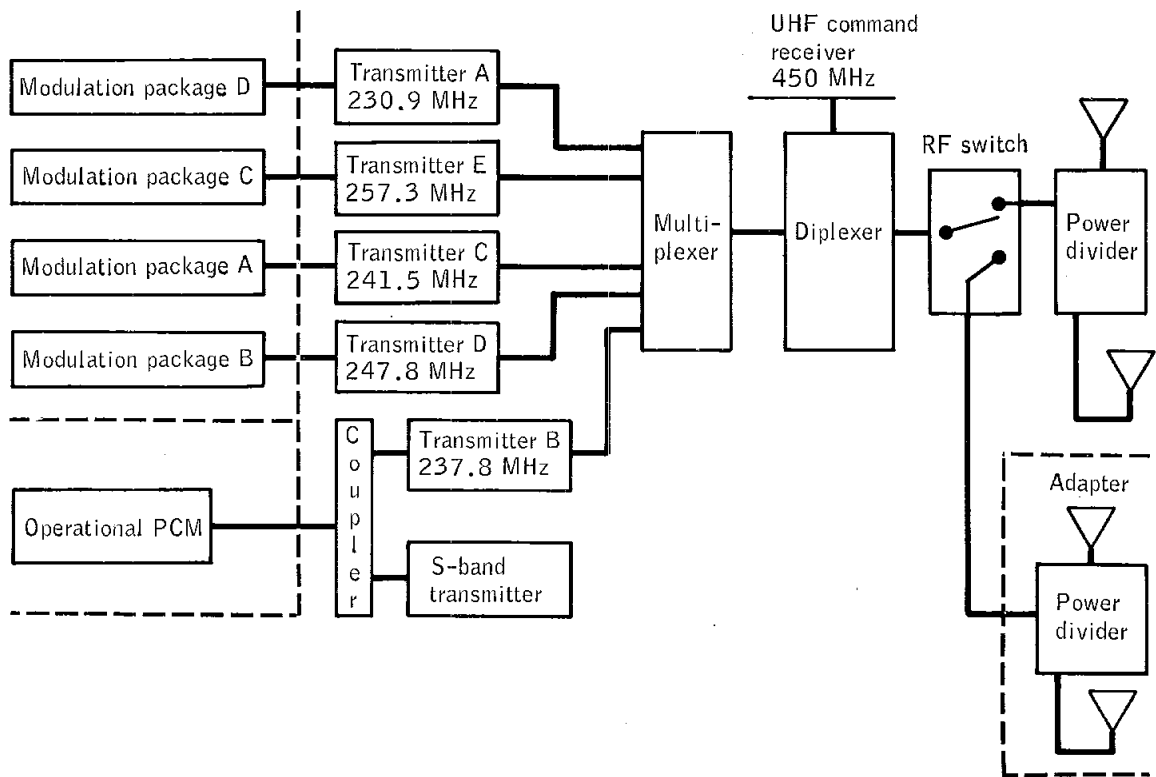


Figure 13.2-14.- Development flight instrumentation data transmission system.

NASA-S-68-2105

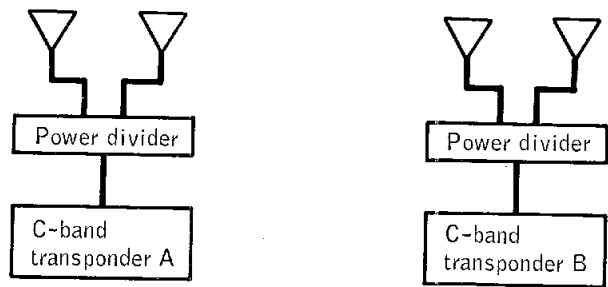


Figure 13.2-15.- Development flight instrumentation ranging and tracking RF system.

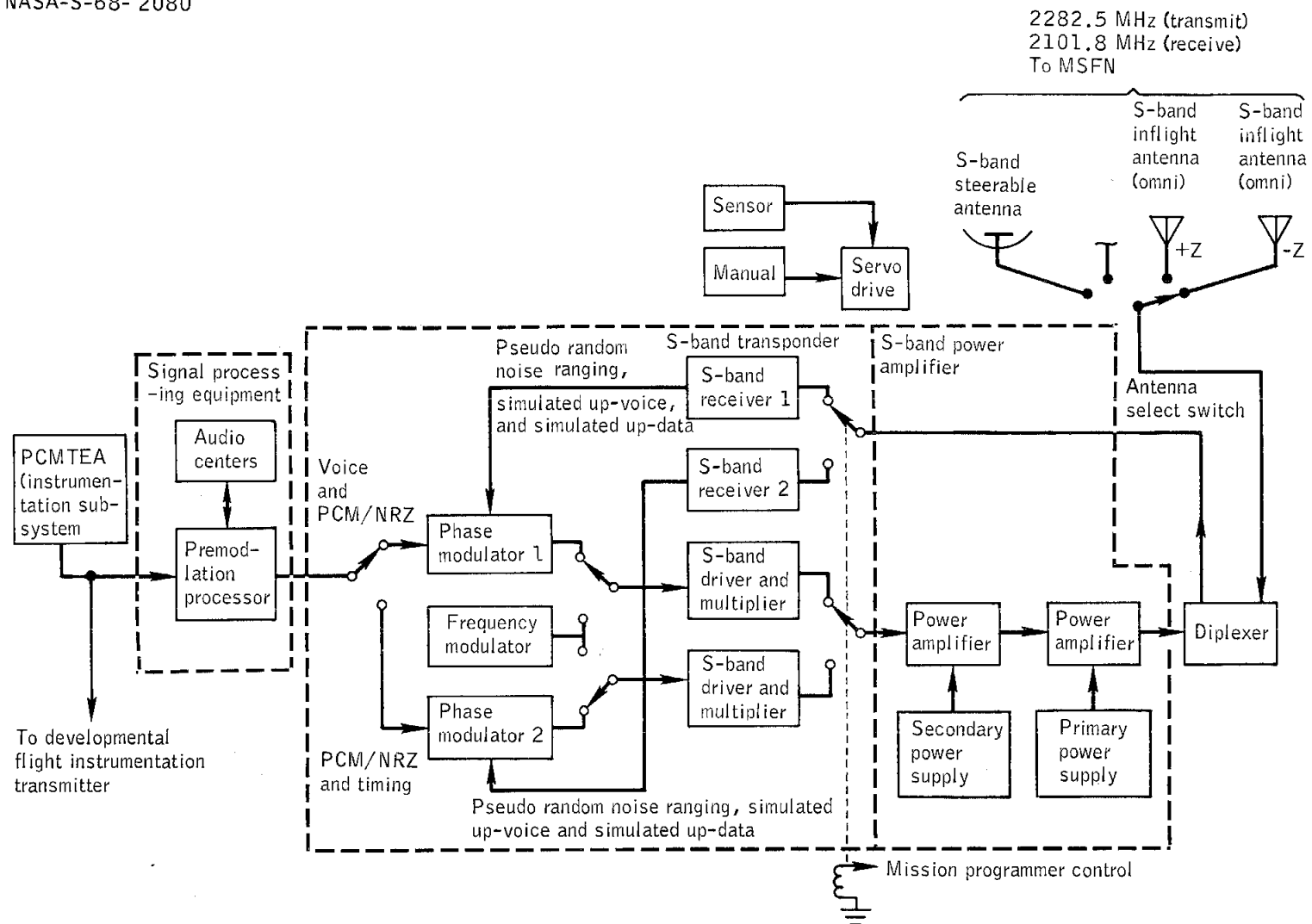
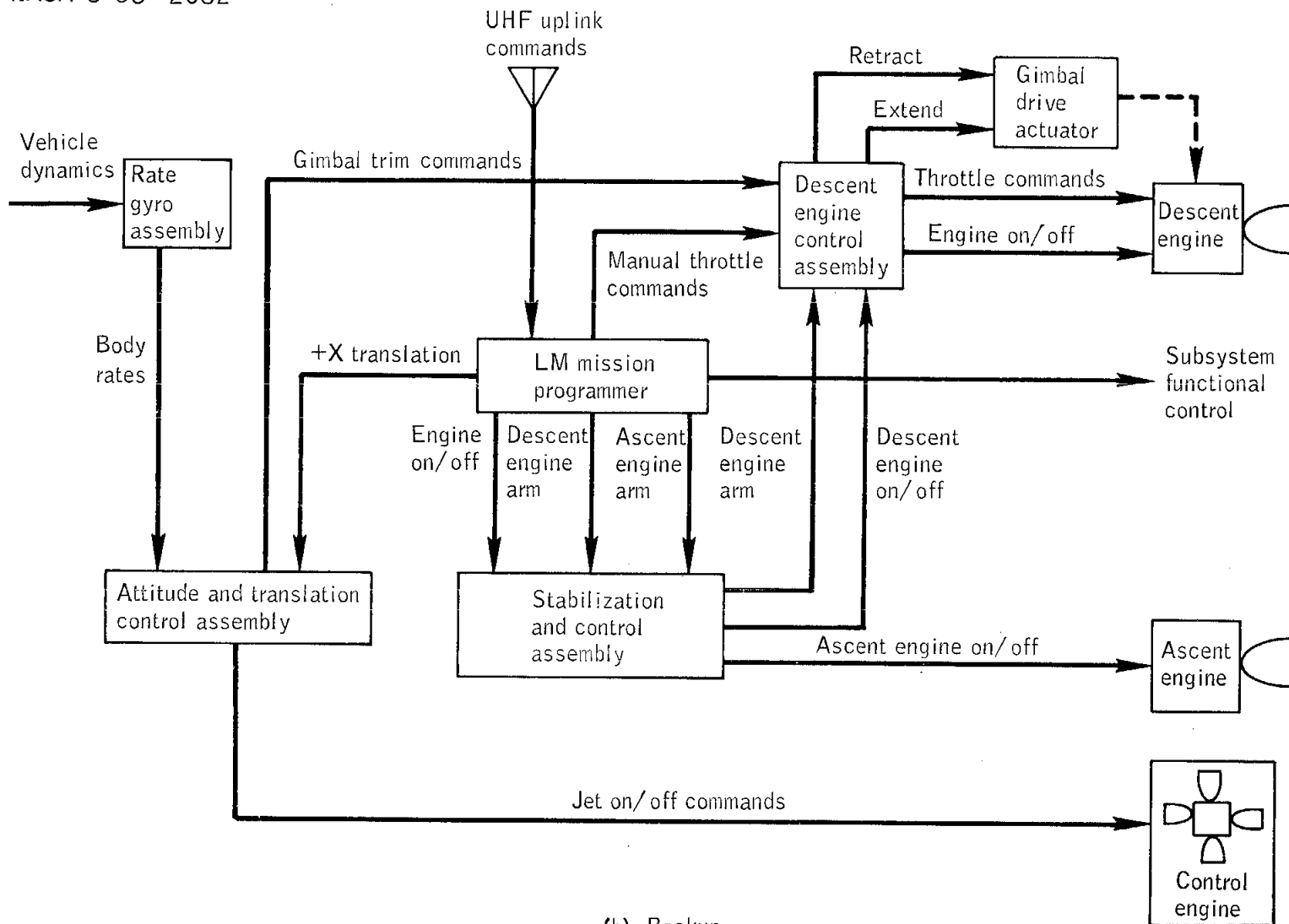


Figure 13.2-16.- Communication system schematic.



(b) Backup.

Figure 13.2-17.- Concluded.

NASA-S-68-2083

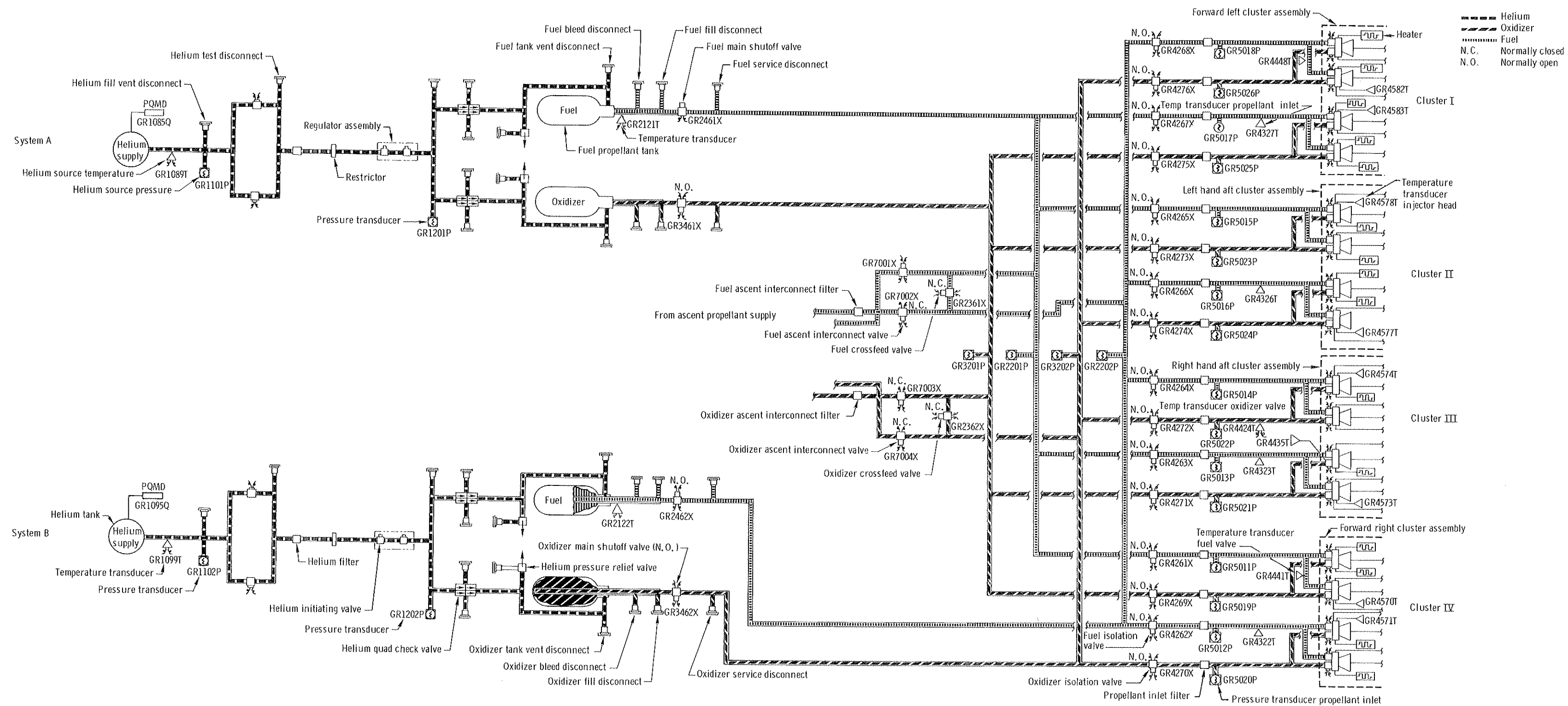


Figure 13.2-18. - Reaction control system.

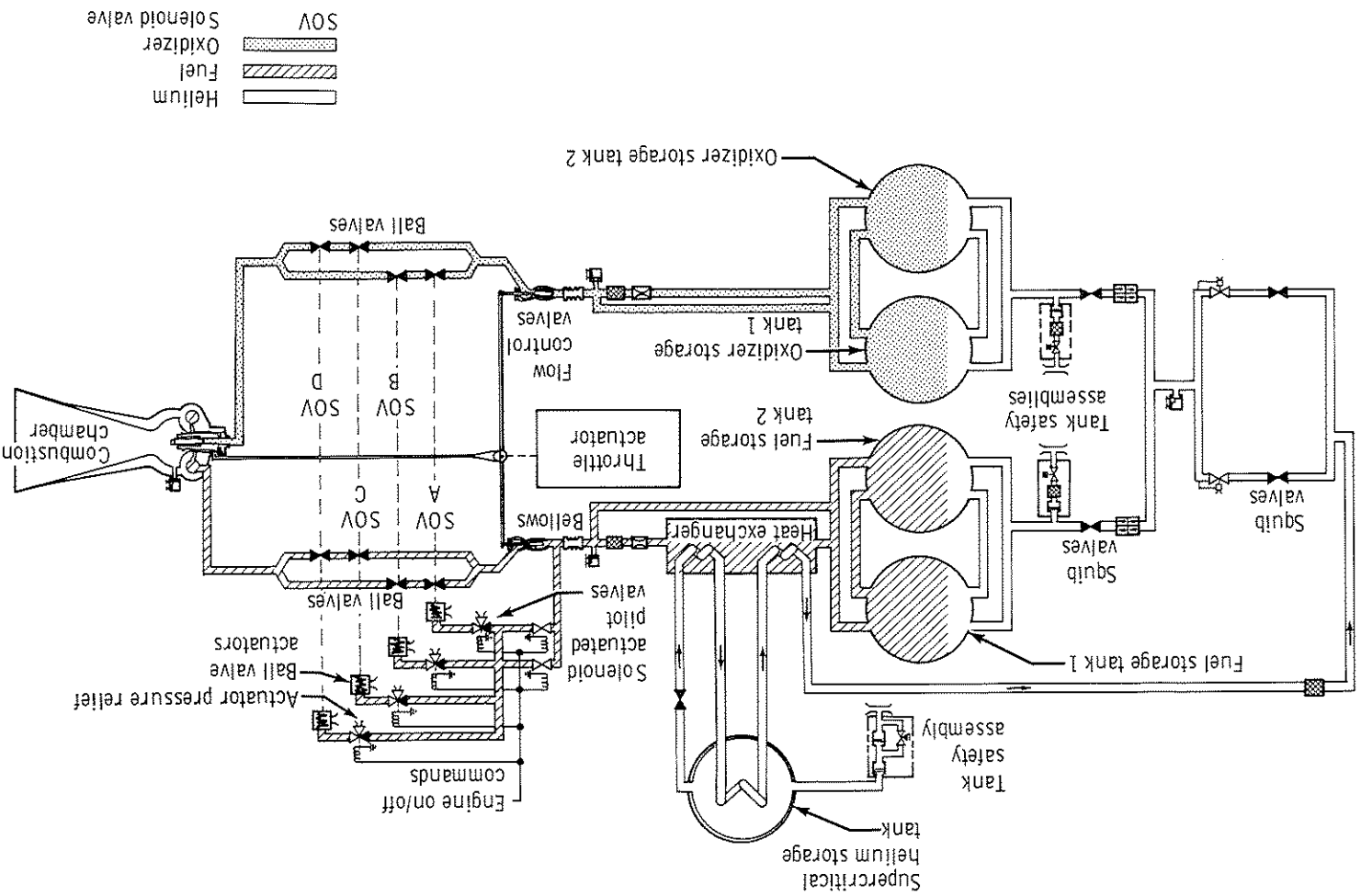


Figure 13.2-19. - Descent propulsion system schematic.

NASA-S-68-2085

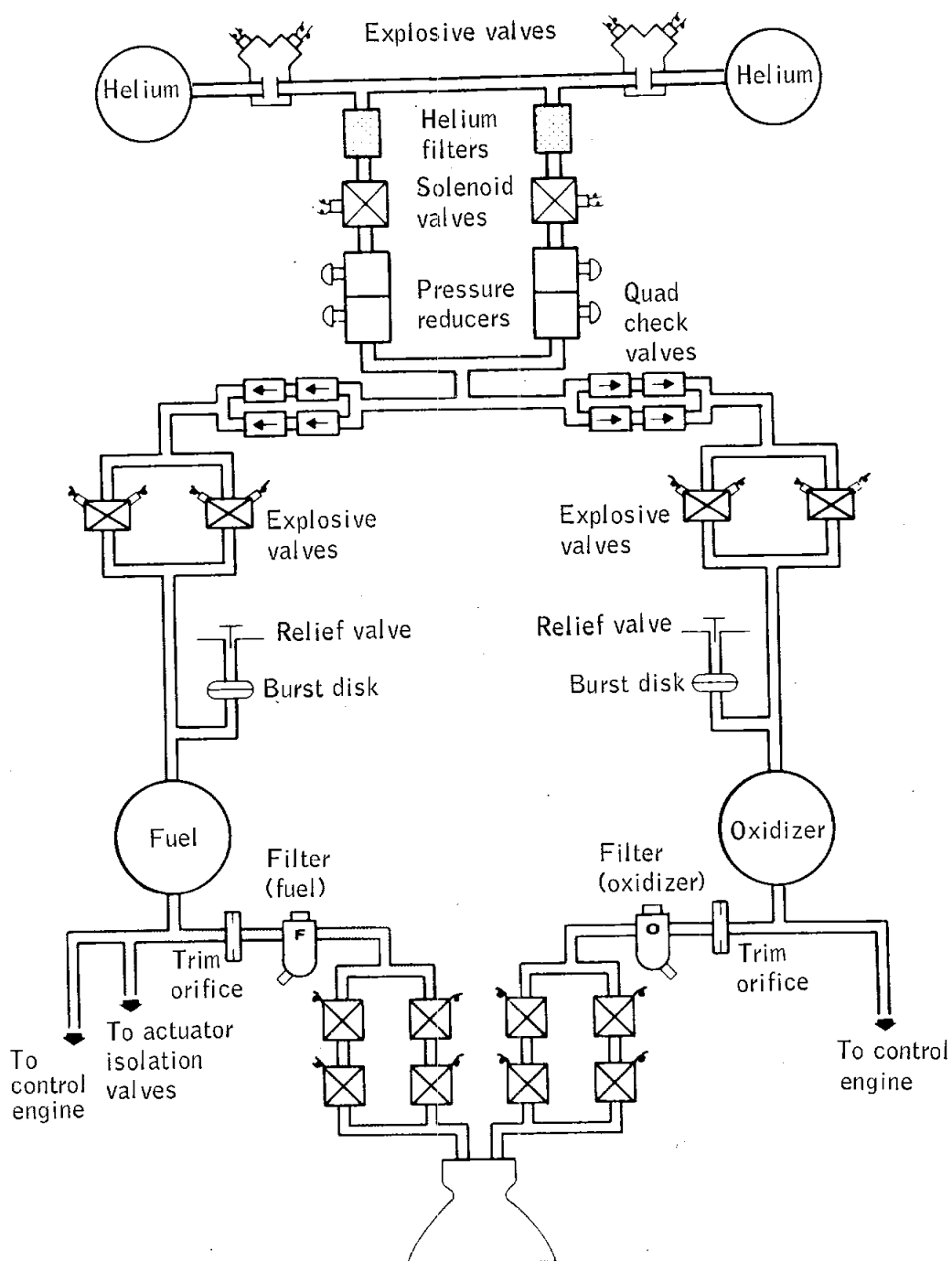


Figure 13.2-20.- Ascent propulsion propellant/ pressurization schematic.

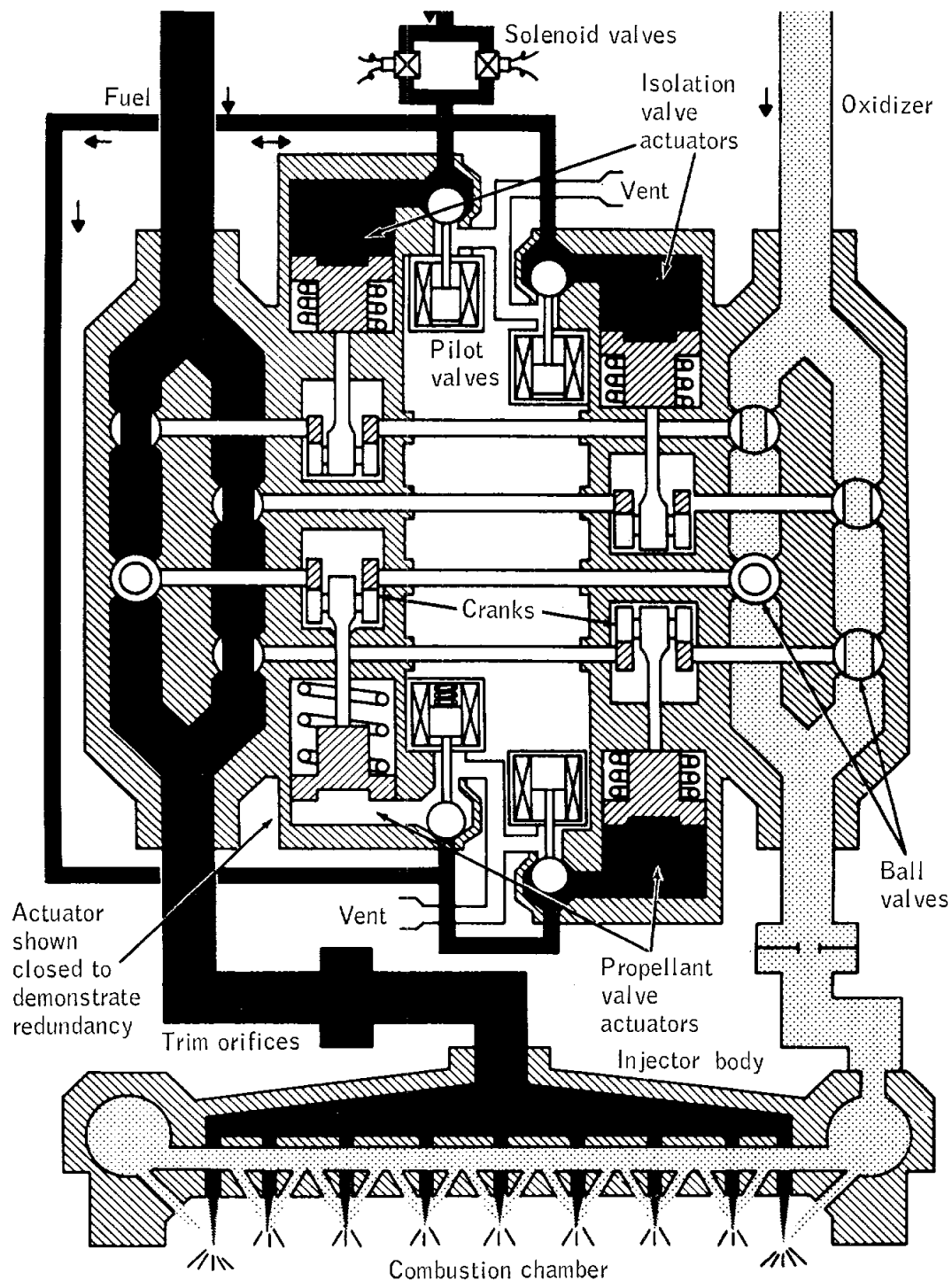


Figure 13.2-21.- Ascent engine schematic.

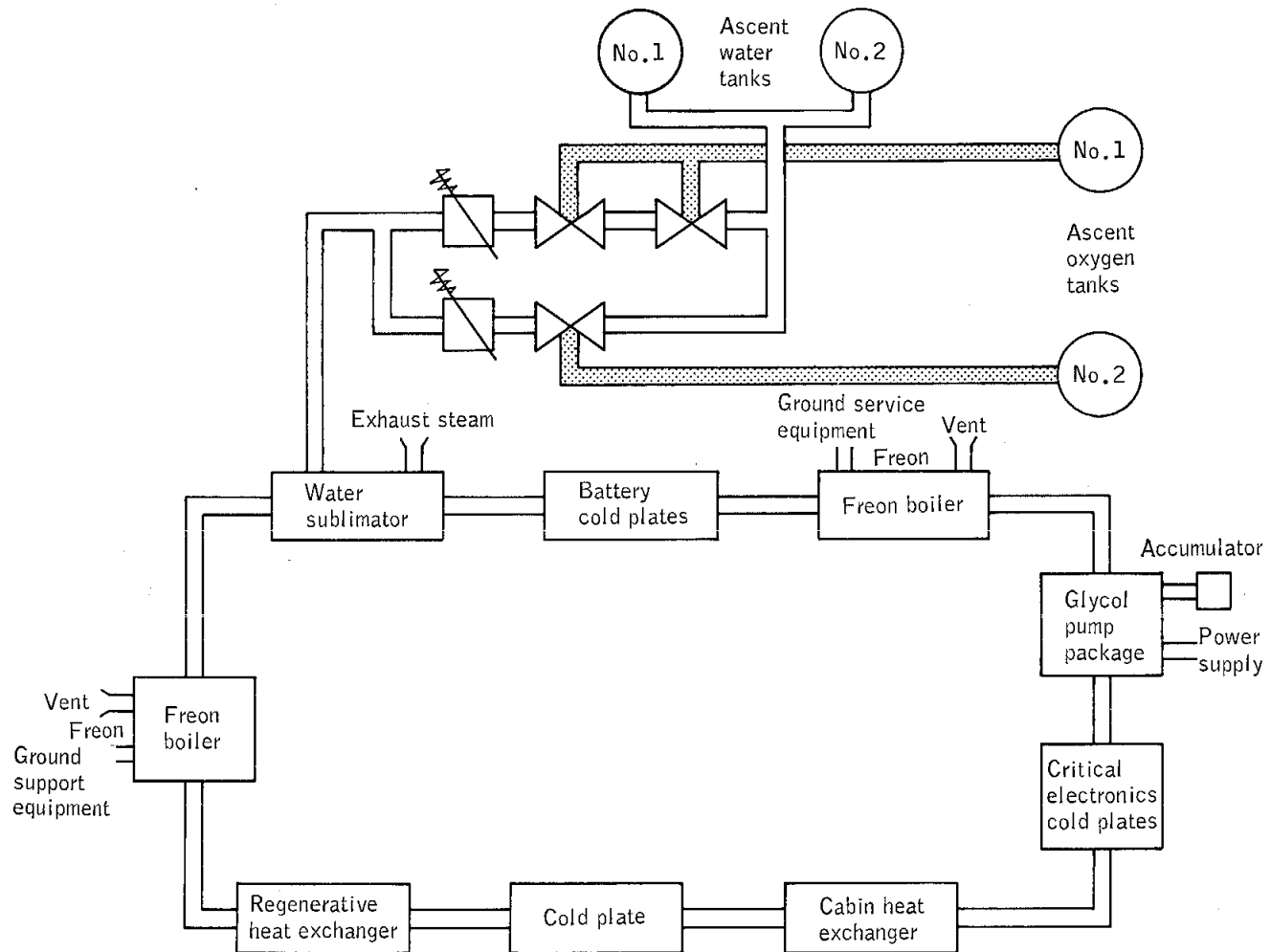


Figure 13.2-22.- Schematic of environmental control system.

13.3 LAUNCH VEHICLE

The flight of launch vehicle AS-204 was the fourth flight to qualify and flight test the Saturn-IB vehicle. It was the first flight of the lunar module with the Saturn-IB launch vehicle. The space vehicle (fig. 13.0-1) was approximately 181 feet long and consisted of an S-IB stage, an S-IVB stage, an instrument unit, an adapter, a nose cone, and a lunar module.

13.3.1 S-IB Stage

The S-IB stage was 80.3 feet long and 21.4 feet in diameter (fig. 13.3-1). A cluster of eight uprated H-1 engines powered the S-IB stage and produced a total sea-level thrust of 1 600 000 pounds. Each of the four outboard engines gimballed in a ± 8 -degree square pattern to provide pitch, yaw, and roll control. The inboard engines were canted 3 degrees and the outboard engines 6 degrees outward from the vehicle longitudinal axis.

Fuel (RP-1) and oxidizer (liquid oxygen) were supplied to the engines from nine propellant tanks arranged in a cluster. Oxidizer and fuel tank pressurization modules regulated the tank pressures during ground operation and S-IB stage flight. Nominal stage propellant loading capacity was 884 000 pounds.

Eight fins attached to the base of the S-IB stage provided vehicle support and hold-down points prior to launch and provided inflight stability. The area of each fin was 53.3 square feet. Each fin extended radially approximately 9 feet from the outer surface of the thrust structure.

Additional systems on the S-IB stage included: (a) flight control, (b) hydraulic (which gimballed the outboard engines), (c) electrical, (d) environmental control (which thermally conditioned the aft compartment of instrument canisters F1 and F2), (e) data acquisition, (f) range safety, (g) propellant utilization, and (h) four solid-propellant retrograde motors. Guidance and control commands for the S-IB stage were received from the instrument unit.

13.3.2 S-IVB Stage

The S-IVB stage (fig. 13.3-2) was 58.4 feet long and 21.7 feet in diameter. A single gimbal-mounted J-2 engine powered the vehicle during

the S-IVB stage portion of powered flight. The engine was mounted on the thrust structure and could be gimballed in a ± 7 -degree square pattern. The engine provided 200 000 pounds total thrust at vacuum conditions when the propellant mixture ratio was a nominal 5:1.

The tanks, fuel forward and oxidizer aft, were separated by a common bulkhead. The fuel (liquid hydrogen) tank consisted of a cylindrical container with a bulkhead at each end. The oxidizer (liquid oxygen) tank consisted of the section between the common bulkhead and an adjacent bulkhead and enclosed by the structural skin.

Oxidizer and fuel tank pressurization modules regulated the tank pressures during ground operations, S-IB boost phase, and S-IVB boost phase. The pneumatic control system used ambient helium to operate the control valves. Nominal propellant loading capacity was 228 500 pounds.

The auxiliary propulsion system of the S-IVB stage provided roll control during S-IVB powered flight, attitude stabilization and reorientation after burnout, and attitude control during coast or maneuvering. The modules were mounted on opposite sides of the S-IVB aft skirt.

Additional systems on the S-IVB stage included (a) flight control (which included auxiliary attitude control and thrust vector control), (b) hydraulic (which gimballed the J-2 engine), (c) electrical, (d) thermoconditioning (which thermally conditioned the electrical/electronic modules in the forward skirt area), (e) data acquisition and telemetry (which acquired and transmitted data for the evaluation of stage performance and environment), (f) ordnance (used for rocket ignition, stage separation, ullage rocket jettison, and range safety), (g) propellant utilization, and (h) three ullage motors. Guidance and control commands were received from the instrument unit.

13.3.3 Instrument Unit

The instrument unit was located just forward of the S-IVB stage. It was a three-segment, cylindrical, unpressurized structure 260 inches in diameter and 36 inches long. The cylinder formed a part of the vehicle load-bearing structure and interfaced with the S-IVB stage and the adapter. Various launch vehicle telemetry and tracking antennas were mounted on the instrument unit. The instrument unit housed electrical and mechanical equipment that guided, controlled, and monitored vehicle performance from lift-off to atmospheric entry of the instrument unit.

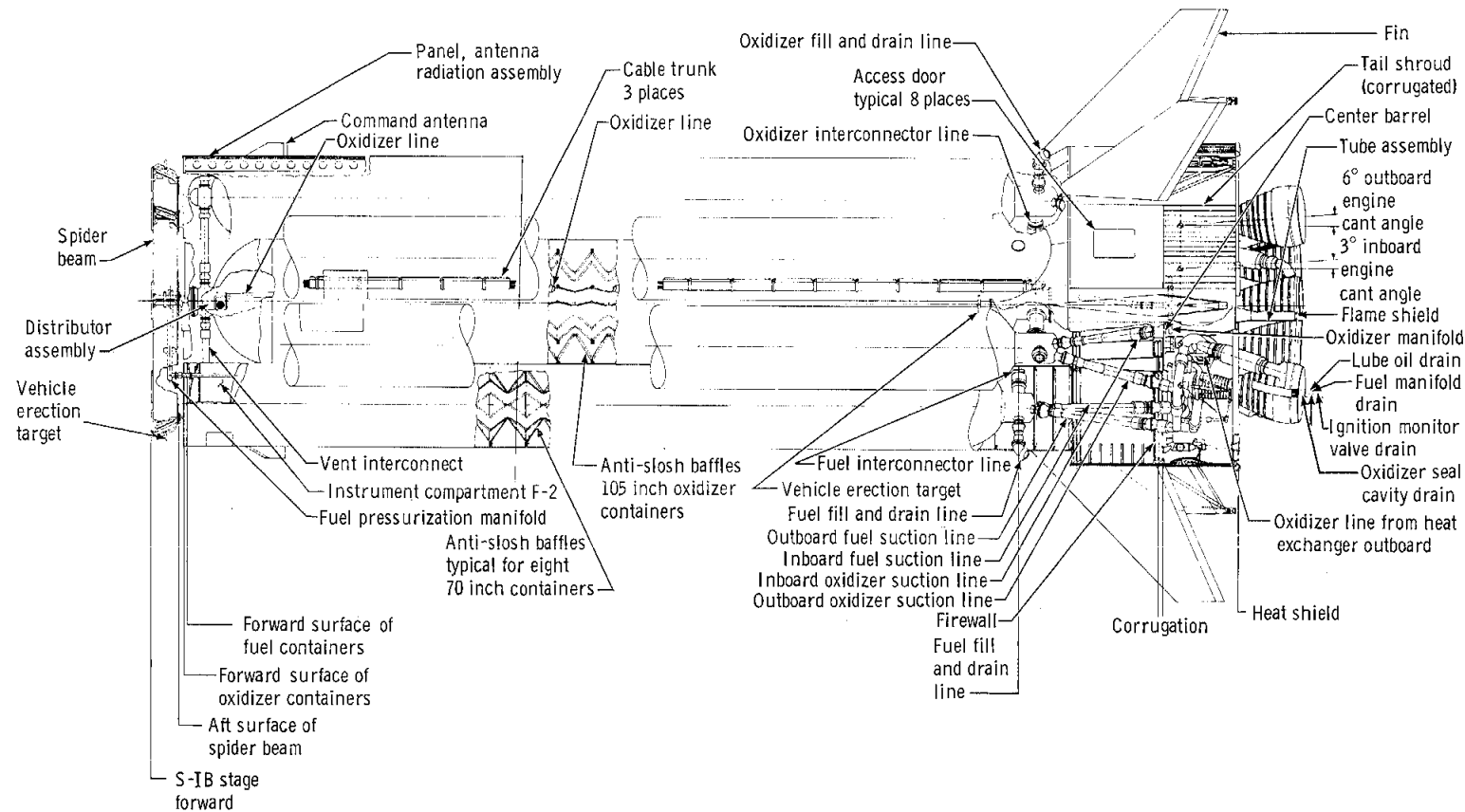


Figure 13.3-1. - S-IB stage.

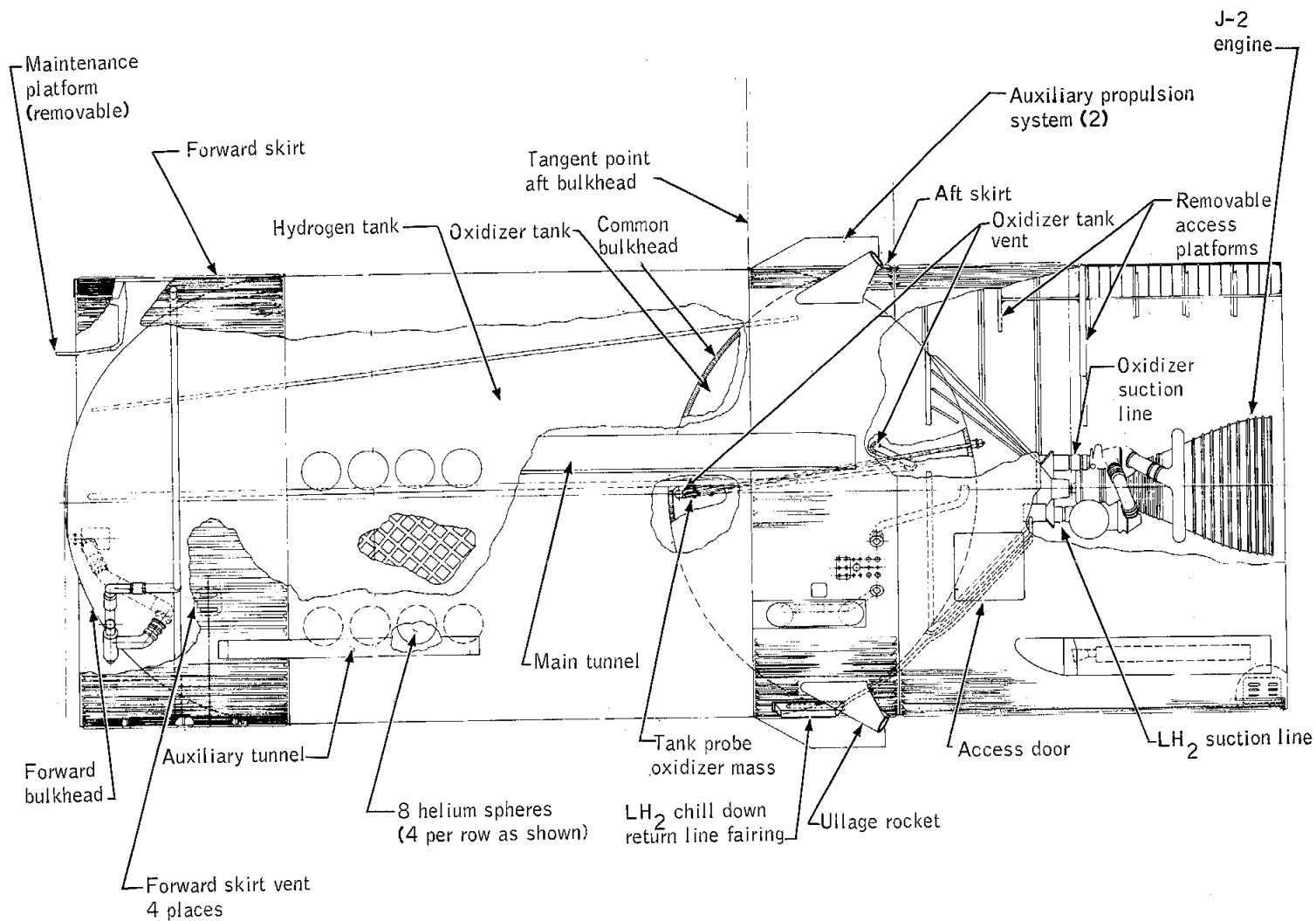


Figure 13.3-2.- S-IVB stage.

13.4 ADAPTER AND NOSE CONE

The adapter structure was an aluminum honeycomb truncated conical shell (fig. 13.4-1). The aft section had four attachment points for the lunar module. The forward section was four panels (fig. 13.4-2) which were separated by a mild detonating fuse explosive train about 9 minutes after the nose cone had been jettisoned. Control engines rotated each panel about an aft hinge line to the open position, where each was retained by a cable retention system.

The spacecraft/lunar module adapter controller accepted commands from the launch vehicle instrument unit to initiate nose cone jettison and adapter panels deploy. The controller also accepted commands from the lunar module mission programmer to initiate separation of the lunar module from the adapter. For a schematic of system A (system B is redundant), see figure 13.4-3.

The two controllers were mounted 90 degrees apart within the adapter below the panels. The sequencer logic was powered by a 5 amp-hr battery and the pyrotechnic devices by a 0.75 amp-hr battery. A total of four batteries were installed: one 5 amp-hr and one 0.75 amp-hr battery to power system A, and a duplicate of each to power system B.

The nose cone (fig. 13.4-2) was furnished by the Marshall Space Flight Center (MSFC). It was a conical shell constructed of aluminum skin, stringers, and ring frames with a cone angle of 25 degrees. The nose cone was detached from the adapter by pyrotechnic devices and was separated from the adapter by 16 springs.

NASA-S-68- 2063

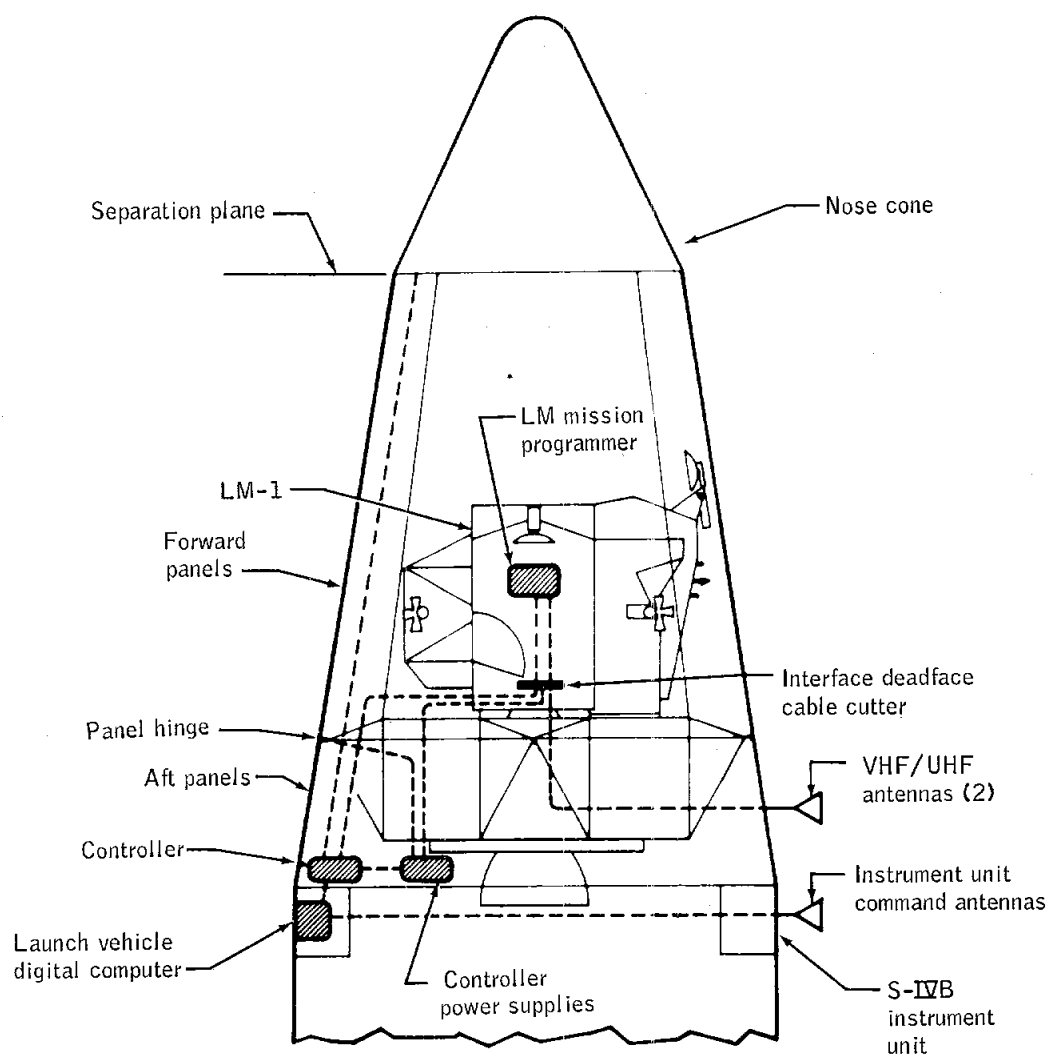


Figure 13.4-1.- Location of lunar module within adapter.

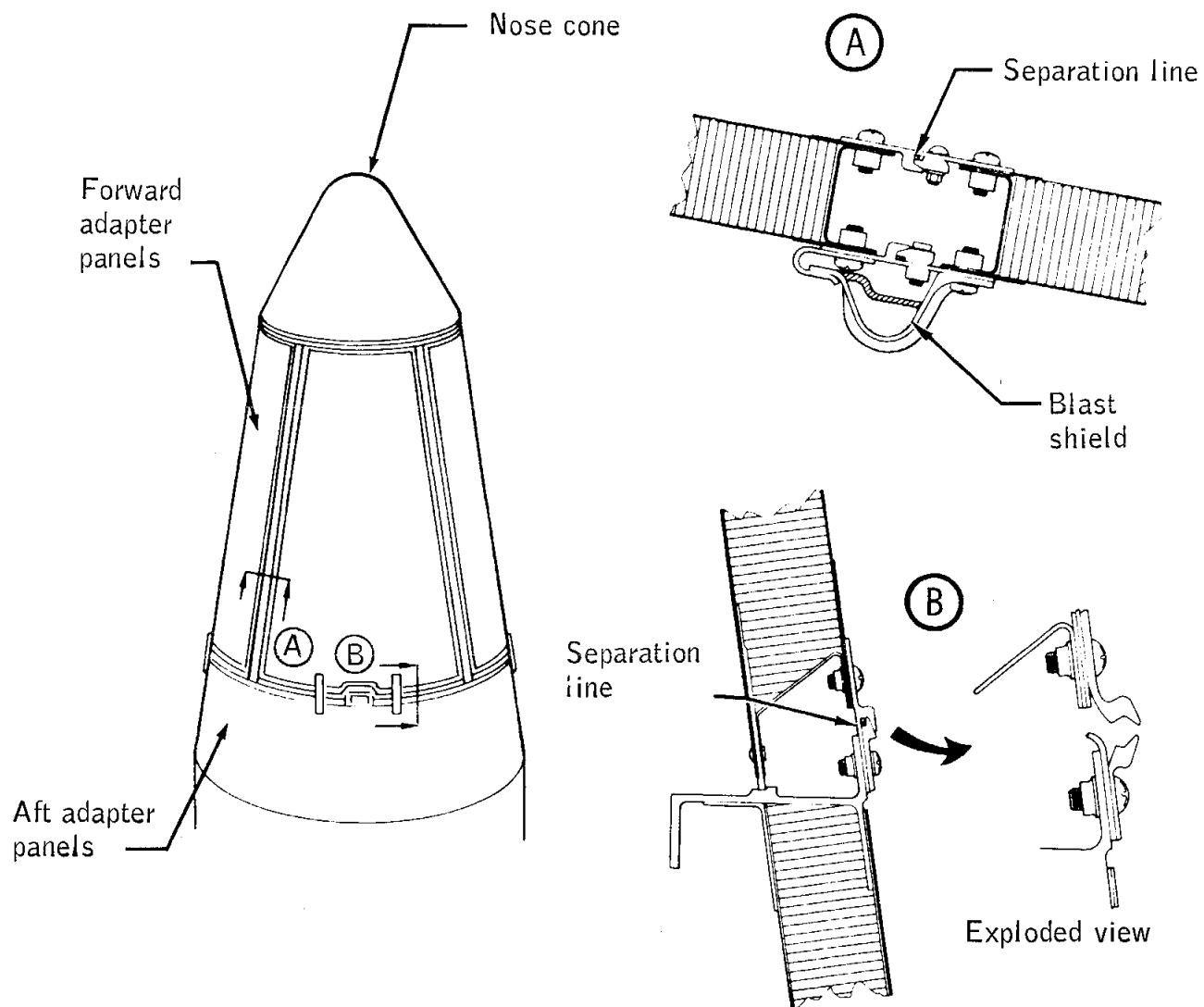


Figure 13.4-2.- Adapter panel separation lines.



Figure 13.4-3.- Nose cone jettison controller, schematic diagram of system A of a redundant A and B system.

13.5 WEIGHT AND BALANCE DATA

The spacecraft mass properties for the Apollo 5 mission are summarized in table 13.5-I. These data represent the actual conditions as determined from postflight analyses of the expendable items loaded and used during the flight.

The weight and the center of gravity were measured for each stage prior to stacking. Inertia values were calculated for the actual weight data obtained. All changes subsequent to measurement and prior to launch were monitored and the mass properties were revised as required.

The mass properties and expendable items loaded at launch did not vary significantly from the predicted values used to establish the operational trajectory. As a result, updating of mass properties and trajectory data was not required prior to launch.

The variations in mass properties were determined for each significant mission phase from lift-off through the end of the second ascent engine firing. The usage of expendables was based on postflight analysis of the mission data. All available ascent and control engine propellants were depleted during the second ascent engine firing, and the vehicle became uncontrollable.

TABLE 13.5-I.- MASS PROPERTIES

	Weight, lb	Center of gravity, in.			Moment of inertia, slug-ft ²		
		X	Y	Z	I _{xx}	I _{yy}	I _{zz}
<u>Launch</u>							
Ascent stage	4 613	257.5	-0.6	0.7	2 560	2 412	1 494
Reaction control propellant	612	276.9	0.0	0.0	292	32	268
Ascent propellant	5 150	227.1	-0.2	0.0	3 547	13	3 546
Descent stage	3 353	157.3	12.8	0.7	2 359	1 487	1 642
Descent propellant	17 800	159.2	0.0	0.0	11 259	7 118	4 627
Total LM at launch	31 528	186.8	1.2	0.2	20 126	22 474	23 096
<u>Launch to first descent engine firing</u>							
LM/adaptor umbilical	-6	209.8	89.0	-29.2	0	0	0
Reaction control propellant	-27	291.9	8.2	-0.5	15	2	14
Environmental control consumables	-23	302.8	-7.6	-4.2	4	1	3
Total LM at first descent engine firing	31 472	186.6	1.2	0.2	20 096	22 338	22 937
<u>First descent engine firing to first coast</u>							
Descent propellant	-15	403.0	0.0	3.6	9	185	185
Total LM at first coast	31 457	186.5	1.2	0.2	20 086	22 371	22 971
<u>First coast to second descent engine firing</u>							
Reaction control propellant	-32	291.1	13.9	-1.8	14	0	11
Environmental control consumables	-10	301.8	0.0	0.0	2	0	1
Total LM at second descent engine firing	31 415	186.3	1.2	0.2	20 070	22 266	22 853
<u>Second descent engine firing to third firing</u>							
Descent propellant	-306	181.8	0.0	0.0	193	93	49
Reaction control propellant	-54	287.3	4.9	-0.5	25	1	20
Total LM at third descent engine firing	31 055	186.2	1.2	0.2	19 851	22 053	22 064

TABLE 13.5-I.- MASS PROPERTIES - Concluded

	Weight, lb	Center of gravity, in.			Moment of inertia, slug-ft ²		
		X	Y	Z	I _{xx}	I _{yy}	I _{zz}
<u>Third descent engine firing to abort staging</u>							
Descent propellant	-179	187.6	-0.3	0.0	113	40	15
Reaction control propellant	-15	257.0	-3.0	-1.0	7	1	6
Total LM at abort staging	30 861	186.2	1.2	0.2	19 732	21 998	22 628
<u>Abort staging to second coast</u>							
Descent stage (jettison)	-3 347	157.3	12.8	0.7	2 359	1 487	1 642
Descent stage propellant (jettison)	-17 300	158.3	0.0	0.0	10 944	6 909	4 488
Ascent engine propellant	-682	242.6	0.0	0.0	468	38	430
Reaction control propellant	3	288.7	-14.8	4.8	1	0	1
Total LM at second coast	9 529	242.8	-0.5	0.4	5 849	3 063	5 382
<u>Second coast to second ascent engine firing</u>							
Environmental control consumables	-8	300.9	0.0	0.0	1	0	1
Reaction control consumables	-377	276.0	4.6	0.5	177	16	159
Total LM at second ascent engine firing	9 144	241.4	-0.7	0.4	5 669	2 947	5 121
<u>Second ascent engine firing to end of firing</u>							
Ascent propellant	-4 282	225.5	0.0	0.0	2 946	3	2 930
Reaction control propellant	-53	267.4	-44.5	4.7	2	2	0
Nozzle ablation	-10	220.2	0.0	0.0	0	0	0
Environmental control consumables	-1	300.2	0.0	0.0	0	0	0
Total LM at end of second ascent stage firing	4 798	255.3	-0.9	0.7	2 698	2 505	1 725

14.0 VEHICLE HISTORIES

Figure 14-1 shows the history of the LM-1 at Bethpage, New York.
Figure 14-2 shows the history of the LM-1 at Kennedy Space Center.

NASA-S-68-2090

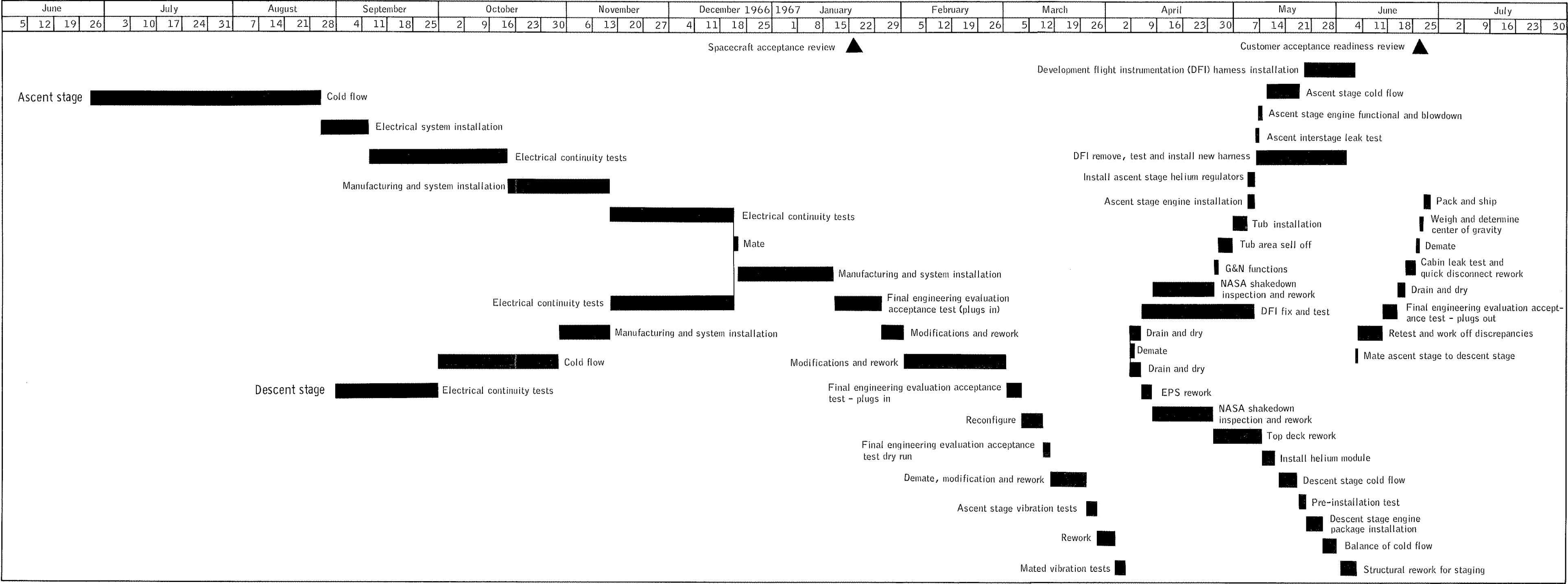


Figure 14-1.- LM-1 history at Bethpage.

NASA-S-68-2091

Week ending dates

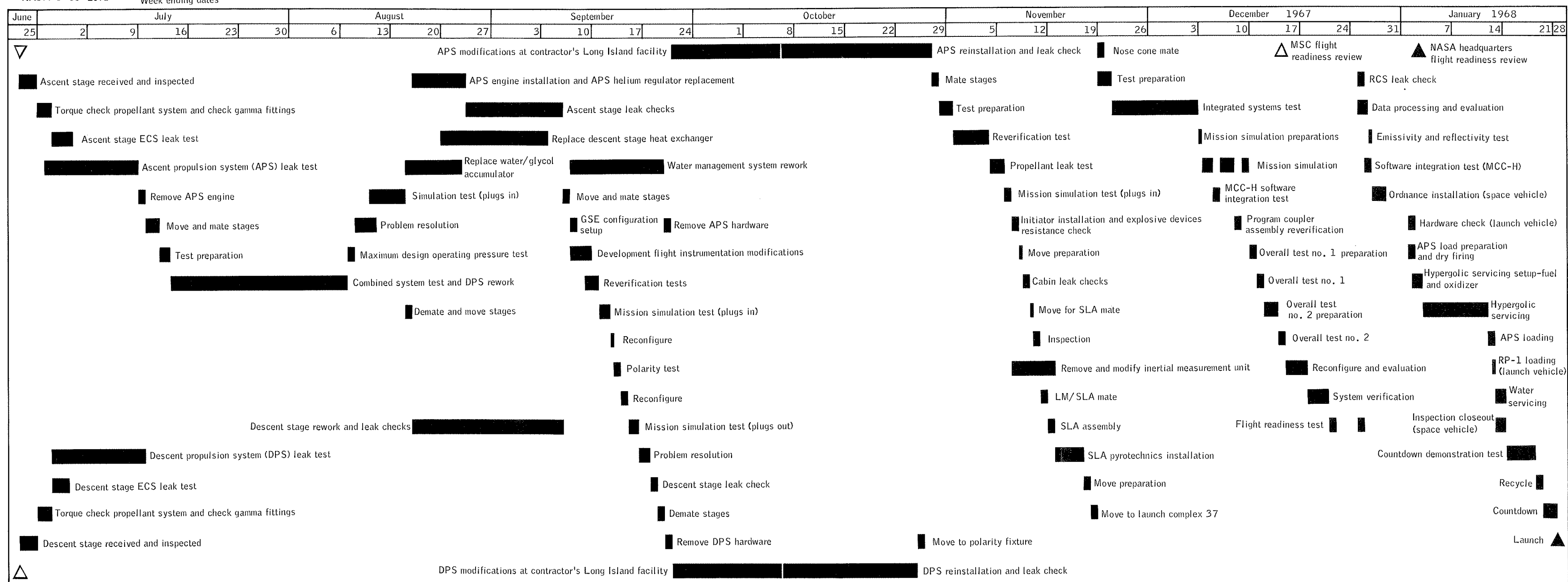


Figure 14-2.- LM-1 history at Kennedy Space Center.

15.0 SUPPLEMENTAL REPORTS

The following table lists the supplemental reports to be published for the Apollo 5 mission:

No.	Subject	Responsible analysis manager	Expected publication date
1	General Supplement (anomalies closeout, errata, and minor supplemental information)	T. J. Grace	5/6/68
2	Apollo 5 Postflight Trajectory Reconstruction Volume I - Analysis Volume II - Trajectory	D. J. Incerto	5/1/68
3	Detailed Analysis of S-band Communications	A. D. Travis	5/3/68
4	Analysis of Digital Autopilot Performance	J. F. Hanaway	4/30/68
5	Apollo 5 Guidance and Navigation Error Analysis - Final Report	J. F. Hanaway	4/15/68
6	Dynamics of LM/S-IVB Stage Separation	J. F. Hanaway	5/1/68
7	Detailed Analysis of Descent Engine Performance	R. B. Ferguson	5/22/68
8	Detailed Analysis of Ascent Engine Performance	R. B. Ferguson	5/22/68

Supplemental reports will not be distributed to all persons who receive the Mission Report. Persons who do not receive supplements may request a specific supplement from BF66, Manned Spacecraft Center, Houston, Texas.

16.0 REFERENCES

1. Chrysler Corporation, Space Division: AS-204/LM-1 Launch Vehicle Operational Flight Trajectory. Revision 1 TN AP-67-255 July 25, 1967
2. Manned Spacecraft Center: Apollo V Mission, AS-204/LM-1 Spacecraft Operational Trajectory. IN 67 FM-194 (3 volumes) December 29, 1967
3. Marshall Space Flight Center: Apollo V Mission Report, Launch Vehicle (This report has not yet been released; therefore, no report number can be cited.)
4. Grumman Aircraft Engineering Corp: LM Instrumentation Installation Photographs, LM-1. LED-360-423 June 23, 1967
5. Manned Spacecraft Center: PA-1 Static Firing. PA 1-7A-005, MSC WSTF, Las Cruces, New Mexico. January 3, 1968
6. Office of Manned Spaceflight: Apollo Flight Mission Assignments (U) OMSF Confidential Document M-D MA 500-11, SE 010-000-1, November 14, 1966
7. National Aeronautics and Space Administration, Manned Spacecraft Center: Apollo Report. SPD7-R-002, Revision 5, December 4, 1967

27.0 DISTRIBUTION

<u>Addressee</u>	<u>Ko. copies</u>	<u>Addressee</u>	<u>No. copies</u>
National Aeronautics and Space Administration Washington, D. C. 20546		National Aeronautics and Space Administration Manned Spacecraft Center Houston, Texas 77058	
MA/S. C. Phillips	1	Apollo Applications Program Office	
MA/G. H. Hage	1	Attention: KA/R. P. Thompson	
MA/W. C. Schneider	1	KA/J. E. Roberts/W. B. Mitchell	1
MAO/J. K. Holcomb	1	KF/Manager, Future Missions Project Office	1
MAF/Program Control Director	1	KX/Manager, Mission Operations Office	2
MAR/G. C. White	1	KP/Manager, Program Control Office	1
MAS/R. L. Wagner	1	KS/Manager, Systems Engineering Office	1
MAT/L. Day	5	KT/Manager, Test Operations Office	1
MC/MSP Field Center Development Director	1	KW/Manager, Orbital Workshop Project Office	1
ME/E. Cortright	1		
ME/C. W. Mathews	1	Reliability and Quality Assurance Office	
MET/M. Savage	1	Attention: RA/A. C. Bond	8
MT/Advance Manned Missions Program Director	2		
R/M. C. Adams	1	Apollo Spacecraft Program Office	
S/J. E. Maugle	1	Office of Program Manager	
T/G. M. Truszynski	1	Attention: FA/G. M. Low	1
JSS-1C/NASA Headquarters Library	2	FA/E. F. M. Rees	1
		PA/X. S. Kleinknecht	1
		PA/C. H. Bolender	1
		PA/S. H. Simpkinson	1
		PA/G. W. S. Abbey	1
		PA/H. W. Tindall	1
		PA/Apollo Files	3
		PD/Chief, Systems Engineering Division	14
		PE/Chief, LM Project Engineering Division	5
		PF/Chief, C&SM Project Engineering Division	3
		PT/Chief, Test Division	15
		PP/Chief, Program Control Division	3
		NASA-RASPO	
		Grumman Aircraft Engineering Corporation	
		Bethpage, New York 11714	
		Attention: PE/A. Kobakan	10
		NASA-RASPO	
		North American Rockwell Corporation	
		12214 Lakewood Blvd.	
		Downey, California 90241	
		Attention: PC/W. H. Gray	13
		Flight Safety Office	
		Attention: SA/A. C. Bond	5
		Director of Science and Applications	
		Attention: TA/W. C. Hess	1
		TD/Manager, Lunar Surface Project Office	1
		TF/Manager, Test and Operations Office	2
		TC/Chief, Space Physics Division	1
		ASPO Acting Manager, KSC	
		Kennedy Space Center, Florida	
		Attention: PSX/A. E. Morse	2
		Coddard Space Flight Center Liaison Office, GSF-L	1
		Attention: GSF-L/W. B. Easter	1
		Marshall Space Flight Center Resident Liaison Office	
		Attention: RL/J. T. Hamilton	1
		Langley Research Center Liaison Office	
		Attention: RAA/A. T. Mattson	1
		DOD Manager's Liaison Office	
		Attention: ZR2/Cmdr. R. E. Colopy	1
		NASA Ames Research Center	
		Moffett Field, California 94035	
		Attention: C. Goodwin	1
		H. J. Allen	1
		Ames Research Center Library	6
		Eastern Test Range	
		Patrick Air Force Base, Florida	
		Attention: Major General V. G. Huston	1
		Colonel R. Olson, EOD Manager	3
		NASA Electronics Research Center	
		565 Technology Square	
		Cambridge, Massachusetts 02139	
		Attention: J. C. Elms	1
		NASA Flight Research Center	
		Post Office Box 273	
		Edwards, California 93523	
		Attention: P. F. Bikle	1
Director of Flight Operations			
Attention: FA/U. C. Kraft, Jr.	1		
FC/Chief, Flight Control Division	10		
FL/Chief, Landing and Recovery Division	5		
FM/Chief, Mission Planning and Analysis Division	1		
FL/Chief, Flight Support Division	3		

Addressee	No. copies	Addressee	No. copies
NASA Goddard Space Flight Center Greenbelt, Maryland 20771 Attention: DIR/John F. Clark	1	Grumman Aircraft Engineering Corporation Kennedy Space Center, Florida Attention: G. M. Skurka	10
506/M. P. Thompson	1		
506/W. P. Varson	1	Grumman Aircraft Engineering Corporation 1740 NASA Boulevard Houston, Texas 77058 Attention: J. M. Buxton	10
550/C. Roberts	1		
800/O. M. Covington	1		
801/H. P. Thompson	1		
810/Manned Flight Engineering Division	5		
820/Manned Flight Operations Division	6	TRW, Incorporated Space Park Drive Houston, Texas 77058 Attention: H1-2058/A. Rosenbloom	6
830/Manned Flight Planning and Analysis Division	5		
840/NASA Communications Division	5		
Goddard Space Flight Center Library	3	Jet Propulsion Laboratory Pasadena, California Attention: DIR/W. H. Pickering	1
John F. Kennedy Space Center, NASA NASA Kennedy Space Center, Florida 32899 Attention: AP/R. O. Middleton	1		
AP-SCG/S. T. Beddingfield	1	North American Rockwell Corporation 12214 Lakewood Blvd. Downey, California 90240 Attention: E. E. Myers	25
AT-SCG/H. E. McCoy	1		
CD/Dr. K. H. Debus	1		
DE/G. M. Preston	1	North American Rockwell Corporation Kennedy Space Center, Florida Attention: B. Hello	5
IN/K. Scandler	1		
LO/R. A. Petrone	1	North American Rockwell Corporation 1840 NASA Boulevard Suite 201 Houston, Texas 77058 Attention: W. T. Short	3
LO/W. L. Kapryan	2		
LS/J. C. Williams	1	The Boeing Company Space Division-Houston P. O. Box 58747 Houston, Texas 77058 Attention: H. J. McClellan	10
LS/A. M. Busch	1		
LS-SRG/S. T. Sasseeen	1	General Electric Company 1830 NASA Boulevard P. O. Box 58408 Houston, Texas 77058 Attention: L. W. Warzecha	10
LS-CAS-42/John F. Kennedy Space Center Library	6		
NASA Lewis Research Center 2100 Brookpark Road Cleveland, Ohio 44135 Attention: Director	1		
Lewis Research Center Library	6		
NASA George C. Marshall Space Flight Center Huntsville, Alabama 35812 Attention: M-Div/W. von Braun	1		
I-MO/F. A. Speer	1		
R-Aero-F/U. P. Lindberg	6		
Marshall Space Flight Center Library	6		
NASA MSC White Sands Missile Range Office of the Manager P. O. Drawer MM Las Cruces, New Mexico 88001 Attention: RA/M. L. Raines	5		
NASA-RASPO Massachusetts Institute of Technology 75 Cambridge Parkway Cambridge, Massachusetts 02142 Attention: EG442/A. C. Metzger	2		
Massachusetts Institute of Technology 75 Cambridge Parkway Cambridge, Massachusetts 02142 Attention: D. C. Hoag	3		
NASA-RASPO AC Electronics Division Milwaukee, Wisconsin 53200 Attention: EG443/W. Swingle	1		
AC Electronics Division, General Motors Corporation Milwaukee, Wisconsin 53200 Attention: H. Brady	3		
Arnold Engineering Development Center Arnold Air Force Station, Tennessee 37389 Attention: General Gossick	1		
Hellcom Inc. 1100 17th Street NW Washington, D.C. Attention: Information Systems Analysis Department Head	1		
Grumman Aircraft Engineering Corporation Bethpage, New York 11714 Attention: J. G. Gavin, Jr.	25		

APOLLO SPACECRAFT FLIGHT HISTORY
(Continued from inside front cover)

<u>Mission</u>	<u>Spacecraft</u>	<u>Description</u>	<u>Launch date</u>	<u>Launch site</u>
Apollo 4	SC-017 LTA-10R	Supercircular entry at lunar return velocity	Nov. 9, 1967	Cape Kennedy, Fla.
Apollo 5	LM-1	First lunar module flight	Jan. 22, 1968	Cape Kennedy, Fla.